NATO Science for Peace and Security Series - C:
Environmental Security

Damage Assessment and Reconstruction after War or Natural Disaster

Edited by
Adnan Ibrahimbegovic
Muhamed Zlatar

Springer

NATO OTAN

This publication is supported by:

The NATO Science for Peace and Security Programme

Damage Assessment and Reconstruction after War or Natural Disaster

NATO Science for Peace and Security Series

This Series presents the results of scientific meetings supported under the NATO Programme: Science for Peace and Security (SPS).

The NATO SPS Programme supports meetings in the following Key Priority areas: (1) Defence Against Terrorism; (2) Countering other Threats to Security and (3) NATO, Partner and Mediterranean Dialogue Country Priorities. The types of meeting supported are generally "Advanced Study Institutes" and "Advanced Research Workshops". The NATO SPS Series collects together the results of these meetings. The meetings are co-organized by scientists from NATO countries and scientists from NATO's "Partner" or "Mediterranean Dialogue" countries. The observations and recommendations made at the meetings, as well as the contents of the volumes in the Series, reflect those of participants and contributors only; they should not necessarily be regarded as reflecting NATO views or policy.

Advanced Study Institutes (ASI) are high-level tutorial courses intended to convey the latest developments in a subject to an advanced-level audience

Advanced Research Workshops (ARW) are expert meetings where an intense but informal exchange of views at the frontiers of a subject aims at identifying directions for future action

Following a transformation of the programme in 2006 the Series has been re-named and re-organised. Recent volumes on topics not related to security, which result from meetings supported under the programme earlier, may be found in the NATO Science Series.

The Series is published by IOS Press, Amsterdam, and Springer, Dordrecht, in conjunction with the NATO Public Diplomacy Division.

Sub-Series

A.	Chemistry and Biology	Springer
B.	Physics and Biophysics	Springer
C.	Environmental Security	Springer
D.	Information and Communication Security	IOS Press
E.	Human and Societal Dynamics	IOS Press

http://www.nato.int/science
http://www.springer.com
http://www.iospress.nl

Series C: Environmental Security

Damage Assessment and Reconstruction after War or Natural Disaster

edited by

Adnan Ibrahimbegovic
Ecole Normale Supérieure
LMT-Cachan, France

and

Muhamed Zlatar
Department of Civil Engineering
University of Sarajevo
Sarajevo, Bosnia and Herzegovina

Published in cooperation with NATO Public Diplomacy Division

Proceedings of the NATO Advanced Research Workshop on
Damage Assessment and Reconstruction after Natural Disasters
and Previous Military Activities
Sarajevo, Bosnia & Herzegovina
5–9 October 2008

Library of Congress Control Number: 2009926509

ISBN 978-90-481-2384-1 (PB)
ISBN 978-90-481-2385-8 (HB)
ISBN 978-90-481-2386-5 (e-book)

Published by Springer,
P.O. Box 17, 3300 AA Dordrecht, The Netherlands.

www.springer.com

Printed on acid-free paper

CONTENTS

EDITORIAL

This book contains the selected contributions from the participants of NATO-ARW 983112 on "Damage Assessment and Reconstruction After Natural Disasters and Previous Military Activities", which was held in October 2008 in Sarajevo, Bosnia and Herzegovina. The meeting was set to provide a critical assessment of the current knowledge and to indicate new challenges that are brought by the present time in dealing with frequent man-made and natural disasters, resulting in damage to structures, infrastructure and human environment. The common ground for all problems of this kind from the viewpoint of scientific contents, which also justifies putting them on the same basis and addressing them within the same meeting, is the need to provide a quick assessment of the destructive action and its consequences, quick reconstruction of infrastructure and human environment, as well as the new basis for a sustainable development of affected areas. The present threat of the terrorist attacks or accidental explosions, the local military conflicts, the climate change that brings soil erosion or yet the destructive earthquake motion that occurs in previously inactive regions, are several examples of the kind of disastrous situations we address herein, along with the best way of reducing their negative impact.

The NATO-ARW Sarajevo meeting constructed a forum for the exchange of ideas among the world leading scientists dealing with different facets of this class of complex problems. All those keynote contributions (along with a couple contributions from invited speakers from partner-country) are gathered in the present book. Among them, we find the lectures dealing with three groups of topics:

(i) Damage of complex structures, damage identification, controlled destruction, quick reconstruction, retrofit
(ii) Damage identification and exploitation of partially damaged infrastructure, water resources, soil pollution, soil erosion
(iii) Case studies of natural and man-made disasters: (explosions, fires, earthquakes, land-slides ...)

We would like to thank all the contributing authors for providing the more lasting impact of our discussions in terms of this book. Last, but not least, we would like to thank NATO Scientific Committee for supporting our meeting.

NATO-country co-director:
Adnan Ibrahimbegovic

Partner-country co-director:
Muhamed Zlatar

PART I

DAMAGE ASSESSMENT AND RECONSTRUCTION OF STRUCTURES

CIVIL ENGINEERING STRUCTURES: MULTISCALE DAMAGE REPRESENTATION, IDENTIFICATION, CONTROLLED DESTRUCTION AND QUICK RECONSTRUCTION

A. IBRAHIMBEGOVIC[1*], A. KUCEROVA[1,3],
D. BRANCHERIE[2], M. HAUTEFEUILLE[1,2], J.B. COLLIAT[1],
N. FRIEDMAN[1,4], AND M. ZLATAR[5]
[1]*Ecole Normale Supérieure, LMT-Cachan, Civil Engineering, 61 avenue du president Wilson, 94235 Cachan, France*
[2]*Unverisity of Technology of Compiègne, Mechanical Engineering, France*
[3]*Technical University of Prague, Civil Engineering, Czech Republic*
[4]*Technical University of Budapest, Civil Engineering, Hungary*
[5]*University of Sarajevo, Civil Engineering, Bosnia and Herzegovina*

Abstract. In this paper we review the large field of research pertaining to damage detection and rebuilding the human environment in urban areas following the natural disasters and past military activities. This domain of current practical interest is highly interdisciplinary and belongs not only to the traditional domain of Civil Engineering, but draws upon to a large extent on domains of Applied Mathematics, Material Science, Physics and Chemistry. In particular, we first review the typical damage to engineering structures and infrastructure in urban zones, which can be caused by the extreme conditions of mechanical or thermal loads, interaction with aggressive environment, from very high-rate (e.g. explosions) to very low-rate applications (e.g. the problems of durability or ageing). We then discuss the topics of current research interest related to the techniques of damage detection in structures and infrastructure, with special emphasis on detection under heterogeneous fields and heterogeneous material properties. We only briefly discuss the techniques for controlled destruction of heavily damaged engineering structures, which are no longer deemed reparable. Finally, we give a quick overview of the techniques for quick reconstruction and the structural systems that can be employed for that purpose.

* To whom correspondence should be addressed. e-mail: ai@lmt.ens-cachan.fr

A. Ibrahimbegovic and M. Zlatar (eds.), *Damage Assessment and Reconstruction After War or Natural Disaster*,

Keywords: Engineering structures, infrastructure, damage detection, controlled destruction, quick reconstruction

1. Introduction

The present time of local conflicts mostly fought in urban areas brings additional challenge of damage detection and quick rebuilding of human environment, which is very important for preventing large emigration flux from the affected areas. The engineering knowledge faces perhaps the most demanding problems in this domain of application, and it needs help by a number of other scientific disciplines, such as Applied Mathematics, Material Science, Physics and Chemistry. A number of questions that need the answer related to this class of problems: first and foremost, how to describe different damage mechanism of engineering structures and infrastructure and how to account for the natural variation of these mechanisms within a complex, heterogeneous structure; in short, the main question pertains to classifying different damage mechanisms in massive structures. The second question we address is how to detect these damage mechanisms, and estimate the parameters of the model that is supposed to represent them. We note in passing that the study presented herein focuses mostly on the mechanical damage identification, with no mention of any other techniques used for non-destructive damage assessment, such as X-ray or ultra-sonar probing. When the excessive damage is found, in a structure that is damaged beyond reparation, we will face a difficult problem of controlled destruction in an urban zone, where other neighboring structures should not be damaged while removing the damaged structure. It turns out that the modeling procedure of controlled destruction calls upon practically all available tools currently used for solving different problems in structural engineering domain. The final goal to be studied pertains to the quick reconstruction and retrofit of damaged structures. The former can be accelerated by the special deployable structures, whereas the latter can be accelerated by the judicious use of modern materials.

In this chapter the most thorough part of discussion is given of the first issue pertaining to the damage mechanisms description in a massive engineering structure, by taking into account the heterogeneities of the material properties and the loading history producing different levels of damage. We draw attention in particular to a very specific form of damage mechanism for a massive structure, where the fracture process zone plays equally important role to the final crack that endangers the integrity of a given structural component. We also show that the finite element interpolation has to be constructed accordingly for the best possible representation of this kind of mechanisms. In the second part of the chapter we review two classes of identification methods based upon forward mode and inverse mode analysis. We show how these identification

methods can be used for precise identification of the parameters for representing nonlinear inelastic behavior of a damaged structural component. We also indicate that it is very likely the inverse mode that has a larger potential in dealing with identification problems for a complex structure. In the last part of the work, we very briefly review the main steps in controlled destruction of a heavily damaged structure, as well as the quick reconstruction problems.

2. Damage in massive civil engineering structures

2.1. NOVEL MODELS FOR DAMAGE ASSESSMENT

Ever increasing demand to achieve a more economical structural design requires that a better understanding be obtained for the non-linear behavior of a particular structural system and reliable estimate of its limit load be furnished. However, the limit state of a complex system often implies that particular components – whose peak resistance has already been defeated – be able to function in the post-peak regime, which induces strain softening behavior. A reliable evaluation of the limit load of the considered system is thus highly dependent upon an efficient and reliable description of the softening branch of the material behavior.

The models for computing the ultimate limit load are not reliable enough as soon as we are facing the heterogeneous structures and heterogeneous stress field; the benchmark competition on a single component (a shear wall) with double notch, submitted to non-proportional loading starting first with shearing and followed by a traction force: The results show very significant difference from the experimental results (which are dominated by more than one damage mechanism), and moreover a large dispersion among them (Fig. 1).

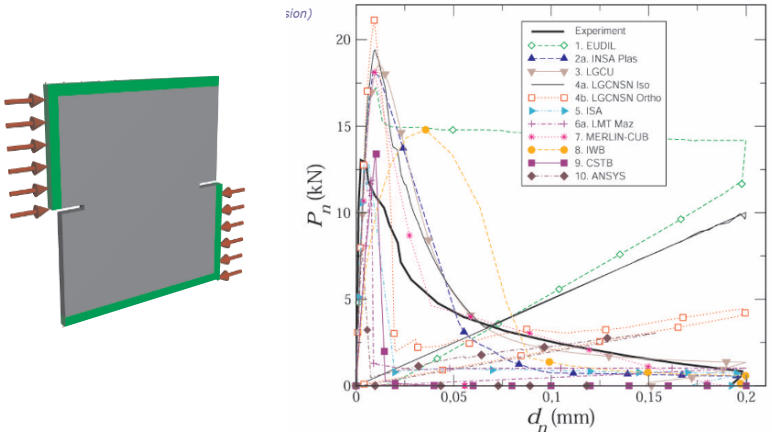

Figure 1. Results of numerical simulations Nooru-Mohamed benchmark of double-edge notched component

With new damage assessment models, most of them developed recently (Ibrahimbegovic and Brancherie, 2003; Ibrahimbegovic and Delaplace, 2003; Ibrahimbegovic and Markovic, 2003; Ibrahimbegovic and Melnyk, 2007; Brancherie, 2003; Brancherie and Ibrahimbegovic, 2006, 2009; Colliat, 2003; Colliat et al., 2005, 2007, 2008; Markovic, 2004; Markovic et al., 2005; Niekamp et al., 2009; Davenne et al., 2003; Dolarevic, 2005; Dominguez, 2005; Herve, 2005; Melnyk, 2007, see also Leger and Tremblay [2008] or Owen et al. [2008] for damage in dynamics), we can obtain not only this global information, but also the local information in a more reliable manner; for example, for the benchmark problem of Nooru-Mohamed, we also obtain close match with crack spacing and opening under non-proportional loading (Fig. 2).

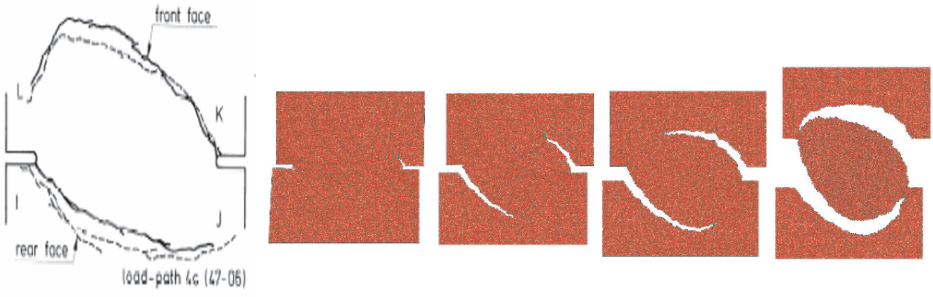

Figure 2. Crack pattern for Nooru-Mohamed benchmark: experimental results versus computations with refined damage models taking into account heterogeneities of material and stress field

The models had for the starting point the fact that no anisotropic damage model is capable of representing correctly the fine details of the solution. The guiding principles for development of new generation of damage models were:

(i) Separate complexities and assign to each mechanism of inelastic behavior its criterion.
(ii) Account for true nature of inelastic dissipation (for example, volume vs. surface).
(iii) Localized failure description cannot be described only by the UMAT kind rules specifying how to compute the stress from strain, but FE representation of strain field has to be constructed accordingly, by taking into account the heterogeneities.

Of special interest for this work is the failure pattern for massive structures, where the creation fracture process zone (FPZ), with a number of tiny cracks of different orientation, proceeds the creation of the macro crack, which endangers the integrity of a particular component of the whole structure (see Fig. 3).

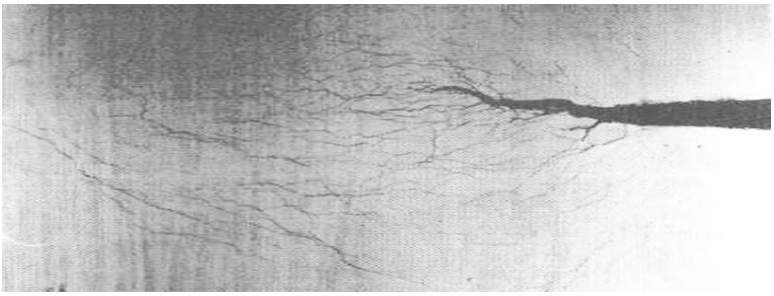

Figure 3. Typical failure pattern of a massive structure, where the fracture process zone (FPZ) precedes the macro crack creation that leads to final failure of the given component or the entire structure

The models of this kind will have at least two dissipative mechanisms, the first related to the fracture process zone and the second related to the localized failure (Fig. 4). Each of mechanisms is described by a particular plasticity failure criterion (we could also choose the damage criteria). We can thus obtain the basic set of governing equations, which can be written and illustrated as:

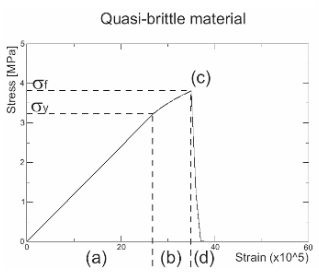

$$
\begin{aligned}
\epsilon &= \epsilon^e + \bar{\epsilon}^p + \bar{\bar{\epsilon}}^p \, \delta x \\
\Psi &\quad (\epsilon^e, \bar{\xi}, \bar{\bar{\xi}}) = \bar{\Psi}(\epsilon^e, \bar{\xi}) + \bar{\bar{\Psi}}(\bar{\bar{\xi}}) \\
\bar{\Phi} &\quad (\sigma, \bar{q}) := |\sigma| - (\sigma_y - \bar{q}) \\
\bar{\bar{\Phi}} &\quad (\sigma, \bar{\bar{q}}) := |t| - (\sigma_f - \bar{\bar{q}}) \\
\dot{\bar{\epsilon}}^p &= \dot{\bar{\gamma}} \frac{\partial \bar{\Phi}}{\partial \sigma} \quad ; \quad \dot{\bar{\xi}} = \dot{\bar{\gamma}} \quad ; \quad \bar{\Phi} \leq 0 \quad ; \quad \dot{\bar{\gamma}} \geq 0 \quad ; \quad \dot{\bar{\gamma}} \bar{\Phi} = 0 \\
\dot{\bar{\bar{\epsilon}}}^p &= \dot{\bar{\bar{\gamma}}} \frac{\partial \bar{\bar{\Phi}}}{\partial \sigma} \quad ; \quad \dot{\bar{\bar{\xi}}} = \dot{\bar{\bar{\gamma}}} \quad ; \quad \bar{\bar{\Phi}} \leq 0 \quad ; \quad \dot{\bar{\bar{\gamma}}} \geq 0 \quad ; \quad \dot{\bar{\bar{\gamma}}} \bar{\bar{\Phi}} = 0
\end{aligned}
$$

Figure 4. 1D representation of failure model for massive structures and governing equations postulating: (i) additive split of total deformation into elastic, smooth plastic and localized plastic field, (ii) strain energy in terms of elastic strain and hardening variables, (iii) plasticity criteria for smooth and localized field, and the evolution equations for the internal variables (note that one over-bar pertains to the FPZ mechanisms, and two bars is used for the internal variables describing the localized failure)

The typical result obtained with models of this kind is given in Fig. 5, for the case of simple tension test, where the global force–displacement diagram indicating three different regimes of response (with elastic, inelastic hardening and inelastic softening) remains the same for different mesh grading.

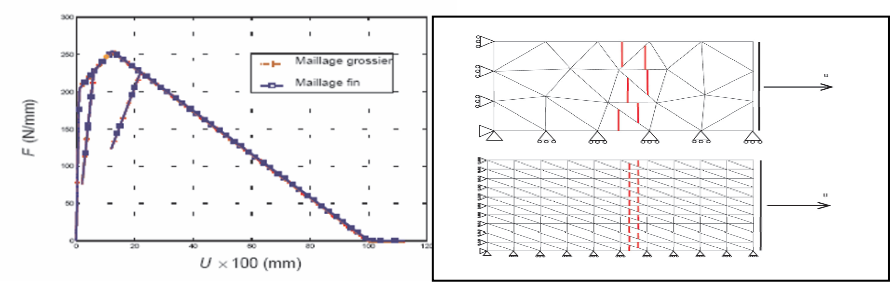

Figure 5. Computed response with failure model for massive structures with FPZ, and crack pattern by using coarse mesh and fine structured mesh

When going one step further along this line of developments, we can look at the reinforced concrete structures (as probably a dominant class of structures in civil engineering practice), where the judicious combination of steel and concrete has provided the best building material in terms of cost. However, the nonlinear inelastic behavior of reinforced concrete is perhaps the most difficult one to comprehend. More importantly, the most adequate model will strongly depend upon the goal of the present analysis, and the estimate of the damage we would like to obtain. In that respect the choice should be made between: i) global integrity of the structure built of reinforced concrete under extreme loading, ii) local integrity of concrete under extreme loading case and iii) durability of concrete under aggressive environment. The models for each of the listed goals get to be more and more detailed; see Fig. 6.

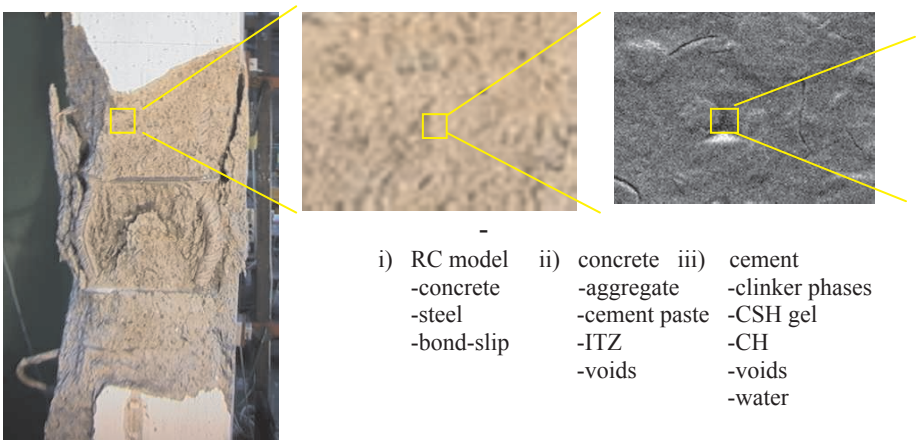

Figure 6. Different models of reinforced concrete for studies of: (**a**) structural integrity, (**b**) material integrity, (**c**) material durability

2.2. HETEROGENEITIES OF REAL STRUCTURES AND SIZE EFFECT

The damage modes on the real structures are very much influenced by the heterogeneities at the structural level, related to the spatial variation of the material properties, as well as the non-homogeneity of the applied stress field. For that reason, the type of structural failure for the same construction material should be explained by accounting for the structure heterogeneities. The case in point concerns the analysis where the material properties are not prescribed in the deterministic manner, but rather as random fields.

In Colliat et al. (2007) and Hautefeuille et al. (2009), we have studied the possibilities of describing the heterogeneities of material properties for the case where the material microstructure or mesostructure properties are known, but their geometric arrangement is random. More precisely, we have looked more closely into the class of concrete models built at the meso-scale, by accounting for Poisson's process distribution of the aggregate within a given component shown in Fig. 7.

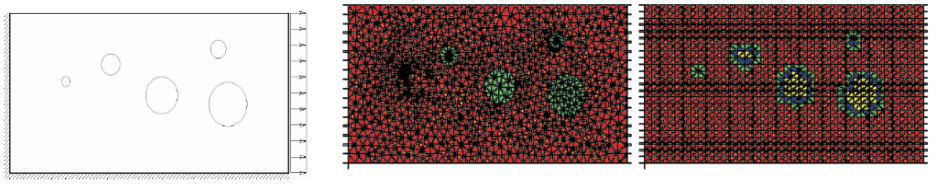

Figure 7. Schematic representation of two-phase meso-structure of concrete as two-phase material taking into account the difference between aggregate and cement paste, and exact and structured mesh representation

We assume the aggregate to remain elastic, and the cement paste constitutive behavior to be governed by the elastic-perfectly-plastic Drucker–Prager plasticity model, and both phases will have deterministic material parameters. The only randomness will stem from the uncertain meso-structure geometric arrangements,

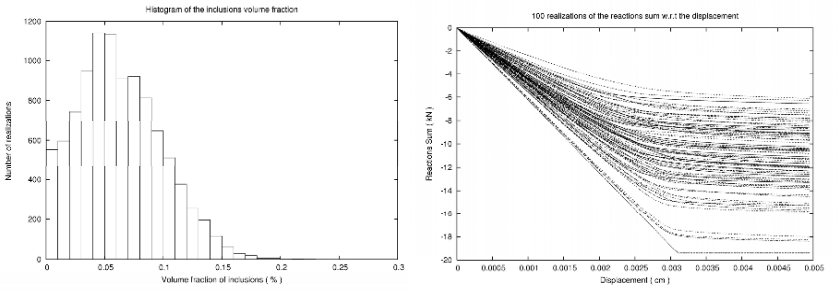

Figure 8. Phase histogram and response dispersion for different realizations of two-phase representation of concrete constitutive model

which are produced by Poisson's random process enforcing minimum and maximum aggregate size and distance. The response statistics is computed with the structured mesh (since it provides much more efficient computational procedure), by using the Monte Carlo method. The results presented in Fig. 8, in terms of phase histogram, and the dispersion of 1D representation of the constitutive behavior.

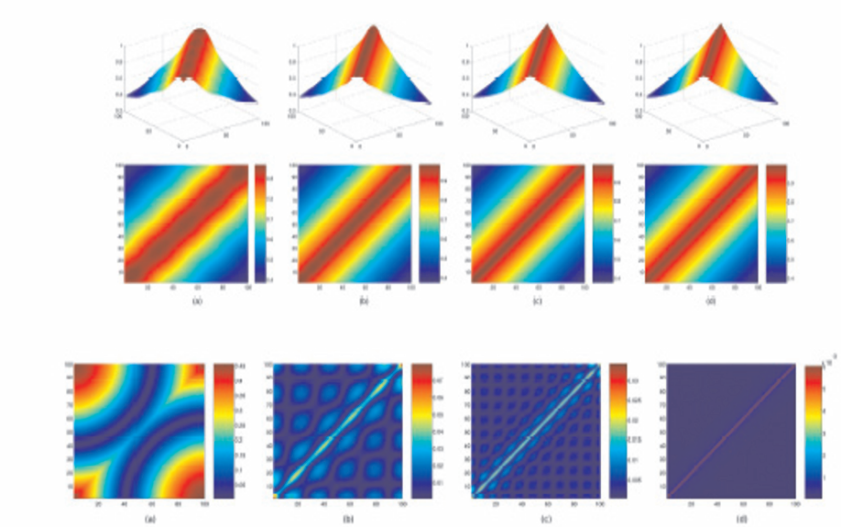

Figure 9. Covariance representation with 5, 10 or 50 Karhunen-Loeve modes versus exact representation (3D – *top* row, 2D – *middle* row, error – *bottom* row)

The main idea pursued further pertain to reinterpretation of the results of this analysis in terms of 1D model for localized failure with FPZ for massive structure defined in Fig. 4. However, the crucial difference now is that the parameters of this model governing activation of diffuse plasticity in FPZ and localized failure are defined as random field. For simplicity, we assume statistically homogeneous material, with the random field parameters characterized by the correlation length; for example, for yield stress we would have the typical space variation described by:

$$cov_{\sigma_y}(x,y) = V exp(-\frac{||x-y||_1}{L_c})$$

where V is the variance of the field, x and y are two points in space and L_c is the correlation length. For the chosen correlation length, the spatial variation of the material parameter then can be expressed in terms of KL modes expansion, with no more than 50 modes needed; see Fig. 9.

The typical realization of material properties variation obtained in this manner for short, medium and long bars are given in Fig. 10.

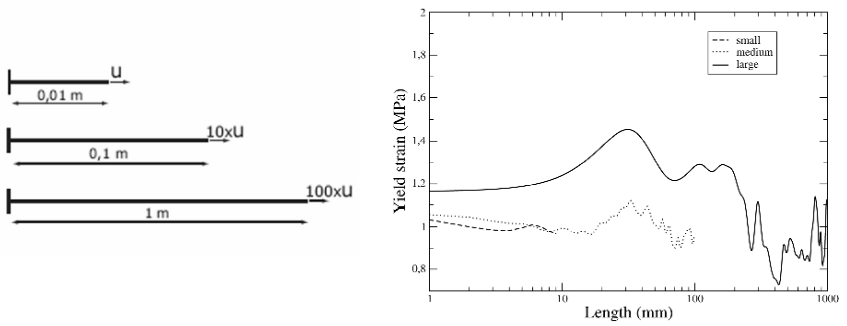

Figure 10. Realizations of yield stress spatial variation for short, medium and long bars

The computations are then carried out with this kind of probabilistic models of structures, computing the failure of each realization. The final results are used to built the cumulative distribution of failure for different structures, with the percentage of broken bar shown in Fig. 11.

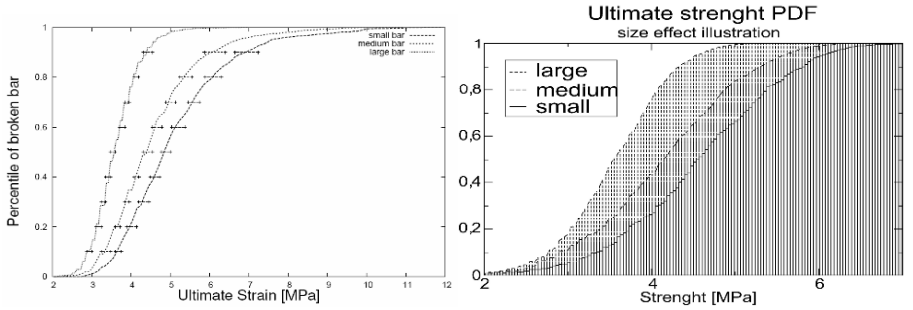

Figure 11. Cumulative distribution with percentage of broken bars for short, medium and long bar, along with the confidence index for each case

The last result can be resented in an alternative manner, by plotting for the percentage of broken bars the corresponding strength (see Fig. 12), which allows us to show that not only the long bars will break sooner (for more likely presence of the weak spot), but that the type of failure will be closer to the one described by classical fracture mechanics (with a negligible FPZ).

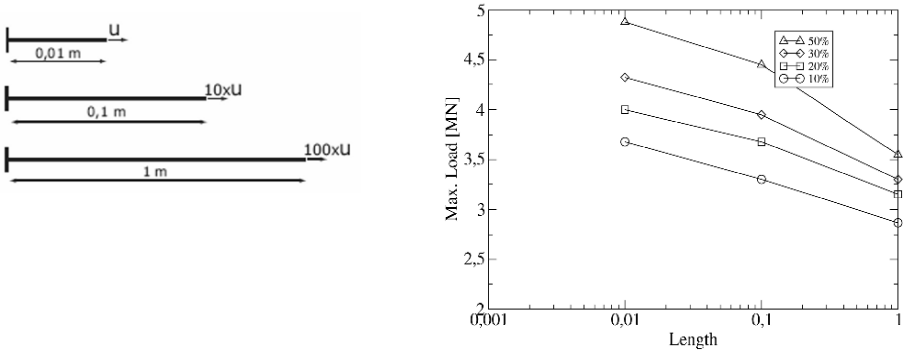

Figure 12. The corresponding values of ultimate strength for short, medium and long bars indicating size-effect, with longer bar breaking sooner with a small FPZ size

Similar effects on material heterogeneities are obvious in response of RC structures, producing rather a different crack spacing that does not remain constant. The case in point is the result presented in Fig. 13, which present the outcome of different RC tie-beam tension tests.

Tirant	Espacement minimal S_{min} (cm)	Espacement maximal S_{max} (cm)
BAP-12-HA	14	19
BAP-16-HA	12,3	18,7
BAP-20-HA	10	21
BV-12-HA	12,5	21
BV-16-HA	11,5	17
BV-20-HA	10	17
BAP-12-Lisse	14	19
BAP-16-Lisse	15,5	21
BAP-20-Lisse	14,5	20

Figure 13. Experimental results of tension test on RC tie-beams producing variable values of crack spacing (from Daoud [2003], doctoral thesis INSA Lyon)

The test of this kind is carried out under displacement control directly imposed upon steel bar, which puts the bar and the surrounding concrete in tension. At certain value of deformation, the concrete can no longer follow the bar deformation, and produces the first crack followed by additional cracks each occurring at certain distance with respect to the previously created crack. We have carried out the numerical simulation of these tests by using the RC model, which consists of the concrete model described in the previous section, the elasto-plastic steel model and the bond-slip model described in Dominguez et al. (2005). The bond slip model of this kind can account for three different phases of slip, the elastic phase, the plastic slip with hardening and the last

phase of large slip with softening. We note in passing that the softening phenomena of bond-slip do not lead to any mesh-objectivity problem, since the length scale is imposed by the presence of the steel bar that connects all the slips along the bar. In Fig. 14, we present the computed results obtained for the cases of: perfect bond between steel and concrete, the constant value of the bond slip resistance, along with the heterogeneity-imposed variation of the bond along the bar with different choices of standard deviation. We can see that the bond-slip do play important role and that its absence (perfect bond) produces rather non-physical results. We can also see that the best match to experimental results for crack spacing is produced by the standard deviation of 5%.

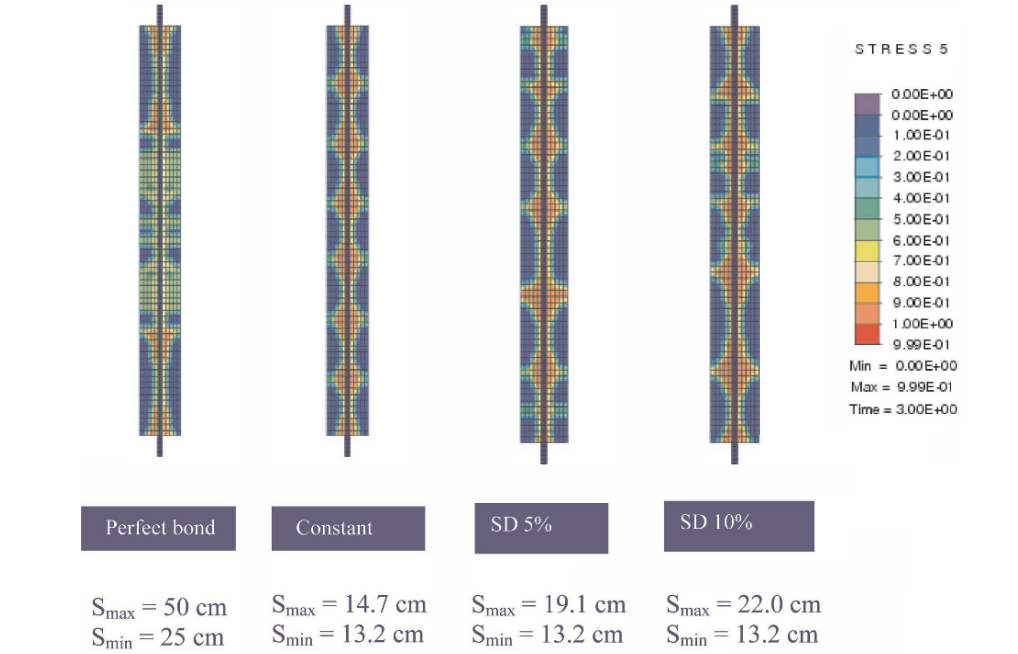

Figure 14. Results of numerical simulations of RC-tie tension test with (from left to right): perfect bond, constant bond-slip resistance, variables resistance with 5% and 10% standard deviation

3. Damage parameters identification in civil engineering structures

In this section we discuss the main issues pertaining to the damage parameter identification, which is the main requirement for successful damage assessment. We start with the methods that are usually used for material damage parameters, and than comment upon the suitable extensions to the methods for structural damage assessment.

The testing procedure for estimating the damage parameters of quasi-brittle materials is very much geared towards the tests under heterogeneous stress field, which are easy to perform. The case in point is three-point bending test, shown in Fig. 15.

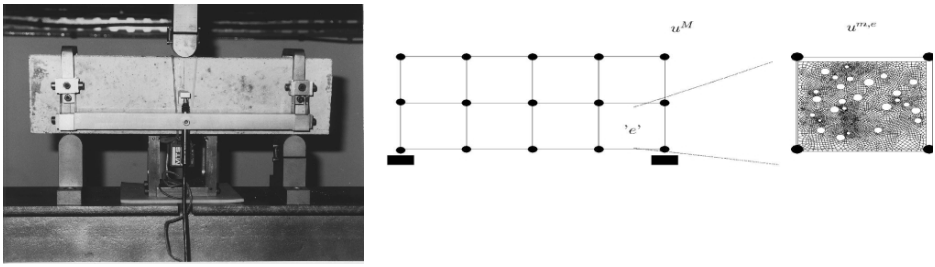

Figure 15. Typical test for quasi-brittle materials: three-point bending test

The typical measurements are no longer only the point-wise observation of the displacement corresponding to a given force, but the optimal measurements spread over certain area, which provides the displacement field throughout that area; see Fig. 16.

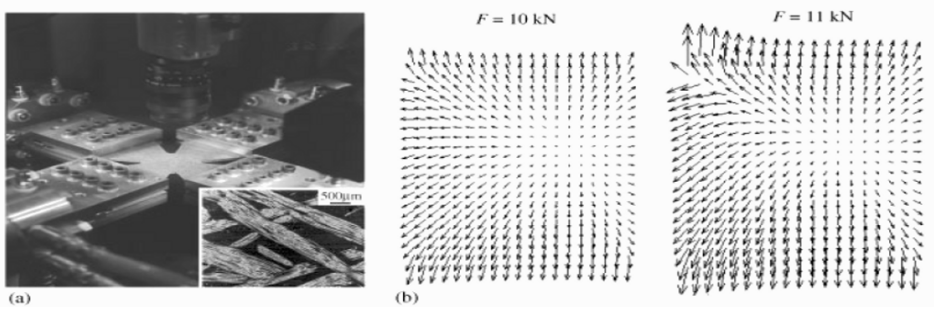

Figure 16. (**a**) Sample of the testing machine ASTRÉE and microstructure of the studied composite, (**b**) Displacement filed in biaxial test measured by digital image correlation for two load levels, with failure load F = 11.1 kN (Claire et al., 2001)

The modern identification procedures are nowadays adapted to this point of view, treating each specimen as the structure. We review briefly two types of methods: the forward and the inverse mode of identification (e.g. see Kucerova [2007] for more details).

3.1. FORWARD MODE IDENTIFICATION

The forward mode indentification provides the estimate of the model parameters from the given experimental measurements. If we denote the set of parameters

of the model as X, the model operation as M and the measurements as Y^E, the forward mode identification reduces to:

$$F(X)=||Y^E-M(X)||$$

This kind of relation can be established either experimentally (results denoted with superscript E) or by means of the model (results denoted with superscript M), as illustrated in Fig. 17.

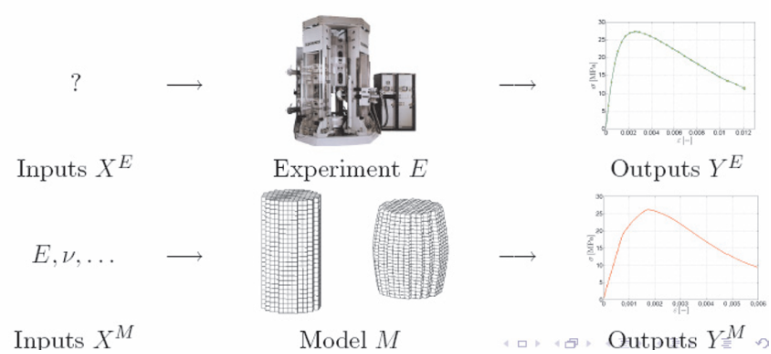

Figure 17. Forward model identification with relationship established either experimentally or by the chosen model

The forward mode identification can be carried out by minimizing the error functional, as a suitably chosen measure expressing the difference between the results computed by the model and the experimental results; see Fig. 18. We also show in Fig. 18 that the results provided by finite element model, the most frequently used kind of model for complex structures nowadays, should first be processed through the verification procedure to provide the sufficient guarantees for model accuracy, before carrying on with the model validation procedure from experiments.

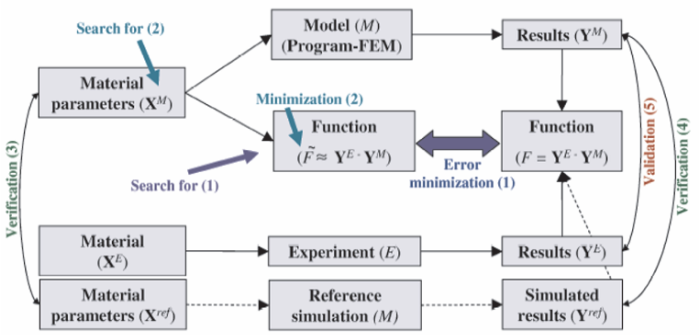

Figure 18. Forward mode of identification and definition of error function

A number of solution tools are used currently in order to improve the efficiency and the robustness of forward mode identification; some of them are listed in Fig. 19 given below (we also refer to Kucerova [2007] for recent state-of-the-art review):

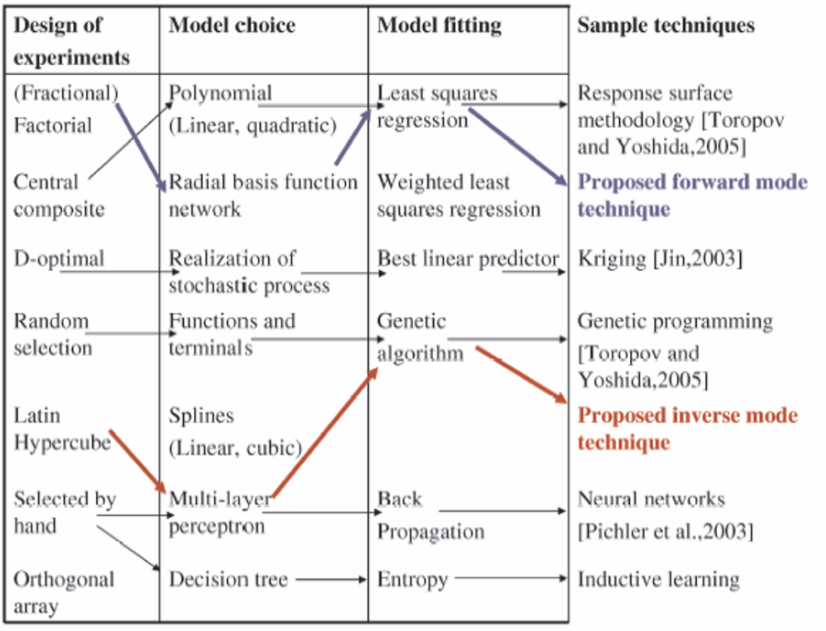

Figure 19. Solution tools for forward mode identification problem

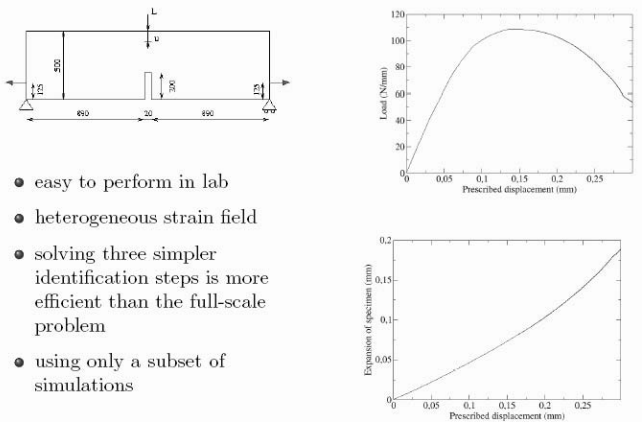

Figure 20. Three-point bending test on notched specimen and typical measurements

The forward mode identification is not very difficult to solve if the chosen model has the sound theoretical foundation with clear interpretation of each and every inelastic mechanism. This is certainly true of the present model for localized failure of massive structures with a significant contribution of the FPZ. The case in point is provided by the results of identification problem from the standard three-point bending testing, performed on the notched specimen shown in Fig. 20.

The robustness of the identification procedure in this case is not only guaranteed by the sound theoretical basis of the model, but also by the judicious solution strategy where the complete set of material parameters is split in several groups, corresponding to three prominent phases of nonlinear behavior, and only one group is identified at the time. This strategy is illustrated in Fig. 21.

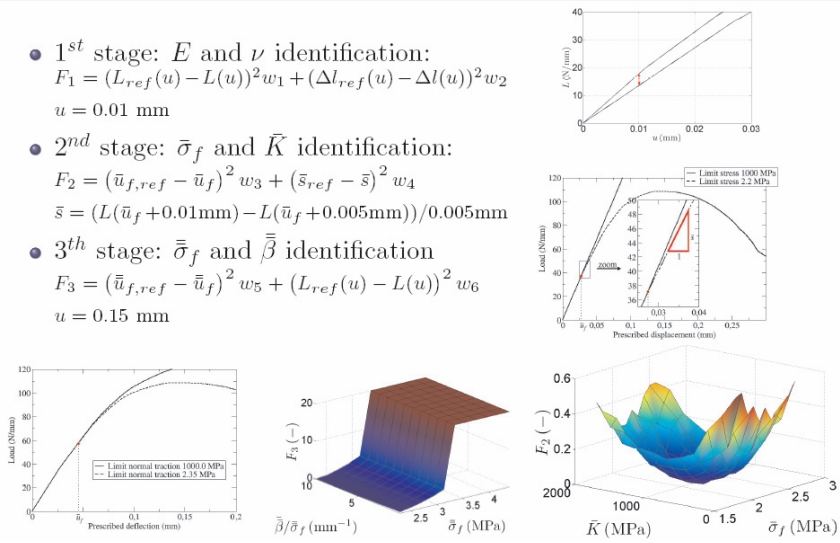

Figure 21. Forward mode identification procedure for three-point bending test, with parameter group identified from different regime measurements

We note in passing that the identification procedure of this kind is very much adapted to the problems of material parameter estimates, where we can choose a sufficiently reliable model of inelastic behavior, and afford the complete destruction of the chosen specimen, which allows us to gather the measurements over all regimes of nonlinear inelastic behavior.

3.2. INVERSE MODE IDENTIFICATION

The inverse mode identification is more suitable for the problems where the system behavior is neither clearly defined nor possible to capture by a sound

theoretical model. The latter can be the consequence of extremely complexity of material behavior, extreme complexity of geometric setting (e.g. complex structures) or inability to carry out the tests and obtain the corresponding measurements over all different regimes of material behavior.

In the inverse mode identification we ought to solve for the approximation to the system behavior, without really having a very precise notion on the kind of model one can use. This can formally be written as:

$$\Rightarrow \text{determination of its } \textit{approximation } M^{INV}$$
$$X^M = M^{INV}(Y^M).$$

where M^{INV} is the inverse approximation to the complex system operator. The illustrative representation of the inverse mode identification is presented in Fig. 22.

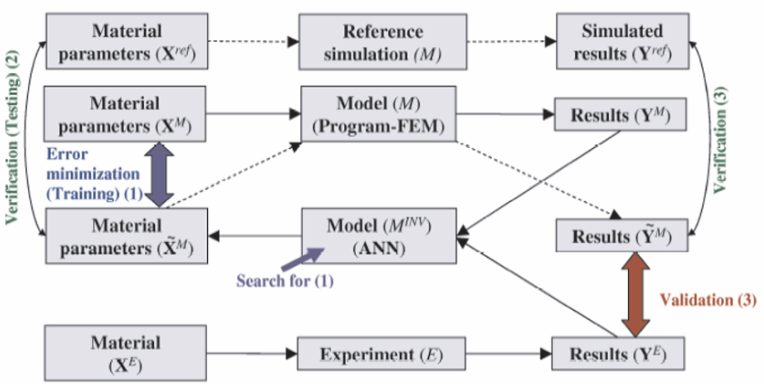

Figure 22. Flow-chart for inverse mode identification procedure

One can count with the most important advantage for such a inverse mode identification, such as the possibility to replace a complex systems rules with the corresponding approximation that allows a frequent and an efficient use of the artificial model, but also with a number of disadvantages, such as the need to carry out an exhaustive exploration of the inverse relationship, inability to solve for multi-modal problems especially with the data with measurement noise. One of the popular approaches for reconstructing the behavior of a complex system relies on neural networks, which can build the equivalent system response as the collection of simpler rules put together as a multi-layer representation (see Fig. 23 for illustration).

$$O_{l,j} = f_{act}\left(\sum_{i=0}^{n_{l-1}} O_{l-1,i} \cdot w_{l,i,j}\right) \qquad f_{act}(\Sigma) = \frac{1}{\left(1+e^{-\alpha/\Sigma}\right)} \qquad \alpha = 0.8$$

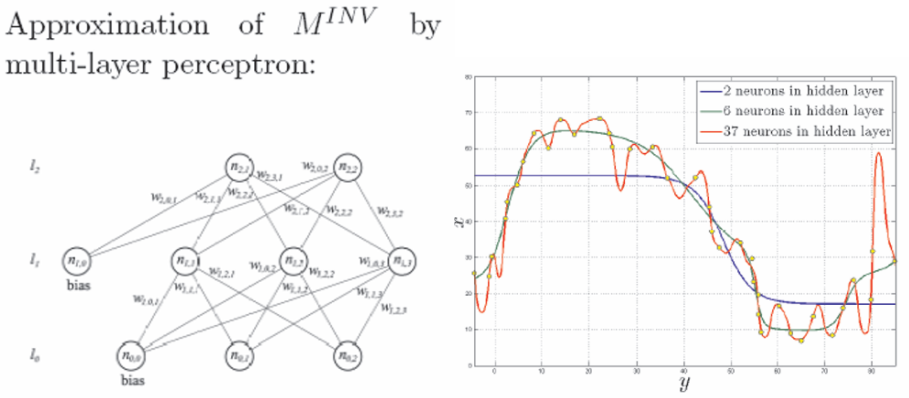

Figure 23. Approximation of M^{INV} by multi-layer representation and computed complex system response in terms of layer complexity

It is also shown in Fig. 23 that the complex system response representation by neural networks is then very much affected by the type of representation and the complexity of each links, in the sense that the increasing complexity can provide a more detailed representation (as opposed to the smoothed, averaged values given by coarse representation). One recent example of inverse mode identification is given in Kucerova (2007), dealing with the system identification capable of representing a very complex behavior of concrete under different stress states of either compression or tensile stress. This kind of behavior was supposed to be represented by the micro-plane "model" of Bazant et al. (2000), which assumes that 1D response in a number of planes (32 for 2D case, and 128 for 3D case, the numbers being imposed by the rules of numerical integration over a circle or a sphere, respectively), without any coupling in axial and tangential direction on each plane, can somehow describe the global response. In that respect, the micro-plane constitutive model can be considered as the model of complex structure whose behavior is influenced by a number of its components (i.e. "micro" planes). The micro-plane model can be packed in the form featuring a number of model parameters, which do not posses (except two: Young's modulus E, and Poisson's ratio v) clear physical meaning.

$$E, v, K_1, K_2, K_3, K_4, C_3, C_{20}$$

The lack of clear physical basis of most of coefficients and the need to understand behavior under different deformation modes make this identification problem very much equivalent to the model estimates for a complex structure from the estimate of its components. The importance of each parameter throughout the deformation history of interest can be obtained by Pearson's product moment correlation coefficient for each parameter (see Fig. 24), which

clearly shows that the system response does not remain equally governed throughout the deformation history.

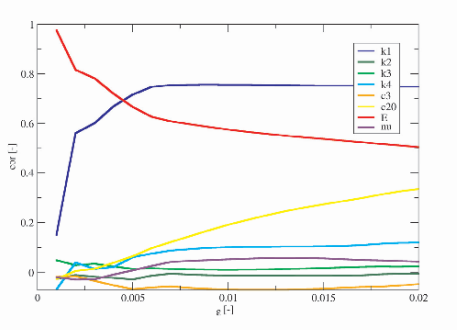

Figure 24. Pearson's product moment correlation for micro-plane model parameters

Bazant and co-workers have proposed several typical tests in order to provide the best estimates of the micro-plane model parameters, with the most of parameters lacking a clear physical meaning. These tests include: uniaxial compression, hydrostatic pressure and triaxial compression; see Fig. 25. We can see that the tests of this kind can reveal the particular sensitivity of the model parameters in the course straining throughout different regimes.

It is very much open question how to achieve the same goal with a complex structure, and especially with the existing one, which might have been partially damaged. The question of this kind will be addressed by several keynote speakers, each focusing upon particular type of structure and particular natural or man-made disaster.

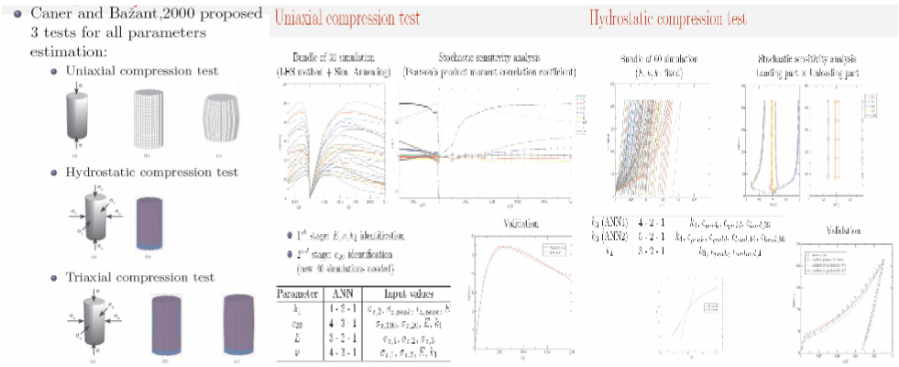

Figure 25. Micro-plane model for concrete: uniaxial compression and hydrostatic pressure tests to determine all model parameters, stochastic sensitivity analysis of parameters and neural network response

4. Controlled destruction of damaged structures and quick reconstruction

Once the damage assessment has confirmed that extent of the structural damage, one are left facing two different possible solutions. The first pertains to the controlled destruction of the structure that is damaged beyond the level that is possible to repair, and the second concerns the reparation and quick reconstructtion of the damaged structural component or the complete structure. In this section, we briefly review the main steps that are necessary for either of these two tasks. More detailed presentations are given in keynote lectures of Breysse (2008) or Bruhwiler (2008).

4.1. CONTROLLED DESTRUCTION OF DAMAGED STRUCTURE

Any structure that is damaged beyond possible reparation or retrofitting, which has to be removed, posses quite a difficult problem if placed in the urban area where the uncontrolled destruction can induce to a significant damage to any neighboring structure. As briefly shown in this section, it is in fact more difficult to destroy the partially damaged structure in a controlled manner, than to understand the damage mechanisms and carry out the damage assessment. Namely, not only do we need to provide the reliable estimates of the damage mechanisms accounting for possible heterogeneities (as described in the previous sections), but also to carry out the simulation of the complete structural failure in post-stable regime. This kind of problem was studied both experimentally and numerically in a collaborative project involving four university teams in Germany (see Hartmann et al. [2008]), for the particular structure shown in Fig. 26.

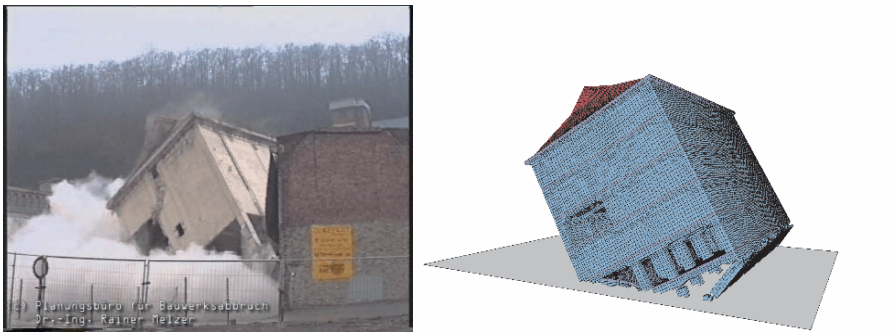

Figure 26. Typical residence building used for experimental and numerical (finite-element-method-based) studies of complete failure induced by controlled destruction

It is important to understand that the problem of this kind calls for the numerical modeling and simulation tools capable of going beyond the nonlinear

structural mechanics applications into the area of multibody dynamics, so that we can predict the post-critical path of the failing structure. Moreover, we would also need the computational tools for handling the contact problems in order to predict the final position of the failing structures produced upon hitting the ground. These three phases carried out for the chosen building and the corresponding analyses are carried out by FEAP, MBS-code and LS-DYNA computer codes, respectively (see Hartmann et al. [2008]).

However, there is still one important phase missing from the analysis of this kind, which concerns any debris from the fallen structure big enough to induce potential damage in the neighboring structures in the urbane zone. However, this last phase of computation would again require a change of the computational model in that the discrete rather than finite elements should be used for the debris trajectories computations. Among available models of this kind, the most promising appears to be the models of Ibrahimbegovic and Delaplace (2003) or Delaplace and Ibrahimbegovic (2006), using the geometrically exact beams (e.g. see Ibrahimbegovic and Taylor [2003]) for cohesive force representation, which can handle both large displacements and rotations in the invariant manner; an illustrative example for failure modeling in dynamic bending test simulation is given in Fig. 27.

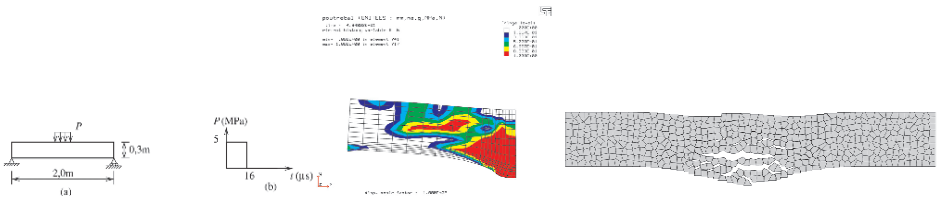

Figure 27. Simulation tools for post-failure modeling and debris computations, based either upon the finite element code (which only predict complete failure of heavily damaged zone) and discrete element code (which can also provide the complete trajectory of detached debris)

4.2. QUICK REPAIRMENTS AND RECONSTRUCTION

If the structural damage is reparable, one should carry out this kind of procedure by using modern materials, such as Ultra-High Performance Fiber Reinforced Concrete or Carbon Fiber, which can help us recover the structural integrity to a desired level. Several keynote lectures are focusing on this particular class of problems (see Bruhwiler [2008], Breysse [2008] or Owen et al. [2008]).

If the structures, however, are damaged beyond the reparation and would take much longer period of time to rebuild, one can then employ the temporary structures, which can re-establish the operations in the urban zones. Case in point is the deployable bridge in Fig. 28, which can be used for quick reconstruction of the city infrastructure.

*Figure 28***.** Deployable bridge in Hamanizuki Park

Such an example is quite typical of deployable structures that ought to be used repeatedly, which are often built as quite slender and lightweight. The latter implies that the deformation of the structure is sufficiently important and ought to be taken into account both in exploitation phase and in deployment. In fact, the deployment of such structure is often facilitated by the snap-through phenomena, which occur in-between the zero-stress-with-zero-displacement initial configuration and the zero-stress-with-finite-displacement final deployed configuration. Such a deployment procedure can be formulated and solved within the framework of real-time control problems, in terms of computing the most suitable sequence of actuators $\boldsymbol{\nu}$ that should bring the structure into the desired form $\boldsymbol{\Phi}$, or rather as close as possible to this form in terms of the chosen cost function, where we will also satisfy the equilibrium equations $G(\boldsymbol{\Phi};.) = 0$

$$\hat{J}(\hat{\boldsymbol{\phi}}(\boldsymbol{\nu}),\boldsymbol{\nu}) = \min_{\forall \boldsymbol{\nu}_t, G(\hat{\boldsymbol{\phi}}^*_t(\nu^*_t);\cdot)=0} \Big|_{\hat{\boldsymbol{\phi}}_d} \hat{J}(\hat{\boldsymbol{\phi}}_t(\boldsymbol{\nu}^*_t),\boldsymbol{\nu}^*_t)$$

An efficient solution procedure can be constructed for this class of problems (e.g. see Ibrahimbegovic et al. [2004]), where the constraints defined through equilibrium equations is brought-up to the same level as the cost function by exploiting the Lagrange multiplier procedure and defining and solving the min–max problem with the following Lagrangian:

$$\max_{\forall \boldsymbol{\lambda}_t} \min_{\forall (\boldsymbol{\phi}_t, \boldsymbol{\nu}_t)} \Big|_{\bar{\boldsymbol{\phi}}_d} L(\boldsymbol{\phi}_t, \boldsymbol{\nu}_t, \boldsymbol{\lambda}_t)\,; \quad L(\boldsymbol{\phi}_t, \boldsymbol{\nu}_t, \boldsymbol{\lambda}_t) = J(\boldsymbol{\phi}_t, \boldsymbol{\nu}_t) + G(\boldsymbol{\phi}_t, \boldsymbol{\nu}_t; \boldsymbol{\lambda}_t)$$

The solution for this kind of problem is rather difficult to obtain by the traditional solvers, since they often lead to a set of stiff nonlinear algebraic equations. Namely, the nonlinear mechanics problem is already prone to solution difficulties brought by an important difference between the soft, bending-dominated modes against the stiff, membrane-deformation modes; one can expect additional difficulties brought about by an arbitrary choice of the cost function,

which can lead to a set of highly heterogeneous equations. We reported on two different solution procedures (e.g. see Ibrahimbegovic et al. [2004]), one based upon the surface response techniques constructed by a judicious application of diffuse approximation (e.g. see Brancherie et al. [2008]) and the genetic or rather evolutionary algorithms. The performance of this method is illustrated in a typical control problem presented in Fig. 29, where we can see that the dominant control components converge quickly during evolutionary algorithm, but the secondary components (whose contribution is far from being dominant) will require many more steps and would impair convergence.

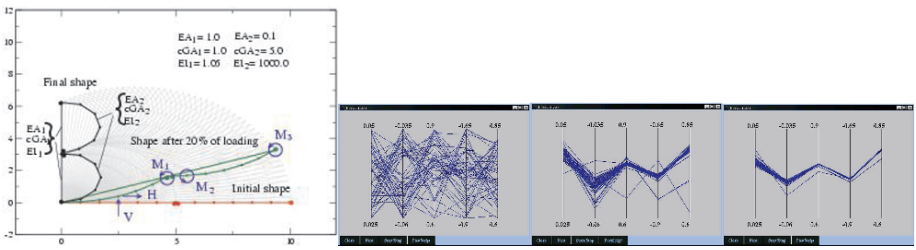

Figure 29. Control problem of placing flexible multibody system in final position, and selected results of solution procedure based on evolutionary algorithm presenting first, 4th and 18th step

5. Conclusions

In this works we have briefly reviewed the very broad class of problems focusing upon the damage assessment and reconstruction of structures and infrastructure in the urban zone, following natural disasters and previous military activities. The most thorough discussion is given for a reliable description of damage mechanisms, including the special form of damage for massive structure where the fracture process zone provides the same order dissipation as the macro-crack that is likely to endanger the integrity of a particular structural component.

We have also presented on how to account for heterogeneities of the material properties, as well as the heterogeneities induced by different loading history for each structural component and its nonlinear behavior. The most important result in this sense pertains to explanations of size-effect from the statistic on different interplays between main damage mechanisms.

The main methods for solving identification problems, both forward mode and backward mode identification are illustrated within the context of material parameters estimates for a particular damaged structural component. How to carry out the damage identification and assessment for a complete, complex structure is still an open question.

The problem of controlled destruction of a heavily damaged structure in a urban zone, without damaging the neighboring structures, brings about a very

interesting combination of modeling tools, starting with the finite element models of inelastic nonlinear behavior, going over to multi-body dynamics systems and finally to the contact problem. If the debris area computation is of strong interest, we ought to use yet another model based upon the discrete models, with cohesive forces represented by the geometrically exact beams that can provide a reliable estimate of the mass and velocity of particles which split from the main structure.

The quick reconstruction and retrofit of damaged materials and structures is also an important goal for this class of problems. The reconstruction pertains both to reparation by special materials (such as Ultra-High-Performance Fibre-Reinforced Concrete), as well as the quick replacement of a destroyed structure or a heavily damaged structural component by deployable structures.

Acknowledgements: this work was supported by the French Ministry of Research (funding for DB, JBC, MH, AK, NF), Alexander von Humboldt Research Award (to AI) and Slovenian Research Agency Award (to AI). This support is gratefully acknowledged.

References

Bazant Z.P., F.C. Caner, I. Carol, M.D. Adley, and S.A. Akers, Microplane model M4 for concrete. Part I: Formulation with work-conjugate deviatoric stress, Part II: Algorithm and calibration, ASCE Journal of Engineering Mechanics, 126, 904–961 (2000)

Brancherie D., Doctoral thesis on "Continuum and discrete models for localized fracture of ductile and brittle materials". (doctoral thesis defended on December 17, 2003)

Brancherie D. and A. Ibrahimbegovic, Méthode à discontinuités fortes, dans La méthode des éléments finis (ed. P. Breitkopf), traité MIME, Hermes-Lavoisir (2006)

Brancherie D. and A. Ibrahimbegovic, Novel anisotropic continuum-discrete damage model capable of representing localized failure. Part I : theoretical formulation and numerical implementation, International Journal of Engineering Computations, 26, 100–127 (2009)

Brancherie D., P. Villon, and A. Ibrahimbegovic, On a consistent field transfer in nonlinear inelastic analysis and ultimate load computations, Computational Mechanics, 42, 213–226 (2008)

Breysse D., Non destructive assessment of concrete damage: interest, difficulties and research needs, Proceedings NATO-ARW (eds. A. Ibrahimbegovic and M. Zlatar), GF Sarajevo (2008)

Bruhwiler E., Improving safety and durability of civil structures, Proceedings NATO-ARW (eds. A. Ibrahimbegovic and M. Zlatar), GF Sarajevo (2008)

Claire D., F. Hild, and S. Roux, A finite element formulation to identify damage fields: Equilibrium gap method, International Journal of Numerical Methods in Engineering 61, 189–208 (2001)

Colliat J.B., Doctoral thesis on "Thermodynamics coupling and fire resistance of brittle structures" (doctoral thesis defended on December 19, 2003)

Colliat J.B., A. Ibrahimbegovic, and L. Davenne, Saint-Venant multi-surface plasticity model in strain space and in stress resultants, International Journal of Engineering Computations, 22, 536–557 (2005)

Colliat J.B., M. Hautefeuille, A. Ibrahimbegovic, and H.G. Matthies, Stochastic approach to quasi-brittle failure and size effect, Comptes Rendus de l'Academie des Sciences, Part II: Mécanique, 335, 430–435 (2007)

Colliat J.B., M. Hautefeuille, and A. Ibrahimbegovic, Size effect interpretation by inelastic macro-scale model with correlated probabilistic properties defined from micro-structure. In Multiscale Modeling of Heterogeneous Materials: From Microstructure to Macro-scale Properties (eds. O. Cazacu and F. Darve), iSTE, Wiley (2008)

Daoud, Doctoral thesis, INSA Lyon, France (2003)

Davenne L., F. Ragueneau, J. Mazars, and A. Ibrahimbegovic, Efficient approach to earthquake engineering analysis, Computers and Structures, 81, 1223–1239 (2003)

Delaplace A. and A. Ibrahimbegovic, Time-integration schemes for dynamic fracture problem using the discrete model, International Journal for Numerical Methods in Engineering, 65, 1527–1544 (2006)

Dolarevic S., Doctoral thesis on "Soil mechanics CAP plasticity model and soil-structure interaction" (doctoral thesis defended on December 21, 2005)

Dolarevic S. and A. Ibrahimbegovic, A modified three-surface elasto-plastic cap model and its numerical implementation, Computers and Structures, 85, 419–430 (2007)

Dominguez N., Doctoral thesis on "Theoretical and numerical studies of bond-slip phenomena" (doctoral thesis defended on July 1, 2005)

Dominguez N., D. Brancherie, L. Davenne, and A. Ibrahimbegovic, Prediction of crack pattern distribution in reinforced concrete by coupling a strong discontinuity model of concrete cracking and a bond-slip of reinforcement model, International Journal of Engineering Computations, 22, 558–582 (2005)

Hartmann D., M. Breidt, V. Nguyen, and F. Stangenberg, Structural collapse simulation under consideration of uncertainty, Proceedings NATO-ARW (eds. A. Ibrahimbegovic and M. Zlatar), GF Sarajevo (2008)

Hautefeuille M., S. Melnyk, J.B. Colliat, and A. Ibrahimbegovic, Probabilistic aspects of localized failure of massive heterogeneous structures, International Journal of Engineering Computations, 26, 166–184 (2009)

Hervé G., Doctoral thesis on "Choc resistance analysis and design of structures under airplane impact" (doctoral thesis defended on October 28, 2005)

Hervé G., F. Gatuingt, and A. Ibrahimbegovic, On numerical implementation of a coupled rate-dependent damage-plasticity constitutive model for concrete in application to high rate dynamics, International Journal of Engineering Computations, 22, 583–604 (2005)

Ibrahimbegovic A., On the geometrically exact formulation of structural mechanics and its applications to dynamics, control and optimization, Comptes Rendus de l'Academie des Sciences, Part II: Mécanique, 331, 383–394 (2003)

Ibrahimbegovic A., Mécanique non linéaire des solides déformables : Formulation théorique et résolution numérique par éléments finis, Hermes Science Publication – Lavoisier, Paris (ISBN 2-7462-1489-X) pp. 1–604 (2006)

Ibrahimbegovic A., Nonlinear solid mechanics: theoretical formulations and finite element solution methods, Springer, Berlin (ISBN 978-90-481-2330) pp. 1–569 (2009)

Ibrahimbegovic A. and D. Brancherie, Combined hardening and softening constitutive model for plasticity: Precursor to shear slip line failure, Computational Mechanics, 31, 88–100 (2003)

Ibrahimbegovic A. and B. Brank (eds.), Multi-physics and multi-scale computer models in nonlinear analysis and optimal design of engineering structures under extreme conditions, IOS Press, Amsterdam (ISBN 1-58803-479-0) pp. 1–407 (2005)

Ibrahimbegovic A. and A. Delaplace, Microscale and mesoscale discrete models for dynamic fracture of structures built of brittle materials, Computers and Structures, 81, 1255–1265 (2003)

Ibrahimbegovic A. and I. Kozar (eds.), Extreme man-made and natural hazards in dynamics of structures, Springer, Berlin (ISBN-10 1-4020-5654-0) pp. 1–397 (2007)

Ibrahimbegovic A. and S. Mamouri, Energy conserving/decaying implicit time-stepping scheme for nonlinear dynamics of three-dimensional beams undergoing finite rotations, Computer Methods in Applied Mechanics and Engineering, 191, 4241–4258 (2002)

Ibrahimbegovic A. and A. Markovic, Strong coupling methods in multi-phase and multi-scale modeling of inelastic behavior of heterogeneous structures, Computer Methods in Applied Mechanics and Engineering, 192, 3089–3107 (2003)

Ibrahimbegovic A., D. Markovic, and F. Gatuingt, Constitutive model of coupled damage-plasticity and its finite element implementation, Revue européenne des éléments finis, 12, 381–405 (2003)

Ibrahimbegovic A. and S. Melnyk, Embedded discontinuity finite element method for modelling of localized failure in heterogeneous materials with structured mesh: An alternative to extended finite element method, Computational Mechanics, 40, 149–155 (2007)

Ibrahimbegovic A. and R.L. Taylor, Nonlinear dynamics of flexible multibody systems, Computers and Structures, 81, 1113–1132 (2003)

Ibrahimbegovic A., C. Knopf-Lenoir, A. Kucerova, and P. Villon, Optimal design and optimal control of elastic structures undergoing finite rotations and deformations, International Journal for Numerical Methods in Engineering, 61, 2428–2460 (2004)

Ibrahimbegovic A., J.B. Colliat, and L. Davenne, Thermomechanical coupling in folded plates and non-smooth shells, Computer Methods in Applied Mechanics and Engineering, 194, 2686–2707 (2005a)

Ibrahimbegovic A., I. Gresovnik, D. Markovic, S. Melnyk, and T. Rodic, Shape optimization of two-phase material with microstructure, International Journal of Engineering Computations, 22, 605–645 (2005b)

Ibrahimbegovic A., P. Jehel, and L. Davenne, Coupled damage-plasticity constitutive model and direct stress interpolation, Computational Mechanics, 42, 1–11 (2008)

Ibrahimbegovic A., G. Herve, and P. Villon, Nonlinear impact dynamics and field transfer suitable for parametric design studies, International Journal of Engineering Computations, 26, 185–204 (2009)

Kassiotis C., J.B. Colliat, A. Ibrahimbegovic, and H. Matthies, Multiscale in time and stability analysis of operator split solution procedure applied to thermomechanical problems, International Journal of Engineering Computations, 26, 205–223 (2009)

Kucerova A., Doctoral thesis on "Identification of nonlinear mechanics model parameters based on softcomputing methods" (doctoral thesis defended on November 27, 2007)

Kucerova A., D. Brancherie, A. Ibrahimbegovic, J. Zeman, and Z. Bittnar, Novel anisotropic continuum-discrete damage model capable of representing localized failure of massive structures. Part II: identification from tests under heterogeneous stress field, International Journal of Engineering Computations, 26, 128–144 (2009)

Leger P. and R. Tremblay, Earthquake ground motion for seismic damage assessment and re-evaluation of existing buildings and critical facilities, Proceedings NATO-ARW (eds. A. Ibrahimbegovic and M. Zlatar), GF Sarajevo (2008)

Mang H., S. Scheiner, C. Hellmich, and B. Pichler, Avoiding damage of NATM-tunnels during the construction stage: micromechanics-supported hybrid analyses, Proceedings NATO-ARW (eds. A. Ibrahimbegovic and M. Zlatar), GF Sarajevo (2008)

Markovic D., Doctoral thesis on "Multiscale analysis of inelastic nonlinear behavior of heterogeneous structures" (ENS-Cachan thesis defended on June 12, 2004)

Markovic D. and A. Ibrahimbegovic, On micro-macro interface conditions for micro-scale based FEM for in elastic behavior of heterogeneous materials, Computer Methods in Applied Mechanics and Engineering, 193, 5503–5523 (2004)

Markovic D. and A. Ibrahimbegovic, Complementary energy based FE modeling of coupled elasto-plastic and damage behavior for continuum microstructure computations, Computer Methods in Applied Mechanics and Engineering, 195, 5077–5093 (2006)

Markovic D., R. Niekamp, A. Ibrahimbegovic, H.G. Matthies, and R.L. Taylor, Multi-scale modeling of heterogeneous structures with inelastic constitutive behavior. Part I : Mathematical and physical aspects, International Journal of Engineering Computations, 22, 664–683 (2005)

Markovic D., K.C. Park, and A. Ibrahimbegovic, Model reduction strategy for transient analysis of large structures with inelastic behavior, International Journal of Engineering Computations, 26, 45–68 (2009)

Matthies H., Natural and man-made hazard estimates and probability aspects, Proceedings NATO-ARW (eds. A. Ibrahimbegovic and M. Zlatar), GF Sarajevo (2008)

Melnyk S., Doctoral thesis on "Multiscale modeling approach and optimal design of heterogeneous materials with inelastic behavior" (doctoral thesis defended on November 2, 2007)

Niekamp R., D. Markovic, A. Ibrahimbegovic, H.G. Matthies, and R.L. Taylor, Multi-scale modeling of heterogeneous structures with inelastic constitutive behavior. Part II : Software coupling and implementation aspects, International Journal of Engineering Computations, 26, 6–28 (2009)

Owen D.R.J., Y.T. Feng, J.M. Rance, and A.T. Bere, Predictive modeling of damage in structures and the development of retrofitting or mitigating strategies, Proceedings NATO-ARW (eds. A. Ibrahimbegovic and M. Zlatar), GF Sarajevo (2008)

Stein E., M. Ruter, and S. Ohnimus, Computational validation and verification of engineering structures via error controlled mode and discretization adaptivity, Proceedings NATO-ARW (eds. A. Ibrahimbegovic and M. Zlatar), GF Sarajevo (2008)

Villon P. and A. Nace, Crisis management in water distribution networks, Proceedings NATO-ARW (eds. A. Ibrahimbegovic and M. Zlatar), GF Sarajevo (2008)

NON-DESTRUCTIVE ASSESSMENT OF CONCRETE DAMAGE: INTEREST, DIFFICULTIES AND RESEARCH NEEDS

D. BREYSSE*
University Bordeaux 1, Ghymac, Avenue des facultés, 33405 Talence cedex, France

Abstract. Damage assessment of reinforced concrete structure is required for maintaining the building and infrastructures asset at a good level of performance. Non-destructive techniques provide a way towards this assessment. They however suffer from several shortcomings, since are only indirect measurements of engineering properties, and they are sensitive to many influent factors. In addition, the influence of material variability is not easy to sort out of the measurement variability, when it has a big influence on the assessment reliability. Some main results of several cooperative research programs are discussed, highlighting the conditions for a better use of combination of several non-destructive techniques. It is shown how to quantify and account for material variability and for the influence of environmental potential bias factors. Data are taken both from in-site measurements and laboratory studies. Applications are analyzed for corrosion assessment and for in-site strength assessment.

Keywords: Corrosion, damage, material variability, non destructive assessment, reliability, strength assessment

1. Interest and Key Challenges of Non Destructive Assessment of Concrete

For the maintenance or the refurbishing of their structures, engineers need to assess their condition. When detecting or getting suspicion of possible pathology from visual inspection, they need to know first the origin of this problem, then if there is a possible evolution and more over at what rate, and finally what is

* To whom correspondence should be addressed. e-mail: d.breysse@ghymac.u-bordeaux1.fr

A. Ibrahimbegovic and M. Zlatar (eds.), *Damage Assessment and Reconstruction After War or Natural Disaster*,

the level of the problem, its extent and location. Another common objective is the quantitative evaluation of the safety level of the structure. Any parameter useful for this safety quantitative evaluation will be called "*engineering property*". The more common are stiffness (Young's modulus) and strength. Non-destructive techniques (NDT) can be used to assess the structural condition, even if they only provide an indirect approach to their performances (De Lorenzis and Nanni, 2004). The aims of NDT can be classified as being able to: (a) *detect* (a defect or a variation of properties, between two structures or inside one structure), (b) *build a hierarchy* (i.e. to rank on a scale), regarding a given property, between several areas in a structure or between several structures, (c) *quantify* these properties, e.g. compare them to allowable thresholds. Detection, ranking and quantification can be regarded as three levels of requirements, the last being the strongest and the more difficult one.

Much research has been devoted to the development of techniques or of data processing for a better assessment of building materials. Some authors have tried to synthesize the abilities of techniques with respect to given problems (Bungey and Millard, 1996; Uemoto, 2000; Breysse and Abraham, 2005) or to define the most promising paths for future developments (OECD, 1998). The general agreement is that the quality of assessment is limited due to sources of uncertainties arising at various levels and caused: by the testing method, by systematic interferences with the environment, by random interferences (due to material intrinsic variability), by human factor influence and by data interpretation (Gehlen et al., 2006). Thus, reducing any of these sources of uncertainties can provide for an improved damage assessment.

Among the main challenges about concrete assessment, one can cite:

- *Stiffness and strength assessment.* The knowledge of the elasticity modulus or the compressive strength of concrete is necessary to perform any structural evaluation. They can be evaluated from coring, which offers only an image of the properties at the point where the specimens have been taken. Thus it is difficult to obtain a representative view of the mechanical properties, since the material as well as the damage level can be highly spatially variable. NDT provides an interesting alternative since it enables to easily cover wide areas, the difficulty being to correlate the values of the physical measurements obtained via NDT to the mechanical properties. Rebound measurement and ultrasonic pulse velocity (UPV) are among the more adapted NDT regarding this purpose (Malhotra, 1981) and a recent European standard has given formal solution on how concrete strength from in-situ testing (NF EN 13791, 2007).
- *Water content (or moisture content) assessment*, for two reasons: a large value of water content can be the sign of the bad quality of the material (often due to delaminating in concrete), but it can also be the sign that a

potential vector of future damage is present, since the water is the more common agent for deterioration (salt ingress, dissolution, freeze...). Many NDT are sensitive to both a material condition parameter (e.g. Young's modulus) and to water content. Due this double dependency, one cannot easily decide what is the cause of the measured variation in the NDT parameter.

– *Corrosion assessment*, since many reinforced concrete structures suffer severe damage due to corrosion (due to chlorides in marine environment, de-icing salts, or other causes). The cost of corrosion is estimated to be about 3–4% of GNP in Western countries. The material and structural assessment of such structures is a key point when one wants to evaluate its residual capacity, to design a reinforcing solution or to plan maintenance. Some techniques have been standardized which enable to assess the material condition of corroding structures but it will be seen that many questions still remain unanswered.

These three questions regard partly mechanical assessment, partly durability assessment, but the boundary between the two domains is not well defined, since the mechanical properties of tomorrow are often dependent on the deterioration process of today.

2. Non-Destructive Evaluation of Concrete: Objectives, Means and Difficulties

2.1. DIFFICULTIES COMING FROM THE COMBINED INFLUENCE OF MANY FACTORS

When wanting to address material condition, the expert can try to get only a qualitative view, for instance by identifying spatial variations in the measured parameters. He can be more ambitious, wanting to quantify these variations, for instance because he needs some input values for structural computations before repair or for reliability assessment. If expertise is required in the first case, it is not sufficient in the second one that also requires a validated methodology such as to ensure the quality of estimates. Much research has been devoted to the development of techniques or of data processing for a better assessment of building materials. Many case studies exist where several techniques have been combined on a given structure (or on laboratory specimens), but we think that real added value will be obtained only when the question of coupling has been correctly analyzed (Dérobert et al., 2005). This added value can be defined in terms of: (a) accuracy of estimation of properties, (b) relevance of physical explanations and diagnosis, (c) shorter time to reach a given answer.

Table 1 illustrates the sensitivity of four different non-destructive techniques to several important properties of concrete. It is drawn from a national review of the state of the art recently established in France (Breysse and Abraham, 2005) and from results obtained in a benchmark research program (Balayssac, 2005). The + or − signs correspond to a positive (consequence varies with cause) or negative (consequence varies against cause) sensitivity.

TABLE 1. Supposed sensitivity of NDT to several important concrete properties ("0" denotes no significant influence, "?" denotes uncertainty)

	Radar	Capacimetry	Electrical resistance	Ultrasonic waves
Water content	Velocity: – Amplitude: –	–	–	Velocity: + Attenuation: −
Porosity	–	–	–	Velocity: YES (+ if saturated, − if dried)
Chloride content	Velocity: – Amplitude: 0	0?	–?	0
Re-bars	Bias		Bias	Bias

It is crucial to understand why and how the combination of techniques can bring some added value. Two remarks can be made:

- When two parameters to which a given technique is sensitive are varied simultaneously, one cannot identify the reason for the observed variation without additional information. Such is usually the case when a variation in water content (due to varying environmental conditions) is superimposed on a variation in the concrete microstructure (porosity of the paste for instance). In this case, it is not possible to establish a direct link between the observed variation of the measured property (wave velocity, electrical resistance ...) and the physical cause. This is, of course, a crucial point for diagnosis since a variation of the microstructure can reveal some defect or damage when the variation in water content (which can also depend on the microstructure, since the water content in a highly porous saturated concrete will be larger than in a dense saturated concrete) also depends on the environmental context (temperature, exposure to the sun, dominant wind...).
- The combination of two non-destructive techniques can provide additional information only if the sensitivity to the two parameters is different for the two techniques.

Several levels of uncertainty arise, some from physical considerations, others from the measurement process itself, and a third part from the material variability. One needs to take some insight in the physics of the involved phenomena for a better understanding. The physical property measured with the NDT is usually not the parameter one wants to evaluate. Let us call:

– Y the property that we are looking for (dimension, strength, modulus, durability…) and
– T the measured property (electrical resistance, magnitude or time of arrival of a signal…)

The assumption on which NDT is based is that a correlation exists between Y and T, for instance between a length and the time of arrival of a signal. However, this correlation is not perfect, since, in fact, these two properties are usually macroscopic properties which result from some combination of physical material properties at the micro-scale (porosity, water content, crack-shapes, connectivity, strength of bonds in the composite…). Let us denote with X these basic physical properties.

Figure 1 illustrates what kind of relations can exist between various material properties and why NDT interpretation is so much a complex task. The black and gray arrows denote some correlation between properties and the red arrows denote some sensitivity of a technique to parameters. At the center, one finds material properties X (in blue boxes), which are representative of the material: porosity and connectivity on one hand, water content and saturation rate on the other hand. The former can be considered as constant with time (at least at short term, since they can vary due to chemical processes), while the latter can vary due to environmental changes, since timber, concrete or stone are hygroscopic materials. On the left part of the diagram, one has the engineering properties Y which are related the material properties (gray double arrows), even if the relations are very complex. Finally, on the right part, one has physical properties T measured through NDT (here electrical conductivity and UPV), which depend on material properties (red double arrows) but also on some bias factors, for instance temperature at the time of the measurement (orange arrows). Environmental factors have also been taken into consideration, they influence the T factors, probably because they interfere on X properties.

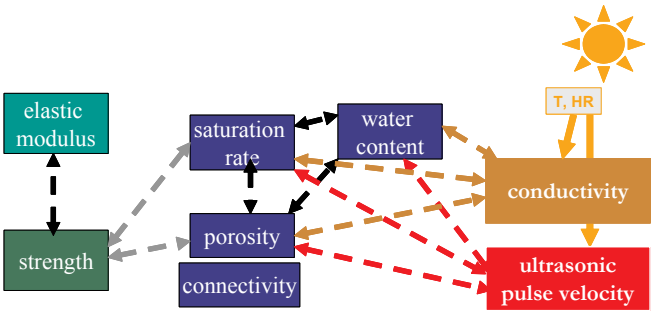

Figure 1. Generic diagram of relations between engineering properties, physical parameters, NDT measurements and sources of noise

This graph shows that:

- The assessment of Y parameters does not reduce to a direct and simple Y = f(T) relation.
- Any existing correlation between two techniques (here radar and resistance) will also follow a very complex way, which must be understood before being used.

When addressing the question of quantification, a common problem is that the NDT measurements can be sensitive to both the engineering parameter (like strength or stiffness), which are mainly stable with time, and to the water content, which can vary at short term according to environmental conditions. If it is the case:

- One cannot tell if the measured variations result from a variation in the engineering parameter or in the water content.
- One has to account for this sensitivity if he wants to quantify the engineering parameter.

This question is a central one, since it is the main cause that weakens the practical ability of NDT. Considering that a measurement is sensitive to a first parameter (whose value is expected) and to one or several "bias factors", the effects of these "bias factors" have to be eliminated during the data processing.

2.2. THE POSSIBLE ADDED-VALUE OF COMBINATION OF TECHNIQUES

The combination of techniques can follow various objectives, like for instance confirming with a second technique what has been observed with a first one, zoning the area where a more sophisticated investigation will be performed in the following, decreasing the number of borings. These questions have recently been formalized (Breysse et al., 2008a) with a series of practical examples. A more ambitious objective can be to use two (or several) techniques relying on the fact that a second technique can provide additional information, enabling to reduce uncertainty or to eliminate a bias factor to which the first technique is sensitive. This point will be detailed here.

The generic problem comes from the use of ONE NDT, which is sensitive to TWO parameters. In this situation, a second technique, also sensitive to these two parameters (or only to the second one) can enable to capture and eliminate the effect of the second one. The second parameter can be a material property (internal) or an environmental one (e.g. air temperature and humidity whose changes with time and environmental conditions will affect all electrochemical measurements).

In practice, since this problem has been known from a long time, engineers have developed strategies to account for it, for instance by building and using some charts in which the correction is accounted for. One of the best known example is that of the "SonReb" method in which Ultrasonic Pulse Velocity (UPV) and rebound number are used to estimate on site concrete strength (Malhotra, 1981). The water content influence is a key question, since many common NDT used to quantify heterogeneities and potential damage (UPV, ground penetrating radar, resistance ...) are also sensitive to water content. Thus, how is it possible to make the part between the two potential causes of variation of the measurements?

Figure 2 shows the variation of compression wave velocity (frequency 250 kHz) as a function of the 28 days compressive strength of six concrete mixes, measured both on saturated specimens and on specimen maintained at a 40% saturation rate. It shows how the measured parameter (here UPV) is sensitive to both sources of variations. Thus any measurement of UPV without any additional information would be totally unable to make the part between the two possible explanations, whose magnitude of influence is comparable.

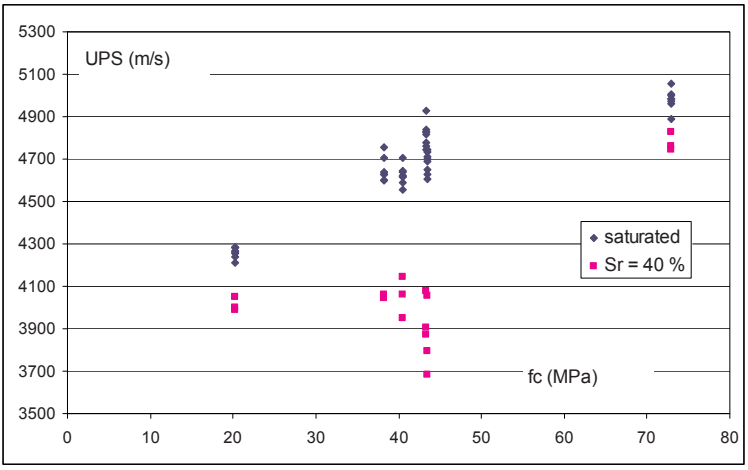

Figure 2. Influence of saturation rate and concrete properties on UPV

2.3. DIFFICULTIES ARISING WHILE COMBINING TECHNIQUES FOR IMPROVING THE ASSESSMENT

Many authors have pointed the fact that the comprehension and modeling of the relations between X, Y and T values is difficult. For instance (Popovics, 2001) has written: "Unfortunately, improvement cannot come from science because there is no theoretically justifiable relation between strength and pulse velocity

even for homogeneous, linearly elastic materials, let alone for concrete. Considerable value can, however, still be derived from formulas for improved nondestructive strength estimation obtained by circumventing the lack of scientific approach and selecting an engineering approach: mathematical modeling".

One way is the development of empirical laws, based on statistical analysis or on models, like the Mori-Tanaka model. Literature study shows that many empirical models have been proposed for relying UPV and strength and/or modulus. We will not question here their theoretical validity but only their practical ability to be used for a more accurate material assessment. These correlations are somehow material dependent and calibration curves must be used, for instance from cores on which both series of measurements are performed. Another difficulty comes from the fact that both physical and mechanical properties depend on various influent factors (intrinsic like porosity or varying with exposure like water content). As long as these factors are not mastered, the calibration will itself be of poor quality.

The "SonReb" (from sonic and rebound") method has been proposed to offer an original way for strength assessment, using charts made of a series of curves (for different rebound values) giving the strength as a function of UPV. This approach has been used for all types of concrete, including young age concrete (Soshiroda et al., 2006) and high strength concrete (Pascale et al., 2000; Khan et al., 2004). The question of the calibration of such curves is a key point, since many kinds of mathematical expressions are available in the literature (IAEA, 2002) providing an extensive state-of-the-art. The best correlation laws can be identified from an extensive experimental program (Samarin, 1991; Soshiroda et al., 2006) varying aggregate type and age of concrete, but this is not adapted to the context of practical in-situ assessment. We will show in Section 5 that fundamental limits can be encountered and that the real added value of combination will depend on several factors, whose each of them can be quantified. Let us have a look first on the influence of water content on the measurements.

Sonic and ultrasonic measurements are the more widely used NDT for the condition assessment of building materials. The first reason is that, for elastic materials, it exists a theoretical relation between the velocity of longitudinal waves and the elasticity modulus:

$$E = c\, V_L^2\, \rho \qquad \text{or} \qquad V_L^2 = E \,/\, c\rho \tag{1}$$

where V_L is the velocity of longitudinal waves, ρ is the mass density and c is a constant which depends on the Poisson's ratio. Thus, assuming linear elasticity and providing a value to ν and ρ will lead to a direct assessment of Young's modulus.

One question is that of the influence of the water content on measurements. The variation in moisture or in water content can change both volumetric mass (by replacing air by water, assuming the total volume remains unchanged) and modulus (changes in the internal stresses due to capillarity forces for low wat er content f.i.). The dependence to water content however shows contrasting results, depending on the material. These effects have been widely studied in timber construction and, at a lesser degree in stone construction, where non-linear effects have been encountered (Homand and Duffaut, 2000; Ezzdine et al., 2008). In concrete, to the best of our knowledge, few studies have been devoted to this question. The dominant paradigm was that the wave velocity increases with the water content. Recent results obtained within the SENSO project have proved that the behavior is, opposite to what was supposed, similar to that of limestone (Villain et al., 2008). Figure 3 shows some of these results. In fact, a "dry" concrete can be obtained (with some difficulties) in the laboratory but it does not correspond to a common situation in practice.

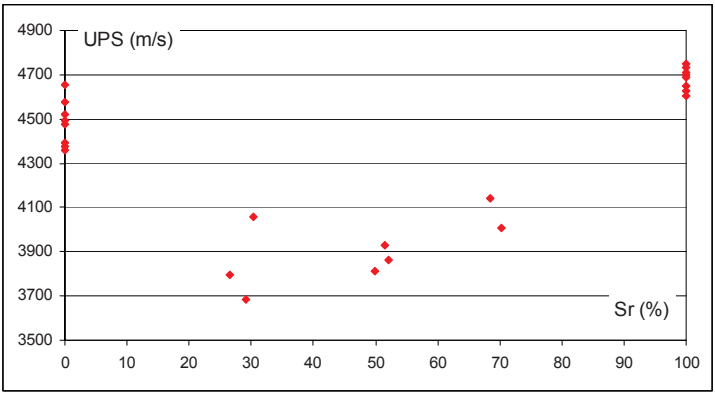

Figure 3. Variation of the UPV with saturation rate (one concrete mix)

Since the minimum point on the saturation/velocity curve seems to be around 40%, the assumption of velocity increase with large water content can be seen as a good approximation in the practical range of use. However, extrapolating any relation identified in this domain to the dry material would be grossly erroneous. In Eq. (1), there is a conflicting influence between the increase of the mass density and that of the Young's modulus. One has also to remain careful with too simplistic explanations based on the linear elastic model, since many other effects, among which viscosity can be invoked for explaining the exhibited response.

These non-monotonous variations have to be superimposed to those due to other factors: contrast between different materials (for instance different concrete

mixes), heterogeneity in the material, temperature effects... We must account for these questions when addressing the question of material assessment.

3. Variability and Reliability of Assessment: A Corrosion Case Study

3.1. USUAL MEANS FOR ASSESSING CORROSION

Corrosion of reinforced concrete infrastructures, often due to chloride ingress, has practical consequences on the condition and safety level of infrastructures. To reduce the cost of maintenance and repair while keeping these infrastructures at a correct level of safety, managers can use non-destructive techniques to assess the condition state. When relevant models are used, life cycle cost analysis becomes possible and the maintenance of structures can be optimized (Stewart, 2005; Li, 2004). The non-destructive assessment of corrosion is usually carried out by combining the following three techniques (NEA, 2002):

- Half cell potential measurements, which provide an indication of likelihood of corrosion activity at time of testing, through a value of potential (ASTM C876-91 standard puts in relation the value measured and a probability of corrosion).
- Measurement of the concrete resistance, which informs about the moisture content in the concrete.
- These two first measurements give no information about the corrosion rate, which can be estimated by measuring the polarization resistance, which gives an indication of corrosion rate of the reinforcement at time of testing.

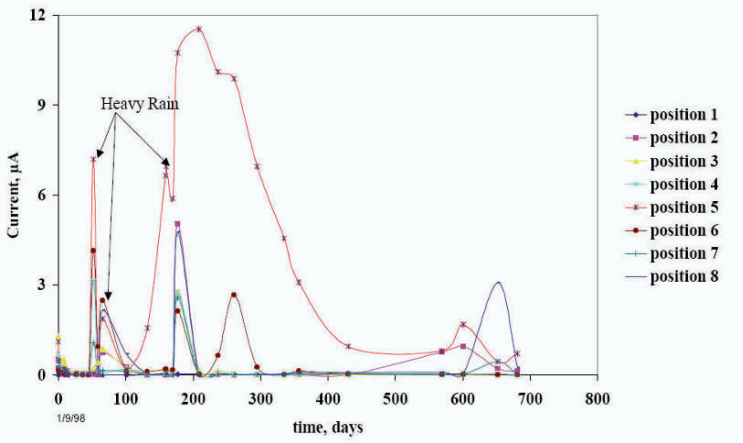

Figure 4. Temporal variability of the current of corrosion (in µA) and its relation with humidity (After Klinghöfer et al., 2000)

A value of the corrosion current density i_{corr} is derived, whose magnitude is put in relation with the corrosion rate (e.g. the corrosion is said to be negligible if it is lower than 0.1 $\mu A/cm^2$ and high if it is larger than 1 $\mu A/cm^2$). The problem is however more difficult regarding interpretation. Standards only provide some information on thresholds which have to be considered as "relative thresholds" and need to be taken with a lot of care.

It is well known that all these techniques must be used by qualified and experienced operators, and that they mainly provide qualitative data (or relative variations) instead of quantitative ones. The main reason is that NDT only give information at the time of the measurement, and that this information is very sensitive to environmental conditions (Jäggi et al., 2001; Burgan Isgor and Ghani Razaqpur, 2006), as it can be seen on Fig. 4.

Continuous monitoring combined with NDT on Skovdiget bridge, near Kopenhagen has shown that, due to temperature effects, NDT inspections during autumn months tend to provide conservative measurements of the corrosion potential (and thus corrosion risk). The corrosion development is itself very dependent on moisture content and temperature, which are responsible for the electrolyte continuity (pore connectivity) and for the oxygen availability at the steel surface. Moisture influences the electrical resistance, which is the most comprehensive parameter determining the corrosion current. Since moisture and temperature vary with time, and may also vary from place to place in the concrete, an assessment of concrete that should be independent of these variations becomes difficult. Since many influencing factors can explain any observed variability of the measurements, it is important to quantify these potential effects, such as to sort out any "real signal", i.e. real variation with time or space, of the effective corrosion degree (Breysse et al., 2007).

Collective efforts have been undertaken in the recent years to gather data about time and space variability in relation with service life prediction and structural reliability (Duracrete, 2000; Samco, 2006). The measured on-site variability can be due either to material and exposure conditions variability or to uncertainty in the measurement process (e.g. lack of repeatability or influence of environmental conditions at the time of measurement). The first cause is representative of the structure and of its condition. The spatial variability of the material properties results from the construction process and concrete placing. It must be accounted for in a probabilistic approach, the residual service life becoming a probabilistic variable, whose value is distributed in the structure (Stewart, 2001; Li, 2004). The second type of uncertainties can be reduced with a more cautious approach and with the modelling of environmental effects on the measurements. Data obtained at the laboratory, repeating for instance electro-chemical measurements under varying ambient conditions, can be processed and used for this purpose. In fact, the vast majorities of probabilistic studies

whose purpose is to analyze the consequence of material variability on the structure reliability do not make the part between the two components of variability: the real one (random uncertainty), due to the material, and the superimposed one (epistemic uncertainty), which only comes from imperfect knowledge one has of the structure after measurement.

3.2. BARRA BRIDGE CHARACTERISTICS AND INVESTIGATION PROGRAM

The structure. The Barra Bridge is located on km 0 + 824 of E.N.109-7 over Ria de Aveiro. It has a 578 m length, between the support axes on the abutments. The central span has 80 m and the access viaducts, symmetric as refers to the central span, have 249 m, each being formed by seven spans of 32 m and a last one of 25 m (Fig. 5).

In a first inspection made in the Barra Bridge (in May 2006), two piers and one of the abutments were inspected. The piers were the P13 and P15, which are in land, and the abutment was the E2. The inspected zones are on the right part of the bridge, which is the farthest from the sea, since the sea is about 300–500 m from the left end of the bridge. Regarding their location respectively to the river, the inspected areas on the piers are denominated as "upstream" and "downstream" (depending on what column it is referred to) and in "left" and "right" side.

Figure 5. Barra Bridge

The inspection included visual observation of the structure, the selection of different areas to be studied (differing in elevation, part of pier and side), concrete cover over the reinforcements in the selected areas, half cell potential and corrosion rate measurements. Cores were extracted for laboratory tests, mainly for chloride characterization but also for concrete compressive strength and for microstructural characterization.

In pier 13, six areas were analyzed, three in the left side of the pier and three in the right side (Fig. 6). Concrete cover, potential and corrosion rate measurements were performed and cores were taken in five of those areas. In the last one, it has been only proceeded to concrete coring.

These areas are denominated as follows: 13JE (2.5 m) – downstream, left side at about 2.5 m above ground level; 13JE (10 m) – downstream, left side, above 10 m; T13E – transverse beam, left side; 13MD (2.5 m) – UPVtream, right side at about 2.5 m; 13MD (10 m) – UPVtream, right side, above 10 m; T13D – transverse beam, right side.

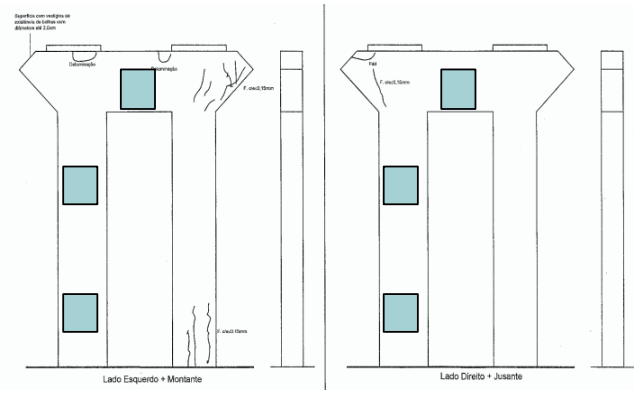

Figure 6. Location of investigated areas on pier 13 (*left* face and *right* face)

3.2.1. *Spatial Variability*

The cover was measured using a scanning cover depth meter. The mapping of corrosion potential was performed with a German Instruments GD-2000 Mini Great Dane system, and the determination of the corrosion rates was done by the polarization resistance method using the equipment GeCor 6. The detailed results of each area, regarding the cover of each rebar, the potential values and the corrosion rate measurements were analyzed in terms of variability. For instance, regarding the 13MD (10 m) area (whose size is about 1 m^2), the investigation performed on 15 May 2006 has provided:

- A corrosion current density i_{corr} in the 0.085–0.359 $\mu A/cm^2$ interval
- A half cell potential (measured with $Cu/CuSO_4$ reference electrode) varying from −72.7–30.4 mV
- A cover depth between 29 and 35 mm (horizontal re-bars) and 38–40 mm (vertical re-bars)
- A carbonation depth (from cores) between 10 and 14 mm

Therefore, the 13MD (10 m) area, which can be regarded as a "homogeneous" area regarding the corrosion degree (at least from visual inspection) exhibits some spatial variation of its characteristics. It is thus interesting to analyze the reasons of this variability and to understand if it requires a statistical analysis or if it suffices to consider representative values (either mean values or conservative estimates) to have a good image of the area.

3.2.2. *Temporal Variability and Consistency*

A second series of investigations was undertaken two months later (on 27 July 2006), to check the stability of the non-destructive results with time, and to gather additional information. The two series of measurements have been

performed in different atmospheric conditions (this information was not recorded at the time and place of the measurements):

- On 15 May 2006, the temperature was average (about 20°C) and the weather was rather dry (RH about 80%)
- On 27 July 2006, the temperature was higher (about 25°C) but the weather was wet (RH about 90%)

Regarding the 13MD area, the results were:

- A corrosion current density i_{corr} in the 0.363–0.783 μA/cm^2 interval,
- A potential (measured with Cu/$CuSO_4$ reference electrode) varying from –47.5 to −17.3 mV.

This shows that the non destructive results (corrosion current density or potential) cannot be simply viewed as reference values, which can be compared to normalized threshold, and that a correct assessment of the structural condition requires a lot of care. It is well known that the environmental context (mainly temperature and humidity) can influence the electrical response of the structure.

However, the repeatability of the NDT measurements can be checked by comparing the two series of measurements (Fig. 7). On this area 13JE (but the same conclusions has be drawn for others areas), the overall consistency between the two series of measurements is good, even if one has some scatter. The "local noise" which corresponds to the scatter is about +/− 15 mV.

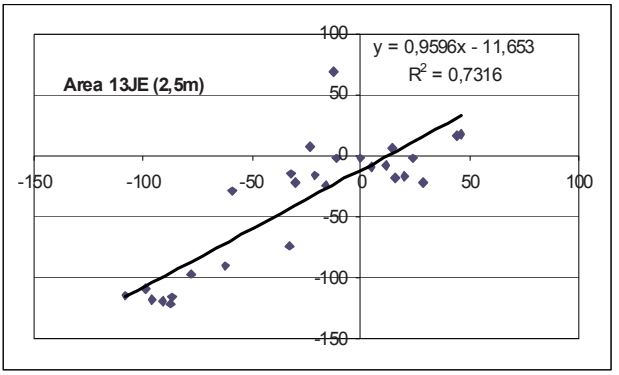

Figure 7. Repeatability of potential measurements (in mV) for area 13 JE

Regarding the measured values for the corrosion current density, they are very different for the two series of measurements, as summarized in Table 2. The average value of i_{corr} has been multiplied by about 2 between May and July (multiplying factor = 1.86 calculated on 11 measurements on Pier 13).

TABLE 2. Average values for i_{corr} ($\mu A/cm^2$) measurements at two different times

Area	May	July	Difference (%)
13 JE	0.31	0.62	+98
13 MD	0.31	0.53	+75
13 – : T beam	0.22	0.48	+123
all	0.29	0.54	+86

3.2.3. *Cover Depth Variability*

All data regarding cover have been synthesized, such has to quantify the variability at various scales (within an area, within a pier, for the whole bridge). A significant difference has been noted between horizontal and vertical re-bars (due to obvious design reasons), with an average cover depth that is 7–8 mm larger for vertical rebars. A significant difference has also been noted between Pier 13 and Pier 15, which can only be explained by variability in the rebar positioning:

- Pier 13: average horizontal cover depth 29.1 mm, average vertical cover depth 37.7 mm
- Pier 15: average horizontal cover depth 37.3 mm, average vertical cover depth 44.8 mm

More detailed measurements of cover depth have been performed during the second series of investigations, to quantify the longitudinal variation of cover depth along a given rebar. For instance, one has measured between 30 and 35 mm when the cover depth had at first been estimated as being 34 mm. The coefficient of variation (c.o.v.) along a rebar is between 3% and 10%, with an average value of 7%. For a given 1 m^2 area, and a given set of re-bars (horizontal or vertical) the c.o.v. ranges between 9% and 16%. It jumps to 20–30% if one combines the two directions of reinforcements in a given area. This value is much larger than that of an individual rebar. When a whole pier is considered, the coefficient of variation is about 30%.

3.3. LABORATORY ANALYSIS AND DEVELOPMENT OF A CORRECTION PROCESS

3.3.1. *Experimental Program Definition and Analysis*

Moisture content in the concrete and humidity are the most influencing factors affecting the corrosion development, but also the electrochemical properties assessed via non-destructive techniques. It is also well known (Andrade and Alonso, 1996; Gonzalez et al., 1996) that other influencing factors are the quality of concrete, the chloride content, the oxygen content. Since the measurements are also performed through the cover concrete, the cover depth also appears as a

potential influent parameter. Thus an experimental program has been designed such as to quantify the influence of some of these parameters on the corrosion development and on the current of corrosion.

Specimens were cast with two w/c ratios (0.45 and 0.65) and two cover depths (1 and 3 cm). Two prisms with 20 × 20 × 25 cm^3 were prepared for each concrete type and cover depth. Chlorides have also been added to the mix, such as to ensure the initiation of corrosion (3% total chlorides related to cement content). All specimens were subjected during ten months to varying conditions regarding relative air humidity (20% < RH < 100%) and temperature (2°C < T < 50°C). Regular measurements of polarization resistance have been performed, from which corrosion current density has been deduced.

Statistical analysis has been performed on the whole series of measurements, such as to identify the most influencing factors and to provide, via multi-linear regression analysis, a quantitative model for i_{corr}. Due to the fact that the i_{corr} values can vary in a large range, $\ln(i_{corr})$ values have been considered in the model. As it was expected from previous studies, moisture is the most important parameter. Figure 8 shows how it is positively correlated with $\ln(i_{corr.})$, the diagram excluding RH = 100% values, since this value involves different physical phenomena limiting the corrosion rate. Accounting for the linear influence of RH for explaining $\ln(i_{corr})$ variability reduces by a factor of 2 the total experimental variance.

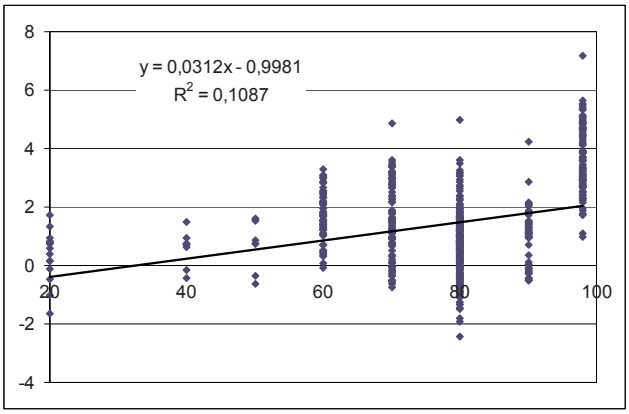

Figure 8. Correlation between RH (in %, x-axis) and $\ln(i_{corr.})$ (y-axis)

The other parameters bring less information but the effect of temperature, cover depth and water to cement ratio are significant. Each of them leads to an additional reduction of variance of about 10%. Two other parameters (total time since the beginning of experiment, and time elapsed since the beginning of the

new level of (RH, T) are not statistically significant). The multi-linear regression analysis leads to:

$$\ln i_{corr} = 0.0312\ RH - 4736/T + 1.695\ w/c - 0.391\ d + 14.589 \quad (2)$$

Thus the resulting model can be written as:

$$i_{corr} = A\ e^{0{,}0312\ RH}\ e^{-4736/T}\ e^{-0.391\ d}\ e^{+1.695\ w/c} \quad (3)$$

where RH is the air relative humidity (in %), T is the air temperature (in K), d is the cover depth (in cm), w/c is the water to cement ratio, A is a constant (in $\mu A/cm^2$).

This empirical model quantifies the combined influence of the four parameters (RH, T, d, w/c) on the measured value of the corrosion current density. The unexplained variance of the model which accounts for the combined influence of these four parameters is only 36% of the total experimental variance, giving an idea of the "quality" of this model. It must be added that the model can only be used for RH < 100%, since when the concrete is saturated the involved mechanisms are different. It thus makes possible the correction of the measurements to cancel the effects of these parameters when they are varying with time and/or space. The model can also be fitted with renormalized variables, such as to have coefficients without units. The model confirms that the corrosion current density is larger when RH increases, T increases and d decreases. It also confirms that the temperature and moisture are the most influencing parameters. For instance:

– It is multiplied by a factor 1.37 if RH varies from 80% to 90%.
– It is multiplied by a factor 1.70 if T varies from 15°C to 25°C.
– It is multiplied by a factor 1.48 if d varies from 3 to 2 cm.

3.3.2. *Correction Process for Temporal and Spatial Variability*

If we focus on the influence of the variation of the (RH and T) environmental parameters and of the cover depth on the i_{corr} measured value for a given concrete, it is possible to define an arbitrary reference set $S_{ref} = \{RH_{ref}, T_{ref}, d_{ref}\}$ and to consider the real set S = {RH, T, d} at the place and time of the measurement. Since i_{corr} is measured with S, the question is to correct it (using a multiplying factor), such as to obtain an $i_{corr\ ref}$ reference value which would have been measured under the conditions of the reference set. The obtained reference value would then be independent of any time variation in the environmental conditions (temperature, humidity) as well as of any spatial variation in the cover depth of rebars. Writing Eq. (3) a first time for the real set S and a second time for the reference set S_{ref}, thus eliminating A, it comes:

$$i_{corr\ ref} = k\ i_{corr} \quad (4)$$

with

$$k = e^{0,0312\,(RH - RHref)}\, e^{-4736(\,1/T - 1/Tref)}\, e^{-0,391\,(d - dref)} \quad (5)$$

Considering the following arbitrary reference set: {RH_{ref} = 80%, T_{ref} = 293 K, d_{ref} = 3 cm}, one can calculate the correcting factor for any set at the time and place of measurement. The Table 3 gives some examples of such correcting factors for various sets. The last series on Table 3 gives the factor (k = 0.558) by which one would have to multiply the July measurements to compare them with the May measurements. It is totally compatible with what has been observed on site (1/1.86 = 0.54), but the lack of any accurate recording of atmospheric conditions prevents us to conclude further on this point.

TABLE 3. Correcting factor on i_{corr} for several sets ({RH_{ref} = 80%, T_{ref} = 20°C, d_{ref} = 3 cm})

RH (%)	T (°C)	d (cm)	k	RH (%)	T (°C)	d (cm)	k
65	20	3	1.597	80	35	3	0.455
95	20	3	0.626	80	20	2	0.676
80	5	3	2.390	90	25	3	0.558

Equation (5) giving k value can also be helpful in interpreting the level of significance of any spatial variation that can be noted on site, when T and RH can be assumed as constant (during the series of measurements). Variations in measured values of i_{corr} can be due either:

- To a different degree of intensity of corrosion, which is the purpose of NDT measurement
- To the variation of an influent parameter, like the cover depth
- To the variation of any other influent parameters (for instance local micro-structure of concrete) or to any noise in the measurement process

It is easy to quantify the variability on i_{corr} resulting from any variability on the cover depth. The cover depth variability has been assessed on the Barra Bridge at three scales: that of a given rebar, that of a 1 m^2 area (Area 13MD for

TABLE 4. Measured variabilities of cover and of corrosion current density at three scales (c.o.v. indicates coefficient of variation)

Scale	c.o.v.(d)	c.o.v.(i_{corr})
One rebar	7% (between 3% and 10%)	Not enough measurements
1 m² area	9–16%	15% (on 5 measurements in May) to 22% (on 4 measurements in July)
Pier 13	20–30%	36% (11 measurements)

instance), that of the whole series of measurements on a given Pier (Pier 13 for instance), all re-bars being combined in the same population. Table 4 summarizes the measurement results. Variations in the corrosion current density can be expected as a result of the measured variability on cover depth (independently from any variability in the environmental conditions and noise measurement).

If we consider d = 3 cm as a central reference value, it appears that the measured variability (c.o.v. = 36% at the scale of the pier) can logically be expected as a consequence of the simple variability of cover depth at the same scale.

3.3.3. *Generalizing the Approach to Improve the Material Condition Assessment*

The correction factor expression Eq. (5) has been fitted from the laboratory experiments and it remains empirical. One has all reasons to think that it would have been slightly different with another concrete mix. However, the expression can be assumed to be, more generally:

$$k = e^{a\,(RH - RHref)}\, e^{-b(\,1/T - 1/Tref)}\, e^{-c\,(d - dref)} \qquad (6)$$

a, b and c being positive constants which would have to be fitted in any particular case (given structure, given concrete, given history...). The strategy to fit their value is however simple. It would suffice, on the studied structure, to monitor the current of corrosion under varying ambient conditions (24 h would suffice to have varying T, and perhaps few weeks to cover a wide range of variations for RH). Thus a and b can be derived from the regression between i_{corr}, RH and 1/T.

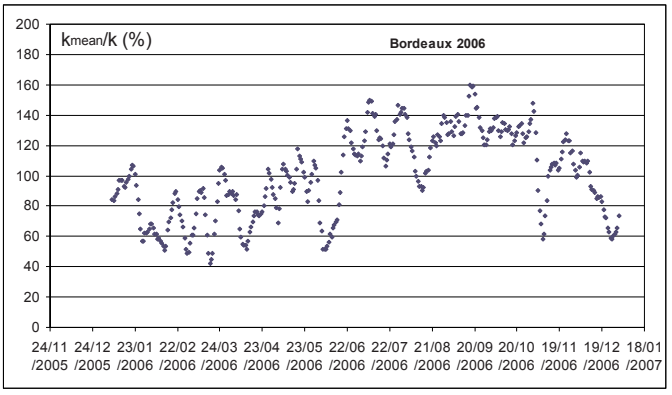

Figure 9. Ratio between k_{mean} (yearly average of k) and k (averaged on 1 week)

We can also apply the empirical model of Eq. (5) to the question of the representativity of a punctual measurement of corrosion rate. For this, we have used meteorological chronicles recorded in the city of Bordeaux, France, which is located 40 km from the Atlantic Ocean, in Atlantic climate. For the year 2006, we have considered average daily temperature and air moisture and computed the value of k coefficient according to Eq. (5) (one must keep in mind that k is the value by which one must multiply what is measured to obtain "what would have been obtained with" reference condition measurements).

The k value varies in a large range, from less than 1 during summer (the meteorological conditions approaching the reference ones) to more than 4 or 5 on some dry and cold days of winter and spring. The average value over the whole 2006 year equals $k_{mean} = 1.72$. If one considers that, for active corrosion, i_{corr} is directly proportional to the steel loss, this value is representative of the corrosion intensity over the year. Thus any isolated measurement of i_{corr}, during a "random" day, only provides a random estimation of this corrosion intensity, which is an overestimation if the measurement is performed during summer (corrosion is, in our case, more active than average between mid-June and end of October) while it is an underestimation if it is provided at other periods. Figure 9 highlights this point by quantifying the k_{mean}/k ratio, which can be put in parallel with the relative corrosion activity along time. It is wholly compatible with what was illustrated on Figure 4 from on-site monitoring of structures.

Thus this kind of model opens interesting tracks towards a more reliable assessment of corrosion, enabling to replace the results of punctual measurements in a wider panorama, being assumed that meteorological information (at the time of the measurements as well as for the usual service condition) are known.

4. Variability and Reliability of NDT: Point of View from the Lab

4.1. AN AMBITIOUS APPROACH FOR UNCERTAINTY MODELLING IN NDT: THE SENSO PROGRAM

An effective optimal combination of techniques for a better assessment of material properties requires one knows:

- The existing relations (whatever linear or not) between what we will name "observables" (T parameters in Section 2, that can be directly measured, like R and V in the SonReb method) and what we will call "indicators" (X and Y parameters in Section 2, that we want to assess, like strength and modulus in the SonReb method)
- The magnitude of uncertainties linked to each assessed value of observable quantities

SENSO, is the name of a specific research program which has been designed under the auspices of French National Agency of Research (ANR) such as to quantify both these relations and these uncertainties for a large series of NDT observable quantities and concrete material properties (indicators), namely: strength, modulus, porosity, water content, carbonation depth, chloride content, magnitude of micro-cracking. The full program will not be described here, but only the methodology used for gathering useful data, building the relevant relations and performing first improved assessments.

The first part of the programme consists in analyzing the effects of water content and porosity variations on the NDT observables for several concrete mixes, on laboratory specimens. Specimens are concrete slabs taken from nine mixes in which are varied w/c (from 0.30 to 0.90), kind, size and shape of aggregates. Eight slabs have been cast for each mix and all NDT measurements are performed on all slabs. The first series of measurements is focused on porosity and water content influence, thus the saturation of slabs is controlled, and varied from a "saturated" reference state to a "dry" one. Many NDT techniques have been used by five research teams and consist in radar measurements, acoustical measurements, electrical measurements, infrared thermography measurements and capacimetry measurements. Each technique can provide a series of observable quantities (f.i., for radar, velocity, magnitude or attenuation at several frequencies, shape of the signal...), thus about 60 observable quantities have been defined and estimated on each specimen.

Knowing the various sources of variability, the measurement process is defined such as to quantify, for each observable, several variance estimators (Fig. 10).

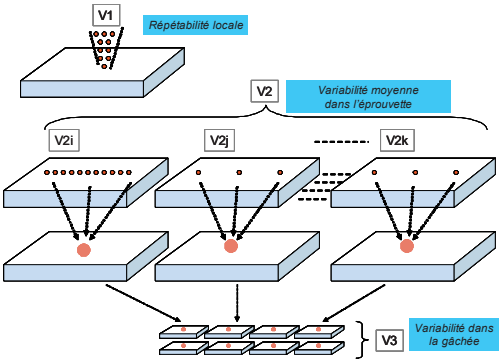

Figure 10. Meaning of V1, V2 and V3 variances

V1 comes from the lack of local repeatability of any measurement, at a given point, when the measurement is done several times. It is estimated after ten repetitions. **V2** comes from the internal slab variability (due to the concrete fabric, to boundary effects, to the non-homogeneity in water content...). It is

estimated by moving the sensors within each specimen and evaluated after ten points of measurements. **V3** comes from the mix variability. It is evaluated by comparing the average measurements obtained on the eight specimens of each mix. **V3a** comes from the mix lack of repeatability. It is evaluated by comparing the measurements on specimens originating from a twinned reference mix, with w/c = 0.45. **V4** corresponds the to the overall contrast between all mixes and specimens. It is evaluated by comparing the average values for each mix.

4.2. BUILDING AND QUALIFYING RELEVANT OBSERVABLE QUANTITIES AND MODELS

When one aims at material condition assessment, the relevancy of a given ND technique depends on:

- The accuracy of the technique: thus V1 has to be as low as possible.
- The exactness of the technique: thus values obtained of similar specimens have to be the same, thus V3a has to be as low as possible.
- The sensitivity of the technique to what is looked for, thus the contrast V4 has to be as large as possible.

Based on these findings, a first step has consisted, for each observable, in quantifying of variances and in building synthetic indexes, which have been named:

- The “quality index”, which is larger when V1, V2 are small with regard with V3.
- The “relevancy index”, which is larger when the technique is more sensitive to the material property.

Thus, the “quality index” mostly qualifies the techniques when the “relevancy index” qualified its ability to find the results that are expected. All measurements are processed, and these two indexes are quantified for all observable quantities, enabling to sort out what are the most efficient for a given purpose (at this stage, for assessing water content and porosity, which are both known to be very influent on strength and modulus).

Before using and combining two (or several techniques), a further step must be done, that of analyzing and quantifying the relations between indicators and observable quantities. At this stage, linear regressions can be tested for all relations (or non linear ones if they seem more adapted from literature survey, as it is the case for instance for resistance measurements which are know to depend on porosity and water content following a power law). Figure 11a and b illustrates what is obtained for the relation between ultrasonic wave velocity (observable) and porosity (indicator). The Fig. 11a plots only average values for

all mixes while Fig. 11b plots all individual values on specimens. The linear regressions give:

$$V\ (m/s) = 5332 - 65.4\ p\ (\%) \qquad r^2 = 0.72$$
$$V\ (m/s) = 5272 - 61.0\ p\ (\%) \qquad r^2 = 0.64$$

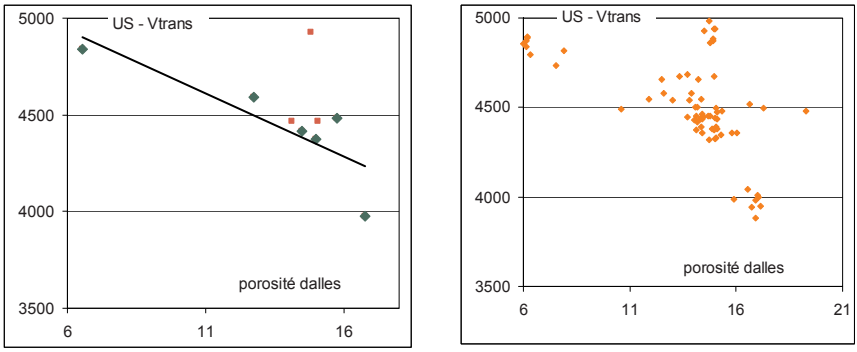

Figure 11a, b. Correlations between ultrasonic wave velocity and concrete porosity

The difference between the two graphs clearly shows the influence of V3 variability, whose result a small « cloud » of points around the average point for each mix. It has the consequence of decreasing the quality of the regression equation, thus the quality of the assessment if one wants to predict the porosity from the velocity measurement.

An additional interesting remark can be done, since on the first graph, the green points correspond to mixes in which only w/c has been varied, when the three small red points correspond to additional mixes, for which the aggregate has been changed (either in size, or in shape, or in nature). It can be seen that a point widely departs from the general relation. It corresponds to a mix in which siliceous aggregates have been used instead of limestone, like in all other mixes. It can be clearly seen that the regression equation cannot predict accurately the properties in this situation, since the velocity is 500 m/s larger than for the basic mixes. This points fundamental limits on all strategy aiming at using NDT for material quantitative assessment if the relations between indicators and observable quantities have not been identified and validated on similar materials. A last step is the selection of series of observable quantities whose combination will be helpful regarding a given purpose. This point will be addressed below.

5. Combination of Techniques for an Improved Reliability of Assessment: Strength Assessment Case Study

5.1. WHY COMBINATION OF TECHNIQUES HAS SOME LIMITS? STRENGTH ASSESSMENT WITH THE SONREB EXAMPLE

5.1.1. *Framework of Simulations*

We will here privilege a synthetic approach, using random simulations, to better understand on what basis lays the use of combination of techniques. The demonstration is based on the use of simulations in which we will simulate physical material properties and non-destructive properties of specimens. These measurements will allow building statistical laws that will be used in a second step to assess the material properties. The principles of the simulations are the following ones:

(a) The material is physically described through two properties: porosity p and saturation rate, which are varying at each point in the structure, with the following assumptions:
   – Porosity assumed to be Gaussian (p_m, s(p)), where s(p) is the standard.
   – Saturation assumed to be uniformly distributed (S_{rm} +/– ΔS_{rm}).

(b) The NDT measurement provide two physical properties: ultrasonic wave propagation velocity V and rebound hammer measurement R, whose "true" value is supposed to be a deterministic function of the [p, S] set. However, since the measurement are not perfect, the measured value of the non destructive parameter is not the real value, the magnitude of the difference depending on the quality of the technique, which is taken as a parameter. The measured values (V_{meas} and R_{meas}) are computed by multiplying the true values by a factor (1 + ε()) where the error ε() is a Gaussian variable (mean zero, standard deviation s(ε()) given, depending on the quality of the technique).

(c) The mechanical properties (E, f_c) can also be assessed from laboratory tests, thus the true values differ from the assessed ones. Their measured values (E_{meas} and $f_{c\ meas}$) are computed by multiplying the true values by a factor (1 + ε()) where the error ε is a Gaussian variable (mean zero, standard deviation s(ε()) given, depending on the quality of the test measurement).

(d) Empirical correlations can be drawn from the measured values of V and R on one hand and those of E and f_c the other hand. It will be focused in the following on the strength parameter, but the same logic prevails for E.

To summarize, the input data for simulations are:

- The range of variation porosity and saturation rate, which corresponds in the reality to material variability
- The level of quality of NDT measurement, given by the error values ε(R) and ε(V)
- The level of quality of mechanical measurement, given by the error values ε(E) and εf_c
- The model functions between material properties and NDT properties:

$$(R, V) = f_{th}(p, S) \tag{7}$$

- The model functions between material and mechanical properties:

$$(E, f_c) = g_{th}(p, S) \tag{8}$$

The real relations between mechanical properties and NDT properties thus writes:

$$(E, f_c) = h_{th}(R, V) = h_{th} = g_{th} \times f_{th}^{-1}(R, V) \tag{9}$$

but it cannot be known because of several reasons:

- The measured values differ from true ones, due to various error measurements.
- The exact functions and ar unknown and can only be approached via empirical correlations on measurement results.

5.1.2. *Simulation of the SonReb Method and Influent Factors*

Monte-Carlo simulations are performed, aiming at modulus and strength assessment. The general idea is to randomly generate a set of varying material properties (p, S). Each (p, S) set induces both mechanical properties (through Eq. 8) and NDT properties (through Eq. 7). These properties are estimated with NDT tests (with some errors ε(V) and ε(R)) and with mechanical tests (with some errors ε(E) and $\varepsilon(f_c)$). For each simulation, one obtains then a set of measured values (p_{meas}, S_{meas}, E_{meas}, $f_{c\,meas}$).

Considering the series of Monte-Carlo simulations, one obtains a series of such sets from which empirical correlations can be identified, for instance using linear regressions.

In practice, this strategy is independent of models used for Eqs. (7) and (8). However these "physical" models have been chosen such as to fulfill some requirements: physical consistency, agreement with what is observed in reality in terms of sensitivity and range of variation of the properties. To do that, experimental information given in (Soshiroda et al., 2006) and obtained by some of the authors in the extensive ANR-SENSO experimental program have been used. The models are given in Table 5. The consistency of the whole set of

simulation has been checked by analyzing the range of variations of true properties and that of measured properties, as well as on the empirical correlations that can be drawn from them. We will study below how the strength assessment depends on the quality (or lack of quality) of the NDT measurement. The quality of all measurements is quantified by the magnitude of the measurement error which is varied from 10^{-3} to 0.20, which covers a wide range of usual techniques. Some results of the SENSO program have been used there.

TABLE 5. Models used for simulations

UPV (m/s)	$V = V_o (1 - \alpha_1 p) (1 - \alpha_2/3\ S + \alpha_2 S^2)$	V_o = 5,600 m/s, $\alpha_1 = 0.1$, $\alpha_2 = 0.05$
Rebound hammer measurement R	$R = 10 + R_o (1 - \alpha_3 p)^3 (1 - \alpha_4 S)$	$R_o = 60$, $\alpha_3 = 1.5$, $\alpha_4 = 0.1$
Young's modulus E (GPa)	$E = E_o (1 - p)^3 (1 - p S)$	E_o = 55 GPa
Compressive strength f_c	$f_c = f_{co} (1 - p)^7 (1 - \alpha_5 S)$	f_{co} =140 MPa $\alpha_5 = 0.5$

5.1.2. *Illustration of Effects of Noise on Correlations Between Measurements*

In these simulations, the average material properties are assumed to be p = 13% and S = 80% with a standard deviation of 2% for porosity and a range of +/− 5% for saturation rate. The relation between NDT properties and mechanical properties can be approached with linear regressions, as shown on Fig. 12a and b. These figures show that, even if the real relations are not linear (because of models used in Eqs. 7–8), the quality of fit for true values is good in the experimental range of variation of the parameters. It also shows that the quality of fit is lower for measured values, because of measurement errors. These graphs have been obtained with: $s(\varepsilon(R)) = 5\%$, $s(\varepsilon(V_p)) = 0.5\%$, $s(\varepsilon(f_c)) = 5\%$).

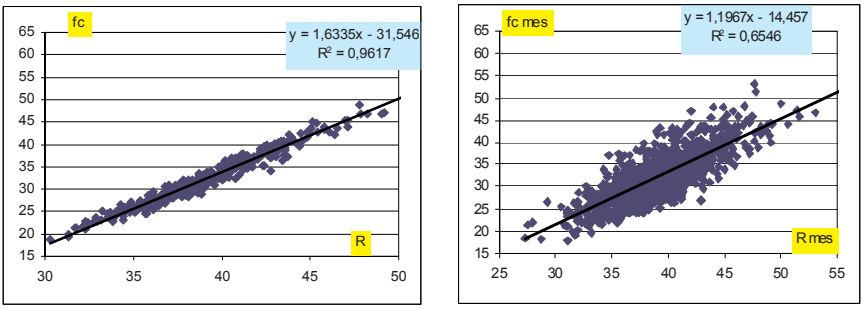

Figure 12a, b. Correlations between Rebound and strength: true values (*left*) and measured values (*right*)

The quality of fit regularly decreases when the quality of the sources of information decreases. It can be either because of one of the NDT quality or

because of the destructive test quality. The direct consequence is that the "cloud" is larger and that the regression which will be used for calibration will be less reliable.

5.1.3. *Simulation of the SonReb Method: Calibration and Strength Assessment*

The regressions obtained between R and f_c (see Fig. 12a and b) or between V and f_c can be used to assess the in-situ strength. The idea is on a first step (calibration stage) to identify these correlations, obtained via sampling on some cores (thus one has both measured values or R (or V) and f_c) and, on a second step, to assess from the NDT measurement only. The best is to perform the calibration on the structure under study, but calibration curves can be used if this is not possible. Here, the calibration stage is simulated.

5.1.4. *Calibration Stage*

From the set of measurements, one can write:

$$f_c = f_{c\,ref} + k_V (V - V_{ref}) + k_R (R - R_{ref}) \tag{10}$$

where the *ref* index refers to "reference", for instance an average value on the specimen population. The k_V and k_R coefficients respectively quantify the sensitivity of strength to any change in V or R. The quality of these equations depends on the quality of the destructive tests themselves, since the measured value of f_c is also noisy.

5.1.5. *Assessment Stage*

Thus, assuming that, the measured values on the specimen are V_p and R, the reference values are known to be respectively $f_{c\,ref}$, V_{ref} and R_{ref}, one can deduce estimation for f_c which accounts for corrections after non-destructive measurements:

$$f_{c\,est} = f_{c\,meas} + k_V (V - V_{ref}) + k_R (R - R_{ref}) \tag{11}$$

By simulations, it is possible to study how these corrections (single correction from V or R or combined correction) are able to improve the estimation of real values. The Fig. 16 shows how f_c is related with V_p and R in two cases (good quality of f_c measurement, poor quality of f_c measurement). As see from the shape of clouds, the quality of the regression is better when the f_c measurement is more accurate.

The level of quality of the technique being given, k_V and k_R values are easily identified (for instance $k_R = 1.1685$ in the left side case and $k_R = 1.1993$ in the right side case) and the assessment can be performed as soon as new value of R are provided. These regressions show that a gain of ten points on the

R scale corresponds to a gain of about 11 or 12 MPa in strength. Since our models have been fitted to real experimental data, this is consistent with what is observed in practice.

5.1.6. *Some Results: Efficiency and Limits of Combination*

We will compare the quality of the strength assessment in three cases:

– Case (a) – the strength assessment comes from the rebound measurement only:

$$f_{c\,est} = f_{c\,meas} + k_R\,(R - R_{ref}) \qquad (12)$$

– Case (b) – the strength assessment is given by the UPV measurement only:

$$f_{c\,est} = f_{c\,meas} + k_V\,(V - V_{ref}) \qquad (13)$$

– Case (c) – both UPV measurement and rebound measurement contribute to the strength assessment:

$$f_{c\,est} = f_{c\,meas} + k_V\,(V - V_{ref}) + k_R\,(R - R_{ref}) \qquad (14)$$

This last case formally corresponds to the SonReb protocol and SonReb charts. Figure 13 enables to compare the *true* values (truth can be known since it is not real world but a synthetic world!) to the assessed ones in the case (c). Figure 14 synthesizes all results when the quality of the two NDT techniques is simultaneously varied. It plots how the correlation coefficient between true and assessed values of strength varies when the error on R increases (from near 0 – very good to 20% – very bad) for three values of error on V (0.1%, 2%, 4%) that respectively correspond to a very good, average and bad quality of the technique.

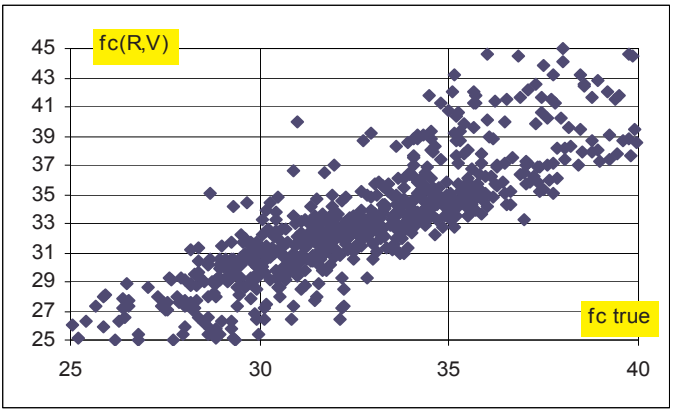

Figure 13. Comparison of true and assessed strength values for case (c) (s(ε(V) = 0.5%, s(ε(R) = 3%, s(f_c(R) = 2%)

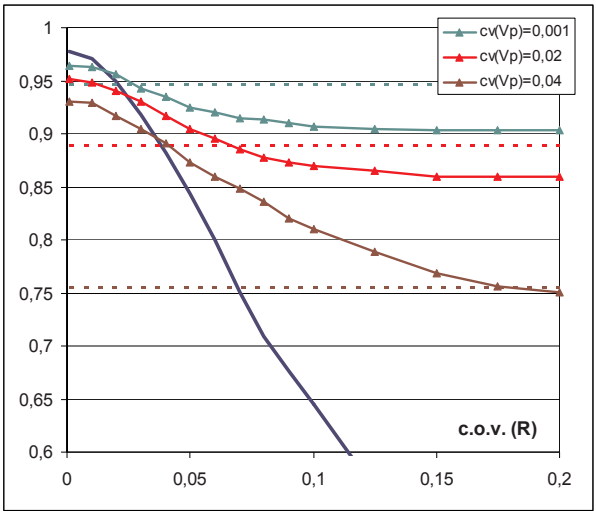

Figure 14. Variation of the quality of strength assessment correlation coefficient between true and assessed values) for varying quality of NDT techniques, with and without combination

Three sets of curves are plotted. The blue bold curve corresponds to the case (a) measurement. It shows that the quality of assessment regularly decreases with the quality of the rebound measurement. The three horizontal lines correspond to case (b) for the three levels of quality of V measurements. They logically show that the quality of strength assessment varies from being good when the error on V is small to being bad when this error is large. The three last curves correspond to the combination (case (c)).

Analyzing these curve is much interesting. If we take for instance the curve corresponding to c.o.v.(V) = 2%, three domains can be seen. On the left part (small c.o.v.(R)) the case (a) gives the best result, since the corresponding curve is the higher. On the right part (high c.o.v.(R)), it is the case (b) which provides the best strength assessment. Between the two (here for 3% < c.o.v.(R) < 6%), the best strength assessment is provided by case (c), i.e. by the combination of techniques. The same can be seen for the other values of c.o.v.(V), even if the boundaries of optimal domains change. SENSO results have shown that we can assume c.o.v.(R) = 3–4% and c.o.v.(V) = 2%, which corresponds to the domain in which the combination really brings something. This confirms the potential interest of this combination.

This conclusion can be generalized, telling that, if any NDT is very accurate, assessing the strength on its simple basis is the best solution, but the combination has an added-value in an intermediate domain, when both techniques are of an average quality. For instance, when c.o.v.(R) = 0.04 and c.o.v.(V) = 0.2, the correlation coefficient jumps from 0.89 (for cases (a) and (b)) to 0.93 (case (c)).

5.2. WHAT CAN BRING THE COMBINATION OF SEVERAL NDT? STIFFNESS ASSESSMENT EXAMPLE

Since UPV measurements are very easy to handle they have been often combined to a secondary technique for material assessment. One interesting idea is to combine them with another technique that is also sensitive to water content. Capacitive measurements (Sirieix et al., 2007), GPR measurements (Saisi et al., 2001; Laurens et al., 2003), IR thermography (Sirieix et al., 2007; Kandemir-Yucel et al., 2007) or electrical resistivity (Sirieix et al., 2007; Breysse et al., 2008b) have been commonly used. However a more formal approach appears to be necessary. This is one of the objective of the SENSO research project on concrete.

The statistical analysis of the measurements when varying the concrete composition and the saturation rate made us capable of selecting the more interesting observable quantities (See Section 4) and of drawing multiple regression laws between properties and NDT measurements. For instance, regarding water content and porosity, the following relations have been derived:

$$Y1 = 1128 + 4.87\ Sr + 26.4\ Esat \quad (15)$$
$$Y2 = 2644 + 8.77\ Sr + 39.1\ Esat \quad (16)$$
$$Y3 = 1.94 - 0.015\ Sr + 0.053\ Esat \quad (17)$$
$$Y4 = 0.541 - 0.0016\ Sr + 0.0014\ Esat \quad (18)$$
$$Y5 = 0.956 + 0.00379\ Sr - 0.0032\ Esat \quad (19)$$

where Sr and Esat are respectively the saturation rate (in %) and the saturated Young's modulus (in GPa) and Y1 to Y5 are NDT observable quantities: Y1 is the group velocity of surface waves (in m/s), Y2 is the UPV of compression waves (in m/s), Y3 is the log of electrical resistance (in Ω.m), Y4 is the magnitude of a radar signal and Y5 is the time of arrival (in ms) of a radar signal;

We have also identified the degree of variability of each measurement, due to the intrinsic material heterogeneity and to the non-perfect repeatability of the measurement (corresponding to the **V3** variance). It can be expressed in terms of signal variance or standard deviation. For instance, for the same five observables, the standard deviations are respectively: sd (Y1) = 41.2; sd (Y2) = 11.5; sd (Y3) = 0.11; sd (Y4) = 0.025; sd (Y5) = 0.020

The smaller is the standard deviation, the more accurate the estimation of {Sr, Esat} will be when using the (15–19) equations for inversion.

Figures 15a and b plot in the Sr-Esat plane the regression line corresponding to the measured value with the five observable quantities Y1-Y5 for two specimens (two slabs) made of the same concrete and kept in the same conditions. If both the measurements and the (statistical regression) models were perfect, all lines would cross in a unique point. If the material was homogeneous, the two graphs

would be identical. Any difference is thus due to one these three explanations: measurements are not perfect, the linear regression model is an approximation, the material is not homogeneous.

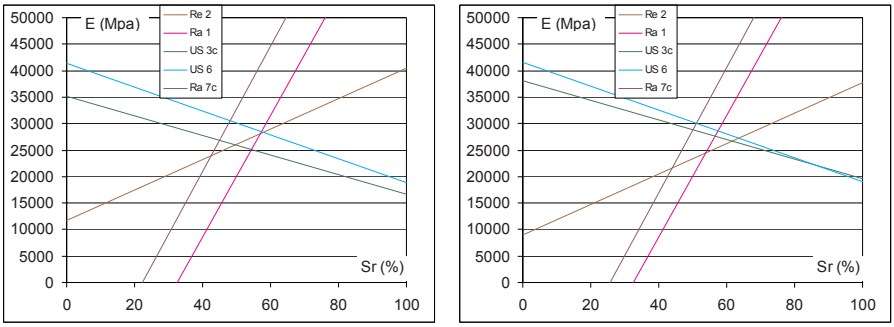

Figures 15 a, b. Use of linear regression model to identify the {Sr, Esat} values for two concrete specimens on two specimens of the same mix

The complementarities of the techniques involved here can be clearly seen through the fact that lines do not follow the same directions. If the two sonic techniques (Y1/US3c and Y2/US6) give parallel lines, the two radar measurements (Y4/Ra1 and Y5/Ra7c) gives two parallel lines very different and the last technique, electric resistance (Y3/Re2) has a very different slope. The more slopes are different, the better the techniques will bring added-value to each other. The diagram plots the results corresponding to five observable quantities (which have been selected from a larger set, since a lot of info has been obtained during the SENSO experimental program), but the method works as soon as two observable quantities are available. Nevertheless, the diagnostic is not perfect, since all lines do not cross in a unique point. To give some basis for comparison, the measured value of Sr, estimated by weighing the slabs is between 47% and 54% and the Young's modulus, measured on cylinders is about 27 GPa. The Sr value seems to be slightly overestimated, but the stiffness is accurately estimated. In addition, the knowledge of the standard deviation for each measurement provides an information about the level of accuracy of the estimate (a slightly different value of the measurement would correspond to a slight displacement of the line in the Esat-Sr diagram). For instance, if one considers the resistance measurement Y3, with sd(Y3) = 0.11, this leads to an uncertainty of about +/− 0.11/0.015 = +/− 6% on Sr and of about +/− 0.11/0.053 = +/− 2 GPa on Esat.

6. Conclusions

We have tried in this paper to review some challenges and some recent research results showing that the high potential of NDT for assessing material condition, including engineering parameters. This discussion was based on a combination of:

- Real on-site measurements, with many sources of noise, due to environmental conditions and the complex history of structure
- Laboratory measurements in which these parameters are controlled
- Synthetic simulations, to better understand what happens and the weight of each factor

We have shown that the important influence of environmental factors (like temperature and humidity) has to be controlled and can even be eliminated, such as to analyze the measurements as if they would have been obtained in "reference conditions".

The high influence of material variability (including cover depth) on the measurements has been confirmed, preventing any reliable statement if one is not able of making the part between the noise of the technique and this material variability. We have shown that it is possible to quantify its influence on measurements, thus to eliminate it if it is measured by a secondary technique.

We have also given the first results of a very ambitious program tending to give a more comprehensive view on the key question of combination of techniques while using NDT. The selection of the more appropriate techniques is possible, on the basis of their intrinsic quality, of their sensitivity to what is looked for and of their complementarities. It has also been shown that in some cases, the use of a second technique brings no additional information and if thus counterproductive.

Of course, all these open tracks remain to be deepened, with the aim of providing experts a more formal methodology for structural condition investigation. The time when it will be able to feed computational models of reliable data on existing structures has not yet come, but it surely will do.

Acknowledgements: It would have been impossible to write this synthetic paper without the contribution of many colleagues who have collaborated, from an experimental or theoretical point of view. I must thank contributors to the European Interreg IIIb-Atlantic space program, Medachs Project 197, driven by Sylvie Yotte; all contributors to the SENSO project and specially Odile Abraham, Jean-Paul Balayssac, Vincent Garnier, Jean-François Lataste, Stéphane Laurens and Marie-Aude Ploix. My acknowledgements also concern Mathilde Larget and Z. Mehdi Sbartai for their fruitful work in data processing, Myriam Chaplain for providing meteorological data used on Fig. 9, and members of

RILEM TC INR 207, and especially Marios Soutsos and Andrezj Moczko. French Agency of Research (ANR) has to thank for funding the SENSO Program and EC for supporting the Medachs Project.

References

Andrade C., Alonso C., 1996, Corrosion rate monitoring in the laboratory and on-site, Constr. Build. Mater., 10(5), 315–328.

ASTM C876-91 Standard test method for half-cell potentials of uncoated reinforcing steel in concrete.

Balayssac J.P., 2005, Evaluation de la dégradation du béton d'enrobage et aide au diagnostic et à la réparation des ouvrages, Projet RGC&U, Contract 01V0550, Final report, 2/2005.

Breysse D., Abraham O., 2005, Guide méthodologique de l'évaluation non destructive des ouvrages en béton armé, Presses ENPC, Paris, 550 p.

Breysse D., Yotte S., Salta M., Pereira E., Ricardo J., Povoa A., 2007, Influence of spatial and temporal variability of the material properties on the assessment of a RC corroded bridge in marine environment, 7th ICASP Conference, 31 July to 1 Aug. 2007, Tokyo.

Breysse D., Klysz G., Dérobert X., Sirieix C., Lataste J.F., 2008a, How to combine several Non-Destructive Techniques for a better assessment of concrete structure?, Cem. Concrete Res., 38, 783–793.

Breysse D., Soutsos M., Lataste J.F., 2008b, Assessing stiffness and strength in reinforced concrete structures: added-value of combination of nondestructive techniques, 1st Medachs Conference, Lisbon, 28–30 Jan. 2008.

Bungey J.H., Millard S.G., 1996, Testing of concrete in structures, 3rd edition, Blackie Acd and Prof., 286 p.

Burgan Isgor O., Ghani Razaqpur A., 2006, Modelling steel corrosion in concrete structures, Mat. Str., 39, 291–302.

De Lorenzis L., Nanni A., 2004, International workshop on preservation of historical structures with FRP composites, Final Report, NSF, July 2004.

Dérobert X., Garnier V., François D., Lataste J.F., Laurens S., 2005, Complémentarité des méthodes d'END, in Guide méthodologique de l'évaluation non destructive des ouvrages en béton armé, ed. BREYSSE D., ABRAHAM O., Presses ENPC, Paris, 550 p.

Duracrete, 2000, Statistic quantification of the variables in the Limit State Function, Brite EURAM Project, 111.

Ezzdine R., Ibanez J., Yotte S., Breysse D., 2008, Analysis of salt crystallisation test applied on Galdacano sanstone and Blaye limestone, 1st Medachs Conference, Lisbon, 28–30 Jan. 2008.

Gehlen C., Dauberschmidt C., Nürnberger U., 2006, Condition control of existing structures by performance testing, Otto-Graf-J., 17, 19–44.

Gonzalez J.A., Feliu S., Rodriguez P., Ramirez E., Alonso C., Andrade C., 1996, Some questions on the corrosion of steel in concrete – Part I: When, how and how much steel corrodes, Mat. Str., 26, 40–46.

Homand F., Duffaut P., 2000, Manuel de Mécanique des Roches, Comité français de Mécanique des roches.

IAEA, 2002, Guidebook on non destructive testing of concrete structures, Training course series 17, International Atomic Energy Agency.

Jäggi S., Böhni H., Elsener B., 2001, Macrocell corrosion of steel in concrete – experiments and numerical modeling, Eurocorr 2001, 1–4 Oct. 2001, Riva di Garda, Italy.

Kandemir-Yucel A., Tavukcuoglu A., Caner-Saltik E.N., 2007, In situ assessment of structural timber elements of a historic building by infrared thermography and ultrasonic velocity, Infrared Phys. Technol., 49, 243–248.

Khan S.RM., Noorzaei J., Kadir M.R.A., Waleeed A.M.T., Jaafar M.S., 2004, Effectiveness of sclerometer test technique on strength assessment of high performance concrete, Int. J. Engn. Tech., 1, 2, pp. 163–168.

Klinghöfer O., Frolund T., Poulsen E., 2000, Rebar corrosion rate measurements fir service life estimates, ACI Fall Convention 2000, Committee 365 "Practical application of service life models", Toronto, Canada.

Laurens S., Balayssac J.P., Rhazi J., Klysz G., Arliguie G., 2003, Non destructive evaluation of concrete moisture by GPR technique: experimental study and direct modeling, NDT-CE'03, 16–19 Sept. 2003.

Li Y., 2004, Effect of spatial variability on maintenance and repair decisions for concrete structures, Master Sc., Tsinghua Univ., Hunan, China.

Malhotra V.M., 1981, Rebound, penetration resistance and pulse velocity tests for testing in place, The Aberdeen Group.

NEA, 2002, Electrochemical techniques to detect corrosion in concrete structures in nuclear installations, Nuclear Energy Agency, OCDE Technical note 21, 19 July 2002.

NF EN 13791, 2007, Evaluation de la résistance en compression sur site des structures et des éléments préfabriqués en béton.

OECD Nuclear Energy Agency, 1998, Development priorities for Non-Destructive examination of concrete structures in nuclear plant, Nuclear Safety, NEA/CSNI/ R(98), 25–39.

Pascale G., Di Leo A., Carli R., 2000, Evaluation of actual compressive strength of high strength concrete by NDT, 15th WCNDT, Roma.

Popovics S., 2001, Analysis of the concrete strength versus ultrasonic pulse velocity, http://www.asnt.org/publications/materialseval/basics/feb01basics/feb01basics.htm

Saisi A., Valle S., Zanzi L., Binda L., 2001, Radar and sonic as complementary and/or alternative tests in the survey of structures, Arch 2000, UNESCO Icomos Conf. 10–12 Sept. 2001.

Samarin, A., 1991, Combining method, in CRC Handbook on Nondestructive Testing of Concrete, CRC Press, Malhotra, V.M., Carino, N.J., pp. 189–201.

Samco, 2006, Work Package 9: Practical bridge management – Interface with current practice, SAMCO Project final report on Bridge Management, March 2006.

Sirieix C., Lataste J.F., Breysse D., Naar S., Dérobert X., 2007, Comparison of nondestructive testing: Infrared thermography, electrical resistivity and capacity methods for assessing a reinforced concrete structure, J. Building Appraisal 3(1), 77–88.

Soshiroda T., Voraputhaporn K., Nozaki Y., 2006, Early-stage inspection of concrete quality in structures by combined nondestructive method, Mat. Str., 39, pp. 149–160.

Stewart M.G., 2001, Risk based approaches to the assessment of ageing bridges, Reliability Eng. Syst. safety, 74(3), 263–273.

Stewart M.G., 2005, Life-cycle cost analysis considering spatial and temporal variability of corrosion-induced damage and repair to concrete surface, ICOSSAR 2005, 1663–1670, Millpress, Rotterdam.

Uemoto T., 2000, Maintenance of concrete structure and application of non-destructive inspection in Japan, Proceedings of the Non Destructive testing in Civil Eng., Elsevier, pp. 1–11.

Villain G., et al., 2008, Effet de la teneur en eau sur la mesure du module élastique dynamique de dalles de béton par ondes ultrasonores, LCPC, Journées Ouvrages d'Art, Bordeaux, juin 2008.

IMPROVING SAFETY AND DURABILITY OF CIVIL STRUCTURES

E. BRÜHWILER*
Ecole Polytechnique Fédérale (EPFL), ENAC-MCS, Institute of Structural Engineering – Maintenance and safety of structures, Station 18, CH-1015 Lausanne, Switzerland

Abstract. Society expects that failure of civil structures is extremely rare and relies on the care and expertise of the professionals involved in the design, construction and maintenance of structures. Analysis shows that human errors are a major source of structural failures. Relevant measures to improve the safety of civil structures include combating human error, applying hazard recognition methods, establishing organisational documents and performing adequate monitoring and maintenance of structures. Nowadays dealing with existing structures is a major engineering task. Safety evaluation of existing structures follows a stepwise procedure with an increasing degree of refinement of investigations. Target safety levels may be defined as a function of the hazard scenario and the characteristics of the structure under consideration. To improve durability of structures an original concept is to use Ultra-High Performance Fibre Reinforced Concrete (UHPFRC) to "harden" those zones of the structure that are exposed to severe environment and high mechanical loading. This conceptual idea combines efficiently protection and resistance properties of UHPFRC and significantly improves the structural performance. The concept is validated by means of a numerical simulation and applications.

Keywords: Structural safety, hazard scenarios, lessons from structural failures, human factors, safety evaluation of existing structures, target safety levels, ultra-high performance fibre reinforced concrete, durability, composite concrete construction, rehabilitation of concrete structures, bridge design, FE-analysis

* To whom correspondence should be addressed. e-mail: eugen.bruehwiler@epfl.ch

A. Ibrahimbegovic and M. Zlatar (eds.), *Damage Assessment and Reconstruction After War or Natural Disaster*,

1. Introduction

1.1. SAFETY OF CIVIL STRUCTURES

Society expects that the failure of civil structures is extremely rare and relies on the care and expertise of the professionals involved in the design, construction and maintenance of structures. This is in particular true for public technical systems such as transportation or energy supply systems and structures such as bridges.

Structural safety may be defined as follows: "*Adequate safety with respect to a hazard is ensured provided that the hazard is kept under control by appropriate measures or the risk is limited to an acceptable value. Absolute safety is not achievable.*" It is thus not the structure as such that is designated safe but rather the people, goods and the environment in its surroundings.

The continued use of existing structures is of great importance because the built environment is a huge economic and political asset, growing larger every year. Nowadays evaluation of the safety of existing structures is a major engineering task, and structural engineers are increasingly called upon to devise ways for extending the life of structures whilst observing tight cost constraints. Also, existing structures are expected to resist against accidental actions although they were not designed for.

Engineers may apply specific methods for evaluation in order to preserve structures and to reduce a client's expenditure. The ultimate goal is to limit construction intervention to a minimum, a goal that is clearly in agreement with the principles of sustainable development.

In Chapter 2, lessons from structural failures are presented first and measures to improve safety in the design, construction and maintenance of structures are deduced. Principles for the safety evaluation of existing structures and a procedure to determine target safety levels are outlined.

1.2. DURABIITY OF CIVIL STRUCTURES

Concrete structures show excellent performance in terms of structural behaviour and durability except for those zones that are exposed to severe environmental and mechanical loading. Rehabilitation of deteriorated concrete structures is a heavy burden also from the socio-economic viewpoint since it also leads to significant user costs. As a consequence, novel concepts for the rehabilitation of concrete structures must be developed. Sustainable concrete structures of the

future will be those requiring just minimum interventions of only preventative maintenance with no or only little service disruptions.

Over the last 10 years, considerable efforts to improve the behaviour of cementitious materials by incorporating fibres have led to the emergence of Ultra-High Performance Fibre Reinforced Concretes (UHPFRC). These novel building materials provide the structural engineer with an unique combination of (1) extremely low permeability which largely prevents the ingress of detrimental substances such as water and chlorides and (2) very high strength, i.e., compressive strength higher than 150 MPa, tensile strength higher than 10 MPa and with considerable tensile strain hardening (up to more than 1‰ of strain) and softening behaviour (with fracture energy of more than 15,000 J/m^2). In addition, UHPFRC have excellent rheological properties in the fresh state allowing for easy casting of the self-compacting fresh material with conventional concreting equipment. Consequently, UHPFRC clearly have an improved resistance against severe environmental and mechanical loading thus providing significantly improved structural resistance and durability to concrete structures.

Chapter 3 presents an original concept of using UHPFRC for the improvement of concrete structures.

2. Lessons from Structural Failures

2.1. BRIDGE FAILURES IN SWITZERLAND

In Switzerland with a stock of about 25,000 bridges, no bridge collapse occurred during service since the failure of the steel railway bridge in Mönchenstein in 1891 that caused 73 deaths (Fig. 1a). As a consequence of this tragic accident, codes were introduced and systematic monitoring and maintenance of bridges has been performed since then in Switzerland. In several cases, partial structural failure could be prevented due to monitoring and subsequent immediate intervention.

In 1987, scour of a bridge pier on the Gotthard highway at Wassen led to significant economic loss for Switzerland and Europe because of the temporary closure of this important highway crossing the Alps (Fig. 1b). Fortunately there were no human casualties.

Two bridge failures occurred during construction in 1973 when the concrete deck slab of the composite bridge at Valangin (Fig. 1c) and the steel work of the composite bridge at Illarsaz were launched.

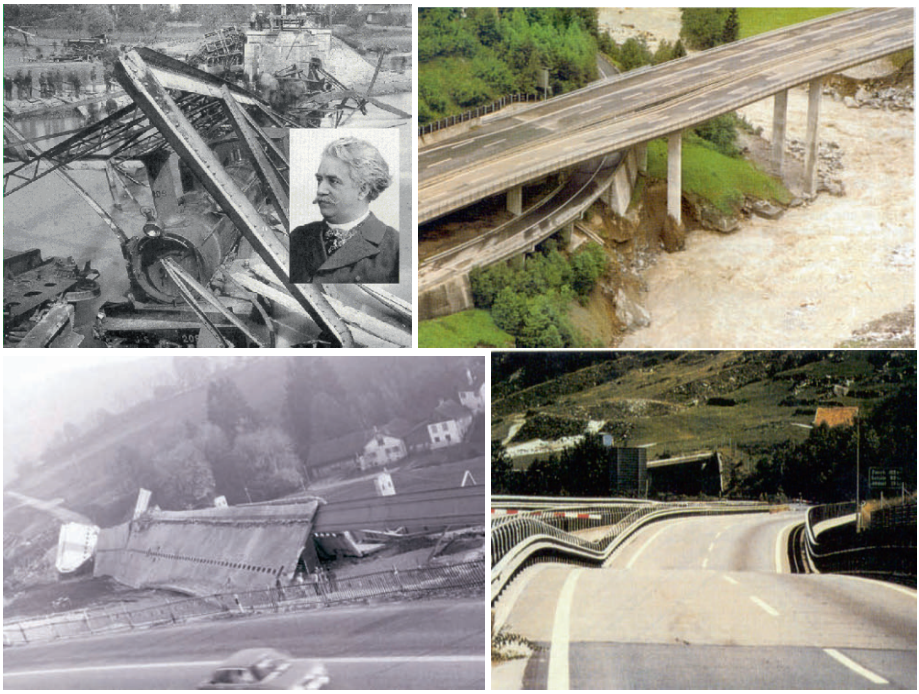

Figure 1. (**a**) Bridge collapse at Mönchenstein in 1891, (**b**) scour at the highway bridge at Wassen in 1987, and (**c**) failure during launching of the deck slab of the composite bridge at Valangin in 1973

2.2. BRIDGE FAILURES WORLDWIDE

A total of 138 cases of bridge failure worldwide have been analysed in Bailey et al. (2001). The following lessons can be learned from this study:

- Most of the bridge failures are due to human error on the part of the structural engineer or an inadequate or unplanned use of the bridge. As a consequence, human behaviour has to be "challenged" in order to reduce structural failures.
- Around 40% of all bridge accidents occurred during construction or during the first two years in service. This shows that more attention should be given to safety aspects relating to the construction phase. Efficient controls (quality assurance) during construction, a conscientious inspection of the structure before opening to service and an intensified monitoring during initial service life may help to prevent and detect defects leading to structural failure.
- Failures due to exceptional natural causes such as earthquake, wind or scour generally occur on bridges for which these hazards have been accepted, not recognised or not correctly considered due to lack of knowledge. Consequently, bridges with conceptual defects should be systematically identified and evaluated in order to improve the safety of a bridge stock.

- Failures due to corrosion or fatigue normally occur at an advanced age of the structure. This points to the significance of adequate monitoring and maintenance of the structure.
- Accepted risks and objectively unknown hazards represent only 8% of all bridge failures.
- No bridge failure could be traced back to items not or insufficiently covered by the codes of practices. This means that the safety level as implicitly applied is – as a rule – sufficiently high.

From these characteristics of bridge failures (not considering gross human errors), it can be deduced that inherently higher structural safety exists for bridges satisfying the following conditions:

- Conceptual design, dimensioning, detailing and construction of the bridge is in accordance with state-of-the-art knowledge and human factors have been considered.
- The bridge has shown a normal behaviour during the first years of service.
- The bridge is subjected to systematic and adequate monitoring and maintenance during its service life.

2.3. MEASURES DEDUCED FROM STRUCTURAL FAILURES

The results of the analysis of structural failures (as shown in Section 2.2 and other similar studies) challenge engineers to learn the lessons and to take the necessary measures. There are four domains where structural engineering has to improve:

2.3.1. *Hazard Recognition Methods*

Safety has a lot to do with the recognition of possible hazards. Once the potential hazards have been recognised, reducing their harmful effects is usually relatively easy. Not having recognised a hazard may lead to one of the worst experiences of an engineer. The objective is thus to recognise all possible hazards because only then a safe solution can be found. This is difficult to achieve.

Hazard recognition requires imagination and creativity from the engineer. There are techniques and methods that are helpful in trying to recognise possible hazards (Schneider, 1997):

- Chronological analysis: Step-by-step the process is considered beforehand (what, where, when will occur).
- Utilisation analysis: It is essential to analyse in advance the way the structure will be used. (what could go wrong? what could break down and become hazardous?)

- Influence analysis: which quantities influence the problem at hand (damaging influences in human activities and shortcomings)? which individually safe components of a situation can in combination become hazardous?
- Energy analysis: what are the energy potentials in the system?
- Material analysis: what properties of building materials can become hazardous (combustibility, explosiveness, toxicity, corrosion)?

Such strategies are used under various names such as Hazard and Operability Study (HAZOP), What-if Analyses or Failure Mode and Effect Analysis (FMEA).

2.3.2. *Organizational Documents*

A principal conclusion from the analysis of accidents is the necessity to establish organisational documents for the design, construction and maintenance of the structure. Preparation and updating of these documents requires a dialogue between all professionals involved in the design, construction and maintenance and in particular with the owner of the structure.

These organizational documents include a "utilization plan" and a "safety plan" ideally to be prepared for all structures in the initial planning phase. From these two basic documents a series of documents are derived which guide the design and construction phase as well as the service phase (utilisation and maintenance), i.e. during the complete life of the structure:

- The *utilization plan* specifies what is wanted. It lists the service states to be considered for the structure and defines the measures to ensure serviceability.
- The *safety plan* is developed on the basis of the utilisation plan and lists the *hazard scenarios* to be considered for the structure and defines the measures to guarantee adequate safety.

Hazard scenarios are critical situations and the conditions which might represent a hazard for a structure. Each hazard scenario is characterised by a predominant action and by one or more accompanying actions. The identification and evaluation of hazard scenarios represent the basis for the planning of measures to be taken to ensure adequate safety.

During the construction phase, co-operation between all those involved in the construction process should be improved and well-planned quality assurance procedures should be adopted.

Monitoring during the service phase of the structure provides the relevant information characterising structural behaviour in order to evaluate structural safety and to enable appropriate maintenance interventions.

Monitoring includes frequent or continuous, normally long-term, observation of structural conditions or actions by means of inspections and measurements. The objective is to detect abnormal structural behaviour or actions as early as

possible; ideally before any damage process is initiated. Measured values may serve as "indicators", "warning signals" or "alerts". Maintenance is routine intervention to preserve adequate structural performance.

A monitoring and maintenance plan should be specified after the construction of a new structure and constantly updated during its service life depending on the utilisation plan and the results of monitoring or evaluation.

2.3.3. *Combating Human Error*

Human errors are clearly the main source of damage and structural failures. They can be combated at several levels (Schneider, 1997):

- *Subjectively unknown hazards* – by improving basic and continuing education and training and by publishing examples of bad experiences
- *Ignored hazards* – by clear allocation of responsibility and competence as well as by rigorously combating all forms of carelessness, negligence and ignorance
- *Unsuitable measures* – by improving expert knowledge, carefulness and overview with all those who plan the measures
- *Improper use of measures* – by requiring clear and unambiguous plans, basic documents and instruction, as well as by creating and maintaining effective control mechanisms
- *Objectively unknown hazards* – by fundamental research and systematic dissemination of experience

2.4. SAFETY EVALUATION OF EXISTING STRUCTURES

2.4.1. *Methodology*

The need to evaluate the safety of an existing structure can usually be related to doubt about the safety. The fundamental question is whether the structure is safe enough. If the answer is no, one of the following interventions has to be performed: demolish the structure and replace it by a safer one, strengthen the structure, ask for reduction of loads or reduce uncertainty by intensifying monitoring. If the answer is yes, then to do nothing and allow the continued operation of the structure may be the most appropriate action. However, intensifying the monitoring of the structure is sometimes beneficial.

Experience shows that a stepwise procedure in the evaluation of a structure is appropriate (ISO International Standard, 2001):

Step 1: *Objectives and hazard scenarios*
First, the objective of the evaluation must be clearly specified in terms of the future use of the structure (remaining service life). Hazard scenarios related to a

change in structural conditions or actions should be specified in the safety plan in order to identify possible critical situations. Furthermore, accepted risks must be identified. As soon as there is some evidence of danger to humans or the environment, protective measures must be taken immediately.

Step 2: *Preliminary evaluation*

The preliminary evaluation consists of a study of documents, an inspection and preliminary structural safety checks to identify the critical deficiencies. The objective of Step 2 is to remove existing doubts using fairly simple methods which must allow proposals to be made for subsequent measures.

Current codes which have proven to provide adequate reliability over a long period of application may be used as a reference but not necessarily as the relevant criterion, and former codes that were valid at the time of construction of an existing structure should be used as informative documents only.

In studying the available documents, a deep insight should be gained into the situation when the structure was designed and built. These are indicators of quality referring to aspects such as design principles and methods, codes, construction methods and materials or working environment. Where there is uncertainty in the actions, action effects or properties of the structure, a detailed evaluation should be performed.

If the doubts that led to the evaluation cannot be overcome in the course of Step 2, further investigational steps must be undertaken in Step 3.

Step 3: *Detailed evaluation*

Detailed structural investigations and updating of information are typical of Step 3. Updating is based on prior information about the structure and on specific additional observations and measurements. In any case, the objective is to verify structural safety.

A detailed inspection of the structure or the structural element in question is extremely important to recognise typical hazard scenarios that could endanger the structure's remaining service life. Furthermore, any defects and damage due to excessive or unplanned loading must be detected.

By means of detailed structural analysis, reserves of strength in structural components may be identified and exploited using ultimate limit state concepts. Deterioration must be analysed as a time-dependent structural reliability problem.

The safety check of an existing structure should be carried out to ensure a target reliability level that reflects the required level of structural performance. The target reliability level may be determined taking into account the required performance level for the structure, the reference period and possible failure consequences.

The conclusion from the assessment shall withstand a plausibility check. In particular, discrepancies between the results of structural analysis (e.g. insufficient

safety) and the real structural condition (e.g. no sign of distress or failure, satisfactory structural performance) must be explained.

2.5. TARGET SAFETY LEVELS FOR EXISTING STRUCTURES

2.5.1. *General Remarks and Concept*

Compared to the design of new bridges, there are two main reasons for treating safety of existing structures differently. Firstly, there are fewer hazards and less uncertainty once a structure has successfully entered service and performed satisfactorily. For example, 40% of bridge accidents occur during construction (see Section 2.2), and there is no need to cover this hazard when evaluating an existing bridge. Secondly, it costs more to increase the safety of an existing structure. As a consequence, target reliability levels for existing structures may be used and justified on the basis of socio-economic criteria, thus following a risk-based safety approach.

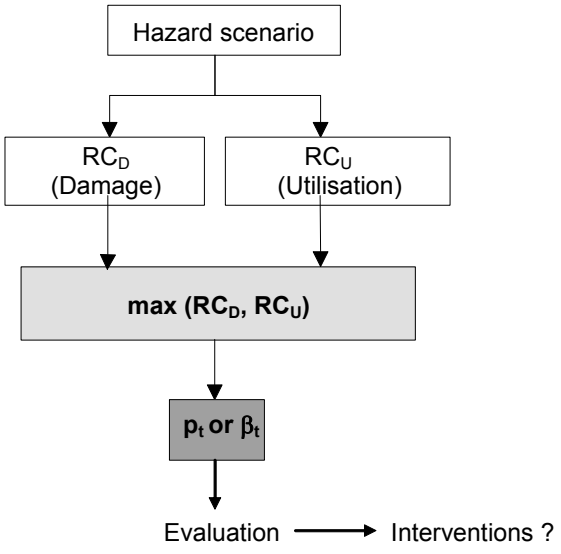

Figure 2. Approach to define the target safety level for a given hazard scenario (RC = Risk Category)

Taking account of the fact that structures are unique, the approach is to define target safety levels as a function of the hazard scenario rather than applying an uniform target safety level to all scenarios and structures. The motivation for this is to rationalize evaluation of existing structures with a view to avoiding interventions on structures that are already adequately safe. (This is

often the case when design codes (for new structures) are simply applied to the evaluation of existing bridges.)

Such an approach to defining target safety levels is suggested in Bailey et al. (2001) involving the following steps (Fig. 2):

- Identification of hazard scenarios
- Definition of the consequences of a given hazard scenario with respect to damage and the economic importance of the structure as characterized by a risk category RC
- Selection of the target safety level p_t as a function of the magnitude of these consequences

It is important to note that the aim of this approach is not to reduce safety levels globally throughout the bridge network, but rather to target a uniform level of acceptable risk.

2.5.2. *Risk Categories*

Risk category for damage: The magnitude of damage can be described in terms of the number of casualties due to structure failure (Table 1). As a function of the hazard scenario and the failure mode, the number of casualties depends on the utilization, geometry and situation of the structure. There is a direct relation between the number of casualties and the mean daily use of the structure by persons.

TABLE 1. Risk categories for damage RC_D (As suggested in Bailey et al. (2001))

Probable number of casualties	Risk category for damage RC_D
<1	I
1	II
5	III
10	IV
50	V
100	VI
500	VII

Risk category for utilisation: A structure is an element of a given system (f.ex. transportation or supply system). The value of utilisation of a structure can be estimated by means of the costs incurred by its failure. In Table 2 risk categories are given as a function of the consequences of structure failure and the relative costs of safety measures. Consequences are defined by a ratio between failure costs C_{fail} (cost of accident, cost of re-construction of the bridge including user costs) and intervention cost C_{int} needed to prevent structure

failure: $\rho = C_{fail}/C_{int}$. User costs depend on the importance of the system in terms of utilization intensity.

TABLE 2. Risk categories for utilisation RC_U (As suggested in Bailey et al. (2001) and adapted from JCSS Probabilistic Model Code)

Relative costs of safety measures	Consequences		
	Minor $\rho < 2$	Moderate $2 < \rho < 5$	Major $5 < \rho < 10$
Large	I	II	III
Normal	III	V	VI
Low	V	VI	VII

2.5.3. *Acceptable Risk Levels*

Acceptable risk levels may be assessed based on historical surveys of the risk associated with structure failures and the risk accepted by the public in daily activities, such as mountaineering and rail travel. These risks are then used to define an acceptable level of risk to be used for evaluating existing structures.

In terms of individual risk of death due to structure failure the study (Bailey et al., 2001) suggests:

- Lower limit: probability of 10^{-6} (deaths/habitant and year)
- Upper limit: probability of $3\ 10^{-4}$ (deaths/habitant and year) (corresponding to the risk of loss of life in a car accident)

2.5.4. *Target Safety Values*

Table 3 presents the target probability of failure p_t and the target reliability index β_t for each risk category. The target risk category is taken as maximum of the risk categories for damage RC_D and for utilisation RC_U (Fig. 2).

TABLE 3. Target probability and reliability indices as a function of the risk category (Bailey et al., 2001)

Risk category RC	Target probability of failure p_t	Target reliability β_t
I	10^{-3}	3.1
II	$5{\cdot}10^{-4}$	3.4
III	10^{-4}	3.7
IV	$5{\cdot}10^{-5}$	4.0
V	10^{-5}	4.2
VI	$5{\cdot}10^{-6}$	4.4
VII	10^{-6}	4.7

2.5.5. *Safety Check*

The target safety level is thus derived as a function of “external” (non-technical or intangible) parameters representing the value and importance of a structure.

This target safety level is then compared to the estimated safety (using engineering methods of calculation of failure probability) which is determined using "internal" (tangible) parameters describing the state of the structure.

In terms of probabilities the safety check is expressed as follows:

$$p_f = p_u \cdot (1 - p_{\text{det}}) \leq p_t$$

with:

p_f : probability of failure of a structure or a structural element
p_u : probability of failure as calculated by structural analysis
p_{det} : probability of detection of an extreme or unplanned load or a damage process decreasing the strength of a structural element
p_t : target probability of failure

This equation also shows that the probability of failure can be reduced by intensifying monitoring of a structural element and thus increasing the probability of the detection.

2.6. CONCLUSIONS

The analysis of structural failures provides a rich and valuable source from which relevant knowledge and measures to improve safety can be deduced. Human errors are clearly the main source of structural failures.

Relevant measures to improve the safety of civil structures include combating human error, applying hazard recognition methods, establishing organisational documents as well as systematic and adequate monitoring and maintenance of structures.

The safety evaluation of an existing structure should follow a stepwise procedure with an increasing degree of refinement of investigations.

For the evaluation of the structural safety of existing structures, target safety levels may be defined as a function of the hazard scenario and the characteristics of the structure under consideration. A methodology to define target safety levels is suggested in this chapter.

3. Improvement of the Durability of Concrete Structures using Ultra-High Performance Fibre Reinforced Concrete

3.1. CONCEPTUAL IDEA

This chapter presents an original concept for the improvement of concrete structures. The basic conceptual idea is to use UHPFRC only in those zones of the structure where the outstanding UHPFRC properties in terms of durability

and strength are fully exploited; i.e. UHPFRC is used to "harden" the zones where the structure is exposed to severe environmental and high mechanical loading. All other parts of the structure remain in conventional structural concrete as these parts are subjected to relatively moderate exposure. Sustainable structures of the future will be those where the number and extent of interventions will be kept to the lowest possible minimum of only preventative maintenance without or only little disruptions of utilization.

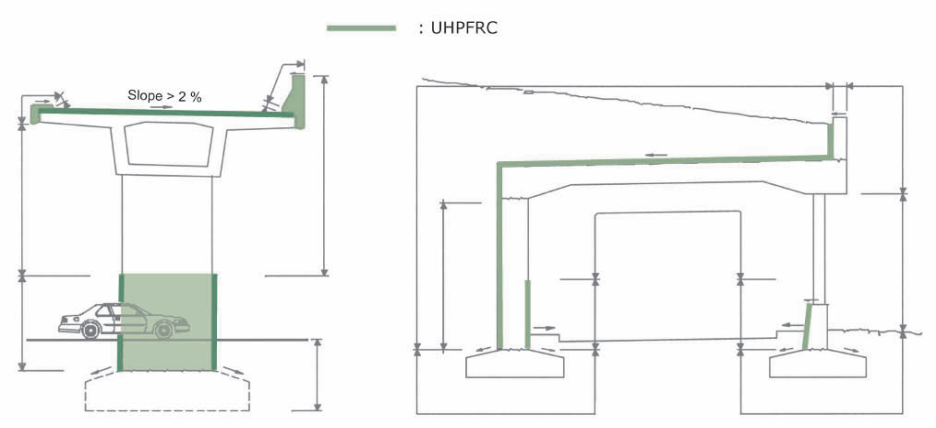

Figure 3. Concept of application of the local "hardening" of bridge superstructures with UHPFRC

This concept is applicable to new structures and for the rehabilitation of existing structures; it necessarily leads to composite structural elements combining conventional reinforced concrete and UHPFRC. The concept of application of UHPFRC is schematically illustrated on Fig. 3. An "everlasting winter coat" is applied on the bridge superstructure in zones of severe environmental and mechanical loads (exposure classes XD2, XD3).

Critical steps of the construction process such as application of waterproofing membranes or compaction by vibration can be prevented, and the associated sources of errors avoided. The construction process becomes then simpler, quicker, and more robust.

The waterproofing capabilities of the UHPFRC exempt from applying a waterproofing membrane. Thus, the bituminous concrete can be applied after only 8 days of moist curing of the UHPFRC. This constitutes a significant time saving with respect to the drying period of up to 3 weeks necessary prior to the application of a waterproofing membrane on a usual mortar or concrete.

The combination of the protective (P) and resistance (R) properties of UHPFRC with the mechanical performance of reinforcement bars (normal or high grade) provides a simple and efficient way of increasing the stiffness and load-carrying capacity with compact cross sections Fig. 4. Depending on the structural and material properties of the composite system, more or less pronounced built-in tensile stresses are induced in the UHPFRC due to restrained deformations at early age. This stress state needs to be analysed and evaluated (see Section 3.4).

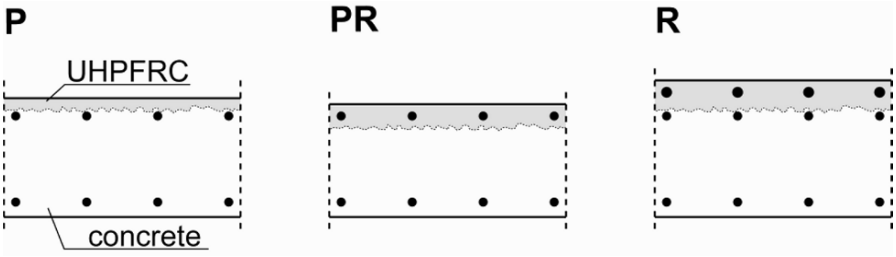

Figure 4. Basic configurations for composite structural elements combining UHPFRC and conventional structural concrete

The original conceptual idea (developed in 1999) has been investigated by means of extensive researches aimed at characterizing UHPFRC materials and the structural behaviour of composite structural members (Kamen et al., 2007, 2008; Charron et al., 2007; Habel et al., 2006a, b, c, d, 2007; Denarié and Brühwiler, 2006). The concept is well-suited for bridges and can also be implemented for buildings, galleries, tunnels or retaining walls.

3.2. PROPERTIES OF UHPFRC

3.2.1. *Tensile Behaviour of UHPFRC*

The uniaxial tensile behaviour of two different recipes of the UHPFRC CEMTEC$_{multiscale}$® type has been determined by means of a tensile test on unnotched dogbone specimens (Denarié and Brühwiler, 2006). The average curves from five tests for each material are represented on Fig. 5, showing the range of possible strain hardening responses. Both recipes are self-compacting.

Recipe CM0 is reinforced with a 468 kg/m^3 of a single type of 10 mm long steel fibres with an aspect ratio of 50. It has a water/binder ratio of 0.140, 1051 kg/m^3 cement, a fluid consistency (slump-flow = 700 mm) and is self-leveling.

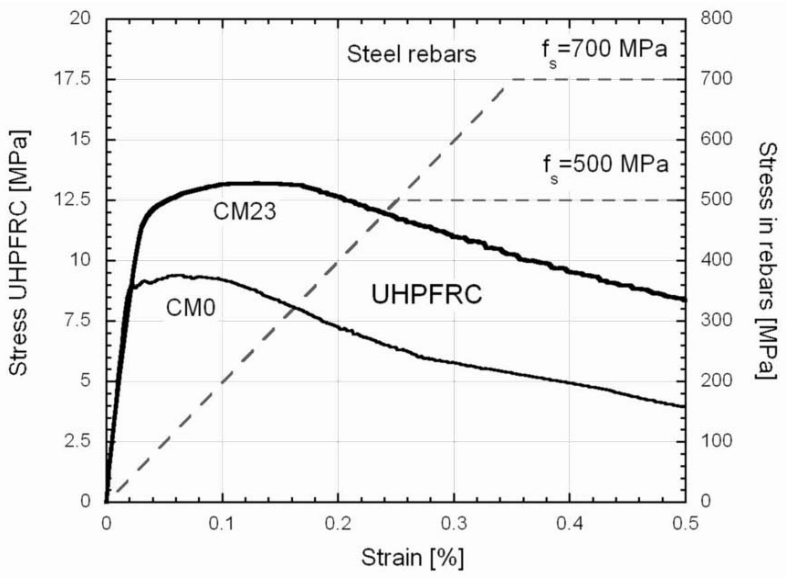

Figure 5. Tensile behaviour of two UHPFRC recipes, CEMTEC$_{multiscale}$®, unnotched tensile tests, fixed rigid boundary conditions, average curves at 28 days

Recipe CM23 has more binder (1,437 kg/m^3 cement) and a lower water-binder ratio (0.125). It is reinforced by a multilevel fibrous mix of macro steel fibres (10 mm long, aspect ratio 50) and microfibres (steel wool) with a total dosage of 705 kg/m^3. It can hold a slope of the substrate up to 2.5%. The effect of the addition of microfibres is revealed on Fig. 5 by three aspects:

1. The significant increase of the pseudo-elastic domain from 8 to above 11 MPa
2. The increase of the strain hardening domain
3. The increase of the load carrying capacity in the descending branch due to the indirect action of the microfibres on the progressive pull-out of the macro fibres

It is worth mentioning that the magnitude of strain hardening of UHPFRC such as CEMTEC$_{multiscale}$® (Rossi, 2002) falls into the range of the yield strain of construction steel, Fig. 5. This property opens up promising domains of combination of UHPFRC with reinforcement bars with high yield strength (700 MPa or above).

The fractured surface of a UHPFRC specimen after a tensile test shows numerous steel fibres, pulled out from the matrix. The work of pull-out of these numerous micro-reinforcements explains the extremely high specific work of fracture of UHPFRC (up to 30,000 J/m^2 compared to 200 J/m^2 for normal

concrete). A significant part of the work of fracture of UHPFRC is dissipated in the bulk of the material, during the strain hardening phase, in the form of finely distributed, multiple cracks.

One should keep in mind that the mechanical response of fibrous composites such as UHPFRC is very much application dependent. Strong anisotropy effects can be induced by the casting procedure of the materials or the width and shape of the moulds and these effects have to be considered for the analysis of test results and for design (Wuest, 2007).

3.3. DESIGN EXAMPLE OF AN OVERPASS BRIDGE USING THE ORIGINAL CONCEPT

3.3.1. *Conceptual Design*

The above described conceptual idea is applied for the design and construction of the overpass bridge (Brühwiler et al., 2007). The principle is to use UHPFRC to "harden" only those zones where the structure is exposed to severe environmental action (direct water contact with deicing salts) and where high mechanical loads have to be taken up. These zones include the top surface of the deck slab, the kerb and sidewalk overlay elements and the zone above the middle support including a unique UHPFRC hinge. All other parts of the bridge structure remain in conventional reinforced and prestressed concrete as these parts are subjected to only moderate exposure. The developed bridge concept consists of a superstructure as a continuous two-span multi-girder system resting on a middle support and the abutments (Figs. 6 and 7).

The main girders are prefabricated in a construction plant and are prestressed and posttensioned in the longitudinal direction. After their alignment on the construction site, the space between the girders over the middle pier is filled out with UHPFRC creating at the same time an UHPFRC hinge over the finger piers (Detail 1, Fig. 8a). Then, a layer of UHPFRC is cast to connect the prefabricated girders along the longitudinal joint (Detail 2, Fig. 8b) and to provide a 3 cm thick (waterproofing) protection layer on the whole top surface of the deck slab. The kerb elements are made of prefabricated UHPFRC elements that are glued to the top surface. UHPFRC is thus applied both on the construction site and in the prefabrication plant by using different adapted mixes (SAMARIS, 2005).

The duration of the construction works shall be limited to a minimum in order to reduce disturbance for the road user. The total time of construction of the superstructure may be optimized and reduced to about 25–30 days. In addition, critical and time consuming steps of the construction process such as application of waterproofing membranes, on-site concreting or compaction by vibration are eliminated, and the associated sources of errors avoided. The construction

process becomes then simpler, quicker and more robust with an optimal use of prefabrication.

The construction cost shall be similar or lower than for a conventional concrete bridge.

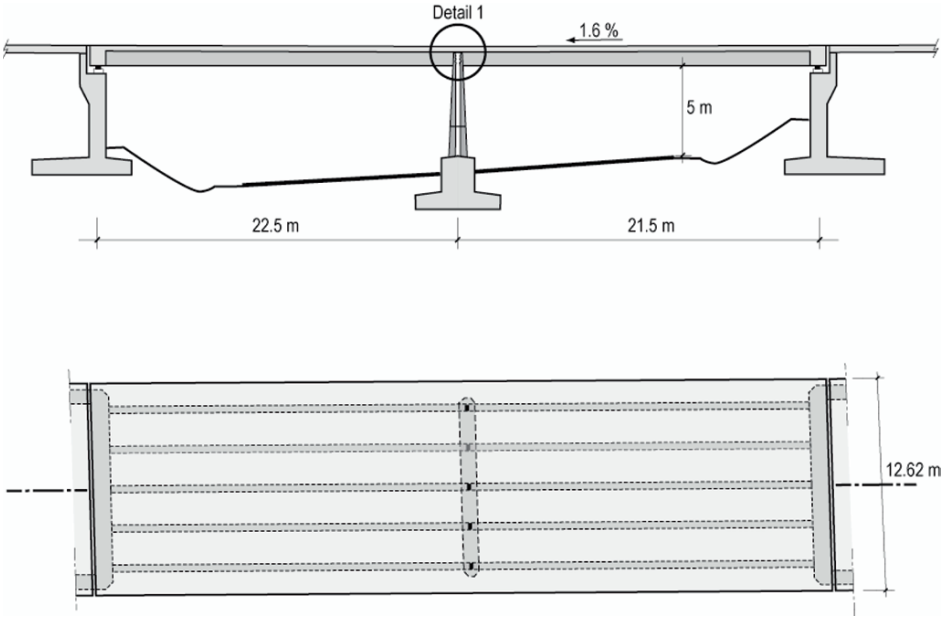

Figure 6. Elevation and plan view

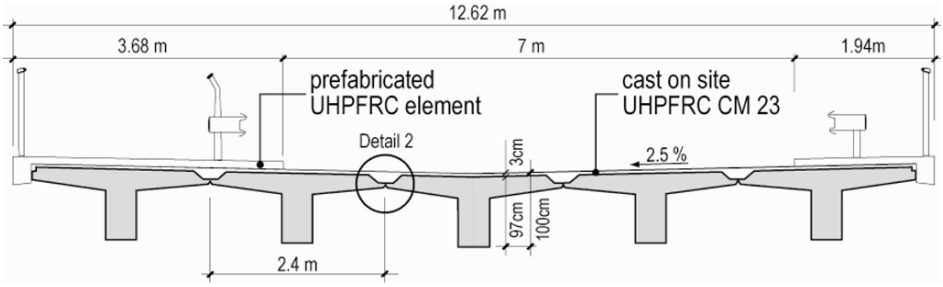

Figure 7. Typical cross section

The originality of Detail 1 (Fig. 8a) resides in the casting of the top part of the pier, hinge and connection between the prefabricated girders in one onsite casting sequence using UHPFRC. The 70 mm wide UHPFRC hinge is subjected to significant rotations requiring certain deformation capabilities of the UHPFRC. The top part of the middle support is a tension chord consisting of UHPFRC

reinforced with steel reinforcing bars to take the tensile forces due to the bending moment over the support.

Detail 2 (Fig. 8b) provides a stiff load carrying connection between the prefabricated girders in the longitudinal direction. The 150 mm thick UHPFRC joint with steel reinforcement bars is highly resistant to account for concentrated wheel loads on the deck slab.

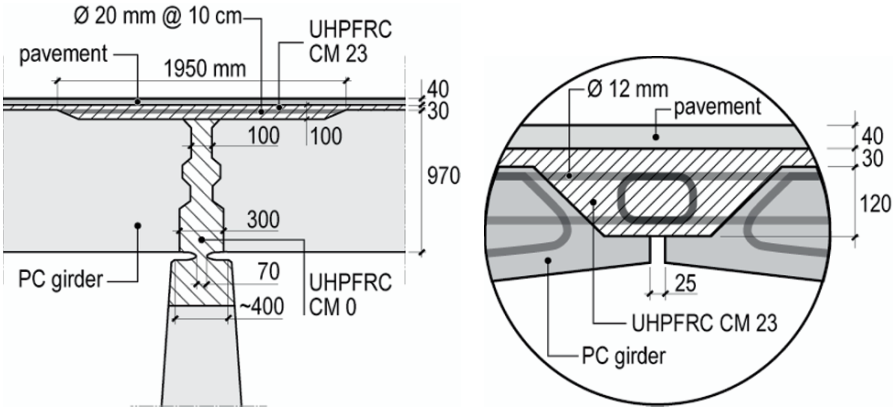

Figure 8. (**a**) Detail 1: middle support, and (**b**) Detail 2: longitudinal joint between prefabricated girders

Previous research indicated that a 30 mm thick UHPFRC layer provides the required mechanical performance and extremely low permeability. This UHPFRC protection layer contributes favourably to the load carrying behaviour of the deck slab in terms of stress membrane resisting against compression and tension forces without undergoing crack formation.

3.4. STRUCTURAL ANALYSIS OF A COMPOSITE BRIDGE GIRDER COMBINING UHPFRC AND REINFORCED CONCRETE

3.4.1. *Introduction*

This section shows findings of a FE-analysis of a conceptual bridge girder design combining a thin UHPFRC overlay with a reinforced concrete substructure (Fig. 7). Besides its load carrying contribution, the UHPFRC overlay replaces conventional waterproofing membrane and therefore has to remain in an impermeable state under service conditions and during the whole service life in order to protect the below conventional reinforced concrete structure effectively.

The present structural analysis focuses thus on the serviceability limit state of the structure.

3.4.2. *Constitutive Material Modeling of UHPFRC*

(a) Requirements

The UHPFRC designed for this application responds to the following general requirements:

- High compressive and tensile strengths
- Strain hardening and softening in tension
- Very low permeability
- Self-compacting fresh mix with the ability to be cast with a slope of 3%
- Low variability of mechanical properties

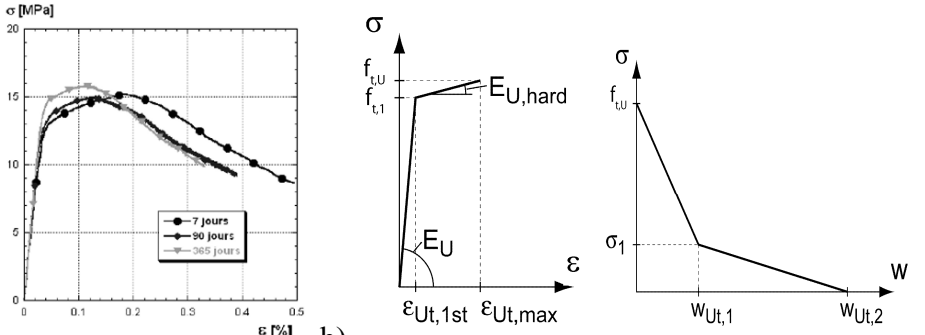

Figure 9. (**a**) Stress–strain diagram from experiments (Wuest, 2007) and (**b**) corresponding constitutive tensile law for FE-analysis input

(b) Tensile behaviour

High tensile strength as well as strain hardening and softening are characterising properties of UHPFRC. The uniaxial tensile behaviour was determined using dogbone specimens. The results of several experiments were averaged (Fig. 9a) and transformed into the constitutive material law for tension (Fig. 9b) as input for the FE-program.

(c) Viscoelastic behaviour

UHPFRC develops important shrinkage (mostly autogenous shrinkage) which leads to Eigenstresses in the composite element due to the restrained deformation conditions. Free shrinkage under drying conditions reaches up to 590 μm/m after 1 year with an evolution of two third of the value after 35 days (Kamen et al., 2007; Habel et al., 2006c). Induced stresses are partly balanced as a function of time by an important creep and relaxation capacity.

The high dosage of fibers prevents microcracking of the matrix and provides a high deformation capacity. Both effects are crucial for the proper working of the UHPFRC-layer regarding mechanical and physical requirements. Input data for the FE-analysis was deduced from comprehensive laboratory tests on the evolution of mechanical and physical properties depending on maturity (Kamen et al., 2007, 2008; Habel et al., 2006c, d).

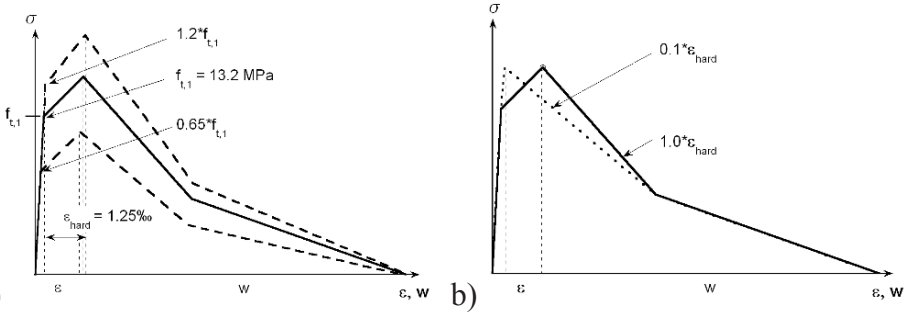

Figure 10. Variation of (**a**) tensile strength f_t and (**b**) deformation capacity ε_{hard}

(d) Variability of mechanical properties

An inherent property of fiber reinforced composites is the non-uniform fiber orientation and distribution depending on the mixing process, casting method and formwork boundaries (Wuest, 2007). This was taken into account in the FE-analysis by varying the values of tensile strength and deformation capacity (Fig. 10).

The tensile strength, defined as elastic limit of the material, was modified to 65% and 120% of the reference value $f_{t,1}$ = 13.2 MPa (Fig. 9a), while the strain hardening, defined as the deformation between $f_{t,1}$ and the ultimate tensile strength $f_{t,U}$, was modified between 10% and 100% of the reference value $\varepsilon_{hard} = \varepsilon_{Ut,max}-\varepsilon_{Ut,1st}$ = 1.25‰ (Fig. 9b). The ultimate tensile strength $f_{t,U}$ is considered to evolve with a constant factor of 1.25*$f_{t,1}$ in relation to the elastic limit.

3.4.3. *FE-Analysis*

(a) Description of the numerical tool

The FE-analysis was done with FEMASSE MLS (Roelfstra et al., 1994). This numerical tool allows to conduct comprehensive analyses including the coupling of age dependent thermal, hygral, chemical and mechanical properties.

In the given 2-D model the deformation in z direction (longitudinal sense of the bridge girder) was not restrained. The UHPFRC layer was applied to inert concrete, cured for 7 days and afterwards exposed to environmental conditions

described by constant values at a temperature of 20°C. The numerical analysis starts at the instant of the UHPFRC overlay casting (time 0).

The structural analysis can be considered as representative regarding the observations made concerning the age-dependent variation of stresses and mechanical properties in the present structural element.

(b) Cross sectional model

The model represents an exemplary transversal cross section of the bridge girder near the support, showing five (prefabricated) T-beams in conventional prestressed concrete with the UHPFRC overlay (Fig. 11). The bottoms of the beams are vertically and horizontally fixed limiting the flexional deformability of the bridge deck to a minimum and increasing the degree of restraint to a maximum.

The loads are transferred laterally by the UHPFRC that also connects the longitudinal beams. The thickness of the layer is increased at the longitudinal joints to 15 cm instead of 3 cm on top of the T-beams.

In general, viscoelastic behaviour of the T-beams is beneficial for the stress evolution in the UHPFRC since it indirectly reduces the degree of restraint but this effect was not considered in the analysis.

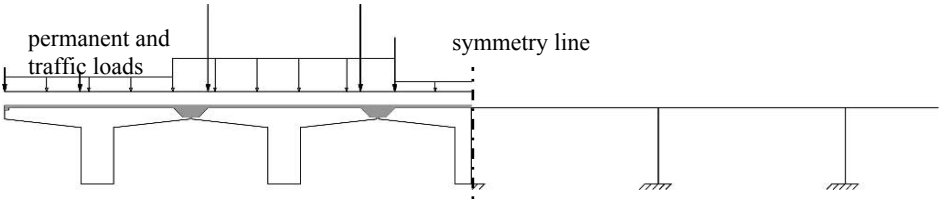

Figure 11. Transversal bridge section with UHPFRC layer, exemplary loading scheme and static system

(c) Load cases

The following load cases were considered in the modelling:

- Permanent loads due to self weight of the structure and the UHPFRC layer
- Permanent loads due to self weight of non-load bearing elements such as the curbs, crash barriers, railings and the asphalt layer, applied at 28 days
- Traffic loads at serviceability limit state including two traffic lanes according to current code provisions, applied at the most unfavourable position regarding stresses in the UHPFRC layer in the transversal sense

All external loads are superimposed to the continuous evolution of the mechanical and physical properties of UHPFRC such as Young's modulus, compressive and tensile strength, shrinkage and viscoelasticity.

3.4.4. *Results*

The results of the numerical simulation are presented exemplary for a typical reference point showing highest stresses:

(a) Restrained shrinkage
Restrained shrinkage is the load case the UHPFRC overlay is subjected to from the very beginning (after casting) and also the one that consumes an important part of the resistance capacity of the material. It is a deformation controlled loading process, and consequently, it is the deformation capacity of the material that predominantly replies to this load case (Fig. 12). The absolute value of the tensile strength is not of great importance here.

Depending on the level of the evolving tensile strength, shrinkage causes Eigenstresses that almost reach the elastic tensile strength $f_{t,1}$ before the external loads are applied. If the UHPFRC overlay is stressed beyond its elastic limit due to restrained shrinkage it enters into the hardening domain where it possesses an important deformation capacity, i.e. the stress increase at this stage will be very small.

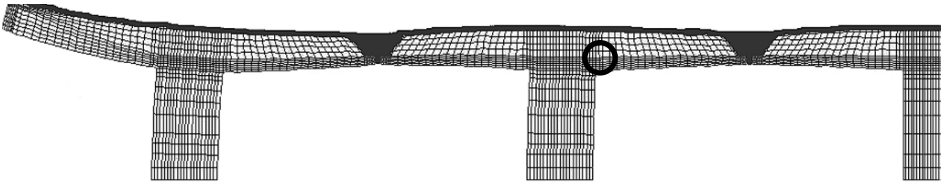

Figure 12. Deformed shape (not in scale) due to shrinkage of UHPFRC (without external loads) and location of the reference point

In this way, the strain hardening behaviour represents a significant stress release potential which is essential for the structural response of the overlay in terms of avoidance of macrocrack localisation and maintaining the low permeability of the UHPFRC layer.

(b) Permanent and traffic loads
Permanent and traffic loads are applied 28 days (672 h) after the application of UHPFRC. They represent a force controlled load case. The UHPFRC layer is subjected to an immediate stress increase which is superimposed to the stresses induced by restrained shrinkage.

Figure 13 shows the stress and strength evolution on the time axis until 42 days (1,000 h) for three cases. The lower dotted lines represent the elastic strength evolution $f_{t,1}$ whereas the upper dotted lines show the evolution of the ultimate strength $f_{t,U}$. The solid lines describe the stress evolution at the reference

point. The step in the solid lines marks the point in time of external load application.

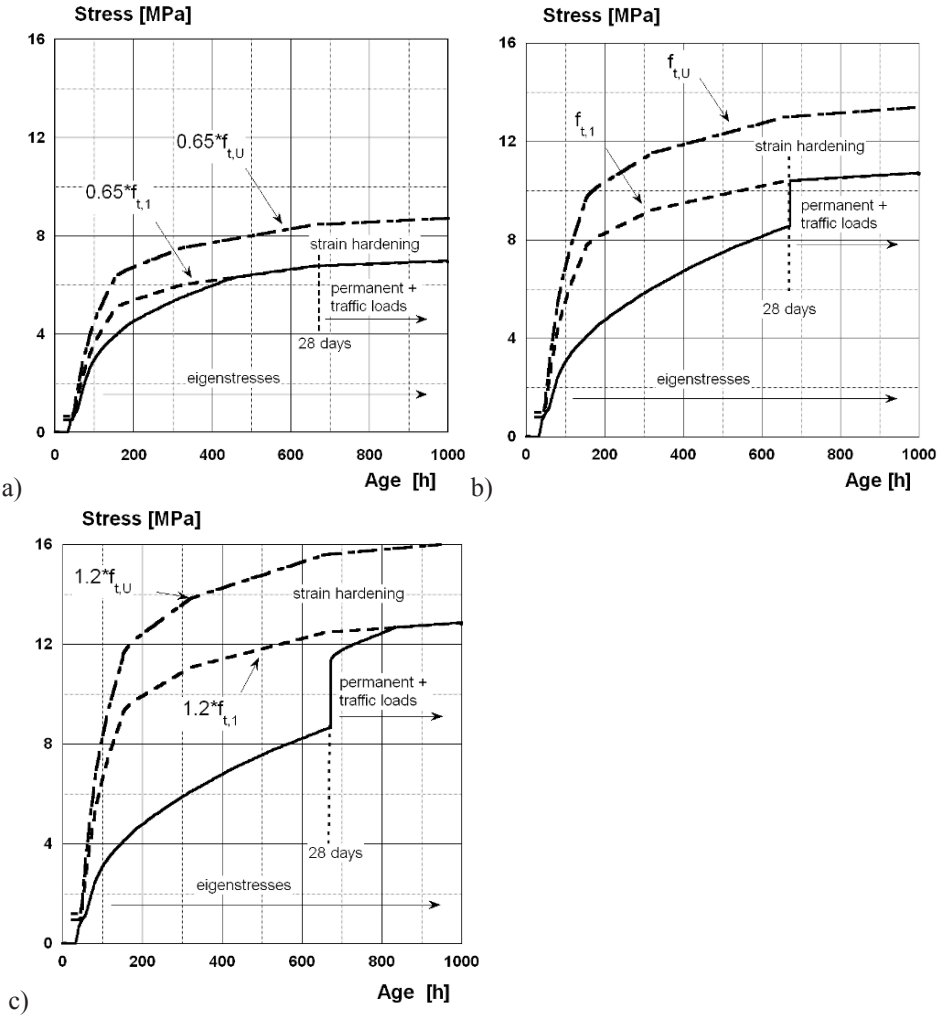

Figure 13. Evolution of stress and strength for (**a**) $0.65*f_{t,1}$; (**b**) $1*f_{t,1}$ and (**c**) $1.2*f_{t,1}$

In case of $f_{t,1} = 0.65*f_{t,1,ref}$ (Fig. 13a) the stresses due to restrained shrinkage reach the elastic limit before the external loads are applied. The application of these creates an inelastic response in the hardening domain. The important deformability of the strain hardening domain keeps the stress level in the UHPFRC layer very close to its elastic limit. The ongoing shrinkage does not

significantly raise the stresses. The stress evolution closely follows the elastic strength evolution.

In case of $f_{t,1,ref}$ (Fig. 13b) the stress increase due to the external loads at 28 days is balanced partly by an elastic response and partly by the strain hardening of UHPFRC. The global behaviour is again similar. Once the stress level exceeds the elastic limit further stress increase is very small.

In case of $f_{t,1} = 1.2*f_{t,1,\ ref}$ (Fig. 13c) external loads lead to a purely elastic response of the overlay. The loads induce a principal tensile stress of approximately 3 MPa at the reference point. Further stress increase is then induced by the continuing shrinkage until the stress level reaches the elastic limit and subsequently follows it.

In all the cases, it can be seen that once the material exceeds its elastic limit strength external loads and continuing shrinkage do not cause a significant further stress increase. The redistribution of loads and increased deformability due to the pronounced strain hardening behaviour and loss of stiffness prevent further stress increase in the UHPFRC layer. Therefore, it is unlikely that the tensile strength $f_{t,U}$ of the UHPFRC is reached. The UHPFRC layer thus remains at the initial stage of multiple microcracking without developing localised macrocracks. The material enters merely very little into the hardening domain, thus keeping its low permeability. It is not subjected to softening within the considered period of 1,000 h.

An exemplary simulation with traffic loads increased by a hypothetical factor of 3 shows that in fact the stress step continues significantly into the hardening domain if the level of loading is sufficiently high (Fig. 14a). Then the

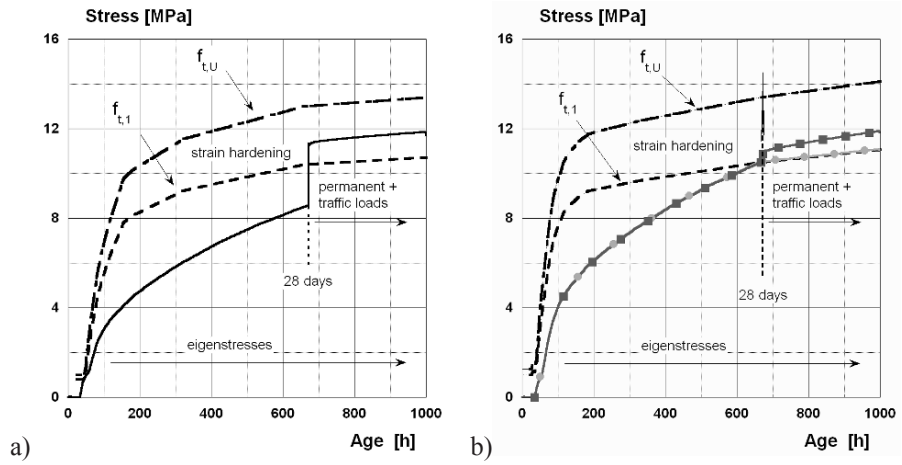

Figure 14. (**a**) Evolution of stress and strength for $1.0*f_{t,1}$ and three times the external loads; (**b**) influence of ε_{hard} on the stress level for $\varepsilon_{hard}=0.1*\ \varepsilon_{hard,ref}$

stresses evolve parallel to the elastic tensile strength but at a higher level. UHPFRC seems to possess enormous reserves in a setup as described above to resist localised cracking even if its elastic tensile strength is exceeded.

In case the strain hardening capacity is reduced significantly the UHPFRC overlay obviously enters far into the hardening domain, (Fig. 14b). The two lines with markers show the stress evolution at a reference point for two materials with $0.1*\varepsilon_{hard,ref}$ (upper line with square markers) and full strain hardening capacity (lower line with round markers).

(c) Serviceability and waterproofing

Charron et al. (2007) have shown for a UHPFRC respecting the requirements given in 2.1 that the water permeability of UHPFRC remains low ($K_{w\ equiv.} < 2 \times 10^{-8}$ cm/s) until a tensile deformation of 1.3‰. This threshold deformation corresponds to a cumulated crack opening equal to 0.13 mm as compared to 0.05 mm for normal concrete.

Since the numerical results show that at all levels of tensile strength the principal stresses in the UHPFRC overlay do not significantly enter into the strain hardening domain, the proposed concept of an "impermeable" and waterproof UHPFRC layer is validated.

3.4.5. *Synthesis of Findings*

A structural analysis of a composite bridge girder combining reinforced concrete and UHPFRC at the serviceability limit state was performed. The structural response under combined loading due to restrained shrinkage and traffic loads was investigated. The obtained results show:

- Restrained shrinkage and external loads may generate stresses close to the elastic tensile strength in the UHPFRC overlay of the composite element with a high degree of restraint. The stresses then follow the age-dependent elastic strength evolution of UHPFRC.
- The evolution of applied stresses in the strain hardening domain is independent of the level of the elastic tensile strength. The loss of stiffness of the UHPFRC layer as it enters into the hardening domain causes a stress release and redistribution.
- The risk of transverse cracking of the UHPFRC layer in the presented structural configuration is unlikely due to the increased deformation capacity and significantly lower stiffness at strain hardening.
- Strain hardening is an essential property for the described type of application since it allows maintaining the low permeability of UHPFRC in its function as waterproofing layer.

3.5. APPLICATIONS

The original concept of application of UHPFRC for the improvement of structural concrete has been validated by means of applications. Four applications have been conducted until today which will be described in the following (Brühwiler and Denarié, 2008).

3.5.1. *Rehabilitation and Widening of a Road Bridge*

A short span road bridge with busy traffic has been rehabilitated and widened using UHPFRC. The entire deck surface of the bridge with a span of 10 m was rehabilitated in three steps during autumn 2004 (Fig. 15).

Firstly, the downstream kerb was replaced by a new prefabricated UHPFRC kerb on a new reinforced concrete beam which was necessary for the widening. Secondly, the chloride contaminated concrete of the upper surface of the bridge deck was replaced by 3 cm of UHPFRC in two consecutive steps such that one traffic lane could be maintained open. Thirdly, the concrete surface of the upstream kerb was replaced with 3 cm of UHPFRC.

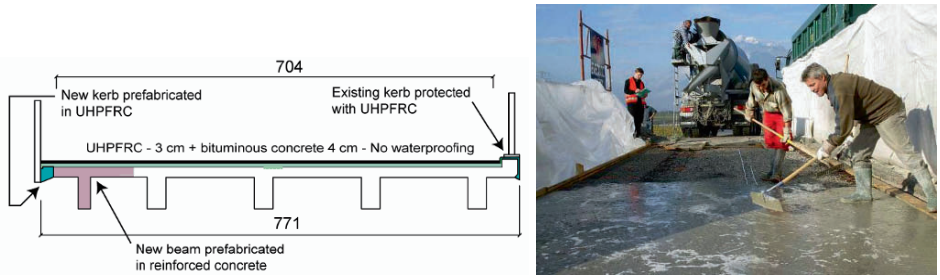

Figure 15. Bridge cross section after rehabilitation (dimensions in cm) and UHPFRC casting.

The fresh self-compacting UHPFRC material was prepared at a local concrete prefabrication plant with a standard mixer, brought to the site by a truck and then poured on the hydrojetted deck surface. The UHPFRC was easy to produce and place with standard tools and very robust and tolerant to the unavoidable particular site conditions. The bituminous pavement was applied on the UHPFRC surfaces after 8 days of moist curing, and the corresponding lane was reopened to traffic the next day. The bridge was fully reopened to traffic one month after the beginning of the construction work.

3.5.2. *UHPFRC Protection Layer on a Crash Barrier Wall*

A layer of UHPFRC has been applied in September 2006 to the concrete crash barrier walls of a highway bridge (Oesterlee et al., 2007). The main design requirement was to obtain long-term durable crash barrier walls since traffic

interruption for future rehabilitation interventions are prohibitive due to the very high traffic volume on this highway. Long-term durability is obtained when transverse macro-cracks in the UHPFRC layer are absent and the permeability of UHPFRC layer to ingress of water and chloride ions is extremely low.

Figure 16 shows the crash barrier wall with a UHPFRC layer covering the areas subjected to splash exposure (Class XD3: reinforcement corrosion induced by chlorides). The rheological properties of UHPFRC were adapted for easy pouring into the 3 cm wide formwork to fill a height of 120 cm including a small horizontal part at the bottom of the wall that provides continuity with the conventional bridge deck with a waterproofing membrane.

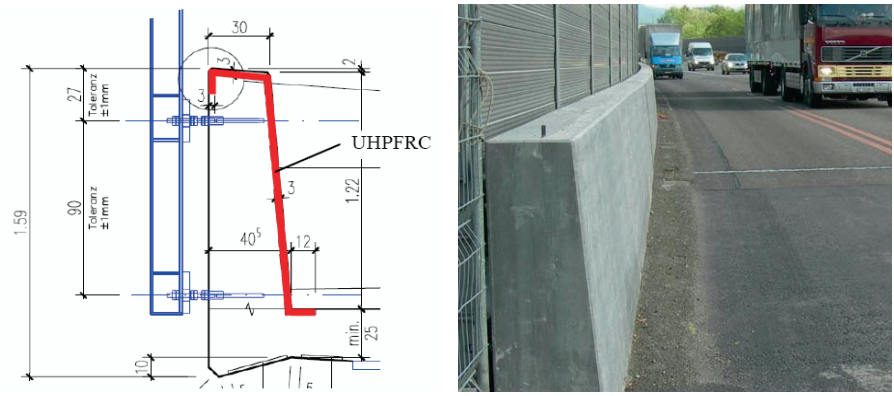

Figure 16. Typical cross section of the crash barrier wall and view after rehabilitation

Due to restrained early age deformation of the UHPFRC (mostly due to thermal and autogenous shrinkage) bonded to the existing reinforced concrete wall, an internal stress state is built up in the composite element including, in particular, tensile stresses in the UHPFRC layer. These tensile stresses, which can cause macrocrack formation, and the capacity of the UHPFRC to resist to these stresses were investigated by means of numerical analyses prior to the intervention.

The fresh self-compacting UHPFRC was fabricated in a conventional ready mix concrete plant, transported to the site by a truck and filled into the thin slot to realize the UHPFRC coating. The required mechanical properties and the protective function of the UHPFRC layer have been confirmed by in-situ air permeability tests and laboratory tests on specimens cast on site. Four months after application no crack could be found confirming the predictions made by the numerical simulations.

3.5.3. *Rehabilitation of a Bridge Pier using Prefabricated UHPFRC Shell Elements*

In this application, 4 cm thick UHPFRC shell elements have been prefabricated to form an outer protection shield for the existing 40 year-old reinforced concrete bridge pier which is located very close to a busy highway which makes it virtually not accessible for future maintenance interventions (Fig. 17).

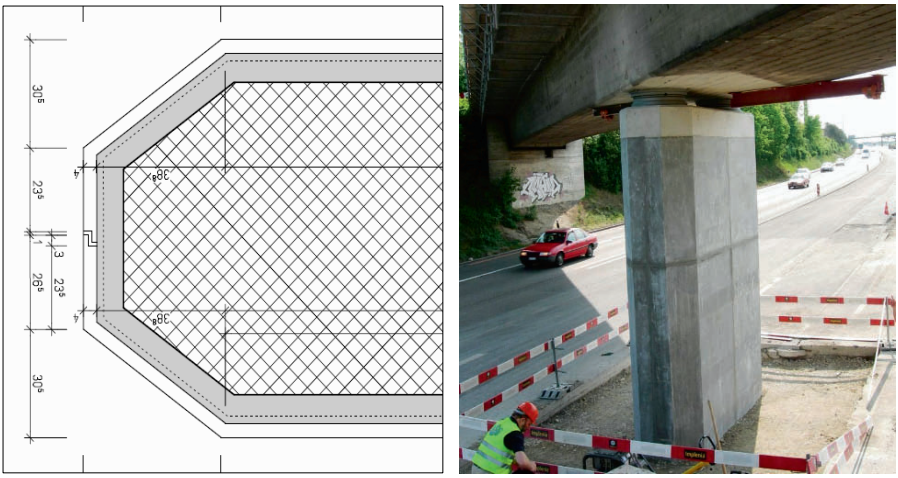

Figure 17. Cross section and general view of the rehabilitated bridge pier

In spring 2007, the UHPFRC elements (maximum element height of 4 m) were cast in a prefabrication plant, transported to the construction site and mounted, after removing of up to 10 cm of chloride contaminated concrete by hydrojetting. The joints between the different UHPFRC shell elements were glued using an epoxy resin. The remaining space between the UHPFRC elements and the existing reinforced concrete was filled with self-compacting mortar.

Long-term durability is expected since transverse cracks in the UHPFRC protection shield are absent and the permeability of UHPFRC for ingress of water and chloride ions is extremely low as confirmed by permeability tests.

3.5.4. *Strengthening of an Industrial Floor*

The 50 year-old drivable reinforced concrete floor of a fire brigade building had insufficient load carrying capacity in view of heavier future fire engines. The concept was to increase the load carrying capacity of the existing slab of 720 m^2 area by pouring a 4 cm thick UHPFRC layer on top of the existing RC slab, as a replacement of the existing cementitious non-load carrying overlay (Fig. 18). The UHPFRC layer leads to a thicker load carrying slab which provides (1) a better distribution of local wheel loads, (2) an increase in static height and (3) a

layer of high strength material capable of resisting both compression and tension stresses.

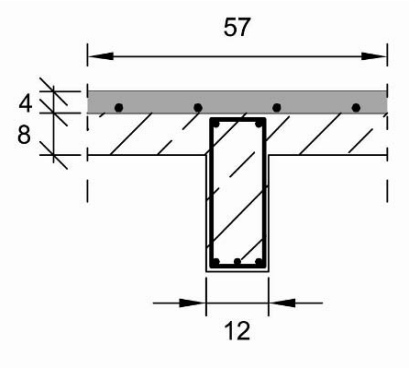

Figure 18. Cross section (dimensions in cm) with UHPFRC layer (in grey) and view of UHPFRC casting performed in autumn 2007

The UHPFRC was again fabricated in a local ready mix concrete plant and transported to the site by trucks. The excellent workability of the fresh self-compacting material allowed for easy casting. The use of the UHPFRC solution turned out to be very economic (compared to the conventional solution of slab demolition and reconstruction). This was also because the utilization of the fire workers building was only slightly restricted during the intervention, holding user costs down.

Acknowledgments: The support of the Swiss National Science Fund, The Swiss Secretary of Education and Research, The Committee of Technology and Innovation, Cemsuisse, Holcim, Swiss Steel AG and the Swiss Federal Roads Office is gratefully acknowledged. The applications were possible thanks to the Road Administrations of the Swiss Cantons of Wallis and Aargau as well as the Town of Geneva.

The UHPFRC Group at MCS-EPFL consists of the following current and former members: Dr. Katrin Habel, Professor Jean-Philippe Charron, Dr. Hamid Sadouki, Professor Minoru Kunieda, Dr. Aicha Kamen, Dr. John Wuest, Dr. Andrin Herwig, Cornelius Oesterlee, Agnieska Switek and Talayeh Noshiravani.

References

Bailey, S.F., Antille, S., Béguin, P., Imhof, D., Brühwiler, E.: *Niveau de sécurité requis pour l'évaluation des ponts-routes existants. (Required safety level for the evaluation of existing road bridges).* Research report No. 550, VSS Zurich, 2001 (in French).

Brühwiler, E., Fehling, E., Bunje, K., Pelke, E., Design of an innovative composite road bridge combining reinforced concrete with Ultra-High Performance Fibre Reinforced Concrete. Proceedings, IABSE Symposium "Improving Infrastructure Worldwide", Weimar, September 2007.

Brühwiler, E., Denarié, E., Rehabilitation of concrete structures using Ultra-High Performance Fibre Reinforced Concrete, UHPC-2008: The Second International Symposium on Ultra High Performance Concrete, March 05–07, 2008, Kassel, Germany.

Charron, J.-P., Denarié, E., Brühwiler, E., Permeability of Ultra High Performance Fiber Reinforced Concretes (UHPFRC) under high stresses, *Materials and Structures*, Vol. 40, No. 3 (March), 2007, pp. 269–277.

Denarié, E., Brühwiler, E., Structural rehabilitations with Ultra High Performance Fibre Reinforced Concretes, *International Journal for Restauration of Buildings and Monuments*, Aedificatio, Vol. 12, No. 5 and 6, 2006, pp. 453–467.

Habel, K., Denarié, E., Brühwiler E., Structural response of elements combining Ultrahigh-Performance Fiber-Reinforced Concretes (UHPFRC) and reinforced concrete, *ASCE Journal of Structural Engineering*, Vol. 132, No. 11, November 2006a, pp. 1793–1800.

Habel, K., Denarié, E., Brühwiler, E., Time Dependent Behaviour of Elements Combining ultra-high performance fiber reinforced concretes (UHPFRC) and Concrete, *Materials and Structures*, Vol. 39, No. 5, June 2006b, pp. 555–567.

Habel, K., Charron, J.P., Denarié, E., Brühwiler, E., Autogenous deformations and viscoelasticity of UHPFRC in structures. – Part I: Experimental results, *Magazine of Concrete Research*, Vol. 58, No. 3, April 2006c, pp. 135–145.

Habel, K., Charron, J.P., Denarié, E., Brühwiler, E., Autogenous deformations and viscoelasticity of UHPFRC in structures – Part II: Numerical Modelling, *Magazine of Concrete Research*, Vol. 58, No. 3, April 2006d, pp. 147–156.

Habel, K., Denarié, E., Brühwiler, E., Experimental Investigation of Composite Ultra-High-Performance Fiber-Reinforced Concrete and Conventional Concrete Members, *ACI Structural Journal*, Vol. 104, No. 1, 2007, pp. 93–101.

ISO International Standard: *Bases for design of structures – Assessment of existing structures.* ISO/TC 98/SC 2/WG6 N35, 2001.

*JCSS Probabilistic Model Code.*www.jcss.ethz.ch

Kamen, A., Denarié, E., Brühwiler, E., Thermal effects on physico-mechanical properties of Ultra-High-Performance Fiber-Reinforced Concrete, *ACI Materials Journal*, Vol. 104, No. 4, July–August 2007, pp. 415–423.

Kamen, A., Denarié, E., Sadouki, H., Brühwiler, E., UHPFRC tensile creep at early age, Materials and Structures MAAS3402, 2008, in press.

Oesterlee, C., Denarié, E., Brühwiler, E., In-situ casting of UHPFRC protection layer on crash barrier walls, Proceedings, Advances in Construction Materials – Symposium in honour of Hans W. Reinhardt, July 2007, University of Stuttgart, Germany.

Roelfstra, P. E., Salet, A. M., Kuiks, J. E. (1994) Defining and application of stress-analysis-based temperature difference limits to prevent early-age cracking in concrete structures. Proceedings n°25 of the International RILEM Symposium: Thermal cracking in concrete at early age, pp. 273–280. Munich, Germany.

Rossi, P., *Development of new cement composite material for construction*, in: K. Dhir, P. C. Hewlett, L.J. Csetenyi (eds.), Proceedings of the International Conference on Innovations and Developments in Concrete Materials and Construction: 17–29, University of Dundee, Dundee, Scotland, 2002.

SAMARIS, 2005, Report D22, *Full scale application of UHPFRC for the rehabilitation of bridges – from the lab to the field,* European project 5th FWP / SAMARIS – Sustainable and Advanced Materials for Road Infrastructures – WP 14: HPFRCC, http://samaris.zag.si/.

Schneider, J., *Introduction to Safety and Reliability of Structures.* Structural Engineering Document 5, IABSE – International Association for Bridge and Structural Engineering, Zurich, 1997, 138p.

Wuest, J., Comportement structural des bétons de fibres ultra performant en traction dans des éléments composés. Doctoral thesis No 3987, Ecole Polytechnique Fédérale de Lausanne (EPFL), 2007, Switzerland.

STRUCTURAL DAMAGE AND RISK ASSESSMENT AND UNCERTAINTY QUANTIFICATION

H.G. Matthies (h.matthies@tu-bs.de)
Institute of Scientific Computing Technische Universität Braunschweig, Brunswick, Germany

Abstract. This article concentrates on the interplay between structural damage and risk assessment on one hand and numerical techniques, especially for uncertainty quantification, on the other hand. It shows the connection between damage assessment and risk quantification, touching on the methods of probabilistic risk assessment (PRA). It then details on how to initially asses the damage, which by necessity will involve some uncertainty, and how to update that initial assessment through additional testing. This is essential a statistical system identification process. The decision making process of finding whether the structure should be repaired or demolished is also mentioned shortly. It should involve a cost/benefit appraisal in the light of the information gained on the extent of the damage. Especially if the damage was caused by environmental forces, e.g. such as seismic action, it may be advantageous to determine the characteristic of this external action which caused the damage. This is a similar problem to the system identification of the structure, only that the testing is purely computational. Having identified the cause and the extent of the damage, one may want to draw lessons as to mitigate the hazard due future extreme environmental effect, in the form of robust design, minimizing vulnerability of life-lines and the fragility of structures.

Keywords: Risk assessment, uncertainty quantification, structural damage

1. Introduction

Structural Damage Assessment means to conduct damage and safety assessments of civil engineering structures and of infrastructure, and to perform structural inspections, and mitigation activities. The capability includes being able to provide contractor management, construction management, cost estimating, technical assistance, and other engineering services to support and manage response and recovery operations.

Here we will look at the role that uncertainty quantification can play in this process. The desired outcome of such an activity is the efficient

A. Ibrahimbegovic and M. Zlatar (eds.), *Damage Assessment and Reconstruction After War or Natural Disaster*,

implementation, management, and coordination of resources, aids emergency response, and recovery operations which restore the affected area to pre-event conditions.

For this to occur future hazards from the sustained damage has to be identified, the exposure to further threats has to be estimated, and the vulnerability of structures, infrastructure, and life-lines has to be considered. This is very similar to the usual risk assessment procedure, only that now the state of the system to be considered is also very uncertain, inasmuch as the amount of damage is not known yet.

For any kind of activity its benefit has to be weighed versus its risk (Starr, 1969). With structures and infrastructure that has been damaged, it is similar. These notes will concentrate on these more fundamental issues as well as on how a general procedure may actually be designed in structural damage and risk assessment, rather than give any specific prescriptions or guidelines on how to actually do the damage assessment, which may be found e.g. in FEMA (2004).

2. Damage, hazard, risk, and uncertainty

First of course it is necessary to dwell a bit on ontology, as to what is really meant by those terms *damage, hazard, risk,* and *uncertainty.*

2.1. ONTOLOGY

Let us start with the simplest of these, *damage*: Legally, as we are concerned with structures and infrastructure, it is a *property damage* we are talking about. It means that the object has changed in some way so that it cannot be used any more in the way originally designed or intended. A moment's thought shows that it is not only the *monetary* damage to objects (structures, infrastructure) which counts; as these may be life-lines for the population living there, a damage can threaten health and maybe even lives. Beyond that the damage maybe hampering economic possibilities, this one could term *opportunity costs* (King et al., 1997). All this of course enters into the decision which structures or infrastructure to repair first in case many have been damaged. Certainly on top of the priority list should be to avoid loss of life or hazards to health. When purely monetary terms count, then of course the opportunity costs have to enter the decision as well.

The term *hazard* is usually understood as the potential to cause harm in some way, i.e. the possibility of something happening which would cause further damage, or even loss of life. The larger the consequences or the potential of a damage or loss, the higher the hazard. To identify hazard, it

is necessary to follow a proper way of reasoning (Pearl, 2000) in order to arrive at valid conclusions.

Hazard then has to be in some way combined with its frequency – or rather *probability* – of occurrence, and a combination of these two is usually taken to define *risk* (Kaplan and Garrick, 1981; Wilson and Crouch, 2001). Often it is the product of these two quantities which are taken as the definition of risk. In quite a number of cases, especially for very high or very low hazards, or very low or high probabilities, this simple combination seems not to be reasonable. It implicitly assumes that the decision-maker taking a certain risk is *risk-neutral*, which most people are not. In fact most people try to *avoid* risk, hence the institution of *insurance*.

The hardest to define of those terms seems *uncertainty* (Lindley, 2006), especially when contrasted with *risk*. While we have already defined – even though not completely specified – risk, it seems now the only thing left is to define uncertainty. But here we have the opinion of Frank Knight (1921), who in his view established a distinction between risk and uncertainty in this way:

> Uncertainty must be taken in a sense radically distinct from the familiar notion of Risk, from which it has never been properly separated. ... The essential fact is that 'risk' means in some cases a quantity susceptible of measurement, while at other times it is something distinctly not of this character; and there are far-reaching and crucial differences in the bearings of the phenomena depending on which of the two is really present and operating. ... It will appear that a measurable uncertainty, or 'risk' proper, as we shall use the term, is so far different from an unmeasurable one that it is not in effect an uncertainty at all.

Douglas Hubbard (2007) on the other hand gives the following distinctions, which by now have found widespread use in quantitative fields such as decision theory and statistics:

Uncertainty is a state where it is impossible to exactly or accurately describe the present state (of some system), or future outcome.

Quantification of uncertainty is the assignment of probabilities to each possible state or outcome.

Risk is a state of uncertainty where some possible outcomes have an undesirable effect, e.g. loss of life or property, damage to property.

Measurement of risk is the combination of quantified uncertainties which represent losses with their respective magnitudes of risk.

Often the term risk is used interchangeably with its measure; and the term state – unless qualified to mean the state of a system – is the state (of information) of the decision maker, or the one who might suffer the loss.

Of course the term *uncertainty* appears from philosophy, psychology, decision theory, probability, information theory to medicine and economics. It is hardly surprising that there are many different views (Tannert et al., 2007). This does not have to involve any philosophical statement on *determinism*, but may simply mean that certain things are not predictable, hence uncertainty is concerned with *unpredictability* and not a fundamental philosophical statement about the nature of the universe.

We will stick to the latter of the two views above (Kaplan and Garrick, 1981), and further only look at what is called *objective* uncertainty (Tannert et al., 2007), although *subjective* uncertainty in the form of *moral* uncertainty certainly enters many decisions concerned with structures and infrastructure and involving the hazards of loss of life and monetary costs. Objective uncertainty we will often think of as further subdivided on one hand into *aleatoric* uncertainty, where *it is in the nature of things* that we cannot give an exact description of future outcomes, and where also this uncertainty cannot be reduced arbitrarily through e.g. further measurements. The other aspect of objective uncertainty we will call *epistemic* uncertainty, i.e. it arises from our lack of information, and could possibly be reduced e.g. by further measurements. In any case one may take the uncertainty as a measure of information, our ability to predict a present state or future outcome.

While most scientists agree that aleatoric uncertainty can be measured via probability theory, and while there are convincing arguments that this is also the proper view for epistemic uncertainty (Jaynes, 2003), there are methods which are claimed to be suitable to model this kind of uncertainty, like propagation of convex sets (containing the uncertain information) (Natke and Ben-Haim, 1997; Ben-Haim and Elishakoff, 1990), or fuzzy methods (Zimmermann, 1992; Uncertainty in Engineering, 2000).

In relation to hazards, *vulnerability* is the extent to which changes can harm a system, i.e. in a certain sense its sensitivity to outside influences, or the susceptibility to damage. A very similar term is *fragility*, i.e. when small damages may yield a structure or infrastructure more or less completely useless.

2.2. INTERDEPENDENCE

To complete the picture, one should also point out the many interdependencies which exist between the various concepts.

A damage may incur further hazards, insomuch as a damage changes the state of the structure. This in turn may change the risk, as it changes maybe also the probabilities of other events stochastically dependent on the damage. It may also change the risk by changing the amount of subsequent

loss. for many interdependent systems, such as an urban area, this may lead to a cascade of risk and uncertainty.

One may now see that structural damage assessment is very similar to any other model building (Pearl, 2000) exercise, and estimation of a state as treated in many control theory texts, and system identification (Ljung, 1999).

Also obvious are similarities with risk assessment (Kumamoto and Henley, 1996), integrity or structural health monitoring (Yao and Kawamura, 2001), and performance prediction and diagnosis (Natke and Cempel, 1997). And certainly risk assessment is an integral part of any kind of risk management (Flyvbjerg, 2006).

Damage and structural reliability (Ditlevsen and Madsen, 1996; Yao and Kawamura, 2001) are similarly linked, first because structural reliability is concerned with avoiding damage, or minimizing the probability of damage occurring, and secondly because after a damage the methods of structural reliability may be used to define subsequent and dependent risks.

3. Methods

A good general overview – although somewhat restricted – for a specific but fairly exemplary application area is contained in (Net, 2000).

Methods to identify damage range from the purely educated visual (FEMA, 2004) which will always be needed as a first guess (Revadigar and Mau, 1999), to further testing (Pearl, 2000), maybe involving the theory of design of experiments (Box and Hunter, 2005), and sequential optimum design (of experiments) (Chernoff, 1972). These techniques, as well as those already mentioned in Section 2.2 in (Ljung, 1999), as well as those used to estimate the state of a system, rely heavily on *Bayesian* statistics (Lindley, 1972), enforcing the view to treat epistemic uncertainties on an equal footing via probability theory, see Section 2.1.

Eventually we want to arrive at a probabilistic risk assessment (*PRA*) (Kumamoto and Henley, 1996). To perform a PRA, an analysts may go through the following steps:

1. Specify the *hazard*, the outcome(s) to be prevented or reduced.
2. Identify initiating events, those that could possibly lead to the specified consequence.
3. Estimate the *frequency/probability* of each initiating event.
4. Assuming that the initiating event has occurred, identify the *combinations* of failures that lead to a specific outcome.

5. Compute the *likelihood* of each combination. The *probabilities* of all those sequences that lead to the same outcome are added. To determine how often this outcome might occur, these probabilities are multiplied by the frequency of the initiating event(s).

As already mentioned, probability theory (Loève, 1977; Krée and Soize, 1986; Jaynes, 2003) is used in most cases to address the uncertainty (Augusti et al., 1984; Ditlevsen and Madsen, 1996), usually on a Bayesian setting (Lindley, 1972; Jaynes, 2003). But combinations with supposedly simpler theories (usually yielding considerably less information) are also proposed. These are e.g. bounds – interval analysis, convex sets – (Natke and Ben-Haim, 1997; Ben-Haim and Elishakoff, 1990), fuzzy analysis (Zimmermann, 1992), and combinations such as *fuzzy probability*, (Uncertainty in Engineering, 2000; Möller and Beer, 1998, 2004; Möller and Reuter, 2007), see also (Elishakoff, 1999). A modification of the Bayesian point of view, which tries to accommodate conflicting information and is based on *belief* and *plausibility* is the *Dempster-Shafer* theory (Dempster, 1968; Shafer, 1976).

The uncertainty then has to be computationally propagated through the system(s). Ideally, given the probability distributions of the input, the numerical models should produce the probability distributions of the outputs, or any other stochastic information desired. This may in the simplest case be sensitivity analysis (Kleiber and Hien, 1992). It may pertain only to (asymptotically) very small probabilities (Ditlevsen and Madsen, 1996). Conceptually the simplest is the Monte Carlo method or its variants (Caflisch, 1998). Overviews are given in (Matthies and Soares, 1997; Schueller, 1997), and more recently in (Matthies, 2007a, b). Modern developments relate to the view of random variables (stochastic processes, random fields) as elements of a vector space, to be approximated through finite dimensional subspaces (Ghanem and Spanos, 1991; Matthies and Bucher, 1999; Matthies and Keese, 2005; Xiu and Karniadakis, 2002) in the sense of weighted residual Galerkin methods, which then also includes collocation methods. In some ways this may be seen as a systematic way of producing *response surfaces* (Khuri and Cornell, 1987).

4. Identifying the damage

As already mentioned, identifying the damage is very similar to system identification. In case damage occurs to a structure, there has to be a quick initial assessment of the kind

- Unsafe, dangerous to enter
- Safe, but unfit for human habitation – occupancy should be restricted

- Lightly damaged, but habitable – occupancy permitted
- Not damaged, not requiring any or only cosmetic repair

This may also involve posting the structures as "unsafe to enter" or just "inspected", meaning safe to enter.

For life-lines and infrastructure similar criteria may be drawn up, and especially for life-lines it is critical to quickly establish whether and/or to what extent are they damaged, are they completely unusable, partly usable, what is the most urgent repair to get them partly on line again? Damage to critical infrastructure includes

- Water and sewage (leaks, damaged pipes de-pressurized?)
- Electric (e.g. exposed power lines de-energized?)
- Oil and gas pipelines (e.g. line breaks sealed?, leaks contained?)
- Gas and propane storage (e.g. tanks inspected, secured by qualified experts?)

This may involve identifying qualified contractors offering damage assessment services, developing damage assessment procedures, developing mitigation plans and procedures, conducting debris assessment, and assessing the requirement for decontamination or safe demolition, removal, and disposition of contaminated debris.

It may include the provision of geo-coded status reports of community, homes and facilities identified as safe or unsafe to re-enter and re-occupy. Situation assessments are conducted using one of following methods (FEMA, 2004):

1. Aerial reconnaissance
2. Remote sensing
3. Computer modelling (e.g., HAZUS [FEMA, 2004])
4. Rapid field assessments/windshield surveys

4.1. INITIAL ASSESSMENT OF DAMAGE

Hereby we mean a more formal assessment than the *first* assessment just sketched, trying to identify the extent of damage and the state of the structure. In a Bayesian setting it may be described as guessing à priori information. Methods used beyond visual inspection are those used in any other system identification process (Revadigar and Mau, 1999), such as vibration test, (ultra-)sound testing, thermal image analysis, etc. (Natke and Cempel, 1997).

The approach yielding finally the most information is to apply a probabilistic modelling, usually on a Bayesian setting (Lindley, 1972; Jaynes, 2003). This then means assigning so-called à priori probabilities, reflecting the state of information. A modification of this is using two measures, belief and plausibility instead of just probability (Dempster, 1968; Shafer, 1976).

Also sometimes used are supposedly simpler theories – yielding less information. These include simple bounds in convex sets (Natke and Ben-Haim, 1997; Ben-Haim and Elishakoff, 1990) fuzzy analysis (Zimmermann, 1992) using possibility instead of probability, and combinations like fuzzy probability (Möller and Beer, 1998, 2004; Möller and Reuter, 2007), see (Elishakoff, 1999) for some examples.

4.2. FURTHER TESTING AND UPDATING

If after the initial assessment described in Section 4.1 the uncertainty on how to class a structure is still too large, especially when deciding whether it is safe or not, and whether it should be demolished or repaired, further testing may be required. This is intended to demonstrate the structural static/dynamic properties of the structure. It is a method to obtain à posteriori information (Lindley, 1972; Jaynes, 2003), through carefully selected experiments. This may use the techniques known as *design of experiments*, and *optimal sequential design* (Chernoff, 1972; Pearl, 2000; Box and Hunter, 2005). The à posteriori information in this approach will come through Bayesian updating of the à priori distributions as new information is included.

Computational models of the structure become very important in this whole phase, as they serve to refine the estimate of the state of the structure. They have to be able to propagate probability/uncertainty information, see the description in Section 3 and the overviews in (Matthies and Soares, 1997; Schueller, 1997). These computational models can be of differing complexity, but they may help in refining the assessment made as described in the beginning of this Section 4.

5. Contribution of decision theory

Decision theory may be used to decide on possible courses of action (Pearl, 2000; Flyvbjerg, 2006), taking care to properly estimate costs, be they due to repair, or demolition and rebuilding. There is a long history of cost-overruns in civil engineering work, and there are methods to obtain an *outside view* (Flyvbjerg, 2006). In any of these decisions, there will be a cost/benefit appraisal (Starr, 1969; Wilson and Crouch, 2001). It involves the allocation of resources for rehabilitation, rebuilding and strengthening.

Again computational models of the structures/infrastructure are very important here, as they help in evaluating different "what if?" scenarios.

If the only purpose of damage assessment was to decide what to do with damaged structures or infrastructure, the task is finished here. But if one wants to learn for the future, especially important if the damage was caused by extreme environmental forces, such as floods, storms, or earthquakes, more analysis is necessary.

6. Reconstructing/identifying the cause

In case of environmental loads leading to damage, it is often desirable to identify the magnitude of those forces, in order to learn for future events. The damaged structure or infrastructure may be used as a "measurement device". Otherwise the whole process is very similar to the one described in Section 4. Only instead of the structure, here the objective is to identify the cause for the damage, or the magnitude and nature of the environmental force. In this process, a computational model capable of propagating uncertainty/stochastic information is definitely needed.

6.1. INITIAL ASSESSMENT OF CAUSE

The initial assessment is similar to the state of the structure an "educated guess" as to the nature and magnitude of the causative action which resulted in the damage, see Section 4.1. This should ideally involve a modelling of the uncertainty of this educated guess, as to express the variation deemed possible for the environmental forces.

Concerning environmental forces, there is common agreement that probabilistic modelling is adequate, usually on a Bayesian setting (Lindley, 1972; Jaynes, 2003). This means assigning so-called à priori probabilities to actions, based on the usually extensive knowledge on how they are generated – e.g. storms, floods, earthquakes.

6.2. COMPUTATIONAL TESTING AND ACTION IDENTIFICATION

This step parallels the one in Section 4.2, only that the testing and updating is performed numerically. The numerical results then may be compared to the estimated state of the damaged structure. The whole process is very akin to system identification, this time not of the structure, but of the environmental action.

The numerical models have to propagate the probability through the system(s), as described in Section 3. As already mentioned the simplest is sensitivity analysis (Kleiber and Hien, 1992). For very small probabilities,

asymptotical methods as in structural reliability may be used (Ditlevsen and Madsen, 1996).

Conceptually the simplest method which can give complete distributional information is the Monte Carlo method or its variants (Caflisch, 1998). Overviews on all such methods is given in (Matthies and Soares, 1997; Schueller, 1997), and more recently in (Matthies, 2007a, b).

Newer developments relate to directly approximating random variables (stochastic processes, random fields) as elements of a vector space through finite dimensional subspaces (Ghanem and Spanos, 1991; Matthies and Bucher, 1999; Matthies and Keese, 2005; Xiu and Karniadakis, 2002). As already mentioned such approximations of the random quantities may be seen as a systematic way of producing response surfaces (Khuri and Cornell, 1987).

In any case, the computational models should help answer the question what are the likely distributions and magnitudes of the environmental actions, in the form of an Bayesian updating to à posteriori distributions of the à priori distributions of Section 6.1, see (Lindley, 1972; Jaynes, 2003).

7. Damage tolerant design

Having identified the type of damage, as well as the environmental actions which caused it, together with their uncertainty quantification, it is now possible to do some kind of improvement/optimization.

7.1. MINIMISE EXPECTED DAMAGE

One way to reduce risks is to reduce the hazard, e.g. to make the structure or infrastructure less prone to certain kinds of exterior actions. Especially for infrastructure life-lines this can often achieved by choosing carefully where they are installed, using redundancy, etc.

The other aspect of risk reduction is the minimization of potential loss in case the hazard *does* occur.

All of these items require a cost/benefit analysis (Starr, 1969); a guideline here may be the so-called "ALARP" principle, an acronym meaning **A**s **L**ow **A**s **R**easonably **P**racticable. It is a very common sense approach regularly practised in the off-shore industry. After a probabilistic risk assessment, the risks – of course forming a continuum – are divided into three main categories. One are those which are considered negligible, here nothing has to be done, no design optimization is necessary. At the other end are risks which are considered unacceptable, and they have to be avoided categorically. In between is the ALARP region, where risks are not negligible,

but the amount of reduction follows the ALARP principle. This means that a risk has to be reduced if this incurs no substantial costs, and all risks are reduced to the point where further efforts yield only marginal risk reductions. At this point it is usually meaningless to try to reduce the risk any further, at least not with the methods applied up to that point. Here a decision has to be taken, as to whether the residual risk is acceptable; if not the activity it is pertaining to has to be stopped, or a completely different design has to be chosen.

7.2. REDUCE VULNERABILITY AND FRAGILITY

The reduction of possible losses has at least two aspects (Douglas, 2007), one is the vulnerability, and the other the fragility.

Reduction of vulnerability may be achieved by reducing the possible impact of the hazard, in general terms moving things out of harms way. Infrastructure development considering vulnerability is especially important, to ensure that life-lines remain operable to as large an extent as possible. Structures may be valued in reference to vulnerability with impact elements, to arrive at some overall idea of vulnerability.

Fragility is a property of the structures or the infrastructure. It may be reduced through robust design, i.e. designs which do not suddenly increase the risk due to smaller damages. It can often represented through so-called fragility curves, showing the risk versus larger magnitude of the actions. In these circumstances a design which has only slowly varying risk with a gradual increase in magnitude is less fragile, there cannot be any unexpected failures. Often, for structures, this boils down to the existence of several load paths, i.e. statically highly indeterminate designs. This is often at variance with traditional design methods, and also often contradict "optimal designs" which are optimal with respect to other criteria, like minimum weight or minimal cost.

Methods used here are similar to those in structural reliability analysis (Augusti et al., 1984; Ditlevsen and Madsen, 1996), where it is also important to estimate the sensitivity of the risk to design parameters.

8. Conclusion

This article has tried to illuminate the issues involved in structural damage and risk assessment, and on the interplay between structural damage and risk assessment on one hand and numerical techniques, especially for uncertainty quantification, on the other hand.

Damage assessment and risk quantification are closely interrelated, once the basic terms have been defined this becomes very clear. Damage

assessment and risk quantification go hand in hand from very simple to more and more sophisticated, such as time and possible expenses allow, and as is meaningful for the questions at hand. The similarities to statistical system identification have been highlighted. Any decision on possible actions involves a cost/benefit appraisal on the basis of present information.

If the damage was caused by environmental forces such as seismic action, one may use the damaged structures as a "measurement device" to determine the characteristic of this external action. This is similar to the system identification of the structure with testing purely computational. Reduction of risk is possible by considering the vulnerability and fragility of design of life-lines, infrastructure, and structures.

References

Augusti, G., Baratta, A., and Casciati, F. (1984) *Probabilistic Methods in Structural Engineering*, Chapman & Hall, London.

Ben-Haim, Y. and Elishakoff, I. (1990) *Convex Models of Uncertainty in Applied Mechanics*, Elsevier, Amsterdam.

Box, G. E., William, G. and Hunter, J. S. H. (2005) *Statistics for Experimenters: Design, Innovation, and Discovery*, Wiley, Hoboken, NJ.

Caflisch, R. E. (1998) Monte Carlo and quasi-Monte Carlo methods, *Acta Numer.* **7**, 1–49.

Chernoff, H. (1972) *Sequential Analysis and Optimal Design*, SIAM, Philadelphia, PA.

Dempster, A. P. (1968) A generalization of Bayesian inference, *J. Royal Stat. Soc. – Ser. B* **30**, 205–247.

Ditlevsen, O. and Madsen, H. O. (1996) *Structural Reliability Methods*, Wiley, Hoboken, NJ.

Douglas, J. (2007) Physical vulnerability modelling in natural hazard risk assessment, *Nat. Hazards Earth Syst. Sci. (www.nat-hazards-earth-syst-sci.net/7/283/2007/)* **7**, 283–288.

Elishakoff, I. (1999) *Whys and Hows in Uncertainty Modelling–Probability, Fuzziness, and Anti-optimization*, Springer, Berlin.

FEMA (2004) *HAZUS-MH Technical Manual*, Washington, DC (http://www.fema.gov/hazus/dl-sr2.shtm).

Flyvbjerg, B. (2006) From Nobel Prize to project management: Getting risks right, *Proj. Manage. J.* **37**, 5–15.

Ghanem, R. and Spanos, P. (1991) *Stochastic Finite Elements – A Spectral Approach*, Springer, Berlin.

Hubbard, D. (2007) *How to Measure Anything: Finding the Value of Intangibles in Business*, Wiley, Hoboken, NJ.

in Engineering, Uncertainly (2000) (http://www.uncertainty-in-engineering.net/).

Jaynes, E. T. (2003) *Probability Theory, The Logic of Science*, Cambridge University Press, Cambridge.

Kaplan, S. and Garrick, B. J. (1981) On the quantitative definition of risk, *Risk Anal.* **1**, 11–37.

Khuri, A. and Cornell, J. (1987) *Response Surfaces: Designs and Analyses*, Marcel Dekker, New York.

King, A., Kiremidjian, S., Basöz, N., Law, K., Vučetić, M., Doroudian, M., Olson, R., Eidinger, J., Goettel, K., and Horner, G. (1997) Methodologies for evaluating the socio-economic consequences of large earthquakes, *Earthq. Spect.* **13**, 565–584.

Kleiber, M. and Hien, T. D. (1992) *The Stochastic Finite Element Method. Basic Perturbation Technique and Computer Implementation*, Wiley, Hoboken, NJ.

Knight, F. H. (1921) *Risk, Uncertainty, and Profit*, Hart, Schaffner & Marx; Houghton Mifflin Company, Boston, MA.

Krée, P. and Soize, C. (1986) *Mathematics of Random Phenomena – Random Vibrations of Mechanical Structures*, D. Reidel, Dordrecht.

Kumamoto, H. and Henley, E. J. (1996) *Probabilistic risk assessment and management for engineers and scientists*, IEEE Press, New York.

Lindley, D. V. (1972) *Bayesian Statistics, a Review*, SIAM, Philadelphia PA.

Lindley, D. V. (2006) *Understanding uncertainty*, Wiley, Hoboken, NJ.

Ljung, L. (1999) *System Identification – Theory for the User*, Prentice Hall, Upper Saddle River, NJ.

Loève, M. (1977) *Probability Theory*, Springer, Berlin.

Matthies, H. G. (2007a) Quantifying uncertainty: Modern computational representation of probability and applications. In A. Ibrahimbegović and I. Kožar (Eds.), *Extreme Man-Made and Natural Hazards in Dynamics of Structures*, NATO-ARW, Springer, Verlag, Berlin.

Matthies, H. G. (2007b) Uncertainty quantification with stochastic finite elements. In E. Stein, R. de Borst, and T. J. R. Hughes, (Eds.), *Encyclopedia of Computational Mechanics*. Wiley, Hoboken, NJ.

Matthies, H. G. and Bucher, C. (1999) Finite elements for stochastic media problems, *Comp. Meth. Appl. Mech. Eng.* **168**, 3–17.

Matthies, H. G. and Keese, A. (2005) Galerkin methods for linear and nonlinear elliptic stochastic partial differential equations, *Comp. Meth. Appl. Mech. Eng.* **194**, 1295–1331.

Matthies, H. G, Brenner, C.E. and Soares, C. G. B. (1997) Uncertainties in probabilistic numerical analysis of structures and solids – stochastic finite elements, *J. Stuct. Safety* **19**(3), 283–336.

Möller, B. and Beer, M. (1998) Safety assessment using fuzzy theory, *In: Proceedings of the 1998 International Computing Congress in Civil Engineering,* ASCE, Boston, MA.

Möller, B. and Beer, M. (2004) *Fuzzy Randomness*, Springer, Berlin.

Möller, B. and Reuter, U. (2007) *Uncertainty Forecasting in Engineering*, Springer, Berlin.

Natke, H. G. and Ben-Haim, Y. (1997) *Uncertainty: Models and Measures*, Akademie, Berlin.

Natke, H. G. and Cempel, C. (1997) *Model-Aided Diagnosis of Mechanical Systems*, Springer, Berlin.

Net, F. R. (2000) (http://www.floodrisknet.org.uk/).

Pearl, J. (2000) *Causality: Models, Reasoning and Inference*, Cambridge University Press, Cambridge.

Revadigar, S. and Mau, S. T. (1999) Automated multi-criterion building damage assessment from seismic data, *J. Struct. Eng.* **125**(2), 211–217.

Schueller, G. (1997) A state of the art report on computational stochastic mechanics, *Prob. Eng. Mech.* **12**(4), 197–321.

Shafer, G. (1976) *A Mathematical Theory of Evidence*, Princeton University Press, Princeton, NJ.

Starr, C. (1969) Social benefit versus technological risk, *Science* **165**(3899), 1232–1238.

Tannert, C., Elvers, H.-D., and Jandrig, B. (2007) The ethics of uncertainty, *EMBO Rep.* **8**(10), 892–896.

Wilson, R. and Crouch, E. (2001) *Risk/Benefit Analysis*, Harvard University Press, Cambridge, MA.

Xiu, D. and Karniadakis, G. E. (2002) Modeling uncertainty in steady state diffusion problems via generalized polynomial chaos, *Comp. Meth. Appl. Mech. Eng.* **191**, 4927–4948.

Yao, J. T. P. and Kawamura, H. (2001) On structural reliability, *J. Temporal Des. Arch. Environ.* **12**, 34–48.

Zimmermann, H. (1992) *Fuzzy Set Theory and Its Applications*, Kluwer, Boston London.

COMPUTATIONAL VERIFICATION AND VALIDATION OF ENGINEERING STRUCTURES VIA ERROR-CONTROLLED MODEL AND DISCRETIZATION ADAPTIVITY

E. Stein[1] (erwin.stein@ibnm.uni-hannover.de), M. Rüter[1], S. Ohnimus[2] and K. Wiechmann[3]
[1] *Institute of Mechanics and Computational Mechanics, Leibniz Universität Hannover, Germany*
[2] *INPRO GmbH, Berlin, Germany*
[3] *Consulting Engineer, Ingolstadt, Germany*

Abstract. In the European Union, codes and rules for guaranteeing safety and reliability of engineering structures are standardized in Eurocode EN 1990 – Basis of Structural Design.

Furthermore, ASME has released the V&V 10 – 2006 Guide for Verification and Validation in Computational Solid Mechanics, treating verified and validated mathematical models as well as verified computer codes. The issues of the ASME V&V Guide are not considered in Eurocode EN 1990 yet.

V&V is realized in Computational Mechanics by error-controlled model and discretization adaptivity of engineering structures, guaranteeing reliability and achieving computational efficiency. This is the main issue of this paper.

In particular, expansive model adaptivity from coarse to fine mathematical models in related subdomains is reasonable and efficient, in contrast to recursive model adaptivity. Validation needs the incorporation of verified measurements from physical experiments.

This paper presents a deterministic methodology for combined verification and model adaptivity by overall error control of quantities of interest. The necessary prolongation of coarse model solutions into the solution space of a fine model for defining a consistent model error is emphasized.

Another noteworthy part of the paper is the structural optimization of engineering structures with elasto-plastic deformations under shakedown conditions, i.e. for load domains. This is motivated by the fact that structural optimization in the presence of elasto-plastic deformations for distinct loading paths does not make any sense.

Finally, this paper also presents some design problems of a very complex structure: the German Pavilion at the World Exhibition 2000 in Hannover with principally new concave glass facades and glass-stiffened pre-stressed steel columns for supporting the huge roof. Especially the safety requirements for the various glass structures are discussed.

Keywords: Verification and validation, finite element method, combined model and discretization adaptivity, structural optimization under shakedown conditions, safety aspects of concave glass facades and glass-stiffened steel columns

A. Ibrahimbegovic and M. Zlatar (eds.), *Damage Assessment and Reconstruction After War or Natural Disaster*,

1. Computational verification and validation for achieving reliability and efficiency requirements

1.1. VERIFICATION AND VALIDATION

Error-controlled adaptivity of (mathematical) modeling and discretization in Computational Mechanics – called AM-FEM – is an important requirement for achieving the *verification* of numerical approximations and the *validation* of models (chosen as coarse as admissible and as fine as necessary in engineering designs), accompanied by experimental data and experience. An approximate numerical solution without error estimation and error bounds is – at least from a mathematical point of view – without any value.

This paradigm involves much deeper and broader knowledge and understanding of all ingredients of Computational Mechanics than for just successfully applying a finite element program, and even more it requires networked thinking, as represented in Fig. 1 by M.C. Escher's Bond of Union, expressing creativity by communication and reproduction.

Model verification is understood as approximately *solving the model equations right* with a given bounded error tolerance of the a posteriori discretization error estimator used.

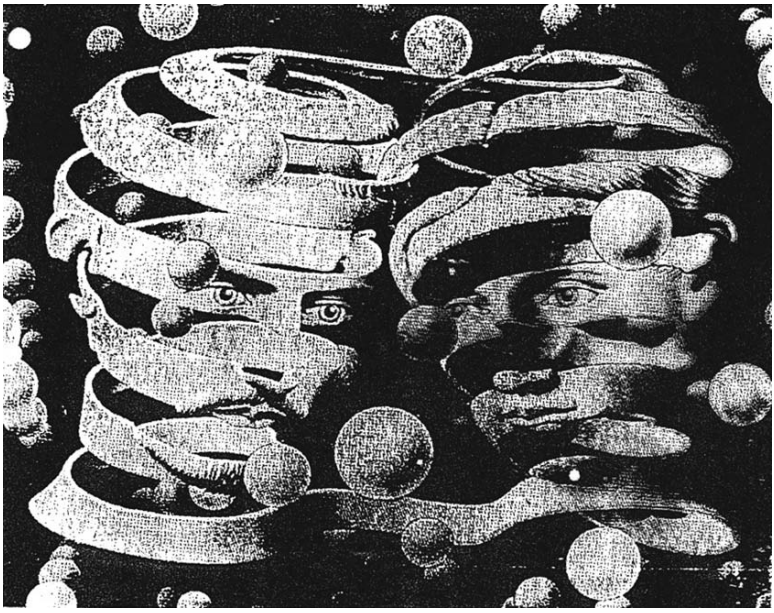

Figure 1. Bond of Union by M.C. Escher, 1956. The M.C. Escher Company B.V.

Model validation is defined as approximately *solving the right (adequate goal-oriented) model equations* with a given tolerance of the a posteriori modeling error estimator used, ensuring by verified experimental data that the mathematical model represents the physical event with a given error tolerance.

This validation includes the identification (or at least calibration) of mathematical and system parameters of the model at least in a deterministic or – if necessary – in a statistical format.

In this paper, only pre-homogenized continua and structures (i.e. macro-models) are regarded as one-scale models. Multi-scale models for micro-heterogeneous materials (e.g. fiber-reinforced epoxies) are not considered here. Moreover, only robust (locking-free) conforming finite elements are used.

The crucial question whether a certain goal-oriented mathematical model – a theory – of a well-defined physical event or process is true, is a complicated matter of the Theory of Science, which was brought up already by Gottfried Wilhelm Leibniz in the 17*th* century, then developed systematically by Immanuel Kant in the 18*th* century, and again treated profoundly by Karl Raimund Popper (1959) in the 20*th* century, regarding the tremendous importance of the validity of mathematical models not only in the technical world, but also in nearly all branches of modern life. Kant's famous statement *that such a theory can never be finally true because it might be falsified by only one new event* has initiated many discussions through the centuries. But according to today's understanding it is also not true to claim that a whole theory is false when specific new events do not fit, see Kuhn (1962) and Roache (1998), and this was already stated by Leibniz.

In this spirit, *post audit prediction by chance* in checking predicted values and so-called *corroboration* as weaker demands than full validation were proposed by Popper.

1.2. EXPLICIT AND IMPLICIT GLOBAL A POSTERIORI DISCRETIZATION ERROR ESTIMATES FOR THE FINITE ELEMENT METHOD

In the stormy developments of Computational Mechanics since the early 1960s – primarily stimulated and enforced by engineers – the crucial mathematical questions of existence, stability and convergence, as well as a priori and a posteriori error estimates have been investigated since the late 1970s, especially by Babuška and Rheinboldt (1978) and Babuška and Miller (1987).

A fundamental result for the a priori error estimator of the discretization error $\boldsymbol{e} = \boldsymbol{u} - \boldsymbol{u}_h$ with the analytical solution $\boldsymbol{u} \in H^2(\Omega)$ for regular boundary conditions and loading and the finite element solution $\boldsymbol{u}_h \in H^1(\Omega)$ in the energy norm is $||\boldsymbol{e}||_E = C_i C_s h^p$ with upper and lower bounds, where C_i and C_s are the interpolation and stability constants, h is the characteristic mesh width of the finite element mesh, and p is the power of the polynomial trial-and-test functions of a finite element. This formula holds for conforming finite elements, approximating mixed boundary value problems of second-order elliptic PDEs.

The following two types of *global explicit relative a posteriori error estimators* are important:

(i) The estimator in the energy norm by Babuška and Miller (1987) and

(ii) The gradient smoothing estimator, expressed in an engineering style by approximated stresses in the complementary energy norm by Zienkiewicz and Zhu (1987) and mathematically proven by Carstensen and Funken (2001)

While the error estimator in the energy norm requires the jumps of the tractions at element interfaces (as strong residua of equilibrium), the gradient averaging estimator needs only information from Gauss points within element domains. This has the important advantage that – at the time – only internal element data are available in commercial computer programs for mesh refinement criteria, but not on element interfaces, e.g. in Abaqus and Ansys.

Both types of relative error estimators are calculated explicitly, i.e. without the solution of algebraic equations.

In contrast to *explicit – or relative – error estimators* with undetermined interpolation constants, the following *implicit – or absolute – a posteriori error estimators* were developed, requiring postprocessing with higher-order test functions, i.e. the solution of further algebraic equations on the element or element patch level:

(i) *Implicit energy-based estimators.*

  (a) In the first type, improved boundary tractions are calculated with locally *equilibrated Neumann problems* on the element level, see Ladevèze and Leguillon (1983), Bank and Weiser (1985), Ainsworth and Oden (1993) and Brink and Stein (1998), the latter for finite elastic deformations.

  (b) *Hierarchical error estimators* were used by Bank and Smith (1993) and

  (c) *Subdomain-based flux-free estimators* were developed by Parés et al. (2006).

(ii) *Implicit gradient averaging estimators* were proposed by Zienkiewicz and Zhu (1992) by choosing enhanced test functions on patches around each element, called SPR (superconvergent patch recovery), which is widely used in engineering practice.

It should be stated once more that convergence – and thus verification – of adaptive *hp*-refinements requires the knowledge of the function space of the true solution as well as the conforming function space of the test functions of the computational model. If, for example, the true solution is contained in the Sobolev space $H^{1-\epsilon}(\Omega), \epsilon < 1$, which holds for plane stress problems with point loads, then the finite element solution in the Sobolev space $H^1(\Omega_h)$ cannot converge to the analytical solution.

1.3. A POSTERIORI DISCRETIZATION ERROR ESTIMATORS FOR QUANTITIES OF INTEREST

A new important type of a posteriori error estimators for errors of quantities of interest has been developed since the mid–1990s, by Eriksson et al. (1995), further with algorithmic enhancements by Becker and Rannacher (1996), and with studying the pollution error in the *h*-version by Babuška et al. (1997). The quantities of interest are defined beneficially as linear or nonlinear functionals, providing reciprocity (symmetry) properties. The error analysis requires the dual numerical problem, which is always linear.

Cirak and Ramm (1998) used Betti's reciprocity theorem for deriving the dual error analysis, and Ohnimus et al. (2001) introduced errors of quantities of interest for error estimators with implicit postprocessing via local Neumann problems, whereas Larsson et al. (2002) used hierarchical bases.

Error estimates for quantities of interest play an important role in fracture mechanics, where the Rice integral (for 2D problems) and more general the energy release rate as the quantity of interest is the predominant searched quantity, see Rüter and Stein (2004).

Concerning 1.2 and 1.3, the textbooks by Verfürth (1996), Ainsworth and Oden (2000), and Braess (2001) are recommended for basic studies, as well as the article by Stein and Rüter (2007).

1.4. COMBINED MODEL AND DISCRETIZATION A POSTERIORI ERROR ESTIMATORS

It is a natural and necessary demand for engineering analysis that the discretization error should be of the same order of magnitude as the modeling error. Usually, it is not possible to find one adequate mathematical model

(e.g. a certain shell theory) in order to cover all essential physical effects of a complex structure with safe load carrying for all given loadings at a prescribed error tolerance. It is obvious that smaller error tolerances for verification and modeling cause finer models in larger subdomains.

Moreover, several models are required mostly in different subdomains, and they might have to be expanded (or enhanced), depending on the deformation process. Thus, boundary layers of elastic plates and shells approximated with 2D theories require enhanced theories or full 3D theory. The same holds for various geometrical and physical irregularities, such as small holes, concentrated loads, or severe changes of physical data. Also structural instabilities and inelastic deformations of stiffened thin-walled structures may arise in the loading process. Nevertheless, it is neither recommendable nor efficient to begin such a structural analysis with the finest model in question that takes care for all expected effects, but to begin with a rather coarse model, e.g. a linear elastic beam model for a wide-spanned bridge, and to expand this theory according to all insufficiencies.

Coupling of finite elements having 1D or 2D kinematics with those having 3D kinematics (dimensional adaptivity) usually requires transition elements in order to avoid locking. This would highly complicate model adaptivity in variable subdomains. Therefore, all finite plate and shell elements are defined with $2\frac{1}{2}$D kinematics here, containing at least constant strains in the transverse (normal) direction. The weak kinematic transitions from 2D to 3D theories are realized by penalized least-squares conditions, see Stein et al. (2007) and Section 3.4.

For efficient convergence, thin plates and shells which are computationally modeled with 3D elements should have different p-orders of the trial and test polynomials in tangential and normal directions. In regular cases, p in tangential directions should be larger than in the normal direction. However, concerning boundary layers, e.g. of a clamped plate calculated with 3D finite elements of the p-version, $p = 5$ in the transverse direction covers all elastic 3D effects.

For advanced applications of pFEM, see Rank et al. (2005) and Düster and Rank (2002).

Hierarchical sequences of approximated linear and nonlinear shell and plate theories are used for model adaptivity, derived from full 3D theory as shown by Bischoff et al. (2004).

The following *strategies have been developed for combined discretization and model adaptivity* for – mainly thin-walled – structures (for surveys see Stein et al. [1997], Stein and Rüter [2007], Oden et al. [2001], Oden and Prudhomme [2002], Düster et al. [2007], and Carey [2006]):

(i) Using a *hierarchical sequence of elastic 2D plate and shell theories by model reduction* from 3D theory, based on the p-version of FEM (see Vogelius and Babuška [1981] and Szabó and Sahrmann [1988]), controlled by the two order parameters p and q (p denotes the polynomial degree in terms of standard shell coordinates, and q holds for the polynomial degree in normal direction of the shell mid-surface).
Computable upper-bound error estimators were given by Schwab (1996), presuming that the resulting 2D PDEs (by reduction) are solved with prescribed error tolerances.

(ii) *Hierarchical $h - pq$ discretization and model adaptivity by reduction* based on a priori hierarchical model and discretization error estimates, as well as an a posteriori estimate for the discretization error, see Oden and Cho (1996). The model and discretization errors are controlled in the whole domain of a system.

(iii) Using a *hierarchical sequence of elastic beam, plate, and shell models with model expansions* by dimensional adaptivity from 1D and 2D to full 3D theories, and correspondingly upgrading the constitutive equations, controlled by combined discretization and model errors (Stein and Ohnimus 1997, 1999; Stein et al. 1992a, 2004, 2007; Niekamp and Stein, 2002). The whole adaptive process starts with the coarsest reasonable goal-oriented low-dimensional model with parallel analysis of the next finer – expanded – model in order to calculate the model error which needs a prolongation of the discretized solution of the coarse model to the solution space of the finer discretized model. The model is automatically expanded (improved) in disturbed subdomains.
In order to avoid locking, $2\frac{1}{2}$D plate elements with at least constant strain modes in the thickness direction are used, see Stein et al. (2007).

(iv) *Local model adaptivity* in small disturbed areas, especially for locally inelastic deformations within mostly elastic systems (Oden and Prudhomme, 2002; Larsson and Runesson, 2005, 2006).

1.5. A STRATEGIC SCHEME FOR VERIFICATION AND VALIDATION IN COMPUTATIONAL MECHANICS

A strategic scheme for verification and validation in computational mechanics is shown in Fig. 2. The problem of identification of material and system parameters – generally taking stochastic phenomena into account has also to be solved herein. This type of problems, however, is not treated in this paper.

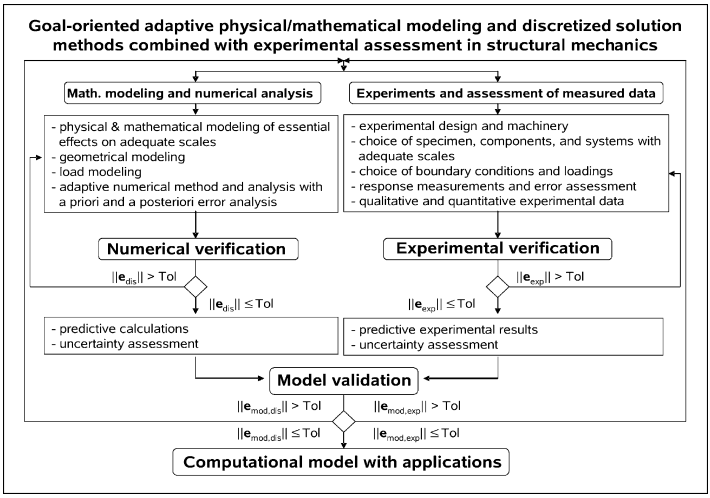

Figure 2. Flowchart of combined error-controlled adaptive modeling, computation and experiments. $\boldsymbol{e}_{\mathrm{dis}}$: discretization error (of quantity of interest), $\boldsymbol{e}_{\mathrm{exp}}$: measuring error, $\boldsymbol{e}_{\mathrm{mod,dis}}$: combined model and discretization error, $\boldsymbol{e}_{\mathrm{mod,exp}}$: combined model and measuring error

1.6. EUROPEAN STANDARDS FOR SAFETY AND RELIABILITY – BASIS OF STRUCTURAL DESIGN

Eurocode EN 1990 (2002) is the basis for guaranteeing safe and reliable resitancies of engineering structures against the effects of actions due to regular and exceptional loads and events in Europe. All the other nine Eurocodes for traditional and new types of materials and structures refer to Eurocode EN 1990 (2002).

Structural safety has to be achieved for the condition:

[design values of structural resistance (R_d)] $\geq$ [design values of the effects of actions for an ultimate load state (E_d), $R_d \geq E_d$].

The safety concept is semi-probabilistic, i.e. probabilistic for the effects of actions (e.g. due to wind loads) and – still – deterministic for material resistances such as material strength data and material parameters in constitutive equations. Split and uncorrelated partial safety factors are used for combined actions of different types of loadings because linear superpositions are not valid in general.

The following types of actions have to be investigated:

(i) Ultimate load limit states for given types of actions (combined loading cases multiplied with partial safety factors); (ii) fatigue limit states; and (iii) serviceability limit states (including limits of deformations for guaranteeing functions.)

The (generally non-linear) calculation of the effects of actions of ultimate limit states has to consider the material strengths including inelastic deformations as well as local and global system instabilities, implementing material and geometric system imperfections according to special codes and rules.

These numerical calculations are usually performed today with non-linear deterministic computational models using commercial finite element programs. But the Eurocodes do not recommend adequate mathematical models for certain problems, e.g. for elastic-plastic buckling of stiffened steel girders, and they do not prescribe error tolerances for finite element solutions.

There is only a remark in Eurocode EN 1990 (2002) that so-called "model factors" can be used for covering "model uncertainties".

Therefore, from the view of verification and validation requirements, see Fig. 2, Eurocode EN 1990 (2002) and all the other related Eurocodes show strong deficits at the important interface to computational modeling and approximation. In the authors' opinion the Eurocodes should be upgraded and adapted to the reality of computational structural design.

2. Variational framework for error-controlled combined model and discretization adaptivity of nonlinear elastic thin-walled structures

2.1. CONCEPT FOR COMBINED MODEL AND DISCRETIZATION ADAPTIVITY BY MODEL EXPANSION

This concept is based on the fact that engineering design begins with rather coarse mathematical and computational models which are then expanded to more refined ones, gradually regarding more and more essential effects for ultimate load behavior. Moreover, this is more efficient than solving very complex and large equation systems from the very beginning.

Therefore, model expansions in related subdomains of the system are used instead of model reductions in order to realize equal tolerances of suitable a posteriori error measures of the model and the discretization errors for essential quantities of interest instead of applying global energy-based or gradient-smoothing error estimates.

The expanded models should be embedded in a hierarchical sequence. Here, the Reissner–Mindlin plate theory is used as the coarse model, enhanced by constant strain terms in transverse direction in order to avoid locking of related $2\frac{1}{2}$D finite plate elements with neighboring 3D finite solid elements, derived from 3D theory of elasticity as the fine (reference) model.

An important issue of expansive model adaptivity is the necessary prolongation of approximated coarse model solutions from the solution space $\mathcal{V}_{m,h}$ into the finite-dimensional solution space $\mathcal{V}_{m+1,h}$ of the fine model in order to define admissible model errors. These matters will be treated in the sequel, see also Stein et al. (1997, 2007).

2.2. THE MODEL ERROR AND THE DISCRETIZATION ERROR

As a starting point to derive error estimates for the model and the discretization error, let us consider the fine model $m+1$ whose domain of interest is given by the closure of a bounded open set $\Omega_{m+1} \subset \mathbb{R}^3$ with a piecewise smooth and polyhedral boundary $\Gamma_{m+1} = \partial\Omega_{m+1}$ such that $\Gamma_{m+1} = \bar{\Gamma}_{m+1,D} \cup \bar{\Gamma}_{m+1,N}$ and $\Gamma_{m+1,D} \cap \Gamma_{m+1,N} = \emptyset$, where $\Gamma_{m+1,D}$ and $\Gamma_{m+1,N}$ are the portions of the boundary where Dirichlet and Neumann boundary conditions are imposed, respectively.

The associated abstract nonlinear variational problem reads: find a solution $\boldsymbol{u}_{m+1}$ in an appropriate Sobolev space $\mathcal{V}_{m+1}$ such that

$$a_{m+1}(\boldsymbol{u}_{m+1}; \boldsymbol{v}) = F_{m+1}(\boldsymbol{v}) \quad \forall \boldsymbol{v} \in \mathcal{V}_{m+1}. \tag{1}$$

Here, $a_{m+1} : \mathcal{V}_{m+1} \times \mathcal{V}_{m+1} \to \mathbb{R}$ denotes a semi-linear form, i.e. it is linear only with respect to its second argument, and $F_{m+1} : \mathcal{V}_{m+1} \to \mathbb{R}$ is a linear functional.

In the coarse model m, we seek a solution $\boldsymbol{u}_m \in \mathcal{V}_m$ such that

$$a_m(\boldsymbol{u}_m; \boldsymbol{v}) = F_m(\boldsymbol{v}) \quad \forall \boldsymbol{v} \in \mathcal{V}_m, \tag{2}$$

where $a_m : \mathcal{V}_m \times \mathcal{V}_m \to \mathbb{R}$ and $F_m : \mathcal{V}_m \to \mathbb{R}$ are the semi-linear and linear forms, respectively, associated with the coarse model m. It is important to point out that the test and solution space $\mathcal{V}_m$ is generally *not* a subspace of $\mathcal{V}_{m+1}$, since, typically, the domains of interest associated with the fine and the coarse model are different whenever the models considered have different dimensions.

Once the coarse model is established, it is usually observed that an analytical solution cannot be determined. We therefore approximate the exact solution by the finite element solution $\boldsymbol{u}_{m,h} \in \mathcal{V}_{m,h} \subset \mathcal{V}_m$ of the coarse model m which solves the discretized variational problem

$$a_m(\boldsymbol{u}_{m,h}; \boldsymbol{v}) = F_m(\boldsymbol{v}) \quad \forall \boldsymbol{v} \in \mathcal{V}_{m,h}. \tag{3}$$

We are now in a position to define the errors resulting from the variational problems presented above. Here, the model error is simply defined as

$$\boldsymbol{e}_{\text{mod}} = \boldsymbol{u}_{m+1} - \mathcal{P}\boldsymbol{u}_m \quad \in \mathcal{V}_{m+1}, \tag{4}$$

where we introduced the linear prolongation operator $\mathcal{P} : \mathcal{V}_m \to \mathcal{V}_{m+1}$. Further properties and the construction of this operator are discussed in Stein et al. (2007).

Next, let us introduce the error obtained while discretizing the variational problem (2) which is naturally defined as

$$\boldsymbol{e}_{m,\mathrm{dis}} = \boldsymbol{u}_m - \boldsymbol{u}_{m,h} \quad \in \mathcal{V}_m. \tag{5}$$

Finally, upon combining the model error (4) and the discretization error (5), we end up with the model and discretization error

$$\boldsymbol{e}_{\mathrm{mod,dis}} = \boldsymbol{e}_{\mathrm{mod}} + \mathcal{P}\boldsymbol{e}_{m,\mathrm{dis}} \quad \in \mathcal{V}_{m+1} \tag{6a}$$

$$= \boldsymbol{u}_{m+1} - \mathcal{P}\boldsymbol{u}_{m,h}. \tag{6b}$$

2.3. ERROR REPRESENTATION

In what follows, we shall derive error representation formulas for the model error $\boldsymbol{e}_{\mathrm{mod}}$ and the discretization error $\boldsymbol{e}_{m,\mathrm{dis}}$. To begin with, we introduce the weak form of the residual $R_{m+1} : \mathcal{V}_{m+1} \to \mathbb{R}$ associated with the fine model, defined by

$$R_{m+1}(\boldsymbol{v}) = F_{m+1}(\boldsymbol{v}) - a_{m+1}(\mathcal{P}\boldsymbol{u}_{m,h}; \boldsymbol{v}). \tag{7}$$

Particularly, R_{m+1} can be split into a part resulting from the model error

$$R_{\mathrm{mod}}(\boldsymbol{v}) = F_{m+1}(\boldsymbol{v}) - a_{m+1}(\mathcal{P}\boldsymbol{u}_m; \boldsymbol{v}) \tag{8}$$

and into a part resulting from the discretization error

$$R_{m+1,\mathrm{dis}}(\boldsymbol{v}) = a_{m+1}(\mathcal{P}\boldsymbol{u}_m; \boldsymbol{v}) - a_{m+1}(\mathcal{P}\boldsymbol{u}_{m,h}; \boldsymbol{v}) \tag{9}$$

such that $R_{m+1}(\boldsymbol{v}) = R_{\mathrm{mod}}(\boldsymbol{v}) + R_{m+1,\mathrm{dis}}(\boldsymbol{v})$.

Let us further consider the weak form of the residual associated with the coarse model, defined by

$$R_{m,\mathrm{dis}}(\boldsymbol{v}) = F_m(\boldsymbol{v}) - a_m(\boldsymbol{u}_{m,h}; \boldsymbol{v}). \tag{10}$$

Now, with (2) and (3) it is evident that the above residual vanishes for all functions $\boldsymbol{v} \in \mathcal{V}_{m,h}$ due to the Galerkin orthogonality. We further remark that the weak residual (8) does not generally vanish for functions $\boldsymbol{v}$ in $\mathcal{V}_{m+1,h}$, since the prolongated solution of the coarse model $\mathcal{P}\boldsymbol{u}_m$ is not obtained by a Galerkin method.

For the sake of simplicity, let us assume that the errors $\boldsymbol{e}_{\mathrm{mod}}$ and $\boldsymbol{e}_{m,\mathrm{dis}}$ are small. In these cases, it is easy to see that the model error can be represented in terms of the variational equation

$$a_{m+1,T}(\boldsymbol{e}_{\mathrm{mod}}, \boldsymbol{v}) = R_{\mathrm{mod}}(\boldsymbol{v}) \quad \forall \boldsymbol{v} \in \mathcal{V}_{m+1}, \tag{11}$$

whereas in the case of the discretization error, we arrive at the error representation

$$a_{m,T}(\boldsymbol{e}_{m,\mathrm{dis}}, \boldsymbol{v}) = R_{m,\mathrm{dis}}(\boldsymbol{v}) \quad \forall \boldsymbol{v} \in \mathcal{V}_m. \tag{12}$$

Here, $a_{m+1,T} : \mathcal{V}_{m+1} \times \mathcal{V}_{m+1} \to \mathbb{R}$ and $a_{m,T} : \mathcal{V}_m \times \mathcal{V}_m \to \mathbb{R}$ are tangent forms (linearizations) of a_{m+1} and a_m, respectively, defined by Gâteaux derivatives.

2.4. GOAL-ORIENTED ERROR MEASURES

Upon introducing the generally nonlinear goal quantity of interest as a linear or nonlinear functional $Q_{m+1} : \mathcal{V}_{m+1} \to \mathbb{R}$, we next introduce the goal-oriented error measure

$$E(\boldsymbol{u}_{m+1}, \mathcal{P}\boldsymbol{u}_{m,h}) = Q_{m+1}(\boldsymbol{u}_{m+1}) - Q_{m+1}(\mathcal{P}\boldsymbol{u}_{m,h}). \tag{13}$$

As with the weak residual R_{m+1}, we may split the error measure E into parts resulting from the model and the discretization errors. Hence, we get

$$E(\boldsymbol{u}_{m+1}, \mathcal{P}\boldsymbol{u}_{m,h}) = E_{\mathrm{mod}}(\boldsymbol{u}_{m+1}, \mathcal{P}\boldsymbol{u}_m) + E_{m,\mathrm{dis}}(\mathcal{P}\boldsymbol{u}_m, \mathcal{P}\boldsymbol{u}_{m,h}) \tag{14}$$

with

$$E_{\mathrm{mod}}(\boldsymbol{u}_{m+1}, \mathcal{P}\boldsymbol{u}_m) = Q_{m+1}(\boldsymbol{u}_{m+1}) - Q_{m+1}(\mathcal{P}\boldsymbol{u}_m) \tag{15}$$

and

$$E_{m,\mathrm{dis}}(\mathcal{P}\boldsymbol{u}_m, \mathcal{P}\boldsymbol{u}_{m,h}) = Q_{m+1}(\mathcal{P}\boldsymbol{u}_m) - Q_{m+1}(\mathcal{P}\boldsymbol{u}_{m,h}). \tag{16}$$

For (nearly) pointwise supports of Q (averaged by the finite element shape functions) we construct a functional $Q_m : \mathcal{V}_m \to \mathbb{R}$ such that the analytical reciprocity property $Q_{m+1}(\mathcal{P}\boldsymbol{u}_m) = Q_m(\boldsymbol{u}_m)$ holds and thus for discretized coarsed models $Q_{m+1}(\mathcal{P}\boldsymbol{u}_{m,h}) = Q_m(\boldsymbol{u}_{m,h})$.

Now, it is easy to see that we are able to replace E_{dis} with

$$E_{m,\mathrm{dis}}(\boldsymbol{u}_m, \boldsymbol{u}_{m,h}) = Q_m(\boldsymbol{u}_m) - Q_m(\boldsymbol{u}_{m,h}) \tag{17}$$

such that the split (14) becomes

$$E(\boldsymbol{u}_{m+1}, \mathcal{P}\boldsymbol{u}_{m,h}) = E_{\mathrm{mod}}(\boldsymbol{u}_{m+1}, \mathcal{P}\boldsymbol{u}_m) + E_{m,\mathrm{dis}}(\boldsymbol{u}_m, \boldsymbol{u}_{m,h}), \tag{18}$$

where no prolongation is required in the term $E_{m,\mathrm{dis}}$.

Since the error measure E is generally nonlinear, we next introduce suitable linearizations in terms of tangent forms of E. In the case of small model and discretization errors we thus obtain

$$E_{\mathrm{mod}}(\boldsymbol{u}_{m+1}, \mathcal{P}\boldsymbol{u}_m) = E_{\mathrm{mod},T}(\boldsymbol{e}_{\mathrm{mod}}) \tag{19}$$

and

$$E_{m,\mathrm{dis}}(\boldsymbol{u}_m, \boldsymbol{u}_{m,h}) = E_{m,\mathrm{dis},T}(\boldsymbol{e}_{m,\mathrm{dis}}), \tag{20}$$

respectively.

2.5. DUALITY TECHNIQUES

In order to derive an error representation formula for the goal-oriented error measure E, we follow the well-established strategy of solving auxiliary dual problems.

Let us first introduce the variational form of the dual problem associated with the fine model (1) which reads: find a dual solution $\overset{*}{\boldsymbol{u}}_{m+1} \in \mathcal{V}_{m+1}$ satisfying

$$a^*_{m+1,T}(\overset{*}{\boldsymbol{u}}_{m+1}, \boldsymbol{v}) = E_{\mathrm{mod},T}(\boldsymbol{v}) \quad \forall \boldsymbol{v} \in \mathcal{V}_{m+1} \tag{21}$$

with dual bilinear form $a^*_{m+1,T} : \mathcal{V}_{m+1} \times \mathcal{V}_{m+1} \to \mathbb{R}$ of the tangent form $a_{m+1,T}$. Furthermore, in the dual problem associated with the coarse model (2) we seek a solution $\overset{*}{\boldsymbol{u}}_m \in \mathcal{V}_m$ satisfying

$$a^*_{m,T}(\overset{*}{\boldsymbol{u}}_m, \boldsymbol{v}) = E_{m,\mathrm{dis},T}(\boldsymbol{v}) \quad \forall \boldsymbol{v} \in \mathcal{V}_m \tag{22}$$

with dual bilinear form $a^*_{m,T} : \mathcal{V}_m \times \mathcal{V}_m \to \mathbb{R}$ of the tangent form $a_{m,T}$.

As with the primal problem, we further establish a finite element discretization of the dual problem (22), which reads: find a solution $\overset{*}{\boldsymbol{u}}_{m,h} \in \mathcal{V}_{m,h}$ such that

$$a^*_{m,T}(\overset{*}{\boldsymbol{u}}_{m,h}, \boldsymbol{v}) = E_{m,\mathrm{dis},T}(\boldsymbol{v}) \quad \forall \boldsymbol{v} \in \mathcal{V}_{m,h}. \tag{23}$$

In the case of small model and discretization errors, an error representation formula in terms of the solutions of the dual problems presented above is now simply obtained by setting $\boldsymbol{v} = \boldsymbol{e}_{\mathrm{mod}}$ in (21) and $\boldsymbol{v} = \boldsymbol{e}_{m,\mathrm{dis}}$ in (22). We thus obtain with (18), (19), (20) and (23)

$$E(\boldsymbol{u}_{m+1}, \mathcal{P}\boldsymbol{u}_{m,h}) = a^*_{m+1,T}(\overset{*}{\boldsymbol{u}}_{m+1}, \boldsymbol{e}_{\mathrm{mod}}) + a^*_{m,T}(\overset{*}{\boldsymbol{u}}_m - \overset{*}{\boldsymbol{u}}_{m,h}, \boldsymbol{e}_{m,\mathrm{dis}}). \tag{24}$$

3. A posteriori error estimation for quantities of interest

3.1. THE GENERAL STRATEGY

Now that we have the error representations for the error measure E at our disposal, we show next how computable a posteriori error estimators can be derived.

To begin with, let us recall the error representation formula (24). For the exact computation of the tangent bilinear forms $a^*_{m+1,T}$ and $a^*_{m,T}$, the

quantities $\boldsymbol{u}_{m+1}$, $\boldsymbol{u}_m$, $\mathcal{P}\boldsymbol{u}_m$, $\boldsymbol{u}_{m,h}$, $\overset{*}{\boldsymbol{u}}_{m+1}$, $\overset{*}{\boldsymbol{u}}_m$ and $\overset{*}{\boldsymbol{u}}_{m,h}$ are required. Clearly, in general, only the finite element solutions $\boldsymbol{u}_{m,h}$ and $\overset{*}{\boldsymbol{u}}_{m,h}$ can be computed exactly. Our objective therefore is to compute suitable approximations of the remaining unknown quantities.

In order to do so, let us assume that we may compute approximate solutions $\boldsymbol{u}_{m+1,h}, \overset{*}{\boldsymbol{u}}_{m+1,h} \in \mathcal{V}_{m+1,h}$ which are improved by a postprocessing technique. These improved approximations will henceforth be denoted as $\tilde{\boldsymbol{u}}_{m+1,h}, \overset{*}{\tilde{\boldsymbol{u}}}_{m+1,h} \in \tilde{\mathcal{V}}_{m+1,h}$ and serve as approximations of the exact solutions $\boldsymbol{u}_{m+1}, \overset{*}{\boldsymbol{u}}_{m+1} \in \mathcal{V}_{m+1}$. Furthermore, we use the same postprocessing technique to improve the finite element solutions of the coarse model m which are denoted as $\tilde{\boldsymbol{u}}_{m,h}, \overset{*}{\tilde{\boldsymbol{u}}}_{m,h} \in \tilde{\mathcal{V}}_{m,h}$. These improved solutions serve as approximations of the exact solutions $\boldsymbol{u}_m, \overset{*}{\boldsymbol{u}}_m \in \mathcal{V}_m$.

Once these approximations are computed and the prolongation operator $\mathcal{P}$ is approximated by $\mathcal{P}_h$, we may establish the computable goal-oriented combined model and discretization error estimator

$$\begin{aligned} E(\boldsymbol{u}_{m+1}, \mathcal{P}\boldsymbol{u}_{m,h}) \approx\ & a^*_{m+1,T}(\overset{*}{\tilde{\boldsymbol{u}}}_{m+1,h}, \tilde{\boldsymbol{u}}_{m+1,h} \\ & -\mathcal{P}_h\tilde{\boldsymbol{u}}_{m,h}) + a^*_{m,T}(\overset{*}{\tilde{\boldsymbol{u}}}_{m,h} - \overset{*}{\boldsymbol{u}}_{m,h}, \tilde{\boldsymbol{u}}_{m,h} - \boldsymbol{u}_{m,h}). \end{aligned} \tag{25}$$

3.2. ON THE COMPUTATION OF THE IMPROVED APPROXIMATIONS

Summarizing the above, all that remains is to show how the improved approximations $\tilde{\boldsymbol{u}}_{m,h}$, $\tilde{\boldsymbol{u}}_{m+1,h}$, $\overset{*}{\tilde{\boldsymbol{u}}}_{m,h}$ and $\overset{*}{\tilde{\boldsymbol{u}}}_{m+1,h}$ can be computed. In this paper, we extend the strategy suggested by Stein and Ohnimus (1997, 1999), i.e. we solve auxiliary Neumann problems on the element level.

To this end, we first recall the error representation (12). Now it is easy to see that the true solution $\boldsymbol{u}_m \in \mathcal{V}_m$ of (2) also satisfies

$$a_{m,T}(\boldsymbol{u}_m, \boldsymbol{v}) = R_{m,\mathrm{dis}}(\boldsymbol{v}) + a_{m,T}(\boldsymbol{u}_{m,h}, \boldsymbol{v}) \quad \forall \boldsymbol{v} \in \mathcal{V}_m. \tag{26}$$

This variational problem is approximated (on the element level) by the Neumann problem of solving

$$a_{m,T,e}(\tilde{\boldsymbol{u}}_m|_{\bar{\Omega}_{m,e}}, \boldsymbol{v}_e) = \tilde{R}_{m,\mathrm{dis},e}(\boldsymbol{v}_e) + a_{m,T,e}(\boldsymbol{u}_{m,h}|_{\bar{\Omega}_{m,e}}, \boldsymbol{v}_e) \quad \forall \boldsymbol{v}_e \in \mathcal{V}_{m,e} \tag{27}$$

for a solution $\tilde{\boldsymbol{u}}_m|_{\bar{\Omega}_{m,e}} \in \mathcal{V}_{m,e} = \{\boldsymbol{v}|_{\bar{\Omega}_{m,e}}; \boldsymbol{v} \in \mathcal{V}_m\}$, defined on an element $\bar{\Omega}_{m,e}$ of the coarse model discretization. In the above, $a_{m,T,e} : \mathcal{V}_{m,e} \times \mathcal{V}_{m,e} \to \mathbb{R}$ denotes the restriction of the bilinear form $a_{m,T}$ to an element and $\tilde{R}_{m,\mathrm{dis},e} : \mathcal{V}_{m,e} \to \mathbb{R}$ denotes the equilibrated (and therefore improved) weak form of the (local) residual which is, in (nonlinear or linearized) elasticity, defined as

$$\tilde{R}_{m,\mathrm{dis},e}(\boldsymbol{v}_e) = \int_{\partial\Omega_{m,e}} \tilde{\boldsymbol{t}}_e \cdot \boldsymbol{v}_e \, \mathrm{d}A - a_{m,e}(\boldsymbol{u}_{m,h}|_{\bar{\Omega}_{m,e}}; \boldsymbol{v}_e) \tag{28}$$

with equilibrated tractions $\tilde{\boldsymbol{t}}_e$, see Ladevèze and Leguillon (1983).

In a similar fashion, the approximation $\tilde{\boldsymbol{u}}_{m+1,h}$ can now be computed. To see this, let us first recall the error representation for the model error (11). As with (26), it is obvious that the true solution $\boldsymbol{u}_{m+1} \in \mathcal{V}_{m+1}$ also satisfies

$$a_{m+1,T}(\boldsymbol{u}_{m+1}, \boldsymbol{v}) = R_{\mathrm{mod}}(\boldsymbol{v}) + a_{m+1,T}(\mathcal{P}\boldsymbol{u}_m, \boldsymbol{v}) \quad \forall \boldsymbol{v} \in \mathcal{V}_{m+1}. \tag{29}$$

In the associated Neumann problem we solve

$$a_{m+1,T,e}(\tilde{\boldsymbol{u}}_{m+1}|_{\bar{\Omega}_{m+1,e}}, \boldsymbol{v}_e) = \tilde{R}_{m+1,\mathrm{mod},e}(\boldsymbol{v}_e) + a_{m+1,T,e}(\mathcal{P}_h\tilde{\boldsymbol{u}}_{m,h}|_{\bar{\Omega}_{m+1,e}}, \boldsymbol{v}_e) \tag{30}$$

for a solution $\tilde{\boldsymbol{u}}_{m+1}|_{\bar{\Omega}_{m+1,e}} \in \mathcal{V}_{m+1,e}$ that holds for all $\boldsymbol{v}_e \in \mathcal{V}_{m+1,e} = \{\boldsymbol{v}|_{\bar{\Omega}_{m+1,e}}; \boldsymbol{v} \in \mathcal{V}_{m+1}\}$. In the above, $a_{m+1,T,e}$ is the local form of $a_{m+1,T}$ defined on an element $\bar{\Omega}_{m+1,e}$ of the fine model discretization. Furthermore, the equilibrated weak residual $\tilde{R}_{m+1,\mathrm{mod},e} : \mathcal{V}_{m+1,e} \to \mathbb{R}$ is now defined as

$$\tilde{R}_{m+1,\mathrm{mod},e}(\boldsymbol{v}_e) = \int_{\partial\Omega_{m+1,e}} \tilde{\boldsymbol{t}}_e \cdot \boldsymbol{v}_e \, \mathrm{d}A - a_{m+1,e}(\mathcal{P}_h\tilde{\boldsymbol{u}}_{m,h}|_{\bar{\Omega}_{m+1,e}}; \boldsymbol{v}_e). \tag{31}$$

Next, we show how the (improved) approximation of the dual problem $\overset{*}{\tilde{\boldsymbol{u}}}_{m,h}$ associated with the coarse model (2) can be computed in much the same way as the approximations of the primal problem. Therefore, let us recall the dual problem (22) which is always linear by definition. The associated Neumann problem on the element level then reads: find a solution $\overset{*}{\tilde{\boldsymbol{u}}}_m|_{\bar{\Omega}_{m,e}} \in \mathcal{V}_{m,e}$ such that

$$a^*_{m,T,e}(\overset{*}{\tilde{\boldsymbol{u}}}_m|_{\bar{\Omega}_{m,e}}, \boldsymbol{v}_e) = E_{m,\mathrm{dis},T,e}(\boldsymbol{v}_e) + \int_{\partial\Omega_{m,e}} \tilde{\boldsymbol{t}}_e \cdot \boldsymbol{v}_e \, \mathrm{d}A \quad \forall \boldsymbol{v}_e \in \mathcal{V}_{m,e}, \tag{32}$$

where $a^*_{m,T,e}$ and $E_{m,\mathrm{dis},T,e}$ are again the local forms of $a^*_{m,T}$ and $E_{m,\mathrm{dis},T}$ defined on an element $\bar{\Omega}_{m,e}$ of the coarse model discretization, respectively.

Finally, we need to compute the (improved) approximation of the dual problem $\overset{*}{\tilde{\boldsymbol{u}}}_{m+1,h}$ associated with the fine model $m+1$. Here, we follow the same strategy as in the case of the primal problem, i.e. we compute $\overset{*}{\tilde{\boldsymbol{u}}}_{m+1,h}$ without solving the discretized global dual problem on the fine model $m+1$. As presented above, we establish the local Neumann problem associated with the dual problem (21) which reads: find a solution $\overset{*}{\tilde{\boldsymbol{u}}}_{m+1}|_{\bar{\Omega}_{m+1,e}} \in \mathcal{V}_{m+1,e}$ such that

$$a^*_{m+1,T,e}(\overset{*}{\tilde{\boldsymbol{u}}}_{m+1}|_{\bar{\Omega}_{m+1,e}}, \boldsymbol{v}_e) = E_{m+1,\mathrm{mod},T,e}(\boldsymbol{v}_e) + \int_{\partial\Omega_{m+1,e}} \tilde{\boldsymbol{t}}_e \cdot \boldsymbol{v}_e \, \mathrm{d}A \quad \forall \boldsymbol{v}_e \in \mathcal{V}_{m+1,e} \tag{33}$$

with local forms $a^*_{m+1,T,e}$ and $E_{m+1,\mathrm{mod},T,e}$ of $a^*_{m+1,T}$ and $E_{m+1,\mathrm{mod},T}$ defined on an element $\bar{\Omega}_{m+1,e}$ of the fine model discretization.

3.3. ORTHOGONALIZATION OF THE MODEL ERROR ON THE ELEMENT LEVEL

As we have seen, the orthogonality relation of the model error with respect to the finite element test functions gets lost. However, for the derivation of upper error bounds on the error measure E, as will be presented in a forthcoming paper, it is advantageous to compute a prolongation operator which fulfills orthogonality relations. This is easily shown by rewriting the error representation (24), which forms the basis for the derivation of upper error bounds, as

$$\begin{aligned} E(\boldsymbol{u}_{m+1}, \mathcal{P}\boldsymbol{u}_{m,h}) =& a^*_{m+1,T}(\underbrace{\overset{*}{\boldsymbol{u}}_{m+1} - \mathcal{P}\overset{*}{\boldsymbol{u}}_m}_{\overset{*}{\boldsymbol{e}}_{\mathrm{mod}}}, \boldsymbol{e}_{\mathrm{mod}}) \\ &+ a^*_{m,T}(\underbrace{\overset{*}{\boldsymbol{u}}_m - \overset{*}{\boldsymbol{u}}_{m,h}}_{\overset{*}{\boldsymbol{e}}_{m,\mathrm{dis}}}, \boldsymbol{e}_{m,\mathrm{dis}}) + a^*_{m+1,T}(\mathcal{P}\overset{*}{\boldsymbol{u}}_m, \boldsymbol{e}_{\mathrm{mod}}). \end{aligned} \tag{34}$$

Now it is easy to see that the last of our terms in the above error representation should vanish. This can be achieved by a pre-multiplied orthogonal matrix $\mathcal{P}^{\mathrm{ort}}$, yielding $\mathcal{P} = \mathcal{P}^{\mathrm{ort}}\mathcal{P}^{\mathrm{kin}}$.

For the sake of simplicity, we restrict our considerations to the linear theory. In this case, the prolongation operator $\mathcal{P}$ should be constructed such that the orthogonality condition

$$a^*_{m+1}(\mathcal{P}\boldsymbol{u}_m, \mathcal{P}\overset{*}{\boldsymbol{u}}_m) = F_{m+1}(\mathcal{P}\overset{*}{\boldsymbol{u}}_m) \tag{35}$$

is fulfilled, which is an equilibrium condition for $\mathcal{P}$. Note that a^*_{m+1} is a bilinear form. In discretized form, the above condition has to be fulfilled for each finite element yielding the following orthogonality condition on the element level.

$$a^*_{m+1,e}(\mathcal{P}_{h,e}\boldsymbol{u}_{m,h,e}, \mathcal{P}_{h,e}\overset{*}{\boldsymbol{u}}_{m,h,e}) = F_{m+1,e}(\mathcal{P}_{h,e}\overset{*}{\boldsymbol{u}}_{m,h,e}). \tag{36}$$

For the approximations $\mathcal{P}_{h,e}\boldsymbol{u}_{m,h,e}$ and $\mathcal{P}_{h,e}\overset{*}{\boldsymbol{u}}_{m,h,e}$ we choose a discrete ansatz of the form

$$\mathcal{P}_{h,e}\boldsymbol{u}_{m,h,e} = \boldsymbol{N}_{m+1}(\boldsymbol{x})\mathcal{P}_{m+1,m,e}\hat{\boldsymbol{u}}_{m,e} \tag{37}$$

for the primal solution and

$$\mathcal{P}_{h,e}\overset{*}{\boldsymbol{u}}_{m,h,e} = \boldsymbol{N}_{m+1}(\boldsymbol{x})\mathcal{P}_{m+1,m,e}\hat{\overset{*}{\boldsymbol{u}}}_{m,e}, \tag{38}$$

for the dual solution. Hence, (36) can be written in the algebraic form

$$\left(\mathcal{P}_{m+1,m,e}\hat{\overset{*}{\boldsymbol{u}}}_{m,e}\right)^T \boldsymbol{k}_{m+1,m+1,e}\mathcal{P}_{m+1,m,e}\hat{\boldsymbol{u}}_{m,e} = \left(\mathcal{P}_{m+1,m,e}\hat{\overset{*}{\boldsymbol{u}}}_{m,e}\right)^T \bar{\boldsymbol{p}}_{m+1,e}, \tag{39}$$

where $\boldsymbol{k}_e$ denotes the local stiffness matrix associated with the bilinear form $a^*_{m+1,e}$. Likewise, $\bar{\boldsymbol{p}}_e$ denotes the local load vector associated with the linear form $F_{m+1,e}$. In order to solve the equation above, we have to eliminate the rigid body modes. Thus, we obtain

$$\mathcal{P}^{\mathrm{red}}_{m+1,m,e}\hat{\boldsymbol{u}}^{\mathrm{red}}_{m,e} = \boldsymbol{k}^{\mathrm{red},-1}_{m+1,m+1,e}\bar{\boldsymbol{p}}_{m+1,e} \tag{40}$$

with $\det \boldsymbol{k}^{\mathrm{red}}_e > 0$. The reduced prolongation operator $\mathcal{P}^{\mathrm{red}}_e$ can be represented as the product of an involutoric orthogonal matrix $\mathcal{P}^{\mathrm{ort}}_e$ (for rotation and reflection) and the reduced (kinematic) prolongation matrix $\mathcal{P}^{\mathrm{kin}}_e$ as

$$\mathcal{P}^{\mathrm{red}}_{m+1,m,e} := \mathcal{P}^{\mathrm{ort}}_{m+1,m+1,e}\mathcal{P}^{\mathrm{kin}}_{m+1,m,e} \tag{41}$$

with $\mathcal{P}^{\mathrm{ort},T}_e = \mathcal{P}^{\mathrm{ort},-1}_e$, $\mathcal{P}^{\mathrm{ort}}_e = \mathcal{P}^{\mathrm{ort},T}_e$ and $(\mathcal{P}^{\mathrm{ort}}_e)^2 = \mathbf{1}$. Inserting (41) into (40) then yields

$$\mathcal{P}^{\mathrm{ort}}_{m+1,m+1,e}\boldsymbol{x}_e = \boldsymbol{y}_e \tag{42}$$

with $\boldsymbol{x}_e := \mathcal{P}^{\mathrm{kin}}_{m+1,m+1,e}\hat{\boldsymbol{u}}^{\mathrm{red}}_{m,e}$ and $\boldsymbol{y}_e := \boldsymbol{k}^{\mathrm{red},-1}_{m+1,m+1,e}\bar{\boldsymbol{p}}_{m+1,e}$.

The matrix $\mathcal{P}^{\mathrm{ort}}_e$ has $\frac{n}{2}(n+1)$ unknowns, where n is the number of equations in (42), and $n + \binom{n}{2} = n + \frac{1}{2}n(n-1) = \frac{1}{2}n(n+1)$ equations are available, amongst them $\binom{n}{2}$ orthogonality conditions of the column or row vectors of matrix $\mathcal{P}^{\mathrm{ort}}_e$. Thus, all matrix elements of $\mathcal{P}^{\mathrm{ort}}_e$ can be uniquely determined.

3.4. NUMERICAL EXAMPLE

Combined model and discretization adaptivity is applied to a continuous flat slab with square fields, haunched at the equidistant columns, see Fig. 3. The coarse model is the 2D Reissner-Mindlin plate theory, enhanced by a constant strain in the thickness direction as a $2\frac{1}{2}$D model. The boundary layers in the vicinity of the columns are modeled with 3D elasticity theory.

The finite elements used are:

– For the $2\frac{1}{2}D$ *RM-plate*: anisotropic Q_2 elements, quadratic in the horizontal directions and linear in the normal direction and

– For the *3D model*: isotropic Q_2 elements

The transition conditions from Reissner-Mindlin plate elements with plane and extensible cross sections to 3D elements are realized by a penalized least squares method. All assembled weak coupling conditions of the system are condensed in the matrix equation $\boldsymbol{G}^T\hat{\boldsymbol{u}} + \boldsymbol{b} = \boldsymbol{0}$, with the rectangular coupling matrix $\boldsymbol{G}^T = [\boldsymbol{g}^T_{xz_1}...\boldsymbol{g}^T_{xz_n}, \boldsymbol{g}^T_{yz_1}...\boldsymbol{g}^T_{yz_n}]$ and the global nodal displacement vector $\hat{\boldsymbol{u}}$. With the global tangential stiffness matrix $\boldsymbol{K}_T$, the algebraic equation system reads $(\boldsymbol{K}_T + \rho\boldsymbol{G}^T\boldsymbol{G})\hat{\boldsymbol{u}} - \hat{\bar{\boldsymbol{p}}} = \boldsymbol{0}$, where $\boldsymbol{G}^T\boldsymbol{G}$ is the positive definite symmetric Gauß-transformed matrix $\boldsymbol{G}$, ρ is the penalty parameter for fulfilling the least squares conditions, and $\hat{\bar{\boldsymbol{p}}}$ is the global nodal load vector, see Stein et al. (2007).

The combined a posteriori error estimator for the averaged bending stress at point P in Fig. 3, calculated for the $2\frac{1}{2}$D model, the adapted $2\frac{1}{2}$D-3D model, and the 3D model are presented in Fig. 4, as are the related effectivity indices. These results show that error tolerances of less than 10% can only be realized by using the 3D model from the beginning of the adaptive process or – more efficient and allowing for engineering understanding – applying the adaptive $2\frac{1}{2}$D–3D modeling.

The process of model adaptivity is illustrated in Fig. 5, showing that the for the meshes 2 and 5 the plate is still modeled with $2\frac{1}{2}$D RM-elements. In mesh 12 the layer zone around the haunches is discretized with 3D elements,

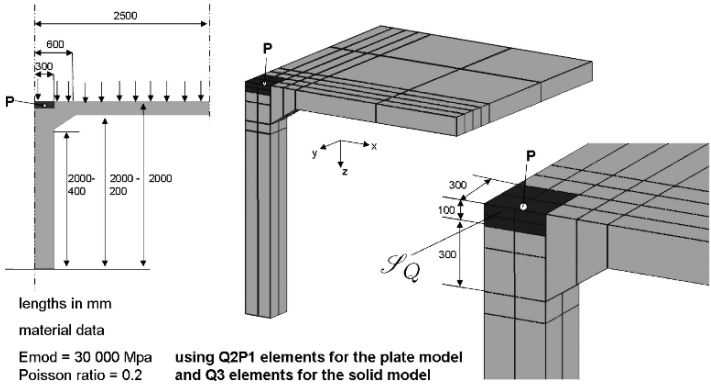

Figure 3. Model and discretization adaptivity of a continuous haunched flat slab with square fields on single columns with a constant static transverse load. Quantity of interest for discretization and model adaptivity, Q_{m+1}: average bending stress $\sigma_x = \sigma_y$ at point P with respect to the local support $\mathscr{S}_Q$

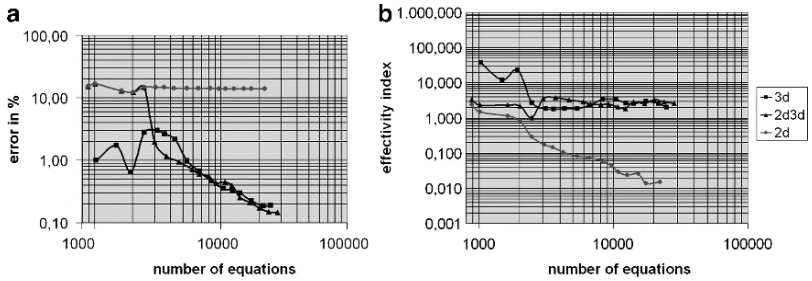

Figure 4. Combined model and discretization error estimates (**a**) and effectivity indices for the combined model and discretization error (**b**) of the average bending stresses $\sigma_x = \sigma_y$ at point P as the quantity of interest for the 2D plate model, the expanded 2D–3D model, and the 3D model. **Symbols:** 3D sol's: □, 2D–3D sol's: △, 2D sol's: ◯

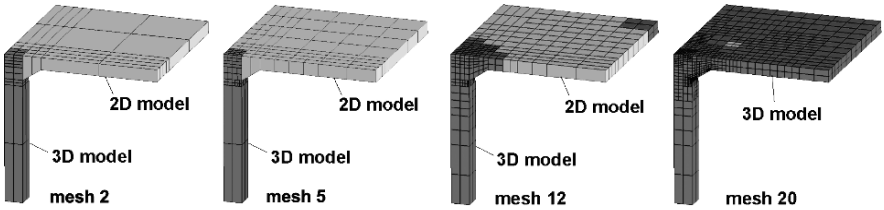

Figure 5. $2\frac{1}{2}$D-to-3D-model-adapted subdomains (dark) for the refined meshes 2, 5, 12, and 20

and for mesh 20 the whole plate has 3D elements. This also illustrates that the lower the combined error tolerance, the more relevant the (fine) 3D model.

4. Structural optimization of elastoplastic structures under shakedown conditions

4.1. MOTIVATION AND CONCEPT

Structural optimization (e.g. weight minimization) is an important matter in engineering. But there are two crucial warnings:

(i) Geometrical imperfections in elastic systems have to be regarded for stability problems because otherwise the primal (linear) critical load can be enlarged significantly but followed by a deep descent in the post-buckling area. Thus, the objective function should not be the maximum primal critical load factor, but the minimum descent from the primal maximum critical value to the minimum postcritical value, for example.

(ii) In case of significant residual inelastic deformations and related residual stresses, the usual optimization algorithms for elastic structures are unsuitable because deformations and stresses depend on the loading paths. Thus, different loading paths for same initial and final static loading create different optimal systems, see Wiechmann and Stein (2006). Moreover, related incremental loading processes need very time-consuming sensitivity analysis and solutions of algebraic equations.

Therefore, a reasonable optimization method for those structures (with proportional and non-proportional loadings) with an arbitrary n-dimensional convex load space can be obtained by applying elastic shakedown conditions, in the most simple way with time-independent unlimited linear kinematic hardening, i.e. displaced yield surfaces, resulting in decoupled local equations for time-independent residual and micro stress fields, see Stein et al. (1992b).

Structural optimization with this material model yields the maximum load parameter (or diameter) of the load space in which arbitrary load paths can be repeated infinitely. This, of course, does not regard low cycle fatigue and creep damage, the first of which can be regarded by reducing the maximum load diameter by the Miner's rule, for example, whereas creep deformations are not contained in the present theory and could be considered by an integrated softening model, which, however, is not a local problem.

The algorithm, based on FEM for structural discretization, a two–fold nested optimization process, see Wiechmann and Stein (2006), as outlined in the sequel.

4.2. ELASTIC SHAKEDOWN ANALYSIS FOR UNLIMITED LINEAR KINEMATIC HARDENING

According to Melan's theorem from 1938, an elastoplastic system will shakedown elastically, if there exist a time-independent residual stress field $\bar{\boldsymbol{\rho}}(\boldsymbol{X})$, a time-independent micro stress field $\bar{\boldsymbol{\chi}}(\boldsymbol{X})$, and a factor $m > 1$ such that the condition

$$\Phi[m\boldsymbol{\sigma}^e(\boldsymbol{X}, t), \bar{\boldsymbol{\rho}}(\boldsymbol{X}), \bar{\boldsymbol{\chi}}(\boldsymbol{X}), \sigma_0] \leq 0 \tag{43}$$

is fulfilled for all points $P(t) \in \mathcal{M}$ and for all $\boldsymbol{X} \in \Omega_0$, where $\mathcal{M}$ is the load space and Ω_0 the system domain.

The maximum enlargement of the load domain $\mathcal{M}$, characterized by the scalar parameter β (the objective function), follows from the optimization problem:

$$
\begin{array}{lrcl}
\text{objective:} & \beta & \rightarrow & \max \\
\text{with the weak} & & & \\
\text{equilibrium conditions:} & \mathcal{G}^{\rho} & = & \int_{\Omega_o} \text{Grad}\ \boldsymbol{\eta} : \bar{\boldsymbol{\rho}}(\boldsymbol{X})\ \mathrm{d}V_o = 0 \\
 & \mathcal{G}^{e} & = & \int_{\Omega_o} \text{Grad}\ \boldsymbol{\eta} : \boldsymbol{\sigma}^{e}(\boldsymbol{X},t)\ \mathrm{d}V_o - \mathcal{G}^{\text{ext}} = 0 \\
\text{and the yield condition:} & \Phi & = & \Phi[\beta\boldsymbol{\sigma}^{e}(\boldsymbol{X},t), \bar{\boldsymbol{\rho}}(\boldsymbol{X}), \bar{\boldsymbol{\chi}}(\boldsymbol{X}), \sigma_o] \leq 0
\end{array}
$$

With the internal stresses $\boldsymbol{y}(\boldsymbol{X}) := \bar{\boldsymbol{\rho}}(\boldsymbol{X}) - \bar{\boldsymbol{\chi}}(\boldsymbol{X})$, the homogeneous equality constraint $\mathcal{G}^{\rho}$ can be eliminated.

Then, the global maximum load factor $\max\beta = \bar{\beta}$ follows from the dimensional reduction as $\bar{\beta} = \min\beta_i$, for $i = 1, ..., NP$. The elastic stresses in the M vertices of the n-dimensional convex polyhedral load domain $\mathcal{M}$ are $\boldsymbol{\sigma}^{e}(\boldsymbol{X},t) = \sum_{j=1}^{M} \alpha_j(t)\boldsymbol{\sigma}^{e}(j), \sum_{j=1}^{M} \alpha_j(t) = 1, t$: the process variable.

4.3. SENSITIVITY ANALYSIS FOR STRUCTURAL OPTIMIZATION

The rather lengthy variational formulas, see Wiechmann and Stein (2006), are presented here only as a brief survey.

For structural analysis with the equilibrium conditions $\mathcal{G}_j^e = \hat{\mathcal{G}}_j^e(\boldsymbol{X}, \boldsymbol{u}_j) = 0$, the sensitivity analysis reads $\delta\mathcal{G}_j^e = \frac{\partial\mathcal{G}_j^e}{\partial\boldsymbol{X}}\delta\boldsymbol{X} + \frac{\partial\mathcal{G}_j^e}{\partial\boldsymbol{u}_j}\delta\boldsymbol{u}_j = 0$. With the shakedown formulation $L_i = -\beta_i + \lambda_j\Phi_j(\boldsymbol{X}, \boldsymbol{u}_j, \beta_i, \boldsymbol{y}_i) = \hat{L}_i(\boldsymbol{X}, \boldsymbol{u}_j, \boldsymbol{z}_i, \lambda_j)$, $\boldsymbol{z}_i = [\beta, \boldsymbol{y}_i]$, the optimality conditions are $\mathcal{L}_i := \delta_{\boldsymbol{z}_i}\hat{\boldsymbol{L}}_i(\boldsymbol{X}, \boldsymbol{u}_j, \boldsymbol{z}_i, \lambda_j) = 0$, and the sensitivities read $\delta\mathcal{L}_i = \frac{\partial\mathcal{L}_i}{\partial\boldsymbol{X}}\delta\boldsymbol{X} + \frac{\partial\mathcal{L}_i}{\partial\boldsymbol{u}_j}\delta\boldsymbol{u}_j + \frac{\partial\mathcal{L}_i}{\partial\boldsymbol{z}_i}\delta\boldsymbol{z}_i = 0$.

The total variation of the weak form of equilibrium has to be zero according to $\delta\mathcal{G}^e = \delta_{\boldsymbol{X}}\mathcal{G}^e + \delta_{\boldsymbol{u}}\mathcal{G}^e = 0$.

The extensive formulas and the numerical algorithm following from this are omitted here.

4.4. EXAMPLE: COMPARATIVE WEIGHT MINIMIZATION OF A STRETCHED SQUARE PLATE WITH A CENTRAL HOLE IN PLANE STRESS STATE

Three optimization problems are calculated for the system and loading in Fig. 6:

1. *Elastic* deformation, one static loading case from zero to final load
2. *Elastoplastic* deformation, one loading case as in 1
3. Elastoplastic *shakedown* problem with a 1D load domain

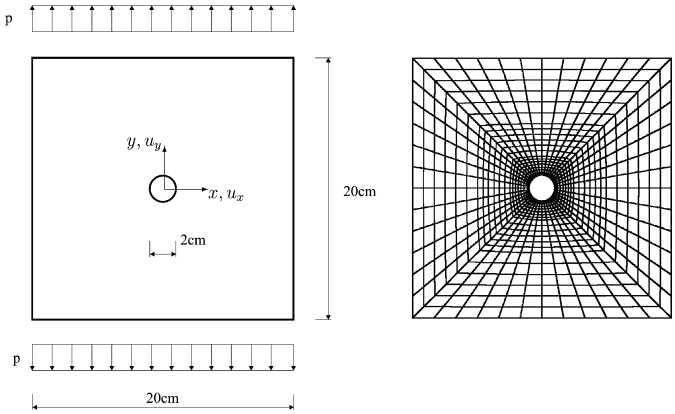

Figure 6. *Left*: Initial geometry and loading; *right*: Refined second finite element mesh with 4×240 Q_1 elements (*right*)

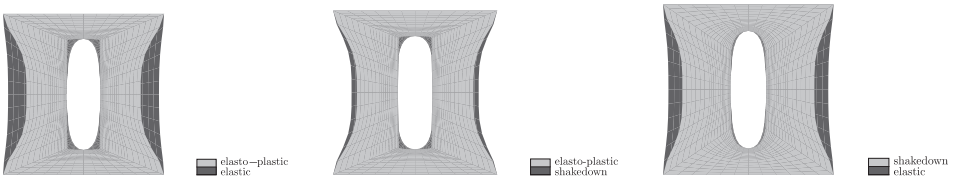

Figure 7. Resulting geometries from weight optimization of a stretched square plate with a central circular hole in the initial state

The main result for the minimized weights is, as reasonably expected, $G_{\text{elastic}} > G_{\text{shakedown}} > G_{\text{elastoplastic}}$.

Figure 7 shows comparisons of the related optimized system geometries. (1) The elastoplastic analysis saves most material compared to the elastic one, but it is unsafe; (2) Shakedown analysis needs a little more material than one load path (elastoplastic analysis), but it is safe. Moreover, the computational cost for shakedown is much less than for elastoplastic analysis; and finally (3) optimization under shakedown constraints yields a noteworthy weight reduction compared to the elastic model because the plastic material properties can be used efficiently.

5. Design and computation problems of the German pavilion at the world exhibition EXPO 2000 in Hannover

After an architectural competition which had failed, only 15 months were left for the new draft, the engineering design, structural analysis, and detailed design accompanied by extensive experiments as well as the whole construction and assembly of the pavilion. It has six steel girders with

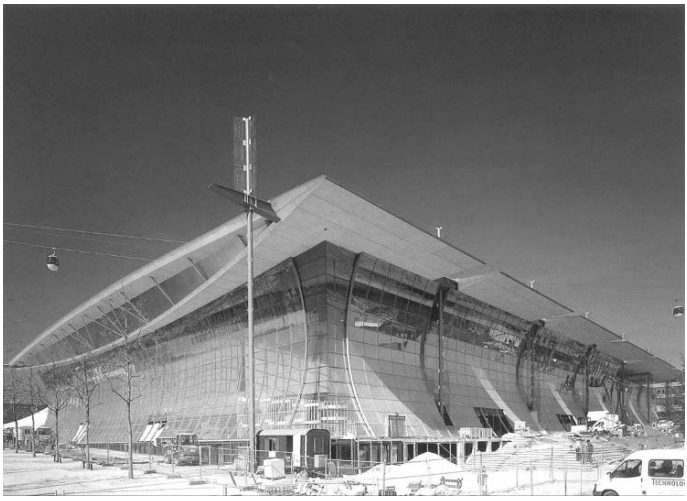

Figure 8. View of the German Pavilion at the EXPO 2000 in Hannover

a span of 88.5 m and a total width of $6 \times 23.4 = 140.4$ m. The owner and architect of the pavilion is Ing. Josef Wund from Friedrichshafen, Germany.

Figure 8 shows a view of the northern part of the pavilion. The design of the pavilion with all its essential components were published in Brandt and Kneib (2001) as well as in Burmeister et al. (2001). The first author of the paper presented here was the official inspection engineer for the German Pavilion, responsible for the safety of design and construction.

The two following conceptually new construction components can be seen in Fig. 8:

(i) The *concave, parabolically curved glass facades* are supported by predeformed steel girders in distances of 1.95 m with the diameter $d = 88.9$ mm and the thickness $t = 20$ mm. The girders have a vertical span of 16 m, supported at the foot and the top by butt hinge bearings. The maximum ordinate of the parabola is 2.3 m, see Fig. 9. The concave parabolic facade girders have constant normal forces for constant wind loads and only little bending moments due to locally concentrated wind loads, but, of course, relatively large vertical reaction forces have to be transmitted in the supports.
The glass plates consist of insulated security glass (by full thermal prestressing) with different sequences in thickness direction in the lower skew area of the facade, the middle part, which is nearly vertical, and the upper area with canopy glazing. In this upper part, one total glass plate consists of (from outside to inside) 10 mm security class, an insulating clearance, then 4 mm partially prestressed glass (TVG), fourfold polyvinyl (PVB) foils, and another 4 mm TVG glass plate.

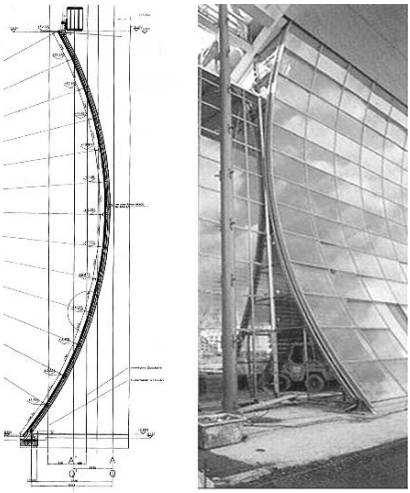

Figure 9. *Left*: Parabolically curved facade girder of the pavilion, vertical section through the facade. *Right*: Photograph of the facade

The two lower areas have different cross-sections, but the total thickness is the same. According to German building laws for energy-saving insulations, the temperature requirement of 19°C for low-temperature workshops is fulfilled.

(ii) The 14 very slender steel columns (tubes with the diameter $d = 355.6$ mm and the thickness $t = 70$ mm) have spans of 15.6 m. Each column is stiffened by three slightly prestressed parabolically curved stainless steel cables in vertical planes with the angles 0°, 120°, and 240°. The shape of the cables, and thus the prestressing, is achieved by 3×9 stiffening glass plates for each column. Each glass plate consists of three composite security glass plates of 10 mm thickness with PVB foils in between, see Burmeister et al. (2001) and Fig. 10.
A major problem was the transmission of unbalanced forces from the steel cables into the glass plates by means of special new bolts (two in each plate), whereas the supports at the column have standard constructions. It is well known that the transmissions of concentrated forces into (brittle) glass plates has to be smoothened. This was realized in the present case with the specially developed so-called HILTI HIT HY50 mortar, consisting of organic and inorganic material with an initial Young's modulus as the average value of steel and glass moduli as well as with well-defined initial creep properties in order to smoothen possible local stress concentrations due to imperfections. This mortar is located between the steel bolt and the glass borehole in a thin annular gap, Fig. 11.

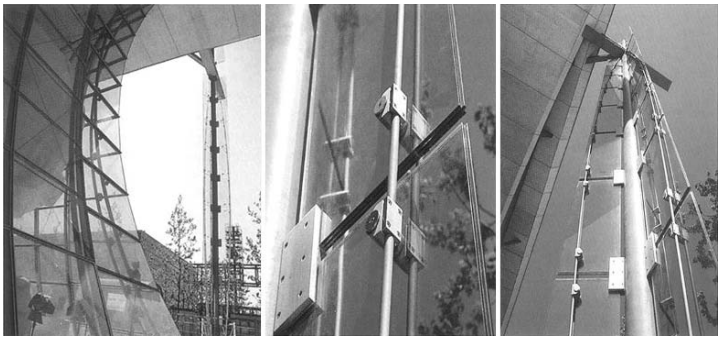

Figure 10. Views of a prestressed glass-stiffened steel column with different scales

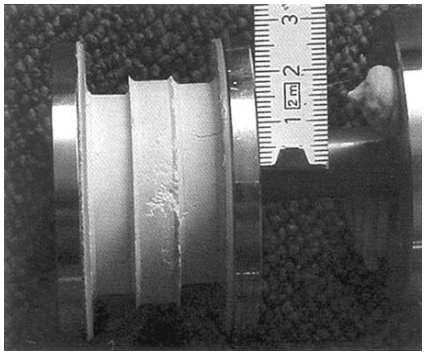

Figure 11. Injection mortar with HILTI HIT HY 50 in glass borehole. The borehole radius of the middle layer is slightly larger than the radius of the outer layers

The computations of the glass facades and the prestressed glass-stiffened steel columns were done with several finite element programs, mostly using 3D elements, accompanied by extensive experiments for the understanding of progressive damage and ultimate load behavior in order to check the desired fail-safe behavior after reaching ultimate loads.

Moreover, the whole roof construction had to be implemented into the overall computational model, i.e. including the facades and the columns. The main reason for this is the low bending stiffness of the steel edge beams above the columns because originally bending-resistant facade components, which only transmit horizontal forces to the edge beams, had been scheduled. With the new membrane type facade, however, large vertical reaction forces had to be carried by the edge beams, and they even had to be strengthened. The vertical displacements of the edge beams had to be limited according to the sensitive horizontal displacements of the facade, where contact between the glass plate joints have to be strictly avoided.

A complicated task was the study of progressing damage and failure scenarios of the glass-stiffened columns which were assumed to be possible by rifle shots hitting the stiffening glass plates, and furthermore studies on damage and partial failure of the glass facades due to fire. The anxious safety actions were motivated by the fact that about 3 million people from all over the world visited the EXPO during its 3 months. As the result of these investigations, the first author had to make a large poster with instructions for the service personnel and the fire fighters for different levels of destruction. As an example, in case that only one glass plate of a column is hit, the hall should not be evacuated that day, and with nine spare glass plates in the cellar, the respective column could be repaired the next day. But in case of three or more damaged glass plates, the hall should be evacuated at once.

All of these safety measures belong to the requirement "fail-safe", i.e. that people and valuable goods can be safed before collapse.

6. Concluding remarks

The paper treats error-controlled adaptive computational methods for combined verification and validation of reliable and efficient goal-oriented nonlinear mathematical models as used in engineering designs. Expansive model adaptivity for quantities of interest is presented, here for the enhancement of 2D elastic plate/shell theories to 3D elastic continuum theory in related subdomains with geometric and physical disturbancies like boundary layers, using efficient a posteriori model and discretization error estimators with upper bounds.

The model error estimator requires the prolongation of discrete coarse model solutions into the finite element solution space of the fine model by which the orthogonality of the model error with respect to the discrete solution of the fine model gets lost. A special orthogonal matrix defined for the finite elements of the fine model (multiplied with the element prolongation matrix) yields the orthogonality and thus the upper-bound property of the error estimator. Reasonably, the model and discretization error should have the same order of magnitude.

In the example of model adaptivity of a continuous plate, haunched at the equidistant columns, and the average maximum plate bending stress (at the edge of the column) as the quantity of interest, $2\frac{1}{2}$D finite plate elements are used for the coarse model which avoid locking at the model interfaces to 3D finite elements.

It is proposed that the requirements of verification and validation will be considered in the future also in the European Codes for structural engineering, especially in Eurocode EN 1990 (2002), the basis for guaranteeing

save and reliable material and structural resistancies against regular and exceptional loads.

Optimized structures play an important role in engineering. The problem of inelastic deformations in subdomains of those structures is treated here by optimization under shake down conditions with kinematic hardening for mild steel, for which the acting loads are defined in a convex polygonal load space. The resulting optimization algorithm is computationally much more efficient than for elasto-plastic load increments, which, moreover, are ambiguous and therefore inadmissible.

Finally, the design and related computational problems of the concave glass façades and the glass-stiffened pre-stressed slender steel columns of the German Pavilion at the World Exhibition EXPO 2000 in Hannover, Germany, are discussed. These examples show the complexity of challenging modern constructions for which verification and validation of the used mathematical models, ensuring safety for complicated ultimate load scenarios are necessary.

Thus, in total, overall error-controlled adaptivity in conjunction with the engineering art of goal-oriented structural modeling is an important paradigm for future developments in Computational Mechanics.

References

Ainsworth, M. and Oden, J. (1993) A unified approach to a posteriori error estimation based on element residual methods, *Numer. Math.* **65**, 23–50.

Ainsworth, M. and Oden, J. (2000) *A Posteriori Error Estimation in Finite Element Analysis*, Wiley, New York.

Babuška, I. and Miller, A. (1987) A feedback finite element method with a posteriori error estimation: Part I. The finite element method and some basic properties of the a posteriori error estimator, *Comp. Meth. Appl. Mech. Eng.* **61**, 1–40.

Babuška, I. and Rheinboldt, W. (1978) A-posteriori error estimates for finite-element method, *Int. J. Numer. Meth. Eng.* **12**, 1597–1615.

Babuška, I., Strouboulis, T., Gangaraj, S., and Upadhyay, C. (1997) Pollution error in the h-version of the finite element method and the local quality of the recovered derivatives, *Comp. Meth. in Appl. Mech. Eng.* **140**, 1–37.

Bank, R. and Smith, R. (1993) A posteriori error estimates based on hierarchical bases, *SIAM J. Numer. Anal.* **30**, 921–935.

Bank, R. and Weiser, A. (1985) Some a posteriori error estimators for elliptic partial differential equations, *Math. Comp.* **44**, 283–301.

Becker, R. and Rannacher, R. (1996) A feed-back approach to error control in finite element methods: Basic analysis and examples, *East–West J. Numer. Math.* **4**, 237–264.

Bischoff, M., Wall, W., Bletzinger, K., and Ramm, E. (2004) Models and finite elements for thin-walled structures, In E. Stein, R. de Borst, and T. Hughes (Eds.), *Encyclopedia of Computational Mechanics*, Wiley, Chichester, pp. 59–137.

Braess, D. (2001) *Finite elements. Theory, Fast Solvers, and Applications in Solid mechanics*, Cambridge University Press, Cambridge 2nd edition.

Brandt, A. and Kneib, W. (2001) Die Dachkonstruktion des Deutschen Pavillons auf der EXPO 2000 in Hannover, *Bauingenieur* **76**, 483–486.

Brink, U. and Stein, E. (1998) A posteriori error estimation in large-strain elasticity using equilibrated local Neumann problems, *Comp. Meth. Appl. Mech. Eng.* **161**, 77–101.

Burmeister, A., Reitinger, R., and Ramm, E. (2001) Der Deutsche Pavillon auf der EXPO 2000. Fassaden und glasversteifte Stützen, *Bauingenieur* **76**, 487–497.

Carey, G. (2006) A perspective on adaptive modeling and meshing (AM & M), *Comp. Meth. Appl. Mech. Eng.* **195**, 214–235.

Carstensen, C. and Funken, S. (2001) Averaging technique for FE – a posteriori error control in elasticity. Part I: Conforming FEM, *Comp. Meth. Appl. Mech. Eng.* **190**, 2483–2498.

Cirak, F. and Ramm, E. (1998) A posteriori error estimation and adaptivity for linear elasticity using the reciprocal theorem, *Comp. Meth. Appl. Mech. Eng.* **156**, 351–362.

Düster, A. and Rank, E. (2002) A p-version finite element approach for two- and three-dimensional problems of the J_2 flow theory with non-linear isotropic hardening, *Int. J. Numer. Meth. Eng.* **53**, 49–63.

Düster, A., Niggl, A., and Rank, E. (2007) Applying the hp-d version of the FEM to locally enhance dimensionally reduced models, *Comp. Meth. Appl. Mech. Eng.* **196**, 3524–3533.

Eriksson, K., Estep, D., Hansbo, P., and Johnson, C. (1995) Introduction to adaptive methods for differential equations, *Acta Numer.* **105**, 106–158.

EuroNorm EN 1990 (2002) *Eurocode. Basis of Structural Design. German version.*, Berlin, Beuth Verlag.

Kuhn, T. (1962) *The Structure of Scientific Revolutions*, University of Chicago Press Chicago, IL.

Ladevèze, P. and Leguillon, D. (1983) Error estimate procedure in the finite element method and applications, *SIAM J. Numer. Anal.* **20**, 485–509.

Larsson, F. and Runesson, K. (2005) Consistent time-cycle approximation for cyclic plasticity coupled to damage. In Onate, E. and Owen, D.R.J. (eds.), *Computational Plasticity VIII, Fundamentals and Application*, Barcelona, Spain, pp. 1102–1105.

Larsson, F. and Runesson, K. (2006) Adaptive computational meso-macro-scale modeling of elastic composites, *Comp. Meth. Appl. Mech. Eng.* **195**, 324–338.

Larsson, F., Hansbo, P., and Runesson, K. (2002) On the computation of goal-oriented a posteriori error measure in nonlinear elasticity, *Int. J. Numer. Meth. Eng.* **55**, 879–894.

Niekamp, R. and Stein, E. (2002) An object-oriented approach for parallel two- and three-dimensional adaptive finite element computations, *Comp. Struct.* **80**, 317–328.

Oden, J. and Cho, J. (1996) Adaptive hpq-finite element methods of hierarchical models for plate- and shell-like structures, *Comp. Meth. Appl. Mech. Eng.* **136**, 317–346.

Oden, J. and Prudhomme, S. (2002) Estimation of modeling error in computational mechanics, *J. Comput. Phys.* **182**, 496–515.

Oden, J., Prudhomme, S., Hammerand, D., and Kuczma, M. (2001) Modeling error and adaptivity in nonlinear continuum mechanics, *Comp. Meth. Appl. Mech. Eng.* **190**, 6663–6684.

Ohnimus, S., Stein, E., and Walhorn, E. (2001) Local error estimates of FEM for displacements and stresses in linear elasticity by solving local Neumann problems, *Int. J. Numer. Meth. Eng.* **52**, 727–746.

Parés, N., Diéz, P., and Huerta, A. (2006) Subdomain-based flux-free a posteriori error estimators, *Comp. Meth. Appl. Mech. Eng.* **195**, 297–323.

Popper, K. (1959) *The Logic of Scientific Discovery*, Harper & Row, New York.

Rank, E., Düster, A., Nübel, V., Preusch, K., and Bruhns, O. (2005) High order finite elements for shells, *Comp. Meth. Appl. Mech. Eng.* **194**, 2494–2512.

Roache, P. (1998) *Verification and Validation in Computational Science and Engineering*, Hermosa, Albuquerque.

Rüter, M. and Stein, E. (2004) Adaptive finite element analysis of crack propagation in elastic fracture mechanics based on averaging techniques, *Comput. Mater. Sci.* **31**, 247–257.

Schwab, C. (1996) A posteriori modeling error estimation for hierarchic plate models, *Numer. Math.* **74**, 221–259.

Stein, E. and Ohnimus, S. (1997) Coupled model- and solution-adaptivity in the finite element method, *Comp. Meth. Appl. Mech. Eng.* **150**, 327–350.

Stein, E. and Ohnimus, S. (1999) Anisotropic discretization- and model-error estimation in solid mechanics by local Neumann problems, *Comp. Meth. Appl. Mech. Eng.* **176**, 363–385.

Stein, E. and Rüter, M. (2007) Finite element methods for elasticity with error-controlled discretization and model adaptivity. In E. Stein, R. de Borst, and T. Hughes (eds.), *Encyclopedia of Computational Mechanics, First Electronic Revision*, Vol. 2, Wiley, Chichester, pp. 1–55.

Stein, E., Rust, W., and Ohnimus, S. (1992)a h- and p-adaptive finite element methods for two-dimensional structural problems including postbuckling of shells, *Comp. Meth. Appl. Mech. Eng.* **101**, 315–354.

Stein, E., Zhang, G., and König, J. (1992b) Shakedown with nonlinear hardening including structural computation using finite element method, *Int. J. of Plasticity* **8**, 1–31.

Stein, E., Rüter, M., and Ohnimus, S. (2004) Adaptive finite element analysis and modelling of solids and structures. Findings, problems and trends, *Int. J. Numer. Meth. Eng.* **60**, 103–138.

Stein, E., Rüter, M., and Ohnimus, S. (2007) Error-controlled adaptive goal-oriented modeling and finite element approximations in elasticity, *Comp. Meth. Appl. Mech. Eng.* **196**, 3598–3613.

Szabó, B. and Sahrmann, G. (1988) Hierarchic plate and shell models based on p-extension, *Int. J. Numer. Meth. Eng.* **26**, 1855–1881.

Verfürth, R. (1996) *A Review of a Posteriori Error Estimation and Adaptive Mesh Refinement Techniques*, Wiley-Teubner, Chichester Stuttgart.

Vogelius, M. and Babuška, I. (1981) On a dimensional reduction method. II. Some approximation-theoretic results, *Math. Comput.* **37**, 47–48.

Wiechmann, K. and Stein, E. (2006) Shape optimization for elasto-plastic deformation under shakedown conditions, *Int. J. Solids Struct.* **43**, 7145–7165.

Zienkiewicz, O. and Zhu, J. (1987) Simple error estimator and adaptive procedure for practical engineering analysis, *Int. J. Numer. Meth. Eng.* **24**, 337–357.

Zienkiewicz, O. and Zhu, J. (1992) The superconvergent patch recovery (SPR) and adaptive finite element refinements, *Comput. Meth. Appl. Mech. Eng.* **101**, 207–224.

PREDICTIVE MODELLING OF DAMAGE IN STRUCTURES AND THE DEVELOPMENT OF RETROFITTING OR MITIGATING STRATEGIES

D.R.J. OWEN[1*], Y.T. FENG[1], J.M. RANCE[2] AND A.T. BERE[2]
[1]*Civil & Computational Engineering Centre, Swansea University, Singleton Park, Swansea, SA2 8PP, UK*
[2]*Rockfield Technology Ltd., Ethos Bld., King's Road, Swansea, SA1 8PH, UK*

Abstract. This chapter discusses computational approaches employed in the modelling of damage caused by blast, impact and natural loading and considers the development of retrofitting or mitigation strategies. An essential prerequisite to the design of retrofitting techniques is knowledge of the stress, displacement and fracture states in the damaged structure. Prediction of the damage induced in solids and structures due to blast and impact loading is therefore discussed and repair strategies based on anchor stitching methods are illustrated. Applications from several relevant areas are presented to illustrate the capabilities of continuum/discrete computational procedures.

Keywords: Impact, blast, reinforced concrete, masonry, continuous/discrete transformation, explosive modelling, retrofitting

1. Introduction

This chapter discusses computational approaches employed in the modelling of damage caused by blast, impact and natural loading and also considers the development of some retrofitting or mitigation strategies. An essential requirement in the simulation of blast or impact loading is the ability to model the creation of discrete fragmentation during the damage event. This then provides the residual stress and fracture states upon which the design of any retrofitting

* To whom correspondence should be addressed. e-mail: d.r.j.owen@swansea.ac.uk

A. Ibrahimbegovic and M. Zlatar (eds.), *Damage Assessment and Reconstruction After War or Natural Disaster*,

technique is based. Alternatively, when designing structures to withstand future blast or impact events, the ability to predict subsequent damage response is equally important. The chapter describes a range of applications related to damage induced by blast and impact loading to illustrate present day computational capabilities in this broad area of research and development.

Key issues related to the successful modeling of the continuous/discontinuous transformation of quasi-brittle materials have been adequately addressed in the literature (for example Klerck et al., 1999, 2003; Klerck, 2000; Pine et al., 2007; Owen et al., 2004, 2006, 2007a–c) and principally involve (i) the development of constitutive models which govern the material failure; (ii) the ability of numerical approaches to introduce discontinuities such as shear bands and cracks generated during the failure and fracture process and (iii) the effective detection and simulation of contact between the region boundaries and crack surfaces both during and after the failure event.

The numerical treatment of multi-fracturing solids necessitates a blend of continuous and discrete computational processes to provide adequate solution. Modelling fracturing solids employing a continuum description alone results in extremely complicated formulations involving an extended range of problem parameters, many of which are non-physical and cannot be derived from standard laboratory tests. Additionally, the modeling of the process beyond initial fracture becomes impossible, which may be vital if the prediction of material flow, throw pattern of fragments, etc. is important. On the other hand, attempts to model fracturing solids by particle methods are inevitably limited by the fact that description of the complex constitutive behaviour involved is restricted to its inclusion only as a particle interface response. Hence, the theoretical frameworks developed in nonlinear continuum mechanics that establish essential thermodynamic, kinematic and energy conservation conditions under fully multiaxial stress/strain states cannot be relied upon and situations involving dynamic loading, where wave propagation/dispersion phenomena must be addressed, are even more problematic. Consequently, a more natural and theoretically rigorous approach is offered by modelling the fracturing process as a continuum to discrete transformation. In addition to providing a more physically realistic representation, the approach provides advantages in allowing a constitutive description of the material that involves a minimum number of parameters that may be identified from standard experimental tests and does not require any "parameter fitting" process. Modelling aspects related to continuum mechanics include the development of constitutive models for a range of materials under a variety of loading conditions, element technology for near-isochoric deformation conditions, adaptive mesh refinement and damage modelling for prediction of the onset of fracture. With the development of fractures, the domain becomes discontinuous in nature and computational issues include

strategies for discrete crack insertion that preserve the system energy, adaptive remeshing to accommodate the fracture distribution, global search algorithms to monitor contact between the resulting particle system, development of appropriate contact interaction models and time integration of the system equations. Implementation of the entire solution strategy within a parallel processing environment is a further issue. For further information on the methodology the reader is directed to the publications cited in the references, but brief details are provided below.

1.1. LARGE-SCALE MULTI-BODY CONTACT

Modelling of the interaction of multiple bodies requires consideration of a number of key algorithmic issues. One of the most fundamental aspects is the development of effective detection procedures for monitoring contact between entities. The extent of the importance of such procedures is further highlighted by the fact that the process of contact detection and resolution must be performed continuously, i.e. at every time integration step, throughout the course of the finite/discrete element simulation (Cottrell et al., 2002). The contact process is composed of two principal activities; firstly the global search whereby a list of potential contacts is efficiently established using a bounding box circumscription and box intersection approach (Feng and Owen, 2002, 2004; Han et al., 2006, 2007). The second task is to process each of the candidate pairs in turn and establish the exact contact state. For each of the contact couples identified as actual contacts the impenetrability condition is then enforced using the well-established penalty algorithm.

Within the present work a local contact couple description based upon resolving the interaction between 2D node-edge contact pairs is used, and for the more complicated 3D case either node–facet or edge–edge contact couples are used. The 2D node–edge couple description produces an adequate level of contact resolution, however investigations (Feng and Owen, 2002) have identified the 3D node–facet contact algorithm as being inferior to the 3D edge–edge description, in that it often provides a non-smooth interface between intersecting facet corner locations.

1.2. CONTINUOUS ADAPTIVE REMESHING STRATEGIES

In order to alleviate the element distortion deficiency of a fixed mesh solution it has now become common practice to frequently update the finite/discrete element mesh using an adaptive remeshing approach. The continuous updating of the mesh can for many cases also lead to a controlled improvement in the numerical accuracy and overall computational expense of the system; this is

typically achieved through restriction of high element density to regions exhibiting significant activity (strain gradients, etc.). An adaptive remeshing strategy provides the flexible option of representing continuous material flow within a Lagrangian mesh description, and this feature proves to be extremely attractive when compared to the often-employed material based erosion techniques for penetration problems (Cottrell et al., 2002).

The remeshing indicator is the process that triggers the adaptive remeshing process by determining the violation of user defined threshold quantities such as the element distortion. Other element and nodal quantities, such as velocity gradients, are also applicable for initiation of the remeshing process. For many applications, improved mesh density prediction for the newly generated mesh is achieved using a criterion such as the accrued inelastic strain or the total incremental strain rate measure. These approaches provide a suitable means of imposing localised high mesh densities in regions that have large amounts of activity. For explosive material representations the use of evolving and reversible measures such as the strain gradient or pressure state are suitable for predicting element mesh densities. Fundamental issues in the computational procedure involve appropriate procedures for mapping solution variables between consecutive meshes (Cottrell et al., 2002).

1.3. DISCONTINUOUS FRACTURE INSERTION STRATEGIES

Traditionally, finite element modelling strategies rest within a continuum description, however, for many applications it is necessary to break-up or fracture a single body into a set of independent physical bodies in order to capture the true physical response. The fracture of a single continuum body has been shown to be paramount in the successful modelling of brittle systems subject to high strain rate impact or blast conditions.

The propagation of discrete fractures into a continuum domain introduces a number of further degrees of freedom into the system; these variables are associated with the nodes introduced to accommodate both crack insertion or crack extension. The process of creating discrete fractures also introduces additional contact surfaces that must be included (or updated) in the numerical solution procedure.

As a consequence, traditional continuum models have often been favoured over their discrete element counterparts due to their reduced computational complexity and cost, however with the rate at which the advancement of processing technology is progressing, computational efficiency is often considered less critical today. At present it is more crucial that robust strategies be developed for the modelling of both material and geometric response and now it is

computationally feasible, on commercial scale problems, to undertake discrete topological updating for simulating a continuous–discontinuous transition.

1.4. BOREHOLE BREAKOUT SIMULATION

As a test of the ability of the computational approach to simulate the response of multi-fracturing quasi-brittle materials, the problem of borehole breakout modeled as a 2D problem, illustrated in Fig. 1, is considered. Specifically, the ability to capture the contrasting failure mechanisms exhibited by strong and weak rocks under different confining pressure conditions, without the need for any adjustments to the constitutive model, is examined.

The initial continuum mesh is shown (Fig. 1a) and the horizontal confining pressure is maintained at a constant value whilst the vertical pressure is incrementally increased at the rate indicated.

The properties that describe the behaviour of the material are provided in Fig. 1b–d, where it is seen that the parameters required are readily identified from standard triaxial and tension tests. In addition to the usual elastic properties, the essential parameters are the tensile strength, compressive strength, fracture energy release rate and the standard Mohr–Coulomb data. An additional parameter is the frictional sliding coefficient on newly created discrete cracks. The material parameters presented correspond to Lac du Bonnet granite (Lee and Haimson, 1993) and the weak sedimentary rock Cardova cream limestone (Haimson and Song, 1993).

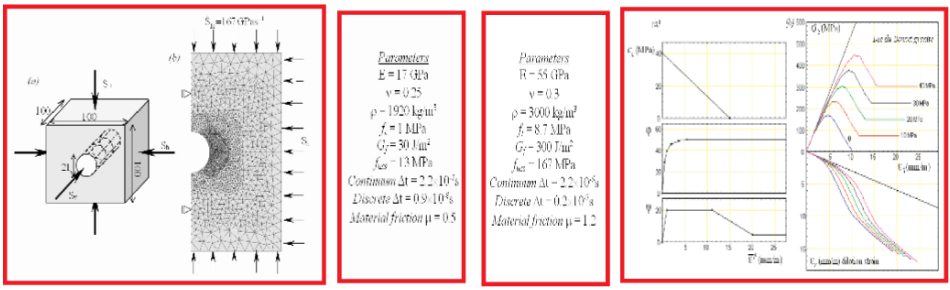

(a) (b) (c) (d)

Figure 1. Borehole breakout example – (**a**) geometry and mesh, material properties; (**b**) granite; (**c**) limestone; and (**d**) Mohr Coulomb data

Figure 2 illustrates the fracture patterns developed for the two materials where it is seen that fundamentally different mechanisms are involved. For the granite specimen, Fig. 2a, failure takes place by the development of sub-vertical fractures at the regions indicated and very good agreement is evident between

the experimental observations (Lee and Haimson, 1993) and the numerical predictions. In Fig. 2b similar comparison is made for the Cardova cream limestone, for which failure takes place by the development of fracture shear bands. In the computational model these manifest themselves as distinct crack bands formed by en-echelon systems of tensile fractures. Again, there is excellent correspondence between the experimental failure mode (Haimson and Song, 1993) and the numerical simulation. It is important to note that the computational model has been able to reproduce these two fundamentally different failure mechanisms by only changing the relevant material parameters.

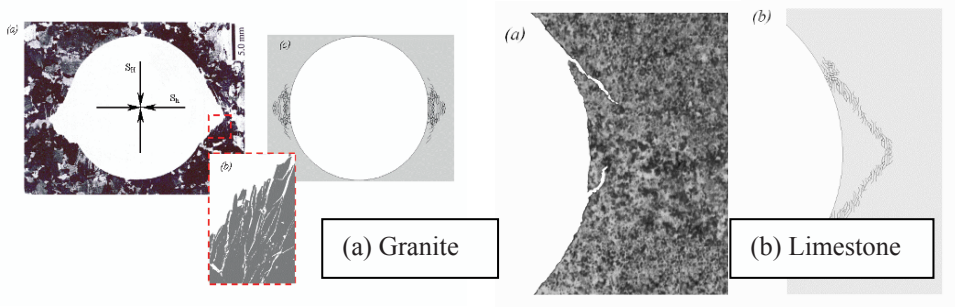

Figure 2. Comparison of experimental and numerically predicted failure patterns for two different materials

2. Impact on Reinforced Concrete Structures

2.1. IMPACT LOADED BEAM

Work has been conducted at Heriot Watt University to assess the response of reinforced beams subjected to impact loading by experimental means (Bere, 2004). The simply supported beams, which are reinforced top and bottom and include shear reinforcement (stirrups), are centrally impacted at low speed. The impact results in the beam reaching a peak loading followed by cracking and load shedding. Although the impact causes failure in a serviceability sense, it is not a catastrophic event, i.e. perforation, penetration or significant scabbing does not occur. Computational modelling of this test serves as a further means of validating the multi-fracturing technology employed. High-speed cameras and load cells are used to assess the effect of the impact on the beam.

The beam is 3 m in length, 200 mm deep and 100 mm wide. The beam is supported 150 mm from each end and is free to rotate about the centre height of the beam. The impactor mass is 98 kg and it is projected towards the beam at 8.3 m/s. The point of impact is on a 12 mm thick section of plywood, which initially rests on the beam.

The numerical model of the beam uses the symmetric properties of the beam to simplify the analysis, whereby only half the beam is modelled. Each aspect of the physical experiment is represented in the numerical model, as displayed in Fig. 3.

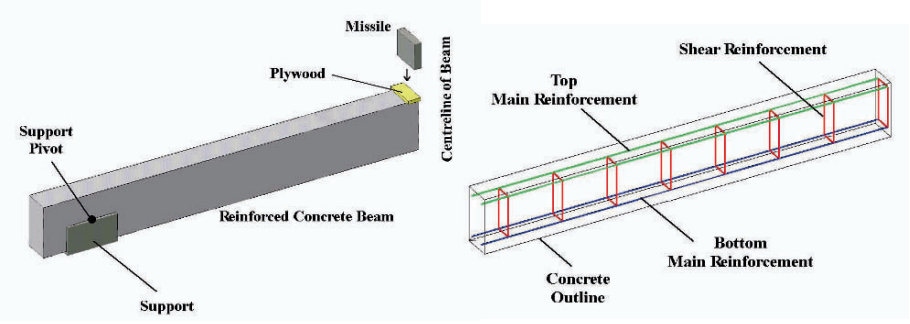

Figure 3. Numerical model setup (*left*) and reinforcement detailing (*right*)

The beam is reinforced with main top and bottom reinforcement (high yield strength – 12 mm diameter bars). Also, along the length of the beam are stirrups (mild steel – 6 mm diameter bars), which pass around the main reinforcement. The reinforcement elements are modelled between nodes that also define the concrete elements and follow an elasto-plastic material response. The modelling technique allows the concrete elements to become detached from the reinforcement with the yield criterion for this bond being equivalent to the tensile strength of the concrete, which is a valid approximation.

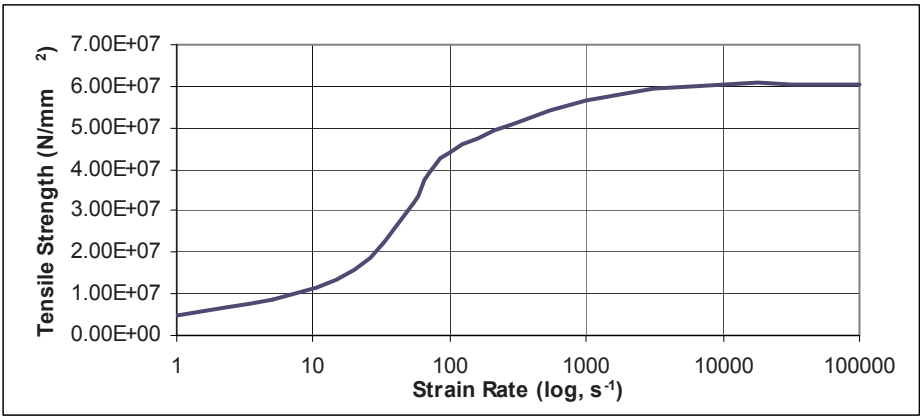

Figure 4. Strain rate dependency of the concrete material

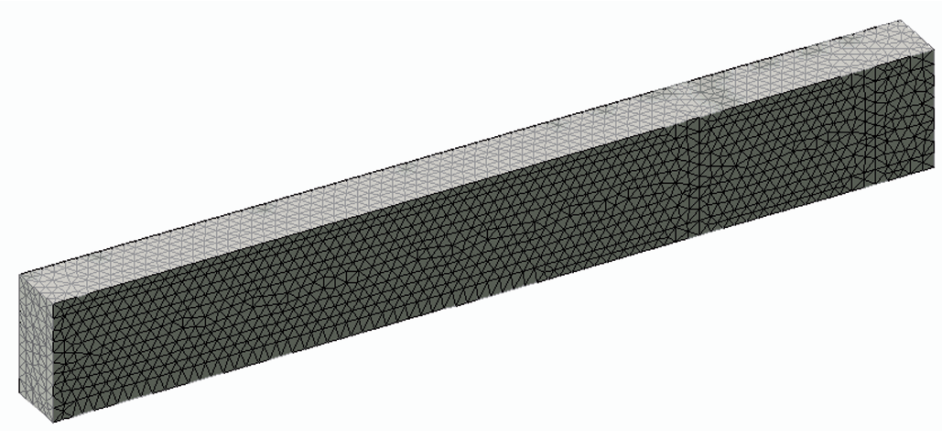

Figure 5. The numerical model mesh

The main reinforcement is composed of high yield bars (Yield stress 560e6 N/m^2, Ultimate stress 630e6 N/m^2) and the stirrups are formed from mild steel bars (Yield stress 250e6 N/m^2, Ultimate stress 280e6 N/m^2). The material properties for the concrete are provided in detail in Bere (2004), but it is worth emphasising the need to include strain rate dependent effects on the material parameters. For example, Fig. 4 shows the increase in tensile strength with increasing local material strain rate.

The numerical model of the beam is analysed with the finite element mesh displayed in Fig. 5. A total of 26,000 tetrahedral elements are used to represent the concrete and 500 beam elements to represent the reinforcement bars. The reinforcement bars are modelled such that they are located along the boundaries of tetrahedral concrete elements.

The experimental results include the time-reaction graph and the final cracking pattern of the beam. The time-reaction curve is a fundamental output as it describes the response of the beam during the impact; which includes non-linear events such as the development of fractures. The reaction reflects the stiffness and capability of the beam to resist failure; and is also dependent on the failure mode of the beam, i.e. whether the load is in continual contact after impact, or if several contact events occur.

Figure 6 displays the comparison of the experimental and numerical time-reactions curves. It can be seen that the duration of loading and the peak loads exhibit good correlation.

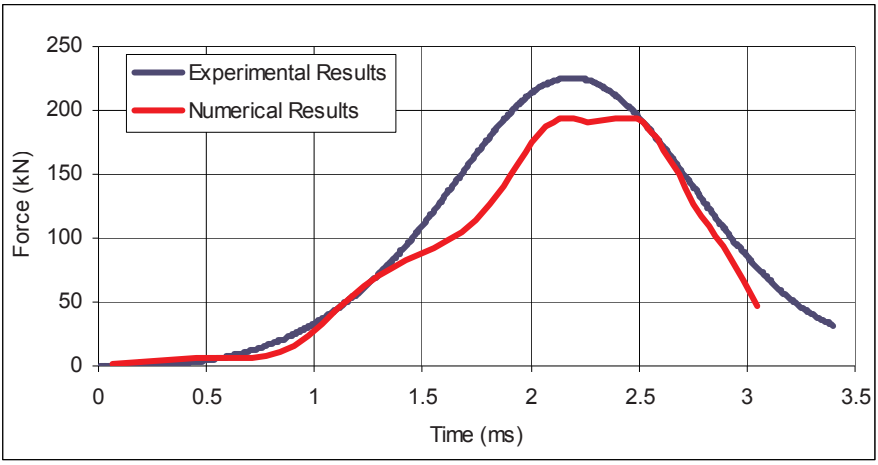

Figure 6. Experimental and numerical simulation results

The initiation of the reactive force can be seen to occur at a low steady rate, followed by a sharp rise in slope to the peak reaction. From the assessment of the numerical results it was seen that the inclusion of a plywood strip at the point of impact was a critical aspect to the beam's behaviour. The low steady increase corresponds to the compaction of the plywood with little deflection of the beam occurring; this indicates that a degree of the missile energy is transferred to the plastic deformation of the plywood and not directly to the beam. As the plywood becomes fully compacted and effectively incompressible, the energy remaining in the missile is transferred directly to the beam, which corresponds to the sharp increase in reaction. It is interesting to note that tests undertaken without a plywood strip resulted in complete destruction of the beam in every case.

(a) Experiment

(b) Numerical Simulation

Figure 7. Final cracking pattern of the experimental test and numerical simulation of the impact of the reinforced concrete beam

The final cracking pattern of the experimental tests, Fig. 7a, contains two main areas of cracking: (1) directly beneath the impact in a cone-like shape and (2) more distributed cracking initiated along the length of the beam. The final cracking pattern obtained by numerical simulation, as shown in Fig. 7b, corresponds with the experimental distribution. A full comparison of the experimental response and computational prediction is undertaken in Bere (2004). By comparison of the fracturing patterns confidence in the simulation of the impact of the beam is gained. Additionally, it is evident that initial fracturing occurs due to the shear cone phenomena, a process which has been widely acknowledged from other observations of such tests. The similarity of the time-reaction curves also supports the validity of the computational model.

2.2. IMPACT LOADED SLAB

The following example describes the numerical simulation of an experimental impact test undertaken by Sugano et al. (1993) in which the impact velocity is considerably higher than in the example presented above. The recorded data was in the form of the impact face crater depth and the size of the crater caused by scabbing of the distal face. The numerical model of the test is illustrated in Fig. 8, where simulation is undertaken using the continuous-to-discrete quasi-brittle fracturing model described above.

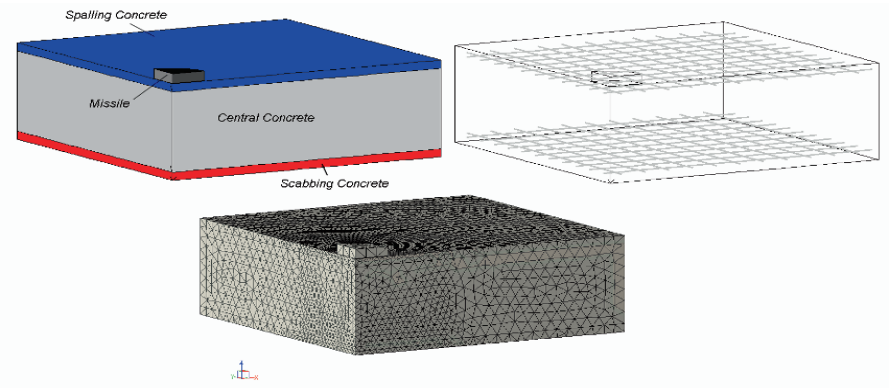

Figure 8. Numerical model: Target material regions, reinforcement layers and finite element mesh

The reinforcement bars are individually modelled as elasto-plastic beam elements and are allowed to separate from the continuum concrete elements. The reinforcement is modelled in two layers, top and bottom, consisting of isotropic bar arrangements. The missile is assumed deformable and can be represented by

a series of three solid components (total scaled mass 25 kg) connected by a spring system, to represent the deformability under impact of a commercial jet engine, as described by Sugano et al. (1993) and summarised in Fig. 9. Sugano et al. assessed the difference between the actual engine and the deformable missile model by conducting static compression tests as well as full-scale impact tests.

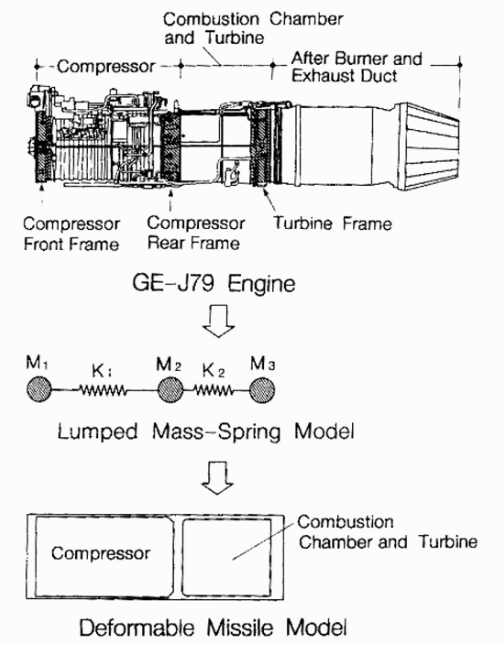

Figure 9. Procedure for modelling the GE-J79 engine as described by Sugano et al. (1993)

The finite element mesh, displayed in Fig. 8, consists of 418,495 tetrahedral elements (representing the concrete and missile), and 3,659 beam elements (representing the reinforcement bars). The missile is projected perpendicular to the surface of the slab at 205 m/s. In view of the loading velocity the concrete is modelled as strain-rate dependent, with the tensile strength being directly related to the local strain-rate, as shown in Fig. 4.

The output from the simulation displayed in Fig. 10 shows the overall fracturing patterns of the impacted face and slab cross sections at complete defeat of the missile and at one instant during the simulation. The fracturing patterns describe the failure method of the slab and are therefore an important aspect of the validation of the analysis and evaluation of the failure process.

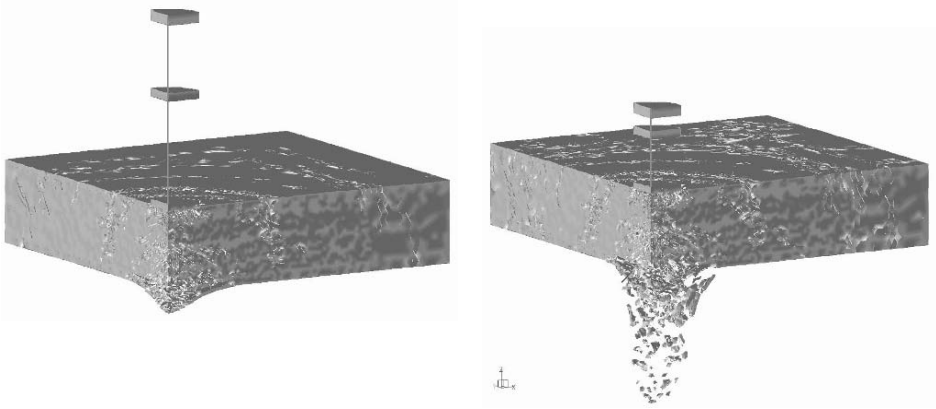

Figure 10. Sequential fracturing patterns of impacted slab and extent of scabbing

Figure 11 displays the displacement of both reinforcement layers when the missile velocity is reduced to zero. It can be seen that the top reinforcement has not significantly deformed, whereas the distal reinforcement shows extensive deformation.

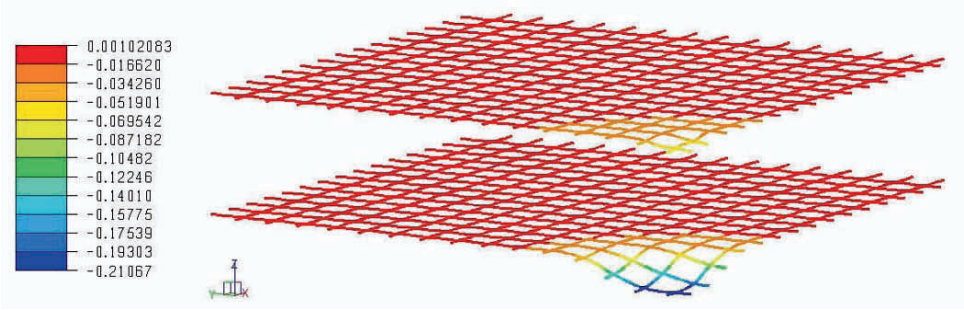

Figure 11. Top and bottom reinforcement layers displacement (m)

In addition to the above results Sugano also predicted, with the aid of high-speed photography, the scabbed particle size and velocity distribution, The majority of the particles tend to detach in the early stages of the analysis with a large velocity. In contrast, the particles with larger mass tend to detach in the later stages of the analysis with lower velocities. The prediction of scabbed particle mass and velocity correlates well with the pattern described by Sugano and the magnitudes of mass and velocity also show good comparison. Further details of the comparison between the experimental results and computational modelling can be found in Bere (2004).

3. Explosive Modeling

Advancement of robust and efficient numerical tools that can aid the understanding of explosive driven structural response is crucial for modeling blast processes. The purpose of this section is to demonstrate that techniques based upon a coupled adaptive finite/discrete element description can be used to obtain well-defined and quality time-resolved results for the modelling of explosively driven processes (Cottrell et al., 2002, 2003a, b). Enhancement of the understanding of the burn propagation and the resulting structural deformation, which can occur for various material configurations, is of primary importance.

Computational strategies in the context of a combined finite/discrete element description for the effective modelling of realistic explosive problems involving multiple phenomena require consideration of: (i) complex constitutive descriptions for providing clear post yielding response for various material types, (ii) the modelling of the ignition and subsequent controlled burn of explosive materials together with accurate pressure evolution (iii) the provision of efficient detection procedures for monitoring contact between large numbers of finite/discrete elements, together with accurate techniques for resolving the interaction between such entities, and (iv) inclusion of adaptive remeshing approaches for the updating of the finite element domain to permit spatial description of the problem throughout the gross geometrical deformations that will take place, as well as providing a means of controlling both the numerical expense and accuracy of the achieved solution. The applicability of the methodologies developed will be illustrated through two practical examples.

3.1. CONSTITUTIVE MODELLING

The Jones–Wilkins–Lee (JWL) equation of state is typically used for the determination of the pressure state resulting from the detonated products of explosive materials (Lee et al., 1973). The JWL equation of state defines the pressure state as a function of the material relative volume (v) and the internal energy per initial volume (e), through the expression

$$P = A\left(1 - \frac{\omega}{r_1 v}\right)\exp\left(-r_1 v\right) + B\left(1 - \frac{\omega}{r_2 v}\right)\exp\left(-r_2 v\right) + \frac{\omega e}{v} \qquad (1)$$

in which the terms A, B, r_1, r_2 and w are specifically defined material parameters, which can be determined from a number of dynamic experiments. In addition, it should be recognised that a set of JWL material parameters are usually considered as a collection of interdependent values, and as such cannot be independently modified without adversely influencing other contributing data.

For the case of metallic based materials the effect of temperature on the flow stresses must be included in a constitutive law to enable an accurate prediction of the material response. Some of the most commonly employed constitutive models include the Johnson and Cook (1983) and Zerilli and Armstrong (1987) viscoplastic strength models. Using these models together with a specific pressure–volume description, provided by an equation of state function, a model that displays both rate, pressure and temperature dependency can be obtained and, more significantly, easily calibrated. Other techniques based upon equation of state formulations are also used to represent the nonlinear pressure–volume response often experienced at high strain rates, temperatures and pressures.

Similarly, for the more complicated case of non-metallic and non-ductile materials such as those typified by quasi-brittle or geomechanical responses, the influence of pressure is equally important and must be well defined within the constitutive law to provide an appropriate material description. Numerous authors have developed constitutive models capable of representing these non-uniform materials, some based on two of the most longstanding Mohr–Coulomb and Drucker–Prager models (e.g. Klerck, 2000; Yu, 1999).

Other more complex descriptions (particularly for more ductile materials) accounting for the additional influence of rate have also been proposed including the Johnson–Holmquist models (Johnson and Holmquist, 1992, 1994) and numerous other variants (Cottrell et al., 2002). Although such responsive model descriptions provide a large flexibility of material description, some constants cannot be easily determined within a controlled laboratory environment, and are often evaluated by way of repetitive “best guess” selection.

3.2. EXPLOSIVE BURN MODELLING

During the initial ignition and subsequent burn of an explosive material, large quantities of energy are rapidly generated. The energy introduced is required for inclusion within the standard Rankine–Hugoniot equations for shock waves governing chemically inert materials. According to the underlying thermodynamic law, the internal energy gained by a local region of material is accounted for through the heat (or energy) input into the region and the work done upon the region by the action of any external pressure forces.

An explosive material can be detonated using a number of techniques within the finite element and discrete element framework (Cottrell et al., 2002); these techniques vary in numerical complexity and are suitable for a large range of problem classes.

- 'Volume controlled burn' – where the explosive energy is added to the energy of the inert material at the start of the numerical analysis
- 'Compression controlled burn' – where the explosive material is initially detonated by a critical value of compressive volumetric strain being exceeded
- 'Time controlled burn' – where the explosive material is initially detonated at a specific initiation point and then the subsequent detonation wave is assumed to travel radially at a (constant) specified velocity

When material detonation occurs, a wave front travels radially away from the initiation point and when the wave front reaches each element Gauss point material ignition occurs. The energy release rate is then specifically defined through combination of the total energy expended per unit volume, the element volume and the post detonation burn time.

3.3. SOIL CRATERING EXAMPLES

The numerical example illustrated in Fig. 12 considers the detonation of an explosive charge that is shallowly buried beneath the surface of a geomechanical material. This type of simulation provides modelling insight to the behaviour of multi-fracturing solids when subjected to explosively driven loadings.

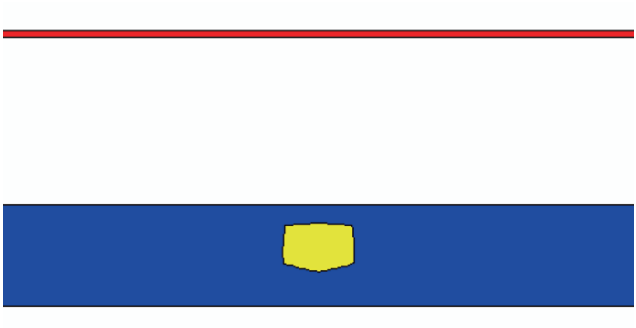

Figure 12. Representation of the initial model geometry, showing the solid medium (blue), the explosive material (yellow), and a steel collection plate (red)

The TNT explosive material is of initial volume 30 mm^3, and is shallowly buried beneath the surface of the material. The explosive is detonated from its centre of mass and the pressure (shock) waves are assumed to travel in a radial direction away from the ignition point using a time-controlled material burn option. The properties representative of the TNT explosive material are given in Cottrell et al. (2002).

In addition to the burn modelling of the TNT explosive material, the soil material is simulated using a compressive fracture model developed specifically for quasi-brittle solids. The tensile/compressive fracture model comprises a failure envelope that encompasses the rate independent but pressure sensitive Mohr–Coulomb criterion together with the anisotropic rate dependent rotating crack strain-softening model (Klerck et al., 1993, 2003; Klerck, 2000). Material properties required for the full description of the tensile/compressive fracture model are given in Cottrell et al. (2002).

The expansion and subsequent deactivation of the TNT explosive material, together with the fragmentation of the surrounding geotechnical medium, and the deformation of the steel collector plate are given in Fig. 13.

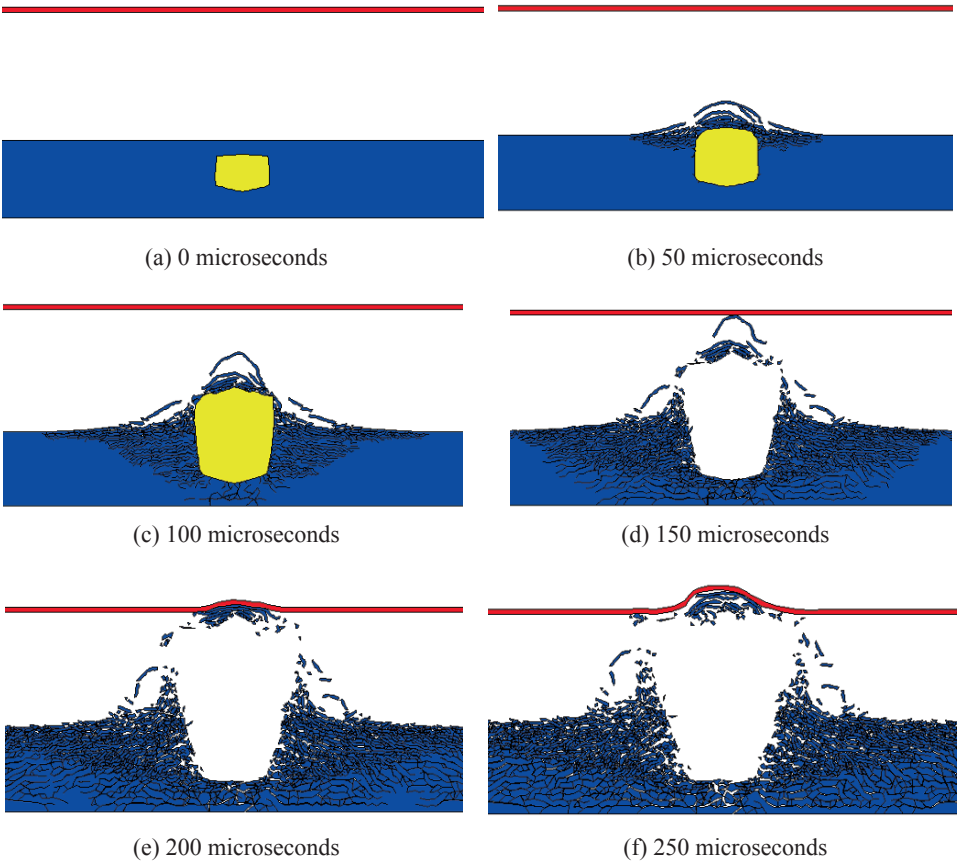

Figure 13. Evolving deformed configurations of the soil material (blue), the TNT explosive material (yellow), and the suspended steel plate (red) at times (**a**) 0, (**b**) 50, (**c**) 100, (**d**) 150, (**e**) 200, and (**f**) 250 μs post initial explosive detonation

The following numerical example considers the detonation of an explosive charge located at the surface of a geomechanical material. This type of simulation demonstrates an approach for modelling continuous type deformations exhibited by some soil materials when subjected to surface located explosive loadings. The problem geometry and loading considered are shown in Fig. 14a.

The PE4 explosive material is of initial diameter 139 mm, and is detonated from its centre and the pressure (shock) waves are assumed to travel in a radial direction away from the ignition point using a time-controlled burn facility. The properties of the explosive model are listed in Table 1. The soil material is modelled using the traditional Drucker–Prager criterion and the relevant properties are given in Cottrell et al. (2002).

The expansion and subsequent deactivation of the PE4 explosive material at 200 μs post detonation, together with the material flow of the surrounding soil medium are given in Figs. 14 and 15.

Within Figure 14 the initial stages of the explosive detonation (<100 μs) are considered. During this stage of the simulation, the explosive surface charge initiates and expands rapidly during the material burn phase.

After 100 μs the explosive material has increased many times in volume but the pressure present within the explosive has dissipated sufficiently to permit deactivation of this material. The irregular shape of the explosive products over the 100 μs interval arises from the use of an unstructured meshing approach, leading to small variations in nodal mass terms. Material flow of the soil after 400–1,000 μs is given in Fig. 15, and indicates formation of a "V" shaped crater.

TABLE 1. Parameters for the PE4 explosive material

Parameter	Notation	Value used
Initial material density (kg/m^3)	ρ	1,600
Elastic bulk modulus (kPa)	K	21,600
Elastic shear modulus (kPa)	G	2,234
Detonation velocity (m/s)	v_D	8,189
Initiation detonation location (m)	X	X = 0.10 y = 0.10 z = 0.0045
Initiation (detonation) time (s)	t_D	0.00
JWL constant A (MPa)	A	707,400
JWL constant B (MPa)	B	12,377
JWL constant w	w	0.25
JWL constant r_1	r_1	4.7
JWL constant r_2	r_2	1.3

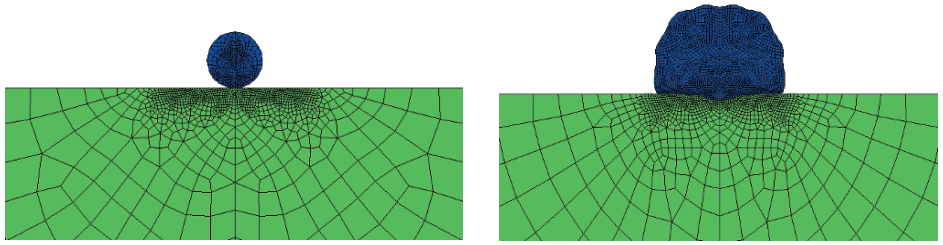

(a) 0 microseconds (b) 50 microseconds

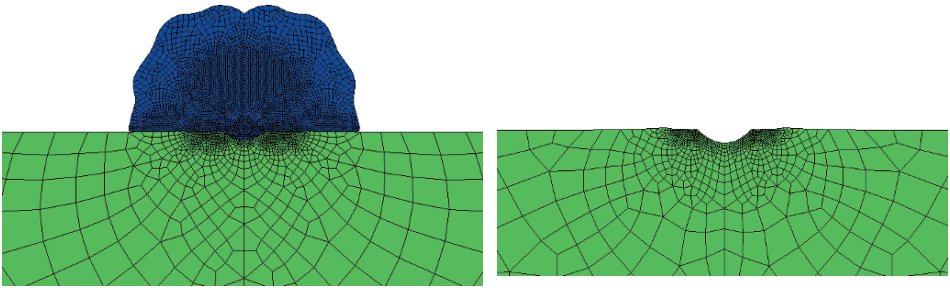

(c) 100 microseconds (d) 200 microseconds

Figure 14. Evolution of the deformed configuration of the soil medium subjected to an explosive charge detonated at surface level, with plots at times (**a**) 0 μs, (**b**) 50 μs, (**c**) 100 μs, and (**d**) 200 μs post initial detonation

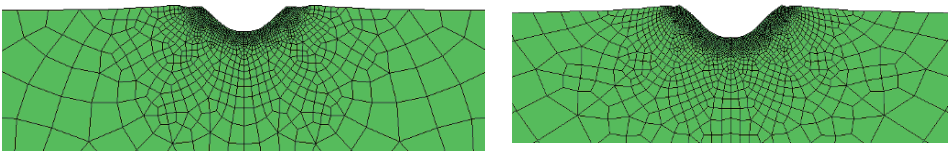

(a) 400 microseconds (b) 600 microseconds

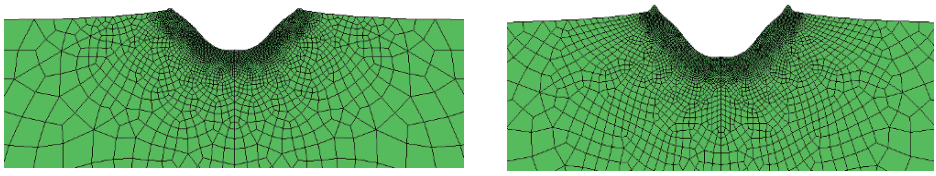

(c) 800 microseconds (d) 1000 microseconds

Figure 15. Evolution of the deforming soil medium subjected to an explosive charge detonated at surface level, with plots at times (**a**) 400 μs, (**b**) 600 μs, (**c**) 800 μs, and (**d**) 1 ms after initial detonation

4. Retrofitting Strategies

One objective of the work described in this chapter is to develop industrially applicable computational procedures to assess alternative repair strategies for damaged masonry structures. In many instances, structures which have been damaged can be successfully repaired by the insertion of anchors, use of prestressing systems, etc. For relatively modern structures the decision to repair, rather than demolish, may be based on economic considerations, but for historic structures the use of remedial techniques becomes a cultural necessity. One major repair strategy involves the insertion of stitching anchors, whereby reinforcing elements are introduced to carry tensile and shear stresses within damaged regions. Currently, appropriate stitching patterns are selected on the basis of previous experience and a major aim of computational modelling is to provide a rational approach to determining an efficient and near-optimal anchor arrangement. In this way, a simulation capability could be provided to aid decision making in quantifying the remnant structural integrity of masonry structures and to examine optional remedial actions.

The predictive modelling of the behaviour of masonry structures, particularly in the non-linear range, remains a challenge, due predominantly to their semi-discrete and composite nature. An adequate computational model must include the fundamental mechanisms that characterise the composite action: (i) sliding along a bed or head joint at low values of normal stress, (ii) cracking of the masonry units (bricks, blocks, etc.) in direct tension and (iii) diagonal tensile cracking of masonry units at values of normal stress sufficient to develop frictional behaviour in the joints. Further aspects which may require consideration include the treatment of reinforcement and/or prestressing in composite construction techniques or repaired structures. To date, most computational predictions have been based on a macro-modelling approach, in which attempts are made to incorporate some or all of the phenomena described above within a continuum description; employing homogenisation concepts to produce a smeared representation of the brick/joint action and classical plasticity concepts to model the tensile/compressive failure of the resulting composite. Such a modelling strategy has, to date, been dictated both by the limits of available computing power and the lack of maturity of other semi-discrete computational techniques.

Whilst considerable fundamental information can be derived from solutions based on a continuum approach, a more natural treatment of this class of problem is offered by use of discrete element methods. Discrete elements are based on the concept that individual material elements are considered to be separate and are (possibly) connected only along their boundaries by frictional/adhesive contact. With present day computational power large scale discrete

element models can be considered and for industrial applications in the field of rock blasting, etc. ~1,000,000 elements are routinely employed.

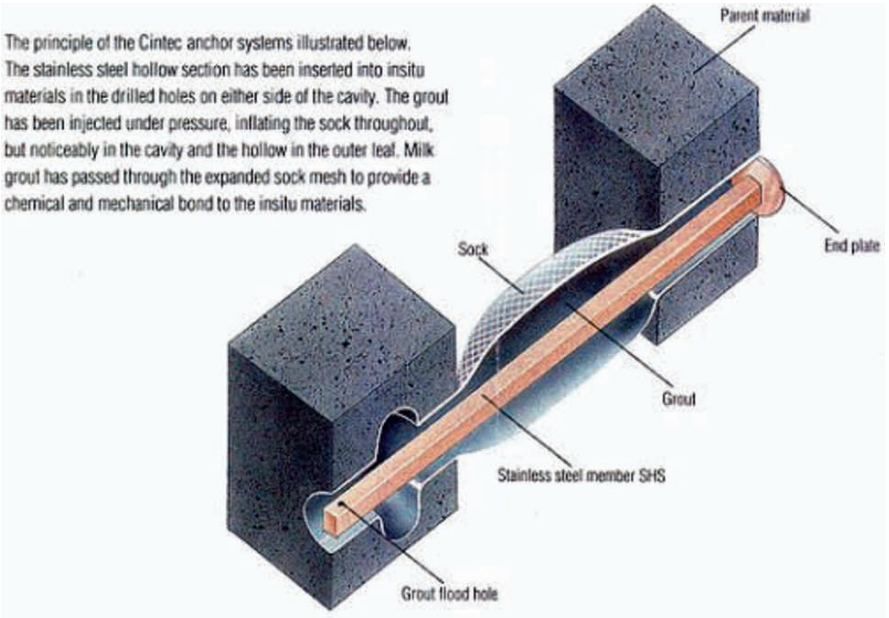

Figure 16. Stitching anchor systems

For repair or mitigation strategies, one particular stitching anchor system is provided by Cintec International (2000). The main steel body of the anchor that carries and transfers loads is completely surrounded by a fabric sock made of polyester fibres. This wrapped anchor is placed in a hole drilled to roughly twice the anchor's diameter. Cementitious grout is injected under controlled pressure through the middle of the anchor. When the grout reaches the end, it flows through a series of grout flood holes back into the fabric sock. The entire assembly then inflates like a balloon and has the advantage that the sock moulds to the shape of any cavities in the masonry, thereby providing additional pull-out resistance. The process is summarised in Fig. 16.

Use of the anchor stitching process in the reinforcement of masonry structures is described below.

4.1. RETROFITTING – BRIDGES

As an illustration of the capabilities of discrete/finite element numerical techniques for predictive modelling of the collapse and subsequent repair of masonry bridges, two examples are presented below. In the first, the Strathmashie Bridge

is considered, where the problem is treated as a combined 2D finite/discrete element problem with the masonry blocks being represented by deformable discrete elements in frictional contact. The bridge and its collapse mode are shown in Fig. 17.

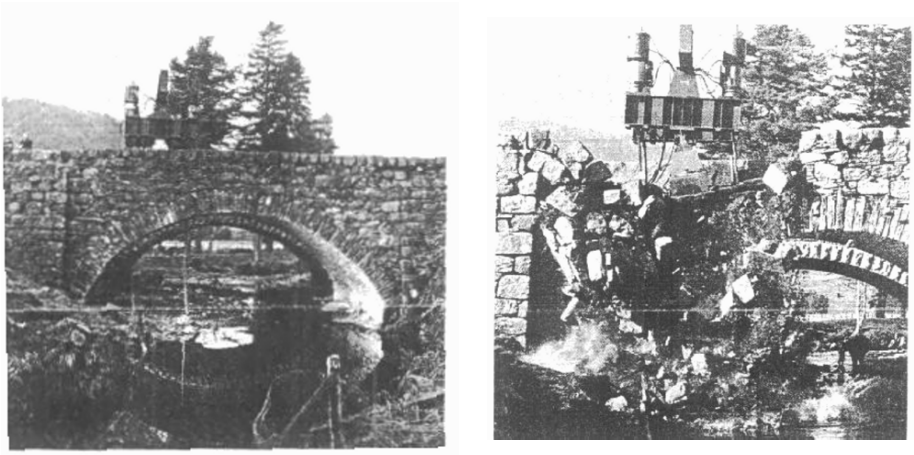

Figure 17. Strathmashie bridge before and at the start of collapse

The computational results obtained are illustrated in Fig. 18. Figure 19 shows the collapse state at the end of the numerical simulation and Fig. 20 shows a comparison between the numerical and experimental load–displacement curves, where a good correlation is evident.

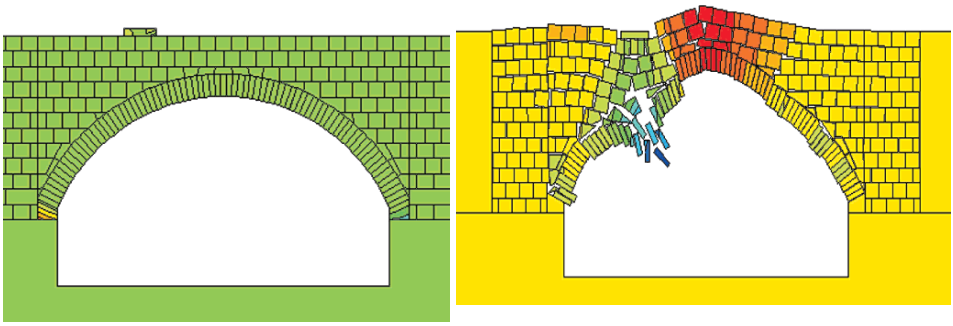

Figure 18. Initial configuration and the beginning of collapse of the numerical model

Figure 19. Collapse stage near to end of thenumerical simulation

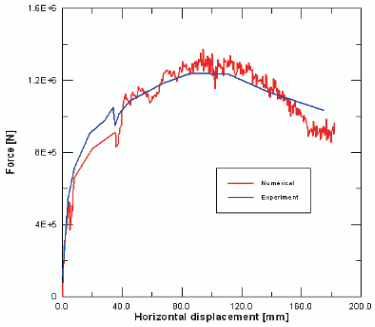

Figure 20. Load–displacement diagram

The second example considers the performance of a three-ring arch bridge, firstly unstrengthened and secondly when reinforced with the Cintec anchor stitching system. Both arches were constructed and tested to destruction under controlled conditions at the Transport Research Laboratory, UK. Each arch was constructed with a layer of wet sand between the three rings to simulate ring separation (delamination). A schematic illustration of the arch, together with the general arrangement of the Cintec anchors, is shown in Fig. 21.

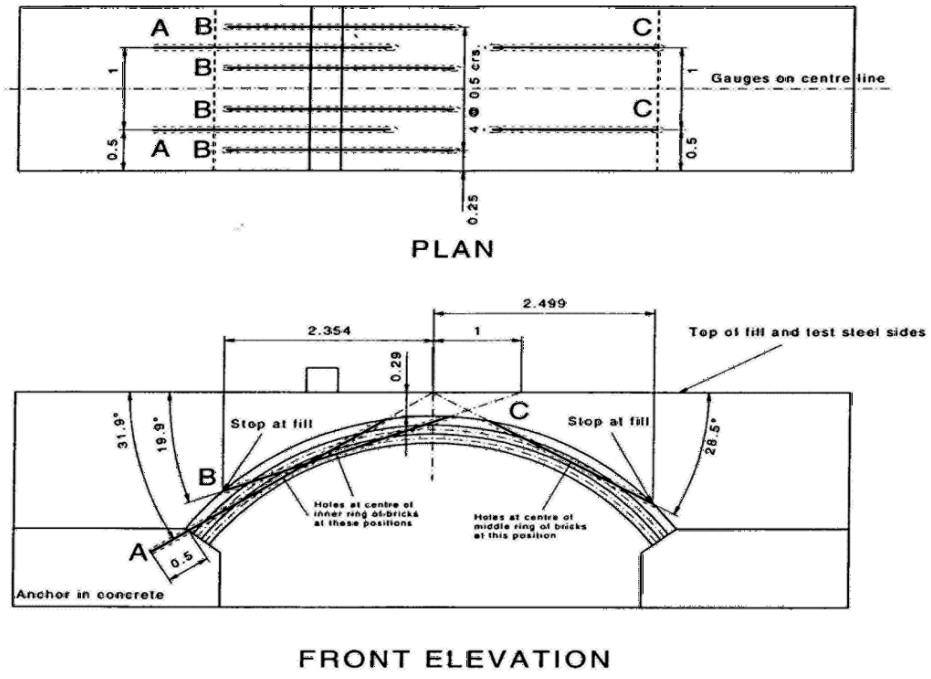

Figure 21. Arch strengthened with Cintec anchor system

Each anchor is modelled as an elasto-plastic steel bar and the grouted bond with the masonry is simulated by prescribing a (non-linear) shear stress/strain relation, whose parameters are determined from laboratory anchor pull-out tests (Roberts, 1999).

The test load was applied at quarter span in 1 t increments with failure occurring in a ductile manner by crushing of the bottom brick at the crown which, for the strengthened arch, lead to the formation of the first hinge at 28 t. During loading to collapse the bottom ring fell away but the remainder of the arch remained held together by the anchors. The arch ultimately failed in a four hinge mechanism. The failure loads for the unstrengthened and reinforced arch were 20 and 41 t respectively. The deformation of the strengthened arch just before the bottom ring fell away is illustrated in Fig. 23.

Figure 22a shows the finite/discrete element idealisation of the unstrengthened arch and Fig. 22b depicts the deformation just prior to collapse. The displacement under the load line with increasing load is shown in Fig. 24, where the prediction for the unstrengthened and reinforced cases are compared. An excellent correlation between the numerical prediction and experimental observation for the peak loads is evident.

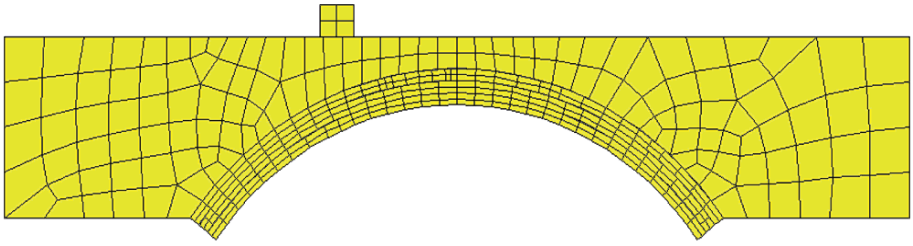

(a) Finite/discrete element idealisation

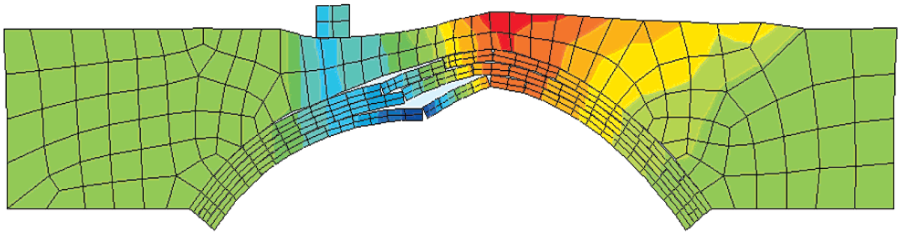

(b) Displacement pattern close to collapse

Figure 22. (**a**) Finite/discrete element idealisation; (**b**) displacement pattern close to collapse

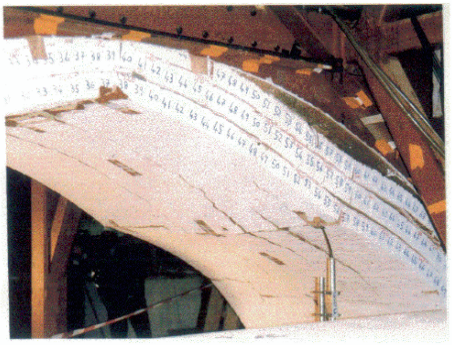

Figure 23. Strengthened arch just before bottom ring fell away

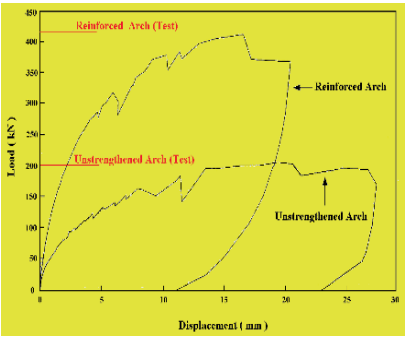

Figure 24. Load–displacement predictions for the unstrengthened and reinforced arches

4.2. RETROFITTING – BLAST LOADING

The following section describes a retrofitting strategy for a wall panel that has been the subject of extensive experimental investigation (see Impact testing). The combined finite/discrete element technology is used to investigate the strengthening of the structure subjected to blast loading. Both unstrengthened and strengthened walls have been simulated and compared against field test results performed at Cranfield University Ordnance Testing Evaluation Centre (COTEC), West Lavington Down, Wiltshire, UK during 1999–2000 and RAF Spadeadam, Cumbria, UK in 2001.

In the field tests, various types of masonry walls consisting of regular brick and concrete block, with and without window apertures have been subjected to a variety of blast loads. The aim of the tests was to investigate the behaviour of the retrofitted reinforced masonry support system under realistic conditions and develop the best techniques for design and installation.

Representation of the interaction of the blast wave with the masonry structure was accomplished using a semi-coupled approach. A CFD analysis was used to predict the propagation of the blast wave and a combined finite/discrete element analysis to predict the response of the masonry wall. Analysis of the blast wave propagation was undertaken using the Air3d (Air3d) software system assuming that the masonry structure was stationary, which is valid since the blast wave passes the wall within 4 ms. The pressure history predicted on the face of the wall was subsequently applied as a loading to the finite/discrete element model.

The test arrangement comprised the masonry wall, a steel reaction frame, concrete support blocks and reinforcing anchors. A detailed representation of the masonry wall was undertaken, with each brick modelled as a discrete elastic solid and a mortar interface model employed between the brick surfaces to

account for the behaviour of the grout. The steel frame utilised an elasto-plastic material model to enable plastic deformation to be captured.

In the case of the reinforced wall, non-linear anchor elements were used to represent the Cintec anchor reinforcement. These anchor elements account for elasto-plastic behaviour of the steel bars and the stiffness of the anchor grout in the direction along the bars (Roberts, 1999).

Loading applied to the structure was gravity and a time-history pressure obtained from the CFD results defined for each brick face. Gravity was applied as a first stage to obtained initial conditions for the subsequent pressure loading. The plots of stress distribution on the reinforced wall taken at varying time intervals are shown in Fig. 25 below.

Figure 25a shows vertical stress contours at 1.0 ms. The stress levels in the compressive zone at the base of wall are high enough to crush the bricks. This zone corresponds to an area on the test wall that exhibited front face brick failure.

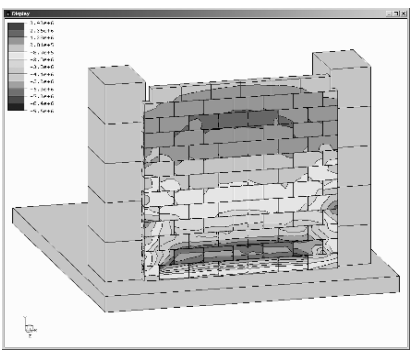

(a) t = 1 ms

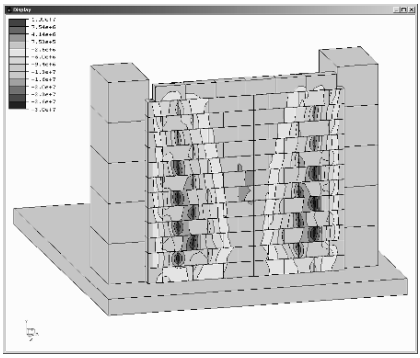

(b) t = 1.5 ms (front face)

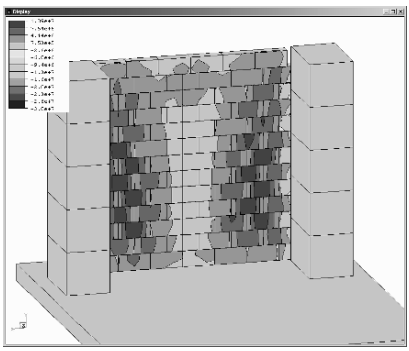

(c) t = 1.5 ms (back face)

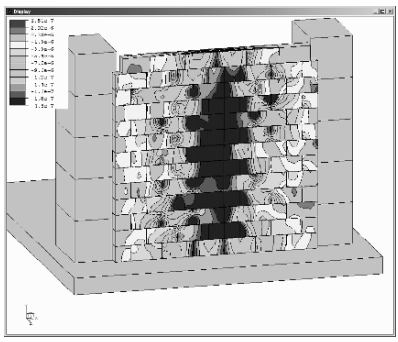

(d) t = 2 ms

Figure 25. Stress distributions for the reinforced wall at different time intervals

After approximately 1.5 ms, the wall starts to bend at the edges and compressive horizontal stresses form at the vertical brick joints on the front face, as shown in Fig. 25b. This compressive force is also large enough to crush some of the brick edges as seen in the tests. A horizontal tensile stress zone also develops on the back face, commensurate with the bending action, as shown in Fig. 25c. The maximum tensile stress occurs at the centre of each brick, reducing horizontally towards the mortar joints. The joints have already failed since stresses are in excess of the mortar tensile strength.

After 2 ms, the bending zones move inwards and meet at the centre of the wall, as depicted in Fig. 25d. Significant horizontal stresses on the back face exceed the tensile capacity of the bricks and initiate vertical cracking. Also, the compressive stress zone meets in the centre of the wall causing significant crushing of the bricks particularly along their vertical edges.

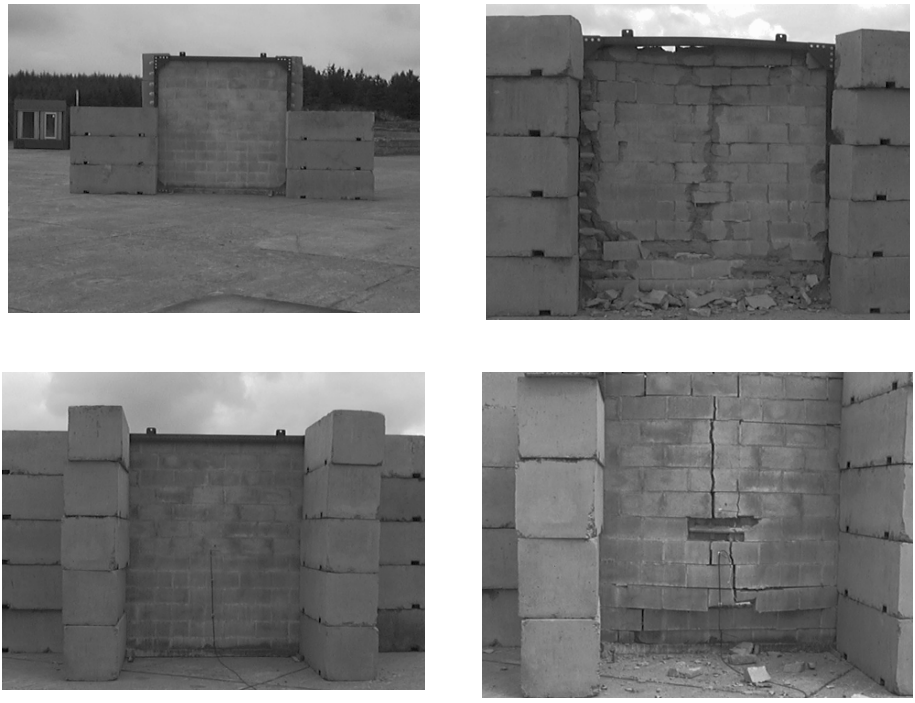

Figure 26. Before (*left* column) and after (*right* column) views of the Spadeadam Wall Test in June 2001. The wall was subjected to a blast load from 200 kg TNT NEQ @ 12.5 m; 534 kPa, 1,274 kPa ms (440 lbs TNT NEQ @ 41 ft; 77 psi, 185 psi ms). The front view is at the top

In order to illustrate the benefits of reinforcement, “before and after” photographs of the Spadeadam Wall Test are reproduced in Fig. 26. The aim of the test was to investigate the behaviour of a hollow concrete block (CMU) wall

subjected to a severe blast load having been reinforced with retrofitted masonry support anchors. The wall measured 3 × 3 m (10 × 10 ft) and was constructed within a steel reaction frame some 8 weeks before the test. Once the wall had cured, it was then diamond drilled at 225 mm (9 in.) vertical centres, corresponding with the masonry gauge. Retrofitted reinforced masonry support system anchors were then installed, inflated and allowed to cure for 28 days before the test.

The displacement plots for the unreinforced wall taken at varying time intervals are shown in Fig. 27 below, where it is seen that total failure takes place. In contrast, it is seen in Fig. 26 that structural integrity is maintained throughout the event for the reinforced wall, as is indeed predicted by numerical simulation of the same case.

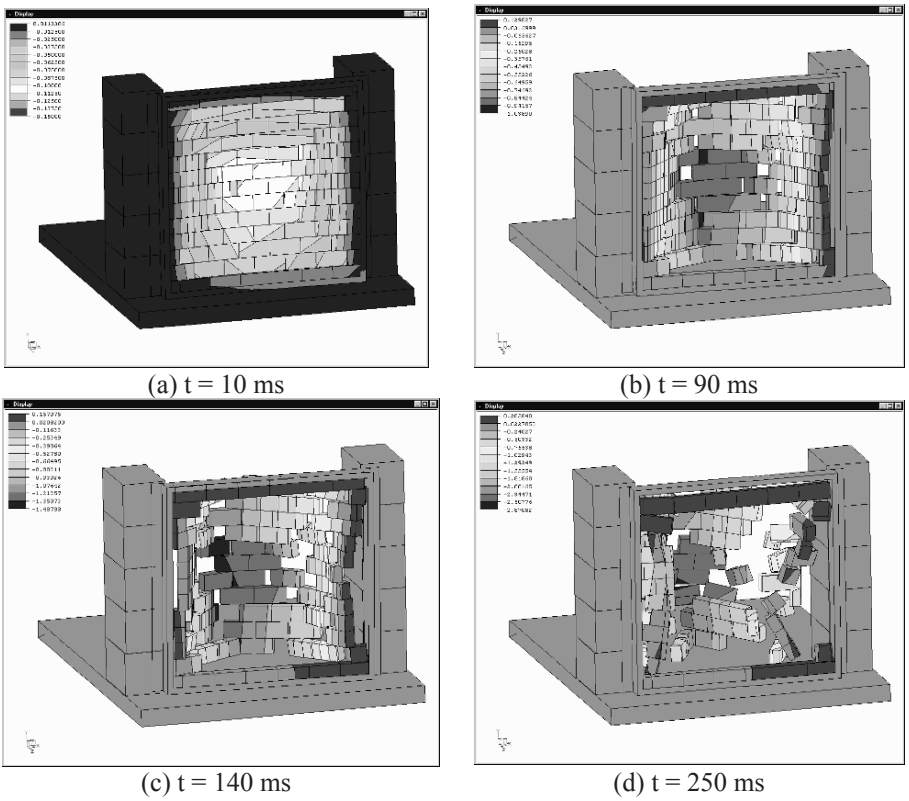

(a) t = 10 ms (b) t = 90 ms

(c) t = 140 ms (d) t = 250 ms

Figure 27. Displacement contours for the unreinforced wall at various time intervals

By combining the discrete element technique with a finite element formulation for the reinforcement, numerical models have been developed that have allowed evaluation of the relative performance of reinforcement based retrofitted

strengthening. The development of strengthening schemes would have been extremely difficult and costly using conventional analysis or testing. Although that the present computational predictions have shown that a good correlation exists with the results of field tests, further work is required to verify in a fully industrial environment that the numerical methodology is capable of simulating the observed behaviour of masonry structures subjected to blast loading.

5. Closing Remarks

This chapter has illustrated the potential that combined discrete/finite element methods offer as an alternative approach to predictive modelling of the failure assessment, and subsequent repair, of structures. As such, the work represents ongoing research and there is considerable scope for further development necessary to improve the robustness and industrial applicability of the methodology. An immediate need involves extension of the procedure to large scale fully three dimensional problems. This clearly extends the scale of the problems to be solved, necessitating the use of parallel processing techniques, but permits a more realistic simulation of the action of a wide range of structures.

As for all computational models, the need for validation is paramount. In this respect the use of field test results is invaluable, particularly for impact and blast loading situations where data is difficult and expensive to accrue.

In view of the complex geometrical configurations existing in an evolving finite/discrete element analysis, the use of visual tools for interpreting the results is mandatory. In addition to employing the more usual on-screen representation of 3D objects, the use of virtual reality techniques to provide a fully immersive environment for the interpretation of results is becoming increasingly attractive and realisable.

References

Air3d, Royal Military College of Science, Cranfield University, Shrivenham, Wiltshire, UK.

Bere, A. T., Computational modelling of large-scale reinforced concrete structures subject to dynamic loading, Ph.D. thesis, University of Wales, Swansea, 2004.

Cintec International Limited. The Cintec anchor system. Newport, Wales, 2000.

Cottrell, M. G., The development of rational computational strategies for modelling high velocity impact, Ph.D. thesis, University of Wales, Swansea, 2002.

Cottrell, M. G., Yu, J. and Owen, D. R. J., The adaptive & erosive numerical modelling of boron carbide subjected to large-scale dynamic loadings with element conversion to undeformable meshless particles. International Journal of Impact Engineering, Vol. 28(9), pp. 1017–1035, 2003a.

Cottrell, M. G., Yu, J., Wei, Z. and Owen, D. R. J., The numerical modelling of ceramics subject to impact using adaptive discrete techniques. Engineering Computations, Vol. 20, pp. 82–106, 2003b.

Feng, Y. T. and Owen, D. R. J., An augmented spatial digital tree algorithm for contact detection in computational mechanics. International Journal of Numerical Methods in Engineering, Vol. 55(2), pp. 159–174, 2002.

Feng, Y. T. and Owen, D. R. J., A 2D polygon/polygon contact model: Algorithmic aspects. International Journal of Engineering Computations, Vol. 21(1–3), pp. 265–277, 2004.

Haimson, B. and Song, I., Laboratory study of borehole breakouts in cordova cream: A case of shear failure mechanism. International Journal of Rock Mechanics and Mining Sciences, Vol. 30(7), pp. 1047–1056, 1993.

Han, K., Feng, Y. T. and Owen, D. R. J., Polygon-based contact resolution for non-circular discrete objects. International Journal of Numerical Methods in Engineering, Vol. 66(3), pp. 485–501, 2006.

Han, K., Feng, Y. T. and Owen, D. R. J., Performance comparisons of tree-based and cell-based contact detection algorithms. International Journal of Engineering Computations, Vol. 24(2), pp. 165–181, 2007.

Johnson, G. R. and Cook, W. H., A constitutive model and data for metals subjected to large strains, high strain rates and high temperatures. Proceedings of the 7th International Symposium on Ballisitcs, The Hague, The Netherlands, pp. 541–547, 1983.

Johnson, G. R. and Holmquist, T. J., A constitutive model for brittle materials subjected to large strains, high strain rates and high pressures. In: Shockwave and High Strain Rate Phenomena in Materials, edited by M. S. Meyers, L. E. Murr and K. P. Staudhammer. Marcel Dekker, New York, pp. 1075–1081, 1992.

Johnson, G. R. and Holmquist, T. J., An improved constitutive model for brittle materials. In: High-Pressure Science & Technology, edited by S. C. Schmidt, J. W. Shaner, G. A. Samara and M. Rodd. AIP Press, New York, 1994.

Impact testing. http://www.sbe.hw.ac.uk/research/structural/impact_test/index.htm.

Klerck, P., Sellers, E. J. and Owen, D. R. J., Discrete fracture in quasi-brittle materials under compressive and tensile stress states. Computational Methods in Applied Mechanics and Engineering, Vol. 193, pp. 3035–3056, 2003.

Klerck, P. A., The discrete element modelling of quasi-brittle fracture, Ph.D. thesis, University of Wales, Swansea, 2000.

Klerck, P. A., Owen, D. R. J., Yu, J. and Crook, A. J. L., A methodology for discretisation objective, discrete, dynamic fracture. In: Mechanics of Quasi-Brittle Materials & Structures, edited by G. Pijaudier-Cabot et al. Hermes Science Publications, Paris, pp. 367–390, 1999.

Lee, E. L., Finger, M. and Collins, W., JWL equation of state coefficients for high explosives. Report No. UCID-16189, Lawrence Radiation Laboratory, University of California, Livermore, CA, 1973.

Lee, M. and Haimson, B., Laboratory study of borehole breakouts in Lac du Bonnet granite: A case of extensile failure mechanism. International Journal of Rock Mechanics and Mining Sciences & Geomechanics, Vol. 30(7), pp. 1039–1045, 1993.

Owen, D. R. J., Feng, Y. T., De Souza Neto, E. A., Wang, F., Cottrell, M. G., Pires, F. A. and Yu, J., The modelling of multi-fracturing solids and particulate media. International Journal of Numerical Methods in Engineering, Vol. 60(1), pp. 317–340, 2004.

Owen, D. R. J., Feng, Y. T., Cottrell, M. G. and Yu, J., Computational issues in the simulation of blast and impact problems: An industrial perspective. NATO Advanced Research Workshop on Extreme Man-Made and Natural Hazards in Dynamics of Structures, Croatia, Springer, pp. 3–36, 2006.

Owen, D. R. J., Feng, Y. T., Lobao, M., Leonardi, C. R., Zhao, S. Y. and Yu, J., Simulation of multi-fracturing rock media including fluid/structure coupling. Proceedings First Canada – US Rock Mechanics Symposium, Vancouver, Canada, May 27–31, 2007a.

Owen, D. R. J., Andrade Pires, F. M. and de Souza Neto, E. A., A computational model for viscoplasticity coupled with damage including unilateral effects. In: Computational Plasticity, edited by E. Onate and D. R. J. Owen, Springer, pp. 145–164, 2007b.

Owen, D. R. J., Feng, Y. T., Han, K. and Leonardi, C. R., Multi-field coupling strategies for large scale problems involving multi-fracturing rock and particulate media. APCOM-EPMESC 07 International Conference, Kyoto, Japan, December 3–6, 2007c.

Pine, R. J., Owen, D. R. J., Coggan, J. S. and Rance, J. M., A new discrete fracture model for rock masses. Geotechnique, Vol. 57(9), pp. 757–766, 2007.

Roberts, D. P., Finite element modelling of rockbolts and reinforcing elements, Ph.D. thesis, University of Wales, Swansea, 1999.

Sugano, T., Tsubota, H., Kasai, Y., Koshika, N., Itoh, C., Shirai, K., vonRiesemann, W. A., Bickel, D. C. and Parks, M. B., Local damage to reinforced concrete structures caused by impact of aircraft engine missiles, Part 1 and Part 2. Nuclear Engineering and Design, Vol. 140, pp. 387–423, 1993.

Yu, J., A contact interaction framework for numerical simulation of multi-body problems and aspects of damage and fracture for brittle materials, Ph.D. thesis, University of Wales, Swansea, 1999.

Zerilli, F. J. and Armstrong R. W., Dislocation mechanics based constitutive relations for material dynamics calculations. Journal of Applied Physics, Vol. 61, pp. 1816–1825, 1987.

ON FUNDAMENTAL CONCEPT OF STRUCTURAL COLLAPSE SIMULATION TAKING INTO ACCOUNT UNCERTAINTY PHENOMENA

D. Hartmann[1] (hartus@inf.bi.rub.de), M. Breidt[1], V. Nguyen[1], F. Stangenberg[2], S. Höhler[2], K. Schweizerhof[3], S. Mattern[3], G. Blankenhorn[3], B. Möller[4], and M. Liebscher[4]
[1]*Institute for Computational Engineering, Ruhr-Universität Bochum, 44780 Bochum, Germany, EU*
[2]*Institute for Reinforced and Prestressed Concrete Structures, Ruhr-Universität Bochum, 44780 Bochum, Germany, EU*
[3]*Institute of Mechanics, Universität Karlsruhe, 76131 Karlsruhe, Germany, EU*
[4]*Institute of Statics and Dynamics of Structures, Dresden University of Technology, 01062 Dresden, Germany, EU*

Abstract. The simulation of controlled structural collapse using explosives faces the problem of the quantification of structural parameters. The latter has to be accomplished on the basis of only few data, which may additionally be characterized by vagueness, e.g. due to uncertain measurements or changing reproduction conditions. This uncertainty has to be taken into account within a consistent analysis. As the simulation of collapses of real world structures with conventional finite element models requires extreme computational effort, this paper addresses an efficient approach for the simulation of structural collapse based on consistently simplified multibody models, that simultaneously allow for the investigation of uncertainty.

Keywords: Demolition, explosives, multi-level simulation, multibody dynamics, uncertainty, fuzzy analysis

1. Introduction

A controlled structural collapse is often requested for dilapidated buildings. To provide a safe as well as an economically reasonable demolition of such structures at the end of their lifespan, a careful planning of the tearing-down process is required. A prime advantage over alternative demolition techniques (e.g. using wrecking balls or special demolition devices) is that the cost intensive application of man power and equipment is primarily

A. Ibrahimbegovic and M. Zlatar (eds.), *Damage Assessment and Reconstruction After War or Natural Disaster*,

limited to drilling holes for the explosive charges in pre-determined zones of the building or structure. The basic idea of a blasting strategy is simply to eliminate vertical supports of the structure by controlled blasting exploiting the forces of gravity in an optimal fashion.

For a long time, the determination of an appropriate blasting strategy has been based upon the acquired experience and knowledge of demolition experts. According to this knowledge, decisions about the number, the placement of the explosive charges applied and the course of the ignition time-points were made. Various accidents and failures at real world blasting events in the past, however, demonstrated that empirical approaches are prone to errors. This is a result of the fact that it is extremely difficult to make prognoses on the accurate dynamic behavior of the induced collapse process. This also holds for the precise position of the explosive charges with respect to the desired collapse result, and also for the ignition time-points as well as ignition sequences of the charges.

To this respect, computer simulations are helpful which form a powerful tool to improve the control of the collapse of buildings, and to figure out optimal blasting strategies.

A lot of research has been carried out on the prevention of hazardous structural collapses. However, only some computer-based investigations on volitional demolitions of moderate complex structures by means of controlled explosives, such as Hartmann et al. (1994), Isobe and Toi (1998) or Kabele et al., (2003) can be found in the literature. In this context, investigations on the dynamic response of structures due to extreme loads like explosion, impact or earthquake have to be mentioned (Meguro and Hakuno, 1992; Meguro and Tagel-Din, 2002; Kaliszky and Logo, 2006). Much of this work is associated with the so-called progressive collapse (e.g. Kaewkulchai and Williamson, 2004; Astaneh-Asl, 2003; Starossek, 2006). One reason for the emergence of the research at this area was the collapse of the Ronan Point Apartment in 1968. Ronan Point was a 23-storey tower block in Newham, East London, which suffered a fatal structural collapse due to a natural gas explosion on 16 May 1968, that caused the progressive collapse of the whole South-East corner of the building. The 9–11-collapse of the world trade center has led to a drastic increase of research in the area of progressive collapse in recent years.

Nonetheless up till now, there is still a lack of generally applicable and holistic simulations for controlled blasting of complex large scale structures. Within this respect the complete basis of modelling has to be considered: The structural model and structural parameters have to be established on the basis of plans, drawings, measurements, observations, experiences, expert knowledge, codes and standards. Structural parameters have to be specified that represent geometry, material and detonation time of

the applied explosives (fuses). Very often, certain information regarding structural models and precise values of structural parameters do not exist.

Thus for realistic structural analysis and safety assessment uncertainty must be appropriately taken into consideration. Different methods are available for mathematically describing and quantifying uncertainty. Characteristic concepts are probability theory (Madsen et al., 1986), including subjective probability approach (Wright, 1994) and Bayes-methods (Stange, 1977), interval mathematics (Alefeld and Herzberger, 1983), convex modelling (Ben-Haim and Elishakoff, 1990), theory of rough sets (Pawlak, 1991), fuzzy set theory (Bandemer and Gottwald, 1995), theory of fuzzy random variables (Krätschmer, 2001) and chaos theory (Kapitaniak, 2000). The selection of one of this models is governed by the existing databases. In our contribution is presumed that the databases require the application of the fuzzy set theory, i.e., the uncertainty model fuzziness.

Summarizing, the focus of the presented project is on the simulation of the controlled collapse of complex large scale structures and the design of blasting strategies based on efficient simulation models using multibody dynamics under particular consideration of uncertainty.

2. Deterministic simulation of progressive collapse

A realistic but also efficient simulation of the collapse of complex large-scale real world structures induced by controlled explosives demands a sophisticated simulation model. This simulation model has to cover the dynamics of the entire collapse process, triggered through the ignition of the explosive charges along with the dead load of the structure. At the end of the collapse process, the debris hill as the final result should be obtained. To map all possible phenomena during the blasting process, the simulation model applied has to be based on a multi-level model.

To this end, a three-level approach is useful to capture most effects: On the first level (local level or micro-level), the effects of the exploding charges are modelled such that the volitional damages can be captured and described. On the second level (near field level or meso-level), the effects of the local damages on adjacent structure components are analyzed. These two levels provide a knowledge basis which allows to model the dynamics of the collapse of the entire structure on the third level in an efficient fashion (global level, far field level or macro-level) including relevant fracture processes and relevant contact mechanisms.

For the uncertainty analysis, which requires a large number of deterministic simulations of the collapse, a very efficient computer model is necessary. Therefore the physical core of the simulation model on the global level is based on a so-called “special multibody system (special MBS)” that

is tailored to the realistic and efficient simulation of structural collapse, particularly to the major collapse kinematics.

2.1. USING MULTIBODY MODELS WITHIN THE SIMULATION OF STRUCTURAL COLLAPSE

The application of rigid multibody models takes advantage of the typical collapse behavior. In such a collapse the deformations of distinct areas of the structure – considering specified periods of time – are small compared to zones of accumulated damage and failure within the structure. Hereby, the zones of accumulated damage are modelled by means of multibody subsystems that are specifically developed for individual load cases and failure mechanisms supported by additional finite element analysis on the global and near field level. Then rigid and non-rigid zones can be defined for certain time segments of the collapse. Figure 1 shows the relation between the individual simulation models.

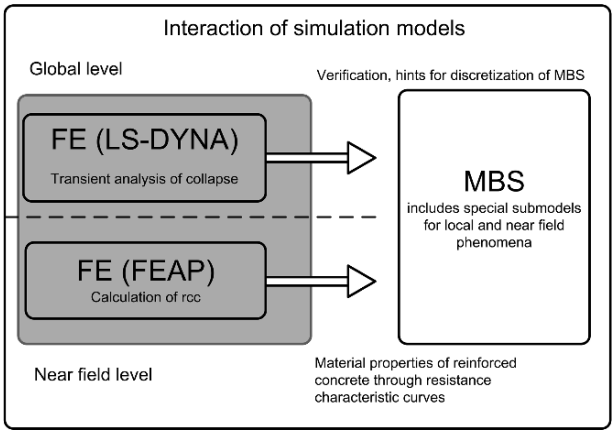

Figure 1. Relation between finite element and multibody models

The multibody subsystems are specifically designed using rigid bodies, constraints and, in particular, appropriate force elements to achieve a realistic approximation of the behavior of reinforced concrete during the collapse process. The force elements use pre-calculated so called resistance characteristic curves (rcc) that are determined by a priori finite element analysis (FEAP) on a near field length scale level using e.g. an elasto-plastic damage model for reinforced concrete.

Also transient finite element calculations (LS-DYNA) are carried out on the global level to gain experience about the proper discretization of the multibody model. This includes the development and selection of appropriate multibody subsystems as well as the distribution of the subsystems

within the entire multibody model. To this respect, the development of the multibody model is linked with global transient finite element methods providing a solid basis for verification of multibody subsystems, see Fig. 2.

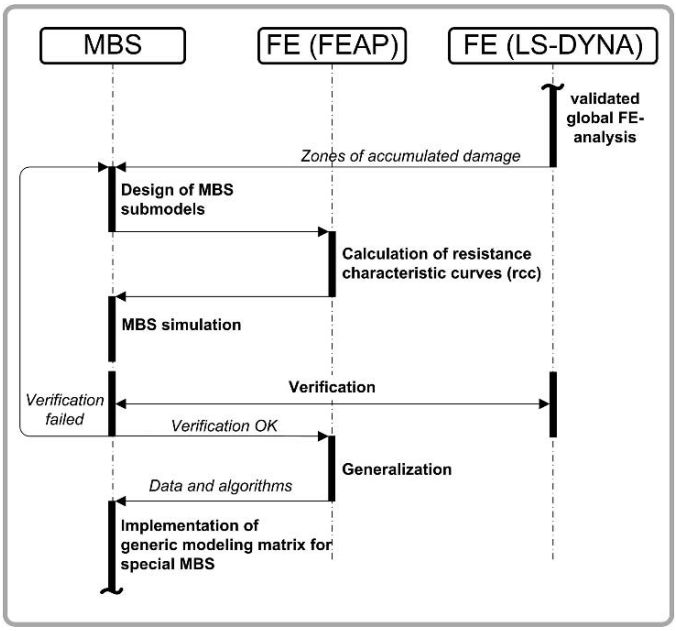

Figure 2. Communication between applied simulation models

Based on validated global finite element analysis of representative real world collapse processes using explicit LS-DYNA (Hallquist, 1998, 2005), typical zones of accumulated damage are identified. The corresponding failure mechanisms are modelled by tailor-made multibody subsystems, that are designed using rigid bodies, constraints and force elements. The nonlinear character of those force elements is calculated by finite element analysis, applying FEAP (Taylor, 2001).

2.1.1. *Reinforced concrete models for zones of accumulated damage and determination of rcc*

To achieve a realistic approximation of the behavior of reinforced concrete during the collapse process, pre-calculated resistance characteristic curves (rcc) are used. Those rcc are determined by finite element analysis using an elasto-plastic damage model for reinforced concrete used in standard structural members of the complete structure. The analysis and the used material model are described in the following.

Material model
The material model applied depends on Krätzig and Pölling (2004) and is a close-to-practice elastic-plastic damage theory model for reinforced concrete. The advantage is the minimum number of material parameters and their determination by standard experiments. It is implemented in the framework of the finite element program FEAP (Taylor, 2001).
To model the behavior of concrete in compression and tension realistically, a combination of plasticity as well as continuum damage theory is used. Both are formulated stress-based which is more fitting for the analysis of the investigated reinforced concrete structures (Pölling, 2000). To avoid localization effects a smeared crack concept and the use of fracture respectively crushing energy is chosen. For details we refer to Hartmann et al. (2008).

Reinforcement is typically used as bars in reinforced concrete structures, so only uniaxial steel behavior is needed. At least elasto-plastic behavior is required for a failure analysis. More applicable models could be found in Hofstetter and Mang (1995) and Chen (1982).

Discretization with finite elements
Reinforced concrete is represented by superposition of the material models of the constituent parts of its components concrete and steel. Depending on the type of problem, the structural part is represented as a volume element or a continuum-based multi layer shell element (Krätzig and Jun, 2002). The reinforcement is either represented by a thin layer within the shell element (Fig. 3a) or a discrete truss element representing each single bar (Fig. 3b). As a consequence perfect bond is assumed. The integration of the constitutive equation is based on the return map algorithm described in Simo and Hughes (1998). Changes and further implementations regarding the specific requirements of the material models for reinforced concrete can be found in (Pfister et al., 2006).

Determination of resistance characteristic curves
The determination of the resistance characteristic curves is conducted based on a FE-Program using the above described material models and elements. It is to be emphasized that the shell element is limited to plates and simple beams due to the complex construction of reinforcement in intersections and columns (stirrups). The stress resultant, which are needed as resistance for the subsystems in the special multibody simulation, can be determined by means of an integration of the stresses. Regularly, the approximation of structural members is made by one shell element representing the height or thickness, so that the stress resultants can be calculated between two

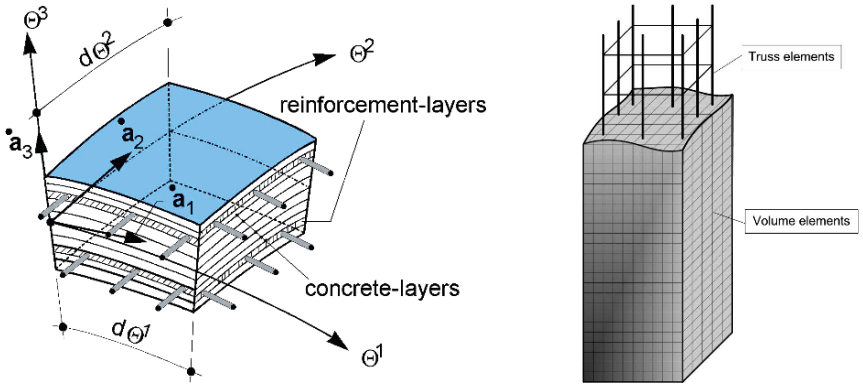

(a) Continuum based multi layer shell element

(b) Volume and Truss elements

Figure 3. Used types of elements

elements. Using volume elements the calculation of the stress resultants requires a given cross section, such that additional data is needed. For one or more locations in the mesh a new arbitrary point of origin is chosen. Along with a defined normal direction, a surface $E: \boldsymbol{p} \cdot \boldsymbol{n} = 0$ is created within the mesh (Fig. 4a). By an intelligent search of the 'corresponding' integration points to this surface, the stress resultants, e.g. $M_y = \int_A \sigma_x \cdot z \cdot dA$, can be calculated. The displacements of the affected nodes lead to the corresponding translational and rotational deformations of the considered zone (Fig. 4b). For different load scenarios the required rcc for the subsystems in the special multibody systems are obtained (Fig. 4c).

2.2. VERIFICATION WITH FINITE ELEMENT ANALYSIS

A verification of the multibody analysis is accomplished with global finite element models of the investigated structures, which are validated against the real collapse process in the form of a visual comparison with video sequences.

To obtain an accurate prediction with finite elements, and consequently to achieve the desired validation of the finite element model, a numerical analysis tool has to provide several capabilities. First of all, the numerical tool must represent the dominant mechanical phenomena which appear during the collapse, e.g. initial wave propagation after detonation, deformations and motions of building parts, emerging local zones of accumulated damage, development of initial kinematics and contacts between building

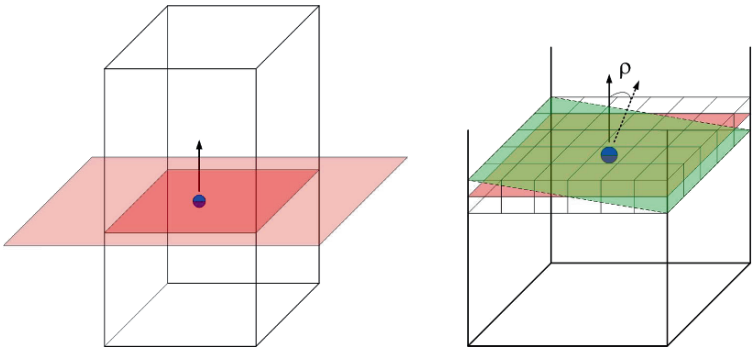

(a) New point of origin

(b) Affected elements and deformed mesh

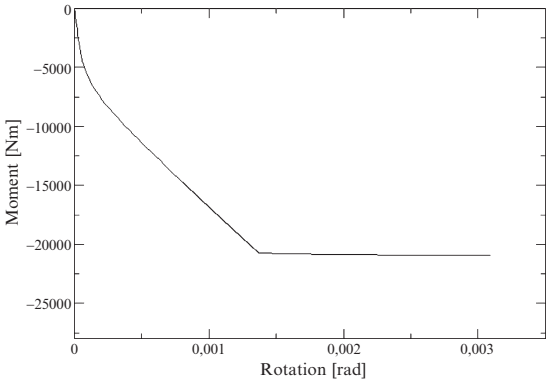

(c) Calculated rcc

Figure 4. Procedure of rcc calculation

fragments. In this contribution, the finite element method is used applying an explicit time integration algorithm (the central difference scheme) as numerical analysis tool. In combination with the central difference method, the finite element method is an efficient and accurate tool, offering great flexibility for analyzing arbitrary geometries and materials. Corresponding analyses are described in detail in Section 5.2.

The modelling and validation process is carried out as follows. First, the geometry is mapped onto a CAD system. The CAD model is then used to discretize the structural system in terms of finite elements. The specific requirements needed for the element and material formulation are described

in Section 5.2. Subsequently, the analyses are performed and compared visually with a sequence of video snapshots in order to evaluate the motion of the collapsing building.

The results of this validation are used to verify the kinematics, obtained by the simulations of the multibody systems. Furthermore, in these models, local zones of accumulated damage which act like hinges can be identified. Parts which are connected to two or more such local zones can be regarded as fragments showing a rigid body like behavior. In this way, the discretization of the multibody system is supported and safeguarded.

3. Investigation of uncertainty

Structural collapse is strongly influenced by data uncertainty. The choice of an appropriate uncertainty model depends on the characteristic of the uncertainty present in the problem description and the boundary conditions. Mostly well developed probabilistic models are applied to take account of uncertainty. In structural collapse simulation however, engineers have to quantify structural parameters on the basis of only few data, which may additionally be characterized by vagueness, e.g. due to uncertain measurements or changing reproduction conditions. Moreover, some expert knowledge and linguistic assessments are required to be incorporated into the modelling. Hence, engineers only have an idea concerning the range of the values of these parameters and some estimate which values are more possible to occur than other ones. For modelling such information adequately a non-probabilistic uncertainty model that considers sets of parameter values together with subjective weighting information inside the set is needed in this context. Fuzzy set theory and fuzzy probabilistic theory provide the most powerful basis for a realistic and reliable modelling. The former permits the modelling of uncertain parameters, and a subjective assessment of degrees describing on the particular elements belong to the set by means of membership functions. This uncertainty model offers the chance for appropriately taking account non-stochastic uncertainty, which frequently appears in engineering problems without making any artificial assumptions concerning the validity which cannot be proven definitely. The fuzzy probabilistic uncertainty model represents a generalized uncertainty model and joins elements of fuzziness and probability (Möller and Beer, 2004).

Thus in this project it is presumed that the quantification of uncertainty has to be performed exclusively on the basis of vague information and expert knowledge, as it frequently appears in the case of structural collapse analysis of real world examples. This non-probabilistic uncertainty

demands the application of the appropriate uncertainty model fuzziness for uncertainty quantification and the application of the assigned analysis methods designated as fuzzy analysis.

4. Software aspects

In order to model real-world systems for computer-aided destruction, a user-friendly and efficient software system is essential. Efficiency is required because a large number of simulation experiments has to be accomplished. As a consequence, all partial models used for the controlled blasting (e.g. product model, MBS models, MBS subsystems with resistance characteristic curves etc.) need to be modelled efficiently and should be modifiable without major effort. For the development, verification and employment of an efficient and close-to-reality blasting simulation environment, in particular a user interaction along with appropriate visualization capabilities of both the model parameters and the simulation results is crucial.

Experiences in optimization of blasting strategies have shown that the implementation and integration of various acquainted as well as new tools into a simulation system are necessary. In the following, a Java-based prototype software system is presented that serves as a "Computational Steering Environment" providing interactive control and visualization capabilities during blasting simulations.

In this section, a brief overview of the underlying structure of the prototype software system and the used simulation model is given. In addition, the key components of the software architecture are briefly explained.

Figure 5 is a graphical representation of the simulation concept and the different submodels as constituents of the total simulation model. Submodel (a) represents the product model for the "demolition using controlled explosives" which serves as a database containing all relevant data needed for the global level simulation (e.g. geometry, material data of the parts of the building, the details of the preparatory work like modifications of the static structure before ignition of the explosives, potential events such as locations and ignition times of explosive charges). Based on these data, along with the results of the different submodels of the global level (d) as well as the lower levels (e), the submodel "simulation manager" (b) creates a model description of the special MBS (c1).

The modelling process takes into account special knowledge (f) that is implemented in the simulation manager submodel. Then, the modelling process can be executed by means of the simulation system depending for example on upcoming events during the simulation. Hereby, the process can be partitioned into individual time steps according to the needs of

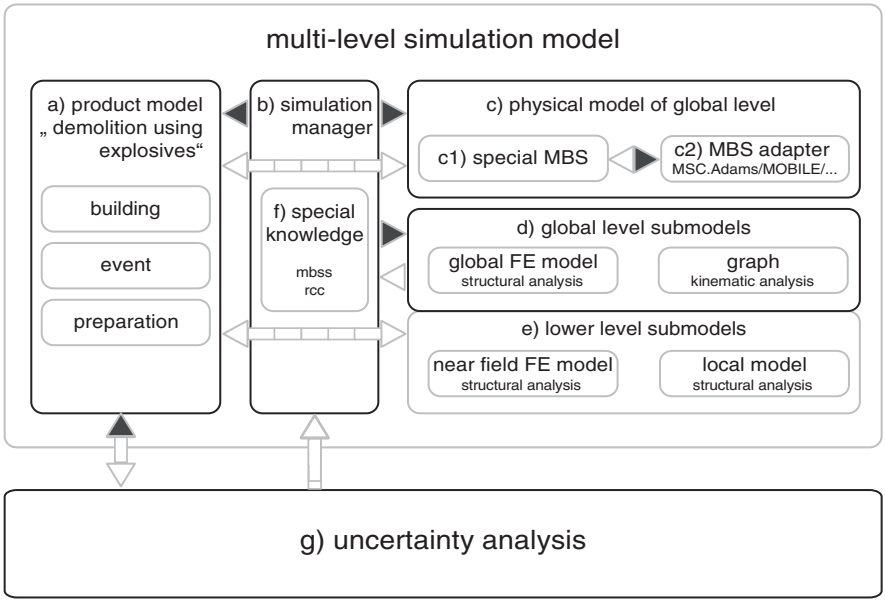

Figure 5. Schematic presentation of the simulation model for the global level of multi-level-problem and coupling to uncertainty analysis

a given problem. The special knowledge for the simulation manager submodel (b), which is providing adequate MBS subsystems, is acquired in collaboration with the involved partner research institutes. In particular, the resistance characteristic curves (rcc) for the nonlinear force elements of the MBS subsystems are computed by the partner Institute of Reinforced and Pre-stressed Concrete Structures in Bochum, based on a near field finite element analysis in zones of accumulated damage. Hereby, specific material models for dynamically loaded reinforced concrete are applied, see Section 2.1.1.

Furthermore, the global MBS models of representative reference systems are verified by transient global finite element (FE) simulations performed by a further partner, the Institute for Mechanics of the University at Karlsruhe, see Section 2.2.

The creation and solution of the system equations of the MBS model is accomplished by a MBS software that is applied by the special MBS submodel via a specific MBS adapter (c2). Currently, the MBS software system MSC.Adams (MSC.ADAMS) is used which fits best. The above mentioned submodels (a) to (c) of the simulation model are implemented as distributed, object-oriented software components that are integrated

into the simulation system to allow for a holistic multi-level simulation of the demolition process. This simulation builds the foundation for the uncertainty analysis (g), see Section 3.

A specific simulation manager has been developed which is further described in Hartmann et al. (2008).

5. A first numerical example

5.1. CHOSEN REFERENCE SYSTEM

As a real world example for the blast simulation, an old storehouse in Thüringen has been chosen which has been deconstructed by blast in 1998 (Fig. 6). The structural system is a seven storey reinforced concrete frame structure with stiffening brickwork outer walls in the first floor and thin concrete walls in the upper floors. The building height as well as length is 22 m, the width is 12 m, leading to an approximate overall mass of about 1,900 t.

In the simulation, the collapse has been carried out in two steps. In a first explosion, two rows of columns in the ground floor has been removed, after 4 s by a second explosion, a third row in the ground floor has been deleted as depicted in Figs. 7 and 9.

The degradation, caused by the first explosion has proved as to be not sufficient to induce the collapse of the building: The structure remained staying for 4 s on the two remaining rows of columns. Only after the destruction of these columns by a second explosion, the building started bending forward, and finally collapsed. First, the complete upper six storeys rotated, then the cuboid approached the ground and started to break into pieces.

Figure 6. Reference structure in Weida/Thüringen

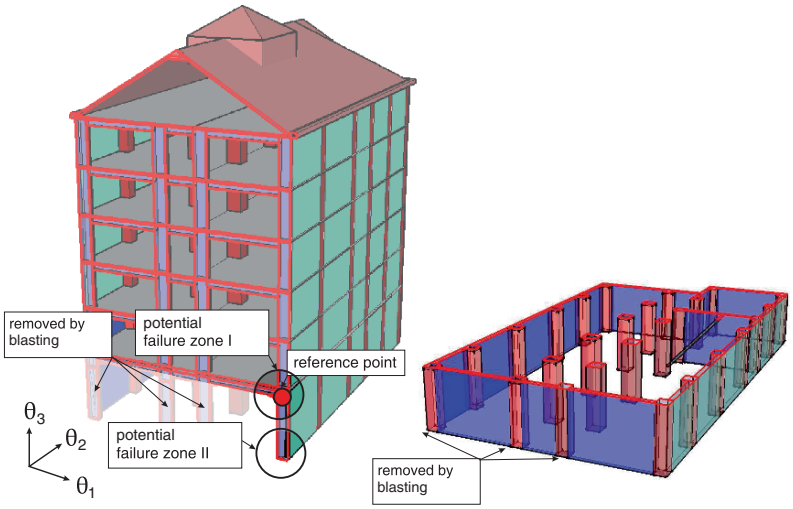

Figure 7. Storehouse – to be demolished with the aid of controlled explosives

5.2. FINITE ELEMENT ANALYSIS

The structural analysis has been based on the commercial FE-program LS-DYNA® which uses a central difference method for time integration (Hallquist, 1998, 2005). For discretization of the structural parts, one-point under-integrated hexahedral elements with hourglass stabilization (Belytschko and Bindemann, 1993) have been chosen, which perform excellently without any locking.

For all concrete parts, a piecewise linear plasticity material model is used. The parameters, describing concrete like behavior were obtained by calibration with rather simple experimental examples. Although, the material model does not allow detailed modifications concerning e.g. reinforcement, the reached approximation for the mass-dominated problems investigated, has rendered reasonable results used to support the generation of the MBS. The potentiality of element failure, which needs to simulate the appearance of local zones of accumulated damage (hinges) during the collapse event, has also been implemented in the material model. Then, every time an element reaches a specific plastic strain, it is removed from the computation. With this procedure the development of rigid body models as mentioned in Section 5.3 is supported and validated. With respect to accuracy, it is acceptable to use the same material model for each simulation. This has to do with limited amount of knowledge and information provided by technical documentation available on the concrete and steel used. Existing lacks of information are, therefore, compensated through application of uncertainty algorithms.

Another approach focusing on a more detailed modelling of the failure of brittle materials is the usage of discrete models described for 2D problems in a rather small scale in Ibrahimbegovic and Delaplace (2003) and Delaplace and Ibrahimbegovic (2006). For the modelling and especially the discretization of multi-storey buildings in practical applications it is a long term goal to include discrete element models, however, the computer resources required are tremendous and beyond the range of the current project described in this paper.

Each time when contacts happen during the collapse, the kinematical configuration of the simulated structure changes abruptly. Hence, also the correct determination of contacts within parts of the building as well as between them and the ground is important to obtain a realistic collapse behavior of the model used. For this reason, fast automatic contact search algorithms are implemented in LS-Dyna®. Albeit these algorithms show very good performance concerning accuracy and computation time, the search for contact consumes a considerable amount of CPU-time within the whole simulation because each surface segment of the FE-mesh has to be considered. The chosen contact formulation is a penalty-based node-to-segment algorithm to capture the baseplate contact, and a segment-to-segment algorithm between building fragments. The baseplate has been modelled using four-node shell elements, assumed as to be rigid, representing the contact segments for the base plate. The discretized structure depicted in Fig. 8b, consists of 82, 867 hexahedral finite elements.

The results of a simulation based on the planned blasting strategy (Fig. 9) can be seen in Fig. 10. Unfortunately, the existing documentation of the real collapse in 1998 is confined to only one video, which makes comprehensive validation of simulations difficult. Nevertheless, the take-off phase of the collapse is fairly realistically mapped with respect to the data quality available.

5.3. MULTIBODY ANALYSIS

The multibody analysis-based simulation of the collapse of the above storehouse is entered after blasting away the first three rows of columns within the ground floor of the structure. In Fig. 11, the created multibody system established is shown schematically.

The zones of accumulated damage are modelled by means of specific multibody subsystems. In particular, the failure of the columns within the ground floor govern the rotation of the structure. Failure areas of columns are modelled by using revolute joints in association with rotational nonlinear force elements. The nonlinear characteristic of the forces has been calculated by a finite element analysis, as described in Section 2.1.1. For

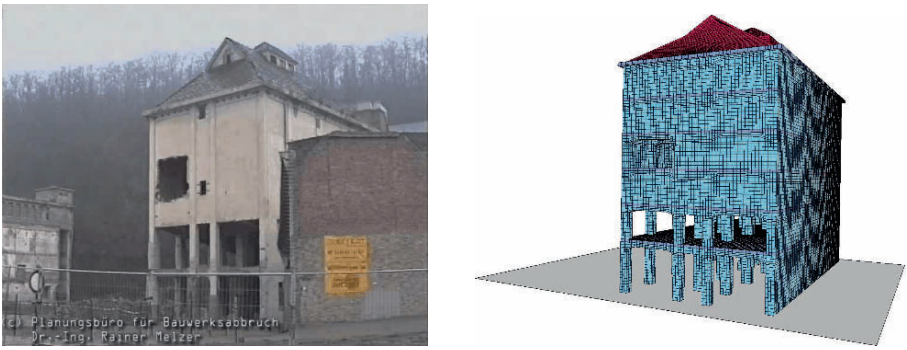

(a) (b)

Figure 8. Reference structure in Weida/Thüringen – photography (**a**) and finite element discretization (**b**)

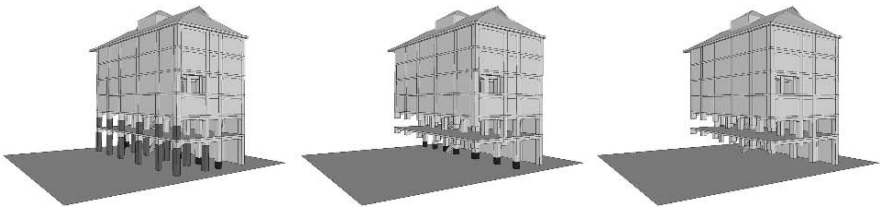

Figure 9. Blasting strategy in order to achieve the collapse kinematics

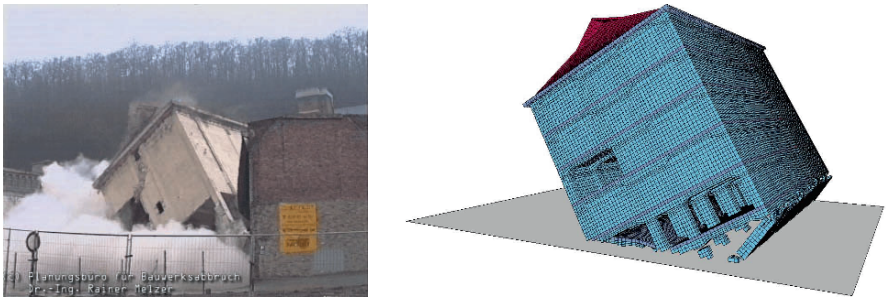

(a) (b)

Figure 10. Reference structure in Weida/Thüringen – video sequence (**a**) compared to simulation results (**b**)

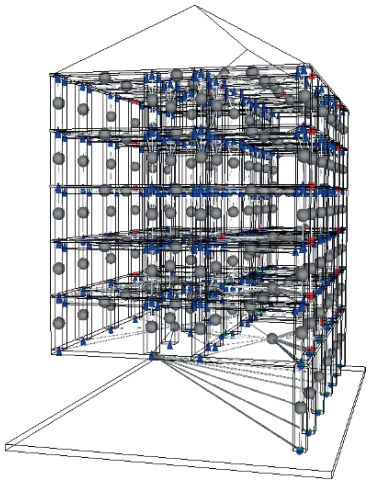

Figure 11. MBS model of reference system

example, for the ground column the dimensions could be taken over from design drawings, whereas the amount and position of reinforcement have been unknown. The same holds for the material data for concrete and reinforcement. To cover these uncertainties fuzzy rcc are determined as described in Section 5.4.

The finite element mesh chosen represents the characteristics of a reinforced concrete column (see Fig. 12a). For the rotational force element a bending moment is required representing the resistance of the column subjected to the rotation of the revolute joint. To take into account the interaction of bending moment and normal force, the weight of the building concerning one column has to be transferred into a normal force. To calculate the stress resultants and deformations, loads corresponding to a normal force and bending moment are applied on nodes of the finite element mesh. By increasing the loads up to the failure of the structure, one obtains the rcc. One deterministic solution of a calculated rcc is shown in Fig. 12b.

Figure 11 shows the simulation of the progressive collapse: After a certain amount of rotation, the structure touches the ground leading to further failures, in particular, within the ceiling.

The model applied contains in total 255 rigid bodies, 19 revolute joints, 43 rigid joints and 639 force elements. Contact of all rigid bodies with the ground is considered. In this case, the computation has been carried out by using the MSC.ADAMS (MSC.ADAMS) program system, applying the penalty regularization-based "Poisson" model with an appropriate coefficient of restitution, see Fig. 13.

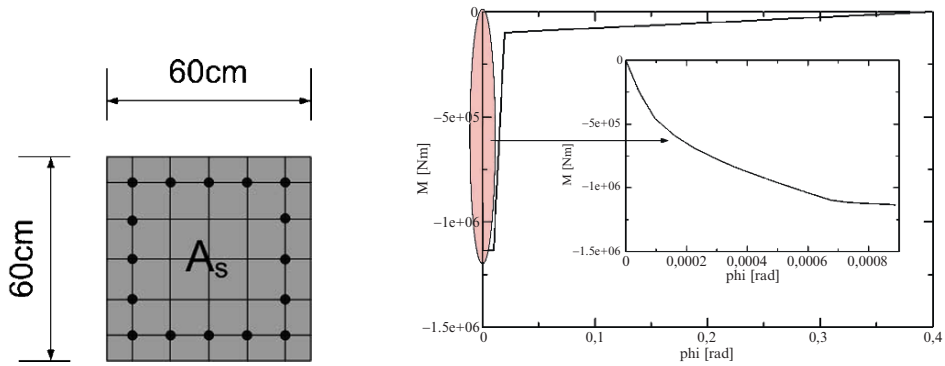

(a) Cross section of rc–column

(b) Calculated rcc

Figure 12. Calculated rcc for the ground column

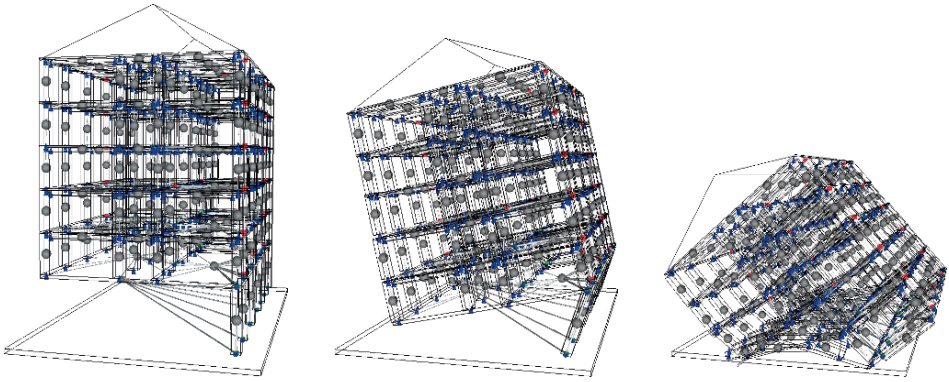

Figure 13. MBS simulation of reference system

The multibody simulation shows an ample coincidence with the finite element analysis for the same process as demonstrated in Fig. 14. It should be pointed out that the comparison of computational costs underline the MBS approach: In contrast to the finite element simulation that requires 31 h for 1.7 s duration in reality, the MBS simulation took only 15 min using a comparable one processor hardware configuration in both cases.

In principle, alternative approaches combining flexible and rigid parts in a single model (see e.g. Ibrahimbegovic et al. [2003] are possible and used in the own global FE verification using LS-DYNA (see Mattern et al. [2006]). Within the concept of this study, however, focus is placed on rigid body systems solely.

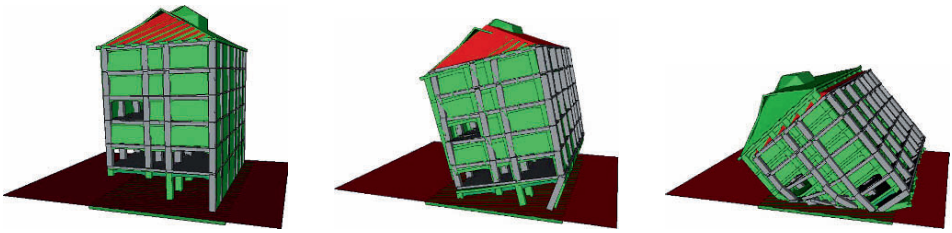

Figure 14. Comparison of finite element analysis (green) and MBS simulation (grey-red)

5.4. FUZZY ANALYSIS

The technical documentation of the structure Fig. 7 as well as the information about the used material and the amount of concrete reinforcement are often incomplete. Therefore a fuzzy structural collapse analysis is required.

This analysis is performed in two steps:

1. Determination of the non-linear fuzzy resistance characteristic curves $\tilde{k}$ of the selected potential failure zones (Fig. 7)
2. Fuzzy multibody analysis of the structural collapse based on the special multibody system, where determined fuzzy rcc $\tilde{k}$ are fuzzy input values

The uncertain results enable engineers to assess the selected blasting strategy forming the basis for improved design and dimensioning.

Determination of fuzzy resistance characteristic curves (fuzzy rcc)
Exemplarily the fuzzy rcc of the potential failure zone I (Fig. 7) is determined. The associated fuzzy function expresses the dependency between the rotation φ_2 and the bending moment M_2. The deterministic fundamental solution as given in (Section 2). Examination of the available data has shown that the following structural parameters possess the uncertainty characteristic fuzziness:

- Modulus of elasticity $\tilde{E}_c$
- Tensile and compressive strength $\tilde{f}_c$, $\tilde{f}_{ct}$
- Yield stress $\tilde{f}_y$ of the reinforcement steel
- Amount of reinforcement in the cross section $\tilde{a}_s$

All fuzzy structural parameters identified are input values of the fuzzy finite element analysis and given in Table 1. Full interaction is assumed between concrete tensile and compression strength according the following equation

$$\tilde{f}_{ct} = 1.40 \cdot \left(\frac{\tilde{f}_c - 8}{10} \right)^{\frac{2}{3}} \quad . \tag{1}$$

TABLE 1. Fuzzy structural parameters

	$\alpha_l = 0$	$\alpha = 1$	$\alpha_r = 0$
$\tilde{E_c}$	$15 \cdot 10^3\,\mathrm{N/mm^2}$	$30 \cdot 10^3\,\mathrm{N/mm^2}$	$52 \cdot 10^3\,\mathrm{N/mm^2}$
$\tilde{f}_c$	$10\,\mathrm{N/mm^2}$	$25\,\mathrm{N/mm^2}$	$45\,\mathrm{N/mm^2}$
$\tilde{f}_{ct}$	$0.479\,\mathrm{N/mm^2}$	$1.994\,\mathrm{N/mm^2}$	$3.349\,\mathrm{N/mm^2}$
f_y	$220\,\mathrm{N/mm^2}$	$420\,\mathrm{N/mm^2}$	$500\,\mathrm{N/mm^2}$
$\tilde{a_s}$	$33.6 \cdot 10^{-4}\,\mathrm{m^2}$	$64.00 \cdot 10^{-4}\,\mathrm{m^2}$	$88.00 \cdot 10^{-4}\,\mathrm{m^2}$

The mapping of the fuzzy input values onto fuzzy result values is performed with the fuzzy finite element analysis as mapping model M.

$$\tilde{E_c},\ \tilde{f}_c,\ \tilde{f}_{ct},\ \tilde{f}_y,\ \tilde{a_s} \rightarrow \tilde{k}_{M_2,\varphi_2}. \tag{2}$$

In Fig. 15 a partial result of the fuzzy rcc $\tilde{k}_{M_2,\varphi_2}$ for positive rotations $\varphi > 0$ is shown.

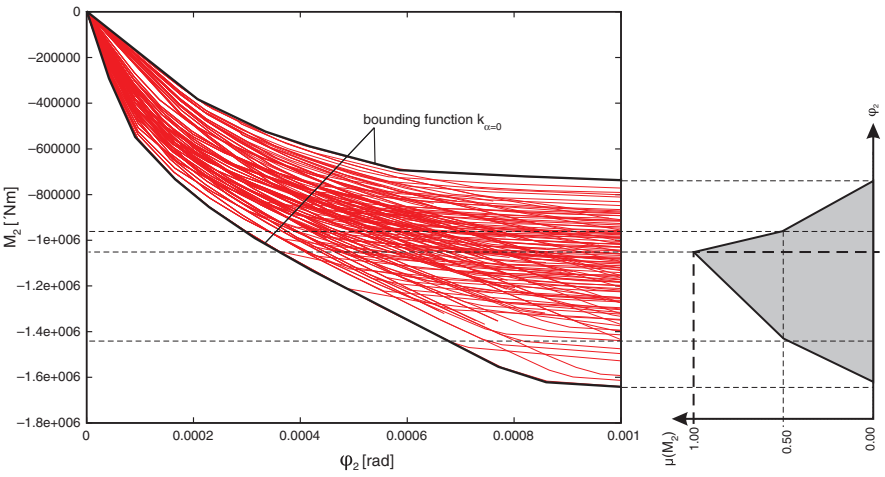

Figure 15. Fuzzy resistance characteristic curves $\tilde{k}_{M_2,\varphi_2}$

Uncertain structural collapse simulation – fuzzy multibody dynamics
The uncertain structural collapse simulation comprises as mapping model the special multibody system (Section 2.1) and the fuzzy rcc of the two potential failure zones I and II (Fig. 7). Depending from the uncertain input parameters different collapse scenarios arise (Fig. 16). The selected blasting strategy, i.e., blasting of the front columns, aims at a tilt collapse.

In the simulation is assumed that hinges develop in the potential failure zone I and II. The resulting kinematics has shown levels for the tilt of the structure. The planned tilt collapse occurs if the displacement $\tilde{d}_{\theta_1}$ (Fig. 16) is zero or negative otherwise a aborted collapse arise. Hereby, the fuzzy displacement function $\underline{\tilde{\theta}}(\tau)$ is used as indicator. This function is obtained as a result of the fuzzy multibody dynamic. The fuzzy functional value $\tilde{\theta}_1(\tau_2)$ at the time $\tau_2 = 1.7$ s represents $\tilde{d}_{\theta_1}$ according to Fig. 16. This result shows that negative displacements may be occur. The question arises which values of the fuzzy input parameters (Table 1) lead to negative $\tilde{d}_{\theta_1}$. An answer can be given by the fuzzy cluster design. According to Eq. (2) five fuzzy input parameters are considered which form a five-dimensional design space $\underline{D}$. The design space $\underline{D}$ may be divided into two subspaces. Points of the permissible subspace $\underline{D}^{[1]}$ lead to a tilt collapse whereas points of the non-permissible subspace $\underline{D}^{[2]}$ cause a vertical collapse. With the aid of the developed algorithm of cluster design (Beer and Liebscher, 2008) the permissible subspace $\underline{D}^{[1]}$ may be determined. For any further details we refer to Hartmann et al. (2008), Möller et al. (2008), Liebscher, (2007).

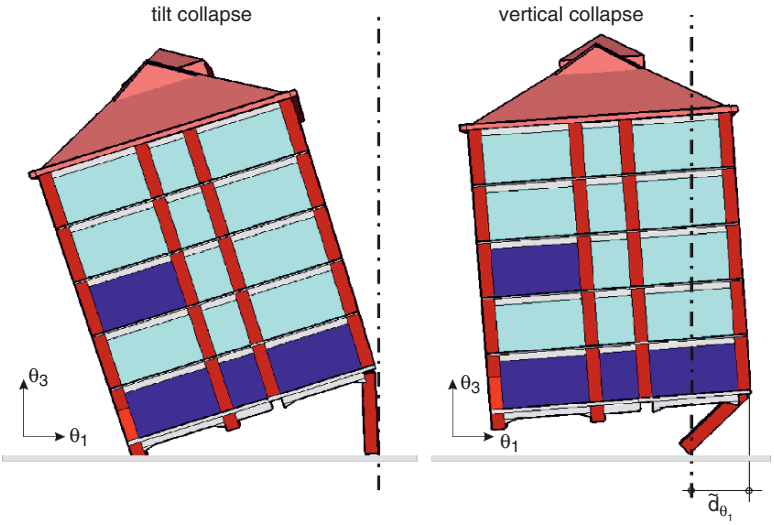

Figure 16. Possible collapse scenarios due to data uncertainty

6. Summary and conclusions

This paper demonstrates that the simulation of the demolition of buildings by means of controlled explosives carried out on the basis of multibody models is efficient and close to reality.

The verification of the multibody models using validated transient finite element calculations evidences the correctness of the approach. Compared to finite element calculations, simplified multibody models are far less time consuming. Considerable reductions of calculation costs are crucial preconditions for a good performance of the uncertainty analysis. In addition MBS models allow practical engineers to judge their blasting strategy more safely and with limited effort.

The presented concept and first results of an ongoing research project show in particular, that the consideration of uncertainty substantially improves the process of designing demolition strategies as well as the safety of a blasting project. Using uncertainty analysis, it is possible to find solutions that could hardly be identified with an solely deterministic analysis because of the complex and non-intuitive behavior of collapsing buildings due to a vague information basis.

Currently, the presented concept is extended to large scale structures in densely populated areas where the demands are even higher.

Acknowledgements

The authors gratefully acknowledge the support of the German Research Foundation (DFG) by funding the interdisciplinary Research Unit (FOR 500) “Computer-aided destruction of complex structures using controlled explosives”.

The authors also thank Dr. Melzer, Dresden, for technical support and for making available video documentations of the reference systems and other materials to allow for a validation of numerical simulations.

References

Alefeld, G. and Herzberger, J. (1983) *Introduction to Interval Computations*, New York: Academic Press.

Astaneh-Asl, A., Progressive collapse prevention in new and existing buildings. Emerging Technologies in Structural Engineering. In *Proceedings of the 9th Arab Structural Engineering Conference,* Abu Dhabi, U.A.E, November 29–December 1, 2003, 1001–1008.

Bandemer, H. and Gottwald, S. (1995) *Fuzzy Sets, Fuzzy Logic Fuzzy Methods with Applications*, England: Wiley.

Beer, M. and Liebscher, M. (2008) Designing robust structures – a nonlinear simulation based approach, *Computers & Structures* **86**, 1102–1122.

Belytschko, T. and Bindemann, L. P. (1993) Assumed strain stabilization of the eight Node hexahedral element, *Computer Methods in Applied Mechanical Engineering* **105**, 225–260.

Ben-Haim, Y. and Elishakoff, I. (1990) *Convex Models of Uncertainty in Applied Mechanics*, Amsterdam: Elsevier.

Chen, W.-F. (1982) *Constructive Equations for Engineering Material*, Elsevier: Amsterdam.

Delaplace, A. and Ibrahimbegovic, A. (2006) Performance of time-stepping schemes for discrete models in fracture dynamic analysis, *International Journal for Numerical Methods in Engineering* **65**, 1527–1544.

Hallquist, J. (1991–1998) *LS-DYNA Theoretical Manual*, Livermore Software Technology Corporation.

Hallquist, J. (1992–2005) *LS-DYNA Keyword User's Manual*, Livermore Software Technology Corporation.

Hartmann, D., Stangenberg, F., Melzer, R., and Blum, R. (1994) *Computer-based planning of demolition of reinforced concrete smokestacks by means of blasting and implementation of a knowledge based assistance system (in German)*, Technisch-wissenschaftliche Mitteilungen Nr. 94-6, Institut für konstruktiven Ingenieurbau, Ruhr- Universität Bochum.

Hartmann, D., Breidt, M., Nguyen, v. V., Stangenberg, F., Höhler, S., Schweizerhof, K., Mattern, S., Blankenhorn, G., Möller, B., and Liebscher, M. (2008) Structural collapse simulation under consideration of uncertainty – Fundamental concept and results, *Computers & Structures* p. doi:10.1016/j.compstruc.2008.03.004.

Hofstetter, G. and Mang, A. (1995) *Computational Mechanics of Reinforced Concrete Structures*, Vieweg, Weisbaden, Germany.

Ibrahimbegovic, A. and Delaplace, A. (2003) Microscale and mesoscale discrete models for dynamic fracture of structures built of brittle materials, *Computers & Structures* **81**, 1255–1285.

Ibrahimbegovic, A., Taylor, R., and Lim, H. (2003) Non-linear dynamics of flexible multibody systems, *Computers & Structures* **81**, 1113–1132.

Isobe, D. and Toi, Y. (1998) ASI finite element analysis of dynamic collapse behaviors of framed structures considering member fracture. In S. Idelson, E. Oñate, and E. Dvorkin (eds.), *Computational Mechanics, New Trends and Applications*, 4th World Cong. Comp. Mech., Buenos Aires, p. 283.

Kabele, P., Pokorny, T., and Koska, R., Finite element analysis of building collapse during Demolition. In *Proceedings of 16th International Conference on the Applications of Computer Science and Mathematics in Architecture and Civil Engineering [CD-ROM]*, Weimar: Bauhaus-Universität Weimar, 2003, ISSN 1611-4086.

Kaewkulchai, G. and Williamson, E. B. (2004) Beam element formulation and solution procedure for dynamic progressive collapse analysis, *Computers & Structures* **82**, 639–651.

Kaliszky, S. and Logo, J. (2006) Optimal design of elasto-plastic structures subjected to normal and extreme loads, *Computers & Structures* **84**, 1770–1779.

Kapitaniak, T. (2000) *Chaos for Engineers: Theory, Applications, and Control*, Berlin: Heidelberg New York Springer.

Krätschmer, V. (2001) A unified approach to fuzzy random variables, *Fuzzy Sets and Systems* **123**, 1–9.

Krätzig, W. and Jun, D. (2002) Multi-layer multi-director concepts for D-adaptivity in shell theory, *Computer & Structures* **80**, 719–734.

Krätzig, W. and Pölling, R. (2004) An elasto-plastic damage model for reinforced concrete with minimum number of material parameters, *Computer & Structures* **82**, 1201–1215.

Liebscher, M. (2007) Dimensionierung und Bewertung von Tragwerken bei Unschärfe – Lösung des inversen Problems mit Methoden der explorativen Datenanalyse, Ph.D. thesis, Institut für Statik und Dynamik der Tragwerke, Technische Universität Dresden.

Madsen, H., Krenk, S., and Lind, N. (1986) *Methods of Structural Safety*, Englewood Cliffs, NJ: Prentice-Hall.

Mattern, S., Blankenhorn, G., Breidt, M., Nguyen, V., Höhler, S., Schweizerhof, K., Hartmann, D., and Stangenberg, F. (2006) Comparison of building collapse simulation results from finite element and rigid body models, In *Multiscale Problems in Multibody System Contacts*, IUTAM Symposium, Stuttgart, **1**, 257–267.

Meguro, K. and Hakuno, M. (1992) Simulation of collapse of structures due to earthquakes using the extended distinct element method, In *Earthquake Engineering, 10th Word Conference*, Balkema Rotterdam.

Meguro, K. and Tagel-Din, H. (2002) Applied element method used for large displacement structural analysis, *Natural Disaster Science* **24**, 25–34.

Möller, B. and Beer, M. (2004) *Fuzzy Randomness – Uncertainty in Civil Engineering and Computational Mechanics*, Berlin: Springer.

Möller, B., Liebscher, M., Schweizerhof, K., Mattern, S., and Blankenhorn, G. (2008) Structural collapse simulation under consideration of uncertainty – Improvement of numerical efficiency, *Computers & Structures* p. doi:10.1016/j.compstruc.2008.04.011.

MSC.ADAMS, Website, http://www.adams.com.

Pawlak, Z. (1991) *Rough Sets. Theoretical Aspects of Reasoning About Data*, Dordrecht: Kluwer.

Pfister, T., Petryna, Y., and Stangenberg, F. (2006) Damage modelling of reinforced concrete under multiaxial fatigue loading, In G. Meschke, R. de Borst, H. Mang, and N. Bicanic (eds.), *Computational Modelling of Concrete Structures*, Proceedings of EURO-C 2006, 27–30 March 2006, Mayrhofen, Tirol, Austria, 421–429.

Pölling, R. (2000) A close-to-practise elasto-plastic damage model for reinforced concrete for structural analyses (in German), Ph.D. thesis, Ruhr-Universität Bochum.

Simo, J.C. and Hughes, T.J.R. (1998) *Computational Inelasticity*, New York: Springer.

Stange, K. (1977) *Bayes-Verfahren, Schätz- und Testverfahren bei Berücksichtigung von Vorinformationen*, Berlin Heidelberg New York: Springer.

Starossek, U. (2006) Progressive collpase of structures: Nomenclature and procedures, *IABSE, Structural Engineering International* **16**, 113–117.

Taylor, R.L. (2001) FEAP – A Finite Element Analysis Program, Programmer Manual.

Wright, G. (1994) *Subjective Probability*, Chichester: Wiley.

EARTHQUAKE GROUND MOTIONS FOR SEISMIC DAMAGE ASSESSMENT AND RE-EVALUATION OF EXISTING BUILDINGS AND CRITICAL FACILITIES

P. LEGER* AND R. TREMBLAY
Department of Civil, Geological and Mining Engineering, École Polytechnique de Montréal, Montréal University, Quebec, Canada

Abstract. This paper presents different methods that can be used to develop ground motion accelerograms that are compatible with a prescribe target response spectra in the seismic evaluation of buildings and critical facilities. Scalar multiplier methods, frequency domain and time domain spectral matching techniques are discussed. Seismic damage assessments are presented for elasto-plastic single-degree-of-freedom systems and an eight story concrete shear wall building. The results have been shown to be sensitive to the spectrum matching strategy used. For nonlinear analysis of ductile structures, time domain and frequency domain spectral matching are able to produce peak structural response parameters that are comparable for systems with period, T, ranging from 0.2 to 1.5 s. For longer periods ($T \geq 1.5$ s) time domain spectral matching is preferred if no real accelerogram consistent with the site characteristics and with significant energy content in the period range of interests are available.

Keywords: Earthquake safety, buildings, critical structures, nonlinear dynamic analyses, ground motion scaling, spectral matching, ductility demand

1. Introduction

The seismic damage assessment and structural safety re-evaluation of existing buildings and critical facilities such as nuclear power plants (NPP) and large dams are very challenging problems. The consequences of failure for the exposed

* To whom correspondence should be addressed. e-mail: pierre.leger@struct.polymon.ca

A. Ibrahimbegovic and M. Zlatar (eds.), *Damage Assessment and Reconstruction After War or Natural Disaster*,

population and the requirements for the owners to provide earthquake resistant facilities with limited economic resources requires to use efficient assessment tools and optimal rehabilitation strategies, if need be (Fig. 1).

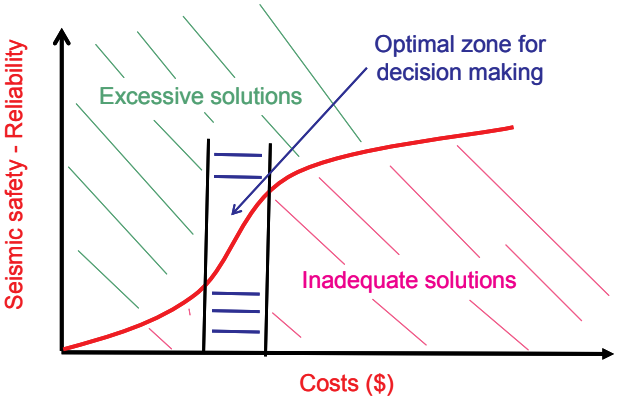

Figure 1. Optimal zone for making decision to increase seismic safety

Nowadays, this is done in the context of performance based assessment where nonlinear dynamic analysis plays a major role. The following steps are typically performed: (1) define site specific input ground motions, (2) use nonlinear dynamic analyses to compute internal forces and displacements demand, (3) compute demand to capacity ratios for structural components, and (4) make decision related to the adequacy of the components and the structural system. Unfortunately, the first step, which is the most important one, is also the most uncertain. Site specific input ground motions are first defined from probabilistic or deterministic seismic hazard analyses. Elastic target response spectra are developed for the selected earthquake return period and non exceedence probability level (median, mean or 84%). They usually exhibit smooth spectral shapes and are prescribed by building codes or developed by seismologists and approved by regulatory agencies in the case of large dams and NPP facilities. Nonlinear dynamic analyses require the definition of ground motion acceleration time histories with spectral ordinates covering adequately the smooth target spectrum. Three basic alternatives could be used:

1. Selecting real historical accelerograms from ground motion databases with characteristics as consistent as possible with the specific site conditions (magnitude [M], distance [R], duration [D], soil condition [SSI])
2. Use simulated ground motions from a seismological model of fault rupture mechanisms

3. Use synthetic or artificial ground motions generated strictly from filtered with noise

Then a strategy must be defined such that the accelerograms match the target spectrum. Two basic options could be considered (1) scaling spectral ordinates without altering the spectral shape, or (2) scaling the spectral ordinates and modifying the spectral shape to match the target spectrum. Ideally for nonlinear analysis the use of scaled real historical accelerograms without altering the spectral shape is preferred. This is because nonlinear displacement and ductility demands are sensitive to the details of the ground motions containing sequences of peaks and valleys as well as long duration pulses (Fig. 2). Several methods could be used to scale an accelerogram without altering its shape. However ASCE (2005) mentions that as many as 30 recorded ground motions could be required to meet the spectral matching criteria for NPP infrastructures. ATC-63 (2008), in its latest recommendations to assess existing buildings using nonlinear analysis, recommends that two sets of records should be used. ATC-63 provides 22 near field records ($R \leq 10$ km) and 28 far field records ($R \geq 10$ km) for a total of 40 records (this means 120 ground motion components for 3D analyses). As an alternative some building codes (NBCC, 2005) and nuclear regulations (ASCE, 2005) mention that it is acceptable to use a limited number (at least three) *modified* recorded accelerograms. The scaling of the spectral ordinates and *modification of the spectral shape* could be done in the frequency domain or in the time domain.

For structural damage assessment, the effect of the spectral matching technique used on the modification of the ground motion characteristics and their related damage potential should be clearly understood. There is currently a lack of knowledge related to this issue.

To address this need the outline of this paper is the following. We first define ground motions and structural response parameters to characterize the damage potential of an earthquake record. Different methodologies to generate ground motions for damage assessments using scalar scaling methods and spectral matching methods are described. We finally presents the results of extensive parametric analyses conducted on nonlinear behaviour of SDOF structures with different force reduction factor, and on an eight-story reinforced concrete shear wall building. We are also providing an extensive bibliography on the subject at the end of the paper for those interested to study in more details the concepts presented in the paper.

2. Structural Damage Indicators for Earthquake Response

2.1. GROUND MOTIONS INDICATORS

Several ground motion parameters could be computed to assess the intensity, frequency, and energy contents of earthquake records. Some of these parameters are often correlated with the destructive potential of the record. In this paper the following parameters have been considered:

- PGA; PGV; PGD: Peak ground acceleration (PGA), velocity (PGV), and displacement (PGD).
- a/v: ratio of the peak acceleration, (a), to the peak velocity, (v), an indicator of the frequency content of a record (high a/v correspond to high frequency content).
- ad/v^2: ratio of peak acceleration, (a), times the peak displacement, (d), to the square of the peak velocity (v^2), this ratio is representative of the energy characteristics of the record.
- D3: The significant duration corresponding to the interval of time over which a proportion (between 5% and 95%) of the total Arias intensity is accumulated.
- AI: Arias intensity

$$\text{AI: } \frac{\pi}{2g}\int_0^{\infty}\left[a(t)\right]^2 dt$$

- SIv: Velocity spectrum intensity

$$SIv = \int_{0.1}^{2.5} Sv(\xi = 0.05, T)\, dT \cdot$$

- SIa: Acceleration spectrum intensity

$$SIa = \int_{0.1}^{0.5} Sa(\xi = 0.05, T)\, dT \cdot$$

- RMSA: Root mean square of acceleration

$$RMSA = \sqrt{\frac{1}{tr}\int_0^{tr}\left|a(t)^2\right| dt} \cdot$$

- NZC: number of zero crossing.
- PPS: Predominant period of strong shaking = 2*D3/[(NZC in D3].
- A*: Area under an accelerogram between two consecutive null values (pulse area).

- DP: Duration of pulse (A*).
- TP: time at which the pulse (A*) begins.

Figure 2 illustrates a ground motion recorded at Pacoima dam in the 1971 San Fernando earthquake. The time variation of the intensity, and the duration of strong shaking are shown. The accelerogram is seen as a series of peaks and valleys, sometimes with long acceleration pulses. The details of the ground motions and the presence of peaks and valleys of different forms could be conceptually simplified to the cases of (i) periodic, (ii) impulsive or (iii) a combination of both.

2.2. STRUCTURAL DAMAGE INDICATORS

Typical parameters to assess seismic structural damage of building and critical structures are:

- μ: ductility demand corresponding to the ratio of the maximum to the yield displacements (u_{max}/u_{yield})
- δ: maximum roof displacement in MDOF structures
- Δ: interstorey drift
- $\mu\phi$: curvature ductility demand corresponding to the ratio of maximum curvature to the curvature at yield (ϕ_{max}/ϕ_{yield})
- V: maximum base shear
- M: maximum base moment

Of course, several other indicators related to cumulative damage such as cyclic ductility demand and energy dissipation could be also defined.

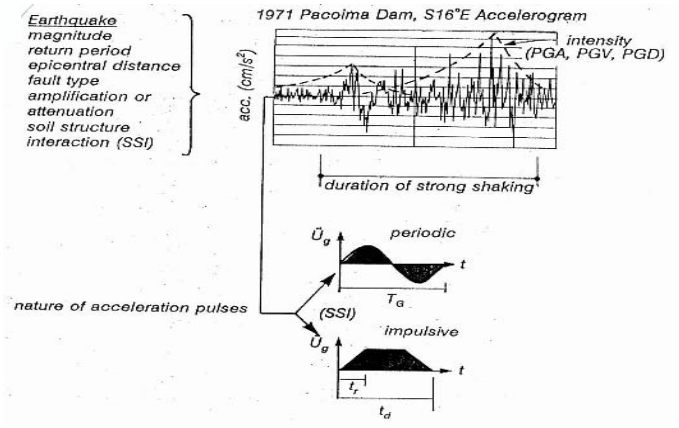

Figure 2. Ground motion records as a sequence of pulses

Figure 3 illustrates that the nature of ground motion acceleration pulses, either periodic or impulsive in this example, has very different effects on the seismic response of SDOF as characterized by the linear and nonlinear response spectra. For elastic structures the most critical form of ground motions is periodic as resonance is possible. However, periodic ground motions are not critical if the system enters in the nonlinear range. On the other hand, long acceleration pulses, that is inertia forces applied in the same direction for a long time while the structure is yielding is very detrimental as the ductility demand increases significantly.

It is thus important to characterise the details of ground motions through various indicators and study how scalar or spectral matching methods can change these characteristics.

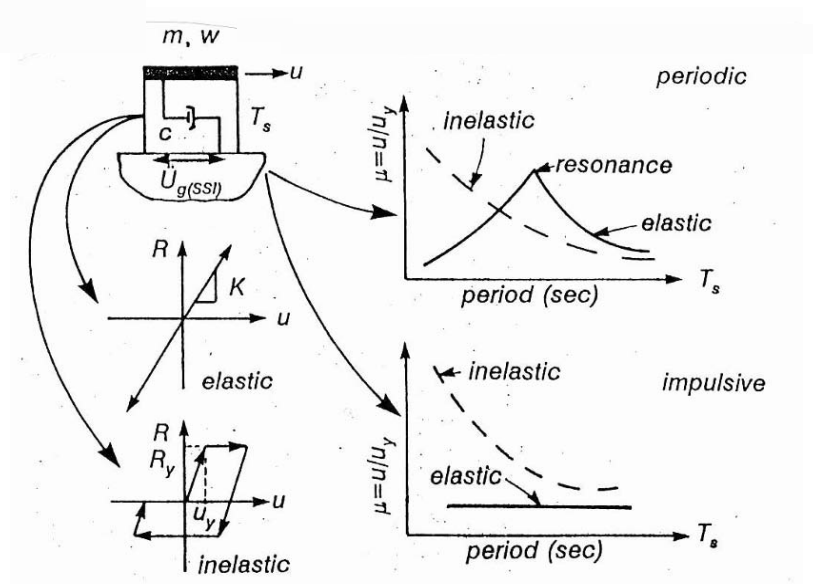

Figure 3. Elastic and inelastic SDOF subjected to periodic or impulsive ground motions and resulting response spectra

3. Guidelines Requirements for Buildings and Critical Facilities

Figure 4 illustrates a typical design spectrum prescribed in building codes (the target spectrum at, say, 5% critical damping). It is most often considered as representative of the minimal earthquake loads that will pose an unacceptable risk to human life in the case of an earthquake. More refined alternatives could be defined in the context of performance based design but this is outside the scope of this paper. Before using this type of spectrum (Fig. 4), one must

recognize four important differences with those of real earthquake records: (1) the target spectrum is smooth, (2) the target spectrum does not return to PGA for a zero period, (3) there is a cut off in peak Sa in the short period (high frequency) range, and (4) the code defined target spectrum tends to deliberately overestimate the Sa in the long period range. When site specific spectra are developed, the frequency at which the peak Sa should equal the PGA is not well known, varying from 33 to 100 Hz. A cut off in peak Sa is admitted because high frequency motions are known to impose very small destructive displacement. The Sa is raised in the long period range to avoid designing flexible buildings with nearly zero inertia forces. This is a potentially unsafe situation if one considers uncertainties in the period of vibration and characteristics of ground motions. For regulatory agencies, the target spectrum is the legally accepted description of the ground motions for damage assessment. It is obvious that no historical accelerogram can provide spectral ordinates, Sa, covering the target spectra in the entire period range to meet the legal requirements of the target spectra.

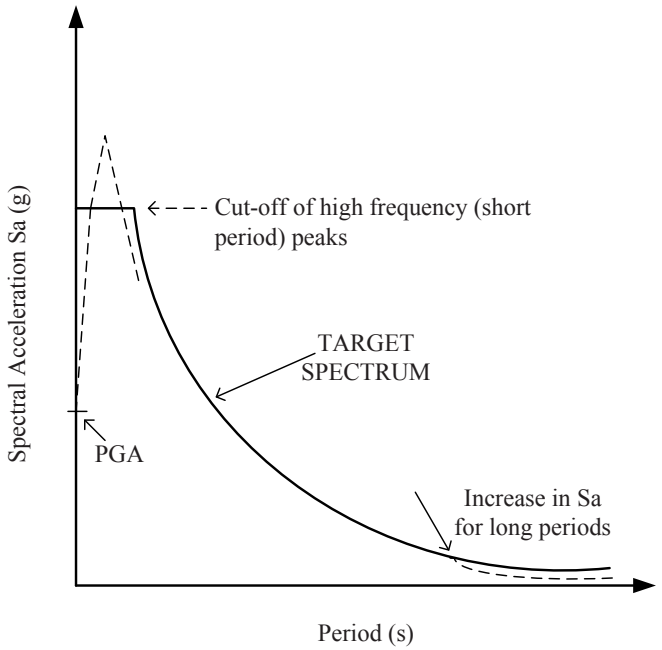

Figure 4. Target code type design spectrum (solid line) and typical response spectrum from earthquake records (dash line)

Very often, small magnitudes earthquake records at close distances to the site are used to cover the short period range of the spectrum. Large magnitude earthquake records at larger distances from the site are used to cover the long

period range of the spectrum. These earthquakes records are scaled by applying a scalar multiplier modifying the spectral ordinates without altering the spectral shape. Alternatively spectral matching techniques could be used as explain in Section 4.

4. Generation of Ground Motions for Damage Assessment

Figure 5 shows the NBCC (2005) target spectrum for the city of Montreal (Quebec, Canada) with a return period of 2,500 years on firm soil. The PGA is 0.43 g. Earthquakes record in Eastern North America (ENA) are known to have a rich content in high frequency (around 10 Hz or T = 0.1 s) (Tremblay and Atkinson, 2001).

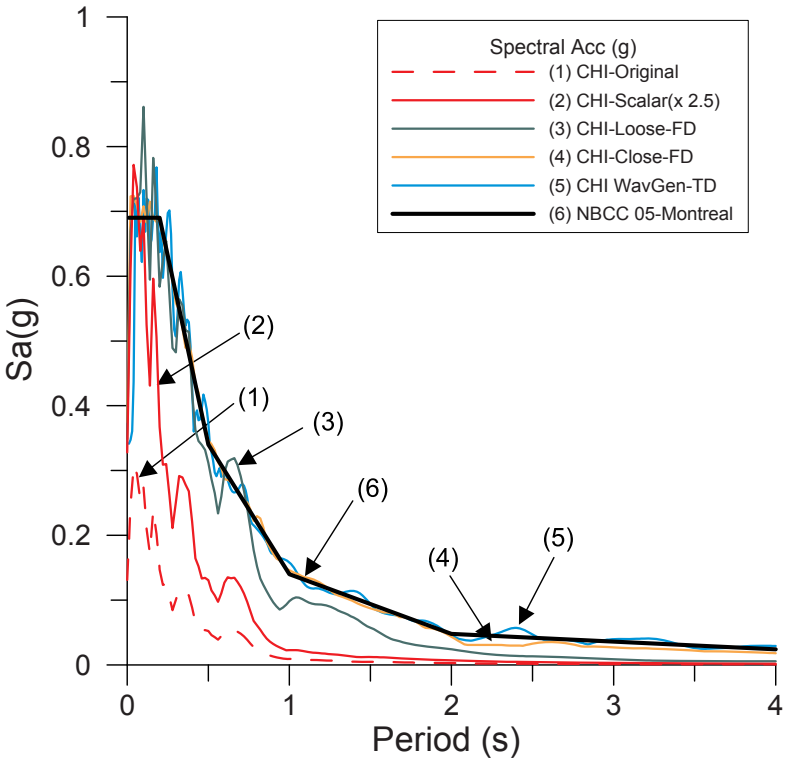

Figure 5. NBCC 05 target spectrum and response spectra from the CHI ground motion records

The response spectra of one record from the 1988 M5.7 Saguenay earthquake with a PGA = 0.13 g recorded on rock near Chicoutimi (CHI) at a hypocentral distance of 52 km in Quebec is also shown (line 1). The corresponding high frequency ground motion record is shown in Fig. 6.

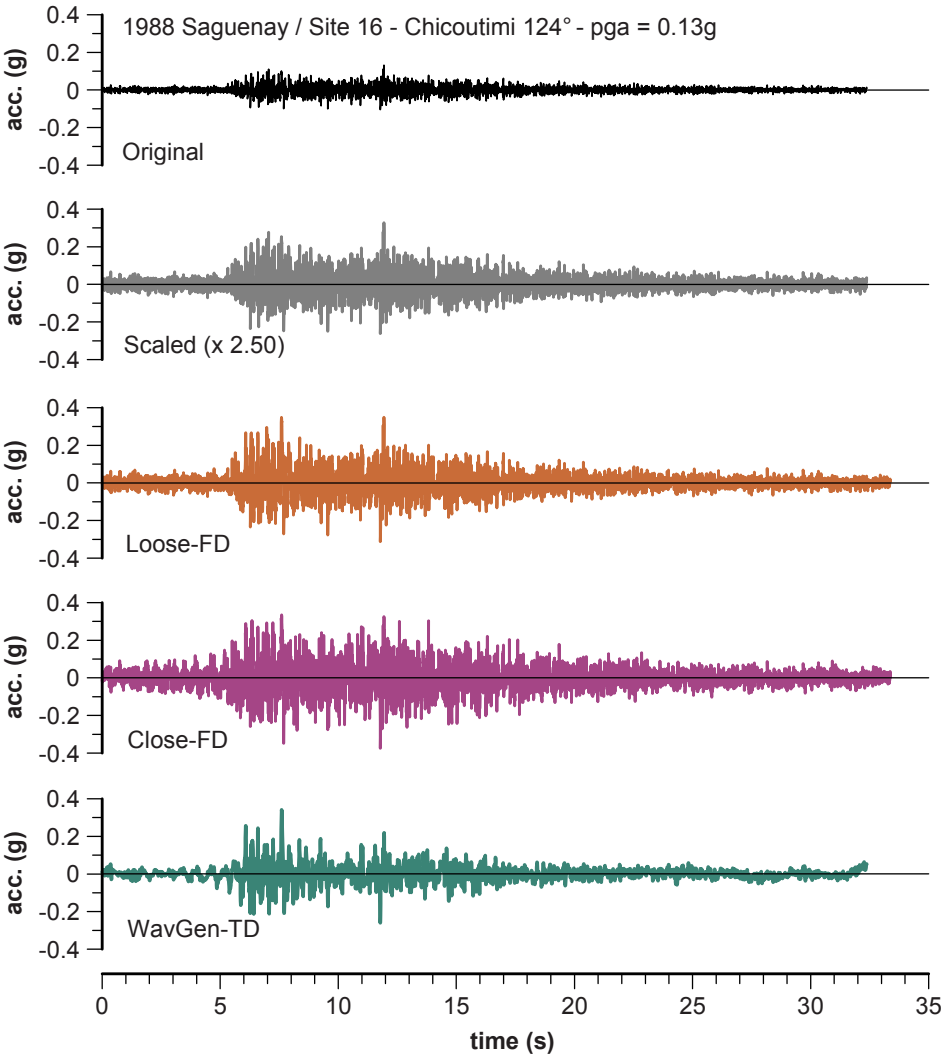

Figure 6. Historical, scaled and spectrally matched CHI ground motion records

4.1. SCALING HISTORICAL OR SIMULATED RECORDS

Several techniques have been proposed to scale historical or simulated ground motion records without altering the spectral shapes. Some of these techniques are described below:

- Scalar: A scalar multiplier is applied to the original accelerogram. It is based on judgment to achieve a “good” fit between the response spectrum and the target spectrum.

- PGA: The accelerogram is multiplied by a scalar to have the same peak ground acceleration (PGA) as that of the site specific data.
- Sa(T_1): The accelerogram is multiplied by a scalar value to obtain the same spectral ordinate at the fundamental period of vibration of the structure studied (T_1) as that of the target spectra.
- SIv: The accelerogram is multiplied by a scalar value to obtain the same velocity spectrum intensity as that of the target spectra.
- SIv + SIa: The accelerogram is multiplied by a scalar equal to the product of the scalar required to obtain the same SIv (as above) and a new scalar required to obtain the same SIa as that of the target spectra.
- Least squares (LS): (Somerville et al., 1997) The accelerogram is multiplied by a scalar that minimizes the weighted sum of the errors (differences) between the accelerogram response spectrum and the target spectrum. The weights used are 0.1, 0.3, 0.3 and 0.3 for the periods 0.3, 1.0, 2.0, and 4.0 s, respectively.
- T_2 and 1.2 T_1: (Naumoski et al., 2004) This method requires that the area under the acceleration response spectrum between the second mode period of vibration, T_2, and 1.2 times the first mode period of vibration, T_1, be the same as that of the target spectrum. The magnification of period T_1 is good practice because a structure that becomes inelastic (damaged) experiences a period elongation.
- PSa: (Naumoski et al., 2004) This method requires that the area under the accelerogram response spectrum and the target spectrum be equal for the period range 0–2 s.
- ASCE 7 (2005): This method requires that the average value of the spectral ordinates should not be smaller than those of the target spectra for the period range 0.2 T to 1.5 T where T is the fundamental period of vibration (T_1) of the structure. For the accelerogram response spectra, the spectral ordinates are computed at a fixed period increment. The same increment is used to obtain the spectral ordinates of the target spectrum.

4.2. SPECTRAL MATCHING – FREQUENCY DOMAIN

The magnitude of the Fourier spectrum coefficients of the record are modified while preserving the phase angle to match the response spectrum of the record to that of the target spectrum. The following iterative procedure is used (Léger et al., 1993):

- Compute the response spectrum and the Fourier transform of the accelerogram. For each frequency multiply the Fourier coefficients by the ratio between the spectral ordinates of the target spectrum and that of the response spectrum.
- Generate a new modified time history by inverse Fourier transform with the modified Fourier coefficient combined with the original phase angles.
- Compute the response spectrum of the modified time history and compare it to the target spectrum. Iterate until acceptable spectrum-compatibility criterion are obtained. For example CSA (1981) requires that "no more than 6% of the total number of points used to generate the spectrum from time history shall fall below the target response spectrum, but by no more than 10% at any point".
- Apply a baseline correction to the record to obtain zero mean velocity and zero final displacements.

4.3. SPECTRAL MATCHING – TIME DOMAIN

Elementary wavelets are added to, or subtracted from, the original record. Different types of wavelets could be used corresponding to the impulse response of a SDOF or tapered sinusoid. The timing for introducing the wavelets is selected to modify the accelerogram such that its response spectra, match the target spectra. The specific procedure used in this study is described by Mukherjee and Gupta (2002).The accelerogram is first decomposed using wavelets analysis into a finite number of time-histories with energy in non-overlapping frequency bands. Those time histories are then iteratively scaled to a suitable amount to achieve spectrum compatibility. The modified motions preserve the non stationary characteristics of the original motion. The procedure has been implemented in a computer program WavGen that could be downloaded from the Web (Gupta, 2002).

4.4. APPLICATIONS

Application 1 – NBCC 05 and CHI record (Fig. 5): For spectral matching in frequency domain (FD) or time domain (TD), the process is to start with a record that is scaled (scalar method – Fig. 5 line 2) to be near to the target spectrum in the period range of interest. In our implementation of the spectral matching in the frequency domain (FD) procedure we define a "loose-FD" spectral matching to be one that is obtained after a single iteration of the

procedure (Fig. 5 line 3). In this case, the resulting spectrum oscillates around the target spectrum. For the "close-FD" spectral matching using ten iterations are performed (Fig. 5 line 4). The results of the time domain spectral matching is noted as line 5 in Fig. 5. In Fig. 5, line 4 (close-FD) and line 5 (WavGen-TD) exhibit very similar response spectrum with good spectral matches with the target spectrum, even in the long period range. However, one can note some differences in the corresponding time histories (Fig. 6).

Application 2 – Scaling and spectral matching of CHI record for a MDOF structure with $T_1 = 0.56$ s and $T_2 = 0.09$ s (Fig. 7).

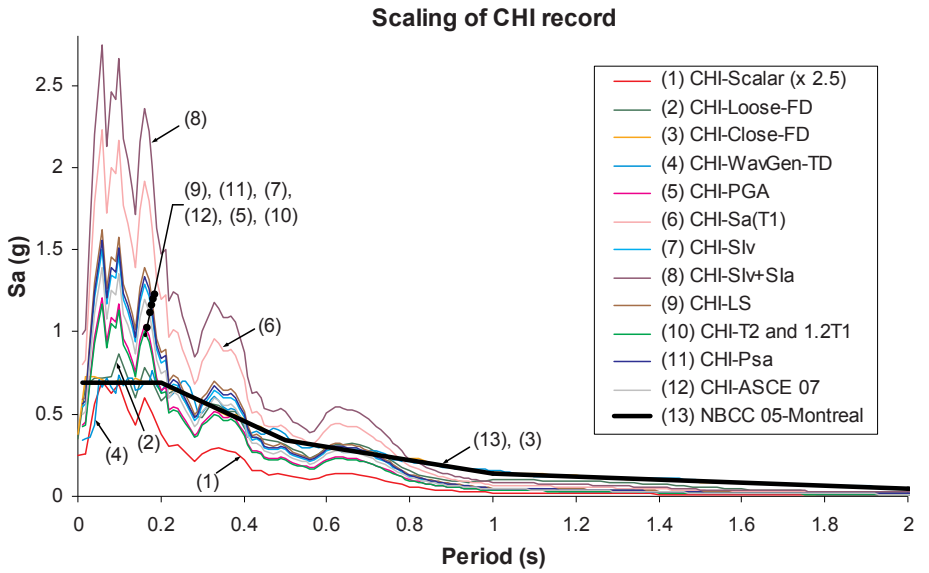

Figure 7. Scaling and matching of the CHI record for a MDOF structure

Figure 7 shows the application of different scaling and spectral matching procedures. Lines 3, 4 (and the corresponding methods) produce very good matching over the complete period range. Lines 5, 7, 9, 10, 11, 12 (and the corresponding methods) provide adequate matching between 0.2 and 0.7 s but they overshoot and undershoot significantly in the short and long period ranges.

Application 3 – Scaling and Matching a Simulated Record with M = 7.0, R = 70 km in ENA (Montreal) for a MDOF structure with $T_1 = 0.56$ s and $T_2 = 0.09$ s.

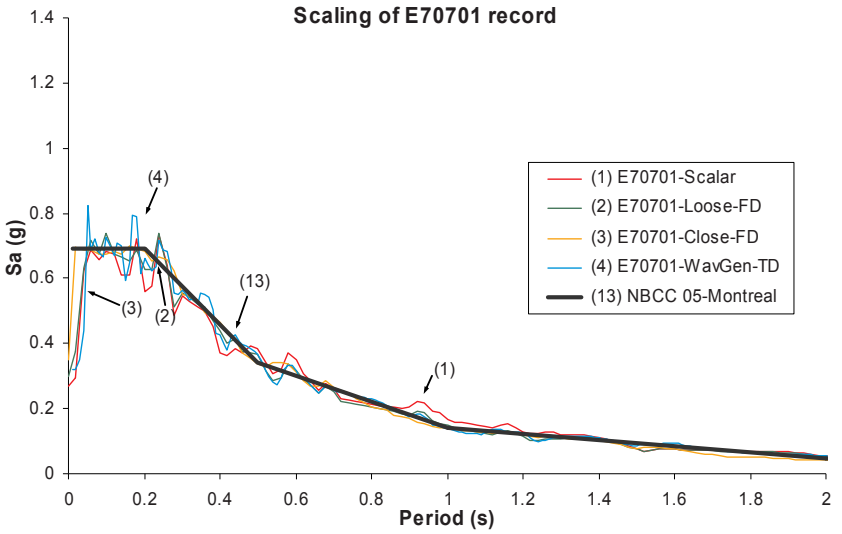

Figure 8. Spectral matching of the E70701 simulated record – Montreal target spectrum

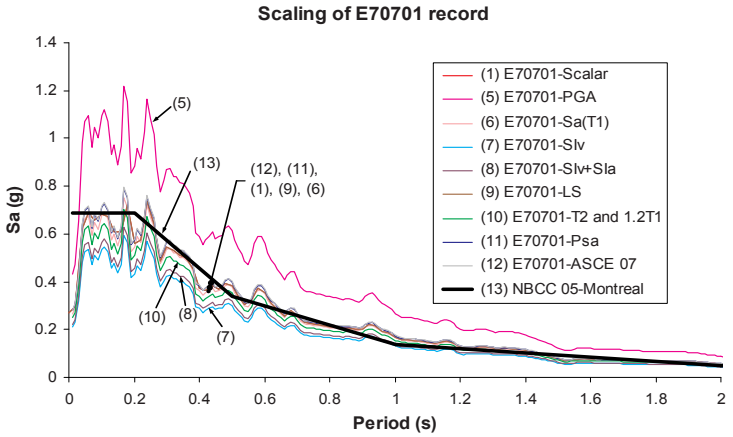

Figure 9. Scaling of the E70701 simulated record to the Montreal target spectrum

Figures 8 and 9 illustrate the spectral matching and the scaling of a simulated earthquake record that was developed by G. Atkinson (Engineering Seismologist) for ENA. In Fig. 8, line 3 (Close-FD) and line 4 (WavGen-TD) provide a tight spectral matching of the target spectrum. In Fig. 9 it is clear that PGA scaling is inappropriate (line 5). The other scaling methods (lines 1, 6, 9,

11, 12) are appropriate although they tend to lack energy content in the short period range <0.2 s.

Application 4 – Scaling of a Loma Prieta earthquake record (M7.0, R = 100 km and NBCC 05 for Vancouver) for a MDOF structure with T_1 = 0.56 s and T_2 = 0.09 s.

For comparison purposes, the NBCC-05 target spectra for Vancouver (British Columbia, Canada) located in Western North America (WNA) is also considered. WNA earthquake records are known to have lower frequency content than ENA records with spectral peaks in the 0.5 s range (2 Hz).

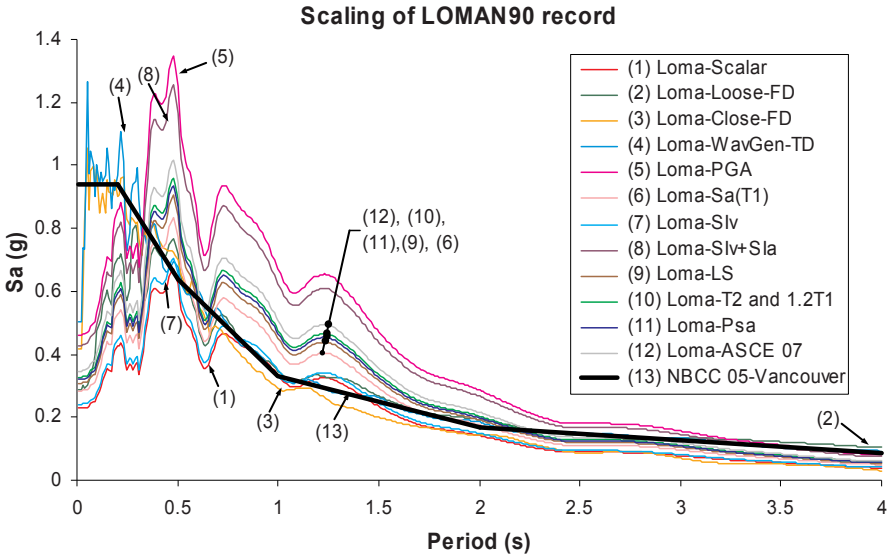

Figure 10. Spectral matching and scaling of the Loma Prieta record to the target spectrum for Vancouver

A WNA record of the 1989 M7 Loma Prieta earthquake (near San Francisco) with R = 100 km is used as the starting historical accelerogram. Figure 10 indicates that only the Loma (Close FD, line 3) and the Loma (WavGen-TD, line 4) are able to provide adequate spectral ordinates in the short period range. This is because the historical earthquake inherently lacks sufficient energy content in the short period range. Scaling of the record near the fundamental period, T_1 = 0.56 s, does not ensure good spectral matching for either the short or the long period range. It this case, it is appropriate to scale another WNA earthquake record (smaller magnitude M and shorter distance R) that is richer in energy in the short period range.

4.5. CHARACTERISTICS OF SPECTRALLY MATCHED AND SCALED TIME HISTORIES

Table 1 indicates the frequency independent scaling factors that have been computed from the different scaling methods for the two ENA types of records. It is shown that there is a wide variation among the computed values. The scaling approach has the advantage that the accelerograms retain their "natural characteristics" in the time domain and in their response spectra (except for the scaling of the record). Some "natural" characteristics (e.g. pulses, peak and valleys) are modified if different components of a record (Fourier coefficients) are scaled with different coefficients. The advantage of the spectrum matching approach is to limit the number of analysis and satisfy the legal Target spectrum.

TABLE 1. Scaling factors for different methods for ENA type of records (T_1 = 0.56 s, T_2 = 0.09 s)

	Scalar	PGA	Sa(T_1)	SIv	SIv + SIa	LS	T_2 + 1.2 T_1	Psa	ASCE 07
CHI	2.500	1.727	3.182	2.151	3.922	2.320	1.667	2.223	1.990
E70701	0.900	1.588	0.981	0.776	0.821	1.000	0.917	1.032	1.040

TABLE 2. Characteristics of spectrally matched and scaled historical accelerograms – CHI

Montréal	PGA (g)	PGV (cm/s)	a/v (g·s/m)	ad/v^2	D3 (s)	AI (m/s)	SIv (cm)	SIa (g·s)	RMSA (g × 100)	PPS (s)
CHI										
NBCC 05	0.43	–	–	–	–	–	46.84	0.22	–	–
Scalar	0.249	6.23	3.99	2.94	15.86	0.62	21.77	0.12	3.53	0.06
Loose-FD	0.34	12.41	2.80	9.36	16.81	1.41	50.09	0.21	5.25	0.1
Close-FD	0.37	15.31	2.44	31.14	18.55	2.19	60.40	0.22	6.52	0.04
WavGen-TD	0.34	18.78	1.81	32.64	17.26	0.95	64.06	0.22	4.36	0.18
PGA	0.43	10.76	3.99	2.94	15.86	1.85	37.61	0.21	6.10	0.06
Sa(T_1)	0.79	19.84	3.99	2.94	15.86	6.31	69.30	0.39	11.24	0.06
SIv	0.53	13.41	3.99	2.94	15.86	2.88	46.84	0.26	7.60	0.06
SIv + SIa	0.97	24.45	3.99	2.94	15.86	9.58	85.42	0.48	13.86	0.06
LS	0.57	14.46	3.99	2.94	15.86	3.35	50.52	0.28	8.19	0.06
T_2 + 1.2 T_1	0.41	10.39	3.99	2.94	15.86	1.73	36.31	0.20	5.89	0.06
Psa	0.55	13.85	3.99	2.94	15.86	3.07	48.40	0.27	7.85	0.06
ASCE 07	0.49	12.40	3.99	2.94	15.86	2.46	43.34	0.24	7.03	0.06

Tables 2–5 present the characteristics of the spectrally matched and scaled accelerograms for ENA. The alteration to the time histories depends on the sensitivity of the characteristic parameter to change in amplitude and frequency content of ground motions (USACE, 2003). The numerical algorithm selected for spectral matching either in the frequency domain or the time domain also appears to have a significant effect on the modified ground motion characteristics. Spectrum matching increases the strong motion duration, D_3, because the AI is modified and the energy content and characteristics, as indicated by AI and (ad/v^2) that were also altered significantly. It is interesting to note that the number of zero crossing (NZC) is significantly increased by frequency domain spectral matching (FD) while it is reduced by the time domain matching (TD), when compared to that of the natural records. The characteristic pulses, that is the larger pulse and the longest pulse, do not occur at the same time for the spectral matching methods compared to the other scaling methods. Moreover, they have different duration that may alter the ductility demand in nonlinear earthquake response analysis.

TABLE 3. Ground motion pulse characteristics for the spectrally matched and scaled historical record – CHI

Montréal	NZC total	NZC in D3	Largest pulse in D3			Longest pulse in D3		
			A* (g·s)	DP (s)	TP (s)	A* (g·s)	DP (s)	TP (s)
CHI								
NBCC 05	–	–	–	–	–	–	–	–
Scalar	1,112	523	0.0205	0.17	7.58	0.0085	0.22	8.08
Loose-FD	2,276	1,033	0.0407	0.25	7.555	0.0407	0.25	7.555
Close-FD	2,543	1,275	0.0423	0.23	7.555	0.0423	0.23	7.555
WavGen-TD	678	395	0.0434	0.24	7.555	0.0189	0.39	14.29
PGA	1,112	523	0.0354	0.17	7.58	0.0148	0.22	8.08
$Sa(T_1)$	1,112	523	0.0653	0.17	7.58	0.0272	0.22	8.08
SIv	1,112	523	0.0441	0.17	7.58	0.0184	0.22	8.08
SIv + SIa	1,112	523	0.0805	0.17	7.58	0.0336	0.22	8.08
LS	1,112	523	0.0476	0.17	7.58	0.0198	0.22	8.08
$T_2 + 1.2\ T_1$	1,112	523	0.0342	0.17	7.58	0.0142	0.22	8.08
Psa	1,112	523	0.0456	0.17	7.58	0.0190	0.22	8.08
ASCE 07	1,112	523	0.0408	0.17	7.58	0.0170	0.22	8.08

TABLE 4. Characteristics of spectrally matched and scaled simulated accelerograms – E70701

Montréal	PGA (g)	PGV (cm/s)	a/v (g·s/m)	ad/v^2	D3 (s)	AI (m/s)	SIv (cm)	SIa (g·s)	RMSA (g × 100)	PPS (s)
E70701										
NBCC 05	0.43	–	–	–	–	–	46.84	0.22	–	–
Scalar	0.27	13.55	1.99	5.65	16.95	1.80	60.34	0.21	6.96	0.24
Loose-FD	0.29	19.11	1.55	18.42	16.93	2.06	58.99	0.21	7.61	0.1
Close-FD	0.34	15.93	2.18	16.93	17.41	3.09	56.98	0.22	9.33	0.16
WavGen-TD	0.32	20.07	1.59	17.41	16.99	1.99	60.28	0.22	7.32	0.18
PGA	0.43	21.51	1.99	5.65	16.95	4.54	95.83	0.33	11.06	0.24
Sa(T_1)	0.26	13.29	1.99	5.65	16.95	1.73	59.18	0.20	6.83	0.24
SIv	0.21	10.51	1.99	5.65	16.95	1.08	46.84	0.16	5.40	0.24
SIv + SIa	0.22	11.12	1.99	5.65	16.95	1.21	49.56	0.17	5.72	0.24
LS	0.27	13.55	1.99	5.65	16.95	1.80	60.34	0.21	6.96	0.24
T_2 + 1.2 T_1	0.24	12.42	1.99	5.65	16.95	1.51	55.32	0.19	6.38	0.24
Psa	0.27	13.98	1.99	5.65	16.95	1.91	62.27	0.21	7.19	0.24
ASCE 07	0.28	14.09	1.99	5.65	16.95	1.94	62.76	0.21	7.24	0.24

TABLE 5. Ground motion pulse characteristics for the spectrally matched and scaled simulated record – E70701

Montréal	NZC total	NZC in D3	Largest pulse in D3			Longest pulse in D3		
			A* (g·s)	DP (s)	TP (s)	A* (g·s)	DP (s)	TP (s)
E70701								
NBCC 05	–	–	–	–	–	–	–	–
Scalar	530	400	0.0166	0.18	10.96	0.0153	0.22	9.41
Loose-FD	630	472	0.0172	0.19	9.95	0.0172	0.19	9.95
Close-FD	803	634	0.0176	0.11	11.92	0.0109	0.14	18.63
WavGen-TD	479	351	0.0181	0.18	10.96	0.0132	0.22	14.69
PGA	530	400	0.0263	0.18	10.96	0.0243	0.22	9.41
Sa(T_1)	530	400	0.0162	0.18	10.96	0.0150	0.22	9.41
SIv	530	400	0.0129	0.18	10.96	0.0119	0.22	9.41
SIv + SIa	530	400	0.0136	0.18	10.96	0.0126	0.22	9.41
LS	530	400	0.0166	0.18	10.96	0.0153	0.22	9.41
T_2 + 1.2 T_1	530	400	0.0152	0.18	10.96	0.0140	0.22	9.41
Psa	530	400	0.0171	0.18	10.96	0.0158	0.22	9.41
ASCE 07	530	400	0.0172	0.18	10.96	0.0159	0.22	9.41

5. Seismic Damage Assessment of Elasto-Plastic SDOF Systems

Series of elasto-plastic single-degree-of-freedom systems have been defined according to NBCC (2005) with periods ranging from T = 0.1 s to T = 3 s for Montreal and Vancouver response spectra with force reduction factors ranging from R_dR_o = 1 (elastic behavior) to R_dR_o = 4. The parameter R_dR_o is equivalent to the parameter q in EC8 (2003). The value of the force reduction factor is based on the equal displacement principle between elastic and elasto-plastic SDOF. In this case, R_dR_o corresponds to the ductility assumed in the design of the SDOF according to the code. Nonlinear dynamic analyses were then performed for different earthquake records obtained using frequency domain spectral matching (loose or close) and time domain spectral matching (WaveGen). Figures 11–16 present the computed ductility demand μ for the systems analyzed. For Montreal (simulated record E70701, M = 7.0, R = 70 km), and Vancouver (simulated record W72701, M = 7.2, R = 70 km), it is shown that the different spectral matching techniques give consistent results in the T = 0.2 s to T = 1.5 s period range. In all cases, the computed ductility demand in that period range is close to the force reduction factor R_dR_o.

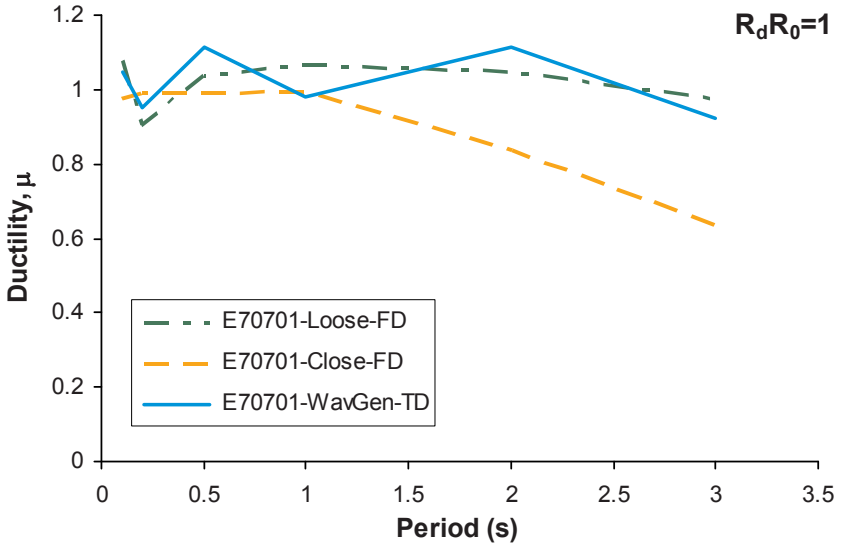

Figure 11. Ductility demand for different SDOF periods (E70701 record with R_dR_o = 1)

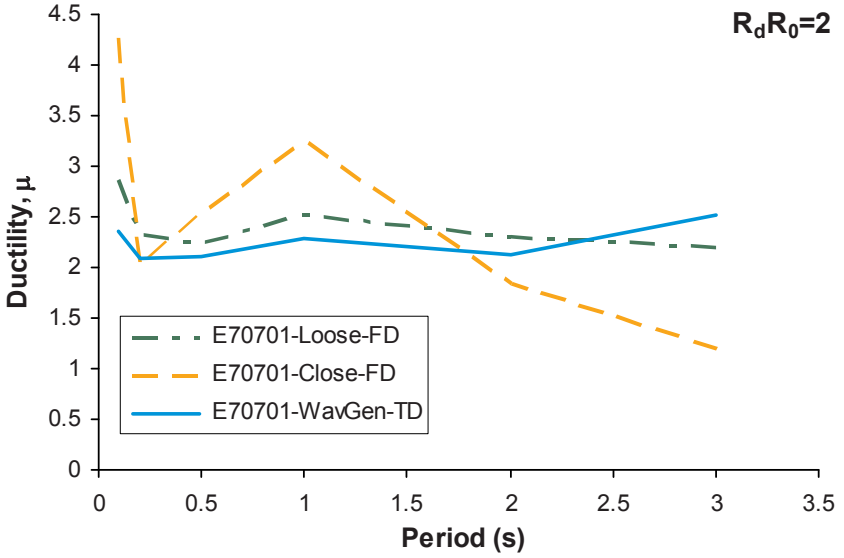

Figure 12. Ductility demand for different SDOF periods (E70701 record with R_dR_o = 2)

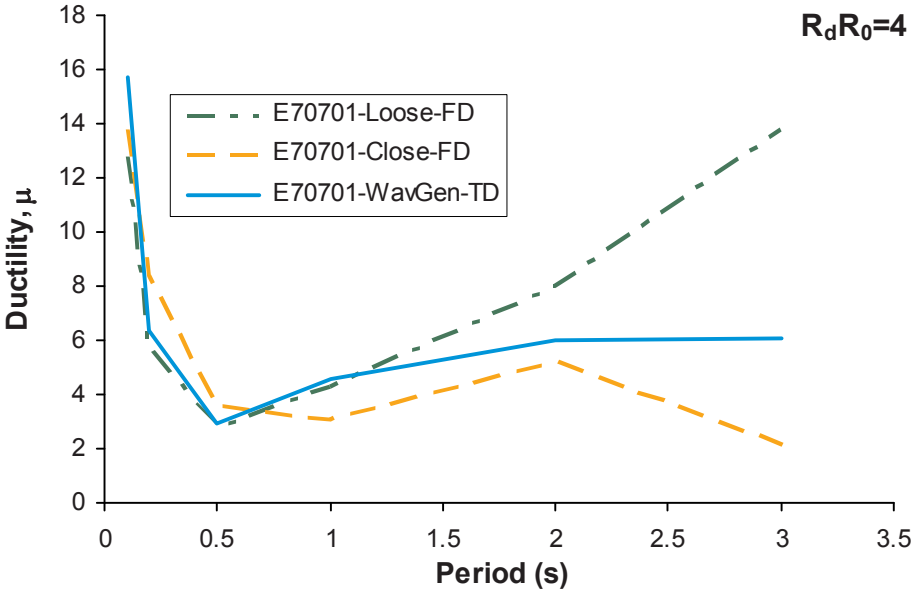

Figure 13. Ductility demand for different SDOF periods (E70701 record with R_dR_o = 4)

As expected, the ductility demand for short periods T < 0.2 s becomes very high as T approaches zero because this is a singularity point. However, for longer periods (T > 1.5 s) the results clearly show that time domain spectral matching (WavGen) generates earthquake records that have energy consistent with the design spectra, maintaining the computed ductility close to the R_dR_o value. This is not the case for the close frequency domain spectral matching. This is a significant result for earthquake engineering because periods of vibration typically tend to elongate as systems accumulate damage. It is interesting to note that "loose frequency domain" spectral matching tends to give results that are closer to those from time domain matching (WavGen) compared to the results of the "close frequency domain" spectral matching (except for T > 1.5 s when R_dR_o = 4 in Fig. 13). Close frequency domain spectral matching of an earthquake record with initially high frequency content appears to lower its ability to produce ductility demand consistent with the design assumptions. As a general observation pending more investigations, if the period range of interest is beyond 1.5 s, either the loose-FD or the WavGen-TD are the most suitable spectral matching techniques.

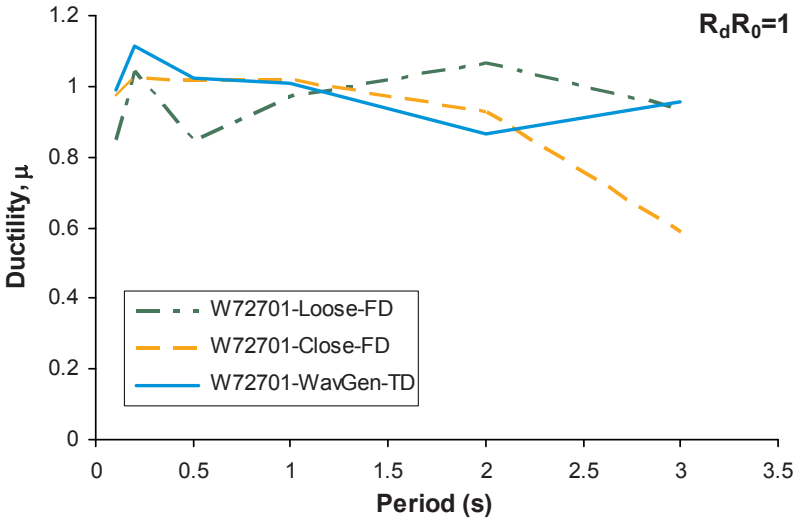

Figure 14. Ductility demand for different SDOF periods (W72701 record with R_dR_o = 1)

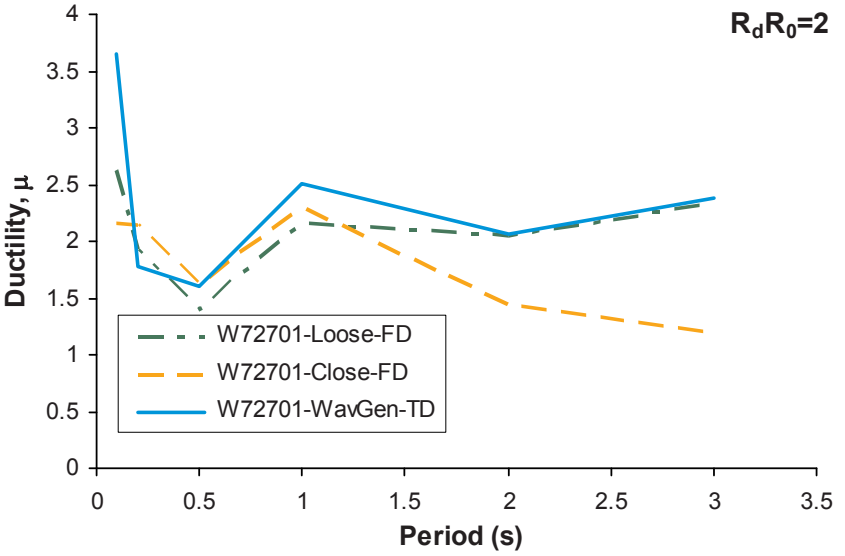

Figure 15. Ductility demand for different SDOF periods (W72701 record with $R_dR_o = 2$)

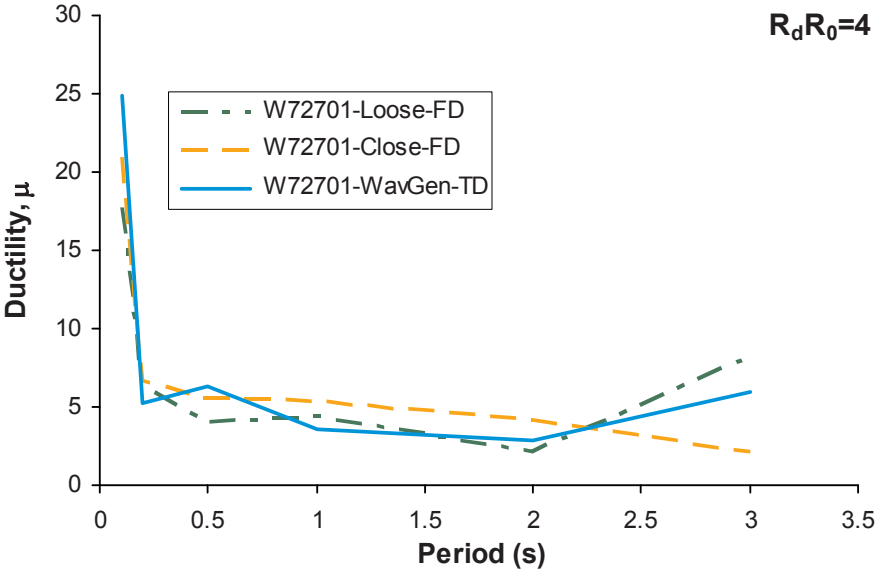

Figure 16. Ductility demand for different SDOF periods (W72701 record with $R_dR_o = 4$)

6. Seismic Damage Assessment of Shear Wall Concrete Buildings

In the last example, the nonlinear seismic response of a reduced scale model of an eight-story reinforced concrete shear wall to be tested on the shake table at Ecole Polytechnique de Montreal is examined. The height of the model, h, is 9 m and the periods of the model in its first two modes of vibration are T_1 = 0.56 s and T_2 = 0.09 s. It is assumed that the prototype structure is located in Montreal and the force reduction factor assumed in the design is R_dR_o = 2.8. The reinforced concrete constitutive model is based on the modified Takeda stiffness degrading hysteresis loop with plastic hinges concentrated at the ends of the beam-column elements (Fig. 17). The results under the E70701 record are given in terms of peak response parameters in Table 6. The base moment is shown to be nearly constant regardless of the spectral matching or the scaling method used because of the formation of a plastic hinge. On the contrary, the base shears vary significantly among the methods with the time domain spectral matching (WavGen) providing the largest value (187.7 kN). The results obtained by scaling on PGA should be discarded because this method provided excessively large spectral ordinates across a large period range of the target spectrum.

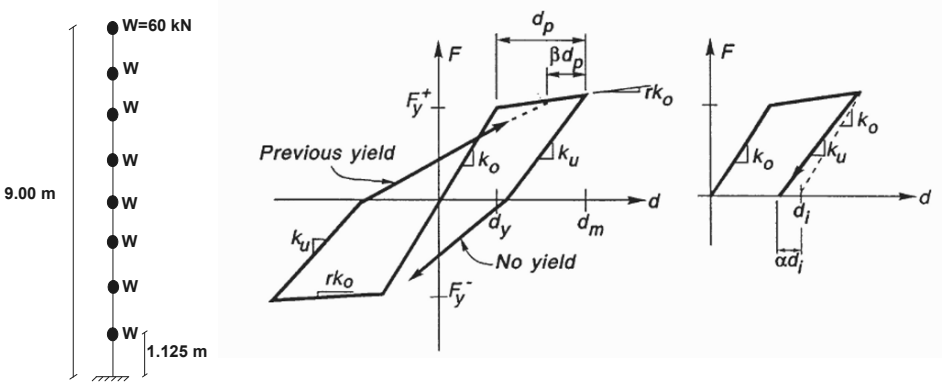

Figure 17. Eight-story shear wall model to be tested on the shake table at École Polytechnique de Montréal

The curvature ductility demand is consistent among the different spectral matching and scaling methods (except PGA). There are slight variations in the curvature ductility demand in the sixth story ($\mu\phi$ sixth) with the highest value being obtained from the close spectral matching in the frequency domain. Of the "loose" and the "close" frequency domain spectral matching techniques, the "loose matching" one appears to preserve more the "natural" characteristics of

the record. However, it appears that a design based on the time domain spectral matching is overly conservative in terms of the base shear to be resisted.

TABLE 6. Peak structural response parameters for an eight-story R/C shear wall building model

Montréal	V (base) (kN)	M (base) (kN m)	Δ Top (mm)	Δ Top (% h)	μϕ base	μϕ sixth
E70701						
Scalar	157.5	351.1	22.80	0.34	2.532	1.527
Loose-FD	168.2	351.1	23.19	0.34	2.588	1.582
Close-FD	170.0	350.9	21.89	0.35	2.269	2.311
WavGen-TD	187.7	351.0	25.42	0.38	2.498	1.894
PGA	178.0	353.4	47.70	0.62	5.820	4.523
$Sa(T_1)$	157.2	351.1	22.50	0.34	2.522	1.435
SIv	168.5	350.9	19.12	0.29	2.282	1.139
SIv + SIa	172.3	351.0	19.77	0.30	2.371	1.272
LS	157.5	351.1	22.80	0.34	2.532	1.527
$T_2 + 1.2\ T_1$	164.8	351.0	21.95	0.32	2.483	1.305
Psa	150.8	351.1	24.18	0.35	2.589	1.722
ASCE 07	150.1	351.2	24.50	0.35	2.645	1.768

7. Conclusions

This paper presents different methods that can be used to develop ground motion accelerograms that are compatible with a prescribe target response spectra in the seismic evaluation of buildings and critical facilities. Scalar multiplier methods, frequency domain and time domain spectral matching techniques are discussed. Seismic damage assessments are presented for elasto-plastic single-degree-of-freedom systems and an eight-story concrete shear wall building model. The following conclusions can be made from this study:

- Different record scaling methods can provide an adequate match to the target spectrum in a period range of interest. Scaling on peak ground acceleration was found inappropriate.
- While using Frequency domain iteration techniques, one could limit the number of iteration to one and obtain a “loosely” matched spectrum that provides less alteration to the details of the original ground motion (pulse characteristics).
- The “closely matched” frequency domain technique and time domain spectral matching method alters the characteristics of a time history in a

different way. This deserves further studies as several alternatives could be used for time domain spectral matching.

- The use of the closely matched records using frequency domain technique led to the best match with the Target NBCC spectrum in terms of velocity spectrum intensity SIv, and acceleration spectrum intensity, SIa.
- It is not enough to achieve a good match for some ground motion intensity characteristics SIv, SIa to ensure that the nonlinear response will not be altered significantly by the spectral matching technique used.
- To reproduce correctly the nonlinear ductility demand of long period structures ($T_1 > 1.5$ s), the time domain spectral matching and "loose" frequency domain methods are recommended. The spectrally closely matched record appears to be deficient in that regard.
- The inelastic response analysis of the eight-story building model with $T_1 = 0.56$ s showed that base shear appears to be maximized when using the time domain spectral matching method whereas the curvature ductility demand at the sixth story was maximized by the "Close" frequency domain matching method. A good compromise appears to use the "loosely" matched frequency domain method.
- Formal matching criteria, as defined in the literature, should be reviewed to avoid excessive alteration of the natural characteristics of original earthquake records. For MDOF systems with $T_1 < 1.5$ s, a good approach appears to use a limited number of loosely matched records that will then be multiplied by a single scalar to achieve the required degree of spectrum compatibility.

This study was limited to a few ground motion records and structural systems. It is recommended that further similar study be carried out on broader record ensembles and on seismic systems exhibiting various hysteretic behavior.

Acknowledgements: The authors wish to thanks V. Proulx-Brisson, I. Ghorbanirenani and M. Leclerc that provided assistance to produce the analysis results presented in this paper. The financial support provided by the National Science and Engineering Research Council of Canada and the Fonds Quebecois for Research in Nature and Technology is also gratefully acknowledged.

Bibliography

Antoniou, S. and Pinho, R., 2008. *SeismoSignal. Version 3.2.0*. [Logiciel]. SeismoSoft.

ASCE/SEI 41-06, 2007. Seismic Rehabilitation of Existing Buildings, American Society of Civil Engineers.

ASCE/SEI 43-05, 2005. Seismic design criteria for structures, systems and components in nuclear facilities. American Society of Civil Engineers.

ASCE 4-98, 2000. Seismic analysis of safety-related nuclear structures and commentary, American Society of Civil Engineers.

ASCE 7-05, 2005. Minimum Design Loads for Buildings and Other Structures, ANSI/SEI 7-05 Including Supplement No.1, American Society of Civil Engineers, Reston, VA.

ASN/Guide/2/01, 2006. Autorité de Sûreté Nucléaire (France) – Prise en compte du risque sismique à la conception des ouvrages de génie civil d'installations nucléaires de base à l'exception des stockages à long terme des déchets radio actifs (www.asn.fr).

ATC-63. 2008. Quantification of Building Seismic Performance Factors ATC-63 Project Report – 90% Draft FEMA P695/April 2008. Applied Technology Council, Redwood City, CA.

Atkinson, G. and Pierre, J., 2004. Ground-motion response spectra in Eastern North America for different critical damping values. Seismological Research Letters, 75(4), 541–545.

Atkinson, G.M. and Beresnev, I.A., 1998. Compatible ground-motion time histories for new national seismic hazard maps. Canadian Journal of Civil Engineering, 25(2), 305–318.

Atkinson, G.M. and Elgohary, M., 2007. Typical uniform hazard spectra for eastern North American sites at low probability levels. Canadian Journal of Civil Engineering, 34(1), 12–18.

Aziz, T.S. 2004. Design Earthquake Ground motions for Nuclear Power Plants, Proceedings, 13th World Conference on earthquake Engineering, Vancouver, B.C., Canada, Paper No. 934.

Barenberg, M.E., 1989. Inelastic response of a spectrum-compatible artificial accelerogram. Earthquake Spectra, 5(3), 477–493.

Bazzurro, P. and Luco, N., 2006. Do scaled and spectrum matched near-source records produce biased nonlinear structural response. Proceedings of the 8th US National Conference on Earthquake Engineering, San Francisco, CA, April.

Beyer, K. and Bommer, J.J., 2007. Selection and scaling of real accelerograms for bi-directional loading: A review of current practice and code provisions. Journal of Earthquake Engineering, 11(Suppl. 1), 13–45.

Bommer, J.J. and Aceveo, A.B., 2004. The use of real earthquake accelerograms as input to dynamic analysis. Journal of Earthquake Engineering, 8(1), 43–91.

Boore, D.M. and Bommer, J.J., 2005. Processing of strong-motion accelerograms: Needs, options and consequences. Soil Dynamics and Earthquake Engineering, 25(2), 93–115.

Boore, D.M., Stephens, C.D. and Joyner, W.B., 2002. Comments on baseline correction of digital strong-motion data: Examples from the 1999 Hector Mine, California, earthquake. Bulletin of the Seismological Society of America, 92(4), 1543–1560.

Canadian Standards Association, 1981. CAN3-N289.3-M81 (reaffirmed 2003). Design procedures for seismic qualification of CANDU Nuclear Power Plant.

Christopoulous, C., Léger, P. and Filiatrault, A., 2003. Seismic sliding response analysis of gravity dams including vertical accelerations. Journal of Earthquake Engineering and Engineering Vibration, 2(2), 189–200.

Christian, J.T., 1988. Developing design ground motions in practice. Geotechnical Special Publication, ASCE, New York, pp. 405–429.

EC8, 2003. Eurocode 8: Design of structures for earthquake resistance. European Committee for Standardisation, Brussels, Belgium.

Fuentes, A. 1998. Bâtiments en zone sismique. Paris: Presses de l'école nationale des ponts et chaussées. p. 35.

Gu, P. and Wen, Y.K., 2007. A record-based method for the generation of tridirectional uniform hazard–response spectra and ground motions using the Hilbert–Huang transform. Bulletin of the Seismological Society of America, 97(5), 1539–1556.

Gupta, V.K. 2002. *WavGen*. [Logiciel], http://home.iitk.ac.in/~vinaykg/wavgen.htm.

Gomes, R.C., Santos, J. and Oliveira, C.S., 2006. Design spectrum-compatible time histories for numerical analysis: Generation, correction and selection. Journal of Earthquake Engineering, 10(6), 843–865.

Hancock, J. and Bommer, J.J. 2007. Using spectral matched records to explore the influence of strong-motion duration on inelastic structural response. Soil Dynamics and Earthquake Engineering, 27(4), 291–299.

Hancock, J., Watson-Lamprey, J., Abrahamson, N.A., Bommer, J.J., Gomes, R.C., Santos, J. and Oliveira, C.S., 2006. Design spectrum-compatible time histories for numerical analysis: Generation, correction and selection. Journal of Earthquake Engineering, 10(6), 843–865.

Hancock, J., Watson-Lamprey, J., Abrahamson, N.A., Bommer, J.J., Markatis, A., McCoy, E. and Mendis, R., 2006. An improved method of matching response spectra of recorded earthquake ground motion using wavelets. Journal of Earthquake Engineering, 10(SPEC. ISS. 1), 67–89.

Hong, X.J. and Xu, Y.L., 2007. Generation of critical and compatible seismic ground acceleration time histories for high-tech facilities. Structural Engineering and Mechanics, 26(6), 687–707.

Iervolino, I., Maddaloni, G. and Cosenza, E., 2008. Eurocode 8 compliant real record sets for seismic analysis of structures. Journal of Earthquake Engineering, 12(1), 54–90.

Kappos, A.J. and Kyriakakis, P., 2000. A re-evaluation of scaling techniques for natural records. Soil Dynamics and Earthquake Engineering, 20(1–4), 111–123.

Kurama, Y.C. and Farrow, K.T., 2003. Ground motion scaling methods for different site conditions and structure characteristics. Earthquake Engineering and Structural Dynamics, 32(15), 2425–2450.

Léger, P. and Leclerc, M., 1996. Evaluation of earthquake ground motion to predict cracking response of gravity dams. Engineering Structures, 18(3), 227–239.

Léger, P., Tayebi, A.K. and Paultre, P., 1993. Spectrum compatible accelerograms for inelastic seismic analysis of short period structures located in Eastern Canada. Canadian Journal of Civil Engineering, 20, 951–968.

Li, Z.-C. and Zhao, F.-X., 2006. Comparison between technical requirements in different standards on synthesis of design ground motion history for nuclear power plants. Nuclear Power Engineering, 27(2), 17–21.

Luco, N. and Bazzurro, P., 2007. Does amplitude scaling of ground motion records result in biased nonlinear structural drift responses? Earthquake Engineering and Structural Dynamics, 36(13), 1813–1835.

Mackie, K.R. and Stojadinovic, B., 2007. Three-dimensional ground motion scaling for highway bridges. Proceedings of the 9th Canadian Conference on Earthquake Engineering, Ottawa, Ontario, Canada, CD.

Markatis, A., McCoy, E. and Mendis, R., 2006. An improved method of matching response spectra of recorded earthquake ground motion using wavelets. Journal of Earthquake Engineering, 10(SPEC. ISS. 1), 67–89.

McGuire, R.K., Silva, W.J. and Kenneally, R. 1999. Hazard- and risk-consistent spectra. Nuclear Engineering and Design, 192(2), 137–145.

Moehle, J.P., 2006. Seismic analysis, design, and review for tall buildings. Structural Design of Tall and Special Buildings, 15(5), 495–513.

Montaldo, V., Kiremidjian, A.S., Thráinsson, H. and Zonno, G., 2003. Simulation of the Fourier phase spectrum for the generation of synthetic accelerograms. Journal of Earthquake Engineering, 7(3), 427–445.

Mukherjee, S. and Gupta, V.K., 2002. Wavelet-based generation of spectrum compatible time histories. Soil Dynamic and Earthquake Engineering, 22(9), 799–804.

Naeim, F., Alimoradi, A. and Pezeshk, S., 2004. Selection and scaling of ground motion time histories for structural design using genetic algorithms. Earthquake Spectra, 20(2), 413–426.

Naiem, F. and Lew, M., 1995. On the use of design-spectrum compatible time histories. Earthquake Spectra, 11(1), 111–127.

NBCC. 2005. National Building Code of Canada, and Commentary. National Research Council of Canada Ottawa, Ontario.

Naumoski, N., Saatcioglu, M. and Amiri-Hormozaki, K. 2004. Effects of scaling of earthquake excitations on the dynamic response of reinforced concrete frame buildings. 13th World Conference on Earthquake Engineering, Vancouver, Canada. Paper No. 2917. CD. 15 pp.

Shibata, H., 2006. Modeling of earthquake motions for seismic design of critical facilities: Revision of licensing criteria of NPP. Journal of Pressure Vessel Technology, Transactions of the ASME, 128(4), 486–501.

Shome, N., Cornell, C., Bazzurro, P. and Carballo, J., 1998. Earthquake records and nonlinear responses. Earthquake Spectra, 14(3), 469–500.

Silva, W. and Constantino, C., 2002. Development of site-specific ground motions in Western and Eastern North America. Soil Dynamics and Earthquake Engineering, 22(9–12), 755–764.

Somerville, P., Smith, N., Punyamurthula, S. and Sun, J., 1997. Development of ground motion time histories for phase 2 of the FEMA/SAC steel project. SAC Joint Venture, Report No. SAC/BD-97/04, California.

Suárez, L.E. and Montejo, L.A., 2005. Generation of artificial earthquakes via the wavelet transform. International Journal of Solids and Structures, 42(21–22), 5905–5919.

Takewaki, I., 2002. Seismic critical excitation method for robust design: A review. ASCE Journal of Structural Engineering, 128(5), 665–672.

Takewaki, I., 2007. Critical excitation methods in earthquake engineering. Elsevier, UK, 270 pp.

Tremblay, R. and Atkinson, G., 2001. Comparative study of the inelastic seismic demand of Eastern and Western Canadian sites. Earthquake Spectra, 17(2), 333–358.

USACE (US Army Corps of Engineers). 2003. Engineering and Design – Time-History Dynamic Analysis of Concrete Hydraulic Structures. (EM 1110-2-6051), http://www.usace.army.mil/publications/eng-manuals/em1110-2-6051/toc.htm.

Vamvatsikos, D. and Cornell, A., 2002. Incremental dynamic analysis. Earthquake Engineering and Structural Dynamics, 31, 491–514.

Vamvatsikos, D. and Cornell, C.A., 2004. Applied incremental dynamic analysis. Earthquake Spectra, 20(2), 523–553.

Wanotkorkul, A. and Filiatrault, A., 2005. Simulation of strong ground motions for seismic fragility evaluation of nonstructural components in hospitals. Technical Report MCEER-05-0005, 206 pp.

Watson-Lamprey, J. and Abrahamson, N., 2006. Selection of ground motion time series and limits on scaling. Soil Dynamics and Earthquake Engineering, 26(5), 477–482.

Zhao, F., Zhang, Y. and Lu, H., 2006. Artificial ground motion compatible with specified ground shaking peaks and target response spectrum. Earthquake Engineering and Engineering Vibration, 5(1), 41–48.

PART II

DAMAGE ASSESSMENT AND RECONSTRUCTION OF INFRASTRUCTURE

DAMAGE ASSESSMENT AND DISASTER PREVENTION IN NATM TUNNELS DURING CONSTRUCTION: MICROMECHANICS-SUPPORTED HYBRID ANALYSES

H.A. Mang (herbert.mang@tuwien.ac.at), S. Scheiner, B. Pichler, and C. Hellmich
Institute for Mechanics of Materials and Structures, Vienna University of Technology, Karlsplatz 13, 1040 Vienna, Austria

Abstract. Knowledge of the stresses in shotcrete tunnel shells is of great importance for assessing their safety against severe cracking or failure. Estimation of these stresses from 3D optical displacement measurements requires shotcrete material models allowing for variation of the water–cement and the aggregate–cement ratio. This is the motivation for employing two representative volume elements within a continuum micromechanics framework: One of them relates to cement paste (with a spherical material phase representing clinker, needle-shaped hydrate phases with isotropically distributed spatial orientations, a spherical water phase, and a spherical air phase, with all phases being in mutual contact), whereas the second one relates to shotcrete (with phases representing cement paste and aggregates, whereby aggregate inclusions are embedded into a matrix made up by cement paste). Elasticity homogenization follows self-consistent schemes (at the cement paste level) and Mori–Tanaka estimates (at the shotcrete level). Stress peaks in the hydrates related to quasi-brittle material failure are estimated by second-order phase averages derived from the RVE-related elastic energy. The latter permits upscaling from the hydrate strength to the shotcrete strength. Experimental data from resonant frequency tests, ultrasonics tests, adiabatic tests, uniaxial compression tests, and nanoindentation tests suggest that early-age (evolving) shotcrete elasticity and strength can be reasonably well predicted from mixture- and hydration-independent mechanical properties of aggregates, clinker, hydrates, water, and air, and from the strength properties of the hydrates. Notably, the model-predicted final strength (at completed hydration) almost perfectly follows the famous Feret formula. At the structural level, the micromechanics model, when combined with 3D displacement measurements, predicts that a decrease of the water–cement ratio increases the safety of the shotcrete tunnel shell whereas standard-type variations in the aggregate–cement ratio, because of rebound during shotcreting, have virtually no influence on the overall structural safety.

Keywords: Micromechanics, shotcrete, hydration, elasticity, strength, tunneling, New Austrian tunneling method

A. Ibrahimbegovic and M. Zlatar (eds.), *Damage Assessment and Reconstruction After War or Natural Disaster*,

1. Introduction

Disasters resulting from damage and failure of civil engineering structures, caused either by short-term influences (earthquake ground motion, explosions, or fires) or by long-term loadings (corrosion, wear, pollution) may occur during service as well as in the construction process itself, in particular, if construction leads to significant changes of the original conditions. This is particularly true for the field of underground tunneling where complicated ground conditions often call for sophisticated methods such as the so-called New Austrian Tunneling Method (NATM) (Rabcewicz 1948, 1964a, b,1965; Karakuş and Fowell, 2004). While being extremely successful in cases where a high degree of flexibility is required, use of this method is also related to what was called 'Britain's worst civil engineering disaster in modern times' (Bishop, 1994), namely, to a series of collapses of thin support shells (Oliver, 1994) during the construction of the Heathrow express station tunnel at London's busiest airport. Installation of such thin support shells or primary linings right after excavation of a small stretch of a tunnel is one of the key elements of the NATM, apart from utilization of the ground surrounding the tunnel as structural element (which may also be reinforced by rock bolts) and from final stabilization of the tunnel by a secondary lining. Since failure of the primary lining is one of the major causes for the disasters that were encountered during NATM tunnel construction, great efforts have been undertaken to monitor the behavior of the freshly installed lining. As of today, 3D optical monitoring systems (Steindorfer et al., 1995; Schubert and Steindorfer, 1996) are the golden standard. Changes of characteristic trend parameters, extracted from 3D displacement measurements, allow to estimate changes in the geological structure of the soil or rock (Schubert et al., 2002).

Understanding of the mechanics of NATM tunnel shells has turned out to be the key to safety increase and disaster prevention in modern NATM tunneling. For almost 2 decades, this was the driving force for theoretical, experimental, and computational mechanics research at the Institute for Mechanics of Materials and Structures (IMWS) of Vienna University of Technology. The present book chapter reviews the Institute's latest achievements in safety assessment and disaster prevention of thin primary support shells, based on an integrated analysis method which combines monitoring data with advanced multiscale mechanics concepts, directly integrating concrete composition and chemical information related to so-called performance-based shotcrete tunnel design. In more detail, the strains in the shotcrete tunnel shell are obtained from the aforementioned 3D optical displacement vector measurements, as proposed by Rokahr and Zachow (1997) on the basis of relative movements of pairs of measurement

points. At the IMWS, this conceptual approach was further elaborated: The strain *fields* can be estimated on the basis of a hybrid method (Hellmich, 1999; Hellmich et al., 1999a, 2001), in which displacement vector fields are approximated through interpolation of measured displacement vectors at discrete points of the tunnel shell. These fields are then prescribed as boundary values for a three-dimensional Finite Element structural model of the tunnel shell. This method was extended to segmented tunnel linings (Macht et al., 2000; Lackner et al., 2002); use of approximations from thin shell theory (Macht et al., 2003; Lackner et al., 2006) turned out to be beneficial for day-to-day use of the hybrid method in engineering practice (Brandtner et al., 2007).

The underlying shotcrete models must represent the creep behavior of the material (Rokahr and Lux, 1987; Schubert, 1988; Lechner et al., 2001) reasonably well. Consideration of hydration-induced, thermal and chemical strains further improves the reliability of estimations of the internal forces of the shell (Hellmich et al., 1999b, c; Sercombe et al., 2000 Lechner et al., 2001). All aforementioned material models rely on shotcrete mixture-specific material properties. Hence, any change in mixture (e.g. a variation of the water–cement ratio, as often encountered *in situ*) can only be considered if additional experiments (related to strength, creep, and shrinkage) are performed on samples with the modified concrete composition. This is often unfeasible so that engineers on site frequently agree on a 'typical' shotcrete for a tunnel track.

Clearly, this situation is unsatisfactory. As a remedy, the shotcrete composition (in terms of the water–cement ratio w/c and the aggregate–cement ratio a/c) needs to be incorporated into the shotcrete material models, within a micromechanical framework: This was recently shown by Hellmich and Mang (2005) for the case of elasticity – following earlier work on concrete by Bernard et al. (2003) and on bone by Hellmich and Ulm (2002). While stiffness is an important factor for attracting stresses to the tunnel shell, strength is the key factor to understand whether these stresses significantly compromise the shell's safety. Also the evolution of strength is influenced by the w/c- and the a/c-ratio (Neville, 1981). Here we review a first micromechanical model for shotcrete elasticity and strength (Pichler et al. 2008a, b). By way of example, we employ this new model to hybrid analysis of a NATM tunnel shell. Extending results published earlier (Pichler et al., 2008b), we not only study the influence of the water–cement ratio on the safety level of the thin primary lining but also the one of the aggregate–cement ratio which typically fluctuates because of varying rebound of aggregates during shotcreting.

The book chapter is organized as follows: After a short review of the fundamentals of continuum micromechanics (Section 2), upscaling of stiffness

and strength properties (Sections 3 and 4) from the hydrate level, via the cement paste level, to the shotcrete level is described. This is followed by experimental validation (Section 5) of the new micromechanics model and by its application to a NATM-tunnel safety assessment (Sections 6 and 7).

2. Fundamentals of micromechanics – representative volume element (RVE)

In continuum micromechanics (Hill, 1963; Suquet, 1997; Zaoui, 1997, 2002), a material is understood as a macro-homogeneous but micro-heterogeneous body filling a representative volume element (RVE) with characteristic length ℓ, $\ell \gg d$, d standing for the characteristic length of inhomogeneities within the RVE, and $\ell \ll \mathcal{L}$, $\mathcal{L}$ standing for the characteristic lengths of geometry or loading of a structure built up by the material defined on the RVE. In general, the microstructure within an RVE is too complicated to describe it in full detail. Therefore, quasi-homogeneous subdomains with known physical quantities (such as volume fractions or elastic properties) are reasonably chosen. They are called material phases. The 'homogenized' mechanical behavior of the overall material, i.e., the relation between homogeneous deformations acting on the boundary of the RVE and resulting (average) stresses, or the ultimate stresses sustainable by the RVE, can then be estimated from the mechanical behavior of the aforementioned homogeneous phases (representing the inhomogeneities within the RVE), their dosages within the RVE, their characteristic shapes, and their interactions. If a single phase exhibits a heterogeneous microstructure itself, its mechanical behavior can be estimated by introduction of an RVE within this phase, with dimensions $\ell_2 \leq d$, comprising again smaller phases with characteristic length $d_2 \ll \ell_2$, and so on, leading to a multistep homogenization scheme.

For shotcrete, we employ two RVEs: The first one relates to cement paste (with phases representing clinker, water, hydrates, and air), and the second one to shotcrete (with phases representing cement paste and aggregates), see Fig. 1.

3. Micromechanics at the cement paste level

3.1. MICROMECHANICAL REPRESENTATION

We consider an RVE_{cp} of cement paste with characteristic length $\ell_{cp} = 0.25$–0.50 mm, see Fig. 1a, consisting of four different material phases with characteristic dimensions $d_{cp} = 1{-}50\,\mu$m (see also Fig. 2): (i) a spherical clinker phase, (ii) needle-shaped hydrate phases with isotropically

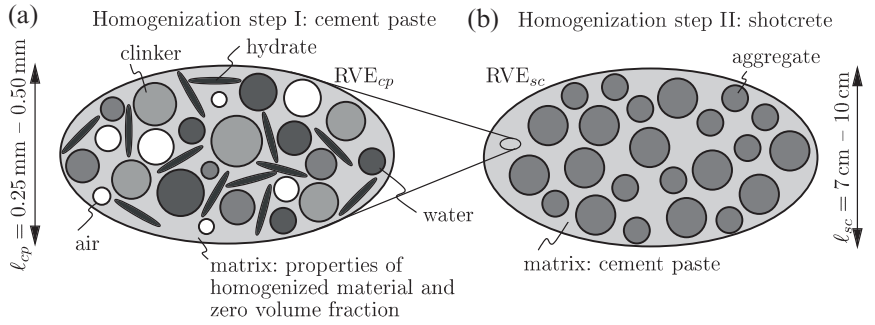

Figure 1. Micromechanical representation of shotcrete microstructure through a two-step homogenization scheme: 2D sketches of 3D representative volume elements (RVEs) – (**a**) the polycrystalline RVE of 'cement paste', RVE$_{cp}$, is built up of clinker, water, needle-shaped hydrates, and air; (**b**) the RVE of the matrix-inclusion composite 'shotcrete', RVE$_{sc}$, is composed of a cement paste matrix with aggregate inclusions

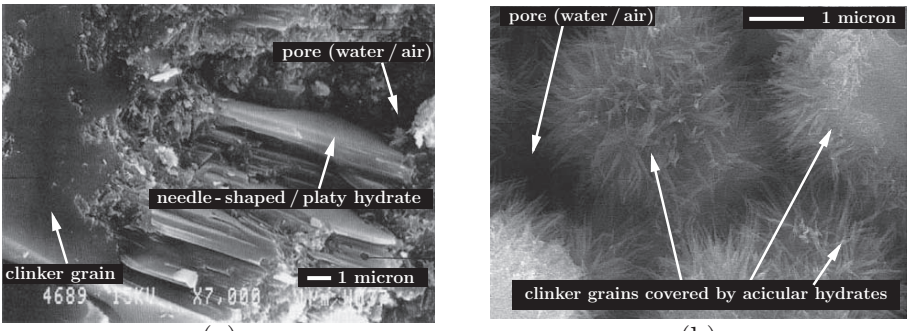

Figure 2. Images of cement paste obtained by Scanning Electron Microscopy showing non-spherical hydrates: (**a**) from Baroghel-Bouny (1994), (**b**) from Tritthart and Häußler (2003)

distributed spatial orientations, (iii) a spherical water phase, and (iv) a spherical air phase.

Macroscopic strains $\mathbf{E}_{cp}$ are imposed at the boundary of the RVE$_{cp}$ in terms of displacement vectors $\boldsymbol{\xi}$ (Hashin, 1983),

$$\text{on } \partial\Omega_{cp} : \boldsymbol{\xi}(\mathbf{x}) = \mathbf{E}_{cp} \cdot \mathbf{x}\,, \tag{1}$$

with $\mathbf{x}$ as the position vector within the RVE$_{cp}$. The geometrical compatibility of (1) with the local microscopic strains $\boldsymbol{\varepsilon}(\mathbf{x})$ within the RVE$_{cp}$ implies

$$\mathbf{E}_{cp} = \frac{1}{\Omega_{cp}} \int\limits_{\Omega_{cp}} \boldsymbol{\varepsilon}(\mathbf{x})\, dV = \sum_p f_p\, \boldsymbol{\varepsilon}_p\,, \tag{2}$$

with $p = clin, H_2O, hyd, air$, Ω_{cp} as the volume of the RVE$_{cp}$, f_{clin}, f_{H_2O}, f_{hyd}, and f_{air} as the volume fractions of clinker, of water, of hydrates, and of air, respectively, and with

$$\boldsymbol{\varepsilon}_p = \frac{1}{\Omega_p} \int\limits_{\Omega_p} \boldsymbol{\varepsilon}(\mathbf{x}) \, \mathrm{d}V \,, \tag{3}$$

as the first-order (spatial average) phase strains. Considering the needle shape of the hydrate phases, the strain average rule (2) takes the form

$$\mathbf{E}_{cp} = \sum_p f_p \, \boldsymbol{\varepsilon}_p + f_{hyd} \int\limits_{\varphi=0}^{2\pi} \int\limits_{\vartheta=0}^{\pi} \boldsymbol{\varepsilon}_{hyd;\varphi,\vartheta} \frac{\sin\vartheta}{4\pi} \, \mathrm{d}\vartheta \, \mathrm{d}\varphi \,. \tag{4}$$

with $p = clin, H_2O, air$, and with the Euler angles φ and ϑ defining the orientations of the hydrate needles, see Pichler et al. (2008b) for details. The average strains in the hydrate needles, $\boldsymbol{\varepsilon}_{hyd;\varphi,\vartheta}$, are defined through

$$\boldsymbol{\varepsilon}_{hyd;\varphi,\vartheta} = \lim_{\Delta\varphi,\Delta\vartheta\to 0} \left(\frac{1}{\Omega_{hyd;\varphi,\vartheta}} \int\limits_{\Omega_{hyd;\varphi,\vartheta}} \boldsymbol{\varepsilon}(\mathbf{x}) \, \mathrm{d}V \right), \tag{5}$$

By analogy to (2), the macroscopic stresses $\boldsymbol{\Sigma}_{cp}$ are equal to the spatial average of the (equilibrated) local stresses $\boldsymbol{\sigma}(\mathbf{x})$ inside the RVE$_{cp}$,

$$\boldsymbol{\Sigma}_{cp} = \frac{1}{\Omega_{cp}} \int\limits_{\Omega_{cp}} \boldsymbol{\sigma}(\mathbf{x}) \, \mathrm{d}V = \sum_p f_p \, \boldsymbol{\sigma}_p + f_{hyd} \int\limits_{\varphi=0}^{2\pi} \int\limits_{\vartheta=0}^{\pi} \boldsymbol{\sigma}_{hyd;\varphi,\vartheta} \frac{\sin\vartheta}{4\pi} \, \mathrm{d}\vartheta \, \mathrm{d}\varphi \,, \tag{6}$$

with $p = clin, H_2O, air$, and with phase stresses $\boldsymbol{\sigma}_p$ and $\boldsymbol{\sigma}_{hyd;\varphi,\vartheta}$ defined analogously to the aforementioned phase strains $\boldsymbol{\varepsilon}_p$ and $\boldsymbol{\varepsilon}_{hyd;\varphi,\vartheta}$, see (3) and (5).

3.2. CONSTITUTIVE BEHAVIOR OF CLINKER, WATER, HYDRATES, AND AIR

We assign linear elastic behavior to all phases, i.e.

$$\boldsymbol{\sigma}_p = \mathbf{C}_p : \boldsymbol{\varepsilon}_p \,, \tag{7}$$

with $\mathbf{C}_p$ as the fourth-order stiffness tensor of phase p, $p = clin, H_2O, hyd, air$. Assuming isotropy for all phases, $\mathbf{C}_p$ reads as

$$\mathbf{C}_p = 3k_p\mathbf{J} + 2\mu_p\mathbf{K} \,, \tag{8}$$

whereby $\mathbf{K}$ is the deviatoric part of the fourth-order unit tensor, defined as $\mathbf{K} = \mathbf{I} - \mathbf{J}$, with $\mathbf{I}$ as the symmetric fourth-order unit tensor with components $I_{ijrs} = 1/2(\delta_{ir}\delta_{js} + \delta_{is}\delta_{jr})$, and with $\mathbf{J} = 1/3(\mathbf{1} \otimes \mathbf{1})$ as the volumetric part of the fourth-order unit tensor, where $\mathbf{1}$ denotes the second-order unit tensor with components δ_{ij} (Kronecker delta), $\delta_{ij} = 1$ for $i = j$, and $\delta_{ij} = 0$ otherwise. The phase stiffnesses $\mathbf{C}_p$, in terms of the bulk modulus k_p and the shear modulus μ_p, are available from experiments (see Table 1): Hydrate stiffnesses follow from nanoindentation experiments (Acker, 2001; Constantinides and Ulm, 2004); we here consider the elastic properties of low-density calcium silicate hydrates (C-S-H) as representative for all hydrates, see also Hellmich and Mang (2005) for details. Clinker properties are taken from Acker (2001). If, upon loading, no water can escape from the RVE_{cp} (sealed or undrained conditions), we consider an elastic water phase with negligible shear stiffness as a very good approximation of 'undrained conditions in the sense of a fully *poro*-micromechanical theory' (Hellmich and Ulm, 2005), whereas a zero water stiffness relates to drained conditions. The zero-stiffness air phase is also in a 'drained' state.

TABLE 1. Intrinsic mechanical properties of microstructural constituents of shotcrete

Phase	Bulk modulus k [GPa]	Shear modulus μ [GPa]	Reference
Clinker	$k_{clin} = 116.7$	$\mu_{clin} = 53.8$	Acker (2001)
Water (drained RVE)	$k_{H_2O} = 0.0$	$\mu_{H_2O} = 0.0$	
Water (sealed RVE)	$k_{H_2O} = 2.3$	$\mu_{H_2O} = 0.0$	
Hydrates	$k_{hyd} = 14.1$	$\mu_{hyd} = 8.9$	Ulm et al. (2004)
Air	$k_{air} = 0.0$	$\mu_{air} = 0.0$	
Aggregate	$k_{agg} = 41.7$	$\mu_{agg} = 19.2$	Wesche (1974), Mehlhorn (1996)

Uniaxial compression tests on cement paste (or shotcrete) samples reveal linear elastic behavior until, close to the compressive strength, axial strains increase overlinearly with increasing axial stresses. Once the peak load is reached, the material exhibits quasi-brittle failure. Hence, the strength of cement paste (or of shotcrete) can be estimated by means of elastic limit analysis (Pichler et al., 2008a). Moreover, it is assumed that the elastic limits of the hydrates govern the elastic limits of cement paste and of the shotcrete. I.e. each hydrate behaves linearly elastic as long as microscopic deviatoric stress peaks remain below a specific critical value. If, because of a (compressible uniaxial) macroscopic load increase, this critical value

is reached in the most strongly stressed region of the hydrate phase, the elastic limit on the microscale is reached, which, in turn, corresponds to the macroscopic elastic limit of cement paste (or shotcrete), associated with failure of the material (under macroscopic uniaxial compression). In more detail, load bearing capacities of the hydrates are being bounded according to a *von Mises*-type elastic limit criterion (Pichler et al., 2008a),

$$\max_{\mathbf{x}\in\Omega_{hyd}} \sigma^{dev}(\mathbf{x}) = \max_{\mathbf{x}\in\Omega_{hyd}} \left[\left(\frac{1}{2}\, \boldsymbol{\sigma}^{dev}(\mathbf{x}) : \boldsymbol{\sigma}^{dev}(\mathbf{x}) \right)^{\frac{1}{2}} \right] \leq \sigma^{dev}_{crit}\,, \tag{9}$$

where $\sigma^{dev}(\mathbf{x})$ is the norm of stress deviator $\boldsymbol{\sigma}^{dev}(\mathbf{x})$ defined by

$$\boldsymbol{\sigma}^{dev}(\mathbf{x}) = \mathbf{K} : \boldsymbol{\sigma}(\mathbf{x})\,. \tag{10}$$

The choice of hydrates as weakest locations inside the RVE$_{cp}$ of cement paste was corroborated by Pichler et al. (2008a) who showed that the single strength-type value for $\sigma^{dev}_{crit} = 26\,\text{MPa}$ allows for prediction of uniaxial cube compressive strength of different cement pastes with w/c ranging from 0.35–0.60 (Boumiz et al., 1996; Sun et al., 2005), at different degrees of hydration ξ.

3.3. HOMOGENIZED ELASTICITY OF CEMENT PASTE

As long as the material phases behave elastically, the relation between $\boldsymbol{\Sigma}_{cp}$ and $\mathbf{E}_{cp}$ reads, analogous to (7), as

$$\boldsymbol{\Sigma}_{cp} = \mathbf{C}_{cp} : \mathbf{E}_{cp}\,, \tag{11}$$

with the 'macroscopic' homogenized stiffness tensor of cement paste, $\mathbf{C}_{cp} = 3k_{cp}\mathbf{J} + 2\mu_{cp}\mathbf{K}$, and where k_{cp} is the bulk modulus and μ_{cp} is the shear modulus. Following the traditional approach in continuum micromechanics (Zaoui, 2002), the dependence of $\mathbf{C}_{cp}$ on the phase stiffness properties (Table 1) will be established on the basis of Eshelby-Laws-type matrix-inclusion problems which are formulated separately for each phase $p = clin, H_2O, hyd, air$. The respective phase is represented by a single ellipsoidal inclusion which is embedded in an infinite matrix with stiffness $\mathbf{C}^0$, subjected to homogeneous strains $\mathbf{E}^\infty$ at infinity. This loading provokes homogeneous strains in the ellipsoidal inclusions which are of the form (Eshelby, 1957; Laws, 1977; Zaoui, 2002)

$$\boldsymbol{\varepsilon}_p = \left[\mathbf{I} + \mathbf{P}^0_p \,:\, (\mathbf{C}_p - \mathbf{C}^0) \right]^{-1} : \mathbf{E}^\infty\,. \tag{12}$$

Thereby, the Hill tensors $\mathbf{P}^0_p$ account for the shape of inclusion (phase) p in a matrix of (isotropic) stiffness $\mathbf{C}^0 = 3k^0\mathbf{J} + 2\mu^0\mathbf{K}$.

Evaluation of (12) for all phases within RVE_{cp} and insertion of the corresponding result into condition (4) yields a relation between RVE_{cp}-related strains $\mathbf{E}_{cp}$ and matrix-related strains $\mathbf{E}^{\infty}$,

$$\mathbf{E}^{\infty} = \mathbf{E}_{cp} : \left\{ \sum_{p} f_p \left[\mathbf{I} + \mathbf{P}^0_{sph} : (\mathbf{C}_p - \mathbf{C}^0) \right]^{-1} + \right.$$
$$\left. + f_{hyd} \int_{\varphi=0}^{2\pi} \int_{\vartheta=0}^{\pi} \left[\mathbf{I} + \mathbf{P}^0_{cyl}(\varphi, \vartheta) : (\mathbf{C}_{hyd} - \mathbf{C}^0) \right]^{-1} \frac{\sin\vartheta}{4\pi} \, d\vartheta \, d\varphi \right\}^{-1} \quad (13)$$

with $p = clin, H_2O, air$. The computation of the Hill tensors for spherical material phases, $\mathbf{P}^0_{sph}$, and for cylindrical material phases, $\mathbf{P}^0_{cyl}(\varphi, \vartheta)$, respectively, is presented in detail in Pichler et al. (2008b). $\mathbf{C}^0$ in (13) is chosen according to the interaction of the phases within the RVE_{cp} (Zaoui, 2002). Since they are largely disordered and in contact with each other, we choose $\mathbf{C}^0 = \mathbf{C}_{cp}$ (self-consistent scheme [Hershey, 1954; Kröner, 1958]), and identify the homogenized stiffness of cement paste, $\mathbf{C}_{cp}$, by inserting (13) into (12), multiplying the corresponding result by $\mathbf{C}_p$, according to the phase elasticity law (7), and inserting the result of the latter operations into the stress average condition (6). Comparison of the final result with (11) yields the desired homogenized stiffness of cement paste as

$$\mathbf{C}_{cp} = \left\{ \sum_{p} f_p \mathbf{C}_p : \left[\mathbf{I} + \mathbf{P}^{cp}_{sph} : (\mathbf{C}_p - \mathbf{C}_{cp}) \right]^{-1} + f_{hyd} \mathbf{C}_{hyd} : \right.$$
$$: \int_{\varphi=0}^{2\pi} \int_{\vartheta=0}^{\pi} \left[\mathbf{I} + \mathbf{P}^{cp}_{cyl}(\varphi, \vartheta) : (\mathbf{C}_{hyd} - \mathbf{C}_{cp}) \right]^{-1} \frac{\sin\vartheta}{4\pi} \, \mathrm{d}\vartheta \, \mathrm{d}\varphi \Bigg\} :$$
$$: \left\{ \sum_{p} f_p \left[\mathbf{I} + \mathbf{P}^{cp}_{sph} : (\mathbf{C}_p - \mathbf{C}_{cp}) \right]^{-1} + f_{hyd} \int_{\varphi=0}^{2\pi} \int_{\vartheta=0}^{\pi} \left[\mathbf{I} + \mathbf{P}^{cp}_{cyl}(\varphi, \vartheta) : \right. \right.$$
$$\left. \left. (\mathbf{C}_{hyd} - \mathbf{C}_{cp}) \right]^{-1} \frac{\sin\vartheta}{4\pi} \, \mathrm{d}\vartheta \, \mathrm{d}\varphi \right\}^{-1}, \quad (14)$$

where $p = clin, H_2O, air$. For detailed explanations regarding the numerical evaluation of (14), see Pichler et al. (2008a, b).

3.4. HOMOGENIZED STRENGTH OF CEMENT PASTE

From loading $\mathbf{E}_{cp}$ (or $\mathbf{\Sigma}_{cp}$) of an RVE_{cp} of cement paste, we are left with estimating the stress peaks $\max \sigma^{dev}_{hyd}(\mathbf{x})$ in the hydrates relevant to the

quasi-brittle failure criterion (9). We have resolved the hydrate phase Ω_{hyd} down to bundles $\Omega_{hyd;\varphi,\vartheta}$ around angles φ and ϑ. Hence, we may specify

$$\max_{\mathbf{x}\in\Omega_{hyd}} \sigma^{dev}(\mathbf{x}) = \max_{\substack{\mathbf{x}\,\in\,\Omega_{hyd;\varphi,\vartheta} \\ \varphi\,\in\,[0,2\pi] \\ \vartheta\,\in\,[0,\pi]}} \sigma^{dev}(\mathbf{x},\varphi,\vartheta)\,. \tag{15}$$

Still, in the maximally stressed bundle, not the (first-order) average phase stresses $\boldsymbol{\sigma}_{hyd;\varphi,\vartheta}$, but stress *peaks* govern the failure of the (φ,ϑ)-oriented hydrate phase (Pichler et al., 2008a). Such peaks can be estimated appropriately through quadratic stress averages over suitably chosen subdomains of the RVE_{cp}, such as 3D subdomains (bulk phases) (Lemarchand et al., 2002; Barthélémy and Dormieux, 2003; Hofstetter et al., 2005) or 2D interfaces (Dormieux et al., 2007; Fritsch et al., 2007). Herein we introduce quadratic (or second-order) deviatoric stress and strain averages over (φ,ϑ)-oriented hydrates, $\overline{\overline{\sigma^{dev}_{hyd;\varphi,\vartheta}}}$ and $\overline{\overline{\epsilon^{dev}_{hyd;\varphi,\vartheta}}}$, averaged, in the sense of (5), over all hydrates oriented in one direction (φ,ϑ),

$$\begin{aligned}\max_{\mathbf{x}\in\Omega_{hyd;\varphi,\vartheta}} \sigma^{dev}(\mathbf{x},\varphi,\vartheta) \;\approx\; \overline{\overline{\sigma^{dev}_{hyd;\varphi,\vartheta}}} = \\ = \lim_{\Delta\varphi,\Delta\vartheta\to 0}\left(\tfrac{1}{\Omega_{hyd;\varphi,\vartheta}}\int_{\Omega_{hyd;\varphi,\vartheta}}\left[\sigma^{dev}(\mathbf{x},\varphi,\vartheta)\right]^2\,\mathrm{d}V\right)^{\frac{1}{2}},\end{aligned} \tag{16}$$

so that, according to (15),

$$\max_{\mathbf{x}\in\Omega_{hyd}} \sigma^{dev}(\mathbf{x}) = \max_{\substack{\varphi\,\in\,[0,2\pi] \\ \vartheta\,\in\,[0,\pi]}} \overline{\overline{\sigma^{dev}_{hyd;\varphi,\vartheta}}}\,. \tag{17}$$

$\overline{\overline{\sigma^{dev}_{hyd;\varphi,\vartheta}}}$ can be related to macroscopic stresses $\boldsymbol{\Sigma}_{cp}$ imposed (in terms of strains $\mathbf{E}_{cp} = \mathbf{C}_{cp}^{-1} : \boldsymbol{\Sigma}_{cp}$) onto the RVE_{cp} of cement paste by means of elastic energy considerations similar to those proposed by Dormieux et al. (2002), Kreher and Molinari (1993), Kreher (1990), yielding

$$\overline{\overline{\sigma^{dev}_{hyd;\varphi,\vartheta}}} = \lim_{\Delta\varphi,\Delta\vartheta\to 0}\left(-\frac{\mu^2_{hyd}}{f_{hyd;\varphi,\vartheta}}\boldsymbol{\Sigma}_{cp} : \frac{\partial\mathbf{C}^{-1}_{cp}}{\partial\mu_{hyd;\varphi,\vartheta}} : \boldsymbol{\Sigma}_{cp}\right)^{\frac{1}{2}}. \tag{18}$$

Setting

$$\max_{\varphi,\vartheta}\overline{\overline{\sigma^{dev}_{hyd;\varphi,\vartheta}}} = \sigma^{dev}_{crit} = 26\,\text{MPa} \tag{19}$$

according to (9), (16), and (18), elastic limits of the hydrates are related to quasi-brittle failure of shotcrete which may be represented by the uniaxial

compressive strength $\Sigma_{cp,11}^{comp,ult}$: The latter follows from insertion of (19) into (18), and evaluation of (18) for $\Sigma_{cp} = -\left|\Sigma_{cp,11}^{comp,ult}\right| (\mathbf{e}_z \otimes \mathbf{e}_z)$,

$$\Sigma_{cp,11}^{comp,ult} = \left\{ \max_{\varphi,\vartheta} \left[\lim_{\Delta\varphi,\Delta\vartheta\to 0} \left(-\frac{\mu_{hyd}^2}{f_{hyd;\varphi,\vartheta}} (\mathbf{e}_z \otimes \mathbf{e}_z) : \frac{\partial \mathbf{C}_{cp}^{-1}}{\partial \mu_{hyd;\varphi,\vartheta}} : \right.\right.\right. \\ \left.\left.\left. : (\mathbf{e}_z \otimes \mathbf{e}_z) \right)^{\frac{1}{2}} \right] \right\}^{-1} \times \sigma_{crit}^{dev} . \tag{20}$$

An algorithm for computation of the aforementioned limit, $\lim_{\Delta\varphi,\Delta\vartheta\to 0}$, is presented in Pichler et al. (2008a).

4. Micromechanics at the shotcrete level

We consider an RVE_{sc} of shotcrete with the characteristic length $\ell_{sc} =$ 7–10 cm, see Fig. 1b, consisting of material phases with characteristic dimensions $d_{sc} =$ 1–15 mm: (i) cement paste with volume fraction $\bar{f}_{cp}$ and stiffness according to (14), and (ii) aggregates with volume fraction $\bar{f}_{agg} = 1 - \bar{f}_{cp}$ and stiffness according to direct experiments on limestone aggregate (see Table 1). Elasticity homogenization results in a macroscopic law of the form

$$\boldsymbol{\Sigma}_{sc} = \mathbf{C}_{sc} : \mathbf{E}_{sc} . \tag{21}$$

The homogenization procedure is similar to the one described in (1) – (14). However, there is one fundamental difference: From a morphological viewpoint, the aggregates constitute *inclusions* in a cement paste *matrix* so that choosing a phase stiffness for $\mathbf{C}^0$, namely $\mathbf{C}^0 = \mathbf{C}_{cp}$, is appropriate rather than the choice of the overall RVE_{sc}-related stiffness, i.e. $\mathbf{C}^0 \neq \mathbf{C}_{sc}$ (Zaoui, 2002).

Accordingly, the homogenized stiffness of shotcrete is of the Mori–Tanaka form (Mori and Tanaka, 1973; Benveniste, 1987), reading as

$$\mathbf{C}_{sc} = \left\{ \bar{f}_{cp}\, \mathbf{C}_{cp} + \bar{f}_{agg}\, \mathbf{C}_{agg} : \left[\mathbf{I} + \mathbf{P}_{sph}^{cp} : (\mathbf{C}_{agg} - \mathbf{C}_{cp}) \right]^{-1} \right\} : \\ : \left\{ \bar{f}_{cp}\, \mathbf{I} + \bar{f}_{agg} \left[\mathbf{I} + \mathbf{P}_{sph}^{cp} : (\mathbf{C}_{agg} - \mathbf{C}_{cp}) \right]^{-1} \right\}^{-1} . \tag{22}$$

The homogenized strength of shotcrete is obtained analogously to that of cement paste. Thus, σ_{crit}^{dev} is related to the uniaxial compressive strength of shotcrete, $\Sigma_{sc,11}^{comp,ult}$, by the homogenized compliance of shotcrete, $\mathbf{C}_{sc}^{-1}$, obtained from (22),

$$\Sigma_{sc,11}^{comp,ult} = \left\{ \max_{\varphi,\vartheta} \left[\lim_{\Delta\varphi,\Delta\vartheta\to 0} \left(-\frac{\mu_{hyd}^2}{\bar{f}_{hyd;\varphi,\vartheta}} (\mathbf{e}_z \otimes \mathbf{e}_z) : \frac{\partial \mathbf{C}_{sc}^{-1}}{\partial \mu_{hyd;\varphi,\vartheta}} : \right. \right. \right. \\ \left. \left. \left. : (\mathbf{e}_z \otimes \mathbf{e}_z) \right)^{\frac{1}{2}} \right] \right\}^{-1} \times \sigma_{crit}^{dev} \,. \tag{23}$$

An algorithm for computation of the aforementioned limit, $\lim_{\Delta\varphi,\Delta\vartheta\to 0}$, is presented in Pichler et al. (2008b).

5. Experimental validation of micromechanics-based material models

The micromechanical model presented in Sections 3 and 4, based on the universal phase properties of Table 1, will be fed with shotcrete mixture and hydration kinetics-specific input data concerning material composition, i.e. with experimental values for the volume fractions of air, water, clinker, hydrates, cement paste, and aggregate: f_{air}, f_{H_2O}, f_{clin}, f_{hyd}, $\bar{f}_{cp}$ and $\bar{f}_{agg}$. For these input data, the model delivers predictions for mixture and hydration-specific shotcrete stiffnesses and strengths. Comparison of these predictions to corresponding experimentally derived values allows for assessing the predictive capabilities of the model.

5.1. MIXTURE-DEPENDENT SHOTCRETE COMPOSITION

The volume fractions inside an RVE_{cp} of cement paste depend on the degree of hydration ξ which can be defined as mass of formed hydrates over the mass of hydrates formed if the entire clinker reacts with water, hence $0 \leq \xi \leq 1$. Besides ξ, the w/c-ratio governs the volume fractions f_{air}, f_{H_2O}, f_{clin}, f_{hyd}, so that we consider, according Acker (2001), that

$$f_{clin}(\xi) = \frac{1-\xi}{1+\frac{\rho_{clin}}{\rho_{H_2O}}(w/c)} = \frac{20(1-\xi)}{20+63(w/c)} \geq 0 \,, \tag{24}$$

$$f_{H_2O}(\xi) = \frac{\rho_{clin}[(w/c)-0.42\xi]}{\rho_{H_2O}\left[1+\frac{\rho_{clin}}{\rho_{H_2O}}(w/c)\right]} = \frac{63\,(w/c-0.42\xi)}{20+63(w/c)} \geq 0 \,, \tag{25}$$

$$f_{hyd}(\xi) = \frac{1.42\rho_{clin}\xi}{\rho_{H_2O}\left[1+\frac{\rho_{clin}}{\rho_{H_2O}}(w/c)\right]} = \frac{43.15\xi}{20+63(w/c)} \,, \tag{26}$$

$$f_{air}(\xi) = \frac{\left(1 + 0.42\dfrac{\rho_{clin}}{\rho_{H_2O}} - 1.42\dfrac{\rho_{clin}}{\rho_{hyd}}\right)\xi}{1 + \dfrac{\rho_{clin}}{\rho_{H_2O}}(w/c)} = \frac{3.31\xi}{20 + 63(w/c)}\,, \qquad (27)$$

with the mass densities of clinker, water, and hydrates, ρ_{clin}, ρ_{H_2O}, and ρ_{hyd}, following from Acker (2001), see also Pichler et al. (2008a): $\rho_{clin} = 3.15\,\mathrm{kg/dm^3}$, $\rho_{H_2O} = 1\,\mathrm{kg/dm^3}$, and $\rho_{hyd} = 2.073\,\mathrm{kg/dm^3}$. The creation of air voids filling f_{air} stems from the fact that hydration products occupy a smaller volume than their reactants, see e.g. Acker and Ulm (2001). In contrast to the volume fractions within the RVE_{cp}, the volume fractions of cement paste and aggregates do not change during hydration of the material. They can be determined from the water–cement ratio (w/c), the aggregate–cement ratio (a/c), and the mass densities of aggregates, water, and clinker, ρ_{agg}, ρ_{H_2O}, and ρ_{clin} (Acker, 2001; Pichler et al., 2008a), through Bernard et al. (2003)

$$\bar{f}_{agg} = \frac{(a/c)/\rho_{agg}}{1/\rho_{clin} + (w/c)/\rho_{H_2O} + (a/c)/\rho_{agg}} \quad \text{and} \quad \bar{f}_{cp} = 1 - \bar{f}_{agg}\,, \qquad (28)$$

with $\rho_{agg} = 2.5\,\mathrm{kg/dm^3}$. The evolution of the degree of hydration is determined by means of adiabatic tests where the measured accumulated hydration heat is considered as an indicator for the hydration progress of the investigated shotcrete specimen (Ulm and Coussy, 1996; Hellmich, 1999).

5.2. EXPERIMENTAL VALIDATION ON CEMENT PASTE LEVEL

Young's moduli and the compressive strengths of cement paste are estimated by the self-consistent homogenization step depicted in Fig. 1a, for mixture- and hydration degree-specific volume fractions, (24)–(28), on the basis of universal phase stiffnesses (Table 1) and strength values (Section 3.2).

The microelastic model of cement paste is validated by comparing model-predicted to experimentally obtained dynamic Young's moduli and dynamic shear moduli, for w/c-ratios ranging from 0.35 to 0.60 (Sun et al., 2005). The agreement between model predictions and corresponding experimental results, obtained under drained conditions, is satisfactory, see Figs. 3a–c and Pichler et al. (2008a).

By comparing model-predicted to experimentally obtained values for the uniaxial strength of cement pastes with different w/c-ratios, a prediction accuracy, quantified by a squared correlation coefficient $r^2 = 97\%$, is obtained, see Fig. 3d. This corroborates the assumption of the single strength-type value for hydrates, $\sigma_{crit}^{dev} = 26\,\mathrm{MPa}$ (Pichler et al., 2008a).

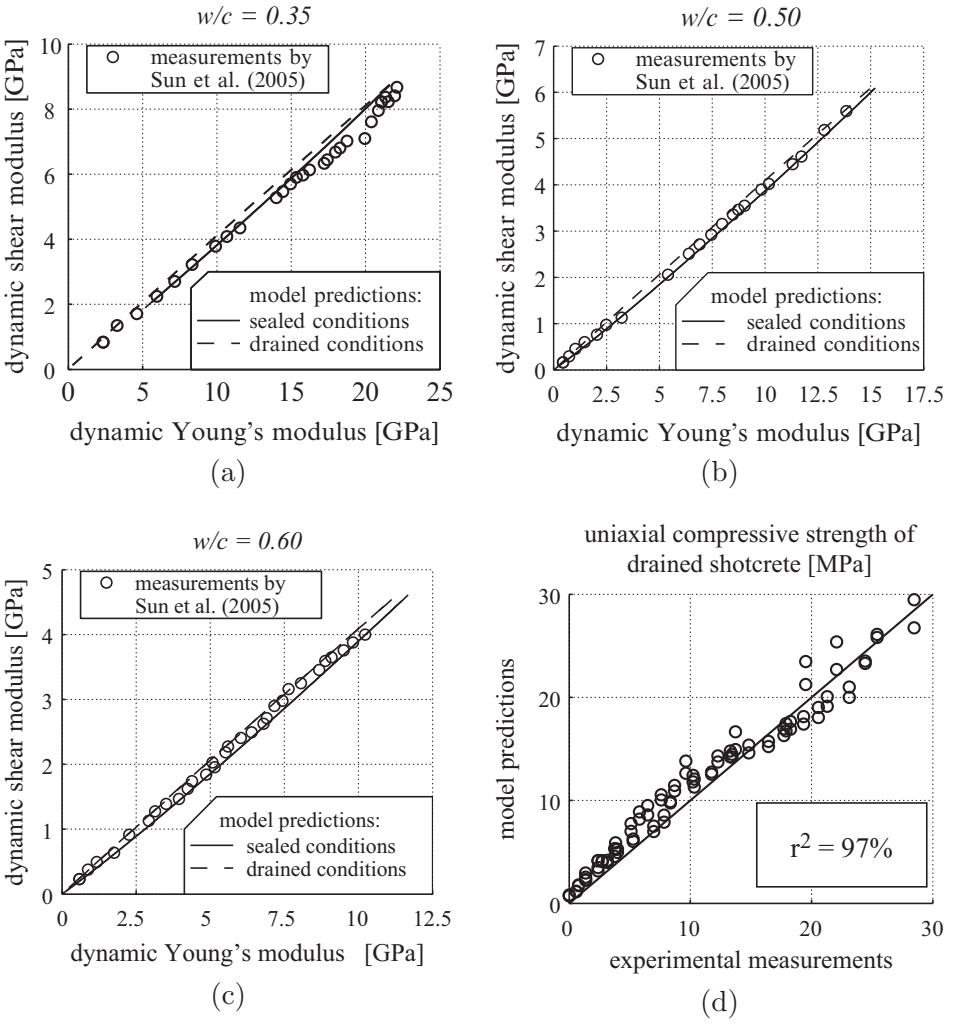

Figure 3. Comparison of model predictions with experimental data characterized by different w/c-ratios ($w/c = 0.35,\ 0.50,\ 0.60$): (**a**–**c**) dynamic shear modulus versus dynamic Young's modulus, and (**d**) uniaxial compressive strength of drained cement paste

5.3. EXPERIMENTAL VALIDATION ON SHOTCRETE LEVEL

A second homogenization step, resulting in a two-step homogenization scheme, is necessary to predict stiffnesses and strengths of shotcrete, see Fig. 1b and Section 4.

For the sake of experimental model validation, the model-predicted Young's modulus of shotcrete is compared to corresponding experimental values of Lafarge (2002) who subjected a shotcrete characterized by $w/c = 0.48$ and $a/c = 5.3$, to resonant frequency tests, see Fig. 4a. The agreement between model predictions and experiments is excellent

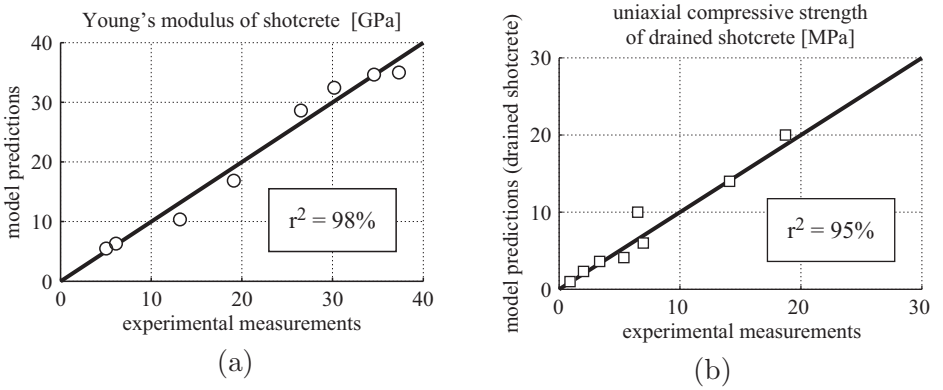

Figure 4. Comparison of model predictions with experimental data characterized by $w/c = 0.48$, $a/c = 5.3$, by $w/c = 0.5$, $a/c = 3.8$, and by $w/c = 0.4$, $a/c = 3.94$, respectively: (**a**) Young's modulus of shotcrete and (**b**) uniaxial compressive strength of drained shotcrete

for sealed conditions (underlined by a mean relative error of 1.0% and a corresponding standard deviation of 6.5%), confirming findings in Hellmich and Mang (2005) that the tests of (Lafarge, 2002) are rather characterized by sealed than by drained conditions. Model predictions related to sealed conditions correlate to experimental results by $r^2 = 98.8\%$, see Fig. 4a.

Experimental validation of the micromechanics-based homogenization of shotcrete strength is carried out according to the experiments of (Lafarge, 1997) and (Pillar, 2002): The applied methodology of experimental strength determination (Hilti gun and penetrometer tests) suggests that model predictions referring to drained conditions are closer to the experimental findings than the ones referring to sealed conditions (Pichler et al., 2008b). The agreement between model predictions (related to drained conditions) and experimental data, characterized by $w/c = 0.5$, $a/c = 3.8$ (Pillar, 2002), and by $w/c = 0.4$, $a/c = 3.94$ (Lafarge, 1997), is quantified by a mean relative prediction error of -5.0% and by a related standard deviation of 19.4%. The relative errors constitute upper bounds (Pichler et al., 2008b), suggesting that the correlation between model predictions and experimental values of $r^2 = 95\%$ is satisfactory, see Fig. 4b.

6. Micromechanics-based shotcrete characterization: influence of water–cement and aggregate–cement ratios on evolutions of elasticity and strength

The experimentally validated micromechanics model (see Sections 3 to 5) allow for predicting hydration degree-dependent evolutions of Young's modulus, Poisson's ratio, and the uniaxial compressive strength of different shotcrete mixtures as functions of their w/c- and a/c-ratios, see Figs. 5 and 6. We observe that Poisson's ratio increases or decreases with

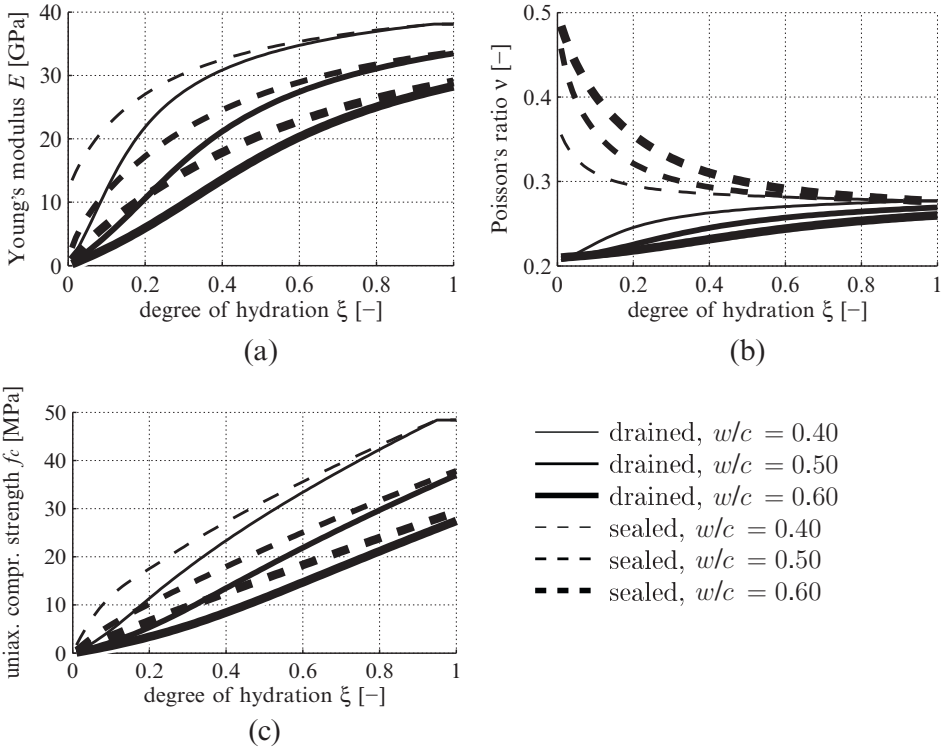

Figure 5. Micromechanics-based input for hybrid analyses of Section 7: Evolutions of (**a**) Young's modulus E, (**b**) Poisson ratio ν, and (**c**) uniaxial compressive strength f_c, respectively, over the hydration degree ξ; diagrams refer to shotcrete with $a/c = 5$, three different w/c-ratios ($w/c = 0.40,\ 0.50,\ 0.60$), under drained as well as under sealed conditions

increasing water–cement ratio, for drained or sealed conditions, respectively, see Figs. 5b and 6c and d. Sealed conditions, as a rule, lead to higher stiffness and strength values when compared to drained conditions, but this difference becomes very small for complete hydration ($\xi \rightarrow 1$), see Figs. 5 and 6. We also observe that both Young's modulus and the uniaxial compressive

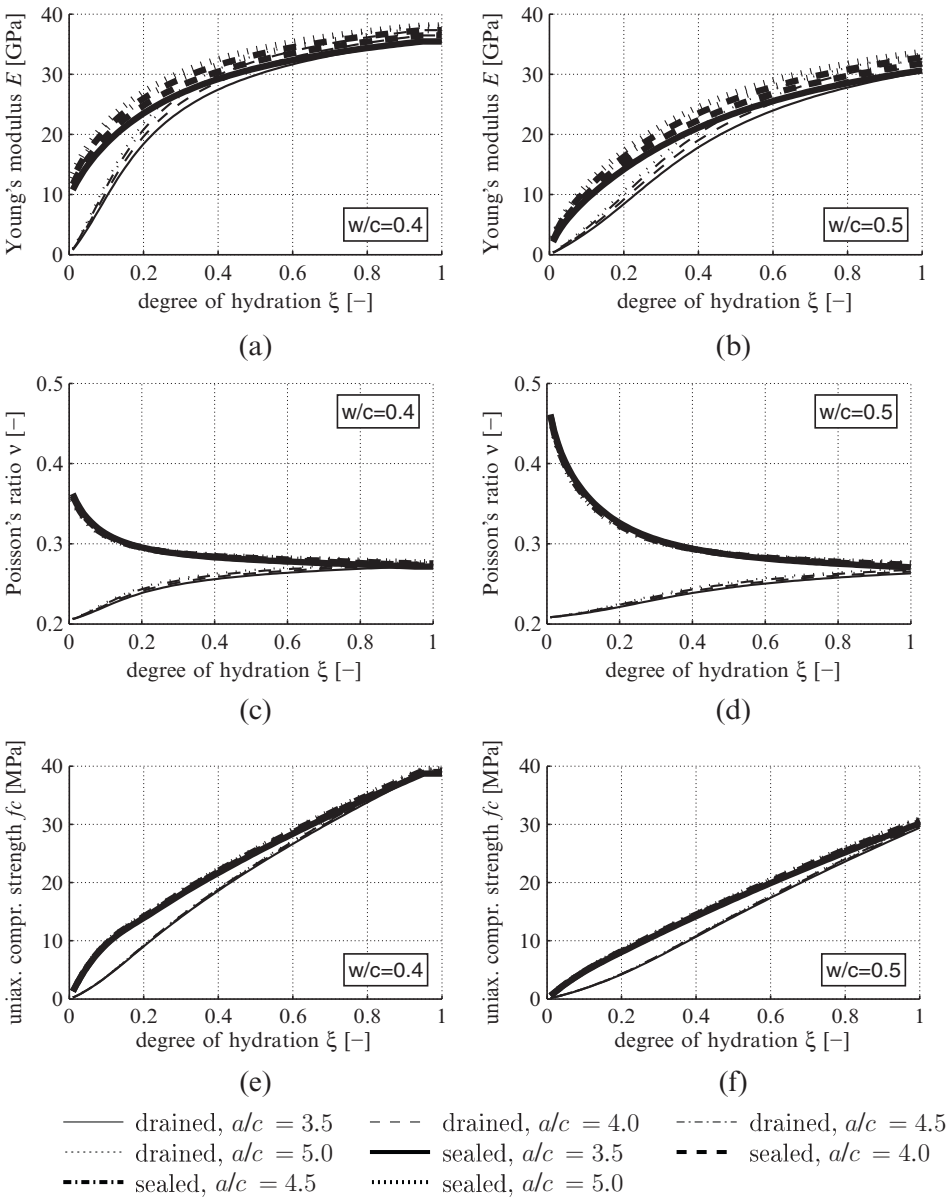

Figure 6. Micromechanics-based input for hybrid analyses of Section 7: Evolutions of (**a**,**b**) Young's modulus E, (**c**,**d**) Poisson's ratio ν, and (**e**,**f**) uniaxial compressive strength f_c, respectively, over the hydration degree ξ; diagrams refer to shotcrete with $w/c = 0.40$ (**a**,**c**,**e**) and $w/c = 0.50$ (**b**,**d**,**f**), four different a/c-ratios ($a/c = 3.5,\ 4.0,\ 4.5,\ 5.0$), under drained as well as under sealed conditions

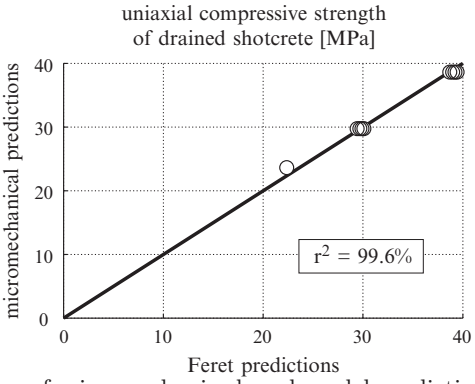

Figure 7. Comparison of micromechanics-based model predictions with predictions of Feret's formula (29) specified for $P = 197.2\,\mathrm{MPa}$

strength decrease with increasing water–cement ratio, whereby the percental decrease of Young's modulus is smaller than that of the compressive strength, see Fig. 5a and c. The loss in final strength (at completed hydration) with increasing water–cement ratio almost perfectly follows Feret's famous empirical relationship (Feret, 1892), stating that the final strength $[\Sigma^{ult}(t=\infty)]$ is proportional to the square of a ratio between the volumes of cement, water, and air contained in a material volume of concrete,

$$\Sigma^{ult}(t=\infty) = P\left[\frac{f_{clin}(\xi=0)}{f_{clin}(\xi=0)+f_{H_2O}(\xi=0)+f_{air}(\xi=0)}\right]^2 \qquad (29)$$

where P is a factor of proportionality. This relationship has proven remarkable usefulness, and it is widely used for mix designs in the cement and concrete industry: The match between this relationship (with $P = 197.2\,\mathrm{MPa}$) and the model-predicted strength at completed hydration, see Fig. 7, further corroborates the relevance of our model, in addition to the experimental evidence given in Section 5 and in earlier publications Pichler et al. 2008a, b.

Remarkably, Feret's formula (29) does not include the aggregate volume, whereas our model directly accounts for the influence of the aggregate-cement ratio. However, increase of the a/c ratio from 3.5 to 5.0 results in an increase of Young's modulus of only up to 10%, see Fig. 6a and b, whereas Poisson's ratio and the uniaxial compressive strength are virtually unaffected by such variations of the shotcrete mixture, see Fig. 6c–f. It is concluded that for typical shotcretes used in NATM tunneling, the a/c ratio plays a minor role in determining the overall mechanical properties – and this is beneficial to the reliability of structural computations as will be detailed in the next subsection.

7. Continuum micromechanics-based safety assessment of NATM tunnel shells

Finally, the continuum micromechanics-based, hydration degree-dependent evolutions of Young's modulus $E(\xi)$, Poisson's ratio $\nu(\xi)$, and the uniaxial compressive strength $f_c(\xi)$ of shotcrete, given in Section 6, serve as input for the assessment of the degree of utilization of shotcrete tunnel shells by means of the hybrid method according to (Hellmich et al., 2001). This will

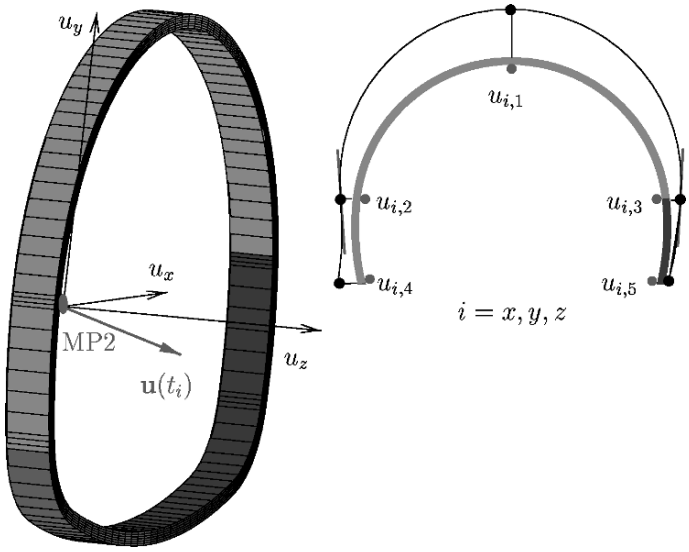

Figure 8. Hybrid method for determination of the level of loading from prescription of measured displacements on a three-dimensional finite element model of the tunnel shell

elucidate the dependence of the structural safety of shotcrete tunnel shells on the shotcrete mixture, governed by the w/c and a/c ratios. Moreover, we examine the role of water with respect to the degree of utilization, by considering both sealed and drained conditions (see Table 1). All other thermochemomechanical phenomena in shotcrete, especially concerning autogeneous shrinkage and creep, are considered macroscopically: In detail, the thermochemomechanical material law proposed by (Hellmich et al., 1999c; Sercombe et al., 2000; Lechner et al., 2001) is employed, considering the relations shown in Fig. 5 for aging elasticity and strength. The remaining material functions (for chemical affinity, creep, and shrinkage) are given in (Lechner et al., 2001), whereby short-term creep is considered according to (Macht et al., 2001).

For simulations based on the hybrid method, displacements measured at km 156.990 of the Sieberg tunnel, in Austria, are prescribed as boundary

conditions for a three-dimensional Finite Element model of the tunnel shell as shown in Fig. 8, compare (Hellmich 1999; Hellmich et al., 1999a, 2001). Simulation results are illustrated in terms of the so-called level of loading $\mathscr{L}$ which can be interpreted as the degree of utilization. The latter is defined as the ratio of the loading (stress) over loading capacity (strength) of the shotcrete tunnel shell. More specifically, it is defined on the basis of a Drucker-Prager failure surface calibrated for uniaxial and biaxial compressive failure, $\Sigma_{sc,11}^{comp,ult}$ from (23), and $\Sigma_{sc,11}^{Bicomp,ult} = \Sigma_{sc,11}^{comp,ult} \times \kappa$, with $\kappa = 1.16 = \text{constant}$,

$$\mathscr{L} = \frac{\alpha \text{tr}\, \mathbf{\Sigma}_{sc} + \sqrt{\Sigma_{sc,ij}^{dev} \Sigma_{sc,ij}^{dev}}}{k} \tag{30}$$

with

$$\alpha = \sqrt{\frac{2}{3}} \frac{\kappa - 1}{2\kappa - 1}, \quad k = \sqrt{\frac{2}{3}} \left(1 - \frac{\kappa - 1}{2\kappa - 1}\right) \Sigma_{sc,11}^{comp,ult} \tag{31}$$

In the present evaluation we focus on the average nature of $\mathscr{L}$ over the tunnel shell thickness h,

$$\overline{\mathscr{L}}(\varphi, t) = \frac{1}{h} \int_h \mathscr{L}(r, \varphi, t)\, dr\,, \tag{32}$$

with r and φ as polar coordinates defining (macroscopic) positions within a circular shell segment, and we designate the maximum value of $\overline{\mathscr{L}}(\varphi, t)$ in the tunnel shell, $\overline{\mathscr{L}}_{max}(t)$, as the 'level of loading' in Fig. 9a and b.

7.1. WATER–CEMENT RATIO-DEPENDENCE OF STRUCTURAL SAFETY

Three shotcrete mixtures are investigated: $w/c = 0.40$ (mix I), $w/c = 0.50$ (mix II), and $w/c = 0.60$ (mix III), each with $a/c = 5$, see Fig. 5. The simulation results show that throughout the observed loading phase the resulting level of loading of the tunnel shell is decisively influenced by the w/c-ratio, see Fig. 8b and c. In detail, the level of loading for $w/c = 0.40$ is around 40% lower than the one for $w/c = 0.60$. At the end of the observed loading phase, 1,120 h after installation of the top heading, simulations based on $w/c = 0.60$ predict a level of loading reaching 100% which would indicate severe cracking or even failure of the tunnel shell, whereas for both $w/c = 0.40$ and $w/c = 0.50$ the tunnel shell is intact, see Fig. 8b and c. The significant increase of the level of loading in the tunnel shell with increasing w/c-ratio can be explained as follows: With increasing water–cement ratio the percental decrease in macroscopic stiffness (e.g. Young's modulus) of shotcrete is smaller than the percental decrease in the uniaxial compressive strength of the material, see Fig. 5a and c. Whereas a slightly reduced elastic

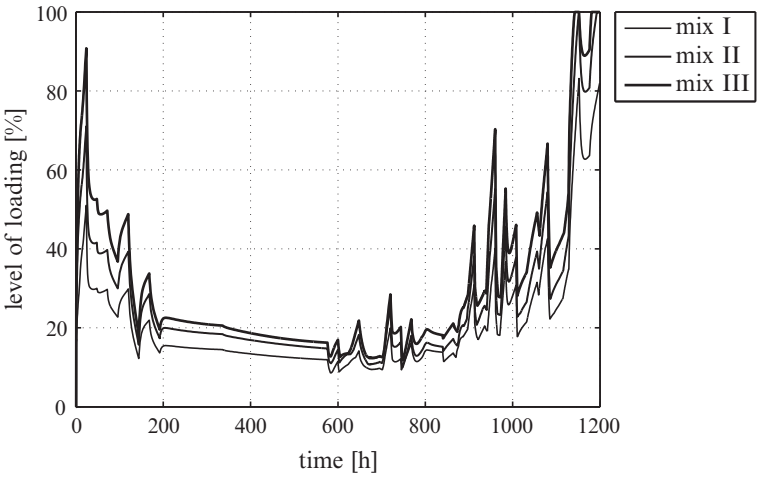

(a) sealed conditions

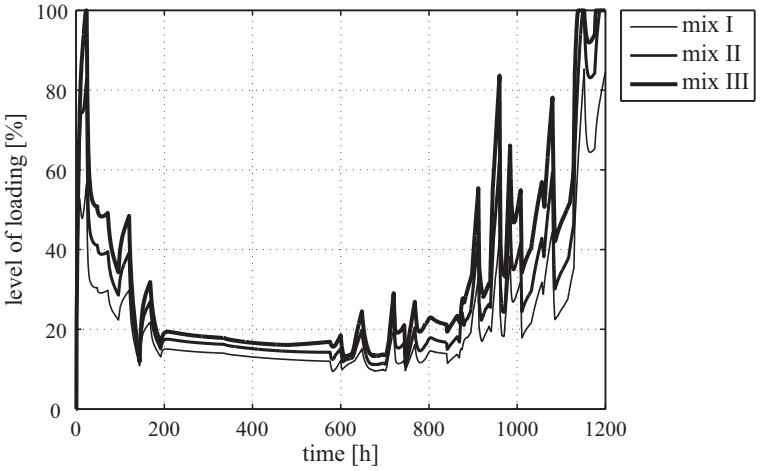

(b) drained conditions

Figure 9. Evolution of the level of loading $\overline{\mathscr{L}}_{max}$ as function of the time after installation of the top heading for (**a**) sealed conditions, and (**b**) drained conditions, determined through hybrid analyses

stiffness activates only slightly smaller forces within the shotcrete tunnel shell, a more pronounced loss in uniaxial compressive strength significantly reduces the load-carrying capacity of the material. Hence, the larger the water–cement ratio, the smaller the material resistance, and the reduced load-carrying capacity cannot be compensated by smaller forces in the tunnel shell caused by the reduced stiffness of the material. It is concluded

that rather small water–cement ratios (that is, high cement contents) are beneficial to shotcrete tunnel shells. This further motivates the development of additives which reduce water contents typically encountered in real-life applications. On the other hand, the deviations between the levels of loading predicted for sealed conditions in the shotcrete, see Fig. 8b, only negligibly differ from those predicted for drained conditions in the shotcrete, see Fig. 8c. Still, we note that, in principal, sealed conditions result in slightly lower levels of loading as compared to drained conditions.

7.2. AGGREGATE–CEMENT RATIO-DEPENDENCE OF STRUCTURAL SAFETY

During shotcreting, shotcrete constituents may detach from the sprayed material, which is referred to as rebound. Assuming rebound to concern aggregates only (m_{clin} = const., m_{H_2O} = const.), the a/c ratio decreases with respect to the targeted a/c ratio, denoted as $(a/c)_{target}$, namely: $a/c = (a/c)_{target} - \Delta(a/c)_{rebound}$. Considering that the targeted mass of shotcrete, $m_{sc,target}$, is composed of the mass of clinker, water, and aggregates,

$$m_{sc,target} = m_{clin} + m_{H_2O} + m_{agg} = m_{clin}\,(1 + w/c + (a/c)_{target})\ , \quad (33)$$

and that the shotcrete mass remaining on the tunnel wall, m_{sc}, is related to $m_{sc,target}$ by rebound R,

$$m_{sc} = m_{sc,target}(1 - R) = m_{clin}\,(1 + w/c + a/c)\ , \quad (34)$$

allows, through substitution of (33) into (34), for estimation of the actual a/c ratio as a function of the rebound R, the water–cement ratio w/c, and the targeted aggregate–cement ratio $(a/c)_{target}$,

$$a/c = (a/c)_{target} - R\,(1 + w/c + (a/c)_{target})\ . \quad (35)$$

For wet shotcreting, as has been used in the Sieberg tunnel, the rebound hardly exceeds 20% (Hague, 2001).[1] In order to elucidate the dependence of the structural safety on rebound-related variations of the a/c-ratio, eight different mixes are investigated (see Table 2 for corresponding rebounds as $(a/c)_{target} = 5.0$): $w/c = 0.40$ and $a/c = 3.5$ (mix IV), $w/c = 0.40$ and $a/c = 4.0$ (mix V), $w/c = 0.40$ and $a/c = 4.5$ (mix VI), $w/c = 0.40$ and $a/c = 5.0$ (mix VII), $w/c = 0.50$ and $a/c = 3.5$ (mix VIII), $w/c = 0.50$ and $a/c = 4.0$ (mix IX), $w/c = 0.50$ and $a/c = 4.5$ (mix X), as well as $w/c = 0.50$ and $a/c = 5.0$ (mix XI), see Fig. 6 for the micromechanics-based material properties.

[1] Dry shotcreting may lead to higher rebounds (Armelin and Banthia, 1998; Pfeuffer and Kusterle, 2001).

TABLE 2. Shotcrete rebound R for given values of w/c and a/c; according to (35); for $(a/c)_{target} = 5.0$

a/c	$w/c = 0.40$	$w/c = 0.50$
5.0	$R = 0.0\%$	$R = 0.0\%$
4.5	$R = 7.8\%$	$R = 7.7\%$
4.0	$R = 15.6\%$	$R = 15.4\%$
3.5	$R = 23.4\%$	$R = 23.1\%$

In contrast to the w/c ratio, the (effective) a/c ratio has no significant influence on the level of loading of the shotcrete tunnel shell, see Fig. 10. This is because the a/c ratio increase-related increase of Young's modulus (see Fig. 6), letting expect higher utilization degrees in the tunnel shell, is compensated by stress redistributions in the tunnel shell. Hence, the level of loading shows no significant dependence on the (actual) a/c ratio for the investigated shotcrete mixtures. This structural behavior can be considered as beneficial: Our calculations suggest that such changes of the (actual) a/c ratio because of shotcrete rebound do not compromise the structural safety of the tunnel shell. Since the investigated shotcrete mixes exhibit a maximum rebound of 23.4% (see Table 2), thus comprising common rebounds in wet shotcreting, the insensitity of the loading level of the tunnel shell with respect to aggregate rebound is a robust feature of the NATM. It suggests that careful *in situ* monitoring of the w/c ratio, as compared to the a/c ratio, is much more critical.

8. Conclusions

We have developed a new micromechanics model which economically accounts for the impact of the shotcrete composition on the elasticity and strength properties of the material. On this basis, we have shown the potentially major influence of the shotcrete composition (in particular of the water–cement ratio) on the forces induced in a NATM-tunnel shell. To further elucidate this role, it is highly desirable to extend the micromechanical description of shotcrete towards consideration of both creep and shrinkage. This is a topic of ongoing research. Another open issue relates to the question whether high levels of loading (such as those encountered in Figs. 8b and c 1,120 h after shell installation) might be overestimations as a result of enforcing $C1$-continuity of displacements between shell components

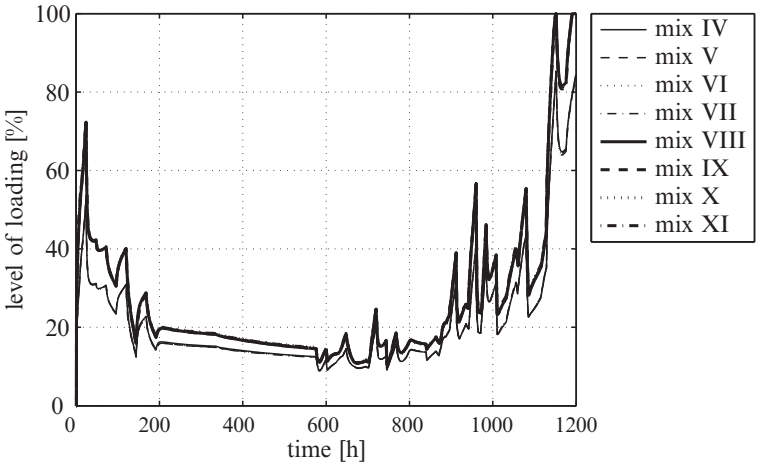

(a) sealed conditions

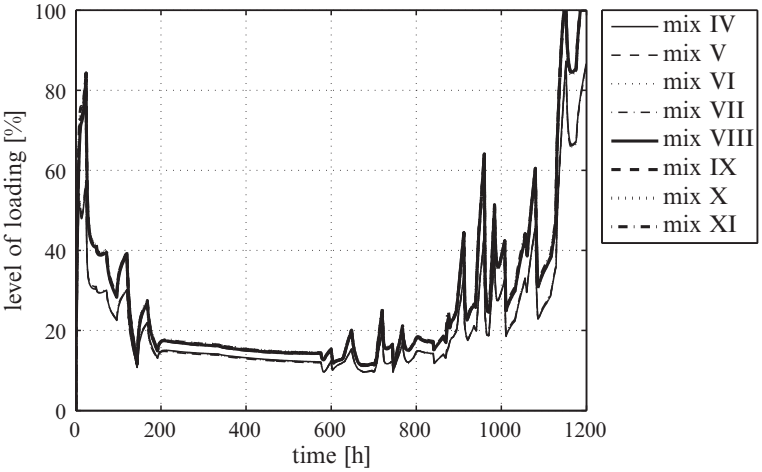

(b) drained conditions

Figure 10. Evolution of the level of loading $\overline{\mathscr{L}}_{max}$ as function of the time after installation of the top heading for (**a**) sealed conditions, and (**b**) drained conditions, determined through hybrid analyses

installed at different time instants, see (Hellmich et al., 1999a, 2001) for details. This underlines that further improvement of data analysis during NATM-tunneling calls for even more refined applied mechanics tools, both at the material level (microstructural level = shotcrete) and at the (macro-) structure level (= tunnel shell).

Acknowledgements

This work was part of the micromechanics-based activities within the integrated project 'Technology Innovation in Underground Construction – TUNCONSTUCT' (http://www.tunconstruct.org), co-sponsored by the European Commission.

References

Acker, P. (2001). Micromechanical analysis of creep and shrinkage mechanisms. In Ulm, F.-J., Bažant, Z., and Wittmann, F., editors, *Creep, shrinkage and durability mechanics of concrete and other quasi-brittle materials*, 6th International Conference CONCREEP@MIT, pages 15–26, Amsterdam: Elsevier.

Acker, P. and Ulm, F.-J. (2001). Creep and shrinkage of concrete: physical origins and practical measurements. *Nuclear Engineering and Design*, 203(2–3):143–158.

Armelin, H. and Banthia, N. (1998). Development of a general model of aggregate rebound for dry-mix shotcrete (Part II). *Materials and Structures*, 31(207):195–202.

Baroghel-Bouny, V. (1994). Caractérisation des pâtes de ciment et des bétons-méthodes, analyse, interprétation [Characterization of cement pastes and concretes-methods, analysis, interpretations]. Technical report, Laboratoire Central des Ponts et Chaussées, Paris, France. In French.

Barthélémy, J.-F. and Dormieux, L. (2003). Détermination du critère de rupture macroscopique d'un milieu poreux par homogénéisation non linèaire [Determination of the macroscopic strength criterion of a porous medium by nonlinear homogenization]. *Comptes Rendus Mécanique*, 331(4):271–276. In French.

Beer, G. (2003). *Numerical Simulation in Tunneling*. Springer Verlag Wien New York.

Benveniste, Y. (1987). A new approach to the application of Mori–Tanaka's theory in composite materials. *Mechanics of Materials*, 6(2):147–157.

Bernard, O., Ulm, F.-J., and Lemarchand, E. (2003). A multiscale micromechanics-hydration model for the early-age elastic properties of cement-based materials. *Cement and Concrete Research*, 33(9):1293–1309.

Bishop, P. (1994). Industry hit by Heathrow implications. *New Civil Engineer*, 27:3.

Boumiz, A., Vernet, C., and Cohen-Tenoudji, F. (1996). Mechanical properties of cement pastes and mortars at early ages. *Advanced Cement Based Materials*, 3(3–4):94–106.

Brandtner, P., Moritz, B., and Schubert, P. (2007). On the challenge of evaluating stress in a shotcrete lining: Experiences gained in applying the hybrid analysis method. *Felsbau*, 25(5):93–98.

Constantinides, G. and Ulm, F.-J. (2004). The effect of two types of C-S-H on the elasticity of cement-based materials: Results from nanoindentation and micromechanical modeling. *Cement and Concrete Research*, 34(1):67–80.

Dormieux, L., Molinari, A., and Kondo, D. (2002). Micromechanical approach to the behavior of poroelastic materials. *Journal of Mechanics and Physics of Solids*, 50(10):2203–2231.

Dormieux, L., Sanahuja, J., and Maalej, Y. (2007). Résistance d'un polycristal avec interfaces intergranulaires imparfaites [Strength of a polycrystal with imperfect intergranular interfaces]. *Comptes Rendus Mecanique*, 335(1):25–31. In French.

Eshelby, J. (1957). The determination of the elastic field of an ellipsoidal inclusion, and related problems. *Proceedings of the Royal Society of London A*, 241:376–396. Reprinted in Markenscoff and Gupta (2006).

Feret, R. (1892). On the compactness of hydraulic mortars [Sur la compacitée des mortiers hydrauliques]. *Annales des Ponts et Chaussées*, 7:5–164. In French.

Fritsch, A., Dormieux, L., Hellmich, C., and Sanahuja, J. (2007). Micromechanics of crystal interfaces in polycrystalline solid phases of porous media: Fundamentals and application to strength of hydroxyapatite biomaterials. *Journal of Materials Science*, 42(21):8824–8837.

Hague, I. (2001). Wet shotcreting – A total system approach. *www.ugc.basf.com* (last download: July 31, 2008).

Hashin, Z. (1983). Analysis of composite materials – A survey. *Journal of Applied Mechanics*, 50(3):481–505.

Hellmich, C. (1999). *Shotcrete as part of the New Austrian tunneling method: From thermochemomechanical material modeling to structural analysis and safety assessment of tunnels*. Ph.D. thesis, Vienna University of Technology, Vienna, Austria.

Hellmich, C. and Ulm, F.-J. (2002). Micromechanical model for ultra-structural stiffness of mineralized tissues. *Journal of Engineering Mechanics (ASCE)*, 128(8):898–908.

Hellmich, C. and Ulm, F.-J. (2005). Drained and undrained poroelastic properties of healthy and pathological bone: A poro-micromechanical investigation. *Transport in Porous Media*, 58(3):243–268.

Hellmich, C., Macht, J., and Mang, H. (1999a). Ein hybrides Verfahren zur Bestimmung der Auslastung von Spritzbetonschalen [A hybrid method for determination of the level of utilization of shotcrete shells]. *Felsbau*, 17(5):422–425. In German.

Hellmich, C., Ulm, F.-J., and Mang, H. (1999b). Consistent linearization in finite element analysis of coupled chemo-thermal problems with exo- or endothermal reactions. *Computational Mechanics*, 24(4):238–244.

Hellmich, C., Ulm, F.-J., and Mang, H. (1999c). Multisurface chemoplasticity I: Material model for shotcrete. *Journal of Engineering Mechanics (ASCE)*, 125(6):692–701.

Hellmich, C., Mang, H., and Ulm, F.-J. (2001). Hybrid method for quantification of stress states in shotcrete tunnel shells: Combination of 3D in situ displacement measurements and thermochemoplastic material law. *Computers and Structures*, 79(22–25):2103–2115.

Hellmich, C. and Mang, H. (2005). Shotcrete elasticity revisited in the framework of continuum micromechanics: From submicron to meter level. *Journal of Materials in Civil Engineering (ASCE)*, 17(3):246–256.

Hershey, A. (1954). The elasticity of an isotropic aggregate of anisotropic cubic crystals. *Journal of Applied Mechanics (ASME)*, 21:226–240.

Hill, R. (1963). Elastic properties of reinforced solids. *Journal of the Mechanics and Physics of Solids*, 11(5):357–372.

Hofstetter, K., Hellmich, C., and Eberhardsteiner, J. (2005). Predicting wood strength from composition and microstructure: Development and experimental verification of a continuum micromechanics model. In Dormieux, L., Kondo, D., and Sab, K., editors, *Colloque en l'honneur du Professeur Jean-Louis Auriault: Microstructure et Propriétés des Matériaux*, pages 217–222. Presses de l'Ecole Nationale des Ponts et Chaussées.

Karakuş, M. and Fowell, R. (2004). An insight into the new Austrian Tunnelling Method (NATM). In *Rockmec'2004 – VIIth Regional Rock Mechanics Symposium*. Sivas, Turkey.

Kreher, W. (1990). Residual stresses and stored elastic energy of composites and polycrystals. *Journal of the Mechanics and Physics of Solids*, 38(1):115–128.

Kreher, W. and Molinari, A. (1993). Residual stresses in polycrystals as influenced by grain shape and texture. *Journal of the Mechanics and Physics of Solids*, 41(12): 1955–1977.

Kröner, E. (1958). Berechnung der elastischen Konstanten des Vielkristalls aus den Konstanten des Einkristalls [Computation of the elastic constants of a polycrystal based on the constants of the single crystal]. *Zeitschrift für Physik A Hadrons and Nuclei*, 151(4):504–518. In German.

Lackner, R., Macht, J., Hellmich, C., and Mang, H. (2002). Hybrid method for analysis of segmented shotcrete tunnel linings. *Journal of Geotechnical and Geoenvironmental Engineering (ASCE)*, 128(4):298–308.

Lackner, R., Macht, J., and Mang, H. (2006). Hybrid analysis method for on-line quantification of stress states in tunnel shells. *Computer Methods in Applied Mechanics and Engineering*, 195(41–43):5361–5378.

Lafarge (1997). Internal report, Lafarge Centre Technique Europe Central. Commissioned by the Institute for Strength of Materials, Vienna University of Technology, Austria.

Lafarge (2002). Internal report, Lafarge Centre Technique Europe Central. Commissioned by the Institute for Strength of Materials, Vienna University of Technology, Austria.

Laws, N. (1977). The determination of stress and strain concentrations at an ellipsoidal inclusion in an anisotropic material. *Journal of Elasticity*, 7(1):91–97.

Lechner, M., Hellmich, C., and Mang, H. (2001). Short-term creep of shotcrete – Thermochemoplastic material modelling and nonlinear analysis of a laboratory test and of a NATM excavation by the finite element method. In Vermeer, P., Diebels, S., Ehlers, W., Herrmann, H., Luding, S., and Ramm, E., editors, *Proceedings of the International Symposium on Discontinuous Modelling of Cohesive-Frictional Materials – Lecture Notes in Physics*, pages 47–62. Berlin: Springer.

Lemarchand, E., Ulm, F.-J., and Dormieux, L. (2002). Effect of inclusions on friction coefficient of highly filled composite materials. *Journal of Engineering Mechanics (ASCE)*, 128(8):876–884.

Macht, J., Hellmich, C., Lackner, R., Schubert, W., and Mang, H. (2000). Assessment of a support system for squeezing rock conditions by means of a hybrid method. *Felsbau*, 18(6):9–15.

Macht, J., Lackner, R., Hellmich, C., and Mang, H. (2001). Shotcrete creep properties – Review of material tests and structural analyses of tunnels. In Ulm, F.-J., Bažant, Z., and Wittmann, F., editors, *Proceedings of the 6th International Conference on Creep, Shrinkage and Durability Mechanics of Concrete and Other Quasi-brittle Materials*, pages 285–300. Amsterdam: Elsevier.

Macht, J., Lackner, R., Hellmich, C., and Mang, H. (2003). *Quantification of stress states in shotcrete shells*, chapter 10, pages 225–248, Wien New York: Springer. In Beer (2003).

Markenscoff, X. and Gupta, A., editors (2006). *Collected works of J. D. Eshelby – The mechanics of defects and inhomogeneities*, volume 133 of *Solid mechanics and its applications*. Springer. Dordrecht, The Netherlands.

Mehlhorn, G. (1996). *Der ingenieurbau: Grundwissen – Werkstoffe, elastizitätstheorie [Basic knowledge in civil engineering: Materials and elasticity theory]*, volume 4, Berlin: Ernst & Sohn. In German.

Mori, T. and Tanaka, K. (1973). Average stress in matrix and average elastic energy of materials with misfitting inclusions. *Acta Metallurgica*, 21:571–574.

Neville, A. (1981). *Properties of concrete*, Pitman, 3rd edition. London, United Kingdom.
Oliver, A. (1994). Heathrow trial runs under question. *New Civil Engineer*, 3:4.
Pfeuffer, M. and Kusterle, W. (2001). Rheology and rebound behaviour of dry-mix shotcrete. *Cement and Concrete Research*, 31(11):1619–1625.
Pichler, B., Hellmich, C., and Eberhardsteiner, J. (2009). Spherical and acicular representation of hydrates in a micromechanical model for cement paste – Prediction of early-age elasticity and strength. *Acta Mechanica,* 203(3-4):137–162.
Pichler, B., Scheiner, S., and Hellmich, C. (2008). From micron-sized needle-shaped hydrates to meter-sized shotcrete tunnel shells: Micromechanical upscaling of stiffness and strength of hydrating shotcrete. *Acta Geotechinca,* 3(4):273–294.
Pillar, N. (2002). *Determination of early age properties of fibre reinforced shotcrete to predict the cracking behavior*. Ph.D. thesis, submitted to the University of New South Wales, Private Communication, Sydney, Australia.
Rabcewicz, L. (1948). Patentschrift. Österreichisches Patent Nr. 165573 [Patent specification, Austrian patent no. 165573]. In German.
Rabcewicz, L. (1964a). The New Austrian Tunnelling Method, Part one. *Water Power*, pages 453–457.
Rabcewicz, L. (1964b). The New Austrian Tunnelling Method, Part two. *Water Power*, pages 511–515.
Rabcewicz, L. (1965). The New Austrian Tunnelling Method, Part three. *Water Power*, pages 19–24.
Rokahr, R. and Lux, K. (1987). Einfluß des rheologischen Verhaltens des Spritzbetons auf den Ausbauwiderstand [Influence of the rheological behavior of shotcrete on the excavation resistance]. *Felsbau*, 5:11–18.
Rokahr, R. and Zachow, R. (1997). Ein neues Verfahren zur täglichen Kontrolle der Auslastung einer Spritzbetonschale [A new method for daily monitoring of the stress intensity of a sprayed concrete lining]. *Felsbau*, 15(6):430–434. In German.
Schubert, P. (1988). Beitrag zum rheologischen Verhalten von Spritzbeton [Contribution to the rheological behavior of shotcrete]. *Felsbau*, 6:150–153.
Schubert, W. and Steindorfer, A. (1996). Selective displacement monitoring during tunnel excavation. *Felsbau*, 14(2):93–97.
Schubert, W., Steindorfer, A., and Button, E. (2002). Displacement monitoring in tunnels – An overview. *Felsbau*, 20(2):7–15.
Sercombe, J., Hellmich, C., Ulm, F.-J., and Mang, H. (2000). Modeling of early-age creep of shotcrete I: Model and model parameters. *Journal of Engineering Mechanics (ASCE)*, 126(3):284–291.
Steindorfer, A., Schubert, W., and Rabensteiner, K. (1995). Problemorientierte Auswertung geotechnischer Messungen [Advanced evaluation of geotechnical displacement monitoring data]. *Felsbau*, 13(6):386–390. In German.
Sun, Z., Ye, G., and Shah, S. (2005). Microstructure and early-age properties of Portland cement paste: Effects of connectivity of solid phases. *ACI Materials Journal*, 102(1):122–129.
Suquet, P. (1997). *Continuum micromechanics*, volume 377 of *CISM Courses and Lectures*, Wien New York: Springer.
Tritthart, J. and Häußler, F. (2003). Pore solution analysis of cement pastes and nanostructural investigations of hydrated C_3S. *Cement and Concrete Research*, 33(7):1063–1070.

Ulm, F.-J. and Coussy, O. (1996). Strength growth as chemo-plastic hardening in early age concrete. *Journal of Engineering Mechanics (ASCE)*, 122(12):1123–1132.

Ulm, F.-J., Constantinides, G., and Heukamp, F. (2004). Is concrete a poromechanics material? – A multiscale investigation of poroelastic properties. *Materials and Structures/Materiaux et Constructions*, 37(1):43–58.

Wesche, K. (1974). *Baustoffe für tragende Bauteile [Building materials for structural components]*. Bauverlag, Wiesbaden, Germany, 3rd edition. In German.

Zaoui, A. (1997). Structural morphology and constitutive behavior of microheterogeneous materials. In Suquet, P., editor, *Continuum Micromechanics*, pages 291–347, Vienna: Springer.

Zaoui, A. (2002). Continuum micromechanics: Survey. *Journal of Engineering Mechanics (ASCE)*, 128(8):808–816.

CRISIS MANAGEMENT IN WATER DISTRIBUTION NETWORKS

P. VILLON[1*] AND A. NACE[2]
[1]*Université de Technologie de Compiegne, Laboratoire Roberval, 60205 Compiegne Cedex, France*
[2]*Suez Environnement, CIRSEE, 38 Rue du President Wilson, 78230 Le Pecq, France*

Abstract. In this article, we present a strategy for managing crisis in water distribution network based on simulation and optimal control tools. First we give some details about the physical problem and the modelling hypothesis; then, we explain how the management of water network can be seen as a mathematical programming problem. Hence, we give an example of anticipating drinking water consumption and detecting network leaks. Optimising the management of a drinking water distribution network means planning how to use the different installations (treatment works, pumping stations, and valves) in order to convey water from many sources (rivers, borings, springs...) to supply areas, while minimizing operating costs (treatment and electricity). SAPHIR is a tool designed to help managers make decisions regarding the optimal operation of the water supply and distribution system. According to daily consumption estimates and operational constraints, SAPHIR calculates, over a 24 h period, volumes to be produced, flows to be transferred and changes in storage levels. Based on the SAPHIR principle, EMERAUDE is designed to monitor and control in real time all the equipment of the network.

Keywords: Drinkable water network, leaks in distribution networks, reservoir safety levels, network flow algorithms

1. Introduction

Classical approach for computing hydraulic networks is classically based on Hardy Cross method (Cross, 1936; Mays, 1999; Munson et al., 1998; Streeter et al., 1998; Viessman and Hammer, 1993; Harel, 1987). This approach requires iterations of

* To whom correspondence should be addressed. e-mail: pierre.villon@utc.fr

A. Ibrahimbegovic and M. Zlatar (eds.), *Damage Assessment and Reconstruction After War or Natural Disaster*,

the nonlinear flows-pressures system. The properties of the pipes (geometry and roughness) have to be well known and the computational time may be excessive for a huge network.

In this work, we are focusing on special types of networks. Their particular topology and their physical properties allow us to use simplified models. In fact, because of the small number of circuits in the graph and, also because we have the transient behaviour, we can consider only the conservation law (Kirchoff's law) in a strong sense and make an approximation about pressure. Then, we obtain a model based on flow network theory. In this context, the system management becomes a linear network optimisation problem (Fulkerson, 1961; Gondran et al., 1984). The methods of this kind have been originally developed for communication networks (Balakrishnan and Altinkemer, 1992), so is not classical in hydraulic engineering. Their performance is so good that we can use it in real time applications. This is the core of the package SAPHIR developed by CIRSEE and Laboratoire Roberval. However, we also need a tool for forecast consumption. For that, we have developed EMERAUDE software, which is based on Dynamic Programming (Barto et al., 1991), with a moving time window (for more details, see Loubeyre et al. [1991], Footohi et al. [1992], Kora et al. [1987]). Combined with EMERAUDE, SAPHIR can be used as a daily management tool to support system operators.

The most important application fields of SAPHIR are computer aided design, daily pumping scheduling, crisis management and future planning on the water supply and distribution systems. The aim of all optimisation studies is to identify potential savings and to find technical improvements (partial automation, tariff modifications...). It can also be utilised to define and schedule maintenance work and evaluate their consequences on the supply management. Furthermore, in this article, we show how SAPHIR can simulate and anticipate crises situations.

2. Problem Formulation

To establish the mathematical model of the water supply and distribution system, a functional schematic is defined. Containing only operator controllable components (valves, pumps, main reservoirs) and based on available technical data, this schematic includes some hydraulic simplifications. Figure 1 shows an example of an established schematic for a small system.

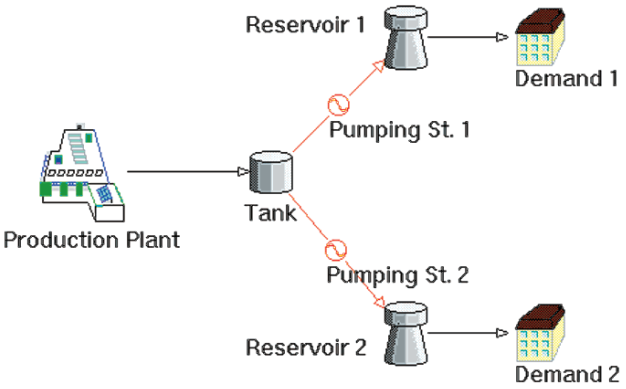

Figure 1. A simple water distribution system

The functional schematic of the water distribution network can be represented by graph where nodes are productions sites, reservoirs or demand areas, and arcs are pumping stations, valves or transfers (Fig. 2).

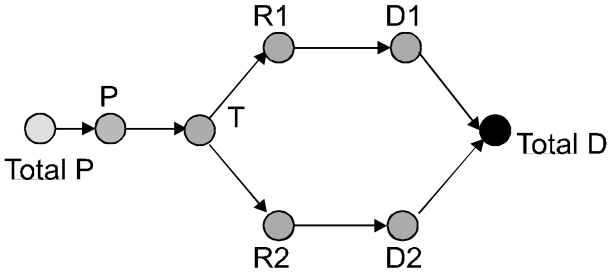

Figure 2. Graph representing the supply system

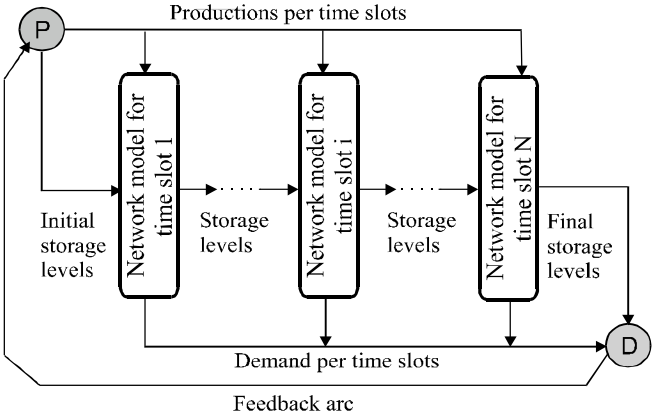

Figure 3. Global graph of the network

In order to represent the water storage on reservoirs and system demand charges during the day, this graph is deployed over 24 time periods. Figure 3 shows the construction and principal of the new graph. Some supplementary nodes and arcs are added to respect mass balance at each node over time.

Finally, the optimal scheduling can be formulated as follows: (problem P)

$$Min \sum_{u \in U1} \alpha_u(\varphi_u)\varphi_u + \sum_{u \in U2} \alpha_u(\varphi_u - \overline{\varphi}_u)^2$$

$$\begin{cases} \forall u \in U, & b_u \le \varphi_u \le c_u \\ \forall i \in X, & \sum_{u \in U^+(i)} \varphi_u = \sum_{u \in U^-(i)} \varphi_u \end{cases}$$

$$U_1 \bigcup U_2 = U$$

$$U_1 \bigcap U_2 = \Phi$$

where X are the nodes and U are the arcs on the graph. U_1 contains piecewise linear cost arcs such as productions, pumps and transfers. U_2 contains quadratic cost arcs used to match final levels of reservoirs. The constraints represent the boundary flow limits on the arcs and the conservation laws on each node. The main difference between our approach and the classical network analysis methods, is that we do not determine system pressures. These are taken into account by using constraints applied to the flows and volumes. On the other hand, we also assume that reservoirs levels do not have a significant influence on transfer flows. In real operations mode, this approximation is acceptable according to demand forecast accuracy.

3. The Solver

The problem (P) is resolved using a primal dual-method, the "Out of kilter" algorithm (Bertsekas, 1991; Edmonds and Karp, 1972; Minoux, 1984). This method was adapted to piecewise linear and quadratic cost functions in order to take into account non-linear pumping costs. As the calculation algorithm has a polynomial complexity, the response time is satisfactory, which allows SAPHIR to be used on large distribution networks.

3.1. THE OUT OF KILTER ALGORITHM

For simplification, we present the method in the case of the standard minimum cost flow problem: find the vector $\varphi = (\varphi_u)_{u \in U}$ which minimizes the cost

function $J(\varphi)=\sum_{u\in U}\alpha_u\varphi_u$ (1) under the conservation constraints $\sum_{u\in U^+(i)}\varphi_u=\sum_{u\in U^-(i)}\varphi_u$ (2) for every node $i\in X$ and the bound constraints $\forall u\in U$, $b_u\le\varphi_u\le c_u$ (3).

$$Min\sum_{u\in U}\alpha_u\varphi_u$$
$$\begin{cases}\forall u\in U, & b_u\le\varphi_u\le c_u\\ \forall i\in X, & \sum_{u\in U^+(i)}\varphi_u=\sum_{u\in U^-(i)}\varphi_u\end{cases}\qquad(1,2,3)$$

The α_u coefficients correspond to the unitary cost flow on the arc u.

If we introduce A, the convexity node-arc matrix, b (respectively c) the lower bound vector (respectively upper bound) vector associated to φ, α the costs vector, the problem (1, 2, 3) becomes:

$$Min\ \alpha^T\varphi \qquad(4)$$
$$b\le\varphi\le c, \qquad(5)$$
$$A\varphi=0 \qquad(6)$$

The linear program (4, 5, 6) has a unique solution (Gondran et al., 1984). If we note τ, the Lagrange multiplier associated to the conservation constraints (6), then τ is solution of the dual linear program (7, 8, 9, 10)

$$\tau A-\lambda+\mu\le\alpha^T \qquad(7)$$
$$\lambda\ge0, \qquad(8)$$
$$\mu\ge0 \qquad(9)$$
$$Max\{-\lambda c+\mu b\} \qquad(10)$$

where λ and μ are the Lagrange multipliers associated to the bounds constraints (5).

For any vector τ, let be v and w, vectors associated to the arcs such that

$$\alpha_u<[\tau A]_u\Rightarrow\left(\left(v_u=\alpha_u-[\tau A]_u\right)\wedge w_u=0\right)$$
$$\alpha_u>[\tau A]_u\Rightarrow\left(\left(w_u=\alpha_u-[\tau A]_u\right)\wedge v_u=0\right)$$
$$\alpha_u=[\tau A]_u\Rightarrow\left(w_u=0\wedge v_u=0\right)$$

Then, we have, in any case, $\alpha - \tau A = v - w$ and, if φ is a flow vector such that (6) occurs, then

$\alpha^T \varphi = v^T \varphi - w^T \varphi$.

If φ verifies (5), and thanks to the fact that v and w are nonnegative, then $\alpha^T \varphi \geq v^T b - w^T c$.

Hence, if φ satisfies (5) and (6) and τ is such that $\alpha^T \varphi = v(\tau)^T b - w(\tau)^T c$, then φ is an optimum flow for the problem (4, 5, 6). The existence of the couple (φ, τ) is a consequence of the complementary slackness theorem.

We can also write $0 = \alpha^T \varphi - (v^T b - w^T c) = v(\varphi - b) + w(c - \varphi)$. Then, if we introduce the tension vector by $\theta = \tau A$, the optimality conditions can be expressed, for the couple (φ, θ):

$$\alpha_u < \theta_u \Rightarrow \varphi_u = c_u \tag{11}$$

$$\alpha_u > \theta_u \Rightarrow \varphi_u = c_u \tag{12}$$

$$\alpha_u = \theta_u \Rightarrow b_u < \varphi_u < c_u \tag{13}$$

When the couple (φ_u, θ_u) verifies (11, 12, 13), we say that the arc u is **in kilter**. The out of kilter algorithm consists of:

(0) initialise (φ, θ)*;*

(1) while there exists an arc u out of kilter repair(u);

The procedure repair(u) modifies (φ, θ) such that u is in kilter and preserves the conformity of the others arcs. It is based on Minty's lemma (for more details, see Edmonds and Karp [1972]). The most important property is that it works in polynomial computational time. The extension to a quadratic cost function is easy.

4. General Software Description

A water distribution network is composed of different installations. Raw water coming from various sources is treated at treatment plants. It is conveyed through pipes by gravity, or by using pumps, to storage reservoirs to meet user demands.

The main objective of water distribution managers is to satisfy all supply area demands, to respect water quality standards and to reduce the operating costs.

Optimal operation should take into account the variations in electricity costs at different moments in the day as well as the treatment costs of each plant and the energy consumption of each pump. On the other hand, operational constraints such as minimum and maximum reservoir water levels, maximum power demands and maximum flow rate variations, must be respected.

In order to improve the operation performances, Lyonnaise des Eaux had developed two optimisation tools for the production and distribution management.

SAPHIR is an off-line system that assists managers in making better decisions regarding optimal scheduling on the distribution network. It calculates production and pump volumes and reservoir levels over a 24 h period, according to the daily demand forecast.

EMERAUDE is an on-line real time control system. Using the last updated water demand forecast and the state of the water network, EMERAUDE calculates the best pumping strategy and sends the controls to the process (Fig. 4).

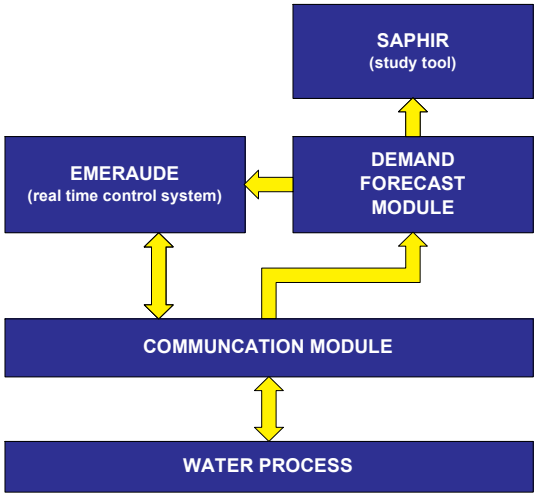

Figure 4. EMERAUDE and SAPHIR main components and process

4.1. SAPHIR

4.1.1. *Overview*

SAPHIR is organized in two main modules: the editor and the simulator. The editor program is used to define the network functional schematic and to describe specific system characteristics. The simulation program allows users to enter constraints related to real situations and to develop optimal production and pump scheduling.

Figure 5 shows SAPHIR input and output data: the horizontal entries represent static data and are entered into the editor program while the vertical data change from day to day and are entered through the simulation program.

Figure 6 shows the various steps involved in the editor and simulation programs.

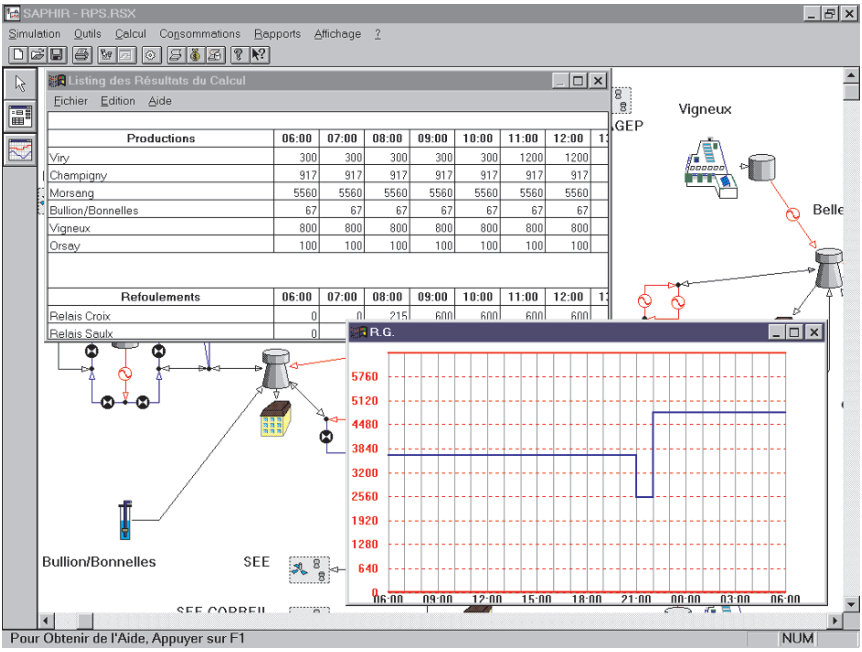

Figure 5. SAPHIR Simulator and results

4.1.2. *Network Description*

The functional schematic of the network is described via the editor. Using a graphical user interface, the operator constructs the network model by first setting network nodes (treatment plants, boreholes, reservoirs, demand areas) and next by linking the nodes with arcs (pipes, pumps and valves).

Each element is then described by the user who enters specific system design data (reservoir volumes and surface areas, pipe capacities...), operational constraints (reservoir minimum and maximum levels, maximum flows in accordance with each electric tariff period,...) and information concerning management criteria (electricity tariffs, energy consumption per pumping rate,...). Furthermore, data modifications and file facilities are available during the editing session.

Figure 7 shows the editor screen: the network schematic is displayed in the background and the editor window in the foreground concerns the pumping station configuration.

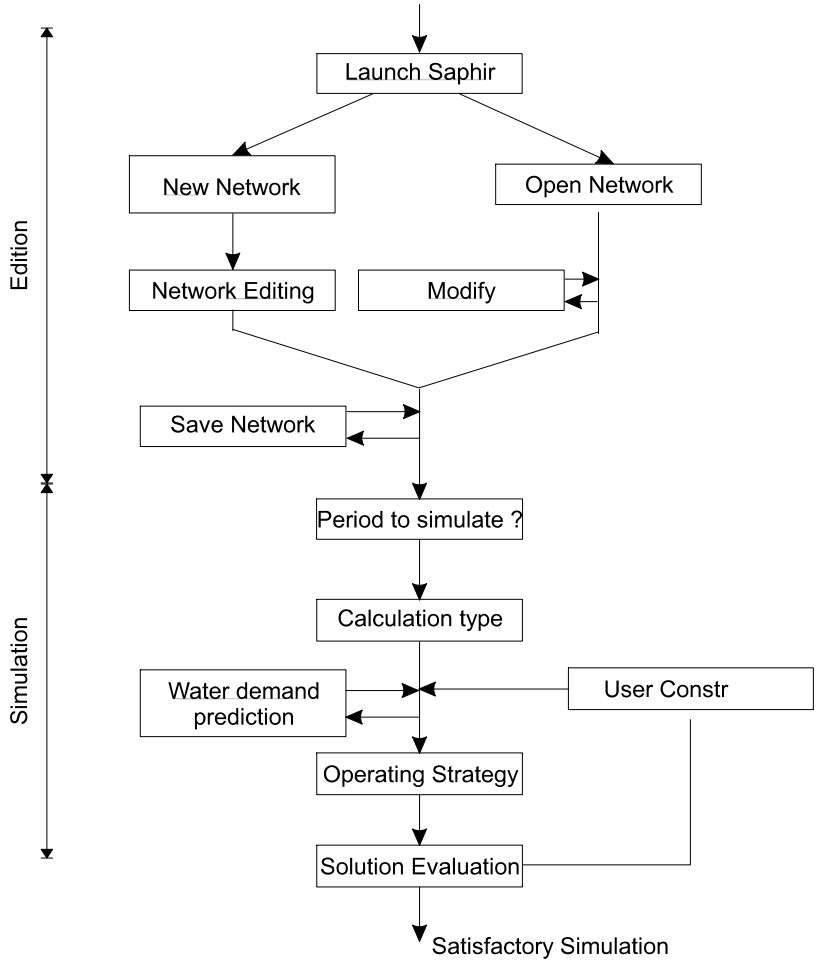

Figure 6. Utilisation schematic

4.1.3. *Defining a Network Situation*

During this phase, the operator enters management constraints and other data in order to define a specific system situation:

Electric tariff periods
Consumption estimates
Additional operating constraints
Initial reservoir levels

The consumption estimates might be set either by the user or could be retrieved from available text files. These files can be generated by an demand

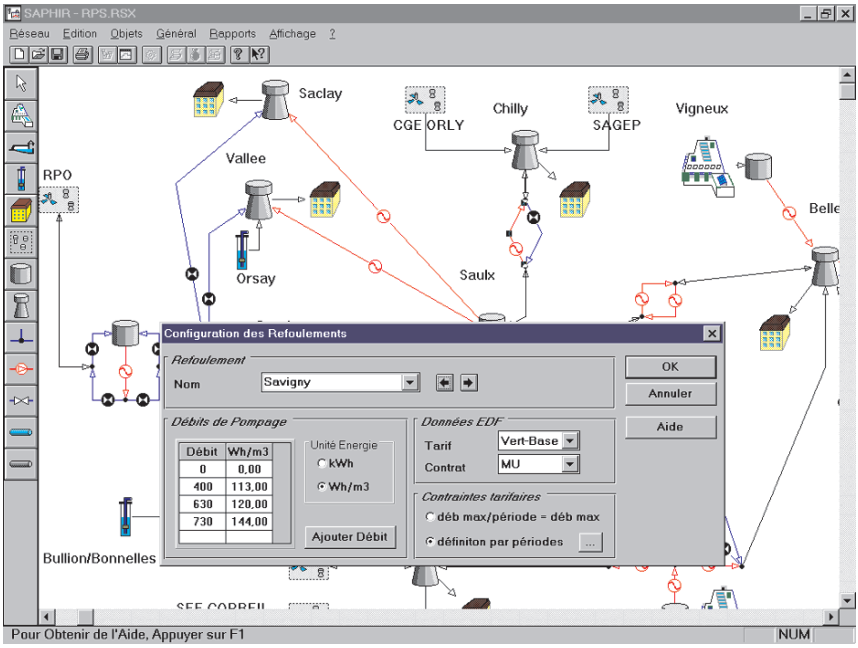

Figure 7. SAPHIR Network Editor

forecast system or by SCADA. Facilities are also provided to retrieve actual reservoir levels for use in the simulation.

Operating constraints, such as component unavailability are entered using the simulator dialogue box.

4.1.4. *Optimisation*

Once the network situation is defined, the user runs the simulator program which calculates the optimum solution for the daily schedule. The calculation takes into account the operating costs and user defined constraints and safety criteria. When a crisis situation is detected by the program, SAPHIR provides information regarding the absence of water per demand point.

Two types of calculation are available:

Daily profile: SAPHIR will find a cyclic operating strategy: initial and final reservoirs levels are calculated by SAPHIR, the objective is to maintain the same reservoir levels at the initial and final stages from day to day.

Follow-up: Users entered into SAPHIR initial and final target reservoir levels. This mode is useful for adapting the programmed schedule to the real situation.

Several outputs are provided to facilitate interpretation and exploitation of optimisation results:

A summary of information such as total production and consumption on the network, treatment and electricity costs

Detailed listings describing the management schedule hour by hour and over 24 h

Analysis listings containing detail information on economic costs

Result curves per system component

Figure 7 shows the calculation results presented on the simulator program screen with typical 24 h pump operation.

4.1.5. *Application Fields*

SAPHIR's most important fields of application are optimisation studies, daily pumping scheduling, crisis management and future planning on the water supply and distribution system.

The aim of all optimisation studies is to identify potential savings and to find technical improvements (partial automation, cost modifications ...).

Combined with a demand forecast system, SAPHIR can be used as a daily management tool to support system operators.

It can also be utilised to help define and schedule maintenance work and evaluate their consequences on the supply management. Furthermore, SAPHIR enables the user to simulate and anticipate crisis situations.

4.2. EMERAUDE

EMERAUDE is a real time system designed to optimise the water network management. It has two main modules:

A water demand forecast (WDF) module. This forecast is auto-corrected in real time, according to the real demand.

An optimisation module which uses the latest updated forecast and computes the best pumping strategy.

An communication module which makes the connection with the water network.

4.2.1. *Water Demand Forecast System*

The goal of this module is to predict the daily consumption curve for each specific consumption site. The calculation of the forecast is performed in two steps:

A initial prediction for the entire day is calculated at the beginning of the day (generally at 4 a.m.).

The forecast is corrected every a quarter of an hour according to the observed water demand.

The first step of the water demand calculation is based on recent historical data (last 2 weeks). A choice of possible prediction methods is proposed and they are chosen according to the specific demand of each site:

An Artificial Neural Network method

Simple Statistical Methods (using the demand of the previous day, day-14, day-7 and day-8)

The second step concerns the real time correction of the original forecast. The prediction module is connected with the state process and calculates in real time the observed water demand. The system analyses errors made and computes a new water demand forecast using a least squares method. The new demand forecast is calculated as a linear combination of independent shape functions defined over a 24 h interval. The principal is based on the fact that consumption curves for each day of the week have a particular shape. Consumption curves for Sundays are different from those on Saturdays. For a fixed day (i.e. Saturday) consumption peaks occur at same instant but with a different amplitude. Everyday, the water demand module constructs, from the previous weeks, the typical profile of the day concerned. Shape functions are based on a calculated typical profile. Demand forecast are then auto-corrected every 15 min, according to errors recorded on the previous forecast. Figure 8 shows an EMERAUDE WDF screen where readers can distinguish between real and predicted consumption.

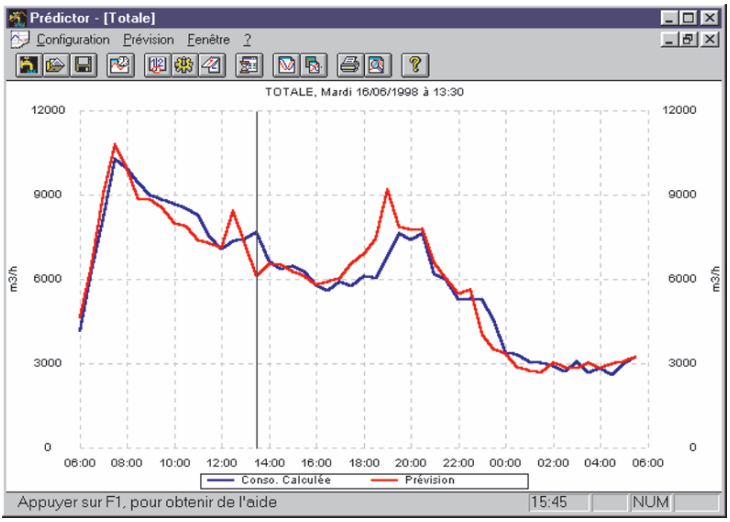

Figure 8. EMERAUDE's WDF screen

4.2.2. *Optimisation System*

The goal of the optimisation module is to produce an optimal scheduling for all main equipment.

With the latest update forecast and the real state of the water network (pump and reservoirs availability), it calculates the best pumping strategy and sends the controls to the process through the communication module.

Every hour, EMERAUDE reconstructs its pumping strategy according to the real state of process.

Monitoring in real time all main equipment (pumps availability, reservoirs level,...), EMERAUDE can decide to start a non-planned optimization if important malfunctions occur.

The Optimisation system shows what it has done and the scheduled pumping strategies.

Figure 9 shows the Morsang sur Seine treatment plant where EMERAUDE was first installed.

Figure 10 represents the Optimisation module's interface where a pumping strategy for a treatment plant with three pumping stations and their associated tank levels are shown.

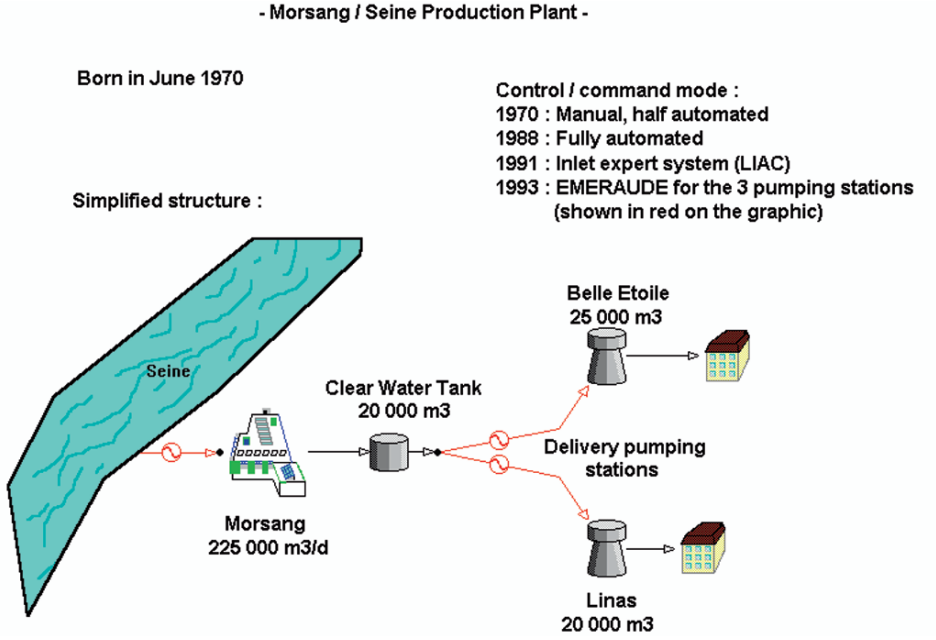

Figure 9. The Morsang sur Seine water treatment plant

Also, EMERAUDE respects the following operational constraints:

Water demand

Minimum and maximum reservoir levels

Maximum power demand

A maximum number of flow variations

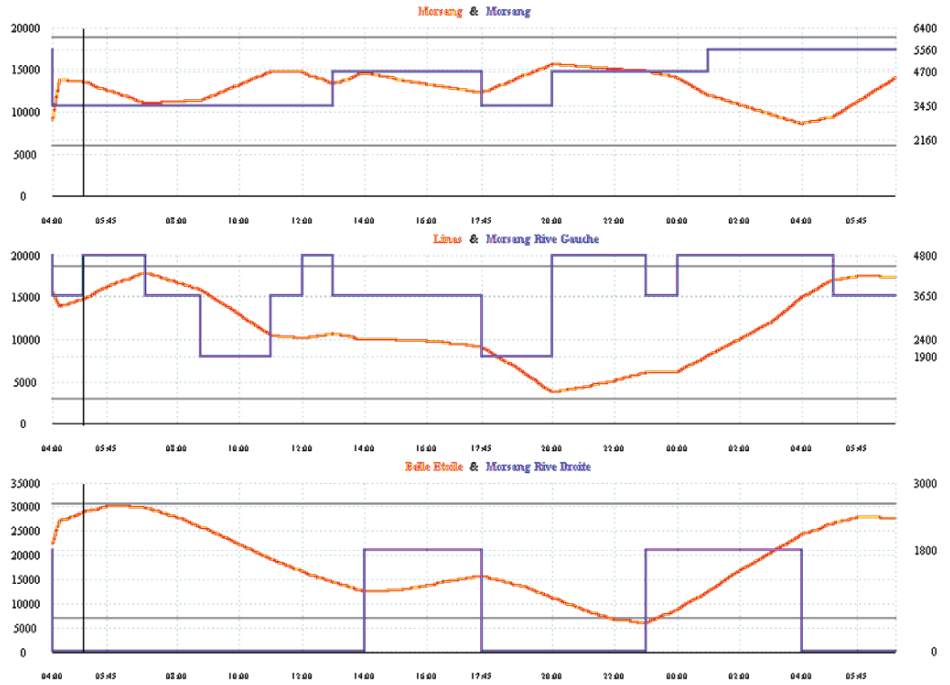

Figure 10. EMERAUDE's graphical interface

Additional constraints are taken into account on the sites where EMERAUDE is installed.

4.2.3. *Method*

The calculation algorithm is a mix of dynamic programming and branch and bound algorithm. The first step is the linear programming algorithm that runs to impose limit conditions on the second step. The branch and bound algorithm solves the optimising problem with discrete variables and equations.

We use this method to reduce the complexity of problem and to have discrete solutions for the schedule of all the equipment on the water network.

In the second step, the hydraulic model is the same as in the SAPHIR tool.

The cost function, used in both steps, takes into account the treatment cost, the electric costs and flow variation penalties. The treatment cost concerns the chemical and biological products used during the treatment process. The electric cost concerns the pumping stations. The unit cost varies during the day and the cost coefficients vary during the year.

4.2.4. *User Intervention*

EMERAUDE is a autonomous system and works without human interventions. But the user can interact with EMERAUDE as follows:

Schedule events on the network like works on pump units (all pumps are stopped), an objective level on a reservoir, decrease the maximum power demand

Indicates an availability of a pump or a reservoir

Schedule a wholesale draft

4.2.5. *Managing Malfunctions*

The following sub-sections describe some of the activities handled by EMERAUDE concerning events that need corrective actions or a new schedule.

When a communication failure comes up, EMERAUDE supposes that the equipment (pumping station, borehole, valve) works in the same way as before the communication failure. It supposes that the PLC will respect the constraints of the electrical contracts. If the communication failure concerns a reservoir, this reservoir is considered unavailable by EMERAUDE.

Any fault in a pump unit might affect the current schedule. If the faulty pump is essential for the execution of the control, EMERAUDE finds a new schedule for the new state of the water network.

The reservoirs levels are carefully followed to avoid violation of the minimum and maximum limits which assigned to each reservoir or tank. EMERAUDE takes a corrective action when such a violation occurs.

In such system, the reservoir level is very important. If a fault in the level measure occurs, EMERAUDE thinks that the reservoir is unavailable and works with the other reservoirs on the network.

When EMERAUDE sends a control to a pump, it verifies the result. If EMERAUDE can't control the pump, it fixes the pump scheduling until the problem is corrected.

4.2.6. *Communication Module*

The communication module makes the connection of the "Water Demand Forecast module" and the "Optimisation module" with the process.

At the moment, this module can communicate with the TOPKAPI SCADA system, the SDG system (a data server) and with other systems which can discuss in MODBUS protocol (PLC for example). EMERAUDE can be adapted to other type of SCADA system or data servers.

5. An Example of Crisis Management

5.1. NETWORK DESCRIPTION

Saphir's objective is to provide survey engineers and dispatchers with the necessary resources so they can formulate an optimal **daily** strategy for managing a network.

Saphir takes into account structural data which do not change over time and which characterise a water network, and temporary and event-based data which describe a particular network situation.

Saphir provides the following output data:

Management strategy: The volumes to produce, the flow rates to transfer and pump, the levels of reserves for a day and **on an hourly basis**.

Missing water: The quantity of water to supply to a demand site in a crisis situation, in order to keep the supply reservoir at 0 level and meet demand. Water shortages constitute criteria for assessing the seriousness of a crisis situation or a situation subject to reduced output.

The operating costs: Saphir provides the treatment and pumping costs for the strategy calculated.

In addition, when the user makes a request, Saphir can:

Display the results curves for each element in the network

Display and print out detailed reports regarding the results and the costs

5.1.1. *Network Element*

The network model is constructed by using the following icons corresponding to a well-defined network element.


Treatment plant


Water source


Borehole


Pumping station


Demand zone


External network


Reservoir


Tower


Connection point


Transfer

"Treatment" is the term used to refer to plants, sources and boreholes. "Storages" refers to towers and reservoirs.

5.1.2. Network Description

Our network model is similar to a real one. However, the electricity or treatment costs and some other characteristics are changed for our simulations purposes.

The water network that will be considered in our simulations is composed of three main treatment plants and three boreholes. The most important treatment plant is Station 3 whose daily maximum capacity is 225,000 m^3.

Production name	Electricity tariffs	Electricity contracts	Treatment cost (/m^3)	Daily capacity (m^3/day)
Station 1	Vert-Base	LU	12.7	48,000
Station 2	Vert-Base	LU	10.4	96,000
Station 3	**Vert-Base**	**TLU**	**9.97**	**225,000**
Borehole O	Vert-Base	TLU	0.5	2,400
Borehole C	Vert-Base	CU	0.9	22,008
Borehole B	Vert-Base	TLU	0.5	1,608

The storage elements (tower and reservoirs) are composed of seven reservoirs and five towers.

Reservoirs and towers	Security level (m)	Max (m)	Useful Volume (m^3)
Courta	4	8	**2,000**
Saulx	1	7.8	**19,550**
Linas	1.5	8.2	**15,075**
B.E.	1.5	5.65	**22,144**
Vallee	2	6.5	**5,693**
Saclay	2	4.8	**1,806**
Chilly	3	7.8	**2,016**
Croix du Bois	3	7	**5,600**
Tower 3	2	4.5	**10,000**
Tower 2	1.18	2.7	**3,861**
Tower 1	1	3	**4,000**
Extension BE	1	6.6	**7,095**

Owing to the useful volume, we can optimise the electrical costs. The treatment plants and the pumping stations will work in priority during the low electrical cost periods. Of course, the surplus production capacity depends essentially on the storage capacities of the towers and reservoirs.

The electrical costs in our simulations are calculated in function of the tariffs used by EDF (Electricité de France). According to those electrical tariffs, the prices from 22:00 to 6:00 are less than during the rest of the day for each period. It means that the production during this period of the day is optimal in financial terms

All our simulations are made upon a 24 h period. In order to make possible the comparisons between our simulations, we suppose that at the end of a simulation; the storage elements of the network must have the same capacity as at the start of this simulation.

The model and the network elements are represented in the following scheme:

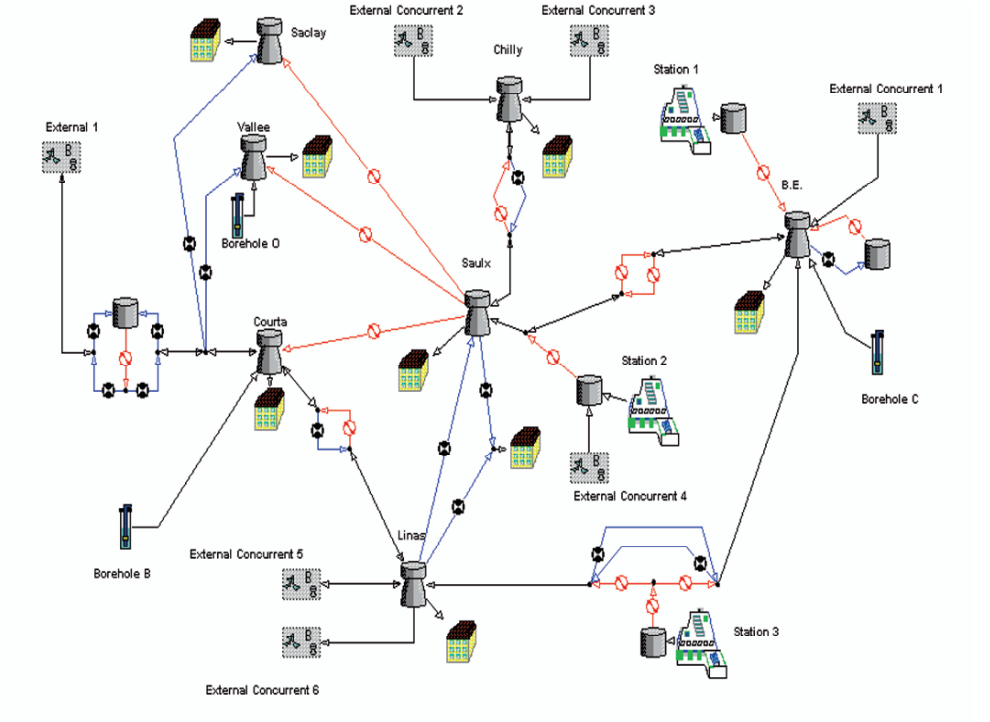

Since the network looks like a graph, we will call pumping stations, valves, transfers and connections "*arcs*", and the other entities "*nodes*".

5.1.3. *Demand profile*

In these simulations, the demand profile considered for each demand zone is the following one:

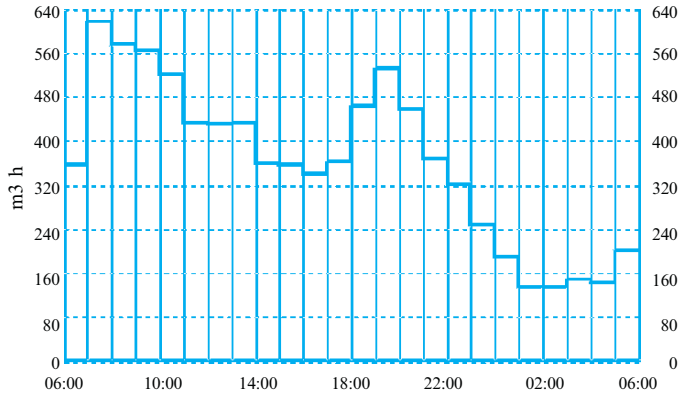

However the user can retrieve demand data from files or can change them manually.

5.2. SIMULATIONS

Our simulations are based on a 24 h period (daily period). On a **daily profile simulation,** the system looks for a management profile for the situation defined. The objective is to fulfil demand, with a minimal economic cost, without loss of volume (initial levels on day D + 1 = initial levels on day D). We use this type of calculation to find a cyclic strategy for managing the network.

5.2.1. *Normal Simulation*

The summary results of this simulation (treatment and electricity costs, demand and production as well as water insufficiencies) are given in the following image:

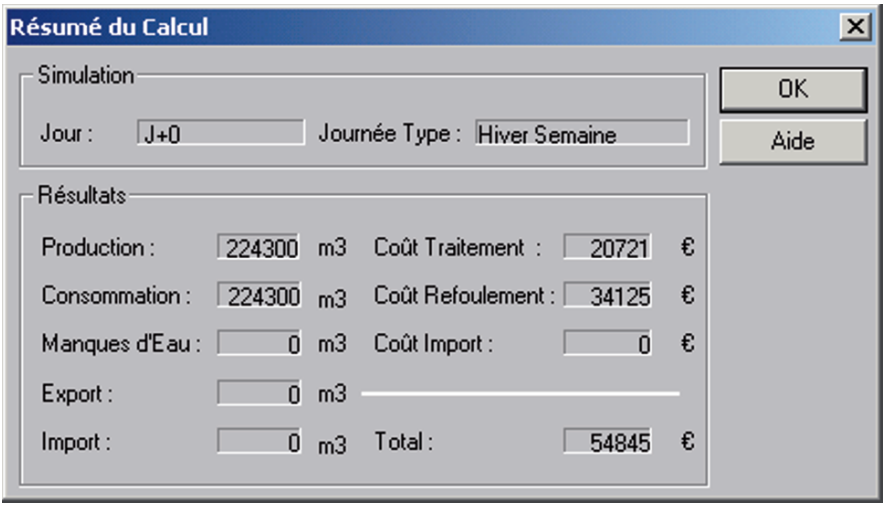

Summary results of the simulation

We remark that there are no water insufficiencies (missing water) in our simulation.

Moreover, all the storages behaviour (see images below) show that they are filled up during the less electricity costs hours. The minimum level is reached always at 22:00.

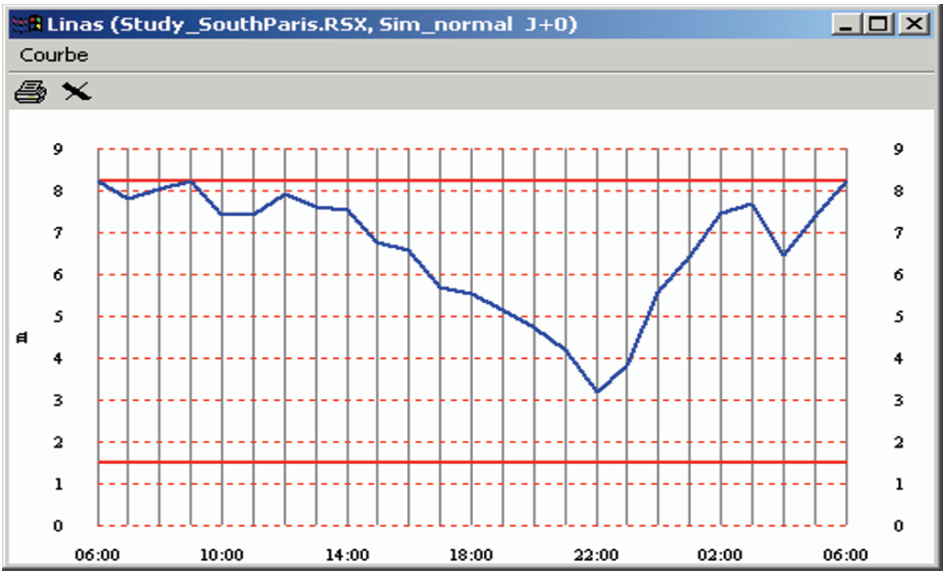

Linas Tower level during the 24-hours simulation

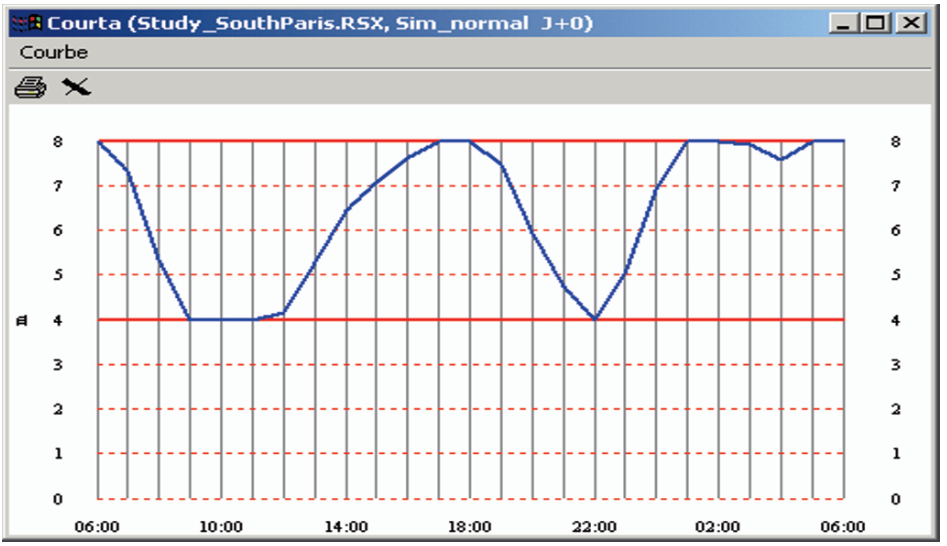

Courta Tower level during the 24-h simulation

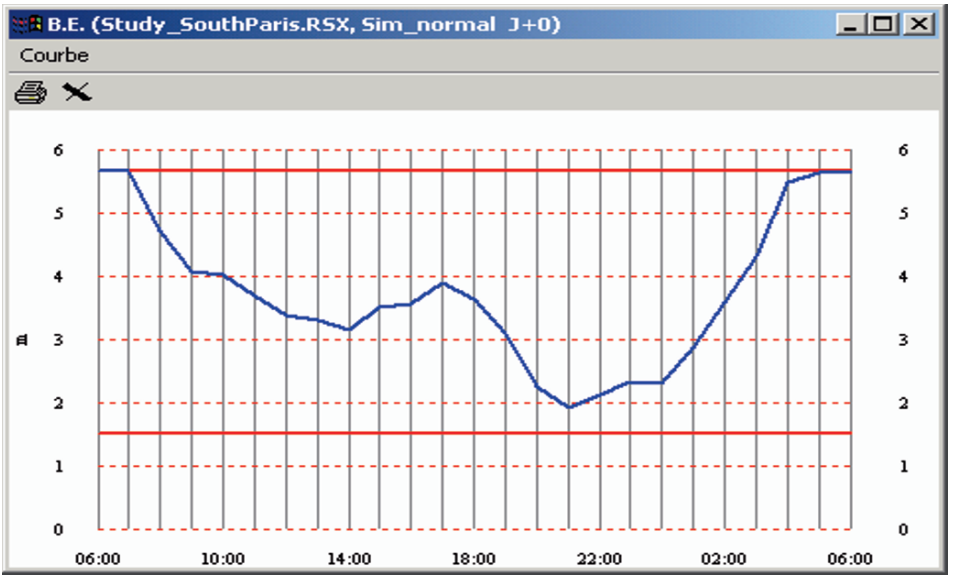

B.E. Tower level during the 24-h simulation

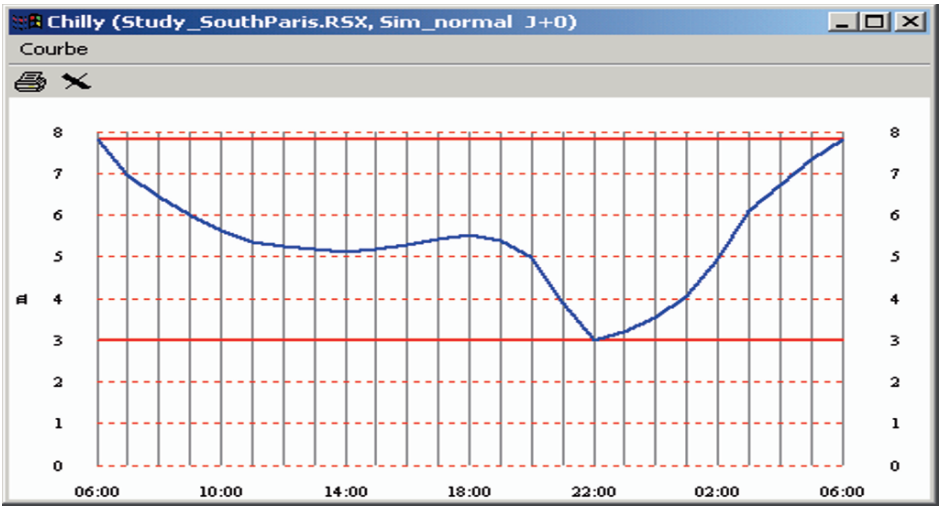

Chilly Tower level during the 24-h simulation

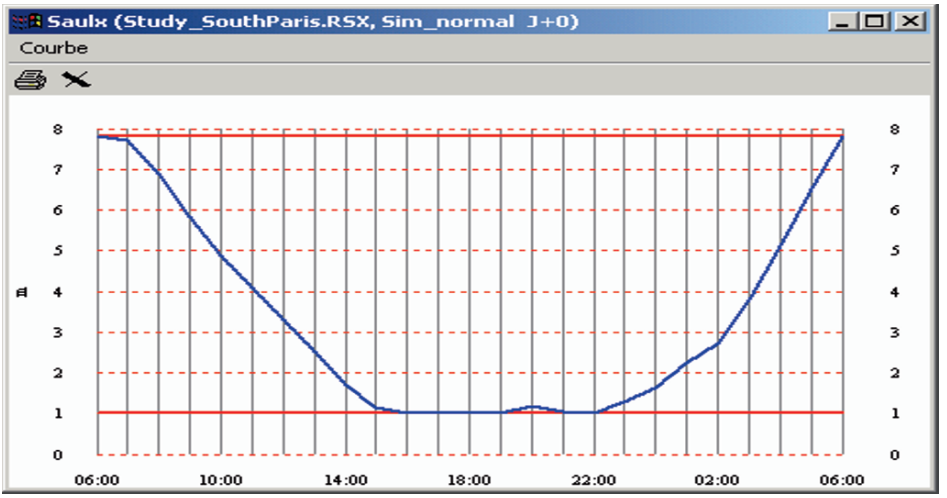

Saulx Tower level during the 24-h simulation

On the other hand, all the treatment plants (see graphics of the treatment plants) show that the capacity per hour during the less electricity cost hours (22:00 to 6:00) is greater than for the rest of the day.

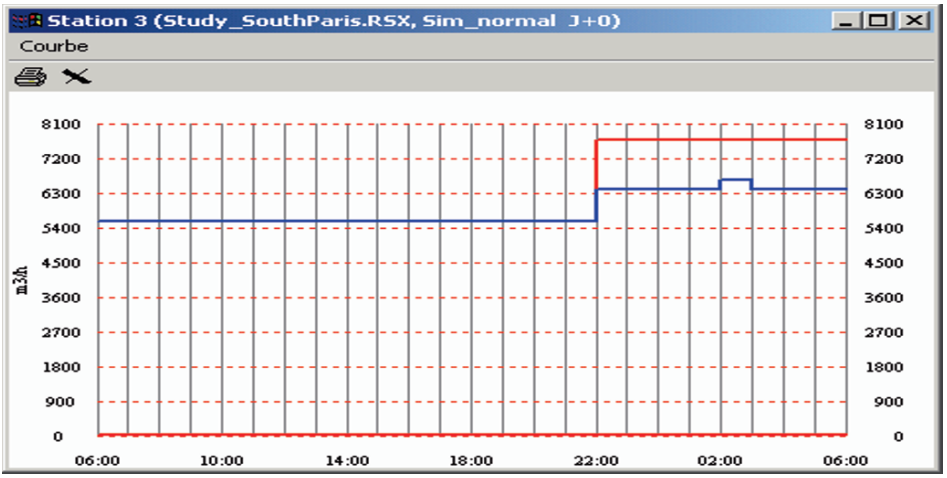

Station 3 production (m^3/h) during the 24-h simulation

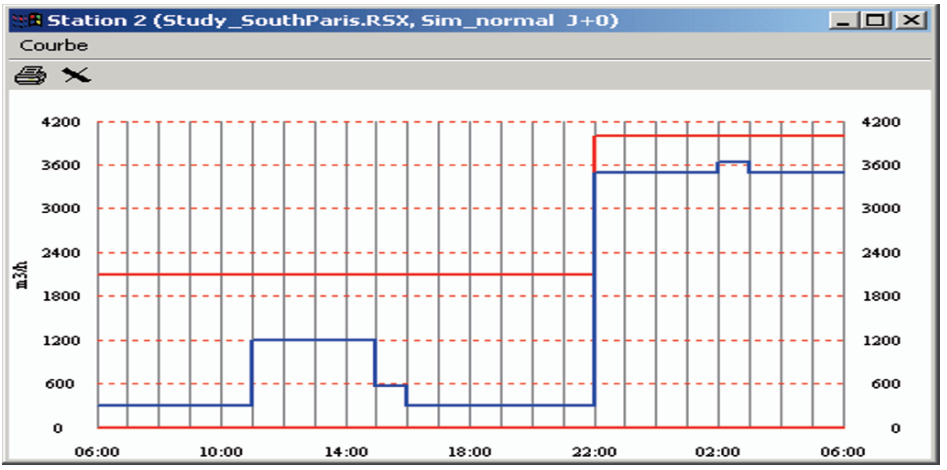

Station 2 production (m^3/h) during the 24-h simulation

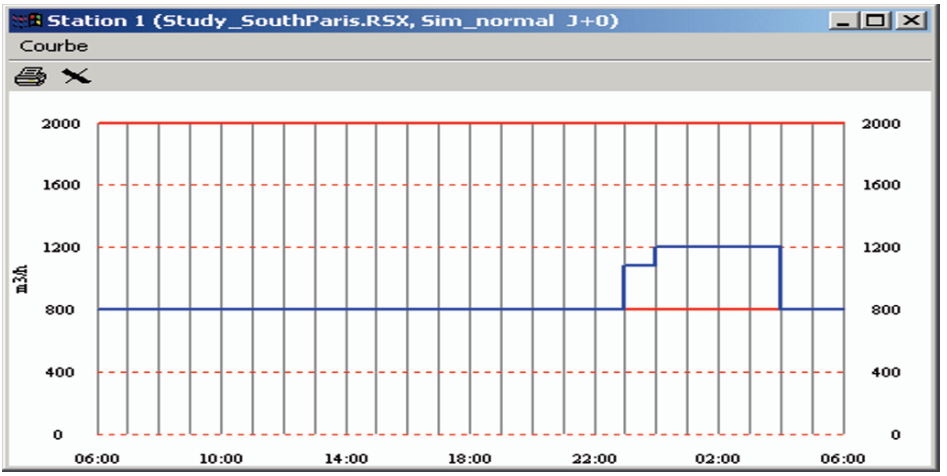

Station 1 production (m^3/h) during the 24-h simulation

5.2.2. *Out of Order Simulation*

The following are a few examples of out of order cases that can be studied:

- Shut-down of a plant from H+0 to H+5.
- Washing one of the compartments in a reservoir for a day: the reservoir's effective volume divided by 2 in the description of the associated event.
- The limitation of pumping flow rates due to a pump breakdown: instead of flow rates of 0, 1,000, 2,000 and 3,000 m^3/h, you can set a maximum flow rate of 2,000 m^3/h for the duration of the event.

In our case, we have considered the most important water treatment in the network. We have supposed that the pumping on the left side of Station 3 is broken down. Thus there is no more possibilities to send water on the left side of this treatment plant.

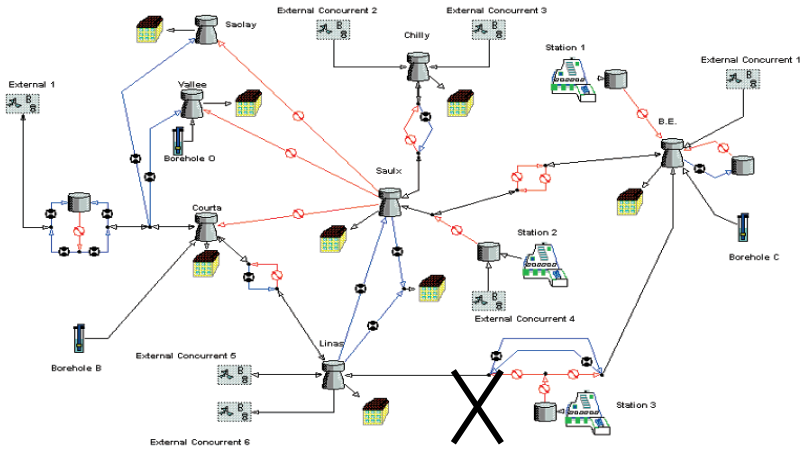

The pumping station on the left side of the Station 3 is broken down.

The summary results of this simulation is given in the following image:

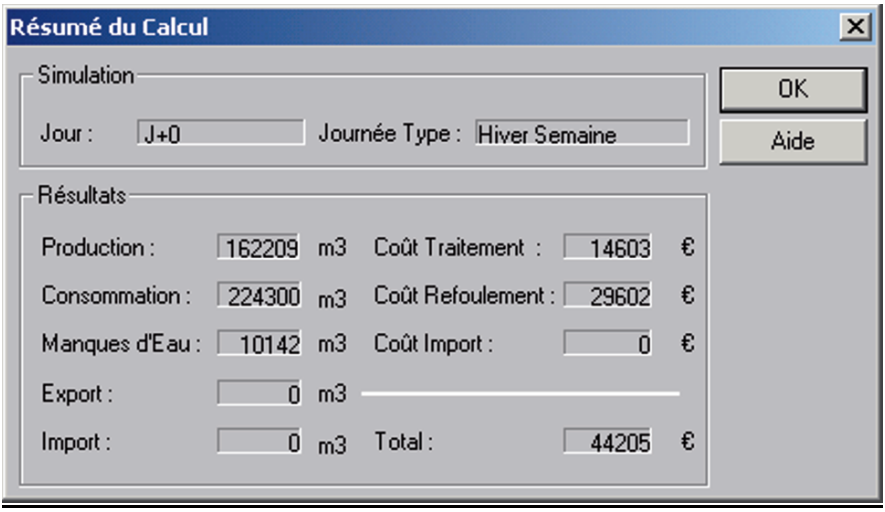

Summary results of the simulation

We remark that there are water insufficiencies (missing water = 10,142 m^3) in our simulation.

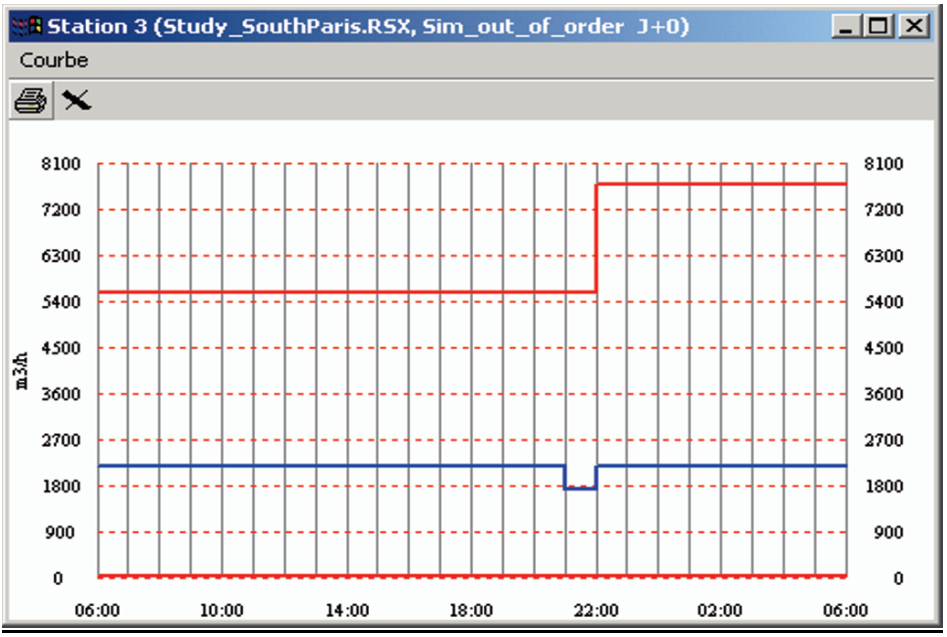

The station 3 is running on less than half of his capacity.

On the other hand, the most dependant towers from left side pumping station of Station 3 can no more satisfy the demand. These tower's levels stay at 0 for many hours.

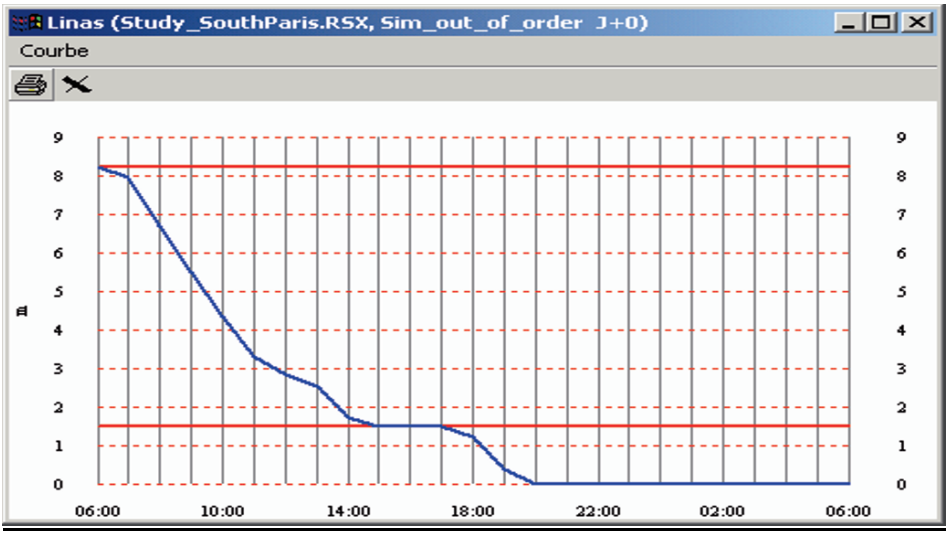

Linas Tower level staying at 0 after 20:00

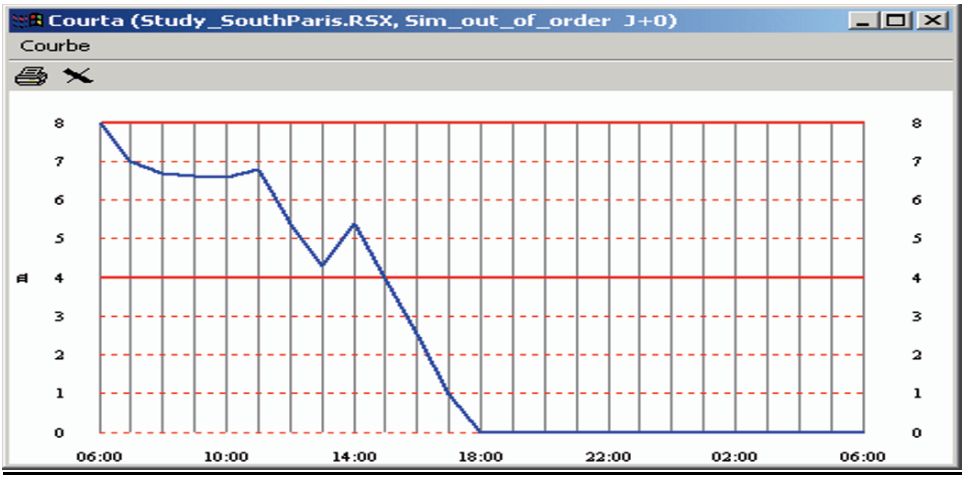

Courta Tower level staying at 0 after 18:00

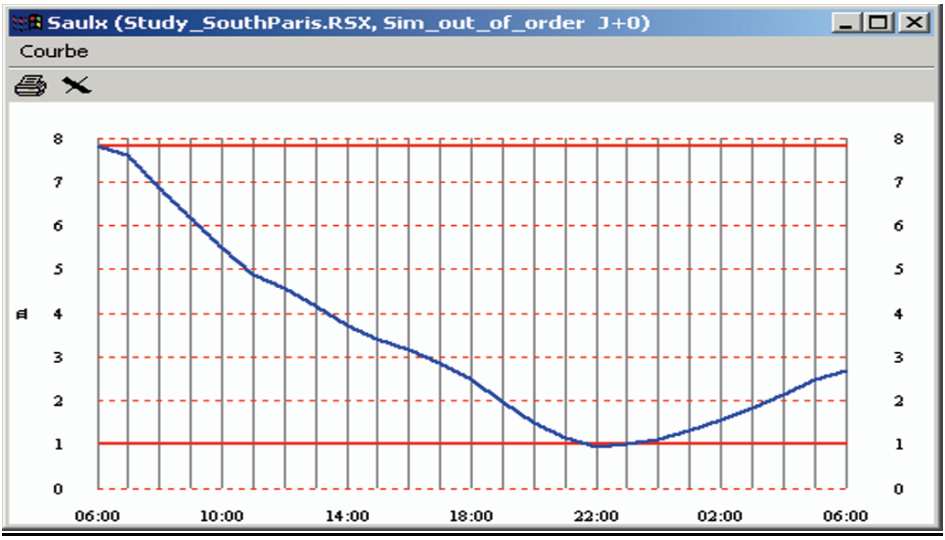

Saulx Tower level can't reach the same level as at the start of the day

It's impossible to manage this kind of situation without an external solution. Our network is connected to seven external networks managed by external companies whose prices are different.

Getting help from an External Network – Solution 1

We use for this simulation only the External 1 which daily capacity is 24,000 m^3.

The summary results of this simulation is given in the following image:

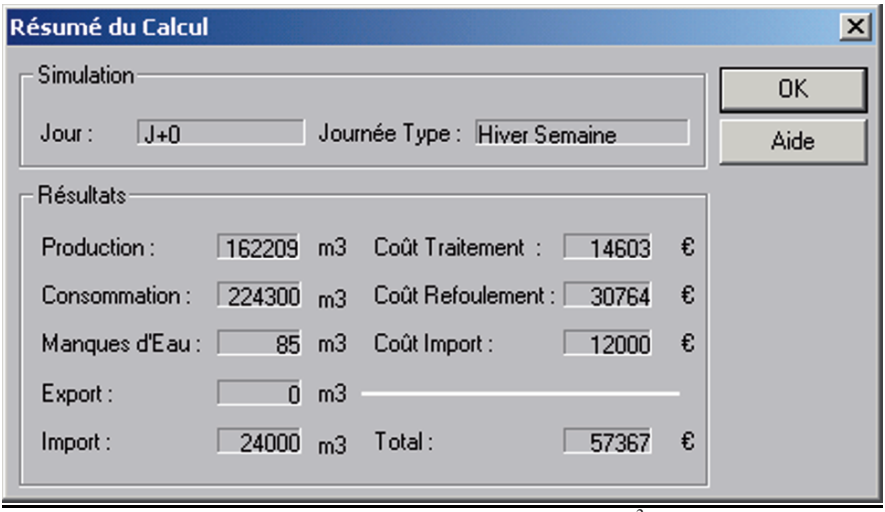

Owing to the water quantity imported (24,000 m^3), the quantity of the missing water has reduced neatly.

However, the Linas Tower can't get any more the start level. At the end of the day it level goes dangerously at 0.

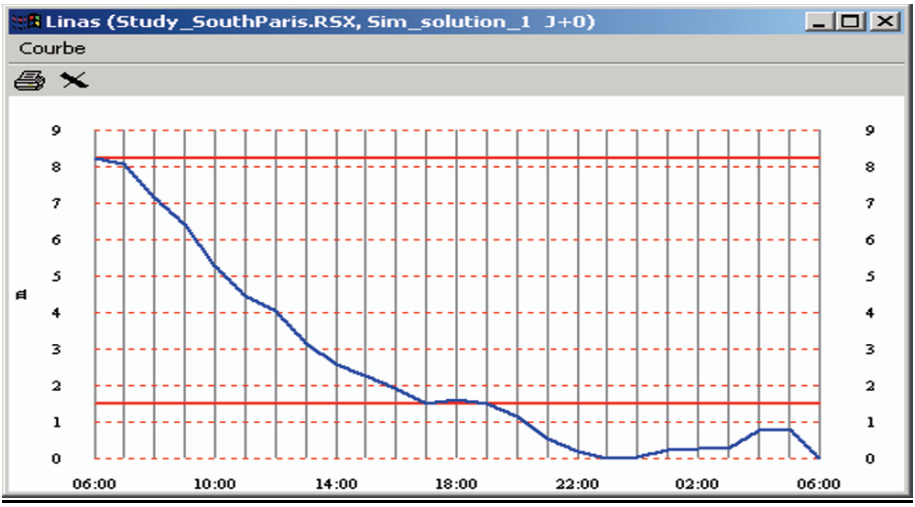

Linas Tower level reaching at 0 at the end of day simulation

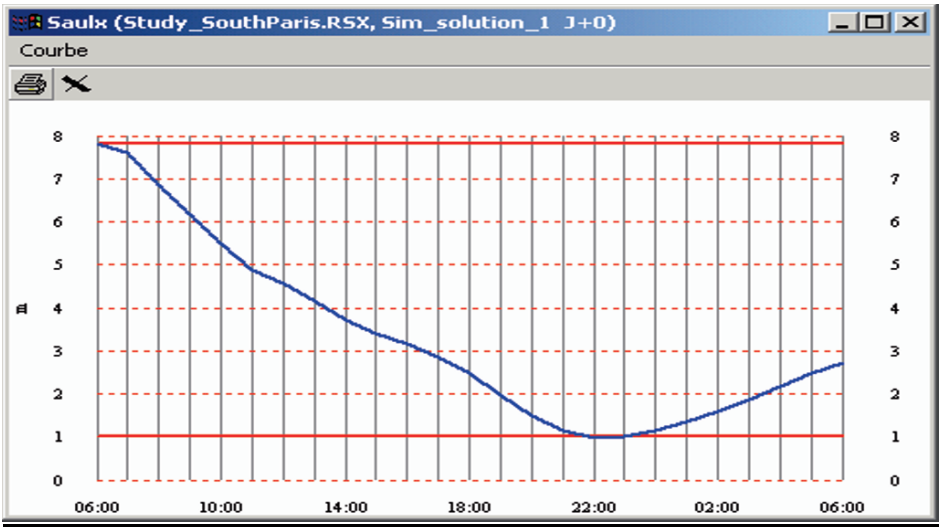

Saulx Tower level can't reach the start level at the end of day simulation

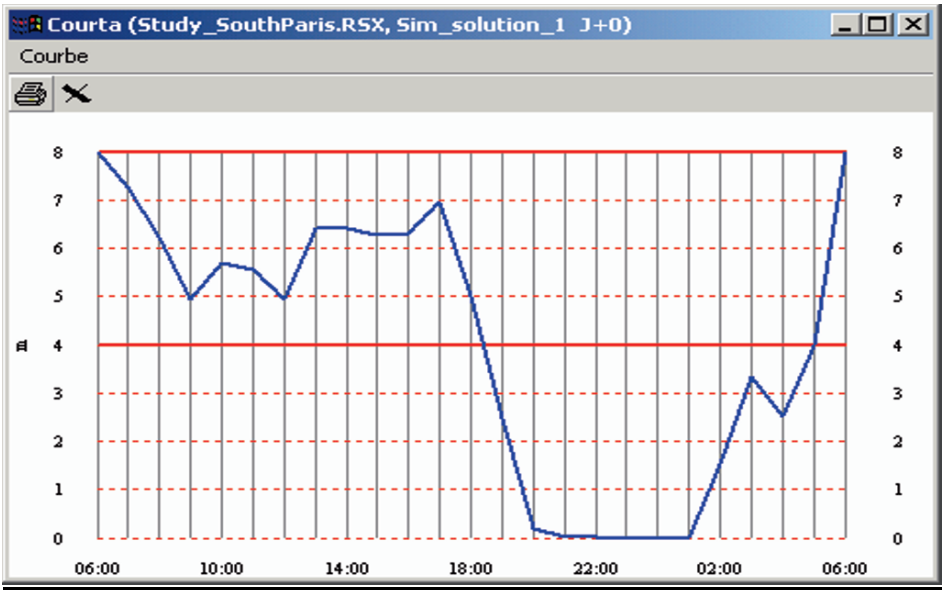

Courta Tower behaviour shows that it can't satisfy the demand from 22:00 to 02:00

Getting help from an External Network – Solution 2

We use for this simulation only the External Concurrent 5 which daily capacity is 50,000 m^3.

Owing to the water quantity imported (50,000 m^3), there is no more missing water in the network. However, the production and the imported water don't reach the demand. It means that at the end of the simulation we can't reach the same levels as the start levels.

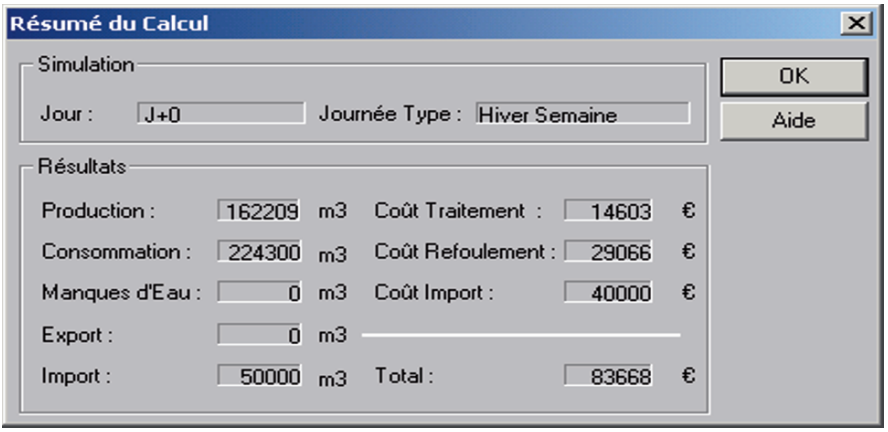

The summary results of Solution 2

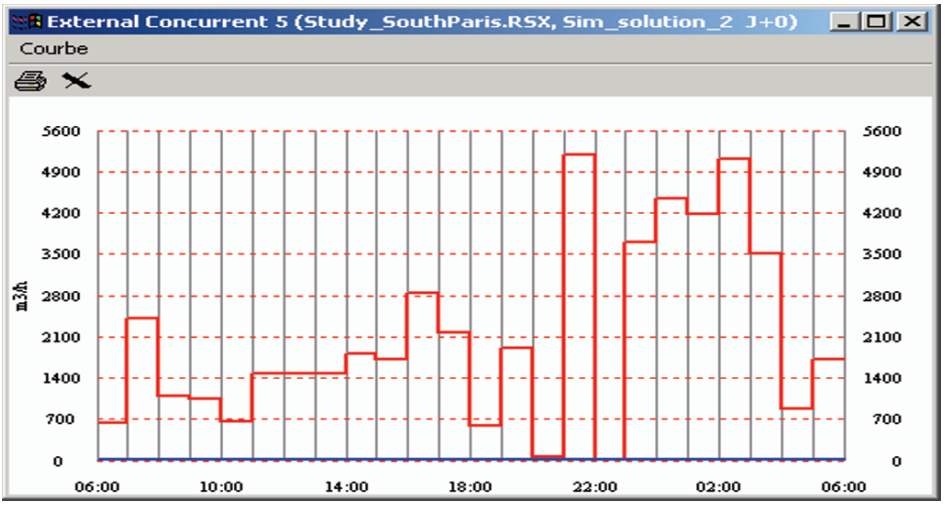

Water imported over a 24-h period

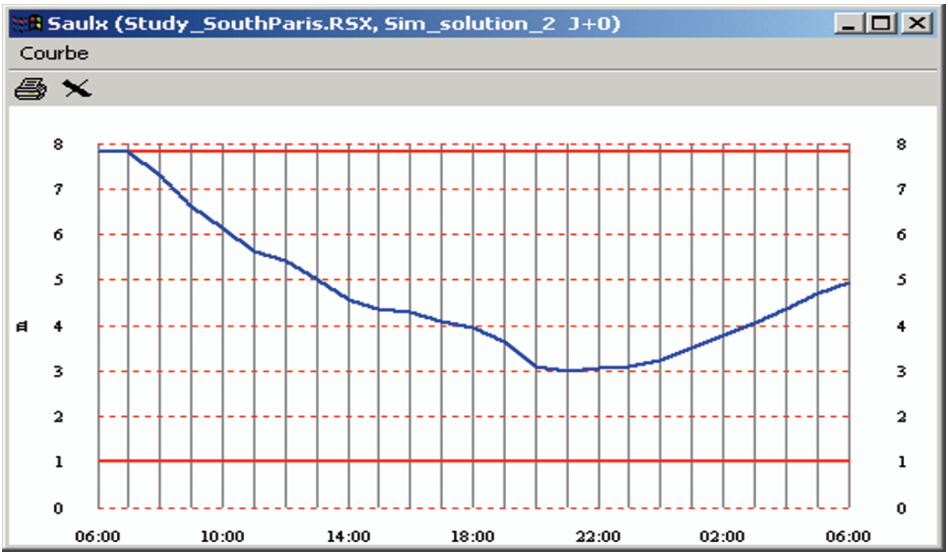

Saulx Tower level can't reach the start level at the end of day simulation

Getting help from an External Network – Solution 3

We use for this simulation External Concurrent 5 which daily capacity is 50,000 m^3 and External 1 which daily capacity is 24,000 m^3.

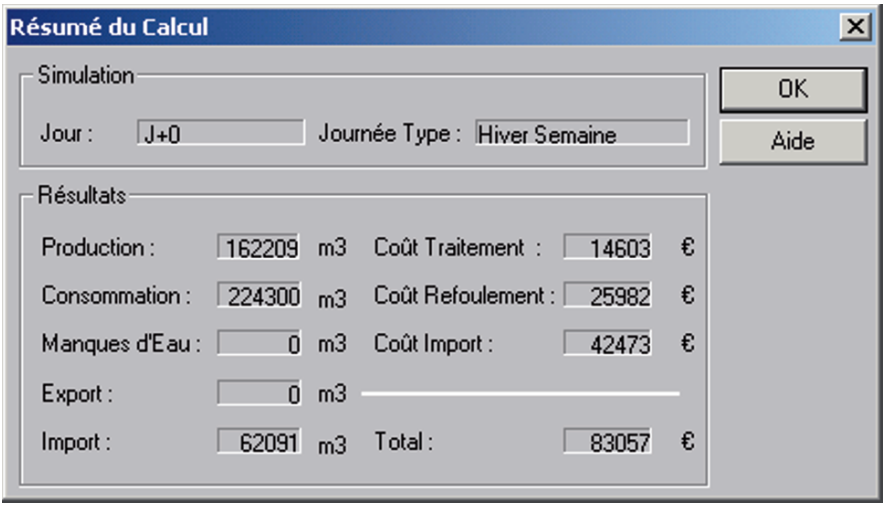

The summary results of Solution 3

There is no more missing water and the quantity of water produced and imported equal the demand of the network. At the end of a day simulation, all the storages come at their starting levels.

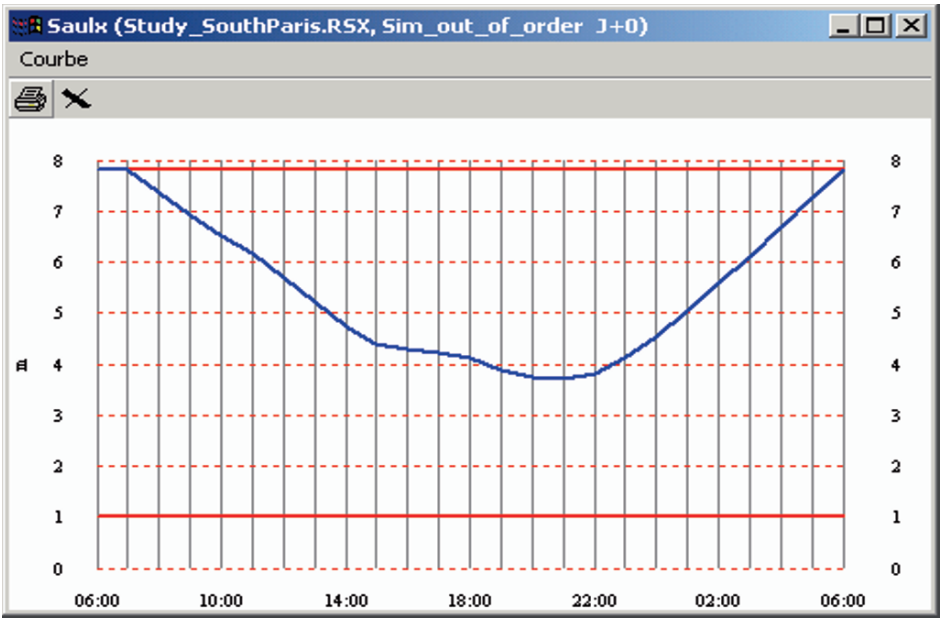

Saulx Tower level reach the start level at the end of day simulation

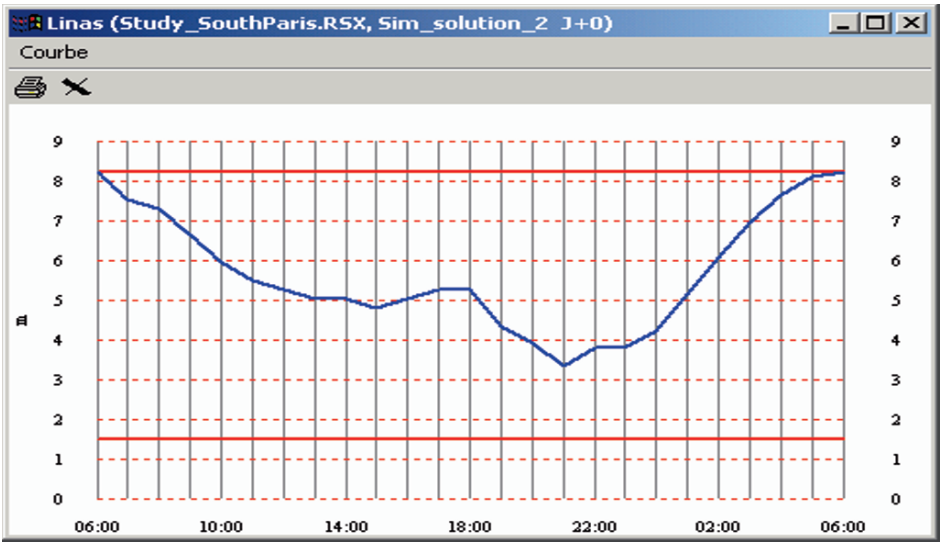

Linas Tower level reach the start level at the end of day simulation

We have bought all the quantity possible from External 1 whose price for cubic meters is lower than the price of External Concurrent 5

Name	Start	Duration (h)	Quantity (m^3)
External 1	06:00	24	24,000
External Concurrent 5	06:00	24	38,091

6. Conclusion

SAPHIR is a Windows based software program designed to solve the scheduling problem for water supply and distribution. Based on a user friendly graphical interface, it provides a invaluable help to network managers. Simplifications made on the optimisation problem formulation remain reasonable on operation mode and give satisfaction in all studied networks.

The SAPHIR product is already installed and used in more than 20 Lyonnaise des Eaux water distribution networks in France (City of Dijon, Paris Sud, Paris West, City of Bordeaux,...), Great Britain (Essex & Suffolk Water, Northumbrian Water) and USA (United Water New York).

EMERAUDE can be considered as a real time application of SAPHIR principle. It gives excellent results from several points of view. First, the stabilization of raw water flow rates has been improved. This objective has been reached thanks to the EMERAUDE's predictive capabilities and it's adapted algorithm compared to what a classical PLC can do. The second point is electrical cost optimisation. This is done by maximizing water transfer at night and by using the best available pumping combination.

Today, the EMERAUDE system is fully operational at six water networks in France: Morsang sur Seine (installed in 1993, production 200,000 m^3), Viry sur Seine (1994, 120,000 m^3), Bischwiller (1996, 35,000 m^3), Creil (1997, 30,000 m^3), Bordeaux (1998, 60,000 m^3) and Dunkerque (1999, 60,000 m^3).

References

Balakrishnan, A. and K. Altinkemer. 1992. Using a hop-constrained model to generate alternative communication network design. ORSA Journal on Computing, 4, 192–205.

Barto, A. G., S. J. Bradtke, and S. P. Singh. 1991. Real-time learning and control using asynchronous dynamic programming, Technical report, University of Massachusetts, Amherst.

Bertsekas, D. P. 1991. Linear Network Optimization: Algorithms and Codes. MIT Press, Cambridge, MA.

Cross, H. 1936. Analysis of flow in networks of conduits or conductors. University of Illinois Bulletin No. 286.

Edmonds, J. and R. M. Karp. 1972. Theoretical improvement in algorithmic efficiency for network flow problems. Journal of the Association for Computing Machinery, 19(2), 248–264.

Fotoohi, F., P. Villon, and R. Loubeyre. 1992. Un outil d'aide à l'exploitation d'un réseau de distribution d'eau potable. *Hydrotop 92*.

Fulkerson, D. R. 1961. An out-of-kilter method for minimal cost flow problems. *S.I.A.M.,* 9(1), 18–27.

Gondran, M., M. Minoux, and S. Vajda. 1984. Graphs and Algorithms. Wiley, New York, ISBN:0471-10374-8.

Harel, D. 1987. Algorithmics: The Spirit of Computing. Addison-Wesley, Reading, MA.

Kora, R., P. Lesueur, and P. Villon. 1987. Sixteenth IFIP Conference on system Modelling and Optimization: A real-time optimal control algorithm for water treatment plant.

Loubeyre, R., P. A. Jarrige, and N. Dembele. 1991. Small water distribution network optimization. Proceedings AWWA, Houston, TX, April 1991.

Mays, L. W. (Ed.) 1999. Hydraulic Design Handbook. McGraw Hill, New York.

Minoux, M. 1984. A polynomial algorithm for minimum quadratic cost flow. North-Holland. European Journal of Operational Research, 18, 377–387.

Munson, B. R., D. F. Young, and T. H. Okiishi. 1998. Fundamentals of Fluid Mechanics (3rd edition). Wiley, New York.

Streeter, V. L., E. B. Wylie, and K. W. Bedford. 1998. Fluid Mechanics (9th edition). WCB/McGraw Hill, New York.

Viessman, W. and M. J. Hammer. 1993. Water Supply and Pollution Control (5th edition). HarperCollins, New York.

NONLINEAR BEHAVIOR OF SOILS AS THE MAIN SOURCE OF DAMAGE OF STRUCTURES

S. DOLAREVIĆ[1*] AND A. IBRAHIMBEGOVIC[2]
[1]*University of Sarajevo, Department of Civil Engineering, Patriotske lige 30, 71000 Sarajevo, Bosnia and Herzegovina*
[2]*Ecole Normale Supérieure de Cachan, LMT, 61 avenue du président Wilson, 94235 Cachan, France*

Abstract. One of standing problems in the practical structure analysis is associated with the issue how to model soil beneath foundations. Usual approach is based on elastic soil models and determination of soil elastic parameters is the main problem. The essence of problem is that nonlinear soil behavior is difficult to describe by two elastic parameters. In this paper we present analysis of soil-structure interaction using elastoplastic cap model for soil. These results are compared with results obtained by elastic soil models for various types of foundations. Results of analysis show that nonlinear models could be used for determination replacing static stress–strain modulus for low level of soil stresses beneath structures.

Keywords: Elastoplasticity, cap model, soil-structure interaction

1. Introduction

Classical approach to the analysis of structure is based on assumption that behavior of soil is elastic. Various model of soil is developed on this assumption, but all of them have the same problem – determination of elastic parameters. These parameters have a key role in structure settlements calculation and, therefore, in structure stresses. These difficulties are clear from Eurocode 7. Here is quoted chapter of Eurocode 7 about this issue:

* To whom correspondence should be addressed. e-mail: sdolar@bih.net.ba

A. Ibrahimbegovic and M. Zlatar (eds.), *Damage Assessment and Reconstruction After War or Natural Disaster*,

3.3.8 Soil stiffness

(1) In assessing the soil stiffness, the following features shall be considered:
- *drainage conditions;*
- *level of mean effective stress;*
- *level of imposed shear strain or induced shear stress, this latter often normalized with respect to the shear strength at failure;*
- *stress and strain history*

(2) These factors are the most important in controlling the stiffness of soils. Other factors influencing the deformation module of soils that may be taken into account include:
- *direction of soil stressing with respect to the orientation of the principal consolidation stress;*
- *time and strain rate effects;*
- *size of the specimen tested in relation to the particle size and macrofabric feature of the soil.*

Reliable measurements of the stiffness of the ground are often very difficult to obtain from field or laboratory tests. In particular, owing to sample disturbance and other effects, measurements obtained from laboratory specimens often underestimate the stiffness of the soil in-site. Analysis of observations of the behavior of previous constructions is therefore recommended.

It is sometimes convenient to assume a linear or log-linear relationship between stress and strain for a limited range of stress change. However, this must always be adopted with caution since the actual behavior of soil is generally significantly non-linear.

The essence of the problem is presence of plastic deformations, which are unavoidable under foundations even in low range of soil stresses. This deformation cannot be described by elastic parameters and it causes difficulties in determination of static stress–strain modulus. On the other hand, elastic models of soil in structure analysis have some advantages. Calculation process is simple and soil stresses are far of failure stresses, because safety factors for allowed stresses in soils are high. Moreover, failure of structure will happen before failure of soil, except in case when structure is built on slides. Therefore, relationship between loads and settlements is usually linear.

Soil failure under footing, stability of slopes and pressure on retaining walls are classical plasticity problems in geomechanics. In these problems soil is modeled as ideal plastic material without any elastic behavior. Absolutely stiff structures are assumed, because this approach does not allow analysis interaction of elastic structures and soil. Nowadays it is possible to connect these problems using elastoplastic constitutive equations for soils and Finite Element Method.

2. Soil Constitutive Model

2.1. MAIN CHARACTERISTICS OF SOIL BEHAVIOR

A good constitutive stress–strain model of soil behavior has to fulfill the following requirements: an adequate description of main characteristics of inelastic soil behavior, a stable and unique mathematical formulation, along with an efficient performance for numerical implementation. At the same time, in order to ensure its practical value, the model should be defined with only a few parameters, whose values are available from standard tests. Due to very complex behavior of soil the former and the latter requirements are usually not compatible. For example, the well-known Coulomb model is simple and has only a couple of parameters, but it is not easy to establish its validity for many practical three-dimension problems in geotechnical engineering, where the Coulomb surface exhibits singularities.

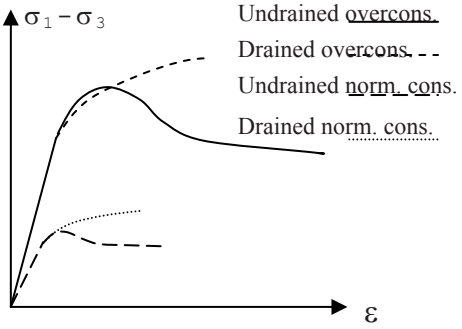

Figure 1. Soil behavior – triaxial test

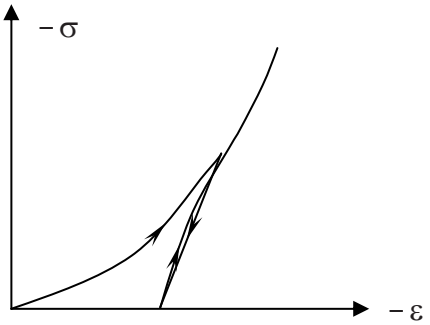

Figure 2. Soil behavior – hydrostatic pressure

Typical stress–strain relationships, obtained by triaxial tests and presented in Fig. 1 are not linearly elastic for the entire range of loading of practical interest. Shear strength of soil depends of many parameters. The most important factors are level of consolidation and rapidity of stress applying. Under hydrostatic state of stresses (Fig. 2) four aspects of soil behavior are obvious: response is path-dependent and nonlinear, during cyclic loading behavior is essentially elastic, unloading exposes plastic strain and loading over the previous load proceeds along the same path as the unloading did not occur. Under pressure solid particles move on voids producing irrecoverable strain and increasing shear resistance of soil. It is possible to simulate these main characteristics of soil behavior by elastoplastic cap models. The cap models fall

according to classical incremental theory of hardening plasticity for materials with temperature- and time-independent properties.

2.2. LOADING FUNCTION OF CAP MODEL

Loading function for cap model in plane of stress invariants shown in Fig. 3 is assumed to be isotropic and consist of three parts: a failure function assumed as fixed Drucker-Prager linear function $f_1(I_1, J_2) = 0$, an elliptic strain-hardening cap $f_2\left(I_1, J_2, \xi\left(\varepsilon_v^p\right)\right) = 0$ which expands isotropically about hydrostatic axis and tension circle $f_3(I_1, J_2, T) = 0$, where are: I_1 – the first stress invariant, J_2 – the second deviatoric stress invariant, ε_v – plastic volumetric strain and

T – tension limit strength. The associated flow rule is assumed. Main problem of multisurface models is singularity of elastoplastic tangent operator in corner regions around intersection points.

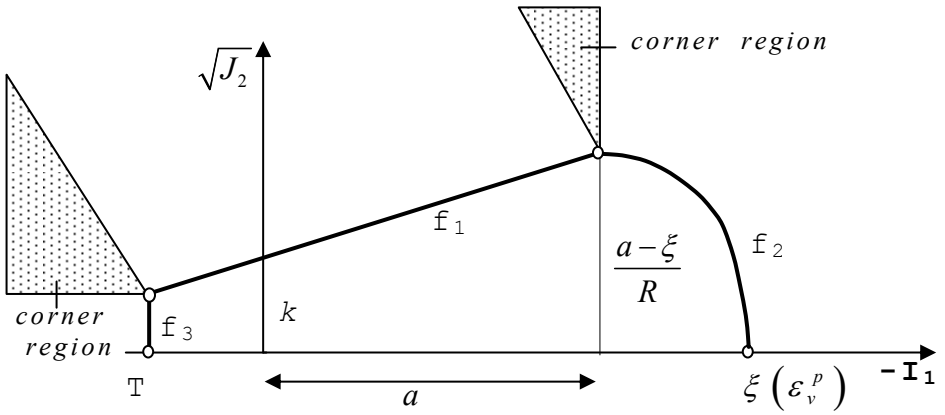

Figure 3. Elliptic cap model in $I_1 - \sqrt{J_2}$ plane

This problem could be avoided by modification of classical cap model. Main characteristic of modified cap model, presented in Fig. 4, is that loading functions intersect in a smooth manner and corner regions are removed (Dolarević and Ibrahimbegović, 2007). Loading function is given by next equations:

$$f_1(I_1, J_2) = \alpha I_1 + \sqrt{J_2 - k} = 0 \qquad I_1^T \geq I_1 \geq I_1^C \tag{1}$$

$$f_2\left(I_1, J_2, \xi\left(\varepsilon_v^p\right)\right) = \frac{\left[I_1 - a(\xi)\right]^2}{R^2} + J_2 - b^2(\xi) = 0 \qquad I_1 \le I_1^C \tag{2}$$

$$f_3\left(I_1, J_2\right) = \left(I_1 - T + R_T\right)^2 + J_2 = R_T^2 \qquad I_1 \ge I_1^T \tag{3}$$

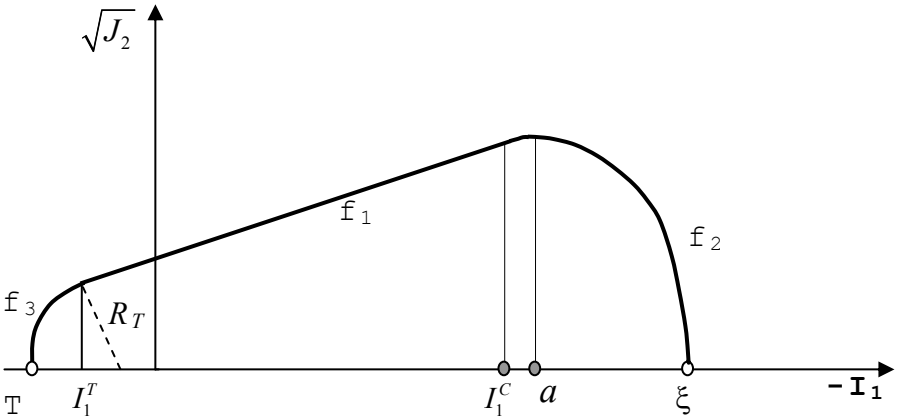

Figure 4. The modified smooth cap model in $I_1 - \sqrt{J_2}$ plane

where

$\xi\left(\varepsilon_v^p\right)$ – Hardening law defined by $\xi\left(\varepsilon_v^p\right) = \frac{1}{D}\ln\left(1 + \frac{\varepsilon_v^P}{W}\right)$ (4)

I_1^T, I_1^C – Ordinates of intersection points between functions f_1 and f_3, as well as f_1 and f_2

$a(\xi)$ – Ordinate of the ellipse center

$b(\xi)$ – Main radius of ellipse

R_T – Circle radius

α, k, R, T, W, D – Material parameters

Since the failure envelope is a straight line, parameters $a(\xi)$, $b(\xi)$, and ordinate I_1, and as well $\sqrt{J_2}$, can be explicitly obtained from the condition that the envelope is tangent to the ellipse in the intersection point and that the ellipse passes through point $(\xi,0)$:

$$b(\xi) = \frac{k - \alpha\xi}{\alpha R + \sqrt{1 + \alpha^2 R^2}} \qquad a(\xi) = Rb + \xi \tag{5}$$

$$I_1^C(\xi) = \frac{k}{\alpha} - \frac{b(\xi)}{\alpha\sqrt{1+\alpha^2 R^2}} \qquad J_2^C(\xi) = \frac{b^2(\xi)}{1+\alpha^2 R^2} \tag{6}$$

If the stress state is described by stress point inside loading surface, model response is elastic. If the stress point lies on Drucker-Prager line (f_1) model behavior is perfectly plastic. Elliptic cap proves strain-hardening model behavior. Location of the hardening cap (ξ) depends of total plastic volumetric strain. As consequence, elastic domain and limit of shear strength increase by increasing of total plastic volumetric strain. On that way main characteristics of soil behavior are connected with porosity, because the plastic volumetric strain is result of soil compaction. In the other words, if some cohesionless soil was not loaded previously, elastic response did not occur at all or in very small range.

On the other hand, dilatancy can be kept quite small on shear failure as required for many soils. With the associated flow rule stress point on Drucker-Prager line causes some plastic volumetric dilatancy and moving cap towards the origin. This moving continues until the top of ellipse coincides with stress point when plastic strain vector becomes vertical and plastic volumetric expansion ceases.

As it is shown, this elastoplastic model is capable to describe main characteristic of soil. It is necessary to determine eight parameters to define this model and all of them are possible to obtain in standard geomechanical tests, what is very important for practical purpose.

2.3. EXPERIMENTAL IDENTIFICATION OF THE MODEL PARAMETERS

Predictive use of any constitutive model in engineering practice depends on our capabilities to determine the model parameters from standard test data. Should this determination be complicated or expensive, the use of a model will remain very limited. In that respect, the proposed model is safe; one of the main advantages of this model is relatively simple determination of parameters. Namely, the parameters needed to completely define the cap model are:

K, G – Bulk and shear moduli
α, k – Plastic parameters
W, D, R – Hardening parameters
T – Tensile strength of material

2.3.1. *Bulk and Shear Moduli*

Since it is assumed that behavior of the cap model is elastic and isotropic during unloading, the corresponding values of elastic moduli could be determined from any standard test. The bulk modulus K is determined from slope of unloading curve under hydrostatic compression test, and could be either constant or a function of I_1. The shear modulus is determined from the slope of unloading curve on deviatoric stress–strain diagram during a triaxial compression test.

2.3.2. *Plasticity Model Parameters*

The standard task in geomechanics laboratory testing of either triaxial compression or direct shear is determination of the Coulomb plasticity parameters. Taking into account that the Drucker-Prager cone has been established as a smooth approximation of the Coulomb pyramid in principal stress space, it is clear that there can be no unique relationship between Coulomb model parameters c, φ and the Drucker-Prager model parameters α, k. For the three-dimensional problems, it is possible to establish this relationship from the condition that the genetrix of cone will match either the compressive meridian of the pyramid, which leads to:

$$\alpha = \frac{2\sin\varphi}{\sqrt{3}\left(3+\sin\varphi\right)}; \qquad k = \frac{6c\cos\varphi}{\sqrt{3}\left(3+\sin\varphi\right)} \tag{7}$$

or the tensile meridian, giving:

$$\alpha = \frac{2\sin\varphi}{\sqrt{3}\left(3-\sin\varphi\right)}; \qquad k = \frac{6c\cos\varphi}{\sqrt{3}\left(3-\sin\varphi\right)} \tag{8}$$

2.3.3. *Hardening Parameters*

Typical form of relationship between the plastic volumetric strain and the first stress invariant I_1 is defined by (4) and shown in Fig. 5. The hardening parameters W and D can be determined from the results of hydrostatic compression test. Physical meaning of parameters W and D is maximum plastic volumetric strain and rate at which soil compaction occurs with pressure increase, respectively.

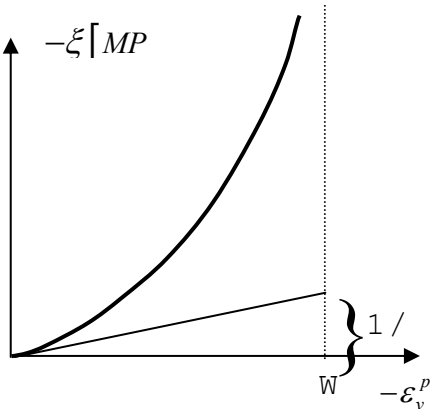

Figure 5. Hardening law in compression

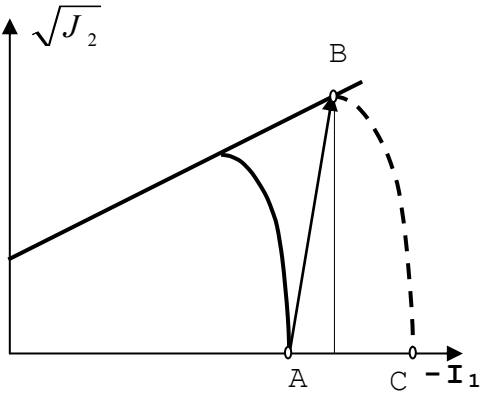

Figure 6. Determination of parameter R from triaxial test

Shape parameter R represents the ratio of major axis to minor axis of the elliptic cap. It may be estimated from the triaxial compression test data with the loading path shown in Fig. 6. The specimen is first compressed under hydrostatic pressure up to point A. Further increasing only one stress component, σ_1, while keeping the others constant, the stress state moves to point B, where the specimen failure will occur. If the parameters D, W and K are obtained from a hydrostatic compression test, the parameter R can be calculated by measuring the total volumetric strain:

$$R = \frac{\left|I_1^C - I_1^B\right|}{\sqrt{J_2^B}} \tag{9}$$

where:

Point A: $I_1^0 = 3 \cdot \sigma^0, \quad \varepsilon_v^{p0} = W \cdot \left(e^{DI_1^0} - 1\right)$

Point B: $I_1^B = 3 \cdot \sigma^0 + \Delta\sigma_1$, $\sqrt{J_2^B} = \dfrac{\Delta\sigma_1}{\sqrt{3}}$

Point C: $I_1^C = \dfrac{1}{D} \ln\left(1 + \dfrac{\varepsilon_v^{p\,0} + \Delta\varepsilon_v^p}{W}\right), \qquad \Delta\varepsilon_v^p = \Delta\varepsilon_v - \dfrac{\Delta\sigma_1}{3K}$

Finally, *the tension cutoff* can be specified with tensile strength of soil that is determined by some form of tension test (Tamrakar et al., 2005).

3. Building Damages Due to Settlements

In Bosnia and Herzegovina numerous of building reconstructions were made. For various reasons, after reconstructions many structures were loaded by additional load. The main problem in such cases is calculation of additional settlements. Basic parameter for this calculation is soil stiffness beneath existing foundation, but it is very difficult to make any test of that soil. In Bosnian regulation it is allowed to increase soil stiffness under foundation "according to state of structure". For illustration, consequences of bad stress–strain modulus estimate are shown in Figs. 7 and 8. Measured settlements of hospital building in Bihać (Bosnia and Herzegovina) are about 30 cm and complete structure of building is damaged.

Figure 7. Measured settlements was 28 cm

Figure 8. Damages on the top (fifth) slab

This problem can be overcome using an elastoplastic constitutive model for soil. If all parameters of elastoplastic model are known, using numerical simulation of loading it is possible to calculate additional settlements under additional loads. Stress state under foundation is heterogeneous even for low level of stresses.

3.1. BEHAVIOR OF CAP MODEL UNDER RIGID FOOT

Behavior of elastoplastic model is analyzed using an analytical model of rigid footing on shallow layer of clay (Zienkiewicz et al., 1975). It is assumed that stratum is supported by a rigid and a very rough base precluding any sliding. The soil weight effect is neglected, so initial stress state is set at the origin of the stress space. The model is analyzed as plane strain problem with material

parameters shown in Table 1. Responses of elastoplastic model are shown in Fig. 9. Figure 9a shows that elements below the footing are in hardening state and others are in elastic state. As the load increases shear yielding zone develops from edge of footing to top of the Prandtl's "rigid zone." The comparison of results obtained by elastoplasic and elastic models, presented in Fig. 10, shows that behavior of these models is similar, but maximal stresses on the edge of footing is higher on the elastoplastic model. Parameters of elastic models are calculated from condition that displacements should be same on both models.

TABLE 1. Parameters of cap model

Elastic parameters	K = 150 MPa, G = 60 MPa
Plastic parameters	c = 30 kPa, φ = 250
	k = 36 kPa, α = 0.189
Hardening parameters	W = 0.003 D = 1.26 mm^2/N
	R = 4
Initial location of cap	$\xi_0 = 240\ kN/m^2$

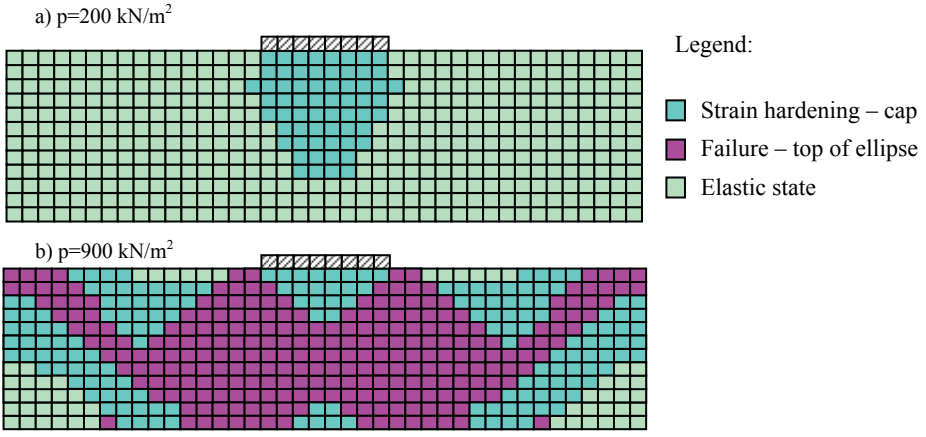

Figure 9. Stress state under rigid foot

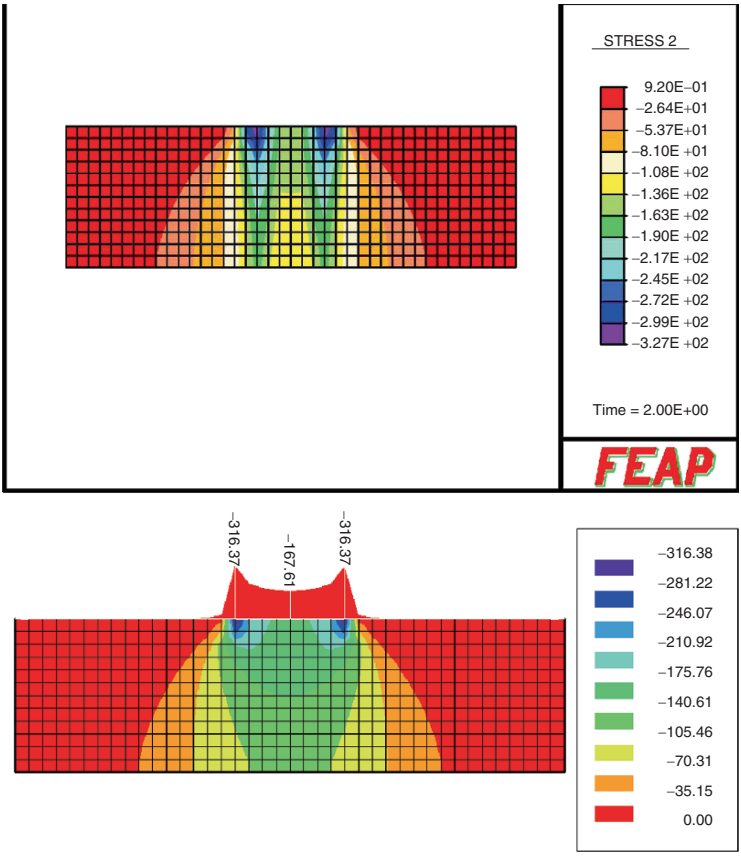

Figure 10. Stress distribution under rigid foot

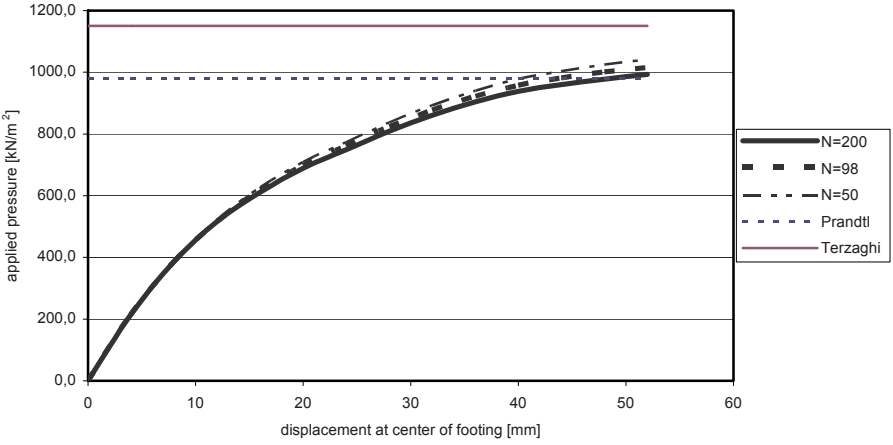

Figure 11. Load–displacement curves

The complete load–displacement response for various number of finite elements is shown on Fig. 11 where the relationship between the applied pressure p and displacement of center of the footing is presented with the well-known Terzaghi's and Prandtl's solutions for bearing capacity. Results show that the computed failure load is close to the Prandtl's solution for chosen hardening parameters.

3.2. BEHAVIOR OF CAP MODEL UNDER FLEXIBLE FOOT

The bearing capacity of a shallow layer of clay is analyzed using a similar analytical model with assumption that stresses beneath the footing are distributed vertically and uniformly.

Stress state at failure load is shown in Fig. 12. The comparison of results obtained by elastoplasic and elastic models, presented in Fig. 13, shows that behavior of these models is similar, but maximal stresses on the center of footing is higher on the elastoplastic model.

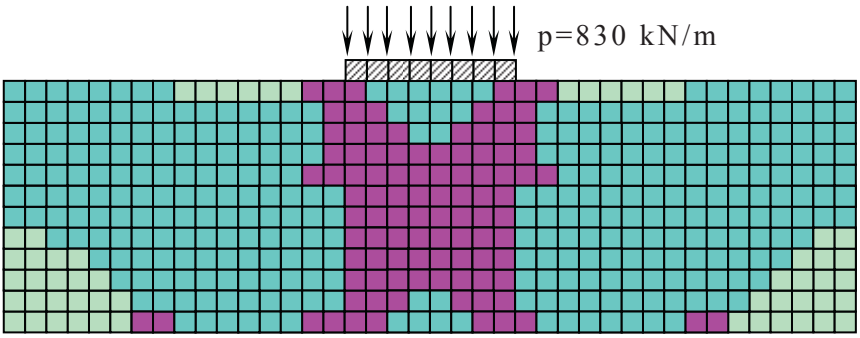

Figure 12. Stress state under flexible foot

This model is used for analysis of influence particular hardening parameters on behavior of cap model. Parameter R is ratio between main ellipse axes. Increasing of parameter R decreases shear strength of model and increases vertical displacements as shown in Fig. 14. It is obvious that higher R value increases deviation from linear behavior of soil. We note in passing that plane cap model is often used as rock model. Loading function of plane cap model is same as elliptic model with R = 0.

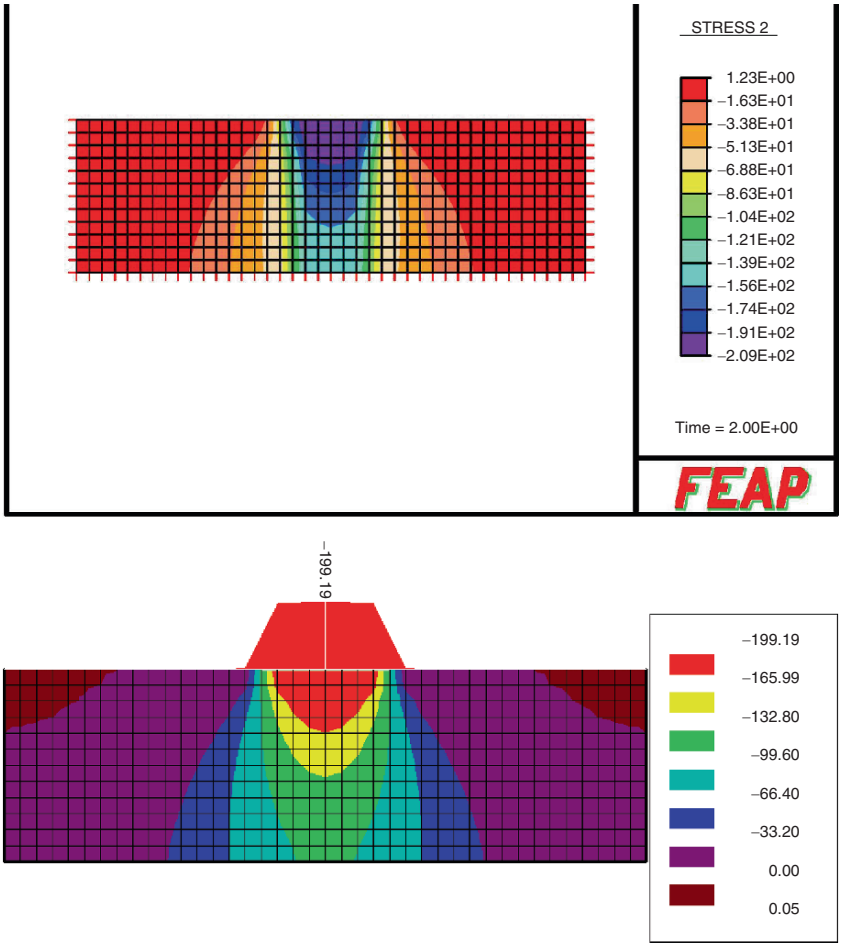

Figure 13. Stress distribution under flexible foot

Parameter W is maximal volumetric strain due to pressure. In other words this parameter shows compressibility of soil. Higher value of parameter W increases displacements at all loading steps and decreases failure load. Hardening parameter D plays the same role. These two parameters have the main influence on the irreversible settlements.

From these theoretical examples it is possible to get following conclusions about comparing elastoplastic and elastic model:

- Stress distribution is similar for low level of stresses. Load-displacement relationship is nearly linear for elastoplastic model. For this range of

stresses hardening cap is employed and more loaded elements become stiffer.

- For higher level of load plastic yielding occurs beneath edge of footing and stresses along footing become nearly constant.
- It is possible to obtain parameters for elastoplastic model and simulate influence of important factors on settlements amount: range of normal stress, stress and strain history, plastic compaction, range of shear strain etc. With two elastic parameters it is not possible consider influence of these factors.

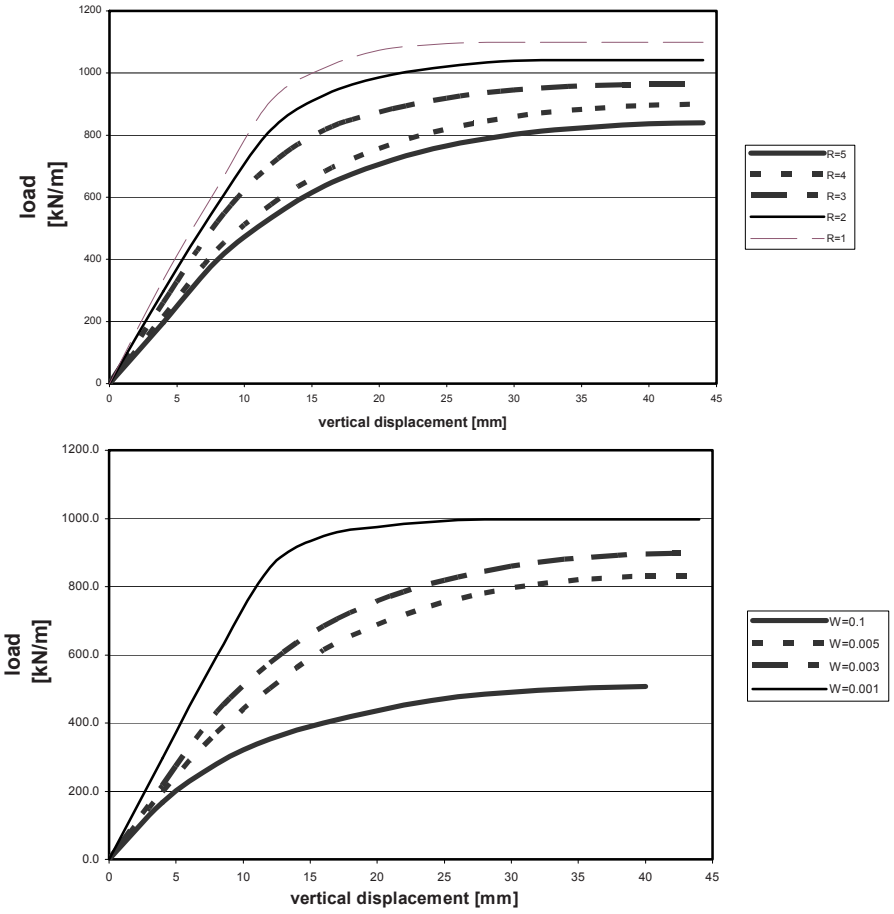

Figure 14. Influence of hardening parameters on model behavior

4. Examples

Several typical examples, where using elastoplastic soil model in problem analysis, are presented in this section.

4.1. FRAME ON FOUNDATION BEAM

Influence of elastoplastic behavior of soil under footings is analyzed on several typical types of foundation. Results of these analyses are compared with results obtained on the same type of structure with elastic model of soil. On Fig. 15 is shown an elastic frame on foundation beam. This example is analyzed by using 2D elastic and elastoplastic models as well as 3D elastoplastic model, since the first yielding occurs in a plane normal to the frame plane. Load is applied in twelve steps from 0 to 160 kN/m.

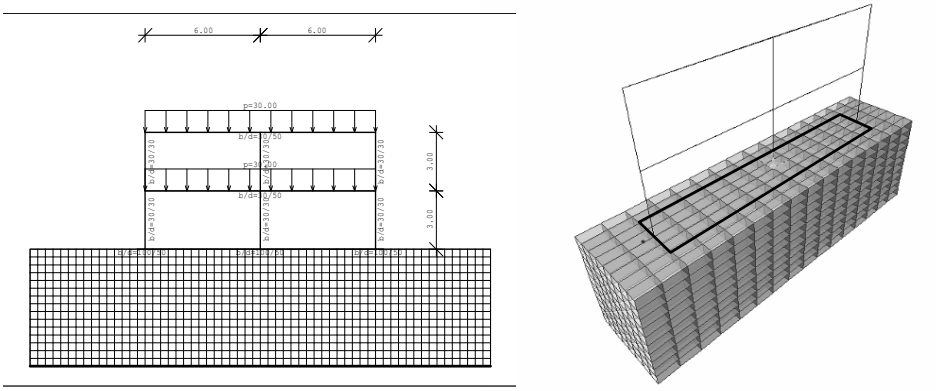

Figure 15. 2D and 3D frame model

Parameters of elastoplastic model of soil are given in Table 1. Parameters of elastic model of soil are calculated using assumption that settlements under middle column are the same for both models.

In Fig. 16 are shown bending moments on foundation beam vs. applied load. Results are closed for loads from 0 to 90 kN/m. On that range load-settlements relationship is linear, and elastoplastic elements are in hardening state.

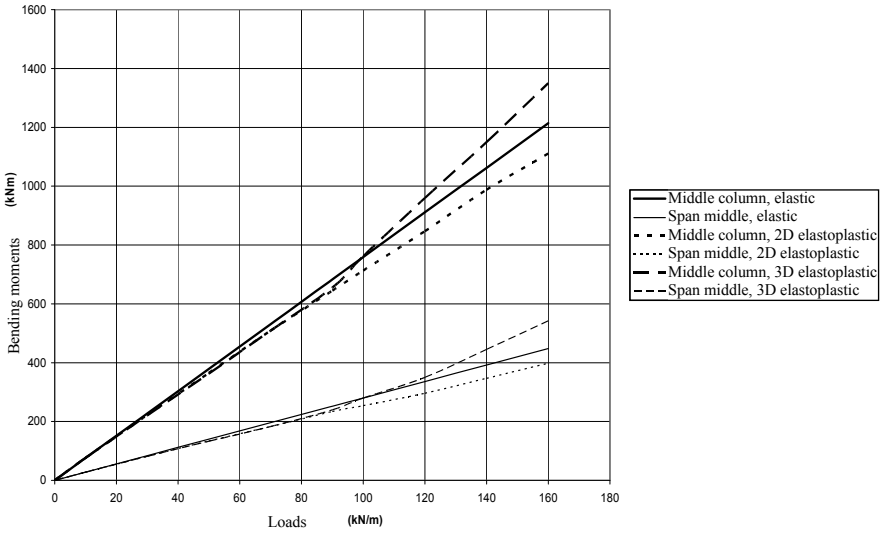

Figure 16. Bending moments on foundation beams

For loads higher then 90 kN/m shear yielding occurs on 3D elastoplastic model. The yielding is in the plane normal to the frame plane. Subsequent to yielding will occur a redistribution of normal stresses along foundation beams. Contact stresses become nearly constant and bending moments are increasing. Failure load of 3D model was about 160 kN/m. For that amount of load, the most of soil elements on 2D elastoplastic model was in the hardening state. On the other side, displacements for loads above 100 kN/m were very high and real structure would be serious damaged due to settlements.

4.2. LANDSLIDE IMPROVEMENT

Traditional approach to design of retaining structures is based on assumption that structures are absolutely stiff. In that case, basic task of designer is proof of structure stability for failure state of soil. This approach was applied in design of landslide improvement in part of Sarajevo called Hambina Carina. Due to landslip on the hither side of drinking water tank it have been seriously damaged as shown in Fig. 17 and water from tank has saturated landslip. Retaining wall supported on solid counterforts was designed. Predicted foundation of counterfort was about 10 m depth where stable layer of marble was situated according to geotechnical investigation. However, excavation of counterfort pit was not possible due to soil quality and high saturation. Therefore, it was decided that counterforts would be replaced by frames. Structural elements of

each frame were two piles 14 m length and the beam which connected the piles. All frames were connected by two beams used for placing geotechnical anchors.

Figure 17. Damages of water tank "Hambina Carina" – upper side

The best approach to calculation of retaining deformable structure in soil is analysis based on elastoplastic model of soil. Analysis was made using plane model shown in Fig. 18. Designed structure is built (see Fig. 19) and displacement was measured for two years. The measured displacements of retaining wall were about three times smaller than those predicted by computations, because all the soil parameter values were assumed on safe side, rather than determined by geotechnical investigations.

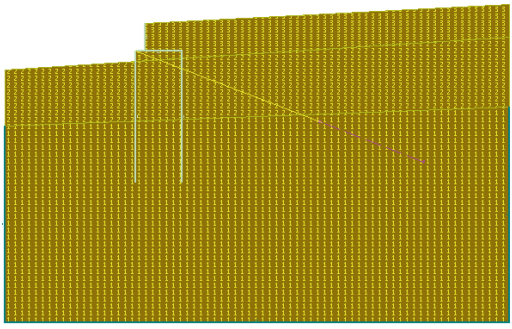

Figure 18. Analysis model

Figure 19. Finished retaining structure

4.3. STRUCTURES NEAR EXCAVATION PIT

The construction of several buildings, with three to five underground floors, has begun in Sarajevo in last 3 years. The main problem in design of excavation pit in urban area is to ensure contiguous buildings. Particularly demanded task was construction of excavation pit near "Unitic" tower in Sarajevo. The edge of excavation pit is 20 m away of tower and depth of excavation is about 13 m. The 20 story-tower is founded on a stiff foundation plate on marl layer 7 m depth.

Design of diaphragm wall was based on equilibrium of plastic state and it was designed as secant pile wall with two rows of pre-stressed geotechnical anchors. According to calculated forces and displacements, dimensions of piles were chosen as well as geotechnical anchors and its pre-stressing forces. In the first days of January excavation was done and inclinometer readings, installed between pit and tower, showed significant movements (see Fig. 20). Geodetic measurements of top of tower were twice times bigger. Tower has inclined, but it was not damaged due to stiff base slab. Further displacements were slowed down by placing the soil ballast in the pit.

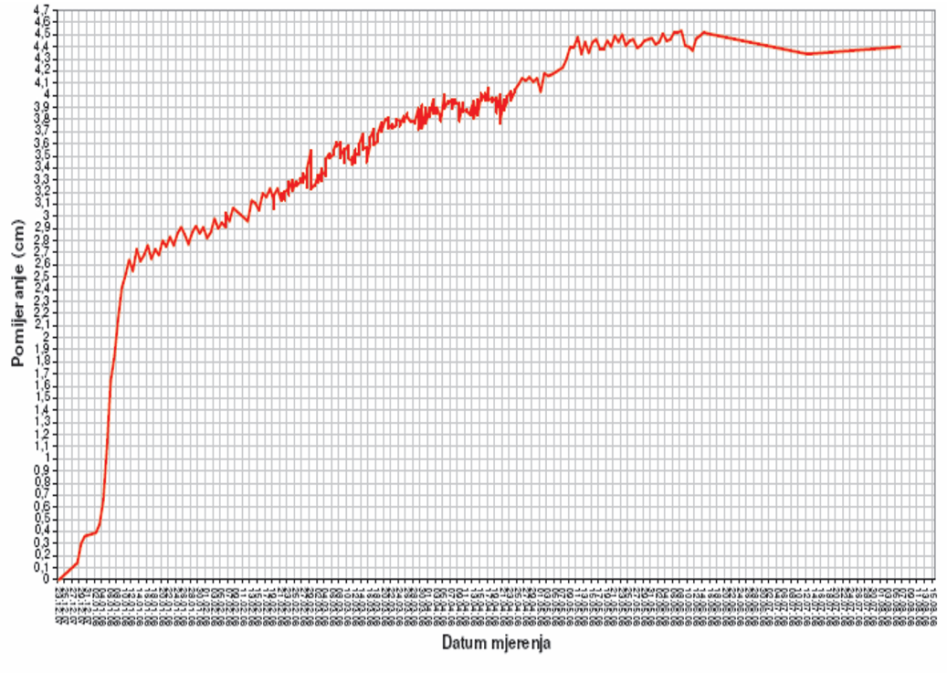

Figure 20. Inclinometer measurements of displacements

New calculation of excavation pit, including tower settlements, was done using Plaxis software with elastoplastic analysis. Calculated vertical and horizontal displacements were much smaller then measured (see Figs. 21 and 22). The problem was in complex characteristics of marl. Namely, marl has a hard quality and all dynamic tests gave 50 blows and more. However, marl is fine structured with layers, so shear strength along the layers is much lower than the obtained ones from the tests. In other words, real marl is anisotropic but model of such material was not available so exact analysis was not possible.

Further excavations, concreting of base slab and building structure was conducted in steps. The underground part of the structure is finalized, and at that moment the total displacement of the tower top is limited to 10 cm. The upper part of the structure is still under construction.

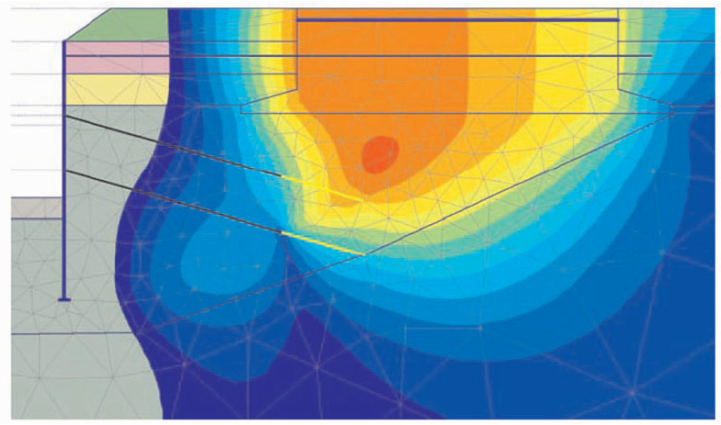

Figure 21. Calculated vertical displacements

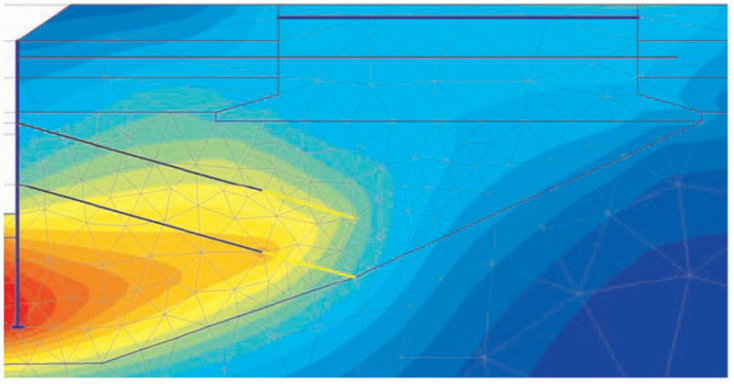

Figure 22. Calculated horizontal displacements

5. Closing Remarks

Linear elastic models of soil provide only limited access to accounting for more realistic support conditions for structures, and the results obtained in that way remain acceptable only for low level of soil stresses and only if adequate elastic parameters are selected. A more realistic representation of soil behavior, which is highly nonlinear and dependent on many parameters, can be provided only by elastoplastic model of soil. Although the models of this kind possess more parameters, they provide much more reliable prediction of soil behavior and

structural damage interpretation from simplified elastic soil model, especially in the parameter values are determined with care.

Nonlinear analysis of soil behavior and its influence on structural damage is not possible to avoid in the following cases: settlements of structures near landslides or excavation pit, structures founded on the heterogeneous soil where redistribution of contact pressure is possible due to local yielding or structures founded on very soft soils where is nonlinear behavior of soil becomes quite significant.

Bibliography

Baladi G.Y., Sandler I.S., Examples of the use of the cap model for simulating the stress-strain behavior of soils, *Plasticity and Generalized Stress-Strain in Geotechnical Engineering*. ASCE, New York, 1981, pp. 649–710.

Bathe K.-J., *Finite Element Procedures in Engineering Analysis*, Prentice-Hall, London, 1996.

Bathe K.J., Snyder M.D., Cimento A.P., Rolph W.D. On some current procedures and difficulties in finite element analysis of elastoplastic response, Computers & Structures, 1980, 12: 607–606.

Chen W.F., Mizuno E. *Nonlinear Analysis in Soil Mechanics*, Elsevier, Amsterdam, 1990.

DiMaggio F.L., Sandler I.S. Material models for granular soils, *Journal of the Engineering Mechanics Division ASCE*, 1971, 97(EM3): 935–950.

Drucker D.C., Gibson R.E., Henkel, D.J. Soil mechanics and work-hardening theories of plasticity, *Transactions, ASCE*, 1957, 122: 338–346.

Dolarević S., Ibrahimbegović A. A modified three-surface elastoplastic cap model and its implementation, *Computers & Structures* 2007, 85: 419–430.

Kojić M., Bathe K.J. *Inelastic Analysis of Solids and Structures*, Springer, Berlin, 2005.

Tamrakar S.B., Mitachi T., Toyosawa Y., and Itoh K. *Development of a New Soil Tensile Strength Test Apparatus*, Geotechnical Special Publications 130–142 & GRI-18; Proceedings of the Geo-Frontiers 2005 Congress, January 24–26, 2005, Austin, Texas.

Taylor R.L., *FEAP – Version 7.5 Theory Manual*, 2003.

Zienkiewicz O.C., Taylor R.L. *The Finite Element Method: Basic Formulation and Linear Problems*, McGraw-Hill, London, 1989.

Zienkiewicz O.C., Humpheson C., Lewis R.W. Associated and non-associated visco-plasticity and plasticity in soil mechanics, *Geotechnique*, 1975, 25(4): 671–689.

FIRE INDUCED DAMAGE IN STRUCTURES AND INFRASTRUCTURE: ANALYSIS, TESTING AND MODELING

A. IBRAHIMBEGOVIC[1*], A. BOULKERTOUS[1], L. DAVENNE[1], M. MUHASILOVIC[2], J. DUHOVNIK[2], AND A. POKRKLIC[3]
[1]*Ecole Normale Supérieure, LMT-Cachan, Civil Engineering, 61 avenue du president Wilson, 94235 Cachan, France*
[2]*Unverisity of Ljubljana, Mechanical Engineering, Slovenia*
[3]*University of Sarajevo, Faculty of Architecture, Bosnia and Herzegovina*

Abstract. In this work we first review the statistical data on large fires in urban areas, presenting a detailed list of causes of fires, the type of damage to structures and infrastructure built of reinforced concrete. We also present the modern experimental approach for studying the fire-resistance of different structural components, along with the role of numerical modeling to provide a more detailed information on quantifying the temperature and heat flux fields. In the last part of this work we provide the refined models for assessment of fire-induced damage in structures built of reinforced concrete, the most frequently used construction material. We show that the refined models of this kind are needed to provide a more thorough explanation of damage and to complete the damage assessment and post-fire evaluations.

Keywords: Fire induced damage, reinforced concrete, structure, infrastructure, fire tests

1. Introduction

The damage of engineering structures and infrastructure due to devastating fire is probably among the most well known natural disasters that the mankind has had to deal with for already more than thousands of years. The most important early risk was widespread use of natural building materials that are quite sensitive

* To whom correspondence should be addressed. e-mail: ai@lmt.ens-cachan.fr

A. Ibrahimbegovic and M. Zlatar (eds.), *Damage Assessment and Reconstruction After War or Natural Disaster*,

to fires (wood, reed, straw), as well as the creation of first large urban zones and increased risks that they represent. Already, at the time of the emperor Neron (64th year B.C.), a large fire broke out in Rome (legend said that Neron himself started it) that in 7 days demolished 10 out of 14 city districts. The fire disasters accelerated with further urbanization and a number of sadly famous disasters have happened throughout the worlds: 'Great Fire' in London (1666), Edinborough (1700), Copenhagen (1728), Stockholm (1750) or Constantinopole (1766). The fire prevention code in urban areas that was proposed and implemented following these disastrous fires (e.g. see ASTM, 1981; Rojtman, 1985), requiring more rigorous rules on construction materials and building space, was partially successful in reducing the number of fires caused by neglect (even though 60% of urban fires are still caused by neglect).

However, these prevention rules are largely insufficient for preventing the fires spread following the natural or man-made disasters, such as earthquakes or explosions. Some known examples of that kind are: the earthquake caused fire in Lisabon (1775) that had about 60,000 victims and the loss of about 85% of the objects; similar post-earthquake fires in San Francisco (1906), or in Tokio and Jokohama (1923); the fire caused by the technical accidents in Fliksboro, England (1974) after pointing of ciklohexane; fire in Mexico City (1984) after the damage on the gas storage; and finally post-accident fire that occurred on the nuclear power plant in Chernobile (1987) which contributed to the more difficult intervention in preventing the leaks of the radioactive particles in the environment. The large fires that occur at war times were numerous, such as fires from last world war in Germany (Hamburg, Drezden) or Japan (Tokio, Jokohama), as well as the wars in Vietnam and Cambodia; and these fires are often as destructive as the military activities. The present day threat of terrorist attacks has further potential of increasing the risk and the damage from accidental fire, with the most recent sadly famous example of the airplane crash into the World Trade Center, which was finally brought down by fire rather than the airplane impact.

Therefore, since we cannot fully control the extreme fire conditions, we focus in this work upon the improvement of the understanding the effects for this kind of disaster and its consequences. Namely, we describe a considerable effort that is spent nowadays to reduce the fire damage by developing and using modern construction materials with enhanced resistance to fire. We also elaborate upon the experimental procedure on testing different structural concepts with respect to fire resistance, along with the numerical procedures for completing the test results in terms of providing the corresponding values of temperature or heat flux distributions. Finally, we also develop numerical models for representing the structural response to fires, which should help provide better damage estimates due to fire for civil engineering structures and infrastructure. We focus herein

upon the most frequently used construction material – the reinforced concrete. The proposed models are quite refined with respect to the usual models used for the same structures under other kind of extreme loading conditions (e.g. earthquake and dead load) and thus require considerable efforts in development, but provide in return much more precise damage estimates. The models presented herein are likely to play important role in constructing the full picture for causes of fire and in providing the complete damage assessment, by running numerical simulations for different fire scenarios.

2. Fire tests and fluid dynamics computations of temperature and heat flux

Fire tests and experimental works, which are carried out currently in routine manner for different construction materials, are often insufficient to decide the fire resistance of structures under heterogeneous temperature and stress fields. Hence, the complementary fire resistance tests are carried out on structure and infrastructure components, trying to enhance understanding of their behavior under sustained devastating fire conditions. No matter how large number of measurements is made in the tests of this kind, one is required in general to supplement those results with the computer aided investigation of the (reactive) fluid flow.

To that end, we will use Computational Fluid Dynamics (CFD) to provide the forecast for movement, propagation of the chemical reaction (during an accidental large-scale fire) and finally important thermodynamic input data on time dependent temperature change and HRR (Heat Release Rate) – flux at the tunnel-cavern or building walls, for further research on resistibility of a RC structures. In this section we present the kind of analysis and typical results that can be obtained for the temperature and flux fields for fires in confined spaces.

We will consider herein the case study of accidental fires in the transformer facilities for the electrical power production (see the photo to the right). We aim at better understanding of the reactive flow phenomena governing the distribution of the gaseous combustion products, which impacts the visibility in first establishing phase of the fire (in such enclosures) and plays decisive parameter that is used in rescuing and protective actions. Further, the influence of heat irradiance that is represented indirectly in the temperature of walls within the cavern, gives the forecast for possible damages in the construction. A thorough understanding of this complex

phenomenon, driven by buoyancy of hot combustion gases in such non-premixed combustion (NPC) can be provided mostly through numerical simulations. Results of the performed study applying the RANS approach for turbulence treatment in the numerically investigated flow in the enclosure of the power-transformer-station show us here the distribution of the temperature-fields and the heat radiation-contours, providing the pertinent information upon thermal loads to be applied on structures.

Several studies of accidental (both pool fires and) fires in enclosures (see Holmstedt et al., 1996; Miles et al., 1999; Wighus, 1994; Fay, 2003; Vidmar and Petelin, 2006), can be consulted for complementary information. The large scale fires are also studied from standpoint of post-event-investigations (see Chow and Kot, 1980; Leitner, 2001; Gabay, 2002) and their negative consequences (Bendelius, 2002), in order to help provide the guidelines of their treatment. Field-model codes that have been tested in CFD-research (see Magnussen and Hjertager, 1976), do report on good capability of these numerical approaches, used in handling the gaseous reacting flows in covered objects. In spite of the first hardware limitations, a decade and half ago, allowing computational domains with few thousands cells (see Kumar and Cox, 1985, 1988), satisfying results were accomplished in attempts of both validating (see Chasse, 1993; Briollay and Chasse, 1994; Kumar and Cox, 1986; Tuovinen, 1994; Kunsch, 2002; McGrattan, 2002) of software tools and aimed CFD-prognoses for particular explored cases of these fluid-flow phenomena (see Beard et al., 1993).

The treating of the turbulent diffusion flames, one of a characteristic of large-scale fires, was incorporated in codes in terms of an extra source term accounting for the effect of buoyancy in turbulent mixing. These developments are carried out and validated for special purpose codes (see Miles, 2006; Magnussen and Hjertager, 1976; Miles and Kumar, 2004) that use the Cartesian mesh only and assume simple one-step chemistry for combustion modeling. The local reaction rate was calculated from a modified version of the eddy break-up mixing model. A comparatively slow mixing of fuel with oxidant (air) is used to control the rate of reaction. Handling both steady and transient flows, treating the turbulence, the RANS models (including variety of boundary conditions and wall functions with modifications for wall roughness) have been compared in latest studies (see Gao et al., 2004). Following up on these studies (see Sanmiguel-Rojas et al., 2007), and trying to investigate transversal prompt-ventilation in the industrial buildings, we performed transient simulation applying k-ε turbulence treatment of large-scale fire in a newly constructed power-transformer unit, where possible accidental scenario was presumed.

In this study the flow phenomena are computed by the Reynolds Averaged Navier–Stokes (RANS) equations, with the turbulence k-ε model (see Britter and Neophytou, 2005), representing the major characteristic of the applied

CFD-investigation-tool of the FLUENT; and handling the buoyancy by applying the Boussinesq approximation. This approach, is not affected by fluctuation of initial conditions, offering more accurate presentation of the time dependent flow – particularly the distribution of the gaseous combustion products (Liu et al., 2004). Since the investigations have shown that the Mach Number was of the order of 0.022, such a flow can be assumed as incompressible (Ferziger and Peric, 2001). Since incompressible, the fluid does not undergo thermal-caused expansion while crossing the reaction front and the reaction makes no impact onto flow-velocity. Further assumption, to have a planar propagation front of combustion in a motionless fluid, leads to the application of the Boussinesq approximation (Baum et al., 1995) without external forces (Vladimirova, 2006). Here, the flow velocity obeys the incompressible Navier–Stokes equation with a temperature-dependent force term.

The change of temperature is described by an advection–reaction–diffusion equation. For this incompressible gaseous reactive flow at low velocity, the governing equations of the combustion-induced flow read:

$$\frac{\partial \overline{v}_j}{\partial x_j} = 0 \tag{1}$$

$$\frac{\partial \overline{v}_i}{\partial t} + \frac{\partial \left(\overline{v}_i \overline{v}_j \right)}{\partial x_j} = -\frac{1}{\rho} \frac{\partial \overline{p}}{\partial x_i} + \frac{1}{\rho} \frac{\partial \overline{\tau}_{ij}}{\partial x_j} - g_i \alpha \Delta \overline{T} \tag{2}$$

$$\frac{\partial \overline{T}}{\partial t} + \frac{\partial \left(\overline{T} \overline{v}_j \right)}{\partial x_j} = \frac{\partial}{\partial x_j} \left(\frac{\lambda}{\rho c_p} \frac{\partial \overline{T}}{\partial x_j} \right) + \frac{1}{z} R\left(T \right) \tag{3}$$

Here $\overline{v}_i$ denotes the average velocity component, $\overline{T}$ the mean local temperature, $\overline{p}$ the pressure, ρ the density, t the time and x_i the space coordinates. The R(T) = ¼ T (1 – T) stands for reaction rate (Vladimirova, 2006) where the reciprocal value of reaction time-scale is represented by z, λ is the thermal conductivity, c_p is the heat capacity at the constant pressure. Temperature T will be used as expression for reaction-progress-variable as well, whose purpose is to distinguished burned, unburned and partially burned state, providing an easy interpretation of flame propagation. The term $-g_i \alpha \Delta \overline{T}$ denotes buoyancy, treated according to the Boussinesq approximation, where $\Delta \overline{T}$ is showing the difference between local and reference temperature. The symbol g denotes the gravity and α is the coefficient of thermal expansion. The model for the stress tensor (Jongen and Gatski, 2000), $\overline{\tau}_{ij}$ is related to the local strain rate:

$$\tau_{ij} = (\tau_{ij})_N + (\tau_{ij})_T \tag{4}$$

where we distinguish between the Newtonian stress $(\tau_{ij})_N = 2\mu\overline{S}_{ij}$ featuring molecular viscosity; and the turbulent Reynolds stress $(\tau_{ij})_T = 2\mu_T\overline{S}_{ij}$, since the stress rate tensor $\overline{S}_{ij}$ is defined as:

$$\overline{S}ij \equiv \frac{1}{2}\left(\frac{\partial v_i}{\partial x_j} + \frac{\partial v_j}{\partial x_i}\right) \tag{5}$$

and the turbulent viscosity:

$$\mu_T = C_\mu \frac{k^2}{\varepsilon} \tag{6}$$

with k the turbulent kinetic energy and ε the dissipation rate of turbulent energy. The applied k-ε model (Leupi, 2005) is a two-equation eddy viscosity model (see Zhang et al., 2002) that uses transport equations for these two variables (see Britter and Woodburn, 1996). One of these equations governs the distribution through the field of k, the local kinetic energy of the fluctuating motion. The other one leads to the energy dissipation rate ε (Malin and Markatos, 1982).

$$\frac{\partial k}{\partial t} - \nabla\cdot\left(C_\mu \frac{k^2}{\varepsilon}\nabla k\right) = C_\mu \frac{k^2}{\varepsilon} P_d - \varepsilon - G_b \tag{7}$$

$$\frac{\partial \varepsilon}{\partial t} - \nabla\cdot\left(C_\varepsilon \frac{k^2}{\varepsilon}\nabla \varepsilon\right) = C_1 k P_d - \frac{\varepsilon}{k}\left(C_3\lambda_v N^2 + C_2\varepsilon\right) \tag{8}$$

The energy term $G_b = \alpha g_i \frac{\mu_t}{Pr_t}\nabla\overline{T}$ is modeling the buoyancy effects, where Pr_t denotes turbulent Prandtl Number (which is of the order of one). The constants are given: C_1=0.126, C_2=1.92, C_μ=0.09, C_ε=0.07.

The applied tool within the CFD-approach (the k-e model) belongs to the state-of-the-art for the turbulence treatment in simulations of the large-scale (accidental) combustion, with no limitation on the shape of the grid. In order to test the grid-independence of computed results, we ran computations with two different grids: one with a grid of 759,646 tetrahedral cells and the other with an unstructured grid of 1,611,723 hexahedral cells – see Fig. 1. The grids were prepared by using the GAMBIT-mesh generator. Both grids were capable of providing sufficient solution accuracy with respect to the computational domain corresponding to the interior the building of power-transformation station, which has the length of 25 m of, the width of 7 m and the height of 8 m.

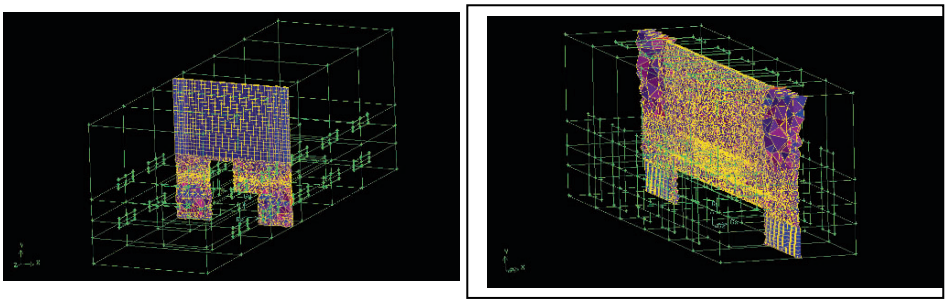

Figure 1. Different grids (with roughly 1,600,000 or 750,000 cells), adapted to the "L-shape" of electric-power-appliance and the interior space of the building of the transformer-unit

For transient simulations (a CFD-mode that was applied in this study (see Brunello et al., 2002) the governing equations must be discretized in both space and time (see Versteeg and Malalasekera, 1995; Sawley and Drotz, 2003). We choose the implicit time-integration and the standard finite volume method (Versteeg and Malalasekera, 1995) for space discretization, along with operator split solution method. The consistent linearization of these equations results in a set of linear equations for each cell in the computational domain, containing the unknown variable at the cell centre as well as the unknown values in surrounding neighbouring cells. In the case when the pressure field and face mass fluxes are not known, FLUENT (Sawley and Drotz, 2003) uses a co-located scheme, where pressure and velocity are both stored at cell centres. The estimation of the boundary conditions in this CFD-based investigation was supported by the experience of some previous studies (Edwards and Hwang, 2005). So were ventilation duct on the roof of the building characterised as open (pressure) boundaries with minor pressure increase or pressure-drop of 10 Pa. The fuel "pool" – the simulated fire-place on the electric-power appliance, was determined by the constant max flux rate of 0.101 kg/m²s having hydraulic diameter of 5.67 m for an approximate 50 MW-heptane fire. The initialisation of computational values for the velocity and pressure was made throughout the whole domain since the global temperature was set to 293 K. The station building walls, were assumed to be adiabatic barriers. This decision was based on some previous research practice. However, a more realistic hypothesis for fire resistance studies of civil-engineering structures would consider the thermal conductivity of walls (e.g. for concrete mixed out of lime-stone sand, we can take $\lambda = 2.3$ W/mK, Gawin et al., 2004) that could provide the appropriate boundary conditions. For our numerical simulations we use wall function boundary conditions in order to avoid a fine meshing in the boundary layer, next to the cavity-walls and we can thus reduce the computational cost. More precisely, the wall shear stress was obtained from the logarithmic law of wall ("wall function") for the distance from the wall, y, the von Karman constant $\kappa = 0.41$ and the constant $C = 9.793$:

$$\frac{\overline{v}}{v_\tau} = \frac{1}{\kappa} ln\, C \frac{v_\tau y}{v} \tag{9}$$

where v_τ denotes the friction velocity, featured within the expression for the wall shear stress:

$$\tau_W = \rho v_\tau^2 \tag{10}$$

The initial conditions of the simulation of this accident, the combustion was assumed to apply to the whole surface that was proclaimed to be fire-source. The numerical solution for the fire-accident in the power-transformer unit is presented in Fig. 2 for the fourth second of this large-scale combustion event. The contours of temperature field show quick fire development with full (negative) impact on the structure.

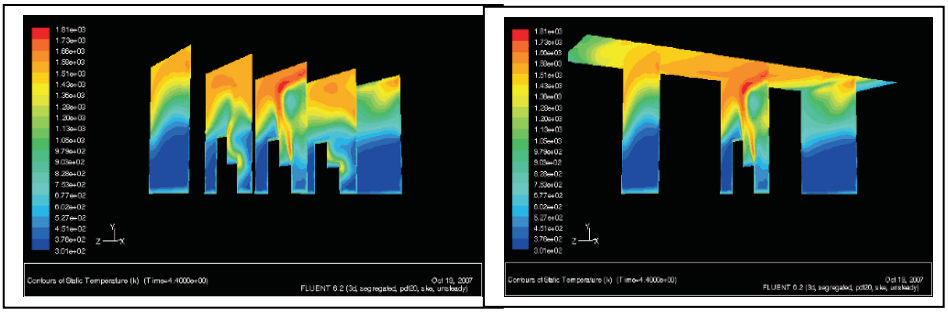

Figure 2. Contours of temperature field in inner space of the power-transformer unit during the simulated accident plotted at several locations within the cavity with typical "mushroom" or "tree-shaped" form of a large-scale pool-combustion; note that the temperature raises over the melting point of the steel in the fourth second of the accidental large-scale fire

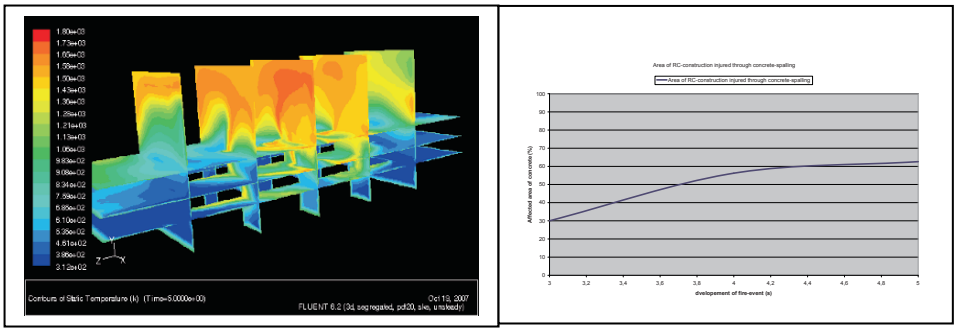

Figure 3. Contours of temperature field in inner space of the power-transformer unit during the simulated accident plotted at several locations within the cavity; note that the temperature raises to the RC spalling temperature in the fifth second of the accidental large-scale fire

For the chosen "fire-size" of this accident is 30 MW as well as a very large volume of inflammable fluid, contained within an electric devices of a power-transformer and switch-unit, contribute to a rather quick fire-spreading accompanying the high thermal power of this confined large-scale accident. The computed results show that after only 5 s (see Fig. 3) of the combustion the temperatures will reach above ~1,100 K (+875°C). The temperatures of this kind can cause a significant damage in structures or infrastructure. In the next section, we review some of the typical damage of most frequently used construction materials.

3. Damage representation due to fire for structures and infrastructure

The reinforced concrete represents the most frequently used construction material for structures and infrastructure. The judicious combination of steel and concrete has provided the best for construction cost, and also the most difficult one to comprehend in terms of its nonlinear inelastic behavior. The most adequate reinforced concrete model depends upon the goal of the present analysis, and the estimate of the damage we would like to obtain. In that respect the choice should be made between: (i) global integrity of the structure built of reinforced concrete under extreme loading, (ii) local integrity of concrete under extreme loading case and (iii) durability of concrete under aggressive environment. The models for each of the listed goals ought to be more and more detailed; see Fig. 4.

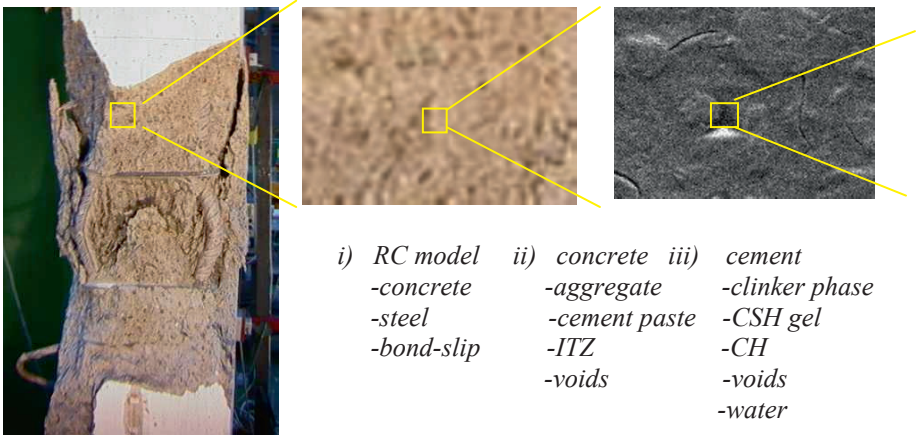

Figure 4. Different models of concrete for computing: (**a**) structure integrity (reinforced-concrete), (**b**) failure criteria (two-phase model of concrete), (**c**) structure durability (multi-phase model of cement)

One of the most dangerous damage mechanisms produced by the large-scale fires, which can especially affect the high-performance concrete, is produced by the spalling phenomena. There exist a couple of competing explanations for spalling (see Bazant and Kaplan, 1996; Ulm et al., 1999; Gawin et al., 2004; Schrefler et al., 2005), illustrated in Fig. 5. The first assumes that the spalling occurs as the joint result of high temperature gradient distribution through the thickness combined with restrained deformation in a massive structure (e.g. tunnel fire, see Tan 2002 and SINTEF 2003), which will jointly produce a compression zone on the surface and the tensile zone in the interior that lead to spalling. The second explanation considers spalling as the results of high temperature gradients accelerating different multi-physics processes, combining thermal (thermal dilatation), chemical (dehydration of cement paste), hydro (evaporation of the liquid pore water, associated by the vapour pressure increase). Accordingly, the main factors that influence spalling are the temperature distribution and its variation inside the concrete element, as well as the characteristics of the considered section (size, shape, permeability, mean pore radius, concrete strength). The vapour pressure can play an important role when a high value is reached during heating, which can produce a kind of explosive spalling, especially in high-density materials like high and ultra high performance concrete.

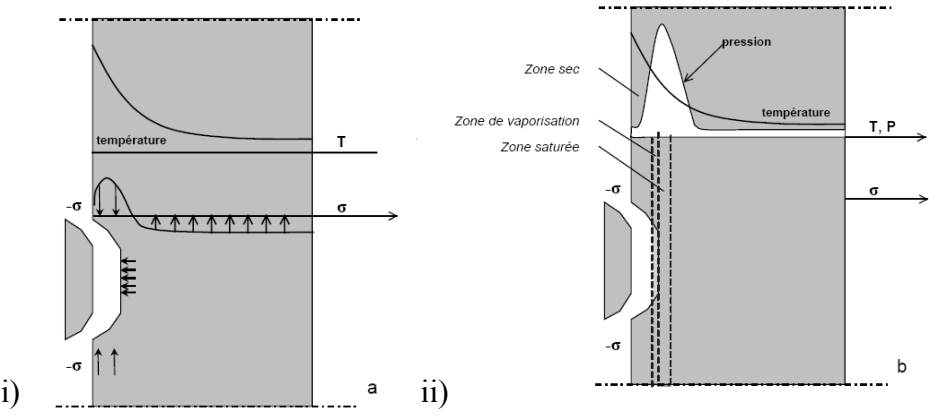

Figure 5. Two different explanations of the spalling phenomena under fire: (**a**) mechanical damage due to high temperature gradient distribution through the thickness, (**b**) pore pressure build-up as a part of hydro-thermo processes under high temperature

The mentioned processes cause an increase of the concrete intrinsic permeability. The joint effect of temperature, gas pressure and material damaging (micro-cracks development) influence the intrinsic material permeability as well. The recent results (see Brunello et al., 2002) indicate that within 5 to 7

min (of fire-combustion only sized as 2.5 MW) inside the concrete walls of a building cavern (at the places differently elevated above the catastrophic fire-place) at the depth of maximum 60 mm from the surface of the concrete, the temperatures of about 700°C are to be noticed – causing the vapour pressure (in the concrete) to reach almost six times higher value than at the ambient, forcing so the kinetics of the thermo-chemical damage.

The spalling phenomena can also be influenced by mechanical damage or cracking of concrete. In fact, it becomes quite important to provide a very reliable representation of the crack spacing and opening in order to evaluate the risk for accelerating the spalling phenomena and the resulting porosity. The key point in that sense is the adequate choice of numerical model for representing the cracks in concrete. The models of this kind will have at least two dissipative mechanisms, the first related to the fracture process zone with a large number of micro cracks and the second related to the localized failure with a large macro crack. Each of mechanisms can be described by a particular plasticity failure criterion (we could also choose the damage criteria). We can thus obtain the basic set of governing equations, which can be written as illustrated in Fig. 6:

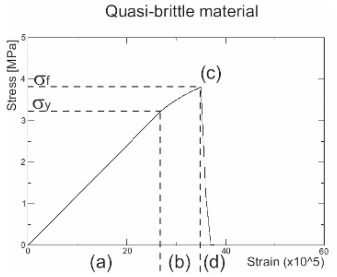

$$
\begin{aligned}
\epsilon &= \epsilon^e + \bar{\epsilon}^p + \bar{\bar{\epsilon}}^p \, \delta x \\
\Psi &\quad (\epsilon^e, \bar{\xi}, \bar{\bar{\xi}}) = \bar{\Psi}(\epsilon^e, \bar{\xi}) + \bar{\bar{\Psi}}(\bar{\bar{\xi}}) \\
\bar{\Phi} &\quad (\sigma, \bar{q}) := |\sigma| - (\sigma_y - \bar{q}) \\
\bar{\bar{\Phi}} &\quad (\sigma, \bar{\bar{q}}) := |t| - (\sigma_f - \bar{\bar{q}}) \\
\dot{\bar{\epsilon}}^p &= \dot{\bar{\gamma}} \frac{\partial \bar{\Phi}}{\partial \sigma} \quad ; \quad \dot{\bar{\xi}} = \dot{\bar{\gamma}} \quad ; \quad \bar{\Phi} \leq 0 \quad ; \quad \dot{\bar{\gamma}} \geq 0 \quad ; \quad \dot{\bar{\gamma}} \bar{\Phi} = 0 \\
\dot{\bar{\bar{\epsilon}}}^p &= \dot{\bar{\bar{\gamma}}} \frac{\partial \bar{\bar{\Phi}}}{\partial \sigma} \quad ; \quad \dot{\bar{\bar{\xi}}} = \dot{\bar{\bar{\gamma}}} \quad ; \quad \bar{\bar{\Phi}} \leq 0 \quad ; \quad \dot{\bar{\bar{\gamma}}} \geq 0 \quad ; \quad \dot{\bar{\bar{\gamma}}} \bar{\bar{\Phi}} = 0
\end{aligned}
$$

Figure 6. 1D representation of failure model for massive structures and governing equations postulating: (i) additive split of total deformation into elastic, smooth plastic and localized plastic field, (ii) strain energy in terms of elastic strain and hardening variables, (iii) plasticity criteria for smooth and localized field, and the evolution equations for the internal variables (note that one over-bar pertains to the FPZ mechanisms, and two bars is used for the internal variables describing the localized failure)

The typical result obtained with models of this kind is given in Fig. 7, for the case of notched specimen under non-proportional loading that starts with tension followed by shear, where we show the spreading of different damage mechanism with contours of micro-cracks and the element-based orientation of macro-cracks. We also show in Fig. 7 the typical sequence of mechanical damage for massive concrete structure, which first starts with micro-cracks followed by macro-cracks.

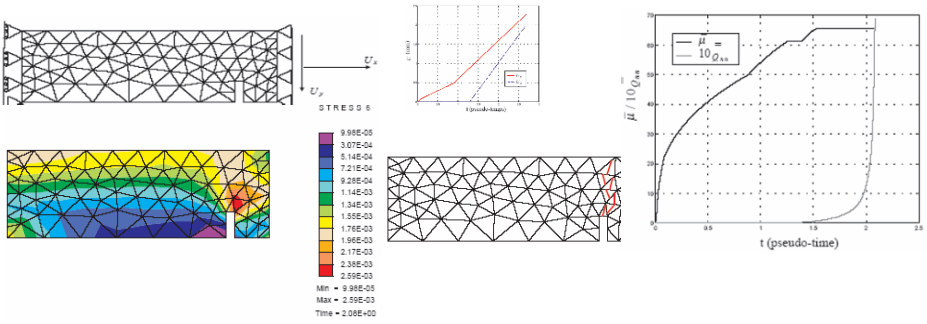

Figure 7. Micro and macro cracks for notched specimen under tensile and shear loading: loading and boundary conditions, contours of micro cracks, orientation of macro cracks, and time evolution of both damage mechanisms

In a recent work (see Ibrahimbegovic et al., 2009) we have developed the predictive model for cracking of reinforced concrete, which integrates the described concrete model for micro and macro cracks representation, along with the bond-slip model for concrete-steel interface (see Dominguez et al., 2005) accounting for frictional sliding and confinement and the standard plasticity model for steel bars including both hardening and softening that can represent different stages of failure mechanism (see Ibrahimbegovic and Brancherie, 2003). The original feature of this model for reinforced concrete concerns the X-FEM based description of the kinematics of the bond-slip that fits within the standard computer program architecture (see Fig. 8):

$$\mathbf{u}(\mathbf{x})|_{\Omega^e} = \sum_{i=1}^{4} N_i(\mathbf{x})(\mathbf{d}_i^c + \sum_{j=1}^{2} M_j(x)\boldsymbol{\alpha}_j) \tag{11}$$

where N_i are standard shape functions of the chosen isoparametric element, d_i^c are concrete nodal displacements, M_j is the corresponding function introducing the global representation of bond-slip along the complete steel bar and , α_j is the nodal value of slip variable. The steel bar nodal displacement is obtained as the sum of the concrete displacement and the nodal value of bond-slip, $d_i^s = d_i^c + \alpha_i$.

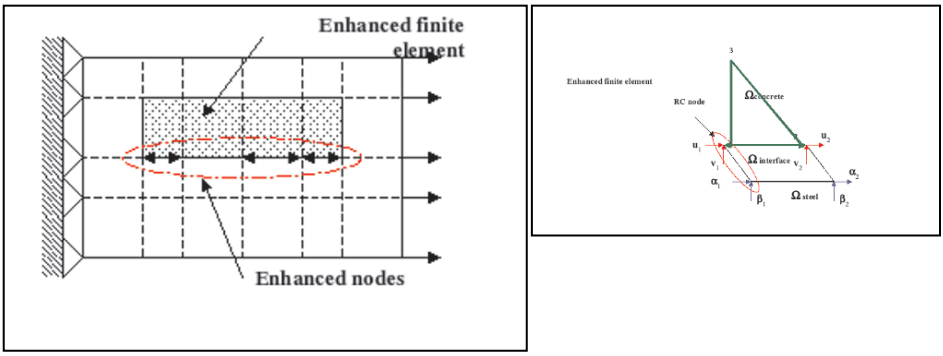

Figure 8. Extended finite element representation of reinforced concrete kinematics

The weak form of equilibrium equations associated with concrete displacements can be written:

$$\begin{aligned}
&\mathbf{r}^{cs} := \mathop{\mathbb{A}}_{e=1}^{n_{el}} \mathbf{f}^{c,int,e}(\mathbf{d}^c_{n+1}) + \mathop{\mathbb{A}}_{e=1}^{n^{bs}_{el}} \mathbf{f}^{s,int,e}(\mathbf{d}^c_{n+1}, \boldsymbol{\alpha}_n) - \mathbf{f}^{ext}_{n+1} = 0 \ ; \\
&\mathbf{f}^{c,int,e}_i(\mathbf{d}^c_{n+1}) = \int_{\Omega^e} (\nabla^s N_i)^T \boldsymbol{\sigma}^c_{n+1}(\mathbf{d}^c_{n+1}) dV \ ; \\
&\mathbf{f}^{s,int,e}_j(\mathbf{d}^c_{n+1}, \boldsymbol{\alpha}_n) = \int_{\Gamma^e_{bs}} (\tfrac{dM_j}{dx})^T \sigma^s_{n+1}(\mathbf{d}^c_{n+1}, \boldsymbol{\alpha}_n) dA \ ; \\
&\mathbf{f}^{ext,e}_{i,n+1} = \int_{\Omega^e} \mathbf{N}^T_i \mathbf{b} dV
\end{aligned} \tag{12}$$

where σ^c and σ^s are concrete and steel stress computed from the corresponding constitutive equations for the fixed value of bond slip. The remaining set equilibrium equations are associated only with the slip variation along a particular reinforcement bar:

$$\begin{aligned}
&\mathbf{r}^{bss} := \mathop{\mathbb{A}}_{e=1}^{n^{bs}_{el}} [\mathbf{f}^{s,int,e}(\mathbf{d}^c_{n+1}, \boldsymbol{\alpha}_{n+1}) + \mathbf{f}^{bs,int,e}(\boldsymbol{\alpha}_{n+1})] = 0 \ ; \\
&\mathbf{f}^{s,int,e}_j(\mathbf{d}^c_{n+1}, \boldsymbol{\alpha}_{n+1}) = \int_{\Gamma^e_{bs}} (\tfrac{dM_j}{dx})^T \sigma^s_{n+1}(\mathbf{d}^c_{n+1}, \boldsymbol{\alpha}_n) dA \\
&\mathbf{f}^{bs,int,e}_j(\boldsymbol{\alpha}_{n+1}) = \int_{\Gamma^e_{bs}} \mathbf{B}^{bs,T} \boldsymbol{\sigma}^{bs}_{n+1}(\boldsymbol{\alpha}_{n+1}) dA
\end{aligned} \tag{13}$$

where σ^{bs} is the bond-slip stress. The operator split computational procedure is proposed for computing the response of this kind of reinforced concrete model can be summarized as follows:

-for $n = 0, 1, 2 \ldots$
-Given: $\mathbf{d}_n^c$, $\boldsymbol{\alpha}_n$, internal variables at t_n
-Find: $\mathbf{d}_{n+1}^c$, $\boldsymbol{\alpha}_{n+1}$, internal variables at t_{n+1}
-Iterate: $(i) = 1, 2 \ldots$
-Iterate: $(j) = 1, 2 \ldots$
compute internal variable evolution for given $\mathbf{d}_{n+1}^{c,(i)}$, $\boldsymbol{\alpha}_{n+1}^{(j)}$

$$\frac{\partial \mathbf{r}^{sbs,(i)}}{\partial \boldsymbol{\alpha}_{n+1}} (\boldsymbol{\alpha}_{n+1}^{(j+1)} - \boldsymbol{\alpha}_n^{(j+1)}) = -\mathbf{r}^{sbs}(\mathbf{d}_{n+1}^{c,(i)}, \boldsymbol{\alpha}_{n+1}^{(j)}) \; ;$$

-Test convergence locally
IF $\| \mathbf{r}^{sbs}(\mathbf{d}_{n+1}^{c,(i)}, \boldsymbol{\alpha}_{n+1}^{(j)}) \| > tol$ NEXT (j)
ELSE $\| \mathbf{r}^{sbs}(\mathbf{d}_{n+1}^{c,(i)}, \boldsymbol{\alpha}_{n+1}^{(j)}) \| < tol \Rightarrow \boldsymbol{\alpha}_{n+1}^{(i+1)} = \boldsymbol{\alpha}_{n+1}^{(j+1)}$ NEXT (i)

$$\left[\frac{\partial \mathbf{r}^{cs}}{\mathbf{d}_{n+1}^{c,(i)}} - \frac{\partial \mathbf{r}^{cs}}{\boldsymbol{\alpha}_{n+1}^{(i)}} \left(\frac{\partial \mathbf{r}^{sbs}}{\boldsymbol{\alpha}_{n+1}^{(i)}}\right)^{-1} \frac{\partial \mathbf{r}^{sbs}}{\mathbf{d}_{n+1}^{(i)}}\right] (\mathbf{d}_{n+1}^{c,(i+1)} - \mathbf{d}_{n+1}^{c,(i)}) = -\mathbf{r}_{n+1}^{cs,(i)} \tag{14}$$

-Test convergence globally
IF $\| \mathbf{r}^{cs}(\mathbf{d}_{n+1}^{c,(i+1)}, \boldsymbol{\alpha}_{n+1}^{(i+1)}) \| > tol$ NEXT (i)
ELSE $\| \mathbf{r}^{cs}(\mathbf{d}_{n+1}^{c,(i+1)}, \boldsymbol{\alpha}_{n+1}^{(i+1)}) \| < tol \Rightarrow \boldsymbol{\alpha}_n \longleftarrow \boldsymbol{\alpha}_{n+1}^{(i+1)}, \mathbf{d}_n \longleftarrow \mathbf{d}_{n+1}^{c,(i+1)}$

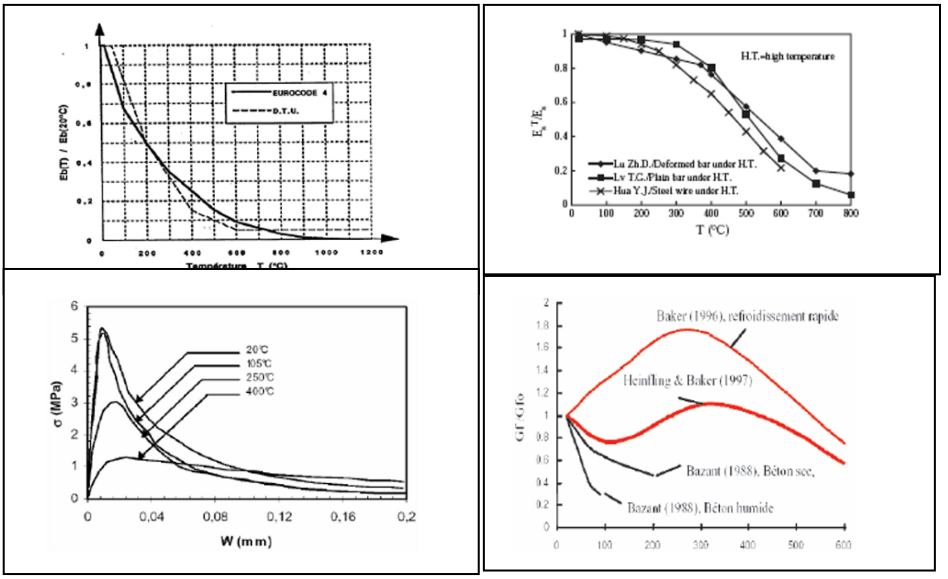

Figure 9. Temperature dependence of concrete and steel material properties showing a drop in Young's modulus values with temperature increase and change in elastic limit and in fracture energy as a function of temperature

The proposed procedure can be placed within the framework of incremental-iterative analysis with no need to change the standard computer program architecture.

When exposed to high temperatures, the material properties of steel and concrete should be modified accordingly. We can see in Fig. 9 that Young's modulus of concrete and steel drop significantly with temperature increase and so does their limits of elasticity (fracture and yield stress, respectively).

This temperature dependence of material properties is taken into account by modifying the corresponding fracture criteria for steel (see Ibrahimbegovic and Chorfi, 2002), bond-slip and concrete. The latter leads to modified form of failure criteria for micro-cracks and macro-cracks, which can be written in terms of the anisotropic damage model:

$$\begin{aligned} \bar{\phi}^c(\sigma,\bar{q},T) &= \sqrt{\sigma\cdot D^e(T)\sigma} - \tfrac{1}{\sqrt{E(T)}}(\bar{\sigma}_f(T)-\bar{q}) \le 0 \\ \bar{\bar{\phi}}^c_n(\sigma,\bar{\bar{q}},T) &= t_\Gamma\cdot n - (\bar{\bar{\sigma}}_f(T)-\bar{\bar{q}}(T)) \le 0 \\ \bar{\bar{\phi}}^c_s(\sigma,\bar{\bar{q}},T) &= t_\Gamma\cdot m - (\bar{\bar{\sigma}}_s(T)-\tfrac{\bar{\bar{\sigma}}_s(T)}{\bar{\bar{\sigma}}_f(T)}.\bar{\bar{q}}(T)) \le 0 \end{aligned} \tag{15}$$

where $D^e(T)$ is the temperature dependent damage compliance produced by micro-cracks in concrete, σ_f is elasticity limit indicating the initiation of micro-cracks, t_Γ is the driving traction at the macro-crack and σ_f and σ_s are the limits to macro-crack activation in mode I and mode II; see Brancherie and Ibrahimbegovic (2009) or Kucerova et al. (2009), for more details about the mechanical form of this model. The computational procedure that accounts for thermomechanical coupling is equivalent to the one developed previously for masonry structures (see Ibrahimbegovic et al., 2005; Colliat et al., 2005; Kassiotis et al., 2009).

We close this section by presenting the results of a couple of numerical simulations for computing the crack spacing and opening in reinforced concrete structures. The current practice of evaluating fire resistance of RC beams is based on standard fire test, in which the beam is exposed to a standard fire such as ISO 834. While standard fire resistance tests are useful benchmarks to establish the performance of RC elements under standard fire condition, they should not be relied upon to determine the survival time of RC elements under realistic fire scenarios, since they can often define less severe heating environments than those encountered in real fires. For example, we illustrate in Fig. 10 the temperature and flux time-evolutions for some realistic scenarios, derived from experimental data used for infrastructure in nuclear industry. It is important to observe in each of those scenarios a decay phase, which can also play an important role in defining the final damage of RC elements. Namely, the cross section enters a cooling phase, in which either the reinforcing steel recovers

parts of its strength and stiffness, and thus the fire resistance increase, or in the opposite produces the cracking upon unloading.

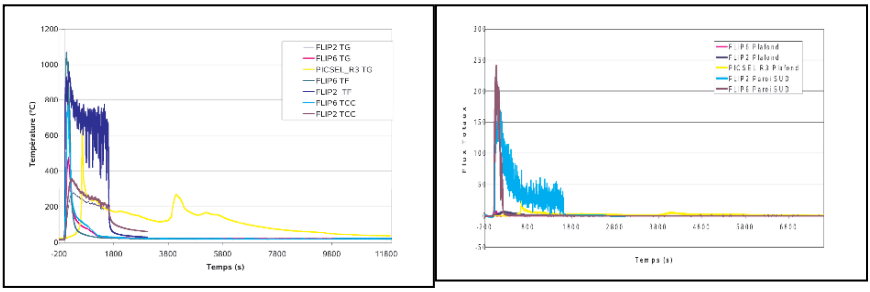

Figure 10. Fire-scenario for nuclear installation in terms of temperature and flux variations

We start with a simple example of plane concrete beam heated on one side only in order to reproduce the corresponding fire-induced conditions with temperature gradient through the thickness. To that end, a simply supported concrete slab (with dimensions: 2,350 × 2,350 × 300 mm) is heated using the critical fire-scenario for nuclear installation (see Fig. 11); applying this kind of loading.

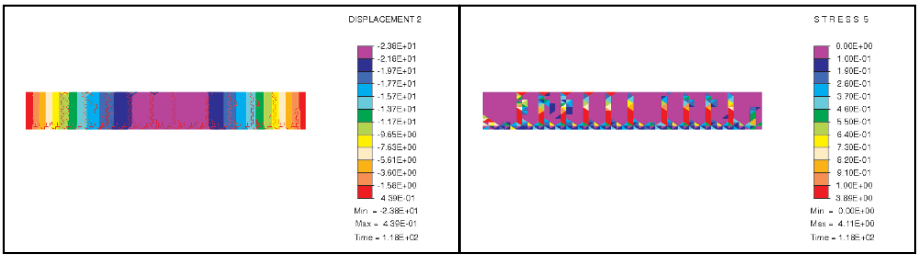

Figure 11. Crack spacing and opening of plain concrete under temperature gradient produced by heating of one side

This scenario characterizes fires were very high temperatures are reached in few seconds. Due to this severe scenario, high thermal gradient is located in a thin layer at the bottom of the slab. This loading generates compressive stresses at the bottom with subsequent traction stresses in the surface layer. It is interesting to note that we can indeed reproduce the mechanism of spalling, with the first cracks appearing in the horizontal direction. Namely, by connecting these cracks, we would finally obtain a part of the surface concrete layer to detach from the rest of the structure; this corroborates the mechanical theory of spalling induced

by steep temperature variation. The further increase in temperature leads to dominant vertical direction of crack propagation. Computed crack opening, in the range of 1–4 mm, can be considered critical in some applications in that is sufficient to allow nuclear waste to dissipate. The crack spacing remains uniform and it is equivalent to deformation mode corresponding to pure bending; this kind of result is the only consequence of homogeneous temperature field imposed on the bottom. It is important to realize that the result on crack spacing can change for a particular fire scenario with the concentrated fire source producing a heterogeneous temperature field.

The second example considers the fire-induced cracking in a reinforced concrete beam, which allows showing the positive influence of reinforcement in preventing or limiting the spalling phenomena. The reinforced concrete slab is loaded with the same critical thermal loading shown in Fig. 12, and has the same dimension as in the previous example. The main difference concerns the present of steel reinforcement with bars of 16 mm of diameter at each 10 *cm*, with a concrete cover of 30 *mm*.

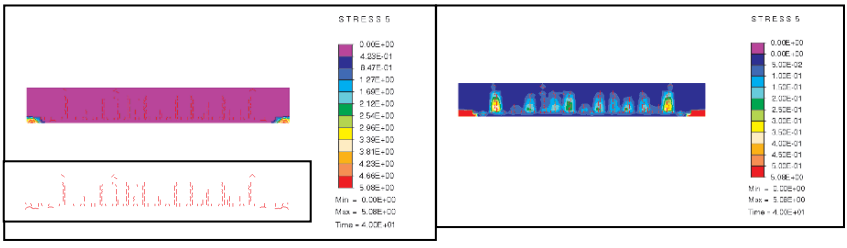

Figure 12. Crack spacing and opening of reinforced concrete under temperature gradient produced by heating of one side

In comparison with the previous case of plain concrete, the crack pattern seems quite different, which confirms that the reinforcement plays an important role. Namely, we observe fewer vertical cracks with smaller width; moreover, there is no horizontal cracks which connect and thus no spalling is observed in this case. Others numerical simulations and parametric studies are performed in order to observe the resulting crack patterns, and the conclusion can be stated as follows:

(i) Increasing the reinforcement ratio reduces the crack width.
(ii) Rising the temperature for the case when the concrete and steel don't have the same expansion coefficient, cracks width can grow slower or faster; more precisely, if steel has small coefficient of expansion relative to concrete, this produces compression in the concrete under temperature increase and hence reduces crack width.

(iii) Formation of cracks continues with the increase in ΔT until a so-called stabilized crack pattern is developed, where no further cracks can form. Hence, the distance between any two cracks cannot be smaller than a certain value called the crack spacing s.
(iv) Temperature gradient corresponding to the stabilized crack pattern is equal to $\Delta T\ s$. Further increase of ΔT beyond $\Delta T\ s$ causes widening of the existing cracks.

4. Conclusions

In this works we have briefly addressed the class of problems of damage assessment of structures and infrastructure exposed to fires. The review of a number of historical case studies show that the extreme loading conditions brought by fire exposure and resulting consequences both in peace and war times. We concluded that since the loading conditions cannot be controlled, one can put the effort in increasing the fire-resistance of modern construction materials and thus reducing the fire-induced damage. The precise thermal loading control can only be achieved in fire-resistance testing, by using additional numerical modeling as shown in this work. The tests of this kind are likely to play an important role in understanding behavior of chosen construction materials and structures and in improving their fire-resistance characteristics. A more detailed study we presented for frequently used construction material of reinforced concrete illustrates well what kind of refined models are needed in order to obtain the full understanding of complex thermomechanical failure phenomena for reinforced concrete structures and infrastructure exposed to fire. Namely, not only do we have to account for thermo-hydro-mechanical coupling at the level of material, but also for more detailed information on crack spacing and opening at the level of structure. Another important advantage of the presented model for cracks prediction in reinforced concrete is to fit within the standard computer code architecture.

Acknowledgements: this work was supported by the French Ministry of Research (funding for AB, LD), Alexander von Humboldt Research Award (to AI) and Slovenian Research Agency Award (to AI). This support is gratefully acknowledged.

References

ASTM 119-81 Standard Methods of Fire of Building Construction and Material, National Bureau of Standards, ANSI Fire Protection Group and American Society for Testing and Materials, Philadelphia, PA, 1981

Baum H.R., et. al., Gravity-current transport in buildings fires. International Conference on Fire Research and Engineering, Orlando, FL, 1995

Bazant Z.P., M.F. Kaplan, Concrete at high temperature: Material properties and mathematical modeling, Longman Harlow – Addison Wesley, 1996

Beard A., D. Drysdale, P. Holborn, S. Bishop, Configuration factor for radiation in a tunnel as partial cylinder. Fire Technology, 29, 391–402, 1993

Bendelius A.G., Tunnel fire and life safety within the world road association PIARC. The 28th ITA General Assembly, Sydney, Australia, 2002

Brancherie D., A. Ibrahimbegovic, Novel anisotropic continuum-discrete damage model capable of representing localized failure. Part I: theoretical formulation and numerical implementation. International Journal of Engineering Computations, 26, 100–127, 2009

Briollay H., P. Chasse, Validating and Optimizing 2D and 3D Computer Simulations for the Offenegg Tunnel Fire Test, Centre d´Etudes des Tunnels, Bron Cedex, France, 1994

Britter R.E., M.K.-A. Neophytou, A simple model for the movement of fire smoke in a confined tunnel. Pure and Applied Geophysics, 162, 1941, 2005

Britter R.E., P.J. Woodburn, CFD-simulations of a tunnel fire – part one. Fire Safety Journal, 26, 35, 1996

Brunello P., B.A. Schrefler, D. Gawin, C.E. Majorana, F. Pesavento, Concrete at high temperature with application to tunnel fire. Computational Mechanics, 29(1), 43, 2002

Chasse P., Sensitivity study of different modelling techniques for the computer simulation of tunnel fire. The 1st CFDS International User Conference, Oxford, UK, 1993

Chow W.K., H.T. Kot, hotel fires in Hong Kong. International Journal of Hospitality Management, 8, 271, 1989

Colliat J.B., A. Ibrahimbegovic, L. Davenne, Saint-Venant multi-surface plasticity model in strain space and in stress resultants. International Journal of Engineering Computations, 22, 536–557, 2005

Dominguez N., D. Brancherie, L. Davenne, A. Ibrahimbegovic, Prediction of crack pattern distribution in reinforced concrete by coupling a strong discontinuity model of concrete cracking and a bond-slip of reinforcement model. International Journal of Engineering Computations, 22, 558–582, 2005

Edwards J.C., C.C. Hwang, The critical ventilation velocity in tunnel fires – a computer simulation. Fire Safety Journal, 40(3), 213–244, 2005

Fay J.A., Spills and fires from LNG and oil tankers in Boston harbour. MIT, Cambridge, MA, 2003

Ferziger H., M. Peric, Computational methods for fluid mechanics. Berlin: Springer, p. 423, 2001

Gabay D., Fire safety: a short history in the Paris-subway. The 28th ITA General Assembly, Sydney, Australia, 2002

Gao P.Z., S.L. Liu, W.K. Chow, N.K. Fong, Large eddy simulations for studying tunnel smoke ventilation. Tunneling and Underground Space Technology, 19(6), 577, 2004

Gawin D., D. Pesavento, B.A. Schrefler, Modeling of deformations of high strength concrete at elevated temperatures, Materials and Structures, 27, 218–236, 2004

Holmstedt G., S. Bengston, H. Tuovinen, Sensitivity calculations of tunnel fires using CFD. Fire Safety Journal, 1, 99, 1996

Ibrahimbegovic A., Nonlinear solid mechanics: Theoretical formulations and finite element solution methods. Berlin: Springer, pp. 1–620, 2009

Ibrahimbegovic A., D. Brancherie, Combined hardening and softening constitutive model for plasticity: precursor to shear slip line failure. Computational Mechanics, 31, 88–100, 2003

Ibrahimbegovic A., L. Chorfi, Covariant principal axis formulation of associated coupled thermo-plasticity at finite strains and its numerical implementation, International Journal of Solids and Structures, 39, 499–528, 2002

Ibrahimbegovic A., J.B. Colliat, L. Davenne, Thermomechanical coupling in folded plates and non-smooth shells. Computer Methods in Applied Mechanics and Engineering, 194, 2686–2707, 2005

Ibrahimbegovic A., G. Herve, P. Villon, Nonlinear impact dynamics and field transfer suitable for parametric design studies, International Journal of Engineering Computations, 26, 185–204, 2009

Jongen T., T.B. Gatski, Nonlinear eddy viscosity and algebraic stress models for solving complex turbulent flows. Progress in Aerospace Sciences, 36, 655, 2000

Kassiotis C., J.B. Colliat, A. Ibrahimbegovic, H. Matthies, Multiscale in time and stability analysis of operator split solution procedure applied to thermomechanical problems. International Journal of Engineering Computations, 26, 205–223, 2009

Kucerova A., D. Brancherie, A. Ibrahimbegovic, J. Zeman, Z. Bittnar, Novel anisotropic continuum-discrete damage model capable of representing localized failure of massive structures. Part II: identification from tests under heterogeneous stress field. International Journal of Engineering Computations, 26, 128–144, 2009

Kumar S., G. Cox, Mathematical modelling of fires in tunnels. The 5th International Symposium on the Aerodynamics and Ventilation of Vehicle-Tunnels, Lyle, France, 1985

Kumar S., G. Cox, Mathematical modelling of fires in tunnels – Validation of JASMINE, Transport and Research Laboratory: Crowthorn, 1986

Kumar S., G. Cox, Radiation and surface roughness effects in the numerical modelling of enclosure fires. Fires Safety Science – The 2nd International Conference, Paris, France, 1988

Kunsch J.P., Simple model for control of fire gases in a ventilated tunnel. Fire Safety Journal, 37, 67, 2002

Leitner A., The fire catastrophe in the Tauern-tunnel. Tunneling and Underground Space Technology, 16(3), 217, 2001

Leupi C., Numerical modeling of cohesive sediment transport and bed morphology in estuaries, in La faculte sciences et techniques de l'íngenieur, EPFL, Lausanne, 2005

Liu S.L., P.Z. Gao, W.K. Chow, N.K. Fong, Large eddy simulations for studying tunnel smoke ventilation. Tunneling and Underground Space Technology, 19, 577, 2004

Magnussen B.F., B.H. Hjertager, On mathematical modelling of turbulent combustion with special emphasis on soot formation and combustion. The 16th International Symposium on Combustion, Pittsburgh, 1976

Malin M.R., N.C. Markatos, Mathematical modelling of buoyancy-induced smoke flow in enclosures. International Journal of Heat Mass Transfer, 25, 63, 1982

McGrattan K.B., Numerical Simulation of the Howard Street Tunnel Fire, NIST: Gaithersburg, 2002

Miles D., S. Kumar, R.D. Andrews, Validation of a CFD model for fires in the memorial tunnel. First International Conference on Tunnel FIres, Lyon, France, 1999

Miles D., S. Kumar, Computer modelling to assess the benefits of road tunnel fire safety measures. The InFlam, Edinburgh, 2004

Rojtman A., Prtotiv pozarnov normirovanie v stroitelstve. Stojizdat, Moscow, 1985

Sanmiguel-Rojas E. et al., Numerical model and validation experiments of atrium enclosure fire in a new fire test facility. Building and Environment, 43, 1912–1928, 2007

Sawley M., A. Drotz, SOCATOP, Lausanne, Switzerland, 2003

Schrefler B.A., F. Pesavento, L. Sanavia, D. Gawin, Multi-physics problems in thermo-hydro-mechanical analysis of partially saturated geomaterials. In Ibrahimbegovic A., B. Brank (eds.), Multi-physics and multi-scale computer models in nonlinear analysis and optimal design of engineering structures under extreme conditions, IOS Press, Amsterdam (ISBN 1-58803-479-0), pp. 1–407, 2005

Simulation of fires in tunnels under construction, SINTEF: Trondheim, Norway, 2005

Tan G.L., Fire fighting in tunnels. Tunneling and Underground Space Technology, 17(2), 179, 2002

Tuovinen H., Validation of ceiling jet flows in a large corridor with vents using the CFD code JASMINE. Fire Technology, 32, 34–45, 1994

Ulm F.J., O. Coussy, Z.P. Bazant, The Chunnel fire: Part I: Chemoplastic softening in rapidly heated concrete. ASCE Journal of Engineering in Mechanics, 125, 378–385, 1999

Versteeg H.K., W. Malalasekera, An introduction to computational fluid dynamics, Longman Group Ltd.: London, 1995

Vidmar P., S. Petelin, Analysis of the effect of an external fire on the safety operation of an powerplant. Fire Safety Journal, 41, 486, 2006

Vladimirova N., Model flames in the Boussinesq limit, ASC/Flash Center, Dept. of Astronomy and Astrophysics, The University of Chicago, Chicago, IL, 2006

Wighus R., Fire at sea-surface, SINTEF: Spitzbergen, Norway, 1994

Zhang W., et al., Turbulence statistics in a fire room model by large eddy simulation. Fire Safety Journal, 37, 721, 2002

APPENDIX: DAMAGE ASSESSMENT TO WAR AND NATURAL DISASTERS IN BOSNIA AND HERZEGOVINA

DAMAGE ASSESSMENT FOR MASONRY AND HISTORIC BUILDINGS IN BOSNIA AND HERZEGOVINA

M. HRASNICA*
Civil Engineering Department, Patriotske lige 30,71000 Sarajevo, Bosnia and Herzegovina

Abstract. Opposite to some common opinions the widest spread structural system of the multistory buildings in Bosnia and Herzegovina is structural wall system with masonry walls and reinforced concrete walls. The country is situated in seismic active region of South-East Europe, divided in seismic zones with PGA of 0.1–0.2 g for 500 year return period, in some parts even PGA of 0.30–0.35 g. Traditional art of building comprises masonry structures from adobe and simple masonry to the one with manufactured brick units. The buildings older than approximate 60 years have usually wooden floors; later the R.C. floors have become the standard art of construction. After the earthquakes in Skopje in 1963 and especially after the earthquake in Montenegro in 1979 the confined masonry became more and more typical art of the masonry structures. Lessons learned form those earthquakes proved the vulnerability of unreinforced masonry buildings. Most of the multistory structures, especially residential buildings, in 1970s, 1980s and 1990s were constructed with R.C. walls, some of them with satisfactory level of earthquake-resistant design. Historic buildings are mostly built as robust unreinforced masonry structures with wooden floors, if any. Seismic vulnerability of buildings with masonry and R.C. walls were analyzed according to the recommendations of European Macroseismic Scale EMS-98 and damage grades were estimated. It is shown that some of the typical masonry buildings could suffer substantial damages when exposed to the earthquake motion, which corresponds to seismic zones in the country. Some structural elements of historical buildings, as domes and arches, crack already by moderate earthquake but without loss of stability. Some analytical procedures and construction methods for retrofit and strengthening are shown.

* To whom correspondence should be addressed. e-mail: hrasnica@bih.net.ba

A. Ibrahimbegovic and M. Zlatar (eds.), *Damage Assessment and Reconstruction After War or Natural Disaster*,

Keywords: Earthquake, multistory building, seismic vulnerability, damage grades

1. Introduction

The existing buildings in Bosnia and Herzegovina are traditionally built as masonry buildings, which include most of historical buildings. After the World War II reinforced concrete structures prevail by the new erected buildings, but masonry structures are further built with apply of new materials. If one wants to assess possible damages, especially those caused by an earthquake, the existing older buildings are more vulnerable compared to the buildings constructed according modern technical codes. Several strong earthquakes that happened in the few last decades, underlined the importance of seismic vulnerability assessment including evaluation of possible strengthening and retrofit measures.

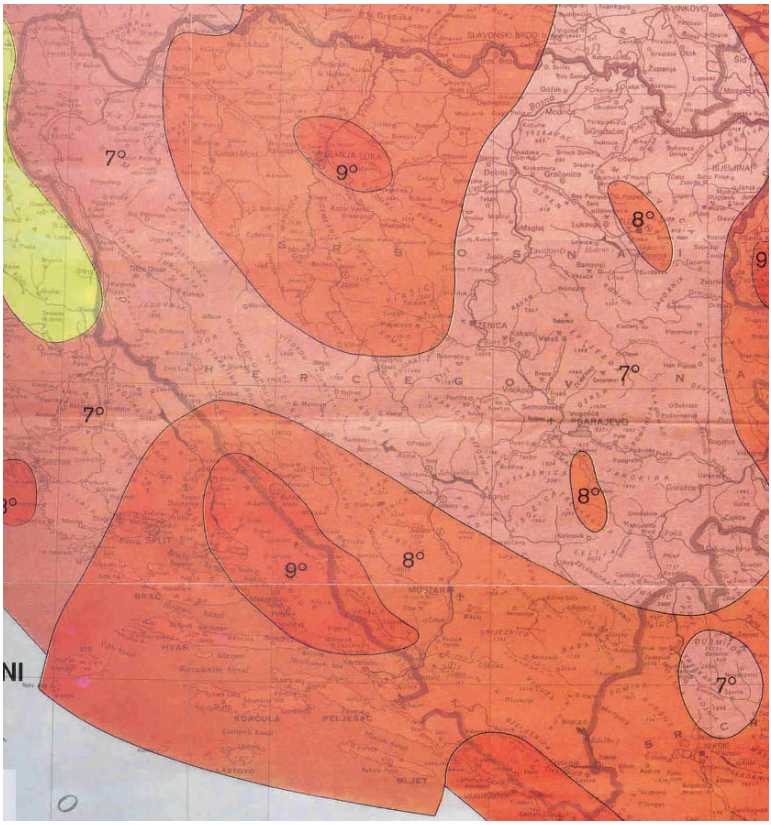

Figure 1. Seismic zones in Bosnia and Herzegovina

The territory of Bosnia and Herzegovina is situated in active seismic region of South-East Europe. Shown on the seismic intensity map of Bosnia and Herzegovina for the reference return period of 500 years (Fig. 1) the greatest part of the country lies in the zones of seventh and eighth intensity degrees according to MCS-scale or the new European Macroseismic Scale EMS. Relatively small part of the territory is situated in the seismic intensity zone 9. Referred to peak ground acceleration (PGA), PGA between 0.10 and 0.20 g corresponds to the greatest part of the territory and even PGA of 0.30–0.35 g in smaller part of the country.

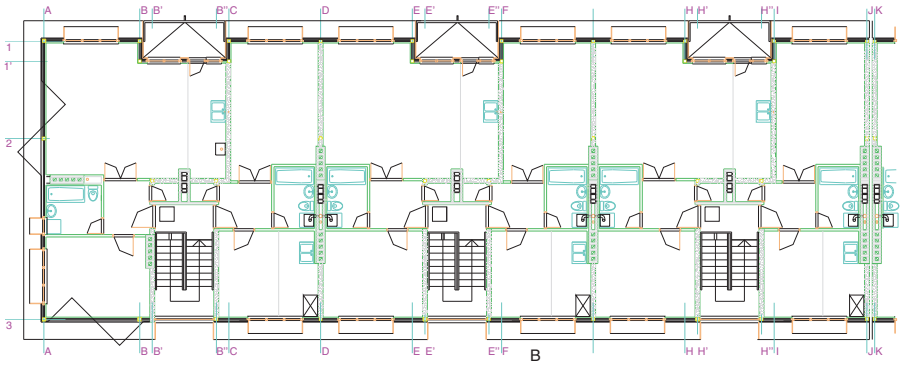

Figure 2. Typical multistory masonry building (Groundfloor + four or five stories), regular structure

Traditional art of construction was masonry building, built as unreinforced masonry (URM) with wooden floors. By the mid 1930s of the last century the first art of half-prefabricated reinforced concrete floors were applied, which was continued after the World War II. The most masonry buildings had up to five stories, but without vertical R.C. confining elements. Seismic resistance was provided by structural walls laid in two mutually orthogonal directions viewed in a plan. Whereby, smaller number of walls in longitudinal direction was caused by functional demands (Fig. 2). After the earthquake in Skopje in 1963, first seismic codes were published and vertical confining R.C. elements were introduced in masonry building. Presently, confining masonry is the common art of masonry structures.

Unlike some enrooted views structural system with walls prevails in reinforced concrete structures of multistory buildings (Fig. 3). It is similar to some Middle European countries, while further to South and South-East, for example Greece and Turkey, frames are usual earthquake resistant system. R.C. walls are predominantly used in last 40 years, especially for multistory residential buildings. During the earthquake in Montenegro 1979 they showed relatively good seismic performance. Most residential areas in the cities, built in 1970s, 1980s and

1990s have this structural system. In older buildings of this type, there was no special detailing concerning acceptable seismic response. Most walls have relatively small amount of transverse reinforcement and generally the criteria of capacity design (Paulay et Priestly, 1992; Bachmann, 1995) are not fulfilled.

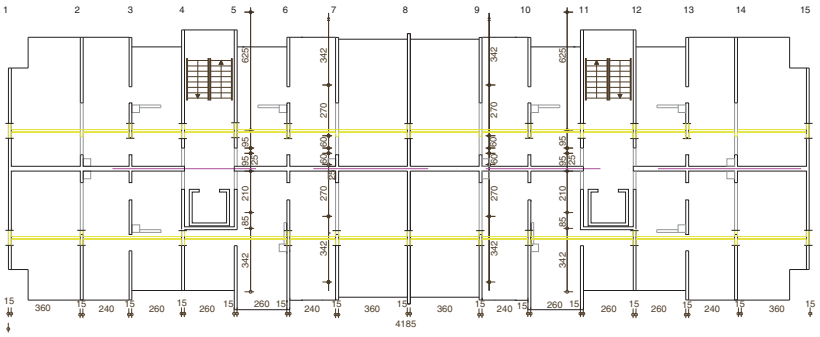

Figure 3. Typical multistory R.C. walls building (Groundfloor + seven/eight stories), regular structure

Reinforced concrete frames filled in with masonry are rarely used in building practice in Bosnia and Herzegovina (should not be mixed with confined masonry, see previous paragraph). The weakness of this system is well known; relatively stiff masonry infill during stronger earthquake could cause serious damages of R.C. frame columns. The earthquakes in Turkey (South-East European Region) in the last 10 years showed significant damages of this structural system.

2. Damages Caused by Past Earthquakes in the Region

Several strong earthquakes hit the region of South-East Europe in the last few decades, some of them in Bosnia and Herzegovina or neighborhood countries. They caused loss of human lives, a lot of injured inhabitants of the hit areas and substantial damages to the building structures.

Some of the recent earthquakes, which caused damages of the buildings, also influenced development of seismic codes for the whole Europe, are listed below:

Earthquake in Skopje, Macedonia in 1963, seismic intensity ninth degree, after this earthquake the first modern seismic code was introduced.

Earthquake in Banja Luka, Bosnia and Hercegovina 1969, seismic intensity eighth to ninth degree, hypocenter was in the country.

Earthquake in Friuli, North-East Italy, seismic intensity ninth to tenth degree, damage analysis are used in development of European Macroseismic Scale EMS.

Earthquake on the Montenegro Coast in 1979, seismic intensity ninth degree, after this earthquake the new seismic code was improved.

The most severe consequences after a strong earthquake are total or partial collapse of the building structures, which were observed for Skopje and Banja Luka earthquake (Figs. 4 and 5). Five-story masonry building without vertical R.C. confining elements could not withstand strong forces induced by the earthquake of the seismic intensity nine and collapsed (Fig. 4). Similar observation can be confirmed by failure of the corner building (Fig. 5).

Figure 4. Total collapse of URM building, Skopje 1963 (Petrovski, 2004)

Figure 5. Partial failure of the masonry building, Banja Luka 1969

Common damages of masonry structures caused by earthquake are diagonal cracks in the walls (Fig. 6). This type of damage on masonry structures was observed after many earthquakes, from minor cracks after less severe ground motion to larger cracks due to strong earthquakes, as illustrated on the figure below. This can lead to the buckling of the damaged wall and collapse of the whole building. The reasons for the diagonal cracks in the masonry walls are in their small resistance in tension. Due to the high level of the horizontal forces induced by an earthquake a sort of truss resistance mechanism is formed in the masonry walls or piers. The truss chords are floor structures, which in the case of R.C. floors can transmit the horizontal forces in efficient way, while the diagonals are formed in the masonry wall itself and fall in tension. The most of the existing masonry buildings in southeast Europe belong to the unreinforced masonry structures and this tradition is preserved. The improvement is made by almost regular built in of the vertical reinforced concrete confining elements, which improve overall structural ductility significantly.

Figure 6. Diagonal crack in masonry walls and loss of corner wall URG masonry' R.C. floors (EMS)

The other, also very frequent type of damage in masonry buildings due to the seismic action is loss of connection between two mutually perpendicular walls in plan. This is also shown on the Fig. 6, where partial loss of connection between two external walls at the corner of building was observed. This building was built as URM with R.C. floors but without vertical confinement.

Traditional stone masonry houses were very often built in the Mediterranean region, where continuous seismic activity is permanently registered. Most of the houses are built with wooden floors. The damages at one of such buildings due to Montenegro earthquake are shown on the Fig. 7. The stone masonry wall collapsed, which caused partial collapse of the floor and the roof structures, leading generally to heavy structural damage of the building.

Figure 7. Stone masonry building with wooden floors, earthquake in Montenegro 1979 (EMS)

The masonry buildings are generally brittle structures, which show relatively satisfactory behavior up to moderate seismicity. In that case most damages can be predicted and also repaired. But, exposed to very strong earthquakes most of the traditional buildings suffer heavy structural damages, whose reparations are not reasonable. Exceptions are important historical buildings. The advantage of the existing masonry building is the structural regularity. Most of them have no large structural eccentricity, viewed in the plan, or there is no important stiffness irregularity along the height of the building, which is not rare in the modern reinforced concrete multi-storey structures (Tomaževič, 2006).

Reinforced concrete walls are generally less vulnerable compared to masonry walls for an equivalent earthquake motion. If they are designed according the newest seismic codes or modern guidelines for the earthquake resistant design, their seismic response could be predicted. That means dissipation of energy induced into the structure by an earthquake, damages on the previously defined parts of the structural elements, and no collapse. These principles are part of the capacity design philosophy, which was developed for earthquake resistant design of the structures. Large number of the damages on the reinforced concrete

buildings, which were registered during recent strong earthquakes, are consequences of the irregular structural system. Non-uniform distribution of stiffness along the height of the building, so called soft-story phenomena, was probably the most mentioned reason for the heavy damages. Especially soft ground floor, very popular among the architects of the buildings. The second place probably belongs to non-uniform distribution of vertical elements, viewed in the plan. Poor detailing, especially absence of the transverse reinforcement in the joints and corner area, as well as absence of appropriate reinforcement ratios could also cause important damages to the structure.

Figure 8 shows collapse of the fresh built reinforced concrete building with structural walls during Montenegro earthquake in 1979. The hotel building had been finished just before the earthquake happened, which means that it was constructed according the latest seismic code. But, two structural irregularities were fatal for it. First, flexible ground floor (soft-story) proved to be very sensitive to strong earthquake motion and then non-symmetrical distribution of the structural walls in the plan of the building. After the lessons from this earthquake the local seismic codes were modified, especially regarding restrictions for the buildings with soft-story.

Figure 8. Soft-story and non-symmetrical structure Montenegro 1979

Typical damage at the bottom of the vertical reinforced concrete element is shown on the Fig. 9. Beyond the yield limit at the bottom of the wall, the plastic hinge is formed. It is marked with the cracks on both sides and very often with spalling of concrete cover. This area is especially vulnerable if there is no enough transverse reinforcement. One of the consequences could be buckling of the vertical reinforcement, which was observed after different earthquakes, even by very robust bridge piers, as it happened during Kobe earthquake in 1995.

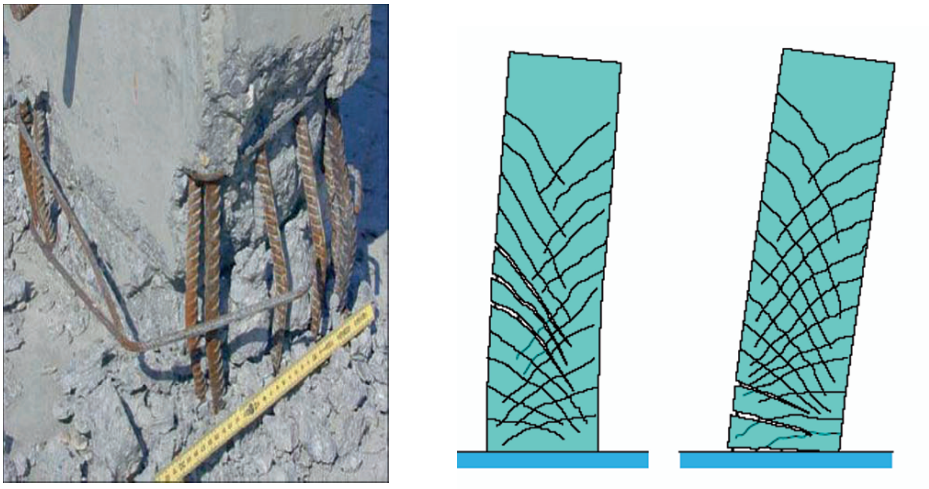

Figure 9. The bottom of the R.C. element, plastic hinge area

Similar damages could be expected during stronger earthquakes in buildings with R.C. walls in Bosnia and Herzegovina.

Masonry infilled reinforced concrete frames represent the specific structure made of relatively ductile R.C. frame, which is designed to carry both, vertical and horizontal loading, and relatively stiff masonry infill wall, which is built as nonstructural element after completing the frame. Due to the infill the structure becomes much stiffer for the horizontal loads. Masonry infill is activated in the case where the building is subjected to seismic loading. At the contacts between the masonry infill and R.C. elements interaction forces could be developed, which can cause unexpected behavior and damages of the main structural system (Fig. 10).

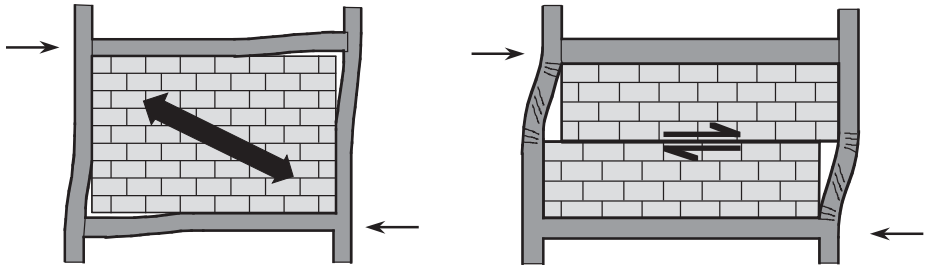

Figure 10. Damages to R.C. frame due to masonry infill wall

During stronger earthquake contact between stiff masonry infill and relatively flexible frame structure could be lost or dangerous sliding of masonry infill along the horizontal mortar joints could occur. As the consequences frame columns

are subjected to additional shear forces, which were usually not taken in account by design. The undesirable shear failure mechanism can be developed in the frame columns, leading probably to the partial collapse of the structure. In some cases, for example under the large window openings masonry infill is partially built in. Due to strong horizontal seismic action high shear forces are developed in the free part of the frame, causing severe damages or shear failure of the column.

Figure 11. Damages on the R.C. frame structure due to masonry infill (SGEB, 2004)

As an example, the damages of the masonry infilled frame structure during earthquake in West Turkey 1999 are shown on the Fig. 11. Frame columns suffered very high structural damages.

It can be concluded that masonry infilled frame structures can perform in an undesirable way during strong earthquake motion producing brittle shear failure of the reinforced concrete frame columns. In the case of lower seismicity the composite structure made of reinforced concrete frame and masonry wall can keep its integrity and act as considerably stiff structure, in some way comparable to reinforced concrete walls, reducing horizontal displacement of the floor structures and preventing the damages of the nonstructural elements.

In Bosnia and Herzegovina R.C. frames filled with masonry are not often constructed. The common type of masonry structures in the last few decades is confined masonry, which is widely accepted, especially for residential houses.

Taking in account damage assessment of building structures, considered in this chapter, it is of great interest to classify typical building structures according to their seismic vulnerability.

3. Vulnerability Classification According to European Macroseismic Scale

Within European Macroseismic Scale (EMS) structural systems of buildings are classified according to vulnerability classes depending on structural type. Vulnerability classes are A–F, where class A is for the weakest seismic structures and class F for those that are expected to have very good seismic performance (Table 1).

TABLE 1. Vulnerability classes according to EMS

Type of structure		Vulnerability Class A	B	C	D	E	F
MASONRY	rubble stone, fieldstone	○					
	adobe (earth brick)	○	⊢				
	simple stone	⊢	○				
	massive stone		⊢	○	⊢		
	unreinforced, with manufactured stone units	⊢	○	⊢			
	unreinforced, with RC floors		⊢	○	⊢		
	reinforced or confined			⊢	○	⊢	
REINFORCED CONCRETE (RC)	frame without. earthquake-resistant design (ERD)	⊢		○	⊢		
	frame with moderate level of ERD		⊢		○	⊢	
	frame with high level of ERD			⊢		○	⊢
	walls without ERD		⊢	○	⊢		
	walls with moderate level of ERD			⊢	○	⊢	
	walls with high level of ERD				⊢	○	⊢

The classification of damage degrees is listed here separately for masonry buildings and reinforced concrete building with walls, two typical building systems in Bosnia and Herzegovina. Damage degrees are from 1 to 5 that means from irrelevant damages or only damages of nonstructural elements that correspond to damage 1, to destruction or even building collapse that corresponds to damage degree 5.

Classification of damage to masonry buildings:

– Grade 1: Negligible to slight damage (no structural damage). Hair-line cracks in very few walls. Fall of small pieces of plaster
– Grade 2: Moderate damage (slight structural damage). Cracks in many walls. Fall of fairly large pieces of plaster

- Grade 3: Substantial to heavy damage (moderate structural damage). Large and extensive cracks in most walls, roof tiles detach
- Grade 4: Very heavy damage (heavy structural damage). Serious failure of walls, partial structural failure of roofs and floors
- Grade 5: Destruction (very heavy structural damage). Total or near total collapse

Classification of damage to R.C. buildings with walls:

- Grade 1: Negligible to slight damage (no structural damage). Fine cracks in walls at the base
- Grade 2: Moderate damage (slight structural damage). Cracks in structural walls
- Grade 3: Substantial to heavy damage (moderate structural damage). Cracks at the base and at joints of coupled walls. Spalling of concrete cover, buckling of reinforced rods
- Grade 4: Very heavy damage (heavy structural damage). Large cracks in the walls with compression failure of concrete and fracture of rebars
- Grade 5: Destruction (very heavy structural damage). Collapse of ground floor or parts of building

Damage degrees of some structural types depend also on earthquake intensity. So, the class of building vulnerability, which depends on the structural type, can be related to damage degrees, which can be expected for different seismic intensities. Within the European Macroseismic Scale there are short descriptions of effects that could be expected for the specific degree of seismic intensity. Further, the focus is on buildings with masonry walls and R.C. walls, typical for multistory buildings in Bosnia and Herzegovina.

4. Seismic Vulnerability Classification of Masonry and R.C. Walls Buildings

The buildings are classified here according to their structural type, seismic intensity, and expected damage degree. In the case of earthquake, the most endangered buildings are those built before the introduction of seismic codes, but that depends very much on regularity of their structures.

Masonry buildings made of rubble stone or earth brick generally belong to vulnerability class A and already for seventh degree of seismic intensity serious damages can be expected, including instability of walls or falling down of ceiling. Such buildings have no many floors, usually ground floor and a story; they are situated in village, often in inaccessible environment.

Further on, there are masonry buildings constructed with bricks produced in factory, but without vertical confining elements. We speak about unreinforced masonry (URM) without confinement. Older buildings have usually wooden floors, while buildings built after World War II generally have R.C. floors. The first belong mostly to vulnerability class B where very heavy damages can be expected for the earthquakes whose intensity corresponds to the seismic zone 8. Masonry buildings with R.C. floors according to EMS classification could stand heavy damages of the structure including falling down of some walls for the intensity degree 9 and they belong mostly to vulnerability class C.

Masonry buildings with reinforced concrete confining elements, usually called confined masonry, are generally classified according to EMS in relatively low class of vulnerability, class D. For ninth degree of seismic intensity significant cracks can appear, roof tiles detach, chimneys can fall down, but there should not be collapse of entire walls. The advantage of confined masonry is evident. After the new seismic codes were introduced this became usual type of masonry building. Yet, most of the existing buildings belong to unconfined masonry.

TABLE 2. Damage grades of typical multistory buildings with wall system in Bosnia and Herzegovina

Type of masonry and R.C. wall buildings typical structures in B&H	Seismic zone according to EMS		
	Zone VII	Zone VIII	Zone IX
Masonry buildings made of earth brick or field stone	3–4	4–5	5
Unconfined masonry, older than approx. 60 years mostly with timber floor structure	2–3	3–4	4–5
Unconfined masonry, younger than approx. 60 years reinforced concrete floors	2	2–3	3–4
confined masonry with R.C. floors, mostly newer masonry buildings	1	2	2–3
Reinforced concrete building with R.C. walls moderate earthquake-resistant design	1	2	2–3
Reinforced concrete building with R.C. walls high level of earthquake-resistant design	–	evt. 1	1–2

There are no reinforced masonry buildings till now in Bosnia and Herzegovina, although this type of structures is favorable, regarding seismic resistance of masonry buildings.

Reinforced concrete buildings with structural walls may be divided into those designed and constructed without or with moderate seismic detailing and those having high level of earthquake resistant design, usually constructed according the newest seismic codes. As the application of structural systems with R.C. walls began in this region by the end of 1960s and the beginning of

1970s of the last century, the existing buildings meet at least some of seismic design criteria, and that places them in average in vulnerability class D. This means that even for the seismic intensity of ninth degree R.C. walls should not collapse, although they would have heavy damages in the form of large cracks, spalling of concrete, especially concrete cover, or instability of some reinforcement bars. R.C. walls designed and constructed according to the newest seismic rules (EC8, 2003) and recommendations would show only smaller, very fine cracks for the earthquake motions corresponding to seismic zones 7 and 8, and only for ninth degree there could be some larger cracks and spalling of concrete cover. All damages are expected to appear in the most stressed part of the wall, at its bottom.

All considerations for different masonry and reinforced building are summarized in Table 2. Taking into account structural type, their vulnerability classification and considerations about expected damages for different seismic intensities the appropriate damage grades are estimated for typical buildings and seismic zones in Bosnia and Herzegovina.

Previous classifications refer to some average design and constructed masonry and reinforced concrete buildings. In the cases of worse construction heavier damages than those described must be taken in consideration. Presented vulnerability classification of masonry and R.C. walls buildings corresponds to relatively regular structures. That means: the layout of the structural walls in a plan is approximately symmetrical and the stiffness is almost uniform or proportional along the height of the building. It has to be stated, that each irregularity increases seismic vulnerability of the structure. It was confirmed in past earthquakes in the region of South-East Europe. Irregular distribution of walls in a plan of the building can produce large eccentricity between mass center and stiffness center (Hrasnica, 2005a). Non-uniform stiffness distribution along the wall height can form soft stories and it is well known source of earthquake damages. The buildings with flexible ground floor are especially vulnerable, which was confirmed in recent strong earthquakes.

5. Damage Assessment of Historical Buildings

Whole Mediterranean area belongs to seismic active regions, which was confirmed by past earthquakes. At the same time Mediterranean countries are rich in historical and cultural buildings and monuments. Those buildings have great importance and value for specific countries and their inhabitants. So they merit special care and protection. This concerns in the same way the historical buildings in Bosnia and Herzegovina. Besides the risk of seismic damages, a lot of them were damaged or even destroyed during the last war.

Assessment of historical buildings presents specific problem considering the ways they were built and the materials, which were used. The damages are sometimes cumulated through many years and many causes, e.g. few moderate or stronger earthquakes.

Another specific problem arises by reparation and necessary strengthening or retrofit, for example to achieve earthquake resistance demanded by modern seismic codes. Speaking about historical buildings and monuments the aim is to preserve and reveal their aesthetic and historical values and to use original materials and original way of construction, if possible. But, where traditional techniques prove inadequate some modern construction and conservation techniques must be implemented. The same problems occur with traditional construction materials. In order to provide necessary resistance and ductility and fulfill the demands of new building codes the contemporary building materials have to be carefully implemented in the structures of those buildings. Many important principles for the assessment of historical buildings and monuments are summarized in the Venice Charter.

Figure 12. The old city of Bam in south-east Iran before the earthquake

The large majority of all historical buildings are built as masonry structures, a lot of stone masonry, but in some regions bricks masonry as well. They are traditionally built as unreinforced masonry without confining elements. In some regions timber confinement was used. Typical curved structural forms as domes, arches and vaults are often part of historical buildings especially the religious one. As they are built as unreinforced masonry structures, the historical buildings are relatively stiff and show generally brittle behavior. So, the first damages in form of cracks appear already by moderate earthquakes on softer structural elements as domes and arches, or ceilings by wooden floors and on partition

walls, if there are any. At the same time the main structure, as dick walls and abutments, is in linear range of the behavior, with no or almost no cracks. But, it's generally not true for very strong earthquake motion.

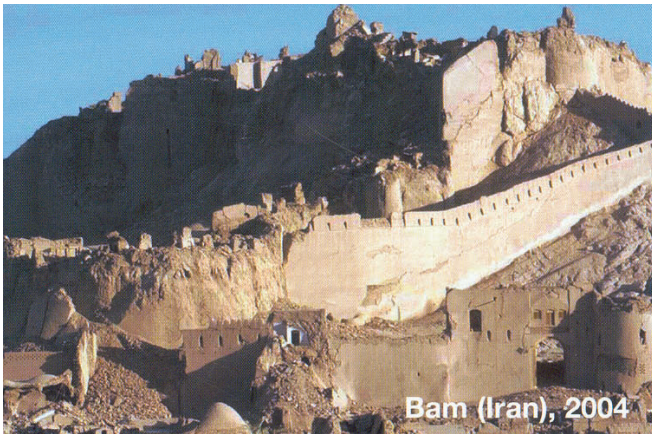

Figure 13. The old city of Bam in south-east Iran after the earthquake 2004

How the strong earthquake can destroy old monumental masonry structure is illustrated on the example of the old city of Bam in southeast Iran. On the Fig. 12 is the view of the city before the catastrophic earthquake in 2004 and on the Fig. 13 after it. The unreinforced masonry structure couldn't withstand high seismic intensity in spite of the probably rather stiff and robust structure.

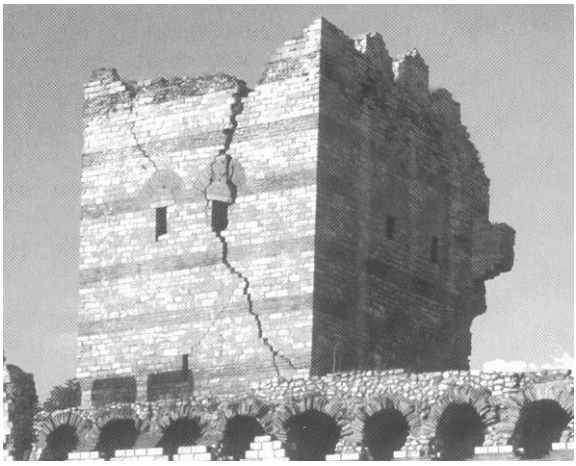

Figure 14. Large diagonal crack in the old tower in Istanbul (Wenk, 2004)

Damages can be accumulated during the history of these old buildings, especially when they are situated in seismic active region. Sometimes it took the time before the decisions are made how to repair these structures and to

preserve their aesthetical and cultural values. On the Fig. 14 is the old tower of the city wall in Istanbul, Turkey, with typical diagonal crack in the masonry wall.

As it was already stated some parts of the old historical buildings are more vulnerable to seismic actions. Masonry structures have rather small resistance in tension and cracks open perpendicular to the direction of seismic forces. Typical example is schematically presented on the following Fig. 15, where the cracks on the dome are opened orthogonal to ring tension forces.

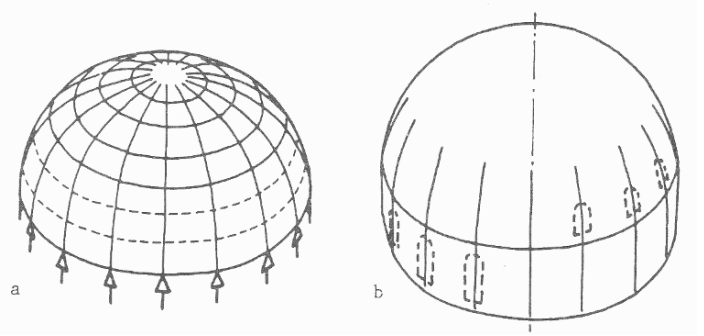

Figure 15. Schematic presentation of dome structural system and cracks in the dome masonry structure

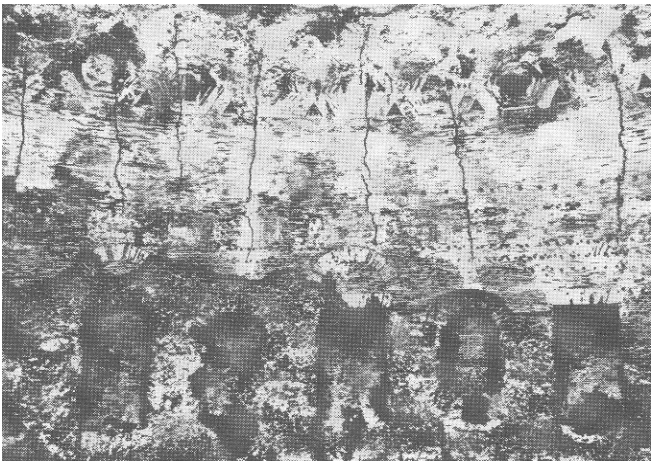

Figure 16. Radial cracks in the old dome masonry structure (UNDP, Vol. 6)

The structural form of the dome as three-dimensional structure is shown on the left side of the Fig. 15; the radial arches in compression and circumferential tension. Masonry dome is usually set on the drum below and very often they are interrupted with window openings. It cracks radially as shown on the right side of the Fig. 15, forming ring of the arches. The illustration of the cracks in an old dome masonry structure is on the Fig. 16.

During last war in Bosnia and Herzegovina many historical buildings, valuable as important cultural heritage, were damaged and even barbarically destroyed. Here, as example, cross-section of the masonry structure of Ferhadija mosque in Banjaluka with its dome, drum and arches (Fig. 17). The mosque is completely destroyed and should be rebuilt respecting former materials, structure and all geometrical dimensions.

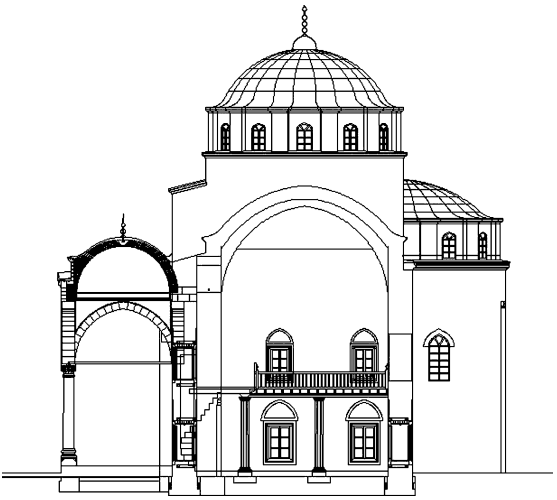

Figure 17. Cross-section of Ferhadija mosque in Banjaluka, Bosnia and Hercegovina (Hrasnica, 2005b)

The building is situated in a seismic zone 9 that means PGA of 0.30–0.35 g. The whole structure should be built in the same way as original one. The main building structure was stone masonry and the dome was brick masonry. The loading from the dome roof is transmitted over the drum further to the arches and walls. The whole building should be constructed as unreinforced masonry and can be classified as rather seismic vulnerable structure (see Tables 1 and 2) with damage grades from 3–5 for the strongest earthquakes. The challenge is how to reinforce and strengthen the mosque structure with respect to aesthetical and cultural value. Traditional methods are reinforced concrete confining elements built in masonry structures or steel ties to keep the integrity of the structure. Modern methods include implementation of new materials as carbon fibers or pre-stressing with high resistance steel wires and ropes.

Another possible but very expensive method in the high seismic areas is base isolation, where the rigid structure of the whole historical building is posted on special elastomeric or similar bearings, which function as isolators and damping elements.

6. Seismic Evaluation and Damage Assessment of Existing Buildings

The existing buildings are more vulnerable to seismic actions than those designed and built according to modern seismic codes. Important percentage of existing buildings represents masonry buildings, which include most of the historical monuments and buildings. The prediction of their seismic performance is very important to assess possible damages. The properties of those buildings and their typical damages were analyzed in the previous chapters. They were also classified according their seismic vulnerability and damage grades, which can occur for different levels of seismic intensity.

The efficient methods for evaluation of existing buildings are pushover analysis and capacity spectrum method (Freeman, 1998; Hrasnica, 2005a). Assuming that the structure responds predominantly in the first eigenmode, using nonlinear static procedure the capacity curve of the building is developed. On the other side, earthquake demand is represented by design spectrum (Fig. 18). The intersection point of two curves simulates the performance point of the structure for the given conditions.

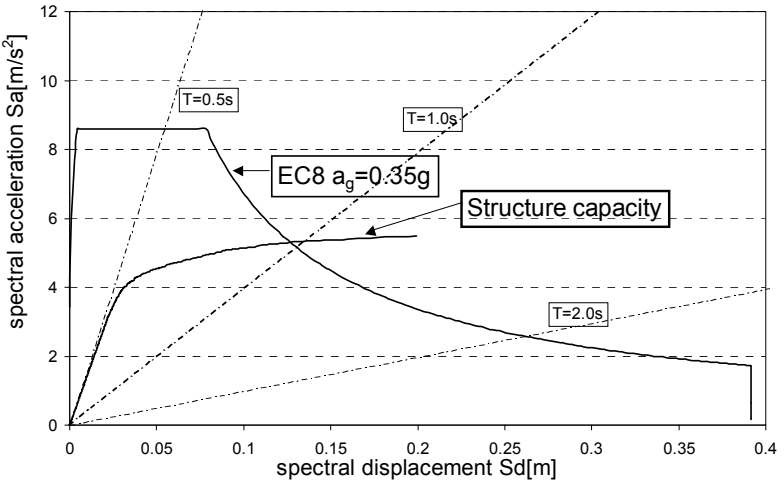

Figure 18. Structure capacity versus earthquake demand

The both curves are presented in acceleration-displacement-response-spectrum ADRS-format. On the Fig. 18 earthquake demand is represented by Eurocode 8 design spectra for the elastic behavior.

This procedure gives very good insight into the structural behavior from the engineering point of view. Position of the structure capacity curve regarding earthquake demand curve shows what kind of measures should be undertaken to improve seismic performance of the building, if it's necessary. Retrofit of the structures concerns three basic structural properties: strength, ductility and

stiffness. Each of them is important for the desirable structural performance during an earthquake. The strength is connected with minimum design capacity, ductility level is important for dissipation of energy induced into the structure by an earthquake and stiffness is important to limit deformations.

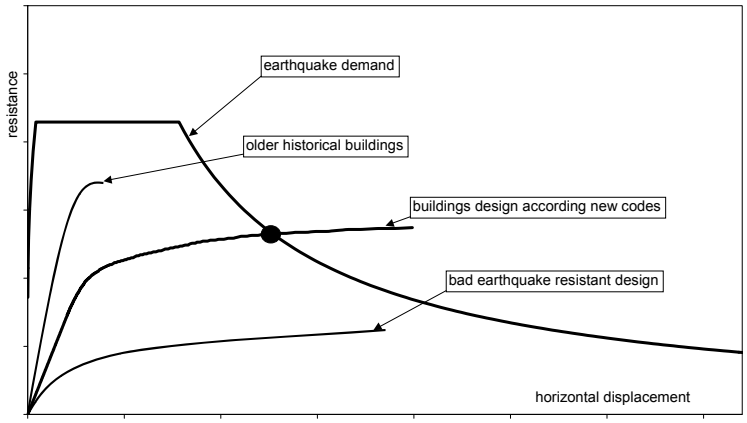

Figure 19. Capacity of different structures regarding their earthquake resistance

On the Fig. 19 the capacity curves for three different structures are compared referring to earthquake demand. The first curve, which does not intersect the demand curve represent behavior of brittle structures with low ductility. This is typical for older historical buildings constructed as robust unreinforced masonry structures. The fundamental period of such structures is usually in the range of high spectral acceleration. If the capacity curve does not go over seismic demand the structure generally cannot survive that earthquake intensity. On the contrary side there are very soft structures, with high ductility but without minimum of required resistance. The capacity curve also does not intersect the seismic demand, here in long period range. It is also example of bad earthquake resistant design.

In order to achieve good earthquake resistant design the structure should have required resistance and appropriate ductility level to assure dissipation of seismic energy. Unreinforced masonry buildings and most of the historical buildings built in a traditional way don't fulfill these requirements.

In the Table 2 (Chapter 4 of this paper) the damage grades for different seismic zones are summarized. To decrease damage grades of the traditional masonry and historical buildings it is obviously necessary to improve their ductility, in the way that the capacity curve intersect the demand curve at the reasonable level of horizontal deformations.

There are many possibilities for repair and retrofit of the masonry or reinforced concrete structures in order to improve their seismic performance. As generally most vulnerable to earthquake a lot of existing masonry buildings should be repaired and strengthened. Two common methods are illustrated here for convenience. Vertical reinforced concrete confining elements built in unreinforced masonry structure improve structural ductility and whole integrity of the building (Fig. 20). The construction begins in the lowest story and continues upward. Good connection between existing masonry and new concrete is of crucial importance.

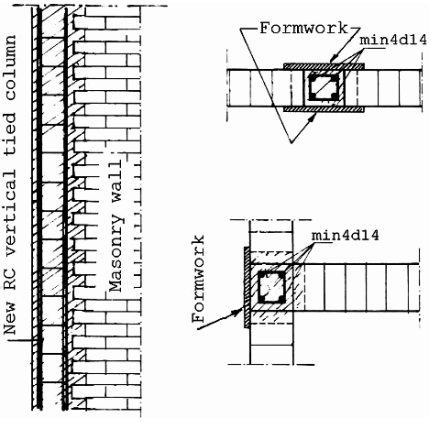

Figure 20. Built in of new R.C. vertical confining elements in existing building

Another very common construction method for masonry strengthening is reinforced concrete jacketing (Fig. 21). It is also logical procedure and at the same time the cracks in the masonry are repaired and covered. The reinforced concrete jackets, 3–5 cm dick, are added, if it's possible on the both sides of the masonry wall. First, wire meshes are fixed by ties on the surfaces of the existing wall and than concrete is added by the shotcrete or some similar method. If the concrete is poured the thickness of the jackets is at least 10 cm.

Vulnerability assessment is important to make decision about retrofit and strengthening of the existing buildings. Seismic evaluation and comparison of structural capacity of existing buildings with seismic demand according to modern seismic codes will result in the necessity of retrofit for the majority of existing buildings, especially for unreinforced masonry buildings. Among them are without doubt very valuable historical buildings, some of them belonging to the world cultural heritage. On the other hand damage statistics from major earthquakes (Otani, 2003) give us the data that after Mexico earthquake in 1985, which was reported as severe, roughly 94% of the buildings suffered light to

minor damages and after Japan earthquake in 1995 about 88% of the buildings survived with light to minor damages. What kind of building structures will suffer heaviest damages; depends not only on structure itself, but local geological and seismological conditions play also important roles. Generally the vertical structural elements have priority when one decides about retrofit and strengthening, because the collapse of building is normally caused by the failure of vertical carrying elements, such as columns and walls. Another important task is to avoid brittle failure of structural elements, as shear failure, which should be examined in retrofit analyzing procedure.

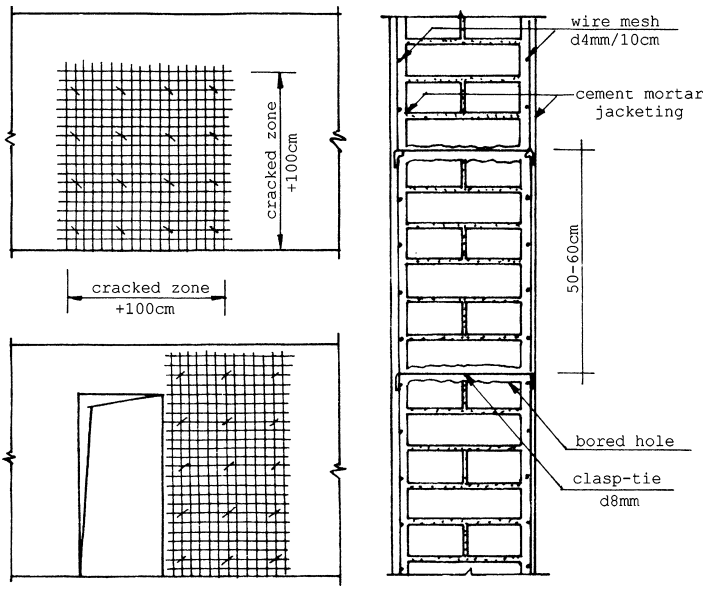

Figure 21. Reinforced concrete jacketing of the existing masonry walls (UNDP, Vol. 5)

7. Conclusions

The existing buildings don't fulfill the requirements of the modern seismic code and they are more vulnerable to an earthquake than the new one. A lot of the existing buildings are built with unreinforced masonry structures. This includes also most of the historical and monumental buildings.

Presented vulnerability classification of typical multistory buildings with masonry and R.C. walls corresponds to regular structures and in average good construction. Irregularities of structural system increase vulnerability class of the building, as well, and it has to be taken in account when making final decision about damage grade of some building for the corresponding seismic zone.

Considering the results from previous chapters, it can be concluded, that for seismic zone 7 (PGA = 0.10 g) prevailing on the seismic map of Bosnia and Herzegovina typical masonry and R. C. wall buildings should not suffer heavy damages or collapse. With the increase of earthquake intensity the possibility of more significant damages also increases, especially in masonry buildings. So, heavy damages of unconfined masonry buildings are real in seismic zone 9. Significant damages can be expected in irregular building structures and in masonry with R.C. confining elements. R.C. walls are, as expected, less vulnerable to earthquake compared to masonry buildings. Their vulnerability significantly increases in the case of irregular structural system. When the earthquake is with PGA between 0.20 and 0.35 g (seismic intensity zones 8 and 9) significant damages of buildings with soft-stories, especially with flexible ground floor, cannot be avoided.

Historical buildings should be classified in the same vulnerability classes as unreinforced masonry buildings. They are generally stiff and show brittle behavior. Significant damages are to be expected during stronger earthquakes, which were confirmed in the past. Some structural elements as dome and arches crack already at lower seismicity level, but those damages are not severe for overall structural stability.

Evaluation of existing building can be efficiently done using pushover analysis and capacity spectrum method. Comparison of structural capacity and seismic demand gives conclusions about retrofit of the structure. Some common method for damaging repair and strengthening of the masonry structures are presented. Strengthening and retrofit have to focus primarily on vertical structural elements, as wall and columns, as well as avoiding brittle shear failure.

References

Bachmann, H. (1995) *Erdbebensicherung von Bauwerken,* Birkhäuser Verlag Basel (in German).

European Macroseismic Scale (1998) EMS-98, Editor G. Grüntal, European Seismological Commission, Luxembourg 1998.

Eurocode 8 (EC8) European Standard prEN 1998-1 (2003), Design of structures for earthquake resistance, Part 1: General rules, seismic actions and rules for buildings, Draft No. 6, January 2003, CEN European Committee for Standardization, Brussels.

Freeman, S.A. (1998) *Development and Use of Capacity Spectrum Method*, 6th U.S. National Conference on Earthquake Engineering.

Hrasnica, M. (2005a) *Seismic Analysis of Building*, Faculty of Civil Engineering, University of Sarajevo, 2005 (in Bosnian).

Hrasnica, M. (2005b) *Reconstruction of Historical and Cultural Building and Earthquake*, Regional Cultural and Natural Heritage Programme for South-Eastern Europe, Tuzla (in Bosnian).

Otani, S. (2003) *Seismic Vulnerability Assessment and Retrofit – State of Practice in Japan*, Proceedings of *fib* 2003 Symposium, May 6–8 Athens Greece.

Paulay, T. and Priestley, M.J.N. (1992) *Seismic Design of Reinforced Concrete and Masonry Buildings*, Wiley, New York.

Petrovski, J.T. (2004) Damaging effects of July 26, 1963 Skopje Earthquake, Middle East Seismological Forum, Cyber Journal of Geoscience Volume Two.

SGEB (2004) Photo Collection Earthquake in West Turkey, Schweizerische Gesellschaft für Erdbebeningenieurwesen.

Tomaževič, M. (2006) *Earthquake-Resistant Design of Masonry Buildings*, Series on Innovation in Structures and Construction – Vol. 1, Imperial College Press, London.

UNDP/UNIDO (1984) *Repair and strengthening of reinforced concrete, stone and brick-masonry buildings*, Building construction under seismic conditions in the Balkan region Vol. 5, Vienna.

UNDP/UNIDO (1984) *Repair and strengthening of historical monuments and buildings in urban nuclei*, Building construction under seismic conditions in the Balkan region Vol. 6, Vienna.

Wenk, T. (2004) *Erdbeben und Kulturgüter: Erkenntnisse aus Ingenieursicht*, Forum 4, BABS Bern (in German).

ENVIRONMENTAL DAMAGE ASSESSMENT, WASTE MANAGEMENT AND OVERVIEW OF THE CURRENT SITUATION IN BOSNIA AND HERZEGOVINA

A. SERDAREVIC*
Department for Sanitary Engineering and Solid Waste, Patriotske lige 30,71000 Sarajevo, Bosnia and Herzegovina

Abstract. How to reduce the negative and harmful environmental impact by production and dissemination of tons of different type of wastes every day? Approach to this issue should always be based on the relevant and valid legislation and on the state or regional strategy for the waste management. The brief information about waste, waste disposal solutions, minimization of the damages caused by wild dumps and others environmental impacts are presented in this paper with an overview of the situation in Bosnia and Herzegovina (B&H). Construction and demolition material, polluted soil, as well as other waste that is a result of eventual natural disaster or military actions are particularly emphasized with a brief overview of situation in Bosnia and Herzegovina after the war (1992–1995).

Keywords: Waste management, environmental impact, landfill, leachate, biogas, pollutions

1. Introduction

According to the Law on Waste, "waste" means any substance or object which the holder discards, intends or is required to discard, and which belongs to one of the categories listed in Law on Waste Management and appears in the List of Wastes. The EU Waste Framework Directive given by European Directive of Waste 75/442/EC defined wastes as following:

* To whom correspondence should be addressed. e-mail: amraserdarevic@yahoo.co.uk

A. Ibrahimbegovic and M. Zlatar (eds.), *Damage Assessment and Reconstruction After War or Natural Disaster*,

"Once a substance or object has become waste, it will remain waste until it has been fully recovered and no longer poses a potential threat to the environment or to human health."

To define what a waste is and to classify all sorts of wastes could sometimes be very difficult, but in general the wastes are divided into several main groups of wastes shown on the Fig. 1.

Figure 1. Main groups of waste (Serdarevic, 2006)

The human control system of many activities and operations related to waste is called waste management. Its aim is to minimize harmful and negative impacts that all types of wastes have on the society and the environment.

2. Waste Management

The waste management concepts vary in different countries and regions. Waste management encompasses different activities and fields of expertise but all of them are aimed at collecting, transporting, treating, recycling or disposing of wastes. The waste management is generally applied in order to reduce negative effect of wastes on human health, the environment or aesthetics aspects in nature. Waste management relates to all activities on recovering resources from wastes. Waste management refers to managing solid, liquid, gaseous non-hazardous or hazardous wastes substances with minimum negative side effects. Waste management includes the prevention of waste production, the reduction of the quantity of waste and its negative impact on the environment, the reduction of the volume or harmful nature of the waste, the planning and control of all activities on the collection of wastes, transport of wastes and final treatment, all activities and operation, closure and aftercare of waste treatment facilities, the environmental monitoring activities during the operational time and post-closure period, raising public awareness and educational activities in connection with waste.

2.1.1. *Waste Management Concepts*

The waste management strategy, in terms of waste minimization, is based on the principles of "3R": reduce, reuse and recycle. The goal of the waste management strategy is to extract the maximum practical benefits from products which should generate the minimum amount of waste. The waste hierarchy is shown on the Fig. 2. Waste management practices vary widely between developed and developing countries. There is an obvious variation in waste management methods between areas for many reasons due to different types of waste material, available areas for waste treatment facilities, nearby land uses and settlements, public awareness and raising it through education and promotion.

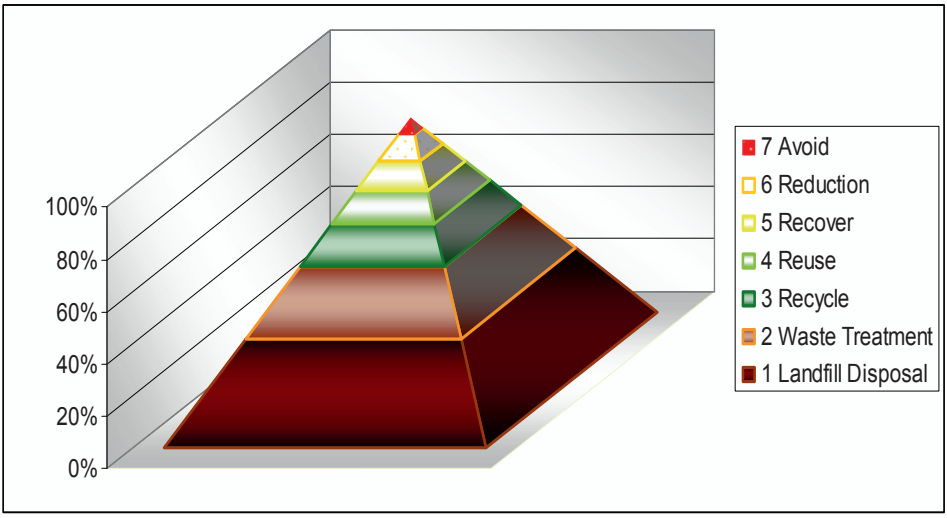

Figure 2. Waste hierarchy (Serdarevic, 2006)

2.1.2. *Waste Management Methods – Waste Hierarchy*

– Avoid and Reduction

To avoid and/or minimize the generation of waste is the best option from an environmental and economic viewpoint. It means that all manufacturers should think about new, "clean" manufacturing and how to re-designing products to improve durability and/or how to make all or some parts of products easy to repair or reuse.

– Reuse

To reuse means to find ways to use the goods again. It could comprise more activities such as collecting, cleaning, and repairing products before we use them again.

– ***Recycle***

Recycling is the processing of waste products aimed at providing raw materials for producing new goods. The recycling process is applied to different materials, but usually it is old newspapers and packaging, aluminium cans, plastic bottles and PET packaging, glass, textiles, etc….

– ***Waste Treatment***

As already mentioned, due to the Waste Management Strategy (depending on the country, regions, municipalities' decision, legislations, etc…) there are various technologies for final waste treatment and disposal. Depending on a number of conditions, such as type of waste and its quantity, available technologies and land uses in the country, technologies used the most are listed below:

1. Landfill
2. Mechanical – biological treatment
   - Mechanical sorting
   - Composting or anaerobic digestion
3. Thermal treatment (Energy recover)
   - Incineration
   - Gasification
   - Pyrolysis
   - Mechanical heat treatment (autoclaving)

2.2. DISPOSAL METHODS

2.2.1. *Landfill*

Landfills have been the most common methods of organized waste disposal and remain so in many places around the world. Smaller landfills can be used for different waste management purposes, such as the temporary storage, consoledation and transfer stations, especially as a part of a regional sanitary landfills concept, or for the treatment of some sort of waste materials (sorting, treatment, or recycling).

Disposing wastes to the landfill is the least environmentally sound waste management option as it requires large areas of land and may cause air and water pollution shown on the Fig. 3. The landfill has to be designed and built in accordance with technical regulations provided by the legislation and EU Directives.

To be commercially and environmentally viable a landfill must be constructed in accordance with specific requirements, which are related to:

- **Location**

  – Distance and location from the urban zones

  - Easy access to transport by road
  - Transfer stations
  - Properties and Land value
  - Type of landfill construction (depending on the geomorphology at the site): abandoned mines and pit-filling, canyon, natural slope or flat area.
- **Stability**
  - Geology cross section
  - Earthquake zones
  - Underground water level
  - Location of nearby rivers, streams
- **Operational data**
  - Operational period
  - Quantity and quality of wastes
  - Density of the wastes
  - Amount of daily cover material
  - Thickness of capping
  - Construction of lining and drainage layers
  - Operational costs
- **Environmental protection**
  - Installation of base liner and collection systems for:
  - Storm water system
  - Leachate collection and treatment
  - Landfill gas collection and using
  - Post closure activities and environmental monitoring

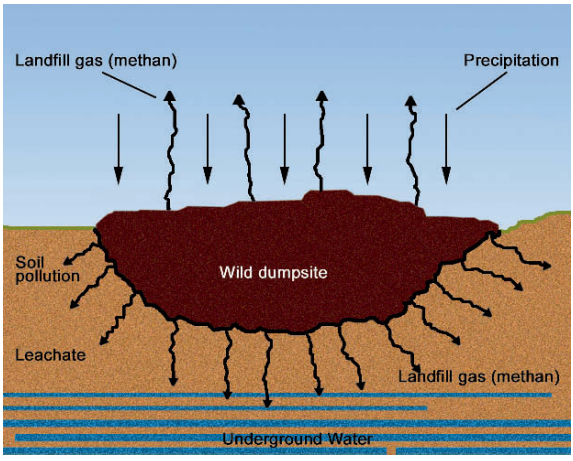

Figure 3. Environmental impact of dumpsite (Serdarevic, 2006)

Potential negative environmental impacts associated with solid waste management include contamination of soil, groundwater, surface water and air quality. These impacts would be associated with construction, collection, transfer and storage, operation of the landfill and leachate and gas emissions from landfills.

Technical safeguard regulations are mainly focused on the isolation liners with low permeability (clay or bentonit layer) in the basis to prevent contamination by leachates migrating downward through the underlying geological formation, operational instruction for disposal waste in the cells with waste compactions, daily covering with layers of soil, and sealing the top of the landfill following recommendations for post-closure environment monitoring activities (Fig. 4).

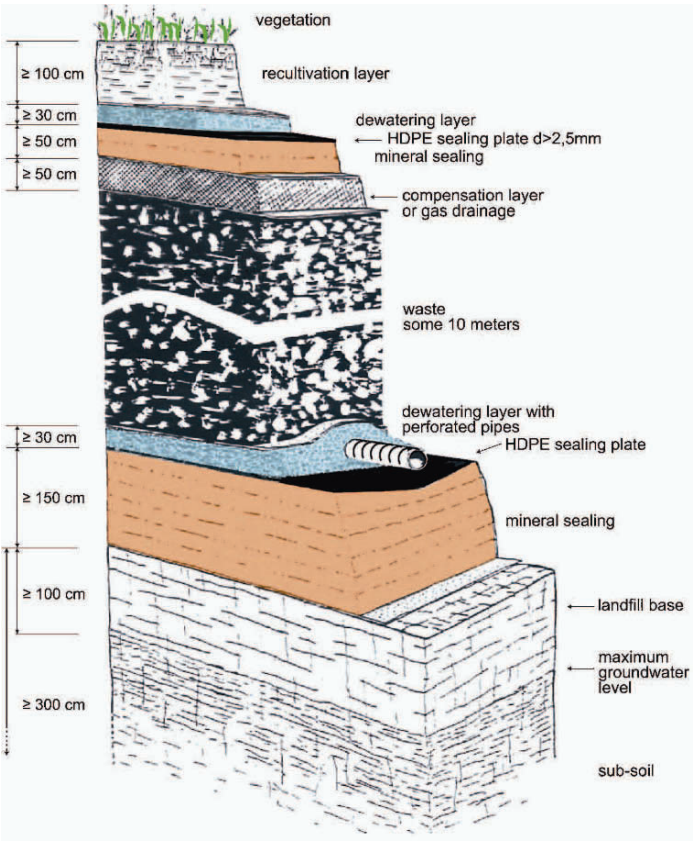

Figure 4. Multi-barriers hazardous waste landfill with double sealing system/German technical regulation on waste 1990 (Thomanetz, 2005)

The biodegradable waste decomposition results in the productions of landfill gas (methane) and leachate. Both have a negative impact on the environment. In order to reduce air pollution and prevent potential explosion, sanitary landfills have to be built with gas pipelines to collect and burn it to produce electricity.

The generation of leachate is caused by precipitation percolating through waste disposed in a landfill. The percolating water becomes contaminated. Additional leachate volume is produced during this decomposition of carbonaceous material. Leachate has to be collected and treated properly before its final disposal to the sewage or streams.

Factors such as daily covering, waste compressibility, waste layer thickness and a number of passes of the compactor over the waste affect the waste density. That could result in decreasing of leachate production as well as the extension of landfill operational time

The possible alternatives to landfills are waste reduction and recycling. In the last decades, alternative methods to waste disposal to landfill and incineration have been accepted. Anaerobic digestion, composting, mechanical biological treatment, pyrolisis and gasification are now being used and they have found their place in the market, especially in developed countries.

Some countries, such as Austria, Germany and Switzerland prohibited disposal of untreated waste in landfills. Only the ashes from incineration plants, inert material or the stabilised material of mechanical biological treatment plants could be deposited on landfills.

2.2.2. *Thermal Treatment*

Using pyrolysis, gasification or incineration as thermal waste treatment, the volume of the waste to final disposal to the landfill are minimized and energy generated as a result of this process can be used for producing electricity or heating systems. Thermal treatment of wastes should be one part of an overall integrated waste management strategy based on reduction of waste production, waste recycles and energy recoveries. Plants for thermal treatment of wastes should be considered upon the analysis of cost-effectiveness, depending on the long-term strategy in waste management, the annual waste production, types of waste, investments and operational costs, taxes, etc.

There are a number of topics and issues which are related to waste generation, waste management, and environmental impact. In addition, the focus will be on the waste generated as a consequence of a natural disaster and/or military actions and an overview of its environmental impacts.

3. Disaster Debris

When natural or man-made disasters, such as storms, floods, earthquakes, tornados or military activities hit a settlement, solid waste management is not the first to be treated, but it always generates huge amount of debris. Debris is the waste stream resulting from natural or man-made disaster and usually includes building materials, sediments, vegetative debris, personal property and other material. The amount of debris generated from a disaster varies from one situation to another. As already mentioned in this paper, depending on the waste management strategy, community has several options on how to manage disaster debris (Fig. 5).

Figure 5. Aftermath of an earthquake and damages in the town due to the torrent (www.ocorn.com)

The waste first has to be classified as a non-hazardous including inert material like concrete, bricks, wood, soil, green waste (e.g. trees, bushes), furniture and personal property, ash, etc., or as a hazardous waste that includes contaminated soil, radioactive material, heavy metals and all hazardous waste classified on the list of hazardous waste by legislation (e.g. EU waste catalogue). This type of waste creates an additional issue which has to be treated urgently by a community already hit by a disaster.

3.1. DISASTER DEBRIS MANAGEMENT PLAN

According to the waste management strategy, the best approach should be to make a plan for disaster debris management before disaster happens. A plan for disaster waste/debris should define options and activities for collecting, sorting, recycling, treatment and final disposal. Main goals should always be protecting

human health and the environment, and preventing generation of additional waste.

Solutions for collecting and removal of non-hazardous disaster debris depend on buildings' damage assessment, restoration or demolition, clean up or repair of structures, infrastructures repair and restorations, as well as the assessment of amount and types of debris caused by wildfire or floods. A disaster debris management plan should include the following components (Fig. 6):

1. Pre-activities: waste and environment related legislations and regulations
2. Identification of debris types and forecast amounts
3. Potential temporary and long-term storage capacity and equipment
4. Debris removal strategy
5. Harmful and hazardous materials – identification and handling recommendations
6. Recycling, energy recovery, reuse and disposal options
7. Environment impacts and protection

Figure 6. Construction and demolition material

3.1.1. *Identification of Debris Types and Forecast Amounts*

Natural disasters, such as earthquakes, floods, winter storms, wildfires, tornadoes, as well as man-made disaster or military actions, can cause damage to buildings, roads, bridges and other structures, causing mainly construction and demolition (C&D) materials generation. Also, the above mentioned disasters can generate large quantities of woods and mixed metals. Further more, disaster debris could include furniture, personal things, electronic waste, white goods and industrial or household hazardous wastes.

Forecast of the amount and type of debris generated during different types and sizes of natural disasters help the planner understand the scope of activities for debris treatment. Due to the unpredictable nature of natural disasters, no

estimation tool will provide a reliable assessment. The estimates could be based on previous experience. The forecast tools can be used for potential man-made disaster, especially for industrial facilities or e.g. for nuclear plants and potential accidents.

3.1.2. *Recycling Disaster Debris*

The process of extracting resources or value from waste is generally referred to recycling, recovering or reusing the material. There are a number of different methods by which waste material is recycled: the raw materials may be extracted and reprocessed, or the calorific content of the waste may be converted to electricity.

Many communities are finding effective ways to recover, reuse, and recycle all kinds of disaster debris. Soil, wood, and some infrastructures and building materials can be recycled or composted into useful commodities. For example (EPA, 2008):

- Green waste, such as trees and shrubs, can be "recycled" into valuable organic material, such as compost or mulch.
- Concrete and asphalt can be crushed and sold for use as sub-base in road building.
- Metal can be recycled and sold by scrap metal dealers.
- Brick can be sold for reuse or ground for use in landscaping applications.
- Soil, gravel, sand and mud can be used as landfill cover or a additionally soil material in construction on the landfill access roads, etc.

In the past, disaster debris was often buried, disposed or burned at the nearest available area. This option is no longer acceptable, however, because of the side effects of smoke and fire from burning and potential (surface and underground) water and soil contamination. The typical methods of recycling and solid waste disposal in sanitary landfills often cannot be applied to disaster debris because of the large volume of waste that can not be added to overloaded existing disposal capacity of landfills. Disaster debris recycling is much easier if the municipality or regions have already established a recycling program.

3.1.3. *Recycling of Construction and Demolition Waste Disaster Debris*

Building materials classified as construction and demolition (C&D) waste are generated by the total or partial destruction of structures as consequences of military actions or disasters and may represent a large portion of waste.

A high proportion of conventional construction and demolition waste and particularly the fraction derived from concrete, bricks and tiles, is well suited to being crushed and recycled as a substitute for newly quarried aggregates in certain lower grade applications, most notably as access roads, filling material

and road sub-base. Also, it is possible to use slightly contaminated soil and demolition debris in earth constructions, in accordance with technical safeguard regulation. These practices have been common in EU states for many years. These materials have a potential to displace equivalent volumes of primary aggregates, thus preserving non-renewable resources, with a minimal need for landfill space for sorting, recycling and partially disposing at the site as material for access roads at the landfill.

3.1.4. *Benefits of Recycling Disaster Debris*

The benefits of recycling disaster debris and an already prepared plan include the following:

- Making a strategy and plans for the reuse of large amounts of materials
- Cleaning up potentially hazardous materials
- Cleaning up temporary storage sites
- Sorting or processing of debris
- Accelerating a recovery period by planning alternatives for recycling, reuse, and disposal

4. Debris Management Sites and Environmental Impact

The sites used for disaster debris management, or for the management of the demolition and potential hazardous wastes after military actions, could be temporary sites or planed through a strategy. The sites should be sufficient in size and with an appropriate geological profile, and be located at an appropriate distance from potable water, streams, rivers and lakes. The sites should not be located in the region of floods or wetlands, as well as in the zones of storm water runoff, erosion or slide slopes.

A number of adverse impacts occur from sites operations. These impacts can vary: fatal accidents like e.g., fire or explosion, infrastructures damage (e.g., damage to access roads by heavy vehicles); pollution of the environment (such as contamination of groundwater and/or aquifers by leakage and soil contamination during temporary usage, as well as after landfill closure and simpler nuisance problems (e.g., dust, odour, vibration of machinery, vermin, and noise). Environmental noise and dust are generated from vehicles and from operations like crushing, sorting and stockpiling of C&D wastes.

There are also visual and aesthetic impacts including littering, which can be considered the most visible form of disaster debris pollution in green fields or urban sites. Other forms of pollution associated with different disaster debris

materials include unregulated disposal of materials on private or public land, illegal dumping and leaching.

Among the many toxins which can be found in disaster debris, one of the most harmful in plastic debris is polychlorinated biphenyls (PCB), which can leach into the surrounding soil and waters. The limit for permitted concentration of PCB in soil and water is provided by legislation, as well as for a number of other substances that can be found in water, soil and air.

In general, environmental, safety and logistical considerations include:

1. Environmental monitoring. Areas used primarily for vegetative and wood debris should be monitored for fires, but areas used for mixed disaster debris, C&D or hazardous wastes need more comprehensive monitoring.
2. Removal of debris from sites according to the plan and in short time. Hazardous waste, mixed and harmful wastes should be remove as soon as possible and be properly treated and stored.
3. Building access roads and limited site access.
4. Minimising noise, vibration and dust side effect on the surrounding areas using the acceptable hours for recycling and reusing, applied technical regulation and modern technologies for recycling in order to prevent air, water and soil pollution.
5. Controlling transport and delivery impacts associated with C&D recycling and reuse.

Regarding the hazardous wastes, technical safeguards are the following:

1. Isolating the sites by double liner of plastic sheeting or a concrete pad
2. Fencing with visible label or orange barricade
3. Obtaining absorbent material or sandbags for accidental spills
4. Using wooden pallets for storage bins, containers, barrels
5. Labelling the bin or barrels with gases, liquids or solids appropriately and storage according technical instructions
6. Providing sufficient fire extinguishers
7. Monitoring the environment around the site

5. Overview of Situation in Waste Management in Bosnia and Herzegovina

5.1. INTRODUCTION OF WASTE MANAGEMENT IN B&H

With regard to waste management, B&H is legging behind developed countries. The problem of collection, treatment and final disposal of waste was not treated adequately even before the war. The destruction caused by the 1992–1995 Bosnian war has only made things worse (Fig. 7).

Figure 7. Sarajevo – Main post office and settlement nearby airport destroyed during the war 1992–1995 (www.paixbalkans.org, http://img57.imageshack.us)

The existing wild dumps should be closed down as soon as possible and turned into sanitary landfills. Following completion of costs evaluation and technical analyses, the regional approach to solid waste management was adopted. This approach includes short term, medium and long term activities in this field including municipal solid waste, industrial waste and hazardous waste.

5.2. LEGISLATION IN DOMAIN OF SOLID WASTE MANAGEMENT IN B&H

State of Bosnia and Herzegovina consists of two entities and one district (Federation of Bosnia and Herzegovina, Republika Srpska and Brcko district).

A legal framework for environmental protection and waste management was prepared in 2002 and 2003. As a result, a set of laws on environmental issues was adopted.

A set of these laws was adopted in Republika Srpska (RS) in September 2002 and published in the RS Official Gazettes number 52/02 and 54/02. In the Federation B&H, these laws were published on 19 July 2003 in the Official Gazette number 33/03 (Fig. 8).

This set of laws includes:

- Law on Environmental Protection
- Law on Nature Protection (Official Gazette FB&H no. 33/03)
- Law on Air Protection (Official Gazette FB&H no. 33/03)
- Law on Water Protection (Official Gazette FB&H no. 33/03)
- Law on Waste Management (Official Gazette FB&H no. 33/03)

Figure 8. Map of Bosnia and Herzegovina

Both entity governments adopted basic laws in the domain of environmental protection with no substantial differences. Also, a number of activities have been undertaken in order to speed up the implementation of the adopted laws.

Apart from this legislation and secondary legislations, some other strategic plans, project and studies regarding the waste management in B&H have been completed, such as:

- National Environmental Action Plan (NEAP) – B&H; it was adopted in 2003
- "Strategy of Solid Waste Management", prepared with EC support
- Feasibility studies for a number of "Waste Allocation Districts" for projects appraised by the World Bank

- "Environmental Protection Assessment Report for Industrial, Medical and other Hazardous Wastes in B&H", a comprehensive study on industrial and hazardous wastes in the country
- "Support for Improved Waste Management in Bosnia and Herzegovina" CARDS 2002, Bosnia and Herzegovina; EC/B&H/02/013

According to the NEAP, eight priorities have been identified and one of them is waste management. This field is divided into two main groups of activities and problems:

(a) Establishing the waste management in B&H
(b) Dumpsites rehabilitation

5.3. LAW ON WASTE MANAGEMENT IN B&H

The Law on Waste Management in FB&H and RS outlines priorities in solid waste management, basic definitions and directions in waste management. Also, each canton has its own plan of waste management within its jurisdiction.

According to this law, some measures have to be taken to enable collection and disposal of waste without jeopardizing health of the population and without environmental risks, such as:

- Risks for water, air, soil, animals and plants
- Odor problems and noise
- Risks for environment and area of special interest

The Law on Waste Management covers all categories of waste, all activities regarding planning waste management, responsibility for waste management, the ways of transporting waste abroad, and supervision of all related activities.

The main purpose of the Law is to encourage conditions which would prevent generation of waste, recycling and re-using waste and its final and safe disposal.

A number of rules and regulations in domain of waste management have been adopted, in accordance with the EU Directives. The catalogue of waste in Federation B&H and RS is in line with the European Waste Catalogue and the EU Directives.

6. Solid Waste Management in B&H

6.1. CURRENT SITUATION IN SOLID WASTE

At the moment, the most used practice in the domain of municipal solid waste and hazardous waste (industrial, medical and other) management in B&H is

disposal at the small, local municipal landfills which do not meet the criteria necessary for the sanitary landfills. Problems are always related to a selection of location and/or technical inadequacy of the existing landfills.

In addition to local municipal landfills, a large number of wild dumps are located on river banks, abandoned quarries, pits and natural depressions. The main difference between wild dumps and sanitary landfills is in their size, location and impact on the environment. Wild dumps often take a relatively small space and contain smaller amounts of waste. Wild dumps exist in almost all municipalities in B&H.

The waste disposed in these wild dumps varies. It includes domestic waste, non-hazardous waste such as old cars, trucks, refrigerators, stoves (even car tires), as well as organic and medical waste of unknown origin.

In municipalities with lots of forests and private sawmills a big problem are sawdust dumps. This problem has been emphasized after the war in Bosnia and Herzegovina, due to the uncontrolled forest/woods exploitation. Such dumps are located mostly in the north-eastern part of the country (Krajina), but also in some other parts of B&H.

In flat, northern part of the country, there is a problem of waste generated at slaughterhouses and chicken farms, and some very dangerous pesticides and herbicides are used in farming.

Collection of domestic waste in small towns and villages is not organized. Also, the treatment and final disposal of the collected waste is not solved appropriately and domestic, hazardous, industrial and demolition wastes are not being separated.

Such inadequate waste management directly jeopardizes local inhabitants in many ways, but a wider area can be polluted too, due to dangerous infiltration of leachate and air pollution.

6.2. REGIONAL SANITARY LANDFILLS IN B&H

6.2.1. *Strategy of Solid Waste Management in B&H*

As part of the implementation of the World Bank projects, the Strategy of the Solid Waste Management in B&H was developed and approved by both entity governments in 2003. It envisages that all activities related to waste management will be divided into several cycles until 2020, such as (Fig. 9):

- Production of waste (domestic, industrial, health care, construction)
- Reduction and recycling
- Disposal (removal of wild dumps, rehabilitation of existing landfills and proposals for regional sanitary landfills)
- Legislation, regulations, standards, guidelines

- Payment for services
- Taxation and incentives
- Enforcement and awareness

The selection of regional sanitary landfills location is the priority in the waste management plans. According to the strategy, the disposal activities will be improved at all levels, moving as rapidly as possible from the present local dump sites to new regional multi-municipality facilities, each designed, constructed and operated in accordance with B&H regulations and the EC directive.

Figure 9. Dumps in Bosnia and Herzegovina towns (Goražde and Tuzla) (Support in Solid Waste Management in B&H, 2005)

The most hazardous dump sites, and especially wild dumps, will have to be closed or rehabilitated as far as is practicable to limit existing pollution or health threats. Existing wild dumps will be analyzed and closure priorities identified. Measures will also be formulated to put a stop to wild dumping. Current disposal practices at local sites will have to be improved if these sites are major causes of pollution and health impacts.

The rehabilitation of existing wild dumpsites, and some formal disposal sites where capacity limits have been reached, should be fixed through the activities planned in short-to-medium term strategy. In undertaking rehabilitation of some sites, wastes will be removed to other locations, thus forming an additional waste arising for which better disposal practices are required.

All of the potential options for the municipal solid waste management, industrial and medical wastes collection, transport and disposal were analyzed as a part of the Strategy for a short (2005), medium (2005–2010) and long term (2010–2020).

The efficient waste management is based on combination of a number of techniques and practices, which vary from country to country, depending on the cost, technical capabilities and waste generation specific for that country. Potential options for the waste management in B&H are shown in Fig. 10.

The Strategy of Waste Management in B&H considers and proposes that medium and long term plans should be based on the approach of multi-municipality landfills (Waste Allocation Districts – WAD). It is proposed that within each of these districts a multi-municipality landfill site is designed, constructed, and operated, with increasingly sophisticated practices and controls introduced, in aiming to approximate to EU landfill standards by 2020.

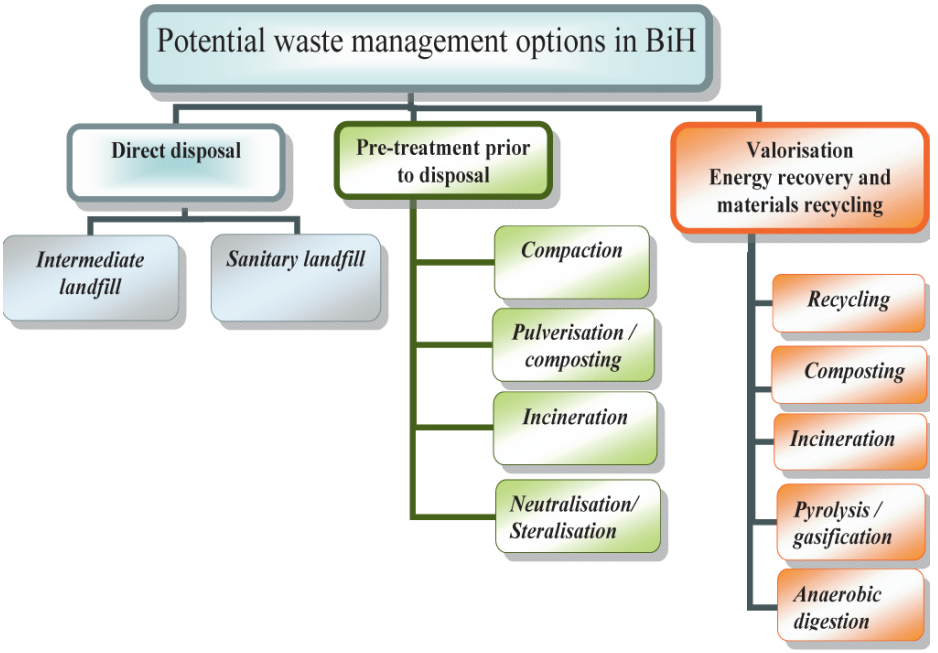

Figure 10. Potential Waste Management Options for Priority Waste Streams in B&H (Startegy, 2000; Serdarevic, 2006)

The most important factor for the Plans for waste management is the part of the Strategy concerning the selection of micro-location for regional sanitary waste landfills. With the exception of the cities of Tuzla and Sarajevo, no other city or municipality in Bosnia and Herzegovina has a sufficient number of residents to generate enough wastes that would justify construction of economical and self-sustainable sanitary waste landfills. The amount of waste which is being collected daily at a disposal site has to be sufficient for the optimal use of a landfill and all the necessary equipment.

For a fully equipped, modern sanitary landfill, established on the cost-effective basis, at least 150–200 t of waste has to be collected every day. Modern cost-effective sanitary landfills can accept upwards of 1,000 t/day of wastes (equivalent to the annual household waste production from around 72,000,000 persons).

If these requirements were met, B&H would need four to five sanitary waste landfills in the future. According to the Strategy, the amount of household waste generated by one person is approximately 250 kg per year. In total, the amount of communal waste generated by one person every year is 500 kg (this is the average rate on the state level). At this rate, 2.1 million tons of communal solid waste is generated every year in B&H.

Also, one of the most important aspects in selecting the location for a new waste landfill for a region is a distance between local transfer stations and a sanitary waste landfill, which should not be more than 100 km. Waste transfer stations will be required in order to provide cost effective transportation of wastes to landfills.

If the general economic situation in the country improves, it can be expected that the quantity of waste generated in B&H will double in the next 15–20 years.

The Strategy envisages a regional approach to the management of communal waste through inter-municipal organizations tasked with waste management and its disposal at regional sanitary waste landfills.

6.2.2. *Micro-Location for Regional Sanitary Landfills*

The problem of solid waste in Bosnia and Herzegovina would be solved exclusively through setting up regional waste landfills.

The Strategy considers several options as interim solutions and they are 16 regional sanitary landfill (on the entity level) and 14 regional sanitary landfill (on the inter-entity level) locations. According to the Strategy, the long term solution due to amount of waste generation, would be establishment of five to eight joint regional sanitary landfills.

It has been suggested that regional waste landfills in the Federation B&H should be built in the regions of: Bihac, Bugojno, Gorazde, Gracanica/Lukavac, Livno, Mostar, Tesanj, Tuzla and Zenica. In RS, the following locations have been proposed: Banja Luka, Bijeljina, Doboj/Teslic, Foca, Gacko, Prijedor, and Vlasenica (Fig. 11).

In January 2003, the World Bank and the entity governments of FB&H and RS approved US$18 million for solving the solid waste management problem and setting up regional sanitary waste landfills over the period of 5 years. The already accepted Strategy was used as a starting point for selection of locations for regional waste landfills.

Before making a final decision on micro-location for new regional waste landfills, approving loans and starting the process of preparing technical documentation and carrying out planned activities, the following problems should be analyzed and solved first:

- Estimation of the amount of waste and cost-effectiveness and self sustainability of a new regional waste landfill
- Establishing of the inter-entity council responsible of a regional waste landfill
- Selection of micro-location in accordance with the regional, inter-entity, and multi-municipal waste management approach
- Selection of locations with minimum 20 ha of land available for a regional waste landfill
- Setting up a sanitary waste landfill in accordance with the European standards (multi-barrier protection, fences, scales, recycling, collecting gases, leachate treatment), and selection of the appropriate technology of waste disposal (compacting, daily covers)
- Obtaining all necessary technical documentation

The proposed selected locations for regional waste landfills must be approved by the development of separate feasibility studies, preliminary designs, main designs of landfills, as well as studies of their impact on the environment.

The regional, inter-entity waste landfills in Bijeljina, Banja Luka, Tuzla, Zenica, Mostar, Sarajevo and Bihac were agreed to be set up first based on afore mentioned pre-activities.

6.3. CURRENT ACTIVITIES ON SETTING UP REGIONAL WASTE LANDFILLS IN B&H

The regional, inter-entity waste landfills were set up near the cities of Bijeljina, Banja Luka, Tuzla, Zenica, Mostar, Sarajevo and Bihac based on the analyses of the regions demands.

A micro-location chosen for the regional waste landfill in Tuzla did not meet the necessary requirements and a search for a new location is underway. Also, a micro-location for a regional sanitary landfill in Mostar hasn't been identified yet.

The regional sanitary landfill "Moscanica" is located 15 km from Zenica, and thus far around US$5 million was invested in its development. The landfill, commissioned in June 2008, was built according to EU directives and standards but still is not full operated.

Region:

1. Bihac	2. Bugojno	3. Mostar
4. Sarajevo	5. Livno	6. Banja Luka
7. Doboj/Tesanj	8. Bijeljina	9. Kladanj
10. Trebinje	11. Tuzla	12. Zenica
13. Gorazde	14. Prijedor	

Figure 11. Strategy for solid waste management in B&H – proposed sites for regional sanitary landfills (Strategy, 2000)

The project "Moscanica" of 8 million BAM in total is financed by local community by the World Bank loan.

The "Moscanica" landfill is one out of two of landfill of solid waste and is part of Waste Management plan in Zenicko-Dobojski Canton. Beside Zenica it

is planned to be used by other six municipalities of Zenicko-Dobojski Canton. Another landfill is planned to be developed in the vicinity of Maglaj. The exact location will be determined by development of the relevant feasibility study.

The sanitary landfill "Ramici" close to Banja Luka is still under construction. It is expected to be commissioned in 2009. The vast amount of old disposed waste has been relocated to the new operational area. The wild dumps (Knezevo) in that region were properly treated and finally closed at the same time.

A feasibility study and main design were presented for the regional waste landfill in Bijeljina and construction works should be start in 2009.

Medical waste is being disposed at the same existing old household waste dump site in Bijeljina, but this problem will be tackled separately.

Some municipalities (Bihac, Trebinje, and Tesanj) have approached the problem of waste disposal through establishing intermediate city sanitary landfills for a period not longer than 3–5 years.

Also, over the last 5 years, some analyses and feasibility studies have been carried out for some other potential regional sanitary landfills, such as Goražde and Bugojno for example, but no further steps have been taken.

The same approach was used for the plans of several intermediate landfills, for medical waste storage and management of the hazardous waste final disposal.

The CARDS project "Support to the improvement of waste management in B&H" funded by EC was finished in 2005. The results of "Support to the improvement of waste management in B&H" project is proposal for planning and construction of three regional sanitary landfills – Doboj, Livno and Trebinje, all in accordance with the inter-entity version of the Strategy for solid waste management in B&H. The regional concept includes waste collection, transport (directly or through transfer stations), and final disposal to the sanitary landfill. This approach also includes allocation and rehabilitation of existing wild dumps in that region.

Finally, the only regional sanitary landfill in B&H which meets the European standards and is operational is the sanitary landfill in Sarajevo (Fig. 12). This landfill receives a huge amount of waste (~265,000 t a year, out of which ~140,000 t are household solid waste) generated by urban areas within the Sarajevo Canton.

The unsolved problem of Sarajevo waste landfill «Smiljevici» was leachate treatment (Fig. 13). The activities on preparation and collecting necessary date and main design were started in 2005 and 2006. The construction of treatment plant has been started and the activities on the site are still in progress. The experience from Sarajevo sanitary landfill should be implemented during the construction of other landfills in the country.

Figure 12. "Smiljevici" – sanitary landfill in Sarajevo, B&H (Serdarevic, 2007)

Figure 13. Membrane – biological reactor (MBR) at the Sarajevo sanitary landfill (Serdarevic, 2008)

The World Bank Executive Board secured financing of the second phase of solid waste management in Bosnia and Herzegovina in November 2008 in the total amount of US$40 million.

The Second Project of Waste Management, using the achievements of current Project of Waste Management, will continue to improve quality, ecological standards, and financial sustainability of solid waste management in the country.

The results of the first project are impressive. The process of establishing and constructing six regional landfills is ongoing. 1.7 million of B&H citizens will be using those landfills. One hundred and forty-five wild dumps were

treated and closed and that resulted in a significantly reduced negative environmental impact.

7. Conclusions

The waste management is a multidisciplinary subject and very complex in its nature.

The approaches for treatment of natural disaster debris or waste generated as a consequence of military actions are described briefly in this paper.

There are actions that should always be considered in the strategy of debris management, such as making plans in advance for the treatment of consequences of natural or man-made disasters, managing disaster debris and assistance to community in solving the problem with generated wastes, as well as protecting population and environment.

Regarding the disaster debris, the following should be considered in waste management strategy:

- Hazardous wastes properly managed
- Storage location placed in acceptable location
- Landfill capacity appropriately used
- Reuse and recycle of construction and demolition material and other disaster debris

The first step to solve disposal problems for disaster debris is to segregate debris material and manage it appropriately. The second task is to consider possibility for recycling and reusing debris materials, as well as protection of human health and the environment, which should be a priority.

When it comes to the solid waste management situation in Bosnia and Herzegovina, the regional approach to municipal solid waste collection, transport and disposal was proved to be the only possible cost-effective option.

Adoption of the legal framework in B&H in accordance with the EU Directives facilitated comprehensive approach to the waste management, as well as procedures for setting up regional sanitary landfills.

Obviously, further progress in this field depends on securing the funding, but also on finding micro-locations and meeting all criteria for setting up self-sufficient and cost-effective regional sanitary landfills.

In accordance with the Strategy, in domain of waste management the following activities should be carried out:

- Completion of the remaining feasibility studies or adjustment plans for intermediate/regional sanitary landfills.

- Completion of main designs for intermediate and/or regional sanitary landfills.
- Setting up the remaining intermediate/regional sanitary landfills.
- Allocation and rehabilitation of wild dumps.
- Improving the system of waste collection, transportation, recycling of selected wastes and improving the payment system.
- Monitoring will be required before a new sanitary site is established, to provide baseline data as part of the required environmental impact assessment. Continuous monitoring will also be required after the site is closed for operations, to ensure that the risk of pollution will be closely controlled.
- Raising public awareness about waste issues and environmental protection.
- Implementation of above mentioned activities should improve the current situation in municipal solid waste management, as well as the construction of intermediate and regional sanitary landfills in Bosnia and Herzegovina.

References

AEA Technology plc. (2000) *B&H Solid Waste Management Strategy*, EU-PHARE Project, Sarajevo, B&H.

C&E (2005) Faculty of Civil Engineering, University of Sarajevo, *Support in Solid Waste Management in B&H*, CARDS EU-Project, Sarajevo, B&H.

EPA (2008) *Planning for Natural Disaster Debris*.

Law of Waste, Official Gazette FB&H no. 33/03.

Law of Waste Management, Official Gazette RS no. 53/02 and 39/05.

National Environmental Action Plan, Republic BH, (2003).

Serdarevic A. (2006) *Sanitary Landfills and Leachate's Treatments*, M.Sc. theses, Faculty of Civil Engineering, University of Sarajevo.

Serdarevic A. (2007) *Current Solid Waste Management in Bosnia and Herzegovina*, Eleventh International Symposium of Sanitary Landfill and Waste Management, Sardinia 2007, Italy.

Thomanetz E. (2005) *Lectures at the Institue SIWA*, University of Stuttgart, Germany, 2005.

www.okorn.net.

Aftermath of an earthquake in Japan (2004) Photograph by Kimimasa Mayama, Reuters, National Geographic.

http://www.paixbalkans.org/images/sarajevo_maisons.gif

http://img57.imageshack.us/img57/757/post1ot9.jpg

ILLUSTRATIVE EXAMPLES OF WAR DESTRUCTION AND ATMOSPHERIC IMPACT ON REINFORCED CONCRETE STRUCTURES IN SARAJEVO

S. MEDIĆ*, J. ĆURIĆ, I. IMAMOVIĆ, N. ADEMOVIĆ AND S. DOLAREVIĆ
Faculty of Civil Engineering in Sarajevo
Patriotske lige br. 30, 71 000 Sarajevo, Bosnia and Herzegovina

Abstract. This article provides an overview of the sort of damage that is typically found on structures that have been recently rehabilitated in the city of Sarajevo. The damage is partly the result of war action that took place during the period from 1992 to 1995. However, the main cause of structure deterioration was the action of atmospheric agents.

The employees of the Institute for Materials and Structures of the Civil Engineering Faculty in Sarajevo conducted sample analysis to determine the degree of damage. The analysis was done with the goal of rehabilitating and restoring the primary function of the structures. However, most of the structures were not rehabilitated immediately after the conflict and some have yet to be rehabilitated because financial assets determine the rhythm of reconstruction and many of these assets have not been forthcoming. As a consequence of this lapse in rehabilitation, there has been further deterioration of the structures, in addition to damage that is not a direct result of war action.

Keywords: Mechanical damage, fire, frost, moisture, material characteristics

1. Determination of the Current State of the Bearing Structure

An analysis of the damaged structures indicated that war action was only one of the causes of their deterioration. Atmospheric agents, for example, have also

* To whom correspondence should be addressed. e-mail: medic@bih.net.ba

A. Ibrahimbegovic and M. Zlatar (eds.), *Damage Assessment and Reconstruction After War or Natural Disaster*,

had an enormous impact on the destruction and devastation of the structures. Consequently, damage can be classified into two groups:

- Damages resulting from mechanical action and fire
- Damages resulting from atmospheric agents

1.1. DAMAGES RESULTING FROM MECHANICAL ACTION AND FIRE

This damage is the result of explosions caused by grenades and mines. Characteristic damage includes the following:

1. Damages to vertical bearing elements (walls and piers). The degree of damage ranges from local destruction of concrete and reinforcement (Fig. 1) to complete removal of wall in one story (Fig. 3).
2. Pier damage which in some cases includes the piers being totally cut off due to direct grenade impact. It is interesting to note that none of these structures have collapsed even though many of their piers have been cut off. (Fig. 2)

Figure 2.

Figure 1.

Figure 3.

3. Destruction of staircases located next to façade walls and large sunroofs.
4. Destruction of the entire roof structure or damage to the waterproofing as a result of shell fragments that led to free penetration of water into the structure.
5. Destruction of all balconies on upper floors of the structure as a result of grenade impacts on those floors triggering a “domino” effect (Fig. 4).
6. Damages to the inter-story structure caused by grenade hits. (Fig. 5).
7. The uplifting of the entire inter-story structure in respect to the piers due to the explosion. This resulted in horizontal and diagonal cracks on the contact of piers and girders. It is important to note that inadequate finishing of the reinforcement with the hook in the beam coming from the pier contributed to the formation of these cracks (Figs. 6 and 7).

Figure 4.

Figure 5.

Figure 6.

Figure 7.

8. Destruction of the concrete cover on the reinforced concrete inter-story structures and the presence of irregular nets of cracks caused by fire. This damage indicates that inadequate concrete cover was another flaw in the design of the original structure. Another consequence are large deflections. (Figs. 8 and 9)
9. Severe local damage to the installations holes caused by fire.

Figure 8.

Figure 9.

1.2. DAMAGES RESULTING FROM ATMOSPHERIC ACTIONS

The economic situation in the country at that time did not allow reconstruction of the structures damaged during the war or their immediate rehabilitation following the destruction. Therefore, atmospheric action contributed in large measure to expansion of the damage and even to the growth of vegetation on the structural elements further accelerating the negative impact of the initial damage.

Characteristic damage includes the following:

1. Damage to partially pre-fabricated inter-story slabs, which consist of pre-fabricated reinforced concrete battens and fillings made of scum blocks with a 2, 5 cm monolithic concrete layer. Damage is exhibited by the separation of the block segments from the structure due to frost (Fig. 10).
2. Separation of the pre-fabricated and monolithic part of “Omnia” slabs. This has led to a significant reduction in the bearing capacity. It should be noted

that two effects have contributed to further destruction: fire and poor construction of the layer between these two parts of the inter-story structure (Figs. 11 and 12).

3. Destruction of the concrete cover and corrosion of the reinforcement, as well as changes in local concrete structure. This damage is evident in all the constructive elements, but is severest in the inter-story structures and bridge decks (Figs. 13, 13–15).

Figure 10.

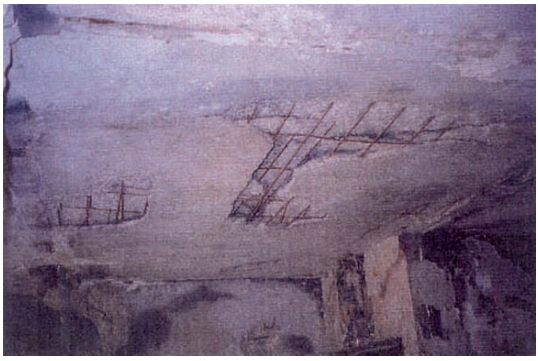

Figure 11.

Figure 12.

Figure13.

Figure 14.

Figure 15.

4. Total destruction of the timber inter-story structures on parts of the structure that had direct contact with the weathering factors. Portions of the inter-story structures that remained intact were also sites where the timber girders were largely destroyed due to moisture, especially in regions where they were resting on walls (Figs. 16 and 17).
5. Deterioration of built in material, mainly mortar in the masonry walls.

Figure 16.

Figure 17.

2. Determination of the In Built Material Characteristics of the Construction Elements

Financial assets were again the cumbersome when quality control of built in material had to be done. The lack of adequate funding resulted in there being no special analysis of the causal factors that could have led to the reduction of these material characteristics. The aim of the analysis that was conducted was only to ascertain whether the built in material continued to satisfies the criterion for its usage in the carrying elements.

2.1. QUALITY CONTROL OF CONCRETE

The testing of concrete material properties was confined to the determination of the concrete strength in compression (Fig. 16). Those tested cylinder samples from the principal structural components often showed a large dispersion of test results, as well as a decrease in the characteristic strength with respect to the one specified by design. This decrease was as high as 50%. In addition to fire and atmospheric agents, another cause of these results dispersion could be poor construction quality of concrete.

The inability to determine the current material quality of pre-fabricated reinforced concrete girders of the inter-story structure (small dimensions of the girder) imposed the in-site testing of damaged structures. Material was used for rehabilitation of the structure and water containers were used to obtain the test loading (Fig. 17).

Figure 16.

Figure 17.

2.2. QUALITY CONTROL OF BUILT IN REINFORCEMENT

Both destructive and non-destructive methods for testing the mechanical characteristics of the built-in reinforcement were utilized depending on the

accessibility of the samples. The results indicated that the built-in reinforcement in most cases did satisfy the quality required by current standards. The exception was welded meshes MAG 500/560 built-in in the inter-story structures that were exposed to fire. This reinforcement underwent severe thermal degradation of yield strength, which practically went back to the value of 240 MP typical of the raw material that is used in the construction of this mesh.

2.3. QUALITY CONTROL OF BUILT IN BRICK AND MORTAR

In order to determine whether the built-in brick satisfied the criterion for the usage in the bearing walls, samples were taken from the walls to test the compressive strength (Figs. 18 and 19). Because tests showed different results in respect to the damage done on different objects, a general conclusion regarding the changes of the characteristics of the built in brick could not be made.

The mortar that was used to connect the masonry was tested for compressive strength and shear strength. However, it must be mentioned that the mortar was usually in such a poor condition that it was not possible to take out samples for testing.

Figure 18.

Figure 19.

3. Additional Static and Dynamic Calculation

In order to assess the possibilities for rehabilitation of the structure, static and dynamic calculation of the structure with new material characteristics and adequate static system were conducted. The main cause for the change in the static system in respect to the designed one was the collapse of the vertical elements of the structure due to mechanical actions.

4. Conclusion

The analyses of the damaged structures indicate that the various causes of the structure degradation can be organized into two characteristic groups with respect to their character of action.

Primary or mechanical damages (damage from explosions) have a local character and do not, in general, present much of a threat to the carrying capacity of the structure.

Those structures that suffered from mechanical damage were left unprotected, so they were exposed to long-term atmospheric action that resulted in additional damage. This secondary damage represents a dominant factor in the degradation of the structure.

The late response due to the financial situation in the country and the inexperience in dealing with the effects of war on civil engineering structures have greatly increased the scale and the cost of the rehabilitation projects. The degree of damage, and thereby the cost of rehabilitation projects, would have been much lower, if the damaged structures were protected from atmospheric action immediately after the war, waiting for rehabilitation to start when the financial resources become available.

Bibliography

V. Hasanović, et al., Report about the state and damage degree of the bearing structure at 3 Emerika Bluma Street in Sarajevo, Institute for Materials and Structures of Sarajevo, 2001

V. Hasanović, et al., Rehabilitation of the damaged RC structure (housing-business complex) in Sarajevo, at 2c and 2d Zagrebačka Street in Sarajevo, Institute for Materials and Structures of Sarajevo, 2001

V. Hasanović, S. Dolarević, F. Biberkić, Report about the state and damage degree of the bearing structure of a housing utility at 7 Lukavička cesta Street in Sarajevo, Institute for Materials and Structures of Sarajevo, 2002

V. Hasanović, M. Hrasnica, S. Dolarević, Report about the state and damage degree of the bearing structure of the House of Parliament and Council of Ministers, Institute for Materials and Structures of Sarajevo, 2003

V. Hasanović, S. Dolarević, F. Biberkić, Report about the state and damage degree of the bearing structure of a housing utility at 30 Kemala Kapetanovića Street in Sarajevo, Institute for Materials and Structures of Sarajevo, 2005

S. Dolarević, F. Biberkić, Report regarding the state of the structure at 2 Koste Hermana in Sarajevo, Institute for Materials and Structures of Sarajevo, 2004

S. Dolarević, Report about the state and damage degree of the "Interšred" Building at Titova Street and rehabilitation measures, Institute for Materials and Structures of Sarajevo, 2007

S. Dolarević, J. Ćurić, Report about the state and damage degree of the bearing structure of a housing utility at 9 Trnovska Street, Institute for Materials and Structures of Sarajevo, 2008

F. Biberkić, S. Medić, Report about the state and damage degree of the bearing structure of a housing utility at 5 Zagrebačka Street in Sarajevo, Institute for Materials and Structures of Sarajevo, 2008

F. Biberkić, S. Medić, J. Ćurić, Report about the state and damage degree of the bearing structure of a housing utility at 3a Zagrebačka Street in Sarajevo, Institute for Materials and Structures of Sarajevo, 2008

AUTHORS INDEX